Carbon Nanostructures

Anish Khan
Mohammad Jawaid
Bernaurdshaw Neppolian
Abdullah M. Asiri *Editors*

Graphene Functionalization Strategies

From Synthesis to Applications

Springer

Carbon Nanostructures

Carbon is intimately connected to almost everything we deal with in a daily basis. Due to its outstanding properties, such as high stability at environmental conditions, different hybridizations, strong covalent bond formation and easy of compounds formation, carbon has been a topic of scientific interest in several areas. Indeed, starting in the 19th century, chemists have devoted a whole field to study carbon-based compounds, which is, nowadays, known as Organic Chemistry. Remarkably, the last 30 years have been witnessing an exponential advance in the science involving carbon and carbon structures. Since the discovery of Fullerenes in 1985, which was awarded the Nobel Prize in Chemistry in 1996, carbon nanostructures have been attracting a great deal of attention from the research community. This public interest dramatically increased after the publications by the Iijima and Bethune groups on single-wall carbon nanotubes in 1993 and found a "new research era" with the isolation of a monolayer of carbon atoms, also called graphene, which conducted groundbreaking experiments demonstrating outstanding phenomena such as the Klein-Tunneling and the fractional quantum hall effect. No wonder, graphene was the object of the 2010 Nobel Prize in Physics.

The "Carbon Nanostructures" book series covers the state-of-art in the research of nanocarbons and their applications. Topics related to carbon allotropes such as diamond, graphite, graphene, fullerenes, metallofullerenes, solid C60, bucky onions, foams, nanotubes and nanocones, including history, theory, synthesis, chemistry & physics, Biophysics & engineering, characterization methods, properties and applications are welcome. Within the "Carbon Nanostructures" book series, the reader will find valuable, up-to-date account of both the newer and traditional forms of carbon. This book series supports the rapid expansion of this field and is a valuable resource for students and professionals in several different areas.

Springer welcomes new book ideas from potential authors. If you are interested in publishing your book in this series, please contact us via mayra.castro@springer.com

**** Indexed by Scopus (2018) ****

More information about this series at http://www.springer.com/series/8633

Anish Khan · Mohammad Jawaid ·
Bernaurdshaw Neppolian · Abdullah M. Asiri
Editors

Graphene Functionalization Strategies

From Synthesis to Applications

Springer

Editors
Anish Khan
Chemistry Department, Faculty of Science
King Abdulaziz University
Jeddah, Saudi Arabia

Center of Excellence for Advanced
Materials Research
King Abdulaziz University
Jeddah, Saudi Arabia

Bernaurdshaw Neppolian
Energy and Environmental Remediation Lab
SRM University
Chennai, India

Mohammad Jawaid
Laboratory of Biocomposite Technology
INTROP
Universiti Putra Malaysia
Selangor, Malaysia

Abdullah M. Asiri
Chemistry Department, Faculty of Science
King Abdulaziz University
Jeddah, Saudi Arabia

Center of Excellence for Advanced
Materials Research
King Abdulaziz University
Jeddah, Saudi Arabia

ISSN 2191-3005 ISSN 2191-3013 (electronic)
Carbon Nanostructures
ISBN 978-981-32-9056-3 ISBN 978-981-32-9057-0 (eBook)
https://doi.org/10.1007/978-981-32-9057-0

This Springer imprint is published by the registered company Springer Nature Singapore Pte Ltd.
The registered company address is: 152 Beach Road, #21-01/04 Gateway East, Singapore 189721, Singapore

Dedicate this book
to his
lovely and precious
Daughter
Aleena Jawaid
Dr. Mohammad Jawaid

Preface

The focus of this book is about the current demand of the technology i.e. functionalization of grapheme oxide by graphting different entities that respond to the different functionalities just like the sensitive core entities. The specialism in grapheme oxide functionalization inaugurated by its outstanding electrical and mechanical properties. Unlike other material, this designed material is combined with resins, carbon materials, nanoparticles to form a high responding functionality as to get the interested in that particular materials. Functionalized grapheme oxide currently stands best among the replacement materials to conventional engineering materials because of its outstanding features such as lightweight, lower cost, environmentally friendly and sustainability. The unique feature of this book is that it presents a unified knowledge of the high-quality material on the basis of characterization, design, manufacture and applications.

This book will help researchers, scientists and industries to understand the need of functionalized graphene for development of safe and sustainable products for different applications. The characterization of functionalized graphene plays a crucial role to find out its potentiality in different real-world application. It elaborates the basic characterization of functionalized graphene or graphene oxide such as; physical, mechanical, thermal and electrical properties. Added with significant morphological and structural properties for clear understanding of this type of materials.

We are highly thankful to all authors who contributed book chapters and provide their valuable ideas and knowledge in this edited book. We attempt to gather all the scattered information of authors from diverse fields around the world (Malaysia, Jordan, USA, Turkey, India, Saudi Arabia, Bangladesh, Oman, and Sweden) in the areas of functionalized graphene nanocomposite and applications and finally complete this venture in a fruitful way. We greatly appreciate contributor's commitment for their support to compile our ideas in reality.

We are highly thankful to Springer-Nature team for their generous cooperation at every stage of the book production.

Jeddah, Saudi Arabia — Anish Khan
Selangor, Malaysia — Mohammad Jawaid
Chennai, India — Bernaurdshaw Neppolian
Jeddah, Saudi Arabia — Abdullah M. Asiri

Acknowledgments

The financial support from Generalitat de Catalunya (Grant 2017SGR1033) and the Spanish Structures of Excellence Mariá de Maeztu Program Grant MDM-2017-0767. This work was supported by the project “Information and Communication Technologies for a Single Digital Market in Science, Education and Security” of the Scientific Research Center, NIS-3317.

Contents

About the Editors

Dr. Anish Khan is currently working as Assistant Professor in Chemistry Department, Centre of Excellence for Advanced Materials Research (CEAMR), Faculty of Science, King Abdulaziz University, Jeddah, Saudi Arabia. Completed Ph. D. from Aligarh Muslim University, India from 2010. Completes Postdoctoral from School of Chemical Sciences, University Sains Malaysia (USM) electroanalytical chemistry in 2010). Working in the field of synthetic Biosensor, polymers composite, organic-inorganic electrically conducting nano-composites. More than 120 research articles, 30 book chapters 10 books published in referred international Publishers and more than 20 international conferences/workshop. Member of American Nano Society, Field of specialization is polymer nano composite/cation-exchanger/ chemical sensor/microbiosensor/nanotechnology, application of nano materials in electroanalytical chemistry, material chemistry, ion-exchange chromatography and electro-analytical chemistry, dealing with the synthesis, characterization (using different analytical techniques) and derivatization of inorganic ion-exchanger by the incorporation of electrically conducting polymers. Preparation and characterization of hybrid nano composite materials and their applications, Polymeric inorganic cation–exchange materials, electrically conducting polymeric, materials, Composite material use as Sensors, Green chemistry by remediation of pollution, Heavy metal ion-selective membrane electrode, Biosensor on neurotransmitter.

Dr. Mohammad Jawaid is currently working as Senior Fellow Researcher (Associate Professor) at Biocomposite Technology Laboratory, Institute of Tropical Forestry and Forest Products (INTROP), Universiti Putra Malaysia (UPM), Serdang, Selangor, Malaysia, and also has been Visiting Professor at the Department of Chemical Engineering, College of Engineering, King Saud University, Riyadh, Saudi Arabia since June 2013. He has more than 14 years of experience in teaching, research, and industries. His area of research interests includes hybrid composites, lignocellulosic reinforced/filled polymer composites, advance materials: graphene/nanoclay/fire retardant, modification and treatment of lignocellulosic fibers and solid wood, biopolymers and biopolymers for packaging

applications, nanocomposites and nanocellulose fibers, and polymer blends. So far, he has published 34 books, 60 book chapters, more than 250 peer-reviewed international journal papers, and 5 published review papers under top 25 hot articles in science direct during 2013–2018. H-index and citation in Scopus are 37 and 6179 and in Google scholar, H-index and citation are 44 and 8594. He worked as guest editor of special issues of *Current Organic Synthesis* and *Current Analytical Chemistry*, Bentham Publishers, UK; *International Journal of Polymer Science*, Hindawi Publishing; Inderscience Enterprises Ltd; IOP Conference Proceeding; and is Editorial Board Member of *Journal of Polymers and The Environment*, *Journal of Asian Science, Technology and Innovation* and the *Recent Innovations in Chemical Engineering*. Besides that, he is also reviewer of several high-impact international peer-reviewed journals of Elsevier, Springer, Wiley, Saga, etc. Presently, he is supervising 18 Ph.D. students (6 Ph.D. as Main Supervisor, and 12 Ph.D. as Member) and 9 Master's students (3 Master as Main Supervisor, and 6 Master as Member) in the fields of hybrid composites, green composites, nanocomposites, natural fiber-reinforced composites, nanocellulose, etc. 12 Ph.D. and six master's students graduated under his supervision in 2014–2018. He has several research grants at university, national, and international levels on polymer composites of around 3 million Malaysian ringgits (USD 700,000). He also delivered plenary and invited talks in international conferences related to composites in India, Turkey, Malaysia, Thailand, the United Kingdom, France, Saudi Arabia, Egypt, and China. Besides that, he is also a member of technical committees of several national and international conferences on composites and material science. Recently Dr. Mohammad Jawaid received Excellent Academic Award in Category of International Grant-Universiti Putra Malaysia-2018 and also Excellent Academic Staff Award in industry High Impact Network (ICAN 2019) Award. Beside that Gold Medal-Community and Industry Network (JINM Showcase) at Universiti Putra Malaysia. He also Received Publons Peer Review Awards 2017, and 2018 (Materials Science) and Certified Sentinel of science Award Receipient-2016 (Materials Science). He is also Winner of Newton-Ungku Omar Coordination Fund: UK-Malaysia Research and Innovation Bridges Competition 2015.

Dr. Bernaurdshaw Neppolian is currently working as a Professor at SRM Research Institute, SRM University, Kattankulathur, Chennai, India since 2012. He has more than 20 years of research experience in the field of photocatalysis. He obtained his Ph.D. degree Anna University, Chennai, year 2000 and then he joined as a Post Doctoral Researcher at Gwangju Institute of Science and Technology, South Korea for two years (2000–2002). Later, Dr. Neppolian had been awarded with Japan Society of Promotion of Science (JSPS), prestigious fellowship to carry out research work at Osaka Prefecture University, Osaka, Japan (2002–2006). Dr. Neppolian had been awarded by KOSEF Brain Pool program to work as a Research Professor in Gwangju Institute of Science and Technology, South Korea for two years (2006–2008). Before joining at SRM University, he worked in Department of Chemistry under the Discovery Project of Australian Research

Council, University of Melbourne, Australia for more than 3 years (2008–2011). He is author of more than 100 publications that have received around 5000 citations with H-Index of 30 and 6 book chapters. He has been working on the preparation of TiO_2 based photocatalysts for energy and environmental remediation studies including splitting of water to produce hydrogen. He is also working on advanced oxidation methods including ultrasound method for the degradation of organic pollutants. Recently, his group started working on Polymer solar cells and Direct methanol oxidation fuel cell using metallic catalysts prepared by ultrasound assisted method. He is currently having 4 research projects from Department of Science Technology and Ministry of New and Renewable Energy, India and guided one Ph.D. student, guiding 8 Ph.D. students and tranined many post and under graduate students. He is potential reviewer for more than 40 reputed international journals inclduing *Applied Catalysis B*, *Enery and Environmental Science*, *Langumir*, etc. He recently received Hiyoshi Environmental Award-2015 from Hiyoshi Corporation, Japan for his outstanding research in the field of environmental protection in India.

Prof. Abdullah M. Asiri is Professor in Chemistry Department—Faculty of Science—King Abdulaziz University. Ph.D. (1995) From University of Walls College of Cardiff, U.K. on Tribochromic compounds and their applications. The chairman of the chemistry department, King Abdulaziz University currently and also The Director of the center of Excellence for advanced Materials Research. Director of Education Affair Unit–Deanship of Community services. Member of Advisory committee for advancing materials, (National Technology Plan, King Abdul Aziz City of Science and Technology, Riyadh, Saudi Arabia). Color chemistry. Synthesis of novel photochromic and thermochromic systems, Synthesis of novel colorants and coloration of textiles and plastics, Molecular Modeling, Applications of organic materials into optics such as OEDS, High performance organic Dyes and pigments. New applications of organic photochromic compounds in new novelty. Organic synthesis of heterocyclic compounds as precursor for dyes. Synthesis of polymers functionalized with organic dyes. Preparation of some coating formulations for different applications. Photodynamic thereby using Organic Dyes and Pigments Virtual Labs and Experimental Simulations. He is member of Editorial board of *Journal of Saudi Chemical Society*, *Journal of King Abdul Aziz University*, *Pigment and Resin Technology Journal*, *Organic Chemistry Insights*, *Libertas Academica*, *Recent Patents on Materials Science*, Bentham Science Publishers Ltd. Beside that he has professional membership of International and National Society and Professional bodies.

Synthesis of Metal/Metal Oxide Supported Reduced Graphene Oxide (RGO) for the Applications of Electrocatalysis and Supercapacitors

Lakshmanan Karuppasamy, Lakshmanan Gurusamy, Gang-Juan Lee and Jerry J. Wu

Abstract Reduced graphene oxide (RGO), atomically thin two-dimensional carbon nanosheets, owns outstanding chemical, electrical, material, optical, and physical properties due to its large surface area, high electron mobility, thermal conductivity, and stability. These unique properties have made reduced graphene oxide an ideal platform for constructing a series of RGO-based functional nanomaterials. Specifically, RGO and RGO derivatives have been utilized as templates for the synthesis of various noble-metal/metal oxide nanocomposites. These hybrid nanocomposites materials are promising alternatives to reduce the drawback of using only transition metal nanoparticles in various applications, such as electrochemical energy storage and conversion technology of supercapacitors and fuel cells. The goal of this chapter is to discuss the state-of-the-art of reduced graphene oxide-based metal and metal oxide nanocomposites with a detailed account of their synthesis and properties. Especially, much attention has been paid to their synthesis and a wide range of applications in various fields, such as electrochemical and electrical fields. This chapter is presented first time with an introduction, followed by synthetic methods of RGO and RGO-based nanocomposites. Then, the application of this novel RGO/metal-metal oxide nanocomposites in fuel cells and supercapacitors are summarized and discussed. Finally, the future research trends and challenges of design and synthesis of RGO/metal-metal oxide nanocomposites are presented.

Keywords Reduced graphene oxide · Metal/metal oxide nanocomposites · Supercapacitors · Fuel cells · Electrochemical reaction

L. Karuppasamy · L. Gurusamy · G.-J. Lee · J. J. Wu (✉)
Department of Environmental Engineering and Science, Feng Chia University, Taichung 407, Taiwan
e-mail: jjwu@mail.fcu.edu.tw

A. Khan et al. (eds.), *Graphene Functionalization Strategies*, Carbon Nanostructures, https://doi.org/10.1007/978-981-32-9057-0_1

1 Introduction

Graphene, a two-dimensional single atomic layer planar sheet with densely packed atomically thin layer of sp^2 hybridized carbon atoms in a honeycomb crystal lattice. Since the first isolation of graphene in 2004 [1]. The appreciation of its significance was followed by the physics noble prize in 2010. The unique and superior physical and chemical properties of graphene, such as a large specific surface area, high-speed electron mobility, strong mechanical strength, and excellent electric and thermal conductivity, are now frequently utilized with new applications [2, 3]. Chemists have taken the advantages of its unique properties by the research on graphene and its nanocomposites, graphene oxide (GO) and reduced graphene oxide (RGO), which have emerged as a promising new nanomaterial for a variety of exciting applications in the fields of chemistry, physics, biology, and many other interdisciplinary fields, such as nanotechnology and nanomedicine. For nearly three decades, carbonaceous materials, such as fullerenes and carbon nanotubes (CNTs), have drawn considerable attention due to their exceptional electronic and mechanical properties [4]. Specifically, after the discoveries of zero-dimensional (0-D) buckminsterfullerene [5] and shortly later one-dimensional (1-D) CNTs [6], enthusiasm in the research of carbon-based nanomaterials has increased further [7]. Both fullerenes and CNTs have been proposed to be derived from 2-D graphene sheets that are viewed as key building blocks of all other graphitic carbon allotropes (Fig. 1), such as "graphite" made up of graphene sheets stacked on top of each other (separated by an interlayer distance of 3.37 °A) [8]. "Fullerenes" and "CNTs" can be virtually made by wrapping and rolling a section of a graphene sheet [9]. In reality, however, they are not synthesized from graphene.

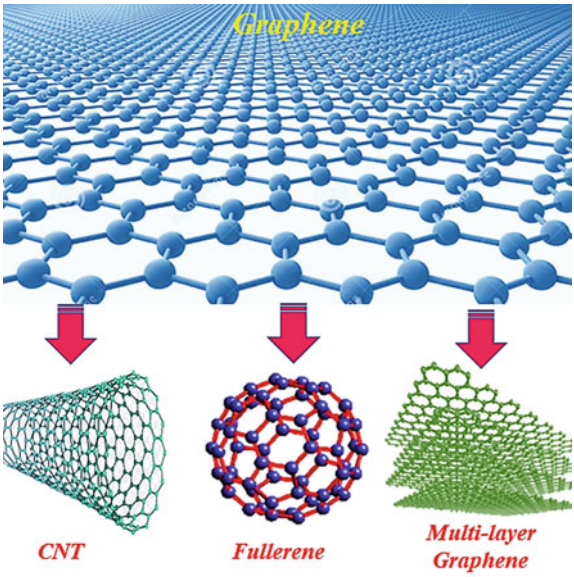

Fig. 1 Graphene is a two-dimensional building block for carbonaceous materials of all other dimensions and it can be wrapped up into 0-D buckyballs, rolled into 1-D nanotubes or stacked into 3-D multilayer graphene

Great contributions have been made in the synthesis of novel catalytic, magnetic, and optoelectronic properties of graphene nanocomposites based on the hybridization with nanoparticles (NPs). It can be noted that hybridization has provided an effective strategy for enhancing the functionality of materials [10]. Particularly, due to the unique sp^2 hybridization of carbon bonds present in graphene, it facilitates the delocalization of electrons to possess excellent electronic conduction [1]. This electronic conduction of graphene can be enhanced by incorporating various inorganic nanoparticles, including different metal and metal oxide NPs. Due to the enhanced electrical and electronic properties and the synergistic effect between graphene and inorganic nanoparticles, graphene/nanoparticle composites offer a great potential for various applications, including energy storage supercapacitor and energy conversion fuel cells devices [11–13]. In order to further enhance the properties and to broaden the applications of graphene, various metal and metal oxide NPs have been decorated on graphene. Apart from enhancing the properties of graphene, the NPs act as a stabilizer against the aggregation of individual graphene sheet, which is caused by strong van der Waals interactions between graphene layers [14]. Therefore, more efforts and new strategies to synthesize graphene-based nanocomposites are indispensable. This chapter has focused on one of such nanocomposites, made of chemically exfoliated graphene and metal oxides. We overview and discuss their synthesis methods, structural features, electrocatalytic applications, and future perspectives.

1.1 Comparison of Energy Storage and Conversion Devices (Electrochemical Supercapacitors, Battery, and Fuel Cells)

Energy and power densities are of two main parameters of an energy storage system. Specific energy, expressed in watt-hours per kilogram (Wh kg^{-1}), determines how much amount of energy could be stored in the system. While the specific power in watt per kilogram (W kg^{-1}) indicates how the energy could be converted. The energy and power density was compared in the electrochemical energy storage system, which is known as a Ragone plot as shown in Fig. 2. The specific energy usually decreases with the increase of specific power. The conventional capacitors have been considered as high-power systems, whereas fuel cells exhibited the high energy density with the combustion engine. Compared with the conventional capacitors, electrochemical supercapacitor (ES) has the ability to store greater amounts of energy due to high surface area carbon nanomaterials combined with pseudocapacitive nature of nanostructured materials. In addition, ES is able to deliver more power than batteries.

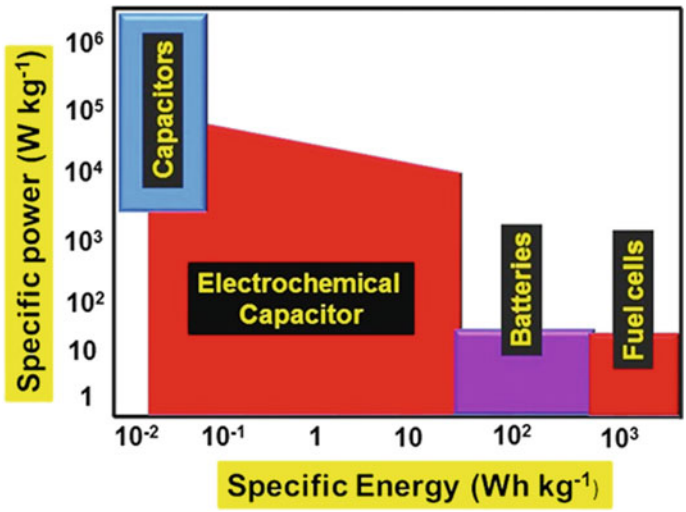

Fig. 2 Schematic diagram of the Ragone plot of energy storage devices [15]

The energy storage mechanism of ES and batteries are fundamentally different. The ES stores the charge on the surface of capacitive materials, whereas batteries store the charge on entire bulk of the electrodes [16, 15]. ESs, batteries, and fuel cells do not always compete with each other. The high power and high-energy resources of electrochemical capacitor have bridged the gap between capacitors and batteries. ES also possess a number of desirable properties that make them an attractive energy storage behavior [17]. For example, the extremely reversible charge and discharge cycle of EDLCs were obtained in a suitable potential window. Moreover, ESs can store or release energy very quickly and can operate over a wide range of temperatures. They also have a high charge and discharge efficiency. The energy loss to heat during each cycle is relatively small. In addition, ESs generally do not contain toxic materials and are much safer than batteries and fuel cells [18].

With the aforementioned advantages, ESs have become a very competitive choice for practical applications of electric vehicles, elevators, digital cameras, mobile phones, pulse laser techniques, and uninterruptible power supplies [19]. For instances, it is very expensive to make frequent replacement of the batteries in the memory back-up system due to their poor cycle life. In a fuel cell or battery electric vehicles, it is difficult to meet peak load requirements of high power, like accelerating or climbing. With the advantages of a long lifetime and high power density, ESs can solve these problems. In the coming decades, the main market targeted by ESs manufacturers may be on the transportation, including hybrid electric vehicles and metro trains [20].

2 Synthesis of RGO and RGO-Based Metal-Metal Oxide Nanocomposites

2.1 Synthesis of Reduced Graphene Oxide (RGO)

A number of methods have been reported already for the synthesis of RGO that can be mainly classified into two different categories, bottom-up approaches and top-down approaches (Fig. 3). The bottom-up synthesis of RGO sheets is an alternative to the micromechanical exfoliation of bulk graphite. For the bottom-up processes, RGO is synthesized by a variety of methods, such as chemical vapor

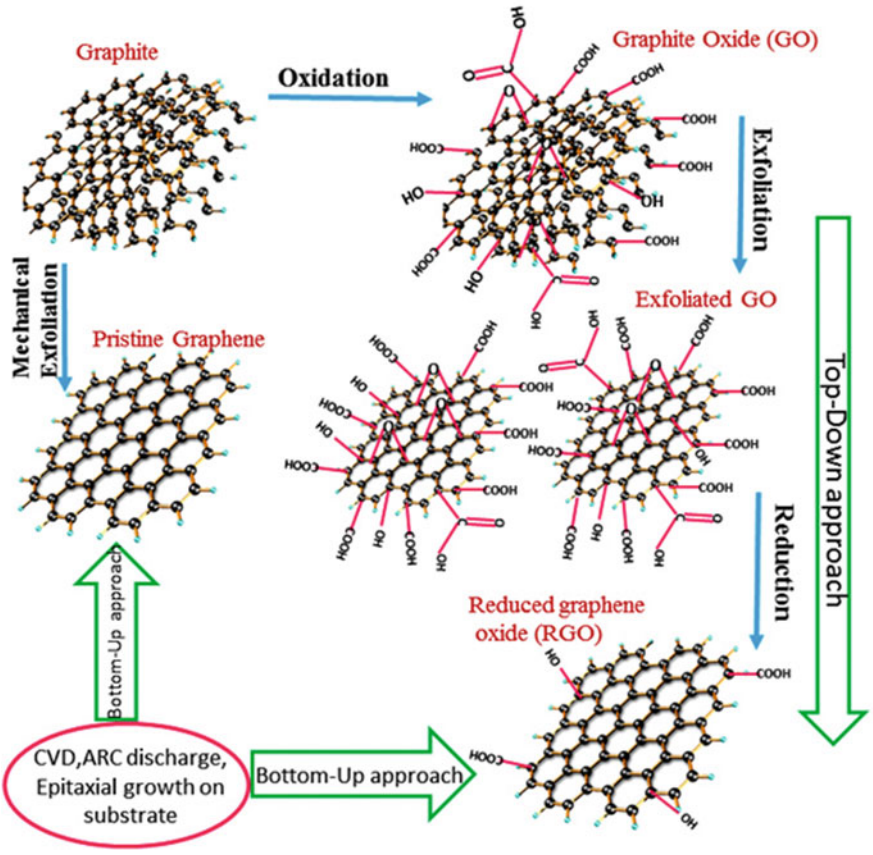

Fig. 3 Schematic representation of the methods used for the synthesis of reduced graphene oxide (RGO), which is classified into top-down and bottom-up approaches. The top-down approach is widely used for the scalable synthesis of graphene that produces a relatively low quality of graphenes like material commonly known as Highly Reduced Graphene Oxide (HRGO) or graphene in the large quantity required for the preparation of graphene-based nanocomposites

deposition (CVD) [21, 22], arc discharge [23], and epitaxial growth on SiC [24]. Using CVD, RGO, and few-layer RGO have been grown on catalytic metal surfaces from carbon-containing gases. The direct synthesis of the CVD method is used for the production of high-quality layers of RGO nanosheets with a large area and low defect concentration, but in small quantities. However, these and other methods revealed before unsuitable for the synthesis of RGO-based nanocomposites, whereas bulk quantities of RGO sheets with a modified surface structure are required. Therefore, for the synthesis of RGO-based nanocomposites, top-down approaches have been used in most cases. These techniques yield low-cost bulk amounts of RGO-like sheets that albeit not defect free, and they are highly processable and can be fabricated into a variety of materials.

The manufacturing of RGO-based nanocomposites generally requires bulk quantities of homogeneously distributed RGO sheets. Therefore, the most common top-down approach for the synthesis of RGO is the reduction of GO by thermal or chemical methods (Fig. 3). The reduction of GO is a low cost and facile technique to yield bulk quantities of RGO nanosheets, where those are highly processable and can be fabricated into a variety of materials. It is now being reinvestigated and receiving intense research interest due to its extensive use as a precursor for the large-scale synthesis of RGO and RGO-based materials. Hence, the application of graphite or graphite derivatives for the synthesis of RGO offers considerable economic advantages over bottom-up methods. Initially, GO was prepared from inexpensive graphite as a raw starting material by the cost-effective and scalable modified Hummers method [25]. Using oxidation and exfoliation of this graphite oxide followed by a reduction process, graphene can be achieved as highly RGO. Like graphite, GO has a layered structure, but the plane of the carbon atoms are heavily decorated by oxygen-containing functional groups, which expand the interlayer distance and make graphite oxide hydrophilic. Exfoliated GO has only one or a few layers of carbon atoms like graphene. GO can be reduced to graphene by removing the oxygen-containing functional groups with the recovery of the conjugated structure. Different reduction processes have been introduced to convert GO into graphene and different reduction processes result in different properties of graphene, which in turn affects the final product and also the performance of the material [26]. Reduced GO has chemically derived graphene, which is also referred to functionalized graphene [27], chemically modified graphene [28], RGO [29], chemically converted graphene [30], or reduced graphene [31]. For the chemical reduction of GO, hydrazine monohydrate and dimethylhydrazine have been used extensively as these do not react with water and have the attractive option for reducing GO in an aqueous dispersion [32–34]. Though hydrazine effectively removes the oxygen functional group from GO, it also introduces heteroatom impurities, such as N_2, which form amines, hydrazones, or other similar functional groups covalently attached on the sheet of graphene [35]. $NaBH_4$ has been demonstrated as being more effective than hydrazine as a reducing agent of GO. $NaBH_4$ is more effective at reducing the C=O group, while it has moderate efficiency in the reduction of epoxide and carboxylic acid [36] (Table 1).

Table 1 Advantages and limitations of the major synthesis procedure of graphene

Synthetic procedure	Advantages	Limitations	Ref.
Micromechanical exfoliation	• Simple process • Few decades • Excellent quality of graphene • Well suited for fundamental research	• Poor reproducibility • Not amenable for large scale production	[37]
CVD	• Large area (up to $\sim$1 cm^2) • A limited number of defects • Mass production • High-quality graphene	• Expensive • Poor scalability	[38]
Epitaxial growth	• High quality of graphene • Few defects	• High cost • High temperature required	[37]
Colloidal suspension	• Scalable • High volume of production • Suitable for multipurpose chemical functionalization	• Significant numbers of defects	[34]
Unzipping of CNTs	• Scalable with controlled widths and edge structures • Better control over chemical functionalization and edge quality	• Low yield • More expensive in respect to chemical exfoliation of graphite or graphite oxide	[39]
Reduction of GO	• Economical and facile technique	• Significant numbers of defects	[40]

Other reductants used for the chemical transformation of GO to graphene include hydroquinone [41], gaseous H_2 [42], alkaline solution [43, 44], and ascorbic acid [45]. Despite the chemical reagent reduction, other reduction processes were used for the conversion of GO to graphene, e.g., microwave irradiation [46, 47], electrochemical reduction [48, 49], thermal annealing [50], photocatalytic reduction [51], solvothermal reduction [52, 53], thermal deoxygenation [54], or chemical deoxygenation [55]. In terms of electrical conductivity, the quality of reduced graphene is lower than that of the graphene nanosheets prepared by CVD. The intrinsic quality of CVD graphene films makes them an excellent candidate for optoelectronic and electronic applications. In brief, the reduction method fits better for the production of small graphene nanosheets. However, the CVD process is more efficient for larger graphene nanosheets.

2.2 Synthesis and Architecture of NPs-RGO Nanocomposites

Graphene derivatives, especially GO and RGO, are good templates or supports for metal and metal oxide nanoparticle nucleation, growth, and attachment, owing to a large number of defects and oxygen functional groups on their surfaces. Thus, for the synthesis of graphene-nanocomposites in most cases, top-down approaches have been used. In another process for the synthesis of graphene-based nanocomposites, graphene or nanoparticles (NPs) could be chemically functionalized firstly and then NPs could be conjugated to the graphene surface by covalent or noncovalent interaction [56, 57]. Graphene is flexible and has a unique 2D sheet-like structure. These sheets can be easily used to wrap or encapsulate NPs with diameters from the nanometer to even the micrometer range. The encapsulated structure is comprised of a single NP encapsulated by a single graphene nanosheet (Fig. 4a), whereas a wrapped structure refers to the case where more than one NP is covered by multiple graphene nanosheets (Fig. 4b). Graphene encapsulated and wrapped structures have advantages compared to bare NPs, including reduced NP agglomeration, as well as increased electrical, electrochemical, and optical properties. Encapsulating NPs with graphene increases the surface-to-volume ratio that is available for sensing [58].

Furthermore, the presence of graphene results in extremely high carrier mobility, high carrier density, and low intrinsic noise for better detection by virtue of the high signal-to-noise ratio. In the anchored structure, electroactive NPs are anchored on the graphene nanosheets (Fig. 4c) [59] and in the mixed structure the graphene and

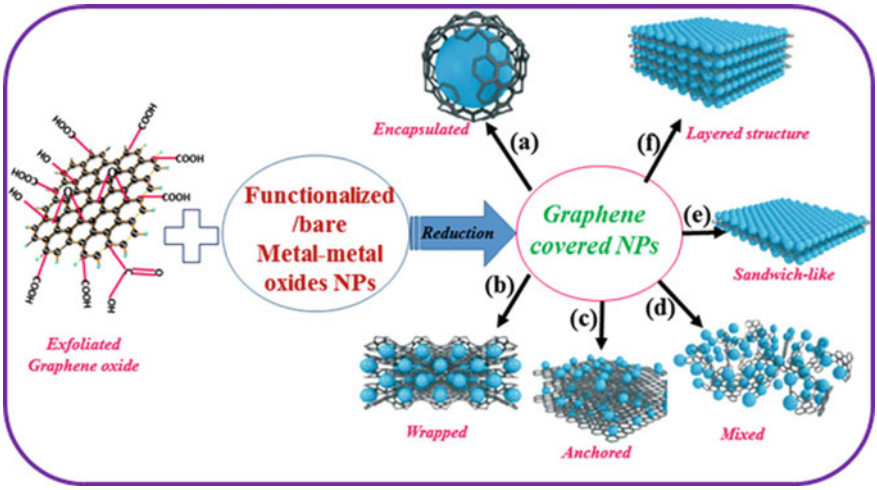

Fig. 4 Schematic presentation of methods used for the formation of graphene–nanoparticles (NPs) composites and different structures of **a** graphene-encapsulated NPs, **b** graphene-wrapped NPs, **c** NPs anchored to graphene nanosheets, **d** mixed graphene–NP structures, **e** graphene–NP sandwich structures, and **f** graphene–NP layered

NPs are synthesized separately and mixed mechanically for application needs in various fields (Fig. 4d) (though mainly used for electrode preparation in Li-ion battery applications). In the sandwich structure, graphene was used as a template to generate the active NP/graphene sandwich structure (Fig. 4e) [60] and in the layer structure, graphene and NPs (Fig. 4f) were alternated. The most research effort has been directed towards the quality improvement of RGO in order to ameliorate the properties of graphene.

2.3 *Synthesis of Metal/Metal Oxide NPs on Reduced Graphene Oxide*

In this section, the synthetic methods of preparing metal and metal oxide NPs on graphene are classified according to the overall strategy and the frequency of their use in the literature (Fig. 5), namely in situ (chemical reduction, hydrothermal and electrochemical methods) and ex situ methods (e.g., physical mixing pre-synthesized NPs with graphene derivatives). Ex situ method involves mixing of

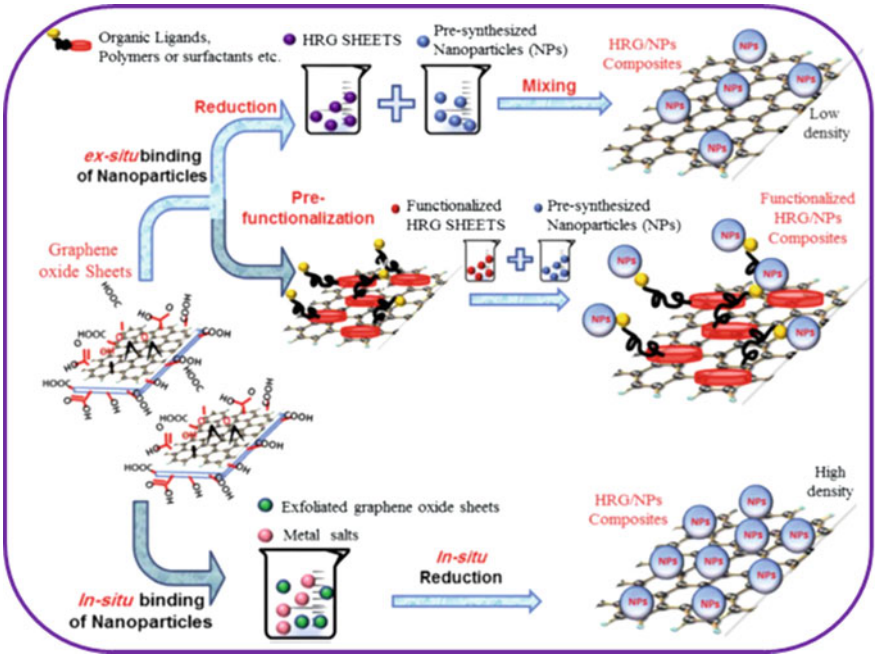

Fig. 5 Schematic illustration of the binding mechanisms of nanoparticles (NPs) onto HRG sheets. The NPs can be loaded onto HRG sheets in two different ways by in situ or ex situ binding. A high density of NPs can be achieved via in situ binding. Both HRG sheets and NPs can be functionalized either via non-covalent p–p stacking or covalent C–C coupling reactions [10]

separate solutions of graphene nanosheets and pre-synthesized NPs. Prior to mixing, the NPs and/or graphene sheets are surface functionalized to enhance the processability of the resulting products. The conjugated graphene sheets can be readily functionalized by non-covalent p–p stacking or covalent C–C coupling reactions. The functionalization of graphene and/or NPs significantly enhances their solubility and hence broadens the opportunities for the preparation of graphene-based composites. However, the ex situ method may suffer from low density and non-uniform coverage of nanostructures by graphene sheets. Therefore, the in situ methods for the preparation of metal and metal oxide decorated graphene-based nanocomposites will be discussed in some detail. In the following paragraphs, we describe the most recent methods for the synthesis of graphene-based metal and metal oxide nanocomposites by in situ methods, i.e. by the simultaneous reduction of graphite oxide or graphene oxide and the respective metal salts.

2.3.1 In Situ Method

Wet-Chemical Method

The chemical reduction method is probably used most frequently because this easy and straightforward method can generate the graphene-based metal and metal oxide nanocomposites [61–63]. In a typical synthesis, the metal precursor (e.g., $HAuCl_4$, K_2PdCl_4 or H_2PtCl_6) is mixed with the graphene compounds in an aqueous solution under a given condition and the reductant (e.g. $NaBH_4$) is then added.

During the synthesis, the metal precursor is reduced to its metallic form, where there are three primary steps: reduction, nucleation, and NP growth, and meanwhile the graphene derivative are also reduced. In this method, GO is the most frequently used graphene compound because the surface functional groups of GO not only afford solubility in water [64–66], but also they stabilize NPs. In a typical case, Hutchings' group adopted this method for preparing GO-stabilized Au–Pd NPs (AuPd–GO) using a "ligand-free" chemical reduction method [67]. GO was introduced into a mixed aqueous solution of $HAuCl_4$ and $PdCl_2$ and the metal precursors were reduced using $NaBH_4$, without the addition of a surfactant, to form AuPd NPs stabilized solely by GO (AuPd–GO) (Fig. 6). Due to the broad AuPd NP size distribution (1–7 nm) and GO stacking, however, AuPd NPs/GO exhibited worse conversion even than PVA-stabilized AuPd/GO counterpart in the solvent-free oxidation of alcohols with molecular oxygen. In order to overcome these problems, the authors then immobilized the TiO_2 NPs, which efficiently inhibited stacking of GO layers, promoted the diffusion of alcohols and oxygen molecules between adjacent GO sheets, and therefore improved the surface catalytic active sites exposure and significantly enhanced the catalytic activity.

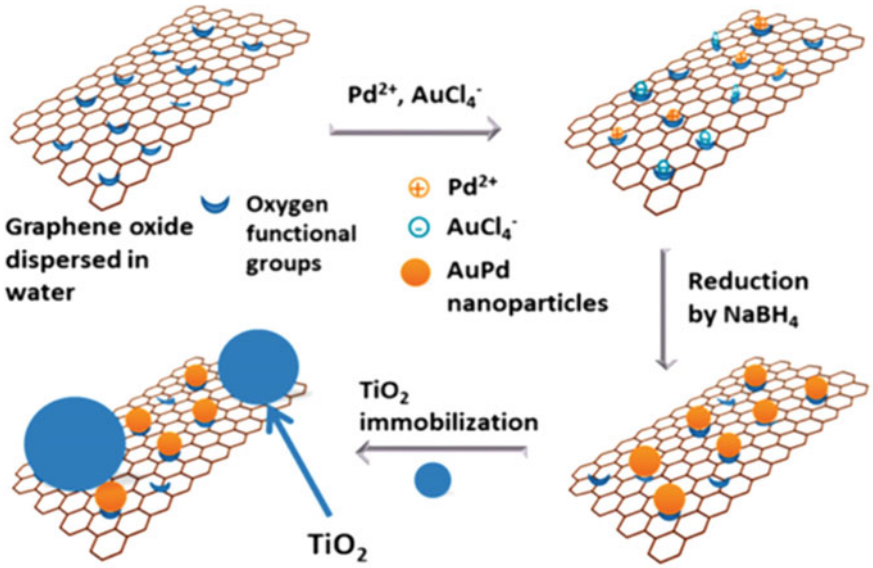

Fig. 6 Preparation of GO-stabilized Au–Pd NPs on TiO_2 (AuPd–GO/TiO_2) using "ligand-free" co-reduction and subsequent sol-immobilization method [67]

Microwave-Irradiation (MWI) Method

MWI is also widely applied for the synthesis of graphene-based nanocomposites. Particularly, the preparation of graphene/metal nanoparticle (NP) composites by simultaneous (in situ) reduction of various metal salts and GO is highly effective. In the case of microwave-assisted reduction to prepare metal-metal oxide/graphene composites, the microwaves caused local dielectric heating of a metal salt solution, thereby resulting in the reduction. The advantage of microwave irradiation-assisted reduction is the uniform and rapid heating that reduces the barriers to the reduction, nucleation, ion incorporation, and NP growth [68, 69]. Thus, in this way, the NPs are obtained with ultrafine NP size and narrow size distribution. For instance, Chen's group reported the microwave-assisted synthesis of CuNPs/GO in the presence of EG (Fig. 7), yielding GO-decorated CuNPs with a 4.1–5.4 nm size that depends on the Cu contents [69]. MWI has attracted much attention due to its ease of processing and scalable production. Moreover, owing to the rapid and uniform heating, MWI prevents the aggregation of graphene layers. A major drawback is the difficulty in controlling the size, uniformity, and surface distribution of NPs on RGO surfaces.

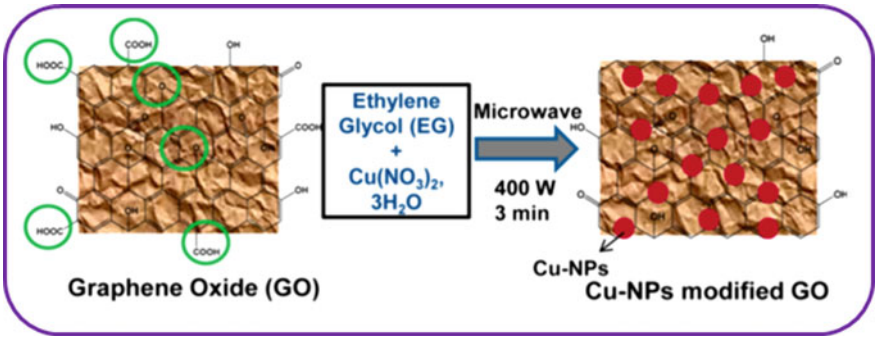

Fig. 7 Microwave synthesis process for GO hybrids decorated with CuNPs [69]

Hydrothermal Method

Hydrothermal and solvothermal reduction processes have been applied for the synthesis of graphene-based metal and metal oxide nanocomposites. It is a low-cost, facile, and template less approach. It generally involves a chemical reaction occurring in a solvent at high temperature above the solvent boiling point and under high pressure in the presence or absence of reducing agent. The NP size, morphology, and crystallinity are tuned upon by adjusting the temperature, pressure, nature of the solvent, and eventually the presence and nature of the reducing agent. Meanwhile, the graphene derivative may also undergo a reduction process to RGO. Moreover, in most of the case, this method allows the synthesis of metal and metal oxide/graphene nanohybrids in one-step. Hydrothermal reactions are sometimes carried out in the absence of reducing agent, but a solvent such as water [70] is necessary. This method is eventually associated with the subsequent annealing treatment to modify the NP morphology. On the other hand, the solvent (EG [71, 72], formic acid [73], EtOH, or DMF) also serves as the reducing agent.

In a typical synthesis procedure [71], the pre-synthesized 3D graphene (3DG) was mixed with $Pd(acac)_2$ and $Co(acac)_2$ in the presence of EG under stirring. The mixed solution was placed in a Teflon-sealed autoclave and maintained at 260 °C for 10 h under high-purity argon protection followed by centrifugation, washing, and oven-drying at 70 °C to obtain the Pd_6Co/3DG catalyst. The resulting Pd_6Co/3DG has a narrow size of Pd_6Co NPs of 5.2 nm that was uniformly distributed on the 3DG, showing a much higher formic acid electro-oxidation activity, the larger peak current density and better stability than Pd/3DG, Pd/C and commercial Pd–C counterparts (Fig. 8). Similarly, Zhang and co-workers reported a facile and cost-effective strategy to synthesize ultrafine Pd NPs supported on N and S dual-doped graphene (NS-G) nanosheets for both direct formic acid fuel cell and direct methanol fuel cell [72]. The NS-G was first prepared by the incorporation of N and S atoms into graphene frameworks via a thermal treatment process, followed

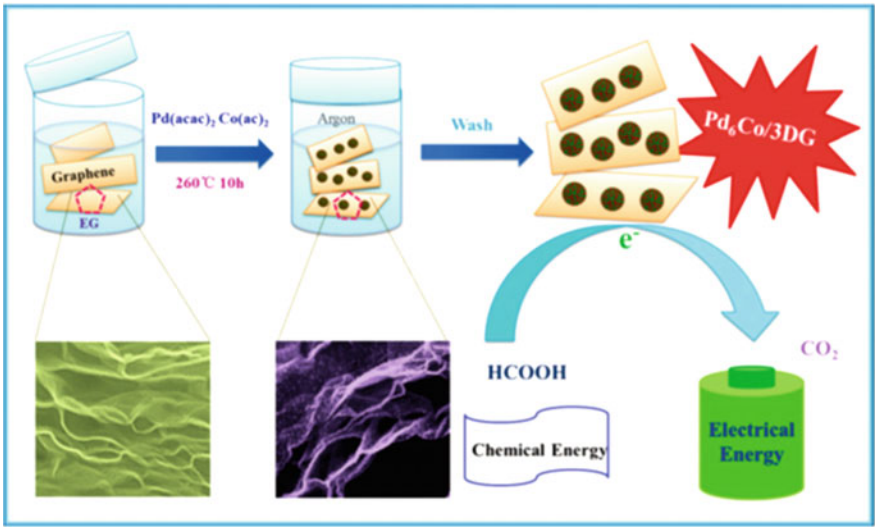

Fig. 8 One-pot hydrothermal process synthesis of a Pd_6Co/3DG catalyst and its application in formic acid oxidation [71]

by the controlled growth of PdNPs on it through a hydrothermal process. The Pd NPs were obtained with an ultrasmall size of 4.6 nm benefiting from the pre-synthesized NS-G sheets that provided sufficient anchoring sites.

Sonochemical Method

The ultrasonic wave irradiation method provides a remarkably facile and versatile route to fabricate various metal nano-architectures in a very short period of time, in which the ultrasonic wave produces various distinctive properties by acoustic cavitation, such as bubbles formation, growth, and implosive the collapse of bubbles in the liquid, which can be well utilized to achieve excellent quality of novel metal nano dendrites with narrower size distribution, larger surface area, and a much smaller size [74]. Nevertheless, limited articles are available on the development of novel metal nano dendrite structures by ultrasonic irradiation for the use as in DEFC. Herein, we have reported a facile one-pot synthesis of Au nano dendrites with branched architectures of RGO nanosheets by sonochemical irradiation method (Fig. 9). The important advantages of this novel method to synthesize Au nano dendrites on RGO nanosheets consist of the following: (1) the Au nano seeds are formed at very short interval of ultrasonic wave irradiation, which can be either act as a catalyst to further growth of Au nano dendrites structures, (2) the size and shape of Au nano dendrites can be easily controlled by ultrasonic irradiation time, concentration of surfactant and reducing agent, and (3) the as obtained Au

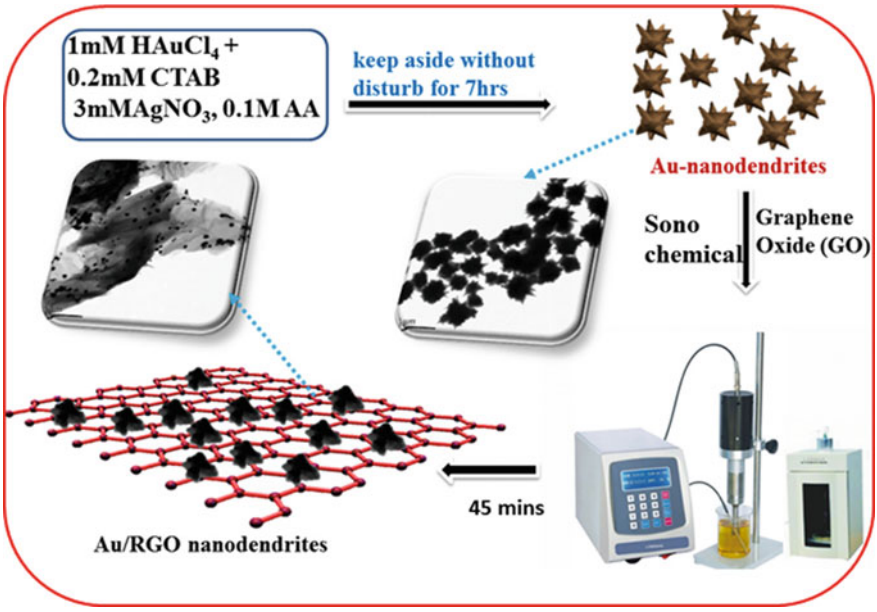

Fig. 9 Sonochemical method for synthesis of an Au/RGO catalyst and its application in electrocatalytic ethanol oxidation fuel cells [75]

nano dendrites with "clean" surfaces on RGO nanosheets can be directly utilized as the electrocatalyst towards ethanol oxidation and oxygen reduction in alkaline medium without further pretreatment.

In a typical preparation of Au-RGO nano dendrites (Fig. 9), firstly 80 mg of graphene oxide (GO) was dispersed in 40 ml DI water (2 mg mL^{-1}) for 10 min by ultrasonication and centrifuged at 10,000 rpm for 15 min. The dispersion and ultrasonication followed by centrifugation of this step repeated 4 times to endorse the discard of unwanted impurities from graphene oxide nanosheets and the final precipitate of graphene oxide nanosheets was dissolved in 20 mL DI waters for further use. Secondly, the fabrication of Au nano dendrites on RGO nanosheets was done by ultrasonic irradiation method (Ti-horn, 20 kHz, and 100 W cm^{-2}) in Ar atmosphere for 45 min (55 s on, 5 s off mode) (synthesis scheme as shown in Fig. 8). The aqueous solution containing 40 mL of 0.2 M CTAB, 1.92 mL of 3.0 mM $AgNO_3$, 40 mL of 1 mM $HAuCl_4$ (Au(III)), and 1 mL of 0.1 M ascorbic acid with 10 min of vigorous stirring and keep aside at room temperature for 7 h without disturbing. After 7 h, the resultant solution mixture followed by adding 10 mL GO suspension was purged with 60 mL min^{-1} Ar for 20 min and then irradiated with the ultrasonic horn for 45 min (ultrasonic bath maintained at 25 °C by a water circulating system). The final product of Au-RGO nano dendrites was collected carefully and washed with absolute ethanol and water by several cycles for the removal of unreacted substrates. Finally, the composite was dried in vacuum air at 60 °C for 24 h.

Electrochemical Deposition Method

Chemical synthesis methods have been widely applied for the fabrication of flower-like PtPd nanostructures. However, these methods suffer from some obstacles, which make the procedure complicated and limit the pervasive application. For example, nanoflowers adhesion on the substrate normally restricted to weak physical or chemical interaction and the surfactants and organic compounds, which usually used in chemical methods, can inhibit the catalytic activity of the resulted nanostructures [76]. However, the electrodeposition method is attractive for achieving high-quality films because of its simple operation, no additional purification step, implementation in low cost, operation in ambient temperature, and no need to various chemical reagents [77]. Besides, the size, morphology, and dispersion of the resulted catalyst nanostructures can be controlled to some extent by the selection of precursor concentration, additives, potential or current density, and so on. In this method, a simple and one-step procedure is employed by keeping the electrode potential at −0.20 V within 300 s at the room temperature to generate the PtPd with a nanoflower structure. In the next step, the modified electrode was removed and rinsed with double distilled water. The prepared electrode in this step is notified as PtPd-NFs/Cu_2O-NSs/RGO. In the following, for comparison the conventional PtPd-NPs deposited on Cu_2O-NPs/RGO were prepared by a similar method as stated above in a solution consisting of 0.002 M of $PtCl_2$ and $PdCl_2$ (1:1 ratio) and 0.1 M KCl. After that, the electrode was taken out and again rinsed thoroughly with double distilled water. The prepared electrode in this step is notified as PtPd-NPs/Cu_2O-NPs/rGO. To better illustrate the electrode modification process, basic steps in electrochemical deposition procedure of Cu_2O and PtPd with different structures are schematically shown in Fig. 10.

3 Application of RGO-Based Metal/Metal Oxide Nanocomposites

The development of alternative strategies for the production of clean energy is one of the biggest challenges for the scientific community. Due to the increasing global warming, air pollution, and growing environmental concerns, the efforts directing toward the development of energy storage and energy conversion devices with high energy densities and power densities have increased tremendously. Graphene-based metallic nanocomposites have gained immense popularity in the field of electrochemical energy storage and conversion [79]. Because of their physicochemical properties, such as high thermal and chemical stability, large surface area, excellent electrical conductivity, and superior thermal and mechanical properties, graphene-based materials have been exploited as electrode materials in electrical energy storage devices. Additionally, their broad potential range and rich surface chemistry have allowed customizing the properties of storage/conversion devices

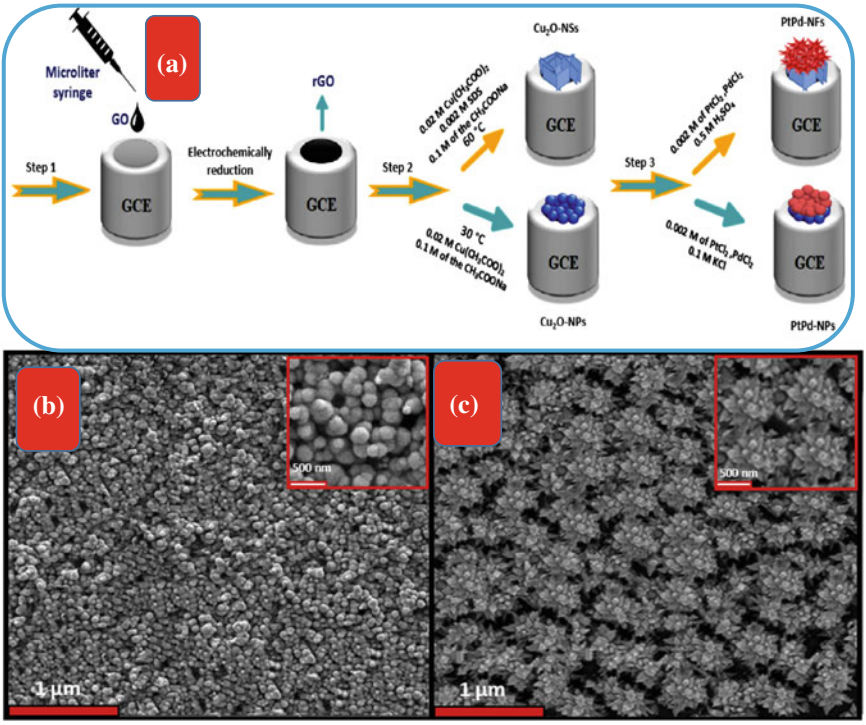

Fig. 10 Electrochemical deposition method for synthesis of a PtPd-NFs/Cu_2O-NSs/RGO catalyst and its application in electrocatalytic methanol oxidation fuel cells [78]

[80–82]. Therefore, graphene-based metallic, bimetallic, and metal oxide nanocomposites have found wide applications in the field of electrochemistry (fuel cells, supercapacitors), photochemistry, and organochemistry (Fig. 11). The most distinguished applications of graphene-based metal/metal oxides in electrochemistry have a long reputation in this area [83]. Indeed excellent electrochemical properties have been disclosed for graphene and its derivatives [84, 85]. The deposition of inorganic nanomaterials, especially metal/metal oxides, onto graphene form interesting metal/metal oxides-graphene nanohybrids, which are expected to present new and intriguing electrochemical properties due to the excellent catalytic activities of metal/metal oxides nanoparticles.

3.1 Electrocatalyst

Electrocatalysis is a special field in electrochemistry that speeds up the rate of an electrochemical reaction occurring on electrode surfaces or at liquid/solid interfaces. There are various types of electrochemical reactions involved in different

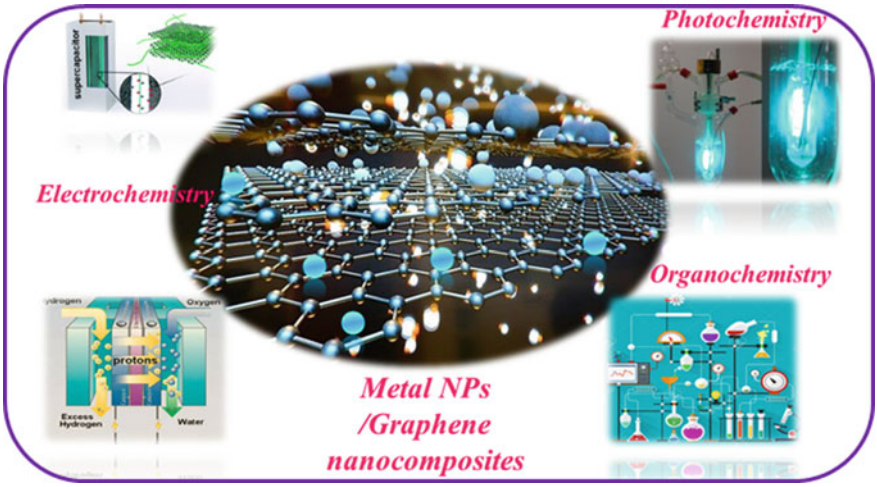

Fig. 11 Schematic illustration of graphene-based metal/metal oxide nanoparticles towards the applications in electrochemistry, organochemistry, and photochemistry

electrocatalytic applications, such as fuel cells, batteries, organic electrosynthesis, and electrode sensor related fields. Among the various electrocatalysts, metal-metal oxide based nanocomposites have received much attention in research owing to their high catalytic activity, stability, selectivity, and tunable properties. Therefore, the novel catalytic and optoelectronic properties of graphene nanocomposites based on the hybridization with nanoparticles are of great significance for the commercialization of electrocatalytic-system-based energy devices. Normally, noble metal-metal oxides are dispersed on catalyst supports for fuel-cell and supercapacitors application. To date, various carbon support nanomaterials have been developed, such as carbon nanotubes, carbon nano horns, and carbon black was incorporated into the hybrids to construct novel noble metal-based nanocomposites. Remarkably, reduced graphene oxide has been extensively used in electrochemistry because of its low price, suitable electrocatalytic activity for a variety of redox reactions, broad potential window, and relatively inert electrochemistry. In this section, we present some examples for the application of reduced graphene oxide (RGO)/metal-metal oxides nanocomposites for different kinds of electrocatalytic reactions

3.1.1 Anodic Oxidation Reaction (AOR)

AOR by RGO Supported Metal-Metal Oxide Nanocomposites

The ever-increasing use of fossil fuels and the increasing concerns of environmentally friendly and sustainable development have pushed direct alcohol fuel cells (DAFCs) to be considered as an excellent candidate because of easy handling,

high-energy conversion efficiency, low pollutant emission, and low operating temperatures. Despite their great potential as an efficient device to convert chemical energy into electrical energy, DAFCs do have their own serious limitations that prevent them from being scaled-up for commercial applications. To date, Pt-based materials have been extensively used as the most effective catalysts for fuel cells, mainly because of their advantages, such as specific activity, high stability, and durability [86]. Unfortunately, high cost, limited resource, and poisoning effect of CO_{ads}-like intermediates on Pt are critical problems, which limited its practical applications [87]. Therefore, the development of new anodic catalysts with low cost and better activity towards fuel oxidation is an urgent need.

In order to surmount these obstacles, two main strategies can be used to reduce the mass of Pt per surface during the fabrication. One strategy is to combine Pt with a cheaper metal to fabricate a bimetallic catalyst. For example, PtPd bimetallic catalysts have captured the interest because of unique characteristics in contrast to their individual counterparts. Also, relatively more abundance of Pd in nature and a lower cost for it, as well as similar catalytic performance with unique tolerance against poisoning effect, have raised more interests for PtPd. Moreover, another strategy to decrease the loading of Pt is to manipulate the shape, size, composition, and structure of the deposited catalyst. In this way, more efforts were devoted to the fabrication of new and unique structures with more active sites, such as edges, corners, steps or more active facets [88]. From this prospect, up to now PtPd catalysts with various structures have been designed, such as cubes [10], dendritic structures [89], nanowires [90], nanotube [91], nanorod [92], and nanoflowers [93]. However, there are some essential drawbacks, such as slow kinetics of methanol electro-oxidation and vulnerability toward intermediate poisoning effects. To overcome these challenges, transition metal oxides as a suitable supporting material can be considered as an appropriate way to enhance the electrocatalytic activity and stability of catalysts [94]. The improved performance as mentioned before can be explained based on the synergetic effects between metal catalysts and transition metal oxides, increasing of the catalyst utilization and excellent proton conductivity. Also, metal oxides increase the superficial hydroxides on catalyst because of spillover of the primary oxide and the partial electron transfer [95]. Among various metal oxides, Cu_2O can be considered as one of the promising candidates given its low-cost, low toxicity, good electrochemical behavior, and high CO tolerance [96].

Based on the above considerations, the aim of the study is to improve the catalytic electro-oxidation of methanol by using a metal oxide (Cu_2O), bimetallic (PtPd) catalyst, and a suitable carbon (RGO) nanomaterial (Fig. 12a, which represents a mechanism of electro-oxidation of methanol over a surface of PtPd NFs/Cu_2O Ns/RGO catalysts). Cyclic voltammetry was used to investigate the electrochemical behavior of the prepared electrocatalysts. Figure 12b depicts the cyclic voltammograms (CVs) of PtPd-NPs/RGO (a), PtPd-NFs/RGO (b), PtPd-NPs/Cu_2O-NPs/RGO (c), and PtPd-NFs/Cu_2O-NSs/RGO (d), where those were recorded in a potential window of −0.25 to 1.3 V in 0.5 M H_2SO_4 for the solution at a scan rate of 50 mVs^{-1}. It can be noted that the prepared nanocomposites essentially have the same voltammetric features, containing hydrogen adsorption/desorption

and PtPd oxide formation/reduction regions. The nanocomposite containing Cu_2O-NSs and PtPd-NFs nanostructures shows higher current densities, reflecting the greater electrochemical active surface areas (EASA). This result can be attributed to the fact that the introduction of Cu_2O into the as-prepared nanocomposites is in favor of the intimate combination of PtPd, Cu_2O, and RGO. Further investigations were carried out to explore and compare the electrocatalytic properties of the prepared nanocomposites towards the methanol oxidation reaction (MOR) by measuring the CV response in 0.5 M H_2SO_4 and 0.5 M methanol solution, as presented in Fig. 12c. It can be seen that anodic peak current densities increase in the order of PtPd-NFs/Cu_2O-NSs/RGO > PtPd-NPs/Cu_2O-NPs/RGO > PtPd-NFs/RGO > PtPd-NPs/RGO. According to the above-mentioned experimental facts, several factors may be considered to explain the mostly enhanced MOR on PtPd-NFs/Cu_2O-NSs/RGO. The probable reasons for this trend are summarized as follows: Firstly, Cu_2O-NSs/rGO provides more active sites and expands the fine dispersion of PtPd catalysts. This result clearly shows that shape and morphology of the Cu_2O and PtPd has a notable impact on the electrocatalytic activity. Thus, unique nanostructures with the larger surface area could provide a high population of the active sites for electrocatalytic applications. Also, Cu_2O nanosheets and RGO

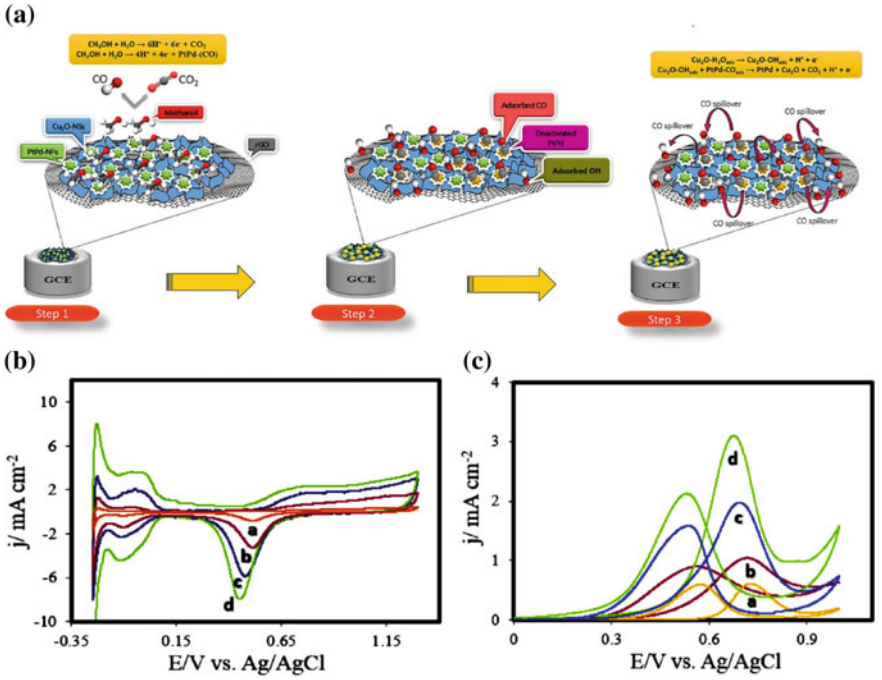

Fig. 12 **a** Electrochemical deposition method for synthesis of a PtPd NFs/Cu_2O Ns/RGO catalyst and its application in electrocatalytic methanol oxidation fuel cells. **b**, **c** Cyclic voltammetry is used to investigate the electrochemical behavior of the prepared electrocatalysts [78]

as suitable support can prevent the unfavorable agglomeration of the catalyst active sites [97]. Furthermore, interconnected nanosheets with porous shapes can improve the transfer electron process, which is also beneficial for the development of electrocatalysts [98]. Secondly, enhancement in the performance of the methanol oxidation can be explained by the co-action and synergistic effect among PtPd, Cu_2O, and rGO [99]. Moreover, the oxophilic nature of the Cu_2O facilitates the formation of OH_{ads} and spillover to PtPd surface [96]. These OH_{ads} can react effectively with carbonaceous intermediate species to produce CO_2, releasing the active sites on PtPd for continuing the electrochemical reaction. In addition, the electronic structure modification due to the partial electron transfer from RGO and Cu_2O to PtPd improves the electrocatalytic capability. The same phenomenon has been reported successfully in the case of CeO_2, MnO_2, and NiO [100]. Relevant reactions can be expressed as the following:

$$Cu_2O + OH^- \rightarrow Cu_2O - OH_{ads} + e^- \quad (1)$$

$$PtPd - (CH_3OH_{ads}) + 4OH^- \rightarrow PtPd - CO_{ads} + 4H_2O + 4e^- \quad (2)$$

$$PtPd - CO_{ads} + Cu_2O - OH_{ads} + OH^- \rightarrow PtPd + Cu_2O + CO_2 + H_2O + e^- \quad (3)$$

AOR by RGO Supported Noble Metal Nanocomposites

The improvement on more efficient electrocatalyst for the direct ethanol fuel cell (DEFC) is one of the important steps in achieving outstanding efficiency. At present time, the noble metals, such as platinum group metals, have been extensively used as electrocatalysts for DEFC. However, the major problem associated with Pt and Pt group metals has been easily poisoned by strongly chemisorbed non-reactive intermediate species, especially CO [101–103]. To overcome the problem of CO-poisoning, the highly effective Au and Au-based functional electrocatalyst may potentially explore an as promising alternative to electrochemical oxidation of ethanol in DEFC. The fabrication of Au nanostructures with controlling morphology has acknowledged considerable attention because of their fascinating physicochemical properties and multi-functional application in catalysis [104, 105].

Generally, a detailed reaction mechanism of ethanol oxidation reaction (EOR) and in particular the rate-limiting steps remain unclear or even contradictory, which produces a variety of intermediate product, such as CH_3CHO, CH_3COOH, and CO. The possible reactive intermediate pathway for ethanol electrooxidation in alkaline condition is: A proposed mechanism of ethanol electrooxidation reaction on Au surface in alkaline aqueous solution at the low potential window (−1.0 to 0.8 V) is described by the following equation as shown in Fig. 13. The earlier research articles by Guo et al. [106] and Rodriguez et al. [107] reported that ethanol electrooxidation on Au electrode mainly yields CH_3CHO (acetaldehyde) and CH_3COOH acetic acid, which means no C–C bond cleavage happens on Au surface. Furthermore, Tateishi et al. [108] confirmed that CH_3CHO (acetaldehyde)

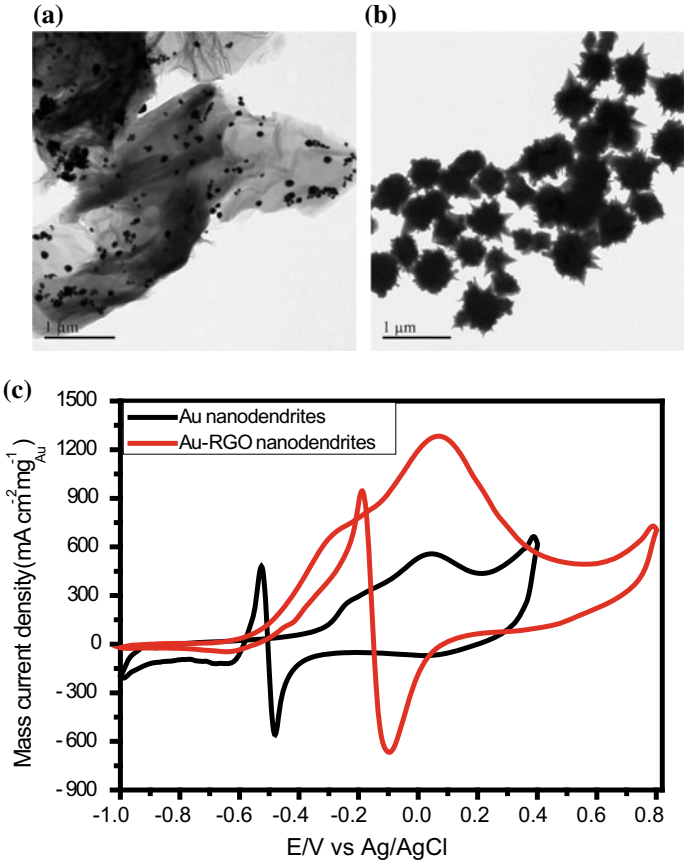

Fig. 13 TEM images of as-prepared freestanding Au nano dendrites and Au-RGO (**a**, **b**) and the corresponding cyclic voltammetry analysis of as-prepared electrocatalysts (**c**) [75]

could be oxidized on Au electrode surface in alkaline medium. Inspired by this, we have ever used the same electrochemical method and the experimental results showed ethanol electrooxidation on Au and Au/RGO nano dendrites possibly through dual pathway mechanism as shown in Fig. 13. The electrocatalytic activity of as prepared electrocatalysts towards the oxidation of ethanol has been evaluated in 1 M KOH + 1 M CH_3CH_2OH with the potential range from −1.0 to 0.8 V at the scan rate of 50 mVs^{-1}. The mass current density of ethanol oxidation was normalized by loading amount of Au nano dendrites on GCE (glassy carbon electrode). For comparison, the CV plots (Fig. 13c) for ethanol electrooxidation of Au and Au-RGO nano dendrites exhibited two strong oxidation peaks in both positive and negative scans. Herein, the peak current density and onset potential for the anodic scan have the two essential limitations to estimate the virtual electrocatalytic performances of the electrocatalyst [109]. During the anodic scan, the current increases

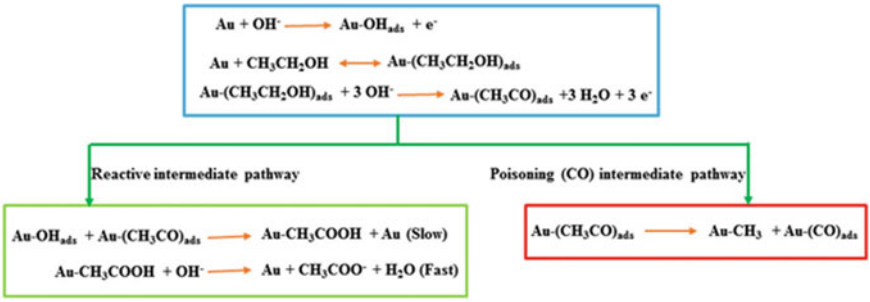

Fig. 14 Scheme for the ethanol electrooxidation reaction pathway of Au electrode in alkaline medium [75]

until the peak seen at about 0.061 V, which is owing to the direct electrooxidation of newly chemisorbed species coming from ethanol adsorption. When the potential scan is negative, the reversed peak at about −0.186 V is corresponding to the removal of poisonous species, which are incompletely oxidized in the anodic scan. It is worth noting that the Au-RGO nano dendrites show much higher catalytic activity towards ethanol electrooxidation compared than that of pure Au nano dendrites (Fig. 14).

3.1.2 Oxygen Reduction Reaction (ORR)

In fuel cells, the ORR at the cathode plays a critical role in determining the energy conversion efficiency of a fuel cell, although the kinetics of the ORR is sluggish, and therefore limits practical applications. The mechanism of the electrochemical ORR is also complicated, which depends on the electrocatalysts, electrode material, and reaction medium, and a variety of reaction intermediates that may be formed during the ORR processes. In brief, the ORR occurs mainly through two pathways: one is the ORR that proceeds either through a four-electron reduction process of O_2 to directly produce H_2O as the final product (i.e., $O_2 + 4H^+ + 4e^- \rightarrow 2H_2O$) and the other is the pathway involving two steps of two-electron reduction, which generates H_2O_2 as an intermediate product (i.e., $O_2 + 4H^+ + 2e^- \rightarrow H_2O_2 + 2H^+ + 2e^- \rightarrow 2H_2O$). According to these pathways, it is obvious that the electrocatalysts catalyze the ORR according to the direct four-electron pathway which is highly favored.

To reduce the usage of noble metals and thus the cost of electrocatalysts, graphene-supported noble-metal single-atom catalysts have also been developed for the ORR in recent years. Different from conventional nanoparticle-based catalysts, single atom catalysts not only dramatically increased interactions with their support, but also reduced the metal–metal coordination effect. These have offered flexibility to tune the catalytic activity and chemoselectivity. Recently, Choi et al. prepared an atomically dispersed Pt catalyst on a sulfur-doped zeolite-templated carbon via the

wet-impregnation method [110]. In the ORR, the as-prepared catalyst did not follow the direct four-electron pathway to produce H_2O. Instead, it followed the two-electron pathway to generate H_2O_2 with nearly 95% selectivity catalyzed by the Pt–S_4 centers. Figure 15 shows the proposed reaction mechanism, which includes the following steps: Fig. 15a shows Pt center was activated by substituting two S atoms of the Pt–S_4 complex with two O atoms of H_2O molecules. Figure 15b appears the first reduction of an O_2 via proton-coupled electron transfer (PCET), forming OOH intermediates. Figure 15c exhibits a two-electron pathway, i.e., the formation of H_2O_2 via the second PCET and the subsequent substitution of an H_2O_2 molecule with an H_2O molecule, recovering the initial state, where Pt is complexed with two thiolates and two H_2O molecules. Figure 15d gives a four-electron pathway, i.e., the formation of H_2O via the second PCET involving O–O bond dissociation. Figure 15e follows a four-electron pathway, i.e., the formation of OH intermediates via the third PCET onto the O atom. Figure 15f demonstrates the fourth PCET to the OH intermediates forms an H_2O, recovering the initial activated

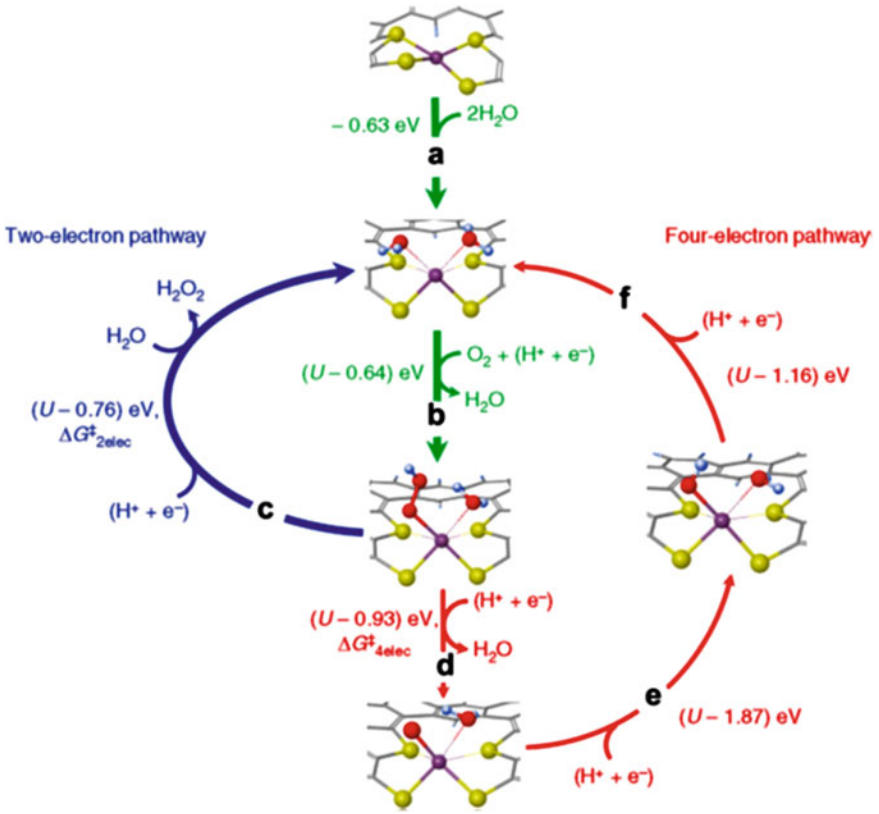

Fig. 15 Proposed ORR mechanism over the single-atom Pt/S-doped zeolite-templated carbon nanocatalyst [110]

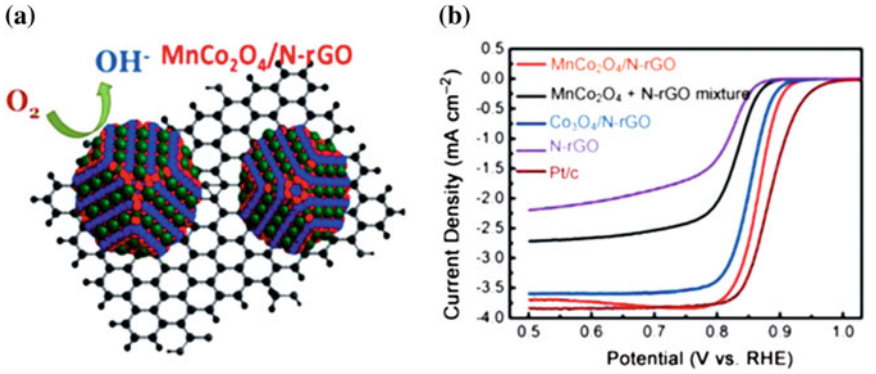

Fig. 16 **a** Representation of the structure of $MnCo_2O_4$/N-RGO hybrid; **b** comparative rotating ring-disk electrode voltammograms of $MnCo_2O_4$/N-RGO hybrid and other electrocatalysts in O^{2-} saturated 1 M KOH at 5 mVs^{-1} at 1600 rpm [111]

state of the Pt–S_4 complex. The blue, red, yellow, and purple balls in the scheme represent H, O, S, and Pt atoms, respectively. Reduced graphene oxide/noble metal-metal oxide based multicomponent hybrids have received considerable interest, which not only avoids the stacking of RGO, but also provides functional electrocatalysts for ORR. Inspired by this, Dai et al. [111] synthesized a novel $MnCo_2O_4$/N-doped reduced graphene oxide (N-RGO) sheet hybrid as a highly efficient electrocatalyst for the ORR in KOH aqueous solution by taking advantage of the high electrocatalytic activity of $MnCo_2O_4$ compared to pure Co_3O_4 and the strong coupling with N-RGO. The nucleation and growth method results in covalent interaction between $MnCo_2O_4$ NPs and N-RGO sheets, giving a rise to much higher activity and durability than the simple physical mixture of $MnCo_2O_4$ NPs and N-RGO (Fig. 16a and b). Moreover, the Mn substitution mediates the size and phase of $MnCo_2O_4$ and increases the activity of catalytic sites of the hybrid materials, which eventually boosts the ORR activity compared with the pure Co_3O_4/N-RGO hybrid.

With the same mass loading, the $MnCo_2O_4$/N-RGO hybrid can even outperform Pt/C in ORR. The current density at the potential of <0.75 V (vs. RHE) with stability superior to Pt/C as shown in Fig. 16c. More importantly, the rotating disk electrode measurements indicate that the ORR catalyzed by $MnCo_2O_4$/N-RGO is mainly through the four-electron pathway.

3.2 Supercapacitor

In the 21st century, energy is one of the most important topics, but the availability of traditional energy-related resources decreases owing to their serious global climate change and more utilization by the rapid growth of the human population [112].

Therefore, considerable attention has been focused seriously on the environmental friendly renewable and sustainable energy materials for effective conversion of energy and storage device, particularly supercapacitor. Supercapacitor is also called electrochemical capacitor, as a kind of energy storage devices, which fulfill the gap between batteries and conventional capacitor owing to their agreeable performance of higher power density and better cycling lifespan over batteries and higher energy density than conventional capacitor [113]. Electrochemical supercapacitors (ES), also called supercapacitors or ultra-capacitors, have been explored as advanced energy storage devices for decades [114]. The energy storage in ES arises from an electrochemical double-layer or reversible redox reaction at the electrode/electrolyte interface [115]. ES could achieve high power density with a combination of porous electrodes and active electrolyte. Compared to batteries, the electrode of ES remains relatively unchanged during charge/discharge cycles, which gives ES excellent cycle stability. The capacitive performance of an ES device is determined by the electrode, electrolyte, and cell configuration [116]. In general, the application of supercapacitor was assembled using two electrodes (cathode and anode), current collector, electrolyte, and separator. A supercapacitor can be further classified as electrical double layer capacitor and the pseudocapacitor according to the different charge storage mechanisms.

3.2.1 Energy Storage Mechanism

Generally, ES can be classified into two types, (i) electrochemical double-layer capacitors (EDLCs, non-Faradaic) and (ii) pseudocapacitors (or) redox-based electrochemical capacitors (Faradaic). In addition, hybrid systems were developed, which combined Faradaic and non-Faradaic process for the charge storage.

Electrochemical Double-Layer Capacitors (EDLCs)

Electrochemical double-layer capacitors (EDLCs) have a similar structure to that of conventional electrostatic capacitors, which store the charge by a non-Faradaic process. Due to the non-Faradaic character, there is no limitation caused by electrochemical kinetics. Therefore, the EDLCs have a higher power density than pseudocapacitors and higher energy density than electrostatic capacitors. In EDLCs, the dielectric is replaced by the electrolyte and the charge does not accumulate on two conductors. Instead, the charge accumulates at the interface between the surface of the conductor and electrolyte as shown in Fig. 17. The accumulated charge hence forms an electric double-layer, the separation of each layer being of the order of a few Angstroms [20]. The obtained capacitance corresponds to the double-layer model was proposed by Helmholtz, in which the double-layer consisted of charged electrode and ions in the electrolyte. The specific capacitance of the Helmholtz model depends on the surface area, the dielectric constant, and thickness of the double-layer. During the charging process, the electrons travel from the negative

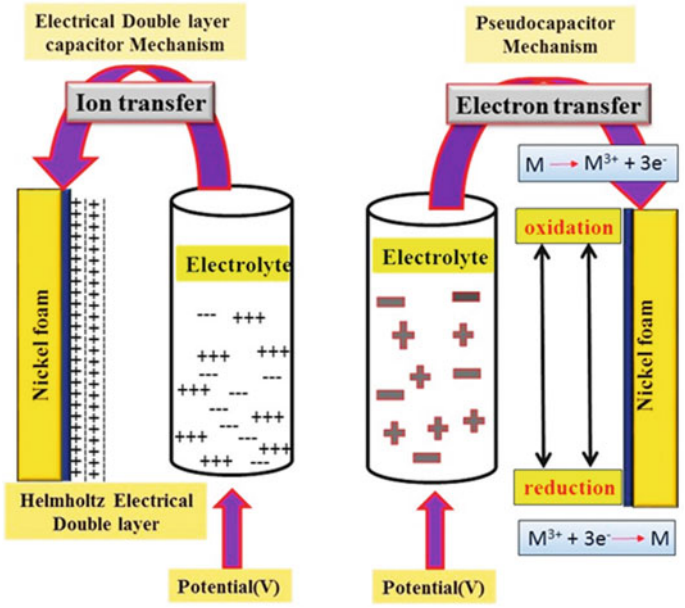

Fig. 17 Schematics diagram of energy storage mechanisms

electrode to the positive electrode by the applied potential window. Within the electrolyte, cations move towards the negative electrode while anions move towards the positive electrode [117]. The EDLC of the carbon electrode is made of high surface-area materials, such as porous carbon or carbon aerogels. The porous carbon electrodes provide the greatest surface area and exhibit a very short distance between electrode and electrolyte. The large surface-areas of porous carbon electrodes have been reported to be as 1000–2000 m^2/g in recent studies.

Pseudocapacitor

Redox pseudocapacitive behavior occurs when ions are electrochemically adsorbed onto the surface or near the surface of a material with a concomitant faradaic charge-transfer. Metal oxides, such as Bi_2O_3, NiO, Co_3O_4 and MnO_2 as well as conducting polymers (Polypyrrole and polyaniline), are classic examples of redox pseudocapacitive materials, which are currently under extensive research. Intercalation pseudocapacitance is a result of ion intercalation into tunnels or layers of a redox-active material, accompanied with faradaic charge transfer process but with no crystallographic phase change [118]. A redox-based electrochemical capacitor is called as pseudocapacitor, of which capacitance arises at electrode surfaces where a completely different mechanism is recognized from the other charge storage mechanism. It is not just an accumulation (or deficiency) of

Table 2 Comparison of EDLCs and pseudocapacitor

Double-layer capacitors (EDLCs)	Pseudocapacitor
Non-Faradaic process	Faradaic process
20–50 μF cm^{-2}	2000 μF cm^{-2} for single-electron transferred process; 200–500 mF cm^{-2} for multi-electrons transferred process
Capacitance is fairly constant with potential, except for the point of zero charges (PZC)	Some single-state materials exhibit marked maximum capacitance
Highly reversible charging/discharging	Quite reversible but has intrinsic electrode kinetic rate limitation
High power compared to pseudocapacitor	High energy compared to EDLCs

electrostatic charge at the interfaces of two electrodes as the double-layer type of capacitor. When an external potential is applied to a pseudocapacitor, a fast and reversible redox reaction occurs on the electrode. It involves the passage of charge between electrode and electrolyte. The mechanisms of charge and discharge of a pseudocapacitor are similar to what occurs in batteries (Table 2).

3.2.2 Electrolyte

The electrolyte, which exists in between the two electrodes and the separator, is also one of the most important components in ES. The electric conductance of the electrolyte reflects the equivalent series resistance (ESR) of the device and thus its power output characteristics. The requirements for the selection of an electrolyte in ES include good electric conductance, high ionic concentration, wide voltage window, high electrochemical stability, low toxicity, and low-cost as well as high purity [119]. The two principal factors involved in conductance of the electrolyte are the concentration of free charge carriers and the ionic mobility, which are in turn determined by the solubility of the salt in the solvent and the degree of dissociation of dissolved salts. Three stages of ion pairing depend on the extent of retention of solvation. Hydration shell contact provides a high fraction of salts as free charge carriers of electric current. The distance of the solvated ions could be significantly reduced when their solvation shells become shared. In poorly solvating solvents, the plus (+) and minus (−) ions come into a contact situation [120]. The conventional liquid electrolytes are used in an ES and they can be classified into three types: (1) aqueous electrolyte, (2) organic electrolyte, and (3) gel electrolyte (or) polymer electrolyte in Fig. 18. Recently, the solid electrolyte or gel electrolyte was obtained from the proton-conducting polymer, which attracted a great attention for the fabrication of solid state of ES.

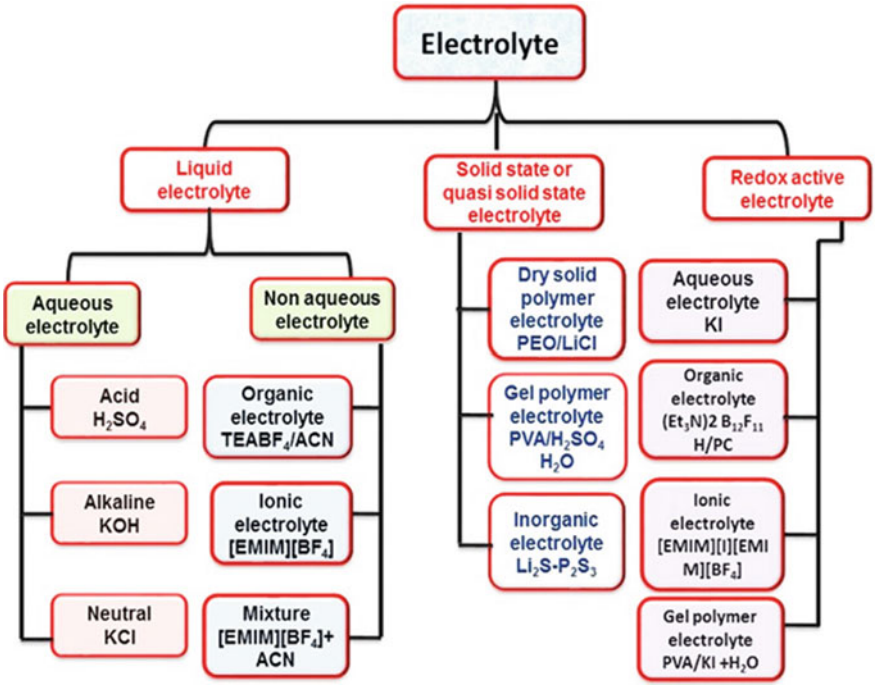

Fig. 18 Schematic diagram of different types of electrolyte [121]

Aqueous Electrolyte

The aqueous electrolytes, such as H_2SO_4, KOH, KCl, and Na_2SO_4, have advantages of low resistance and high ionic concentrations in comparison with organic electrolytes. ES fabricated by the aqueous electrolyte could provide higher power than organic electrolytes due to high conductivity. Furthermore, the aqueous electrolyte can be prepared and utilized without stringently controlling the preparation conditions, while the organic electrolytes need strict processes to obtain an ultra-pure electrolyte. However, the limitation of the aqueous electrolyte is the small voltage window. To improve the voltage window of ES, many efforts have been made to investigate environmentally friendly and cost-effective natural aqueous electrolyte. The results showed that the enlarged voltage window of 1.8–2.2 V was obtained [122, 123].

Organic Electrolyte

The main advantage of organic electrolytes over aqueous electrolyte is large voltage window as high as 3.5 V. Higher voltage window can increase the energy density because the energy density is proportional to the square of voltage. Nevertheless,

most organic electrolytes have the drawbacks of high electric resistance, small power capability, and complex production conditions. Among organic electrolyte, acetonitrile and propylene carbonate (PC), triethylmethylammonium tetrafluoroborate (TEMABF4) are most commonly used solvents. Studies have been made to investigate the relationship between nano-structured activated carbon and the capacitive performance in different electrolytes. As a result, the capacitance of activated carbon compared in aqueous electrolytes (100–300 Fg^{-1}) and organic electrolytes (50–150 Fg^{-1}). Since the effective size of the electrolyte ions of organic solutions is much larger compared with those in water, the number of pores increases in organic electrolytes that are smaller than the ions and decreases the number of pores not contributing to the charge storage. Moreover, the wettability of the electrode belongs to the chemical affinity occurring between the organic electrolyte and electrode surface [124].

Gel Electrolyte or Polymer Electrolyte

The conventional ES consists of two electrodes with a separator between them in an aqueous or organic electrolyte. However, the liquid electrolytes suffer two major drawbacks for practical applications. Firstly, the electrolyte leakage may lead to a reduction in specific capacitance, degradation of electrochemical performance, and even contamination to nearby circuits. Secondly, ES in such configuration is not an integrated one and not able to move relative to each other under strong flexibility. Therefore, all-solid-state ES prepared by the incorporation of gel electrolyte was proposed to provide safe operations for printable, flexible, and wearable devices applications. Commonly, an effective way towards gel electrolyte is to add a polymer, such as polyvinyl alcohol (PVA), polyethylene glycol (PEO), and polyvinylpyrrolidone (PVP), into a proton conducting aqueous solutions, which fix water molecules via the formation of 3-D hydrophilic polymer networks. Significant efforts have been dedicated to developing all-solid-state flexible ES, including film, paper, textile, woven cotton, and fabrics. The increase of proton conductivity for all-solid-state ES is of significance for the development of high-performance ES. The high proton conductivity of polymer electrolyte could be achieved by the fabrication of the thin film with a high degree hydration. Many efforts have been made to improve the water retention capability and reduce the sensitivity to the environment of polymer electrolyte [125].

3.2.3 Metal Oxide on RGO for Supercapacitors Applications

The RGO electrode materials succeeded greatly in both academic and industrial research work for the manufacturing of energy storage devices. The RGO nanostructures were prepared by the lamellar microstructure for the restacked layer of graphene materials. The electrochemical reaction substantially improves the RGO NPs due to numerous conductivity paths of graphene morphology and greater

surface areas with mesoporous architecture. Therefore, the most favorable for interfacial charge transfer is enhanced in between the electrolyte and graphene materials [126, 127]. The pseudocapacitive performance of metal oxide NPs appears with sufficient amount improved by the multiple-pore channel and sufficient surface activities present in the RGO morphology. Thus, both capacity and cyclic stability can be enhanced at high charge/discharge rates. The RGO nanoarchitecture is suitable to support redox species of metal oxide NPs, and this type of integrated anode architectures are promising candidates for a novel pathway to the fabrication for future electrode materials of supercapacitor application [128]. The positive charge of nanosized metal oxide nanoparticle is dispersed on negatively charging with RGO nanostructures framework. Therefore, this kind of hybrid materials has shown ultimate performance for the technology of electrochemical capacitive devices. Furthermore, preventing the agglomeration of metal oxide NPs can afford to increase specific surface area (SSA) and the benefit of their superior interfacial contact with the electrolyte solution will allow the fast ion and electron transport. Inspired this, the most common strategy for that construction of metal oxide supported carbon skeleton nanocomposites have more advantages for synergic effect on the electrodes for supercapacitor application [129, 130].

The RGO materials (EDLCs) were employed for both anode and cathode electrode materials in supercapacitors. The ASC technology hindered by the low specific capacitance and electrical conductivity, charging/discharging rate, decreases electrochemical kinetics and the energy density [131, 132]. These drawbacks have been overcome by using inexpensive transition metals oxides, such as Bi_2O_3, MoO_3, MnO_2, Co_3O_4, and so forth, and those exhibit the highest specific capacitance (SC), multiple oxidation states, and excellent reversibility [133, 134]. The above benefits were made via the metal oxide supported RGO nanocomposites by the guest materials (organic or inorganic species) combined/incorporated into the RGO surface or either throughout the RGO framework. Thus, the metal to carbon (M–C) bond formed by the 'P' orbitals of RGO could overlap with the vacant hybridized orbitals (sp, sp^2, and sp^3) of metal oxide. On the other hand, the overall capacitive performance has been considerably improved by the nano size of the metal oxide particles with excellent surface areas of RGO nanosheets.

Bi_2O_3 on Reduced Graphene Oxide

The Bi_2O_3 nanoparticles dispersed on RGO nanosheets were synthesized by the solvothermal method and followed via different calcination temperatures. Furthermore, the electrochemical performance of Bi_2O_3/RGO nanoelectrode was used in an electrochemical workstation. The reduced size of the Bi_2O_3 nanoparticles have well-defined crystallinity as shown in SEM images of Fig. 19a, b and those are uniformly dispersed on RGO nanosheets by suitable calcination temperature of 350 °C. At this temperature, the perfect morphology of Bi_2O_3/RGO electrode materials is measured in 6 M KOH electrolyte solution for a suitable potential window. The Bi_2O_3/RGO anode materials can achieve the specific capacitance of

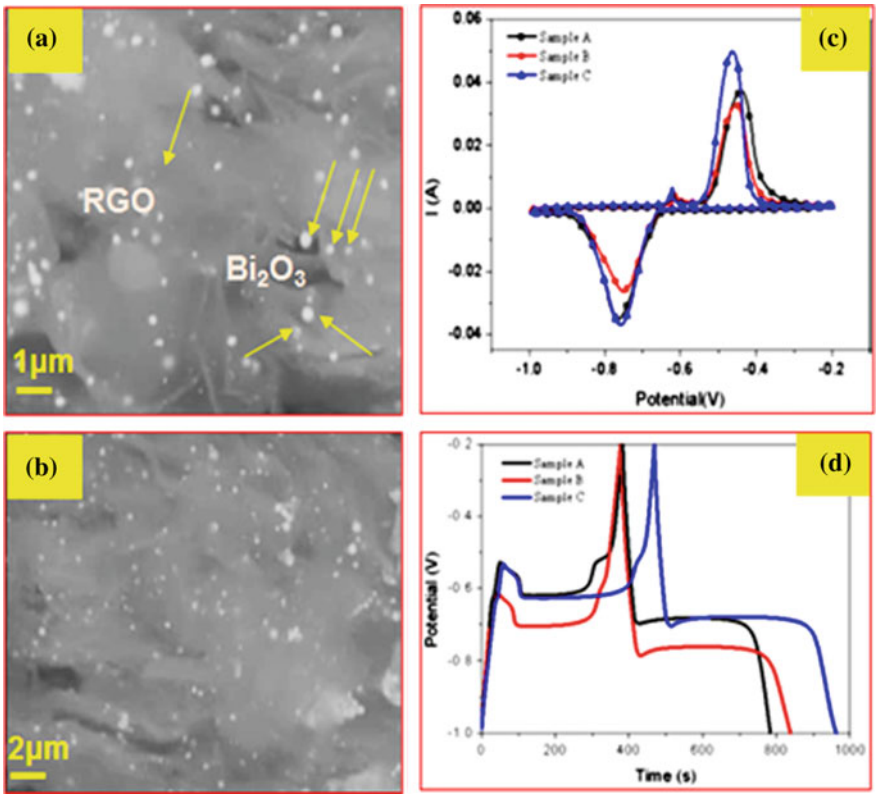

Fig. 19 **a**, **b** is an SEM image and **c**, **d** is a CV and GCD test of Bi_2O_3/RGO anode materials [135]

617 Fg^{-1} at a current density of 1 Ag^{-1}, which indicated that the Bi_2O_3/RGO nanoelectrode could be greatly used for supercapacitor materials as shown in Fig. 19c, d [135].

The positive electrode of $Ni(OH)_2$/GS and negative electrode materials of Bi_2O_3/GS were prepared by a chemical bath deposition method. As a result, the Ni/Bi battery exhibited a high discharge capacity and excellent rate capability. Asymmetric battery achieved with the high energy and power density of 83.2 Wh kg^{-1} at a 143 W kg^{-1} can remain 60.1 Wh kg^{-1} at a 2609 W kg^{-1}, which is demonstrated as promising candidates for energy storage devices [136]. A novel and facile route of Bi_2O_3 nanoparticles supported RGO nano composites were prepared by solvothermal method as displayed in Fig. 20. As prepared electrode materials were obtained from the negative charging of RGO NPs dissolved in N, N-dimethyl formamide (DMF) solution and positive charge of Bi-Cations present in 180 °C. After that, the final product of Bi_2O_3 nanoparticles supported RGO NPs image of Fig. 20a–b was involved in electrochemical measurements. The GCD and cycle life results show the

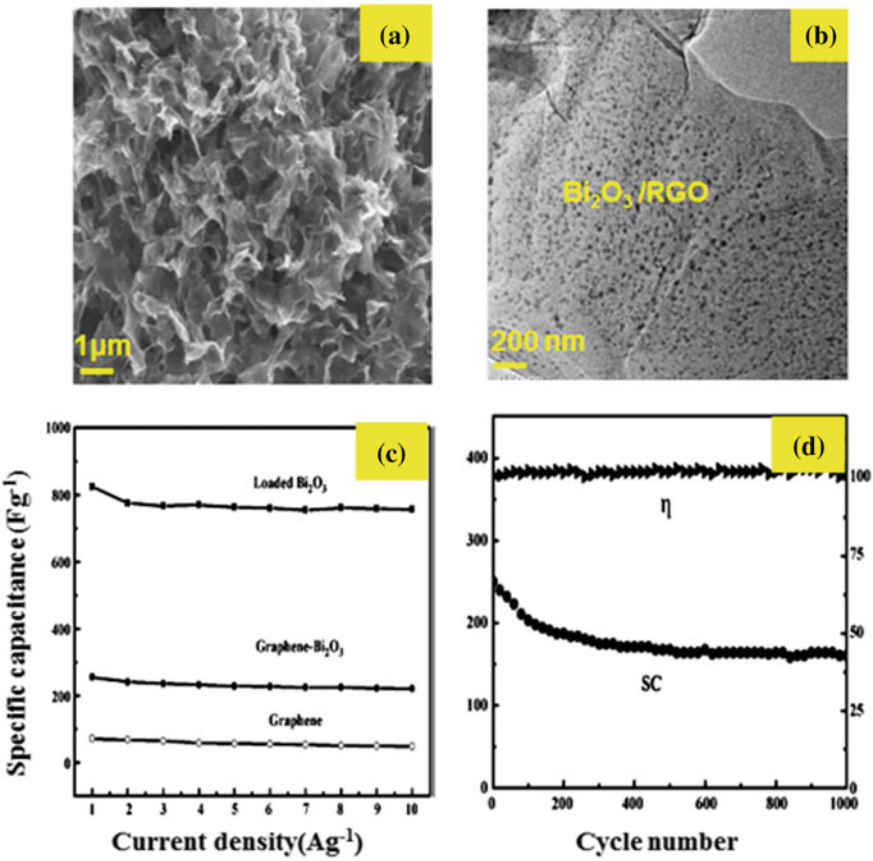

Fig. 20 The low and high magnification of the TEM image shown in **a–b**, **c** is a specific capacitance (Fg^{-1}) versus current density (Ag^{-1}), and **d** cycle number versus specific capacitance of Bi_2O_3/RGO nanosheets [137]

specific capacitance of 255 Fg^{-1} and 65% capacitance retentions after 1000 cycles at 1 Ag^{-1}, which can compare with the pure graphene of 71 Fg^{-1} as presented in Fig. 20c–d. The loaded Bi_2O_3 nanoparticles can achieve the specific capacitance of 757 Fg^{-1} at 10 Ag^{-1} [137].

Co_3O_4 on Reduced Graphene Oxide

The Co_3O_4 nano hexagons derived from the metal-organic framework (MOF) were incorporated into the RGO nanosheets through the hydrothermal route as shown in Fig. 21. The Co_3O_4 hexagons were located uniformly on the RGO nanosheets to help the electron accessibility of the electroactive materials. The as-synthesized

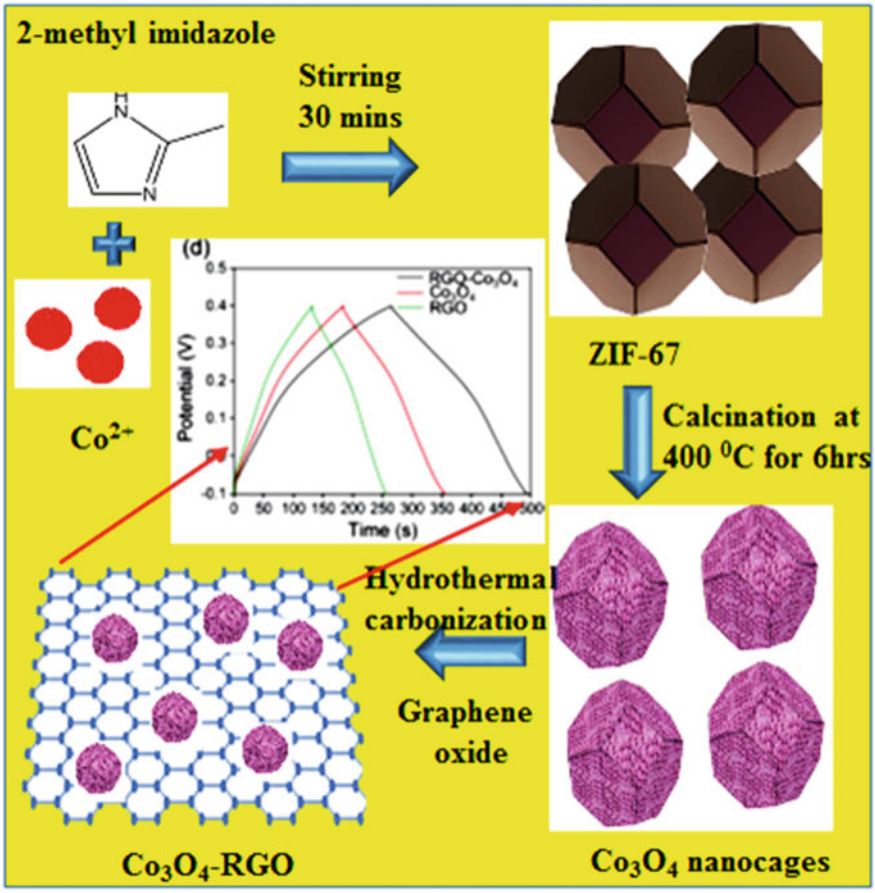

Fig. 21 A schematic diagram of the preparation process of RGO-Co_3O_4 for high-performance supercapacitor applications and inset comparison study of GCD curve [138]

electrode materials can achieve the specific capacitance of 1300 Fg^{-1} at a current density of 4 Ag^{-1} using in 0.1 M KI electrolyte solution. The asymmetric supercapacitor also exhibited the high energy and power density of 65.8 Wh kg^{-1} and 2048 W kg^{-1}, respectively. The 80.5% capacitance retention was exhibited even after 5000 cycles at a current density of 4 Ag^{-1} [138]. The graphene wrapped cobalt oxide-intercalated (GWCI) hybrid structure was synthesized in Fig. 22 using microwave irradiation for supercapacitor applicaiton. The GWCI nanostructure was used to prevent the agglomeration of metal oxide nanoparticles on the RGO surfaces. Additionally, the GWCI electrode materials displayed remarkable cyclic stability over 1000 cycles and greatest rate capability. Besides, the corresponding hybrid materials exhibited high energy and power density of 986.32 W/kg and 52.84 Wh/kg, respectively [139].

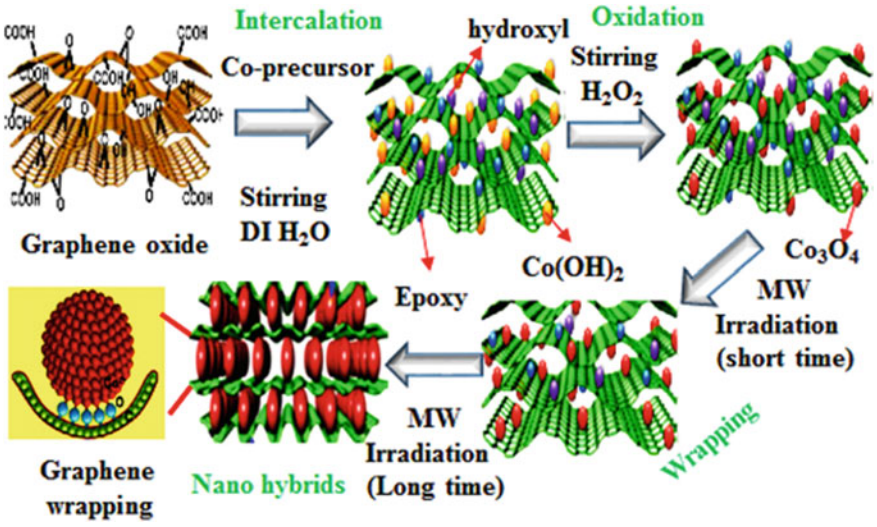

Fig. 22 Schematic illustration of the three-step process for the formation of graphene wrapped Co_3O_4 monohybrid for supercapacitor application [139]

Furthermore, the Co_3O_4 nanocube supported RGO nanocomposite was prepared by the hydrothermal method and the FE-SEM images are shown in Fig. 23. This study was to investigate different molar concentration of cobalt precursor solution for supercapacitor application. The as-prepared electrode of Co_3O_4 nanoparticles exhibited an average crystallite size of 45 nm and excellent interaction of RGO nanosheets as revealed in Fig. 23a–b. Moreover, the electrochemical performance of Co_3O_4 nanocube/RGO was examined by electrochemical workstations. The maximum specific capacitance 278 Fg^{-1} was obtained at 200 mAg^{-1}. The excellent long-term cyclic stability was exhibited after 2000 cycles, which demonstrates the capacitance retention of 91.6% and have the excellent rate capability as presented in Fig. 23c–d. These results suggested that the Co_3O_4 nanocube intercalated RGO matrix play a good role in improved energy storage capability [140].

The porous Co_3O_4 nanoparticles intercalation of layer-by-layer on RGO nanosheets under vacuum filtration with the subsequent thermal annealing is shown in Fig. 24. The resulting electrode materials were presented in high structural integrity for employing a self-electrode. The porous Co_3O_4/RGO is promising electrode materials for electrochemical performances due to highly conductive nature of RGO nanosheets, short ion diffusion path of porous Co_3O_4, strong electrostatic force interaction occurring in between the two layers, and greater ion-accessible areas. The Co_3O_4/RGO electrode exhibited the maximum specific capacitance of 623.8 Fg^{-1} at a scan rate of 5 mVs^{-1}. After that, the capacitance retention remains 87% after 1000 cycles at 20 mVs^{-1} due to their excellent cyclic stability and reversibility [141].

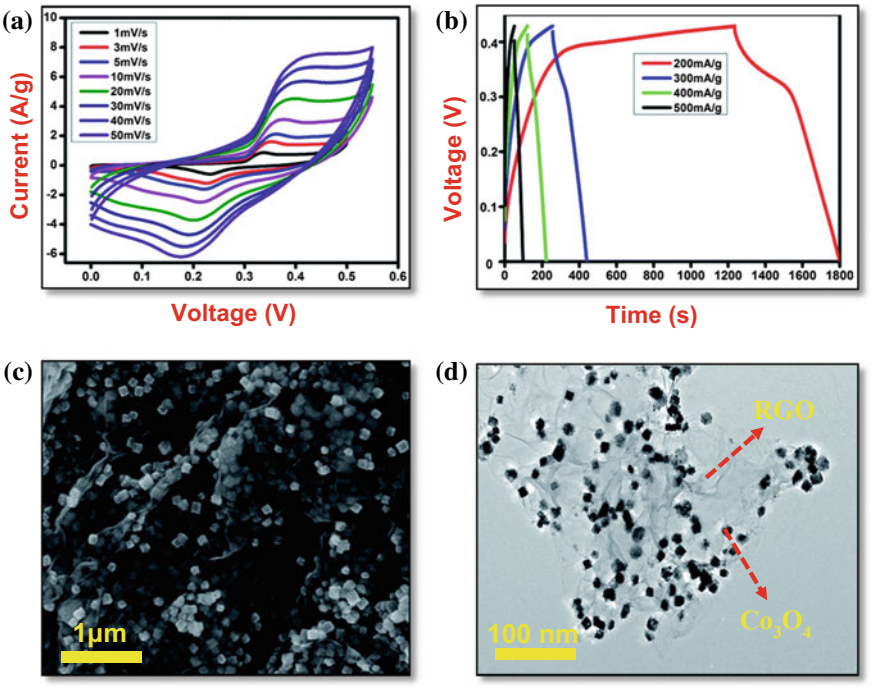

Fig. 23 **a** CV, **b** GCD results and **c–d** FE-SEM images for lower/higher magnification of Co_3O_4 nanoparticles dispersed on RGO nanosheets [140]

MnO_2 on Reduced Graphene Oxide

The MnO_2 nanosheets dispersed on RGO nanocomposites electrode was prepared by the co-precipitation method. Due to the surface charges exchange, RGO nanosheets was used to poly (diallyldimethylammonium chloride (PDDA)) with a negative charge of MnO_2 nanosheets. However, the composite materials exhibited an excellent capacitive performance than pure electrode materials. Obviously, Fig. 25d shows the 89% of original capacitance retention was retained after 1000 cycles due to the good cyclic stability. As shown in Fig. 25a, the CV curves of MnO_2/RGO exhibited rectangular shape of RGO curves and combined with the small redox peak of MnO_2. Based on CV curves, we can see that the MnO_2/RGO exhibited the highest specific capacitance than pure RGO and MnO_2. Furthermore, the triangle shape of the charge/discharge curves were obtained in Fig. 25b and lower resistance values of impedance spectrum indicated the higher electrical conductivity of MnO_2/RGO composite presented in Fig. 25c [142]. The novel graphene wrapped (GW) MnO_2 hybrid materials was synthesized by the honeycomb-like MnO_2 nanospheres associated with the graphene nanosheets through the electrostatic co-precipitation methods. Furthermore, the GW-MnO_2

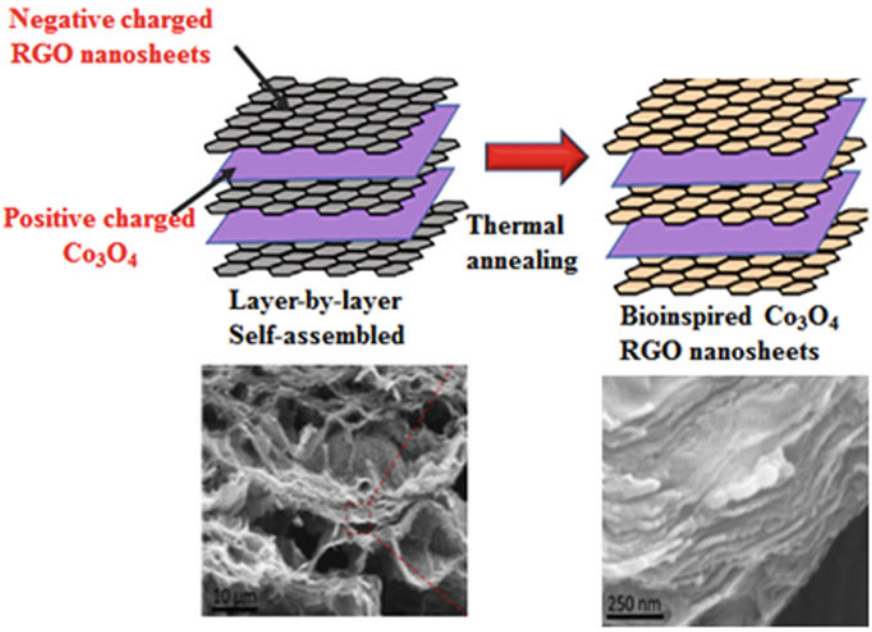

Fig. 24 Synthesis procedure of the bioinspired Co_3O_4 nanoparticles dispersed on RGO layered composite films [141]

hybrid materials exhibited the maximum specific capacitance for 210 Fg^{-1} at 0.5 Ag^{-1} due to the pseudocapacitive properties associated with the excellent electrical conductivity of the electrical double layer (EDL) properties. These hybrid materials exhibited the 82.4% capacitance retention after 1000 charge-discharge cycles [143]. The positive electrode of RGO/MnO_2 and the negative electrode of RGO/MoO_3 in the aqueous electrolyte of 1 M Na_2SO_4 were fabricated as an asymmetric supercapacitor.

The maximum operating voltage was obtained due to the synergetic effect on highly conductive RGO-Ns and pseudocapacitive nature of metal oxides nanoparticles. The hybrid nanostructure of RGO/MnO_2//RGO/MoO_3 achieved the operating voltage window 2.0 V, which displayed the energy and power density of 42.6 Wh Kg^{-1} at 276 W Kg^{-1} and maximum specific capacitances 307 Fg^{-1}. Owing to the micro-porous nanostructure, better charge transport enhanced the capacitive performance. This study demonstrated that hybrid materials follow promising route for next-generation supercapacitors with high energy and high power densities [144]. The needle-like MnO_2 supported graphene nanomaterial has been synthesized through the simple route of water-isopropyl system. Moreover, the as-prepared nanomaterials were found with the excellent electrochemical performances due to the respectable chemical interaction between the GO and MnO_2. The as-prepared electrode materials achieved the specific capacitances of 216 Fg^{-1} at 150 mAg^{-1} and 84.1% capacitance retention remains after 1000 cycles in 1 M Na_2SO_4 [145].

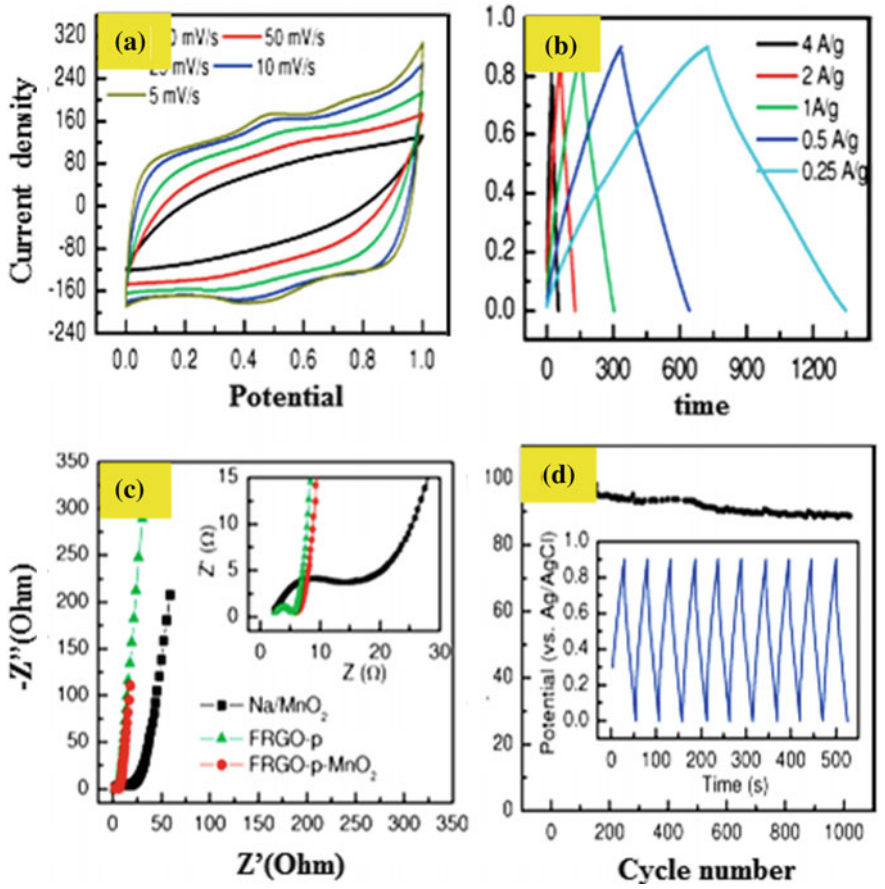

Fig. 25 **a** CV, **b** GCD, **c** EIS, and **d** cycle life of FRGO-p-MnO_2 [142]

MoO_3 on Reduced Graphene Oxide

The porous-RGO/MoO_3 nanocomposites were prepared by the scalable and convenient methods using MOF as a precursor. The obtained RGO/MoO_3 nanocomposites were employed in supercapacitor application. Furthermore, the specific capacitance can achieve 617 Fg^{-1} at 1 Ag^{-1} and 87.5% capacitance retention after 6000 cycles at 6 Ag^{-1} due to the more active surface area for the redox reaction, leading to an enhanced electrochemical performance. Therefore, this nanocomposite can be used for excellent cyclic stability, rate capability, and a long cycle of supercapacitor for practical application of energy storage devices [146]. The RGO/MoO_3 hybrid nanomaterials exhibited the high specific capacitance 724 Fg^{-1} at 1 Ag^{-1} using 12 wt% of RGO. The density functional theory has demonstrated that RGO-Ns (C_{pz}) sub-orbitals can reach the near Fermi-level via the introduction of

RGO in MoO_3, which is responsible for the enhanced capacitance on RGO/MoO_3 hybrid electrode materials [147]. The transition metal oxide nanorods/RGO hybrid materials were prepared by the scalable wet-spinning method. Moreover, the negative electrode of RGO/MoO_3 materials might be employed as an asymmetric supercapacitor. Then, the optimized asymmetric supercapacitor exhibited the potential window of 1.6 V and delivered the high energy and power density of 18.2 mWh cm^{-3} at a 76.4 mW cm^{-3} [148]. The asymmetric supercapacitor exhibited the remarkable cyclic, flexibility, and mechanical stability.

The morphological details were further analyzed in HRTEM images, which displayed the MoO_3 nanocrystals strongly anchored on RGO nanosheets. As shown in Fig. 26a–b, those have demonstrated that the hybrid MoO_3/RGO displayed a highly wrinkled surface and well-defined lattice fringes for 0.38 nm, which is consistent with the (110) crystalline planes of MoO_3 perpendicular to the RGO nanosheets as shown in Fig. 25c. The crystalline planes of MoO_3 [010] direction are anisotropically grown on RGO nanosheets as seen in Fig. 26e–f. The octahedra crystalline structure of MoO_3 was formed by the van der Waals forces involved in the bilayer sheets as shown in Fig. 26d [149] (Table 3).

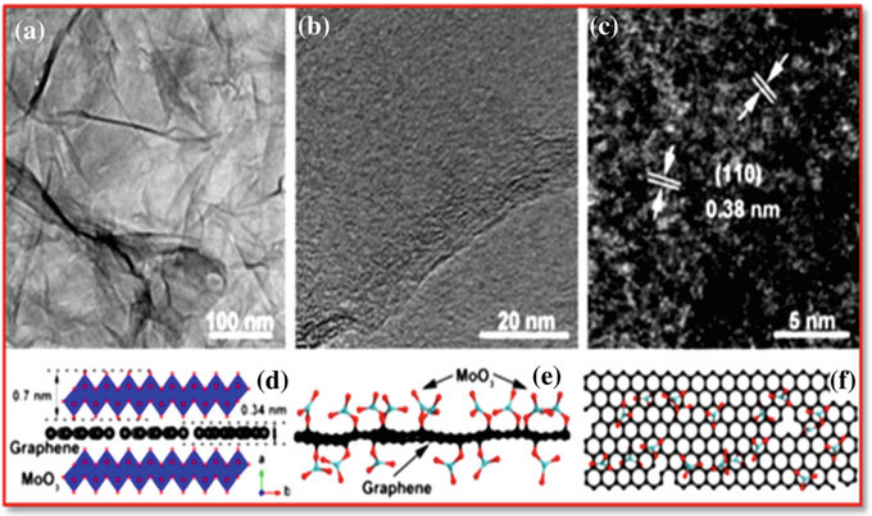

Fig. 26 The low and high-resolution TEM images of MoO_3/RGO nanosheets for **a–b**, **c** STEM image of MoO_3/RGO nanosheets, **d** schematic of MoO_3 self-assembled on RGO nanosheets, **e** and **f** schematic diagrams of MoO_3 bonding with RGO nanosheets [149]

Table 3 Literature survey for a comparative study of the metal oxide nanostructure supported graphene hybrid materials for supercapacitor applications [CR-capacitance retention]

Electrode	Electrolyte	Specific capacitance	Cyclic stability	Rate capability	Ref.
Bi_2O_3/GS	6 M KOH (−1.0 to −0.2)	617 Fg^{-1} at 1 Ag^{-1}	30% CR after 1000 cycles at 5 Ag^{-1}	419 Fg^{-1} at 10 Ag^{-1}	[135]
Bi_2O_3/GS	6 M KOH (−1.0 to 0)	272 Fg^{-1} at 0.5 Ag^{-1}	–	220 Fg^{-1} at 20 Ag^{-1}	[136]
Bi_2O_3/RGO	6MKOH (−0.9 to 0)	255 Fg^{-1} at 1 Ag^{-1}	65% CR after 1000 cycles at 20 mVs^{-1}	198 Fg^{-1} at 10 Ag^{-1}	[137]
Co_3O_4/ RGO	0.1 M KOH (−0.1 to 0.4)	1300 Fg^{-1} at 4 Ag^{-1}	80.5% CR after 5000 cycles at 4 Ag^{-1}	130 Fg^{-1} at 8 Ag^{-1}	[138]
Co_3O_4/ RGO	0.5 M BMIM-BF_4/ CH_3CN (0 to 1.4)	712 Fg^{-1} at 1 Ag^{-1}	55% CR after 10,000 cycles at 7 Ag^{-1}	590 Fg^{-1} at 1 Ag^{-1}	[139]
Co_3O_4/ RGO	1 M KOH (0 to 0.6)	278 Fg^{-1} at 200 mAg^{-1}	91.6% CR after 2000 cycles at 3 Ag^{-1}	145 Fg^{-1} at 300 mAg^{-1}	[140]
Co_3O_4/ RGO	2 M KOH (0 to 0.6)	623.8 Fg^{-1} at 5 mVs^{-1}	87% CR after 1000 cycles at 20 mVs^{-1}	440.4 Fg^{-1} at 20 mVs^{-1}	[141]
MnO_2/RGO	1 M Na_2SO_4 (0 to 1 V)	188 Fg^{-1} at 0.25 Ag^{-1}	89% CR after 1000 cycles at 4 Ag^{-1}	130 Fg^{-1} at 4 Ag^{-1}	[142]
MnO_2/RGO	1 M Na_2SO_4 (0 to 1 V)	210 Fg^{-1} at 0.5 Ag^{-1}	82.4% CR after 1000 cycles at 10 mVs^{-1}	147 Fg^{-1} at 5 Ag^{-1}	[143]
MnO_2/RGO	1 M Na_2SO_4 (−0.2 to 1 V)	350 Fg^{-1} at 200 mAg^{-1}	–	162 Fg^{-1} at 10 Ag^{-1}	[144]
MoO_3/RGO	1 M H_2SO_4 (0 to 0.8 V)	617 Fg^{-1} at 1 Ag^{-1}	87.5% CR after 6000 cycles at 6 Ag^{-1}	374 Fg^{-1} at 10 Ag^{-1}	[146]
MoO_3/RGO	3 M KOH (0 to 0.6)	724 Fg^{-1} at 1 Ag^{-1}	87% CR after 800 cycles at 1 Ag^{-1}	498 Fg^{-1} at 6 Ag^{-1}	[147]
MoO_3/RGO	1 M H_2SO_4 (−0.8 to 0 V)	321.8 F cm^{-3} at 2 mVs^{-1}	97.6% CR after 5000 cycles at 1 A cm^{-3}	130 F cm^{-3} at 50 mVs^{-1}	[148]

4 Conclusion and Perspectives

The recent development of reduced graphene oxide (RGO)-based metal/metal oxide nanocomposites for energy conversion, storage, and various electrochemical applications has been significantly driven by their unique structural features, unusual physicochemical properties, high stability, and low cost. Moreover, the bottom-up strategies can yield a single layer, defect-free graphene, though they are not suitable presently for bulk synthesis of RGO generally required for large-scale production of RGO-based materials. Therefore, considering the great demand for the bulk production of RGO, top-down approaches have gained much attention. Various types of RGO-based metal/metal oxide nanocomposites are synthesized

with a special focus using a top-down approach and the properties are characterized by various techniques as discussed in details. Although a great progress has been made in the synthesis and electrochemical applications of RGO-based metal/metal oxide nanocomposites, problem and challenges are still remaining in the research field. First, the well-defined precise noble metal nanostructure with small size, abundant structural characteristics, and good dispersion on the RGO surface are greatly desirable for applications. However, the controlled synthesis of noble metals with novel nanostructures remains a big challenge. Second, the exact mechanism of how RGO composite is prepared, as a synthetic template for the direct growth of well-defined metal/metal oxide architectures on the RGO surface, is still unclear. An unambiguous understanding of such a mechanism will significantly contribute to the rational design and synthesis of high-performance electrocatalysts and storage materials. Last but not least, the state of the art for the synthesis of novel RGO-based noble metal/metal oxide nanocomposites has only been realized on the small scale. Developing new methods to produce both RGO nanosheets and metal/metal oxide nanostructures in a low-cost, large-scale, and environmentally friendly manner is extremely important toward the practical implementation of these electrocatalysts and energy storage materials. In this chapter, we have discussed the current development of RGO-supported transition metal/metal oxide nanocomposite materials for their electrocatalysts and supercapacitor applications, including their synthesis, key properties, and major applications. Therefore, reduced graphene oxide-based metal and metal oxide composites with anchored, encapsulated, wrapped, layered, and mixed structures have an enormous potential for many industrial applications and they are commercially feasible compared with nanocomposites using other carbonaceous materials. Overall, developments in the quality of reduced graphene oxide will ultimately lead to the synthesis of uniform nanocomposites, which can be fine-tuned for various potential applications, such as electrochemical energy storage/conversion, electrochemical sensors, and so on.

References

1. Novoselov, K.S., Geim, A.K., Morozov, S.V., Jiang, D.A., Zhang, Y., Dubonos, S.V., Firsov, A.A.: Electric field effect in atomically thin carbon films. Science **306**(5696), 666–669 (2004)
2. Guo, S., Dong, S.: Graphene nanosheet: synthesis, molecular engineering, thin film, hybrids, and energy and analytical applications. Chem. Soc. Rev. **40**(5), 2644–2672 (2011)
3. Allen, M.J., Tung, V.C., Kaner, R.B.: Honeycomb carbon: a review of graphene. Chem. Rev. **110**(1), 132–145 (2009)
4. Liang, H.W., Zhuang, X., Brüller, S., Feng, X., Müllen, K.: Hierarchically porous carbons with optimized nitrogen doping as highly active electrocatalysts for oxygen reduction. Nat. Commun. **5**, 4973 (2014)
5. Kroto, H.W., Heath, J.R., O'Brien, S.C., Curl, R.F., Smalley, R.E.: C60: Buckminsterfullerene. Nature **318**(6042), 162 (1985)
6. Ajayan, P.M.: Capillarity-induced filling of carbon nanotubes. Nature **361**(6410), 333 (1993)

7. Kauffman, D.R., Star, A.: Graphene versus carbon nanotubes for chemical sensor and fuel cell applications. Analyst **135**(11), 2790–2797 (2010)
8. Fasolino, A., Los, J.H., Katsnelson, M.I.: Intrinsic ripples in graphene. Nat. Mater. **6**(11), 858 (2007)
9. Antonietti, M., Müllen, K.: Carbon: the sixth element. Adv. Mater. **22**(7), 787 (2010)
10. Khan, M., Tahir, M.N., Adil, S.F., Khan, H.U., Siddiqui, M.R.H., Al-Warthan, A.A., Tremel, W.: Graphene-based metal and metal oxide nanocomposites: synthesis, properties, and their applications. J. Mater. Chem. A **3**(37), 18753–18808 (2015)
11. Zhu, C., Guo, S., Fang, Y., Han, L., Wang, E., Dong, S.: One-step electrochemical approach to the synthesis of graphene/MnO_2 nanowall hybrids. Nano Res. **4**(7), 648–657 (2011)
12. Zhu, C., Zhai, J., Wen, D., Dong, S.: Graphene oxide/polypyrrole nanocomposites: one-step electrochemical doping, coating and synergistic effect for energy storage. J. Mater. Chem. **22** (13), 6300–6306 (2012)
13. Paek, S.M., Yoo, E., Honma, I.: Enhanced cyclic performance and lithium storage capacity of SnO_2/graphene nanoporous electrodes with three-dimensionally delaminated flexible structure. Nano Lett. **9**(1), 72–75 (2008)
14. Huang, X., Yin, Z., Wu, S., Qi, X., He, Q., Zhang, Q., Zhang, H.: Graphene-based materials: synthesis, characterization, properties, and applications. Small **7**(14), 1876–1902 (2011)
15. Porada, S., Weingarth, D., Hamelers, H.V.M., Bryjak, M., Presser, V., Biesheuvel, P.M.: Carbon flow electrodes for continuous operation of capacitive deionization and capacitive mixing energy generation. J. Mater. Chem. A **2**, 9313–9321 (2014)
16. Porada, S., Zhao, R., van der Wal, A., Presser, V., Biesheuvel, P.M.: Review on the science and technology of water desalination by capacitive deionization. Prog. Mater. Sci. **58**, 1388–1442 (2013)
17. Singh, K., Arora, S.: Removal of synthetic textile dyes from wastewaters: a critical review on present treatment technologies. Crit. Rev. Environ. Sci. Technol. **41**, 807–878 (2011)
18. Resch-Genger, U., Grabolle, M., Cavaliere-Jaricot, S., Nitschke, R., Nann, T.: Quantum dots versus organic dyes as fluorescent labels. Nat. Methods **5**, 763–775 (2008)
19. Peng, C., et al.: Carbon nanotube and conducting polymer composites for supercapacitors. Nat. Sci. **18**, 777–788 (2008)
20. Burke, A.: Ultra capacitors: why, how, and where is the technology. J. Power Sources **9**(1), 37–50 (2000)
21. Li, X., Cai, W., An, J., Kim, S., Nah, J., Yang, D., Banerjee, S.K.: Large-area synthesis of high-quality and uniform graphene films on copper foils. Science **324**(5932), 1312–1314 (2009)
22. Capasso, A., Dikonimos, T., Sarto, F., Tamburrano, A., De Bellis, G., Sarto, M.S., Lisi, N.: Nitrogen-doped graphene films from chemical vapor deposition of pyridine: influence of process parameters on the electrical and optical properties. Beilstein J. Nanotechnol. **6**, 2028 (2015)
23. Subrahmanyam, K.S., Panchakarla, L.S., Govindaraj, A., Rao, C.N.R.: A simple method of preparing graphene flakes by an arc-discharge method. J. Phys. Chem. C **113**(11), 4257–4259 (2009)
24. Sutter, P.W., Flege, J.I., Sutter, E.A.: Epitaxial graphene on ruthenium. Nat. Mater. **7**(5), 406 (2008)
25. Hummers Jr., W.S., Offeman, R.E.: Preparation of graphitic oxide. J. Am. Chem. Soc. **80**(6), 1339 (1958)
26. Pei, S., Cheng, H.M.: The reduction of graphene oxide. Carbon **50**(9), 3210–3228 (2012)
27. McAllister, M.J., Li, J.L., Adamson, D.H., Schniepp, H.C., Abdala, A.A., Liu, J., Aksay, I. A.: Single sheet functionalized graphene by oxidation and thermal expansion of graphite. Chem. Mater. **19**(18), 4396–4404 (2007)
28. Sun, X., Luo, D., Liu, J., Evans, D.G.: Monodisperse chemically modified graphene obtained by density gradient ultracentrifugal rate separation. ACS Nano **4**(6), 3381–3389 (2010)

29. An, C., Wang, Y., Wang, Y., Liu, G., Li, L., Qiu, F., Yuan, H.: Facile synthesis and superior supercapacitor performances of Ni_2P/rGO nanoparticles. RSC Adv. **3**(14), 4628–4633 (2013)
30. Xu, Y., Sheng, K., Li, C., Shi, G.: Highly conductive chemically converted graphene prepared from mildly oxidized graphene oxide. J. Mater. Chem. **21**(20), 7376–7380 (2011)
31. Bera, R., Kundu, S., Patra, A.: 2D hybrid nanostructure of reduced graphene oxide–CdS nanosheet for enhanced photocatalysis. ACS Appl. Mater. Interfaces **7**(24), 13251–13259 (2015)
32. Gilje, S., Han, S., Wang, M., Wang, K.L., Kaner, R.B.: A chemical route to graphene for device applications. Nano Lett. **7**(11), 3394–3398 (2007)
33. Stankovich, S., Piner, R.D., Chen, X., Wu, N., Nguyen, S.T., Ruoff, R.S.: Stable aqueous dispersions of graphitic nanoplatelets via the reduction of exfoliated graphite oxide in the presence of poly (sodium 4-styrenesulfonate). J. Mater. Chem. **16**(2), 155–158 (2006)
34. Stankovich, S., Dikin, D.A., Dommett, G.H., Kohlhaas, K.M., Zimney, E.J., Stach, E.A., Ruoff, R.S.: Graphene-based composite materials. Nature **442**(7100), 282 (2006)
35. Shin, H.J., Kim, K.K., Benayad, A., Yoon, S.M., Park, H.K., Jung, I.S., Lee, Y.H.: Efficient reduction of graphite oxide by sodium borohydride and its effect on electrical conductance. Adv. Funct. Mater. **19**(12), 1987–1992 (2009)
36. Wang, G., Yang, J., Park, J., Gou, X., Wang, B., Liu, H., Yao, J.: Facile synthesis and characterization of graphene nanosheets. J. Phys. Chem. C **112**(22), 8192–8195 (2008)
37. Novoselov, K.S., Fal, V.I., Colombo, L., Gellert, P.R., Schwab, M.G., Kim, K.: A roadmap for graphene. Nature **490**(7419), 192 (2012)
38. Reina, A., Jia, X., Ho, J., Nezich, D., Son, H., Bulovic, V., Kong, J.: Large area, few-layer graphene films on arbitrary substrates by chemical vapor deposition. Nano Lett. **9**(1), 30–35 (2008)
39. Jiao, L., Zhang, L., Wang, X., Diankov, G., Dai, H.: Narrow graphene nanoribbons from carbon nanotubes. Nature **458**(7240), 877 (2009)
40. Yin, P.T., Shah, S., Chhowalla, M., Lee, K.B.: Design, synthesis, and characterization of graphene–nanoparticle hybrid materials for bioapplications. Chem. Rev. **115**(7), 2483–2531 (2015)
41. Wu, Z.S., Ren, W., Gao, L., Liu, B., Jiang, C., Cheng, H.M.: Synthesis of high-quality graphene with a pre-determined number of layers. Carbon **47**(2), 493–499 (2009)
42. Fan, X., Peng, W., Li, Y., Li, X., Wang, S., Zhang, G., Zhang, F.: Deoxygenation of exfoliated graphite oxide under alkaline conditions: a green route to graphene preparation. Adv. Mater. **20**(23), 4490–4493 (2008)
43. Boehm, H.P., Clauss, A., Fischer, G.O., Hofmann, U.: Das adsorptionsverhalten sehr dünner kohlenstoff-folien. Z. Anorg. Allg. Chem. **316**(3–4), 119–127 (1962)
44. Fernández-Merino, M.J., Guardia, L., Paredes, J.I., Villar-Rodil, S., Solís-Fernández, P., Martínez-Alonso, A., Tascon, J.M.D.: Vitamin C is an ideal substitute for hydrazine in the reduction of graphene oxide suspensions. J. Phys. Chem. C **114**(14), 6426–6432 (2010)
45. Han, H.J., Chen, Y.N., Wang, Z.J.: Effect of microwave irradiation on reduction of graphene oxide films. RSC Adv. **5**(113), 92940–92946 (2015)
46. Zhu, Y., Murali, S., Stoller, M.D., Velamakanni, A., Piner, R.D., Ruoff, R.S.: Microwave assisted exfoliation and reduction of graphite oxide for ultracapacitors. Carbon **48**(7), 2118–2122 (2010)
47. Zhou, M., Wang, Y., Zhai, Y., Zhai, J., Ren, W., Wang, F., Dong, S.: Controlled synthesis of large-area and patterned electrochemically reduced graphene oxide films. Chem. Eur. J. **15**(25), 6116–6120 (2009)
48. Ramesha, G.K., Sampath, S.: Electrochemical reduction of oriented graphene oxide films: an in situ Raman spectroelectrochemical study. J. Phys. Chem. C **113**(19), 7985–7989 (2009)
49. Kudin, K.N., Ozbas, B., Schniepp, H.C., Prud'Homme, R.K., Aksay, I.A., Car, R.: Raman spectra of graphite oxide and functionalized graphene sheets. Nano Lett. **8**(1), 36–41 (2008)

50. Becerril, H.A., Mao, J., Liu, Z., Stoltenberg, R.M., Bao, Z., Chen, Y.: Evaluation of solution-processed reduced graphene oxide films as transparent conductors. ACS Nano **2**(3), 463–470 (2008)
51. Wang, H., Casalongue, H.S., Liang, Y., Dai, H.: $Ni(OH)_2$ nanoplates grown on graphene as advanced electrochemical pseudocapacitor materials. J. Am. Chem. Soc. **132**(21), 7472–7477 (2010)
52. Yuan, B., Bao, C., Qian, X., Wen, P., Xing, W., Song, L., Hu, Y.: A facile approach to prepare graphene via solvothermal reduction of graphite oxide. Mater. Res. Bull. **55**, 48–52 (2014)
53. Gao, X., Jang, J., Nagase, S.: Hydrazine and thermal reduction of graphene oxide: reaction mechanisms, product structures, and reaction design. J. Phys. Chem. C **114**(2), 832–842 (2009)
54. Pei, S., Zhao, J., Du, J., Ren, W., Cheng, H.M.: Direct reduction of graphene oxide films into highly conductive and flexible graphene films by hydrohalic acids. Carbon **48**(15), 4466–4474 (2010)
55. Wei, Z., Chen, Y., Wang, J., Su, D., Tang, M., Mao, S., Wang, Y.: Cobalt encapsulated in N-doped graphene layers: an efficient and stable catalyst for hydrogenation of quinoline compounds. ACS Catal. **6**(9), 5816–5822 (2016)
56. Lee, J.S., You, K.H., Park, C.B.: Highly photoactive, low bandgap TiO_2 nanoparticles wrapped by graphene. Adv. Mater. **24**(8), 1084–1088 (2012)
57. Zhang, Y., Li, D., Zhang, Y., Zhou, X., Guo, S., Yang, L.: Graphene-wrapped $Bi_2O_2CO_3$ core–shell structures with enhanced quantum efficiency profit from an ultrafast electron transfer process. J. Mater. Chem. A **2**(22), 8273–8280 (2014)
58. Myung, S., Solanki, A., Kim, C., Park, J., Kim, K.S., Lee, K.B.: Graphene-encapsulated nanoparticle-based biosensor for the selective detection of cancer biomarkers. Adv. Mater. **23**(19), 2221–2225 (2011)
59. Wu, Z.S., Wang, D.W., Ren, W., Zhao, J., Zhou, G., Li, F., Cheng, H.M.: Anchoring hydrous RuO_2 on graphene sheets for high-performance electrochemical capacitors. Adv. Funct. Mater. **20**(20), 3595–3602 (2010)
60. Lv, W., Sun, F., Tang, D.M., Fang, H.T., Liu, C., Yang, Q.H., Cheng, H.M.: A sandwich structure of graphene and nickel oxide with excellent supercapacitive performance. J. Mater. Chem. **21**(25), 9014–9019 (2011)
61. Dutta, A., Ouyang, J.: Ternary NiAuPt nanoparticles on reduced graphene oxide as catalysts toward the electrochemical oxidation reaction of ethanol. ACS Catal. **5**(2), 1371–1380 (2015)
62. Li, J., Tang, W., Liu, G., Li, W., Deng, Y., Yang, J., Chen, Y.: Reduced graphene oxide modified platinum catalysts for the oxidation of volatile organic compounds. Catal. Today **278**, 203–208 (2016)
63. Zhou, Y., Hu, X.C., Fan, Q., Wen, H.R.: Three-dimensional crumpled graphene as an electro-catalyst support for formic acid electro-oxidation. J. Mater. Chem. A **4**(12), 4587–4591 (2016)
64. Eigler, S., Hirsch, A.: Chemistry with graphene and graphene oxide—challenges for synthetic chemists. Angew. Chem. Int. Ed. **53**(30), 7720–7738 (2014)
65. Fan, X., Zhang, G., Zhang, F.: Multiple roles of graphene in heterogeneous catalysis. Chem. Soc. Rev. **44**(10), 3023–3035 (2015)
66. Julkapli, N.M., Bagheri, S.: Graphene-supported heterogeneous catalysts: an overview. Int. J. Hydrogen Energy **40**(2), 948–979 (2015)
67. Wang, J., Kondrat, S.A., Wang, Y., Brett, G.L., Giles, C., Bartley, J.K., Hutchings, G.J.: Au–Pd nanoparticles dispersed on composite titania/graphene oxide-supports as a highly active oxidation catalyst. ACS Catal. **5**(6), 3575–3587 (2015)
68. Sun, Y., Du, C., An, M., Du, L., Tan, Q., Liu, C., Yin, G.: Boron-doped graphene as promising support for a platinum catalyst with superior activity towards the methanol electrooxidation reaction. J. Power Sources **300**, 245–253 (2015)

69. Wang, C., Astruc, D.: Recent developments of metallic nanoparticle-graphene nanocatalysts. Prog. Mater. Sci. (2018)
70. Li, D., Xu, H., Zhang, L., Leung, D.Y., Vilela, F., Wang, H., Xuan, J.: Boosting the performance of formic acid microfluidic fuel cell: oxygen annealing enhanced Pd@ graphene electrocatalyst. Int. J. Hydrogen Energy **41**(24), 10249–10254 (2016)
71. Zhang, L.Y., Zhao, Z.L., Yuan, W., Li, C.M.: Facile one-pot surfactant-free synthesis of uniform Pd_6Co nanocrystals on 3D graphene as an efficient electrocatalyst toward formic acid oxidation. Nanoscale **8**(4), 1905–1909 (2016)
72. Zhang, X., Zhu, J., Tiwary, C.S., Ma, Z., Huang, H., Zhang, J., Wu, Y.: Palladium nanoparticles supported on nitrogen and sulfur dual-doped graphene as highly active electrocatalysts for formic acid and methanol oxidation. ACS Appl. Mater. Interfaces **8**(17), 10858–10865 (2016)
73. Zhang, L.Y., Zhao, Z.L., Li, C.M.: Formic acid-reduced ultrasmall Pd nanocrystals on graphene to provide superior electrocatalytic activity and stability toward formic acid oxidation. Nano Energy **11**, 71–77 (2015)
74. Kim, J., Park, J.E., Momma, T., Osaka, T.: Synthesis of Pd–Sn nanoparticles by ultrasonic irradiation and their electrocatalytic activity for oxygen reduction. Electrochim. Acta **54**(12), 3412–3418 (2009)
75. Karuppasamy, L., Chen, C.Y., Anandan, S., Wu, J.J.: Sonochemical fabrication of reduced graphene oxide supported Au nano dendrites for ethanol electrooxidation in alkaline medium. Catal. Today **307**, 308–317 (2018)
76. Zhang, B., Zhang, C., He, H., Yu, Y., Wang, L., Zhang, J.: Electrochemical synthesis of catalytically active Ru/RuO_2 core–shell nanoparticles without stabilizer. Chem. Mater. **22** (13), 4056–4061 (2010)
77. Rao, C.R., Trivedi, D.C.: Chemical and electrochemical depositions of platinum group metals and their applications. Coord. Chem. Rev. **249**(5–6), 613–631 (2005)
78. Shahrokhian, S., Rezaee, S.: Vertically standing Cu_2O nanosheets promoted flower-like PtPd nanostructures supported on reduced graphene oxide for methanol electro-oxidation. Electrochim. Acta **259**, 36–47 (2018)
79. Liu, J., Ma, Q., Huang, Z., Liu, G., Zhang, H.: Recent progress in graphene-based noble-metal nanocomposites for electrocatalytic applications. Adv. Mater. 1800696 (2018)
80. Liu, M., Zhang, R., Chen, W.: Graphene-supported nanoelectrocatalysts for fuel cells: synthesis, properties, and applications. Chem. Rev. **114**(10), 5117–5160 (2014)
81. Li, Q., Mahmood, N., Zhu, J., Hou, Y., Sun, S.: Graphene and its composites with nanoparticles for electrochemical energy applications. Nano Today **9**(5), 668–683 (2014)
82. Xia, B., Yan, Y., Wang, X., Lou, X.W.D.: Recent progress on graphene-based hybrid electrocatalysts. Mater. Horizons **1**(4), 379–399 (2014)
83. Ambrosi, A., Chua, C.K., Latiff, N.M., Loo, A.H., Wong, C.H.A., Eng, A.Y.S., Pumera, M.: Graphene and its electrochemistry—an update. Chem. Soc. Rev. **45**(9), 2458–2493 (2016)
84. Su, D.S., Perathoner, S., Centi, G.: Nanocarbons for the development of advanced catalysts. Chem. Rev. **113**(8), 5782–5816 (2013)
85. Kumar, A., Xu, Q.: Two-dimensional layered materials as catalyst supports. ChemNanoMat **4**(1), 28–40 (2018)
86. Sun, S.H., Yang, D.Q., Villers, D., Zhang, G.X., Sacher, E., Dodelet, J.P.: Template- and surfactant-free room temperature synthesis of self-assembled 3D Pt nanoflowers from single-crystal nanowires. Adv. Mater. **20**(3), 571–574 (2008)
87. Wang, M., Wang, X., Li, J., Liu, L.: In situ synthesis of 3D platinum nanoflowers on porous silicon for monolithic integrated micro direct methanol fuel cells. J. Mater. Chem. A **1**(28), 8127–8133 (2013)
88. Yin, A.X., Min, X.Q., Zhang, Y.W., Yan, C.H.: Shape-selective synthesis and facet-dependent enhanced electrocatalytic activity and durability of monodisperse sub-10 nm Pt–Pd tetrahedrons and cubes. J. Am. Chem. Soc. **133**(11), 3816–3819 (2011)

89. Lu, Y., Jiang, Y., Wu, H., Chen, W.: Nano-PtPd cubes on graphene exhibit enhanced activity and durability in methanol electrooxidation after CO stripping–cleaning. J. Phys. Chem. C **117**(6), 2926–2938 (2013)
90. Li, S.S., Zheng, J.N., Ma, X., Hu, Y.Y., Wang, A.J., Chen, J.R., Feng, J.J.: Facile synthesis of hierarchical dendritic PtPd nanogarlands supported on reduced graphene oxide with enhanced electrocatalytic properties. Nanoscale **6**(11), 5708–5713 (2014)
91. Du, S., Lu, Y., Steinberger-Wilckens, R.: PtPd nanowire arrays supported on reduced graphene oxide as advanced electrocatalysts for methanol oxidation. Carbon **79**, 346–353 (2014)
92. Chen, Z., Waje, M., Li, W., Yan, Y.: Supportless Pt and PtPd nanotubes as electrocatalysts for oxygen-reduction reactions. Angew. Chem. **119**(22), 4138–4141 (2007)
93. Lu, Y., Jiang, Y., Chen, W.: PtPd porous nanorods with enhanced electrocatalytic activity and durability for oxygen reduction reaction. Nano Energy **2**(5), 836–844 (2013)
94. Lv, J.J., Wisitruangsakul, N., Feng, J.J., Luo, J., Fang, K.M., Wang, A.J.: Biomolecule-assisted synthesis of porous PtPd alloyed nanoflowers supported on reduced graphene oxide with highly electrocatalytic performance for ethanol oxidation and oxygen reduction. Electrochim. Acta **160**, 100–107 (2015)
95. Xu, C., Tian, Z., Shen, P., Jiang, S.P.: Oxide (CeO_2, NiO, Co_3O_4 and Mn_3O_4)-promoted Pd/C electrocatalysts for alcohol electrooxidation in alkaline media. Electrochim. Acta **53**(5), 2610–2618 (2008)
96. Rostami, H., Rostami, A.A., Omrani, A.: An electrochemical method to prepare of Pd/Cu_2O/MWCNT nanostructure as an anode electrocatalyst for alkaline direct ethanol fuel cells. Electrochim. Acta **194**, 431–440 (2016)
97. Liu, P., Cheng, Z., Ma, L., Zhang, M., Qiu, Y., Chen, M., Cheng, F.: Cuprous oxide template synthesis of hollow-cubic $Cu_2O@Pd_xRu_y$ nanoparticles for ethanol electrooxidation in alkaline media. RSC Adv. **6**(80), 76684–76690 (2016)
98. Zhang, N., Fan, Y., Fan, H., Shao, H., Wang, J., Zhang, J., Cao, C.: Cross-linked Co_3O_4 nanowalls synthesized by electrochemical oxidation of metallic cobalt layer for oxygen evolution. ECS Electrochem. Lett. **1**(2), H8–H10 (2012)
99. Ye, L., Li, Z., Zhang, X., Lei, F., Lin, S.: One-step microwave synthesis of Pt (Pd)/Cu_2O/GNs composites and their electro-photo-synergistic catalytic properties for methanol oxidation. J. Mater. Chem. A **2**(48), 21010–21019 (2014)
100. Zhao, Y., Zhan, L., Tian, J., Nie, S., Ning, Z.: MnO_2 modified multi-walled carbon nanotubes supported Pd nanoparticles for methanol electro-oxidation in alkaline media. Int. J. Hydrogen Energy **35**(19), 10522–10526 (2010)
101. Zheng, J.N., Li, S.S., Ma, X., Chen, F.Y., Wang, A.J., Chen, J.R., Feng, J.J.: Green synthesis of core–shell gold–palladium@ palladium nanocrystals dispersed on graphene with enhanced catalytic activity toward oxygen reduction and methanol oxidation in alkaline media. J. Power Sources **262**, 270–278 (2014)
102. Wang, S., Iyyamperumal, E., Roy, A., Xue, Y., Yu, D., Dai, L.: Vertically aligned BCN nanotubes as efficient metal-free electrocatalysts for the oxygen reduction reaction: a synergetic effect by Co-doping with boron and nitrogen. Angew. Chem. **123**(49), 11960–11964 (2011)
103. Lv, J.J., Li, S.S., Zheng, J.N., Wang, A.J., Chen, J.R., Feng, J.J.: Facile synthesis of reduced graphene oxide supported PtAg nanoflowers and their enhanced electrocatalytic activity. Int. J. Hydrogen Energy **39**(7), 3211–3218 (2014)
104. Ye, W., Chen, Y., Zhou, F., Wang, C., Li, Y.: Fluoride-assisted galvanic replacement synthesis of Ag and Au dendrites on aluminum foil with enhanced SERS and catalytic activities. J. Mater. Chem. **22**(35), 18327–18334 (2012)
105. Huang, D., Bai, X., Zheng, L.: Ultrafast preparation of three-dimensional dendritic gold nanostructures in aqueous solution and their applications in catalysis and SERS. J. Phys. Chem. C **115**(30), 14641–14647 (2011)

106. Guo, Y., Sun, X., Liu, Y., Wang, W., Qiu, H., Gao, J.: One pot preparation of reduced graphene oxide (RGO) or Au (Ag) nanoparticle-RGO hybrids using chitosan as a reducing and stabilizing agent and their use in methanol electrooxidation. Carbon **50**(7), 2513–2523 (2012)
107. Rodriguez, P., Kwon, Y., Koper, M.T.: The promoting effect of adsorbed carbon monoxide on the oxidation of alcohols on a gold catalyst. Nat. Chem. **4**(3), 177 (2012)
108. Tateishi, N., Nishimura, K., Yahikozawa, K., Nakagawa, M., Yamada, M., Takasu, Y.: Electrocatalytic properties of ultrafine gold particles towards oxidation of acetaldehyde and ethanol. J. Electroanal. Chem. **352**(1–2), 243–252 (1993)
109. Xu, C., Cheng, L., Shen, P., Liu, Y.: Methanol and ethanol electrooxidation on Pt and Pd supported on carbon microspheres in alkaline media. Electrochem. Commun. **9**(5), 997–1001 (2007)
110. Choi, C.H., Kim, M., Kwon, H.C., Cho, S.J., Yun, S., Kim, H.T., Choi, M.: Tuning selectivity of electrochemical reactions by atomically dispersed platinum catalyst. Nat. Commun. **7**, 10922 (2016)
111. Wang, H., Yang, Y., Liang, Y., Zheng, G., Li, Y., Cui, Y., Dai, H.: Rechargeable Li–O_2 batteries with a covalently coupled $MnCo_2O_4$–graphene hybrid as an oxygen cathode catalyst. Energy Environ. Sci. **5**(7), 7931–7935 (2012)
112. Xuan, L., Chen, L., Yang, Q., Chen, W., Hou, X., Jiang, Y., et al.: Engineering 2D multi-layer graphene-like Co_3O_4 thin sheets with vertically aligned nanosheets as basic building units for advanced pseudo capacitor materials. J. Mater. Chem. A. **3**, 17525–17533 (2015)
113. Moosavifard, S.E., Shamsi, J., Fani, S., Kadkhodazade, S.: 3D ordered nanoporous $NiMoO_4$ for high-performance supercapacitor electrode materials. RSC Adv. **4**, 52555–52561 (2014)
114. Lu, X., Yu, M., Wang, G., Tong, Y., Li, Y.: Flexible solid-state supercapacitors: design, fabrication and applications. Energy Environ. Sci. **7**, 2160–2181 (2014)
115. Chen, T., Dai, L.: Carbon nanomaterials for high-performance supercapacitors. Mater. Today **16**, 272–280 (2013)
116. Guo, D., Luo, Y., Yu, X., Li, Q., Wang, T.: High performance $NiMoO_4$ nanowires supported on carbon cloth as advanced electrodes for symmetric supercapacitors. Nano Energy **8**, 174–182 (2014)
117. Hall, P.J., Mirzaeian, M., Fletcher, S.I., Sillars, F.B., Rennie, A.J., Shitta-Bey, G.O., Wilson, G., Cruden, A., Carter, R.: Energy storage in electrochemical capacitors: designing functional materials to improve performance. Energy Environ. Sci. **3**, 1238–1251 (2010)
118. Miller, J.R., Burke, A.F.: Electrochemical capacitors: challenges and opportunities for real-world applications. Electrochem. Soc. Interface **4**(Spring), 53–57 (2008)
119. Conway, B.E.: Electrochemical Supercapacitors: Scientific Fundamentals and Technological Applications, 2nd edn. Kluwer Academic/Plenum Publishers, New York (1999)
120. Trasatti, S., Kurzweil, P.: Electrochemical supercapacitors as versatile energy stores. Platinum Met. Rev. **38**, 46–56 (1994)
121. Zhong, C., Deng, Y., Hu, W., Qiao, J., Zhang, L., Zhang, J.: A review of electrolyte materials and compositions for electrochemical supercapacitors. Chem. Soc. Rev. **44**, 7484–7539 (2015)
122. Carter, R., Cruden, A.: Strategies for control of a battery/supercapacitor system in an electric vehicle. In: 2008 International Symposium on Power Electronics, Electrical Drives, Automation and Motion, vol. 1–3, pp. 727–732. IEEE (2008)
123. Gao, Q., Demarconnay, L., Raymundo-Pinero, E., Beguin, F.: Exploring the large voltage range of carbon/carbon supercapacitors in aqueous lithium sulfate electrolyte. Energy Environ. Sci. **5**, 9611–9617 (2012)
124. Fic, K., Lota, G., Meller, M., Frackowiak, E.: Novel insight into neutral medium as electrolyte for high-voltage supercapacitors. Energy Environ. Sci. **5**, 5842–5850 (2012)
125. Zhang, Q., Rong, J., Ma, D., Wei, B.: The governing self-discharge processes in activated carbon fabric-based supercapacitors with different organic electrolytes. Energy Environ. Sci. **4**, 2152–2159 (2011)

126. Wan, L., Sun, S., Zhai, T., Savilov, S.V., Lunin, V.V., Xia, H.: Multiscale porous graphene oxide network with high packing density for asymmetric supercapacitors. J. Mater. Res. 1–12 (2017)
127. Yang, J., Hu, J., Zhu, M., Zhao, Y., Chen, H., Pan, F.: Ultrahigh surface area meso/microporous carbon formed with self-template for high-voltage aqueous supercapacitors. J. Power Sources **365**, 362–371 (2017)
128. Jana, A., Scheer, E., Polarz, S.: Synthesis of graphene–transition metal oxide hybrid nanoparticles and their application in various fields. Beilstein J. Nanotechnol. **8**, 688–714 (2017)
129. Fan, H., Niu, R., Duan, J., Liu, W., Shen, W.: Fe_3O_4@carbon nanosheets for all-solid-state supercapacitor electrodes. ACS Appl. Mater. Interfaces **8**, 19475–19483 (2016)
130. Wu, Z.-S., Zhou, G., Yin, L.-C., Ren, W., Li, F., Cheng, H.-M.: Graphene/metal oxide composite electrode materials for energy storage. Nano Energy **1**, 107–131 (2012)
131. Frackowiak, E.: Carbon materials for supercapacitor application. Phys. Chem. Chem. Phys. **9**, 1774–1785 (2007)
132. Hu, C.-C., Chang, K.-H., Lin, M.-C., Wu, Y.-T.: Design and tailoring of the nanotubular arrayed architecture of hydrous RuO_2 for next generation supercapacitors. Nano Lett. **6**, 2690–2695 (2006)
133. Cheng, Q., Tang, J., Ma, J., Zhang, H., Shinya, N., Qin, L.-C.: Graphene and nanostructured MnO_2 composite electrodes for supercapacitors. Carbon N. Y. **49**, 2917–2925 (2011)
134. Deng, W., Ji, X., Chen, Q., Banks, C.E.: Electrochemical capacitors utilising transition metal oxides: an update of recent developments. RSC Adv. **1**, 1171–1178 (2011)
135. Shanshan, L., Yansu, W., Zhiling, M.: Bi_2O_3 with reduced graphene oxide composite as a supercapacitor electrode. Int. J. Electrochem. Sci. **13**, 12256–12265 (2018)
136. Jinfeng, S., Zhangpeng, L., Jinqing, W., Wei, H., Peiwei, G., Ping, W., Zhaofeng, W., Shengrong, Y.: Ni/Bi battery based on $Ni(OH)_2$ nanoparticles/graphene sheets and Bi_2O_3 rods/graphene sheets with high performance. J. Alloy. Compd. **643**, 231–238 (2015)
137. Huan-Wen, W., Zhong-Ai, H., Yan-Qin, C., Yan-Li, C., Zi-Qiang, L., Zi-Yu, Z., Yu-Ying, Y.: Facile solvothermal synthesis of a graphene nanosheet–bismuth oxide composite and its electrochemical characteristics. Electrochim. Acta **55**, 8974–8980 (2010)
138. Ezhil, V.A.T., Bose, D., Murugananthan, R., Seung-Kyu, H., Chang-Soo, J., Yun Suk, H., Young-Kyu, H.: Hexagonal Co_3O_4 anchored reduced graphene oxide sheets for high-performance supercapacitors and non-enzymatic glucose sensing. J. Mater. Chem. A **6**, 14367 (2018)
139. Rajesh, K., Hyun-Jun, K., Park, S., Anchal, S., Il-Kwon, O.: Graphene-wrapped and cobalt oxide-intercalated hybrid for extremely durable super-capacitor with ultrahigh energy and power densities. Carbon **79**, 192–202 (2014)
140. Arshid, N., Navaneethan, D., Fatin, S., Mahipal, Y.K., Ramesh, K., Ramesh, S.: Enhanced electrochemical performance of cobalt oxide nanocube intercalated reduced graphene oxide for supercapacitor application. RSC Adv. **6**, 34894 (2016)
141. Chengen, H., Yachao, L., Pengyuan, G., Long, C., Dean, S., Xiaolin, X., Robert, K., Yiu, L., Yingkui, Y.: Bioinspired Co_3O_4/graphene layered composite films as self-supported electrodes for supercapacitors. Compos. B **121**, 68–74 (2017)
142. Jintao, Z., Jianwen, J., Zhao, X.S.: Synthesis and capacitive properties of manganese oxide nanosheets dispersed on functionalized graphene sheets. J. Phys. Chem. C **115**, 6448–6454 (2011)
143. Jiayi, Z., Junhui, Y.: Facile synthesis of graphene-wrapped honeycomb MnO_2 nanospheres and their application in supercapacitors. ACS Appl. Mater. Interfaces **4**, 1770–1776 (2012)
144. Jian, C., Meihua, J., Fei, Y., Tae Hyung, K., Viet Thong, L., Hongyan, Y., Fethullah, G., Bing, L., Arunabha, G., Sishen, X., Young Hee, L.: Asymmetric supercapacitors based on graphene/MnO_2 nanospheres and graphene/MoO_3 nanosheets with high energy density. Adv. Funct. Mater. **23**, 5074–5083 (2013)
145. Sheng, C., Junwu, Z., Xiaodong, W., Qiaofeng, H., Xin, W.: Graphene oxide-MnO_2 nanocomposites for supercapacitors. ACS Nano **4**, 2822–2830 (2010)

146. Xiehong, C., Bing, Z., Wenhui, S., Jian, Y., Zhanxi, F., Zhimin, L., Xianhong, R., Chen, B., Qingyu, Y., Hua, Z.: Reduced graphene oxide-wrapped MoO_3 composites prepared by using metal–organic frameworks as precursor for all-solid-state flexible supercapacitors. Adv. Mater. **27**, 4695–4701 (2015)
147. Alok, P., Abhijeet Sadashiv, G., Satyajit, R., Brahmananda, C., Chandra Sekhar, R.: Enhanced pseudocapacitance of MoO_3-reduced graphene oxide hybrids with insight from density functional theory investigations. J. Phys. Chem. C **12**, 18992–19001 (2017)
148. Wujun, M., Shaohua, C., Shengyuan, Y., Wenping, C., Wei, W., Yanhua, C., Meifang, Z.: Flexible all-solid-state asymmetric supercapacitor based on transition metal oxide nanorods/reduced graphene oxide hybrid fibers with high energy density. Carbon **113**, 151–158 (2017)
149. Kai, Z., Weijia, Z., Xiaojun, L., Yuanhua, S., Shaozheng, J., Wei, L., Jia, L., Ligui, L., Wenhan, N., Hong, L., Shaowei, C.: Ultrathin MoO_3 nanocrystals self-assembled on graphene nanosheets via oxygen bonding as supercapacitor electrodes of high capacitance and long cycle life. Nano Energy **12**, 510–520 (2015)

Functionalized Graphene-Metal Nanoparticles Nanohybrids as Electrochemical Sensors

Ankita Sinha, Dhanjai, Jiping Chen and Rajeev Jain

Abstract Graphene (GR) and its derivatives are highly interesting carbon nanoforms which possess layered morphology and unique structural/chemical/physical features. These extraordinary properties make GR materials highly applicable for multiple scientific applications, however, zero band gap, hydrophobic nature are among few limitations which make its functionalization a mandatory step to expand its practical applications. To achieve the best out of GR materials, different covalent and noncovalent functionalization schemes have been proposed governed by disruption of sp^2 lattice in case of covalent scheme and retention of its structural integrity in case of noncovalent functionalization. The chapter addresses a brief discussion on different GR functionalization schemes. Moreover, it focuses on noncovalently functionalized GR nanohybrids with metal based nanoparticles (MNPs) as electrochemical sensors taking some relevant examples. Synergistic effects of GR materials and MNPs enhance the electro-activity of nanohybrids for electrochemical detection of different targets.

Keywords Graphene (GR) · Functionalization · Metal nanoparticles (MNPs) · Electrochemical sensors

A. Sinha
Key Laboratory of Industrial Ecology and Environmental Engineering (Ministry of Education, China), School of Environmental Science and Technology, Dalian University of Technology, Dalian 116024, People's Republic of China

Dhanjai (✉)
Department of Mathematical and Physical Sciences, Concordia University of Edmonton, Edmonton, AB, Canada
e-mail: dhanjai83@gmail.com

Dhanjai · J. Chen
CAS Key Laboratory of Separation Science for Analytical Chemistry, Dalian Institute of Chemical Physics, Chinese Academy of Sciences, Dalian 116023, People's Republic of China

R. Jain
School of Studies in Chemistry, Jiwaji University, Gwalior 474011, India

A. Khan et al. (eds.), *Graphene Functionalization Strategies*, Carbon Nanostructures, https://doi.org/10.1007/978-981-32-9057-0_2

1 Introduction

Graphene (GR) is interestingly one of the most popular carbon allotropes arranged in a honeycomb pattern. It is two-dimensional sp^2 hybridized sheet of carbon atoms which has been extensively studied and experimented since its discovery in 2004. GR is considered highly promising for multiple scientific applications with unique layered morphology and superior chemical/thermal/mechanical properties [1, 2]. GR is commonly prepared using top down (e.g. chemical vapor deposition) and bottom up (e.g. micromechanical exfoliation) approaches [3, 4]. In top-down approach, the stacked 3D graphite layers are exfoliated by physical/chemical/thermal treatments and are able to produce large quantities of GR. However, it is difficult to produce single-layered GR through these methods. In contrast, bottom up approaches can produce GR sheets of better quality and larger surface areas by growth on suitable substrates. However, in these methods, GR is subjected to high temperature and pressure under suitable experimental conditions. There have been various reports available discussing different synthetic approaches for GR production. Graphene oxide (GO) is the oxidized form of GR in which oxygen atoms are bound with the carbon scaffold (Fig. 1a). Interestingly GR is considered to be hydrophobic while GO is hydrophilic in nature. Notably, it is the basic difference between GR and GO, however, GO possesses both sp^2 (aromatic) and sp^3 (aliphatic) domains [5]. Graphene oxide (GO) has been also used as a precursor to prepare GR. In general, GO is obtained by the Hummers and Offeman method [2]. 3D graphite layers which possess various hydroxyl, epoxy and carboxylic groups at basal and edges planes, can be easily converted into graphite oxides by chemical treatments. The hydrophilic graphite oxides are then subjected to thermal exfoliation/sonication in water followed by the reduction of the GO generating reduced form of GO (rGO). A multi layer GR material contains about 5–10 stacking layers. GO is single-layered with high oxygen functional groups classified by carbon-oxygen (C/O) atom ratio which is less than 3.0 and close to 2.0 whereas rGO shows higher C/O ratio than GO [3]. Both GR and GO materials are highly applicable to multiple applications such as catalysis, energy, flexible electronics, sensors etc. due to their superior ion transport properties, mechanical/thermal strength and high surface-to volume ratio. Recent studies suggest superior catalytic activities of GR materials over other carbon nanoforms [1]. Owing to their high surface area, GR/GO provides an excellent interface for immobilization of highly dispersed nanomaterials for the fabrication of variety of transducing interfaces in sensing devices [3]. However, zero band gap and hydrophobic nature of GR weaken the competitive strength of GR for their application as sensors [4]. Further, it is easy for pristine GR to aggregate due to delocalized π electron system and large surface area making it difficult to be dispersed. Therefore, band gap opening and avoiding aggregation of GR is necessary for expanding their potential utilization in sensing and biosensing applications. Moreover, GO is an insulator due to the disruption of the p-orbital structure during oxidation reactions and thus is not suitable for electronic applications. This enables the production of rGO highly important for fabricating GO based electronics.

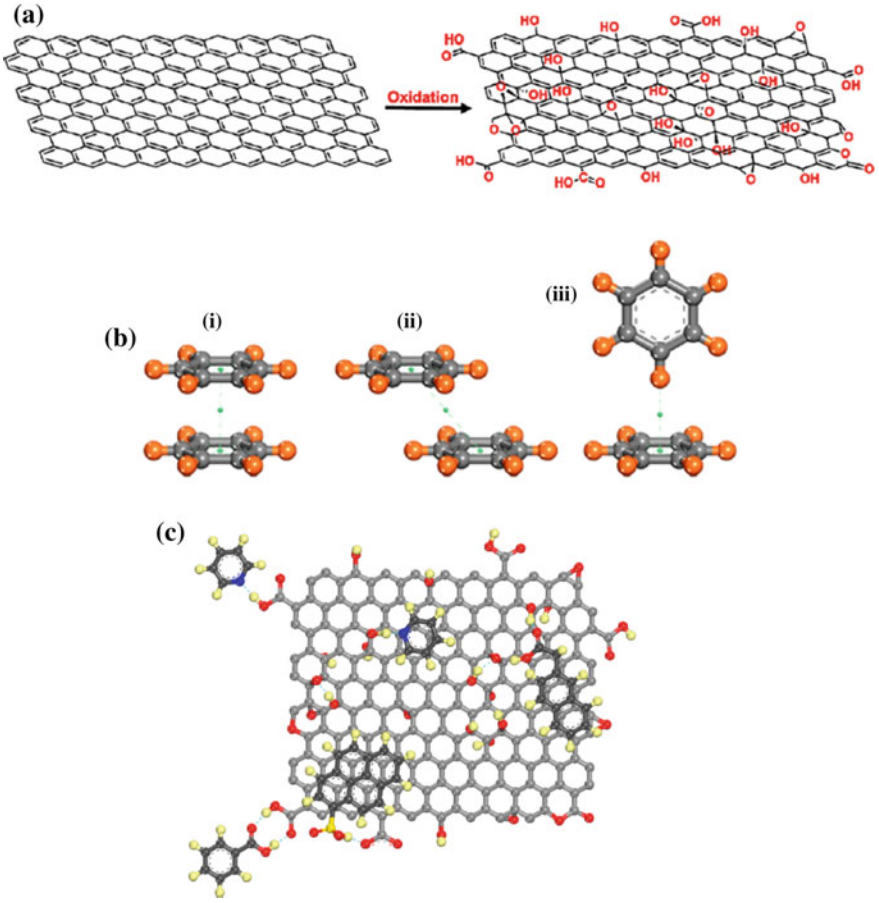

Fig. 1 **a** Graphene oxidation to graphene oxide, **b** (i) π–π interactions face to face (ii) slipped interactions, (iii) C-H-π interactions in benzyl molecules (black balls represent carbon atoms while orange balls represent hydrogen atoms), **c** presentation of π–π stacking and hydrophobic interactions in GO [5]. Reprinted with permission from Ref. [5]

Therefore, functionalization and dispersion of GR materials are of critical importance for their potential practical applications. This can be done by suitable functionalization strategies which include various covalent and noncovalent schemes which can be very effective to achieve best performances out of GR/GO materials [3–5]. Different functionalized GR hybrid materials with metal/carbon/polymer/quantum dots/magnetic nanomaterials have been fabricated to improve their physical and chemical properties. However, the present chapter emphasizes on functionalized GR hybrids with metal based nanomaterials for electrochemical sensing applications taking some relevant examples. The following sections provide brief discussion of different functionalization methods (covalent and noncovalent) of GR materials and their modification modes.

1.1 Covalent Modifications of GR/GO

There has been massive literature survey for emerging applications of GR and GO surfaces modified through covalent bonds and noncovalent interactions [3–5]. Covalent functionalization disturbs the sp^2 domain of GR lattices and results in the formation of defects and loss of electronic properties. Covalent functionalization generally includes addition of free radicals or dienophiles to the sp^2 lattice of GR materials. GR functionalization by free radical addition usually involves thermal and photochemical treatments. The addition reaction converts carbon atoms of GR from sp^2 to sp^3 hybridization form and changes their electronic conductivity by disrupting their aromaticity. Lomeda et al. [6] reported addition reactions of aryl diazonium salts into GR lattice to produce covalently functionalized GR materials. Further, cyclo-addition reactions of GR with dienophiles such as aziridine [7], azomethine ylide [8], carbene and aryne [9] have been successfully applied to produce covalently functionalized GR materials. During cyclo-addition reactions, bond breakage and bond formation processes occur simultaneously through pericyclic reactions which significantly widen the band gap and improve the solubility of GR in aqueous/organic solvents for practical applications. Commonly, [2 + 1] cyclo-addition of carbenes and aziridines, [2 + 2] cyclo-addition of arynes, [3 + 2] cyclo-addition of azomethine ylide and [4 + 2] Diels-Alder reaction are used for GR functionalization [2]. Moreover, covalent linkage of functionalities such as chromophore, polymers and other organic molecules to GO has been also reported [4]. Oxygen moieties such as carboxylic (–COOH), hydroxyl (–OH) and epoxide groups at GO surface and edges of GR can form covalent bonds with amino groups of different biomolecules through carbodiimide reaction with 1-ethyl-3-(3-dimethylaminopropyl) carbodiimide (EDC) or *N*,*N*-dicyclohexyl-carbodiimide (DCC) in the presence of *N*-hydroxysuccinimide (NHS). The produced active esters can react with the amine groups of biomolecules such as poly-L-lysine [10], DNA [6], proteins [9], aminocyclodextrin [11] to form amide bonds and to develop GR functionalized novel electronic sensing interfaces. Covalent attachments of hydrogen or halogen to GR derivatives such as graphene/flourographene have been also reported to produce functionalized GR materials [4].

1.2 Noncovalent Modifications of GR/GO

Noncovalent functionalization schemes of GR introduce new chemical groups on its surfaces without compromising its sp^2 lattice and electronic properties. These schemes lead to enhanced dispersibility and electro-catalytic reactivity of GR for redox applications. The noncovalent functionalization of GR/GO is generally based on π–π or van der Waals interactions with organic molecules/polymers. While π–π

interactions are more common between GR/GO and molecules with similar π systems, the van der Waals interactions occur between GR/GO and molecules of high hydrophobic character [5]. The π–π interactions in GR are seen in the face-to-face and edge-to-face arrangement of the electron-rich and electron-poor regions as shown in Fig. 1b. These interactions can further influence the functionalization of GR with other small molecules (e.g. drugs, biomolecules, polymers) or nanomaterials. Apart from π–π interactions, it is reported that there is also possibility of CH-π interactions occurring at edges planes of GR. Similar kind of π interactions are supposed to occur in GO however unlike GR, additional interactions (e.g. ionic, hydrogen bonding) are also reported due to the addition of hydrogen bond donors-acceptor species from different functional groups (e.g. epoxides, ethers, alcohols, carboxylate, carboxylic). Figure 1c shows the presence of oxygen functional groups at the edges that can help in additional binding.

For a noticeable π–π interactions between GR/GO and organic molecules, their planarity play a significant role. For example, pristine GR monolayer which has a rich extended aromatic π system and planar geometry, interact firmly with small aromatic molecules. GO is considered as a nonaromatic surface with sp^3 carbon atoms with sp^2 domains while rGO possess aromatic character to some extent. Existence of the sp^3 carbon atoms of GO allows it to deviate from the planarity and its ability to interact with aromatic species. However, interactions of GR with π systems vary greatly depending upon the substituents of aromatic molecules, their electron donating/withdrawing ability, size and planarity. Apart from π–π interactions, noncovalent functionalization of GR materials include van der Waals forces towards hydrophobic molecules (e.g. surfactants, ionic liquids, macromolecules) which help to produce GR hybrid materials soluble in aqueous or organic solvents. The similar behavior is not supposed to occur in GO (as it is hydrophilic) but likely to occur in rGO which possess some aromatic character and hydrophobicity. Furthermore, as discussed earlier, GO contains oxygen moieties (mainly carboxylate and hydroxylate) at the edges which take part in ionic/hydrogen bonding with ionic molecules or macromolecules. To some extent this behavior is also noticed in rGO. The hydrophobic interactions (van der Waals) of GR or rGO with the aliphatic part of surfactants results in enhanced stability in aqueous medium. However, interaction of an amphiphilic molecule with GR materials is characterized by ionic interactions where the hydrophobic part enhances their stability in organic solvents. For example, interaction of GO/rGO with quaternary ammonium salts has been demonstrated where polar heads were attached with carboxylate and hydroxylate moieties of GO/rGO and aliphatic part stabilized their solubility and stability of organic medium [4]. In past years, different noncovalent interaction modes of GR materials with organic molecules/macromolecules (e.g. polymers, biomolecules, carbon allotropes, metal based nanoparticles, magnetic nanoparticles, quantum dots, 2D GR analogues) have been justified to produce various GR/GO/rGO hybrid materials for various practical applications [4].

2 Functionalized Graphene-Metal Nanohybrids as Electrochemical Sensors

Graphene based nanohybrids can be obtained through various synthetic methods [12] such as electrospinning [13], chemical reduction [14], electrodeposition [15], electrochemical doping [16], electrochemical polymerization [17], self-assembly [18], in situ polymerization [19] etc. Synergetic effects of GR nanohybrids exert enhanced surface area, high electronic and chemical properties making them suitable candidate for fabricating detection platforms. In this section, we discuss some relevant examples of non-covalently functionalized GR nanohybrids with metal based nanoparticles (MNPs) for fabricating electrochemical sensing interfaces.

Metal nanoparticles such as Au, Ag, Pt, Fe etc. are well known to exert high electronic conductivity due to quantum effects. Noncovalent functionalization of GR materials with such highly conductive MNPs significantly enhances their stability, dispersibility and redox activity than those of individual GR materials. Preparation of GR-MNPs nanohybrids can be achieved by different strategies. For example, one strategy involves firstly the production of GO nanosheets followed by modification with MNPs and finally reduction of GO [20] while other strategy involves reduction of GO and metallic ions in only one system [21]. However, both strategies of preparing GR-MNPs hybrids involve highly complicated processes (e.g. vacuum filtration, spray deposition, spin-coating, chemical vapor deposition) and hazardous reducing agents (e.g. hydrazine hydrate, sodium borohydride) which make the fabrication of GR-MNPs hybrids very difficult. To resolve this, a green synthesis strategy was proposed in which glucose was used to reduce GO and $HAuCl_4$ in one liquid system to prepare rGO-AuNPs hybrid membranes on polyethylene terephthalate (PET) substrate [22]. Formation of self assembled rGO-AuNPs nanohybrid was mainly governed by the Brownian motion and electrostatic interaction between rGO and AuNPs. It was observed that encapsulation of AuNPs in the hybrid membrane could be tuned by changing concentration of $HAuCl_4$. Prepared rGO-AuNP hybrid membranes were found to be very stable in various organic solvents and were used as nonenzymatic biosensor for amperometric detection of hydrogen peroxide (H_2O_2). The rGO-AuNPs nanohybrid biosensor showed high sensing performances for H_2O_2 detection within a wide linear range from 0.25–22.5 mM with detection limit as low as 6.2 mM, high selectivity and stability. Using similar self-assembly approach, rGO-AuNPs nanohybrid was fabricated at liquid-air interface using sodium citrate and ammonia to reduce GO and $HAuCl_4$ simultaneously (Fig. 2) [23]. The prepared rGO-AuNPs film was coated onto glass carbon electrode (GCE) and silicon wafer which were utilized as nonenzymatic amperometric H_2O_2 biosensor. The detection limit towards H_2O_2 at rGO-AuNP-GCE sensor was obtained as 1.7 μM in the concentration range of 10–200 μM.

Furthermore, AgNPs have been also used for preparing various GR/GO nanohybrids [24–26]. In a typical example, electrospinning technique was used to fabricate polyvinyl alcohol (PVA) and GR nanohybrid membrane doped with

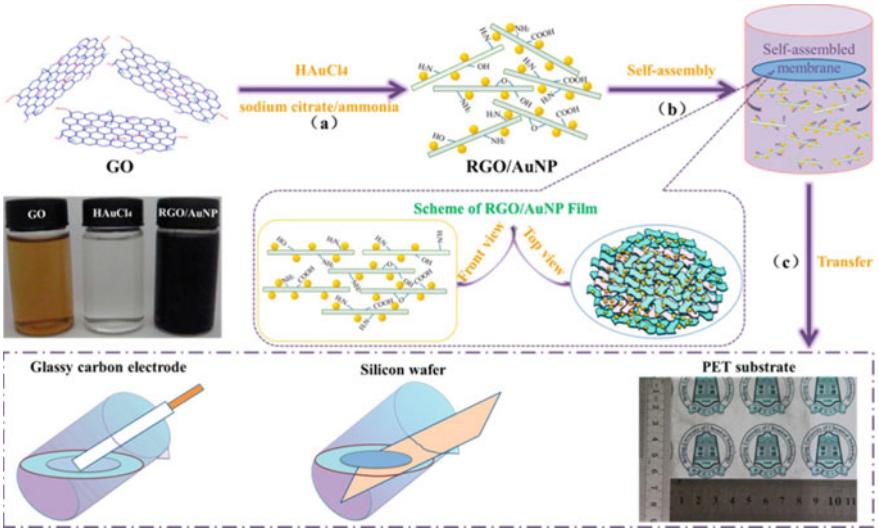

Fig. 2 Systematic presentation of preparation of rGO-AuNPs nanohybrid [23]. Reprinted with permission from Ref. [23]

highly dispersed AgNPs [25]. The PVA-GR-AgNP nanohybrid membrane was directly electrospun onto the surface of GCE for nonenzymatic amperometric detection of H_2O_2. In prepared GR-AgNPs hybrids, the GR sheets were firmly decorated with AgNPs and well dispersed in the PVA nanofibers. This helped to facilitate the electron transfer reaction at the electrode surface towards H_2O_2 detection in the linear detection range from 0.005–47 $\times$ 10^{-3} M to obtain a detection limit of 0.56 $\times$ 10^{-3} M. In another study, rGO-AgNPs nanohybrid was synthesized using microwave-assisted approach and utilized to modify GCE for the sensitive and selective voltammetric detection of nitrite (Fig. 3a) [26]. The study revealed that the rGO sheets were uniformly decorated with AgNPs all over its surface (Fig. 3b, c) and showed high electroactivity towards nitrite. The sensor showed high differential pulse voltammetric (DPV) response towards nitrite detection with detection limit of 0.012 μM within the linear concentration range of 0.1–120 μM (Fig. 3d). Various other MNPs doped GR/GO interfaces have been also applied for nitrite detection in past few years [27–36]. For example, nanohybrids of Co_3O_4 nanospindles doped rGO-GCE [27], AuNPs dispersed halloysite nanotubes (HNTs) composites of rGO-GCE [28], dual metallic nanoparticles Au-PdNPs doped rGO-GCE [29], Cu metal-organic frameworks (MOFs) based CuMOF-rGO-GCE [30], PdNPs-rGO-GCE [31, 32], Cu nanodendrites-rGO-GCE [33], Fe_2O_3-rGO-GCE [34, 35], and flower-like ZnO-rGO-GCE [36] based sensors were successfully applied for electrochemical detection of nitrite using amperometry [27–31, 33, 34, 36] and DPV [32, 34, 35].

In another gentle approach, a ferritin mediated biomimetic synthesis of FePt nanoparticles on GR sheets was carried out in which GR sheets were modified with

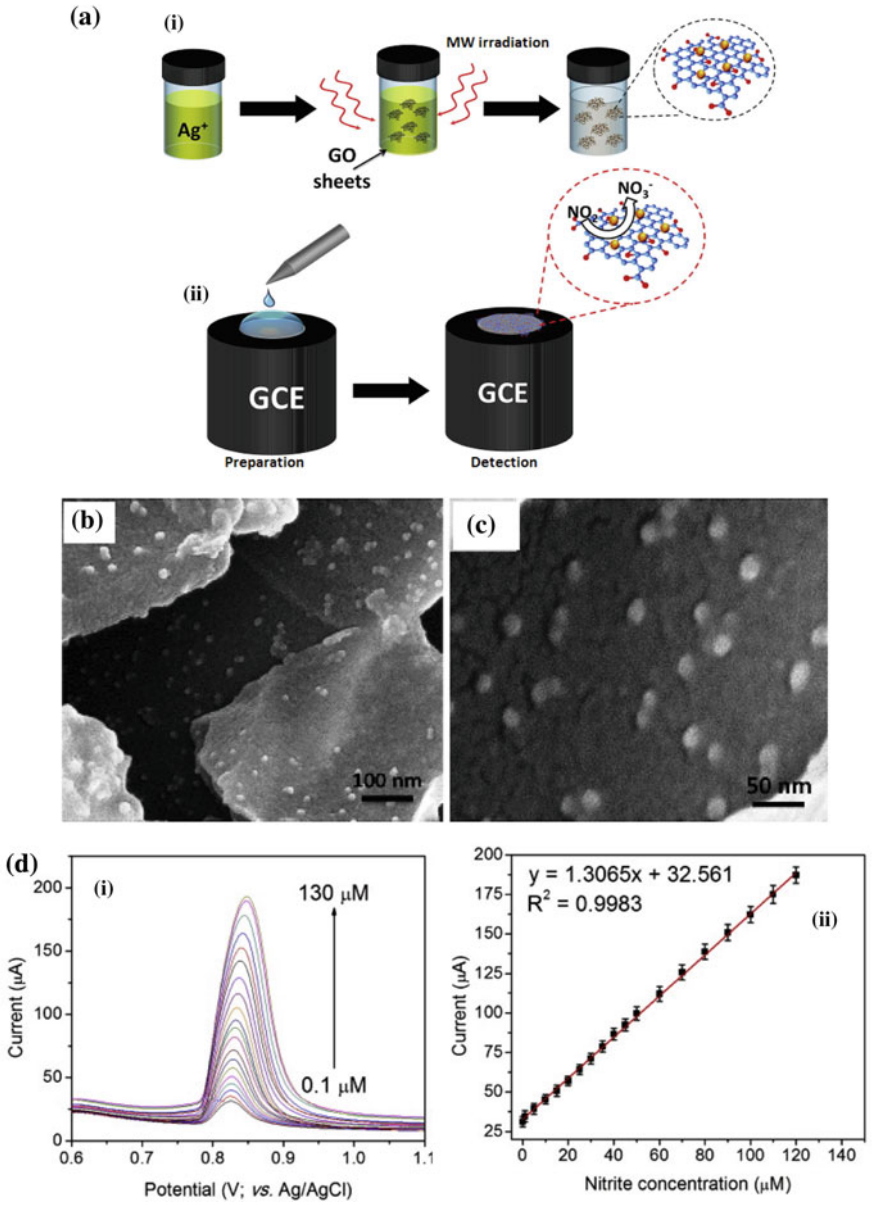

Fig. 3 **a** (i) Microwave assisted synthesis of AgNPs-rGO nanohybrid (ii) preparation of GCE modified sensor for nitrite detection, **b**, **c** SEM of AgNPs-rGO nanohybrid, **d** (i) DPV of AgNPs-rGO-GCE for nitrite detection (ii) calibration curve: current vs nitrite conc. [26]. Reprinted with permission from Ref. [26]

1-pyrenebutyric acid *N*-hydroxysuccinimide ester for efficient binding with ferritin molecules [37]. The FePtNPs were synthesized by chemical reduction of metallic Fe^{2+} and $PtCl_6^{2-}$ and utilized as modified GCE interface for ethanol and methanol oxidation.

In addition, using hydrothermal approach, zinc oxide (ZnO) nanocrystals based rGO nanohybrid was prepared for amperometric detection of hydrazine (N_2H_4) [38]. The size and shape of ZnO nanospindles on rGO surface was controlled by adjusting the mass ratio of Zn^{2+} to rGO. The ZnO-rGO nanohybrid modified GCE sensor showed improved sensing abilities towards N_2H_4 determination compared to pristine ZnO sensor [39–42] suggesting synergistic effects of enhanced conductivity, electro-catalytic activity of ZnO and rGO. The fabricated ZnO-rGO-GCE sensor exhibited a rapid amperometric response to N_2H_4 in a linear detection range of 1.0–33.5 mM with a detection limit of 0.8 mM. Further, a preparation scheme for ZnO-rGO nanohybrid was reported by in situ thermal decomposition method in which zinc benzoate dihydrazinate was used as precursor which was thermally decomposed at the surface of rGO for voltammetric detection of glucose [43]. Moreover, cuprous oxide (Cu_2O) microspheres were successfully grown on the surface of rGO by reducing Cu^{2+} and GO simultaneously in the presence of sodium ascorbate and sodium hydroxide [44]. The size of the microspheres was controlled by tuning the mass ratio of rGO and copper sulphate. The fabricated Cu_2O-rGO-GCE sensor exhibited high amperometric response to H_2O_2 in the linear detection range from 0.005 to 2.775 mM with a detection limit of 0.0108 mM. Further, the sensor showed a detection limit of 7.288×10^{-4} mM for glucose detection in the linear detection range from 0.001 to 0.419 mM. The sensor showed excellent detection performances compared to other pristine Cu_2O and Cu_2O-GR nanohybrid sensors towards H_2O_2 [45–48] and glucose [46, 48] detection. Moreover, a novel nanohybrid of yttrium oxide (Y_2O_3) and GO was used to modify GCE by drop casting technique for electrochemical detection of L-3,4-dihydroxyphenylalanine (L-DOPA) [49]. Aqueous solution of GO was dispersed in pre-prepared nafion solution in ethanol by sonication followed by addition of Y_2O_3 NPs and further sonication. The addition of Y_2O_3 NPs increased the electroactive surface area by inhibiting the aggregation of GO layers and resulted in the enhanced voltammetric performance for detection of L-DOPA with detection limit of 0.05 mM in the linear dynamic range of 0.5–350 mM. Scanning electron microscopic (SEM) image and detection scheme of L-DOPA at Y_2O_3–GO sensor has been shown in Fig. 4a, b respectively. In another example, TiO_2–Mn_2O_3 composites prepared by sol-gel method were decorated on the pristine GR to make TiO_2–Mn_2O_3–GR nanohybrid modified GCE sensor for dopamine (DA) [50]. The pristine GR encapsulated the metal oxides anchoring the metal oxide nanoparticles at the edges planes indicated by the dot and rice pellet structures on GR in transmission electron microscopic (TEM) images (Fig. 5a–d). The prepared TiO_2–Mn_2O_3–GR–GCE sensor exhibited DPV detection limit for DA as low as 0.026 nM within the linear range 0.02–100 nM.

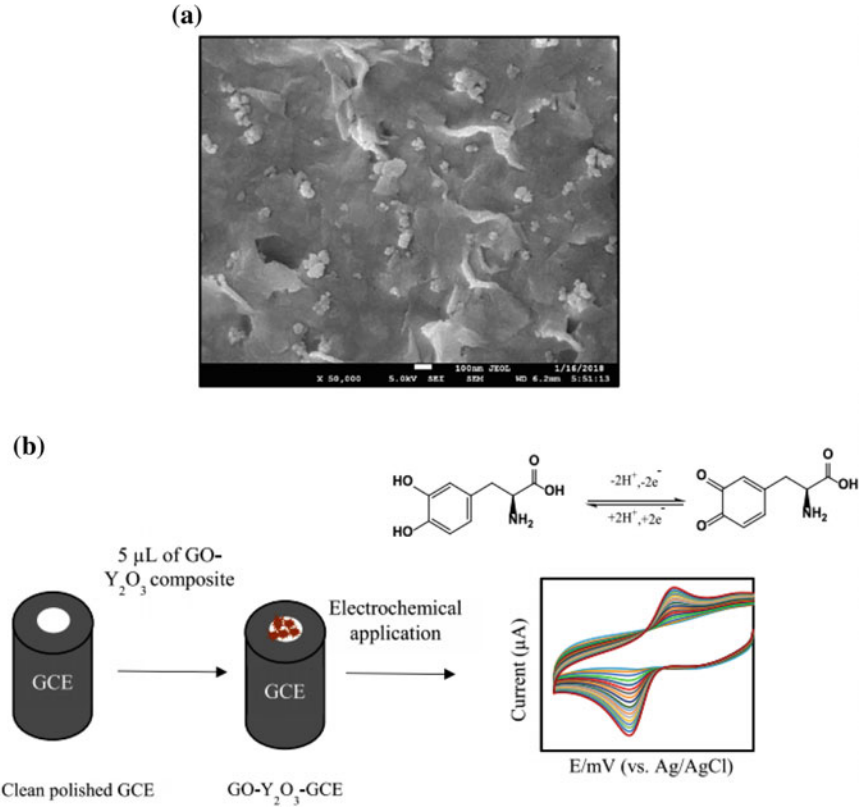

Fig. 4 SEM images of **a** Y_2O_3-GO nanohybrid, **b** detection scheme of L-DOPA at Y_2O_3-GO nanohybrid GCE sensor [49]. Reprinted with permission from Ref. [49]

3 Conclusion

Graphene and its derivatives possess excellent physical and chemical properties which make them attractive candidates as sensors. However, various functionalization schemes have been proposed to improve their sensing performances which include covalent and noncovalent interactions. Various GR nanohybrids have been prepared with different MNPs, polymers, carbon nanoforms, biomolecules etc. The GR-MNPs nanohybrids provide high electrocatalytic activity owing to the synergistic effects of constituting composites. This provides great advantages for GR based nanohybrids such as enhanced surface area, electronic conductivity, less aggregation, high dispersibility in different solvent systems and improved redox activities which are considered highly applicable for electrochemical sensing applications. The defects present at the surface of GR materials (e.g. vacancies, dislocations, grain boundary etc.) helps in the gentle functionalization of GR surfaces. Furthermore, strong π–π stacking and hydrophobic interactions govern the

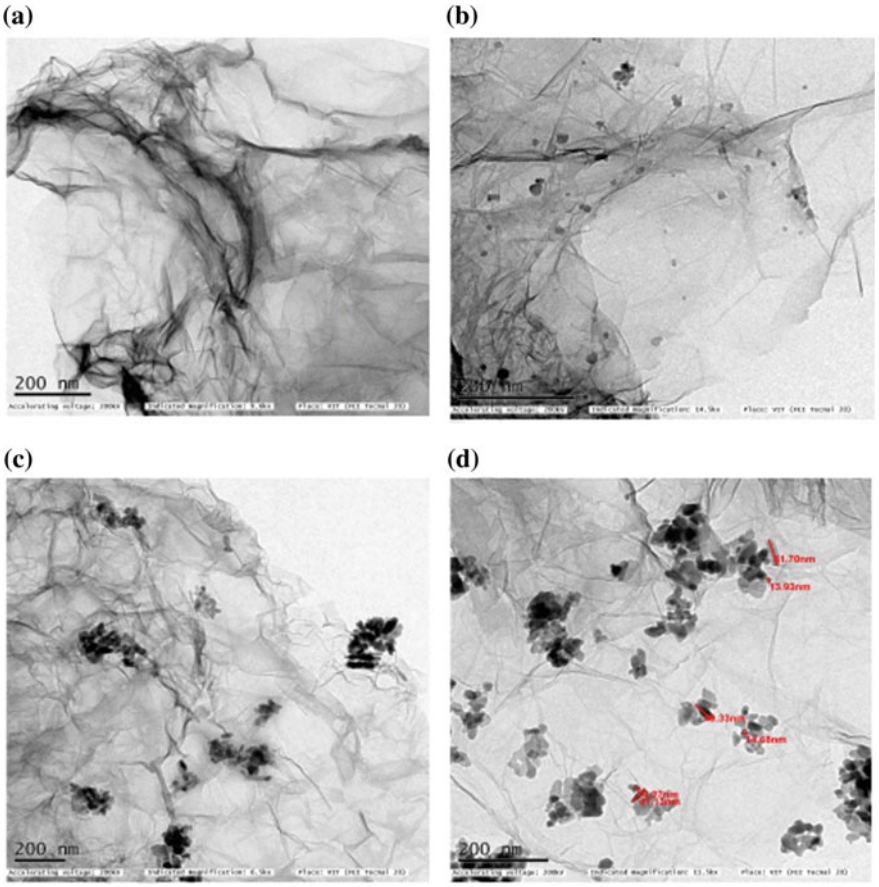

Fig. 5 TEM images of **a** GR, **b** TiO_2-GR, **c** Mn_2O_3-GR, **d** TiO_2-Mn_2O_3-GR nanohybrids [50]. Reprinted with permission from Ref. [50]

noncovalent functionalization of GR materials and stabilize the dispersion of GR in aqueous/organic media. The synergistic effects of GR-metal nanohybrids enhance the effective surface area when immobilized at the transducing surfaces and increase electron transfer rate in the nanohybrids. However, observation of interactions, conformation change and attachment of different nanomaterials/biomolecules onto GR materials is a big challenge to efficiently draw the functionalization mechanisms. Further, production of high quality single layered GR materials by the chemical exfoliation of graphite in various solvent systems is a concerned issue.

References

1. Lawal, A.T.: Synthesis and utilisation of graphene for fabrication of electrochemical sensors. Talanta **131**, 424–443 (2015)
2. Park, C.S., Yoon, H., Kwon, O.S.: Graphene-based nanoelectronic biosensors. J. Ind. Eng. Chem. **38**, 13–22 (2016)
3. Song, H., Zhang, X., Liu, Y., Su, Z.: Developing graphene based nanohybrids for electrochemical sensing. Chem. Rec. **19**, 534–549 (2019)
4. Georgakilas, V., Otyepka, M., Bourlinos, A.B., Chandra, V., Kim, N., Kemp, K.C., Hobza, P., Zboril, R., Kim, K.S.: Functionalization of graphene: covalent and non-covalent approaches, derivatives and applications. Chem. Rev. **112**, 6156–6214 (2012)
5. Georgakilas, V., Tiwari, J.N., Kemp, K.C., Perman, J.A., Bourlinos, A.B., Kim, K.S., Zboril, R.: Noncovalent functionalization of graphene and graphene oxide for energy materials, biosensing, catalytic, and biomedical applications. Chem. Rev. **116**, 5464–5519 (2016)
6. Lomeda, J.R., Doyle, C.D., Kosynkin, D.V., Hwang, W.F., Tour, J.M.: Diazonium functionalization of surfactant-wrapped chemically converted graphene sheets. J. Am. Chem. Soc. **130**, 16201–16206 (2008)
7. Strom, T.A., Dillon, E.P., Hamilton, C.E., Barron, A.R.: Nitrene addition to exfoliated graphene: a one-step route to highly functionalized graphene. Chem. Commun. **46**, 4097–4099 (2010)
8. Georgakilas, V., Bourlinos, A.B., Zboril, R., Steriotis, T.A., Dallas, P., Stubos, A.K., Trapalis, C.: Organic functionalisation of graphenes. Chem. Commun. **46**, 1766–1768 (2010)
9. Zhong, X., Jin, J., Li, S., Niu, Z., Hu, W., Li, R., Ma, J.: Aryne cycloaddition: highly efficient chemical modification of graphene. Chem. Commun. **46**, 7340–7342 (2010)
10. Liu, W.-W., Chai, S.P., Mohamed, A.R., Hashim, U.: Synthesis and characterization of graphene and carbon nanotubes: a review on the past and recent developments. J. Ind. Eng. Chem. **20**, 1171–1185 (2014)
11. Konkena, B., Vasudevan, S.: Covalently linked, water-dispersible, cyclodextrin: reduced-graphene oxide sheets. Langmuir **28**, 12432–12437 (2012)
12. Zhao, X., Zhang, P., Chen, Y., Su, Z., Wei, G.: Recent advances in the fabrication and structure specific applications of graphene based inorganic hybrid membranes. Nanoscale **7**, 5080–5093 (2015)
13. Zhu, P., Nair, A.S., Peng, S., Yang, S., Ramakrishna, S.: Facile fabrication of TiO_2–graphene composite with enhanced photovoltaic and photocatalytic properties by electrospinning. ACS Appl. Mater. Interfaces **4**, 581–585 (2012)
14. Xu, C., Wang, X., Zhu, J.: Graphene–metal particle nanocomposites. J. Phys. Chem. C **112**, 19841–19845 (2008)
15. Yin, Z., Wu, S., Zhou, X., Huang, X., Zhang, Q., Boey, F., Zhang, H.: Electrochemical deposition of ZnO nanorods on transparent reduced graphene oxide electrodes for hybrid solar cells. Small **6**, 307–312 (2010)
16. Zhu, C., Zhai, J., Wen, D., Dong, S.: Graphene oxide/polypyrrole nanocomposites: one-step electrochemical doping, coating and synergistic effect for energy storage. J. Mater. Chem. **22**, 6300–6306 (2012)
17. Hu, L., Tu, J., Jiao, S., Hou, J., Zhu, H., Fray, D.J.: In situ electrochemical polymerization of a nanorod-PANI–Graphene composite in a reverse micelle electrolyte and its application in a supercapacitor. Phys. Chem. Chem. Phys. **14**, 15652–15656 (2012)
18. Huang, Y., Huang, X., Lian, J., Xu, D., Wang, L., Zhang, X.: Self-assembly of ultrathin porous NiO nanosheets/graphene hierarchical structure for high-capacity and high-rate lithium storage. J. Mater. Chem. **22**, 2844–2847 (2012)
19. Wang, X., Hu, Y., Song, L., Yang, H., Xing, W., Lu, H.: In situ polymerization of graphene nanosheets and polyurethane with enhanced mechanical and thermal properties. J. Mater. Chem. **21**, 4222–4227 (2011)

20. Kholmanov, I.N., Stoller, M.D., Edgeworth, J., Lee, W.H., Li, H., Lee, J., Barnhart, C., Potts, J.R., Piner, R., Akinwande, D., Barrick, J.E., Ruoff, R.S.: Nanostructured hybrid transparent conductive films with antibacterial properties. ACS Nano **6**, 5157–5163 (2012)
21. Wang, D., Kou, R., Choi, D., Yang, Z., Nie, Z., Li, J., Saraf, L.V., Hu, D., Zhang, J., Graff, G. L., Liu, J., Pope, M.A., Aksay, I.A.: Ternary self-assembly of ordered metal oxide–graphene nanocomposites for electrochemical energy storage. ACS Nano **4**, 1587–1595 (2010)
22. Zhang, P., Zhang, X., Zhang, S., Lu, X., Li, Q., Su, Z., Wei, G.: One-pot green synthesis, characterizations, and biosensor application of self-assembled reduced graphene oxide–gold nanoparticle hybrid membranes. J. Mater. Chem. B **1**, 6525–6531 (2013)
23. Zhang, P., Huang, Y., Lu, X., Zhang, S., Li, J., Wei, G., Su, Z.: One-step synthesis of large-scale graphene film doped with gold nanoparticles at liquid-air interface for electrochemistry and raman detection applications. Langmuir **30**, 8980–8989 (2014)
24. Li, Y., Zhao, X., Zhang, P., Ning, J., Li, J., Su, Z., Wei, G.: A facile fabrication of large-scale reduced graphene oxide–silver nanoparticle hybrid film as a highly active surface-enhanced raman scattering substrate. J. Mater. Chem. C **3**, 4126–4133 (2015)
25. Li, Y., Zhang, P., Ouyang, Z., Zhang, M., Lin, Z., Li, J., Su, Z., Wei, G.: nanoscale graphene doped with highly dispersed silver nanoparticles: quick synthesis, facile fabrication of 3D membrane modified electrode and super performance for electrochemical sensing. Adv. Funct. Mater. **26**, 2122–2134 (2016)
26. Ahmad, R., Mahmoudi, T., Ahn, M.S., Yoo, J.Y., Hahn, Y.B.: Fabrication of sensitive non-enzymatic nitrite sensor using silver reduced graphene oxide nanocomposite. J. Colloid. Inter. Sci. **516**, 67–75 (2018)
27. Haldorai, Y., Kim, J.Y., Vilian, A.T.E., Heo, N.S., Huh, Y.S., Han, Y.-K.: An enzyme-free electrochemical sensor based on reduced graphene oxide/Co_3O_4 nanospindle composite for sensitive detection of nitrite. Sens. Actuators B: Chem. **227**, 92–99 (2016)
28. Zhang, S., Sheng, Q., Zheng, J.: Synthesis of Au nanoparticles dispersed on halloysite nanotubes-reduced graphene oxide nanosheets and their application for electrochemical sensing of nitrites. New J. Chem. **40**, 9672–9678 (2016)
29. Li, S.S., Hu, Y.Y., Wang, A.J., Weng, X., Chen, J.R., Feng, J.J.: Simple synthesis of worm-like Au-Pd nanostructures supported on reduced graphene oxide for highly sensitive detection of nitrite. Sens. Actuators B: Chem. **208**, 468–474 (2015)
30. Saraf, M., Rajak, R., Mobin, S.M.: A fascinating multitasking Cu-MOF/rGO hybrid for high performance supercapacitors and highly sensitive and selective electrochemical nitrite sensors. J. Mater. Chem. A **4**, 16432–16445 (2016)
31. Zhang, Y., Zhao, Y., Yuan, S., Wang, H., He, C.: Electrocatalysis and detection of nitrite on a reduced graphene/Pd nanocomposite modified glassy carbon electrode. Sens. Actuators B: Chem. **185**, 602–607 (2013)
32. Fu, L., Yu, S., Thompson, L., Yu, A.: Development of a novel nitrite electrochemical sensor by stepwise in situ formation of palladium and reduced graphene oxide nanocomposites. RSC Adv. **5**, 40111–40116 (2015)
33. Zhang, D., Fang, Y., Miao, Z., Ma, M., Du, X., Takahashi, S., Anzai, J.-I., Chen, Q.: Direct electrodeposion of reduced graphene oxide and dendritic copper nanoclusters on glassy carbon electrode for electrochemical detection of nitrite. Electrochim. Acta **107**, 656–663 (2013)
34. Bharath, G., Madhu, R., Chen, S.M., Veeramani, V., Mangalaraj, D., Ponpandian, N.: Solvent-free mechanochemical synthesis of graphene oxide and Fe_3O_4 reduced graphene oxide nanocomposites for sensitive detection of nitrite. J. Mater. Chem. A **3**, 15529–15539 (2015)
35. Radhakrishnan, S., Krishnamoorthy, K., Sekar, C., Wilson, J., Kim, S.J.: A highly sensitive electrochemical sensor for nitrite detection based on Fe_2O_3 nanoparticles decorated reduced graphene oxide nanosheets. Appl. Catalysis B: Environ. **148–149**, 22–28 (2014)

36. Marlinda, A.R., Pandikumar, A., Yusoff, N., Huang, N.M., Lim, H.N.: Electrochemical sensing of nitrite using a glassy carbon electrode modified with reduced functionalized graphene oxide decorated with flower-like zinc oxide. Microchim. Acta **182**, 1113–1122 (2015)
37. Wei, G., Zhang, Y., Steckbeck, S., Su, Z., Li, Z.: Biomimetic graphene–FePt nanohybrids with high solubility, ferromagnetism, fluorescence, and enhanced electrocatalytic activity. J. Mater. Chem. **22**, 17190–17195 (2012)
38. Ding, J., Zhu, S., Zhu, T., Sun, W., Li, Q., Wei, G., Su, Z.: Hydrothermal synthesis of zinc oxide-reduced graphene oxide nanocomposites for an electrochemical hydrazine sensor. RSC Adv. **5**, 22935–22942 (2015)
39. Umar, A., Rahman, M.M., Kim, S.H., Hahn, Y.B.: Zinc oxide nanonail based chemical sensor for hydrazine detection. Chem. Commun. **2**, 166–168 (2008). https://doi.org/10.1039/b711215g
40. Zhang, X., Ma, W., Nan, H., Wang, G.: Ultrathin zinc oxide nanofilm on zinc substrate for high performance electrochemical sensors. Electrochim. Acta **144**, 186–193 (2014)
41. Zhao, Z., Sun, Y., Li, P., Sang, S., Zhang, W., Hu, J., Lian, K.: A sensitive hydrazine electrochemical sensor based on zinc oxide nano-wires. J. Electrochem. Soc. **161**, B157–B162 (2014)
42. Fang, B., Zhang, C., Zhang, W., Wang, G.: A novel hydrazine electrochemical sensor based on a carbon nanotube-wired ZnO nanoflower-modified electrode. Electrochim. Acta **55**, 178–182 (2009)
43. Kavitha, T., Gopalan, A.I., Lee, K.P., Park, S.Y.: Glucose sensing, photocatalytic and antibacterial properties of graphene–ZnO nanoparticle hybrids. Carbon **50**, 2994–3000 (2012)
44. Ding, J., Sun, W., Wei, G., Su, Z.: Cuprous oxide microspheres on graphene nanosheets: an enhanced material for nonenzymatic electrochemical detection of H_2O_2 and glucose. RSC Adv. **5**, 35338–35345 (2015)
45. Xu, F., Deng, M., Li, G., Chen, S., Wang, L.: Electrochemical behavior of cuprous oxide–reduced graphene oxide nanocomposites and their application in nonenzymatic hydrogen peroxide sensing. Electrochim. Acta **88**, 59–65 (2013)
46. Liu, M., Liu, R., Chen, W.: Graphene wrapped Cu_2O nanocubes: non-enzymatic electrochemical sensors for the detection of glucose and hydrogen peroxide with enhanced stability. Biosens. Bioelectron. **45**, 206–212 (2013)
47. Jiang, B.B., Wei, X.W., Wu, F.H., Wu, K.L., Chen, L., Yuan, G.Z., Dong, C., Ye, Y.: A non-enzymatic hydrogen peroxide sensor based on a glassy carbon electrode modified with cuprous oxide and nitrogen-doped graphene in a nafion matrix. Microchim. Acta **181**, 1463–1470 (2014)
48. Zhang, L., Li, H., Ni, Y., Li, J., Liao, K., Zhao, G.: Porous cuprous oxide microcubes for non-enzymatic amperometric hydrogen peroxide and glucose sensing. Electrochem. Commun. **11**, 812–815 (2009)
49. Sunder, G.S.S., Rohanifar, A., Devasurendra, A.M., Kirchhoff, J.R.: Selective determination of L-DOPA at a graphene oxide/yttrium oxide modified glassy carbon electrode. Electrochim. Acta **301**, 192–199 (2019)
50. Grace, A.A., Divya, K.P., Dharuman, V., Hahn, J.H.: Single step sol-gel synthesized Mn_2O_3-TiO_2 decorated graphene for the rapid and selective ultra sensitive electrochemical sensing of dopamine. Electrochim. Acta **302**, 291–300 (2019)

Ultrasound-Assisted Synthesis, Exfoliation and Functionalisation of Graphene Derivatives

Dipanwita Majumdar

Abstract For the last two decades, application of ultrasound in materials synthesis has been a very promising topic especially for the fabrication or modification of various nanomaterials. Simplicity, high efficacy, short reaction tenure along with power saving features are responsible for the popularization of sonochemistry. The physical phenomenon essential for sonochemical process is largely accepted owing to acoustic cavitation, involving formation, growth, and implosive collapse of the micro-bubbles inside liquid. The resulting hot spots/microjets generate very high temperatures $\sim$5000 K and high pressure $\sim$150 MPa due to collapsing bubbles within a nanosecond, with high cooling rates exceeding 10^{11} Ks^{-1} at the local reaction centre, providing necessary activation for faster kinetics. These extreme reaction conditions are not typically attainable through conventional synthesis techniques, generating smarter systems with unique properties. Subsequently, ultrasound techniques have been massively employed in graphene preparation along with its dispersion in various solvents which otherwise requires several days with poor yield using conventional techniques. Graphene has been the material of the millennium owing to its unique large surface area, high charge transport features and mechanical properties and widely employed in nearly every aspects of modern technology. Ultrasonic irradiation offers tuning of graphene layer thickness also. Even oxidation to graphene oxide and subsequent reduction to reduced-graphene oxide at faster kinetics are possible without the use of any external redox agents. Besides, thin-layered functionalized graphenes has been achieved by sonochemistry. Ultrasonic treatment provides scope for direct exfoliation of graphite to graphene layers in presence of suitable intercalating/stabilizing agents with substantial dispersion stability. In addition, various geometries such as scrolled graphene, ribbon or foam graphenes can be purposefully designed. Even smooth and rough edged graphenes have displayed unique implications in energy storage, catalysis, biomedical and other technological fields. Ultrasonic-assisted synthesis of various graphene based composites lead to more homogeneous with diversified nanostructures formation like core-shell, nano-discs, nano-platelets, etc. along with

D. Majumdar (✉)
Department of Chemistry, Chandernagore College, Hooghly 712136, WB, India
e-mail: wbesdmajumdar@gmail.com

A. Khan et al. (eds.), *Graphene Functionalization Strategies*,
Carbon Nanostructures, https://doi.org/10.1007/978-981-32-9057-0_3

specific deposition at the graphene edges have become feasible. This chapter provides comprehensive fundamental concepts of sonochemistry with first hand outline on the sonochemical/ultrasound assisted synthesis of graphene and its various derivatives. Moreover, the ultrasound assisted-dispersion, exfoliation of graphenes and formation of various graphene-based nanocomposites has been emphasized. Important tuneable sonochemical parameters including ultrasound frequency, input power, sonication time, type of sonication probes, etc. have been highlighted to provide an overview of the topic.

Keywords Graphene · Sonochemistry · Ultrasound · Derivatives · Nanocomposites · Functionalisation · Intercalation · Dispersion

1 Introduction

1.1 Ultrasound Energy and Sonochemical Synthesis

Most of the scientific developments deal with expensive instrumentations or specialized appliance usage as well as require substantial extent of expertization for in-depth study of each field. What makes "sonochemistry" a very interesting and exciting branch of science is that it urges quite reasonably priced device to start with and also shows considerable exciting results for certain chemical reactions which otherwise are very complicated to achieve by conventional chemical synthesis techniques.

1.1.1 Definition of Ultrasound

Ultrasound is defined as sound of frequency range of 20–3000 kHz that lies outside the audible range of human perception (i.e. frequency range 16 Hz–16 kHz). It has been applied to a variety of applications in engineering, science, and medicinal fields but its implication in chemistry have emerged recently and accordingly, have been coined the term "sonochemistry". On the basis of frequency range, ultrasound has three categories, i.e. power ultrasound (20–100 kHz), high frequency ultrasound (100 kHz–1 MHz), and diagnostic ultrasound (1–500 MHz) respectively. Among them, power ultrasound is generally employed in sonochemistry [1, 2]. Scheme 1 displays the frequency range of sound waves, different types of ultrasounds and their uses as well as summarizing the various applications of ultrasound [3–6].

When a solution is exposed to ultrasound energy, alternate compression and rarefaction of the medium leads to formation of micro-bubbles. Generally, pure liquids have high tensile strengths and thus, are incapable to producing cavitation on ultrasound exposure. However, majority of the liquids are generally impure and

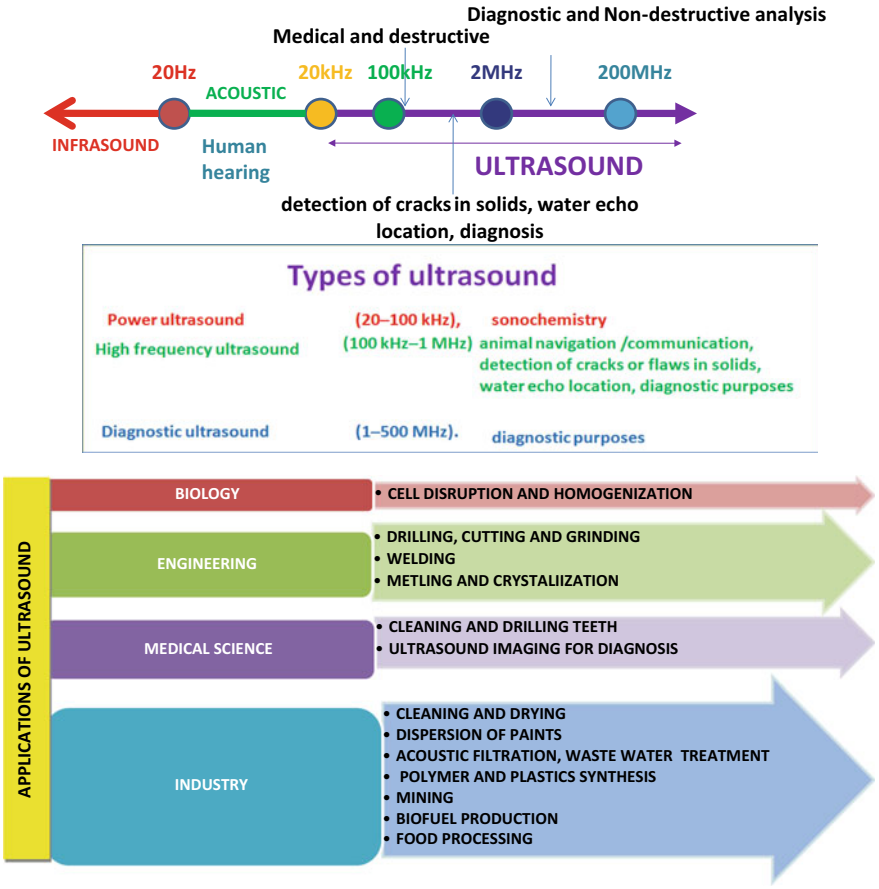

Scheme 1 Frequency range of sound waves, different types of ultrasounds and their uses and summary of various applications of ultrasound

possess low tensile strength due to the presence of impurities such as various small particles, pre-existing dissolved solids, and other contaminants. These impurities in the liquid are sources of nucleation of cavitation bubbles [7, 8].

Two plausible mechanisms exist for bubble formation [9]. The first mechanism proposes the pre-existence of micro-bubbles within the liquid owing to the presence of contaminants or impurities in the medium as well as in the interface of the liquid vessel. The second mechanism which is more popularly accepted considers existence of gas trapped solid particles in the liquid that leads to nucleation. The tiny crevices in the walls of the vessel or containers can also trap gases. Due to pressure difference outside and inside a gas crevice, gases diffuse into the gas pocket, causing it to grow until it reaches a critical size known as its *resonance size*. The resonance size of a bubble is dependent upon the magnitude of applied ultrasound

frequency. The bubbles reach their resonance size by processes called *rectified diffusion or coalescence*, when one of the two events possibly may occur. The bubble may become unstable and collapse, often violently, within a single acoustic cycle or over a small number of cycles. This phenomenon is termed *transient cavitation*. The other possibility is that the bubble oscillates at, or near, the resonance size for large number of cycles, leading to *stable cavitation*.

The imploding/collapsing bubbles generate high local turbulence in the form of shock wave emissions with the release of tremendous energy that can cause sudden increase of temperature to several thousand degrees Kelvin and pressure up to several hundred atmospheres. These extreme effects have been utilized in variety of beneficial applications, especially in chemistry [10]. Figure 1 displays the formation, growth and collapse of micro-bubble over several acoustic cycles of compressions and rarefactions.

Elevated temperatures in the vicinity of collapsing bubble generate "hot spots" that can trigger free radicals formation, mixing and shearing (sonoprocessing), accelerate dissolution or aid the reformation/deposition at the surface of a solid reactant (sonochemistry). Thus, these hot spots can efficiently serve as micro-reactors (primary sonochemistry) or trigger formation of active species that subsequently undergo spontaneous chemical reactions (secondary sonochemistry). Such effects have been employed in various practical application including waste water management, food and beverages processing, protein micro-bubbles generation for image contrast agents, drug delivery mechanisms, electrochemistry, etc. [13–21].

1.1.2 Consequences of Acoustic Cavitations

As discussed in the earlier section, exposure of ultrasound energy to a liquid medium cause the dissolved gases to grow due to rectified diffusion to attain resonance size, mostly followed by bubble coalescence, resulting from primary and secondary Bjerknes forces, due to applied ultrasound as well as so-formed acoustic waves radiated by neighbouring bubbles respectively [22]. During such acoustic cavitation, tremendous condition of high pressures and temperatures results, that triggers several physical and chemical effects inside solution. The Rayleigh-Plesset equation is one of the well-accepted theoretical models for describing bubble dynamics and the calculated localized temperature and pressure was expected to reach up to 5000 K and 150 MPa, respectively [23].

The physical effects are intimately associated to momentum variations from bubble oscillation and its collapse. Again, radial fluctuation of these bubbles leads to restricted liquid flow surrounding them, called *micro-streaming*. As the bubble starts to implode, two consequent effects can occur. When a bubble undergoes a symmetrical collapse, high pressure shock waves propagate across the liquid medium with tremendous velocity gradient of the order of 100 ms^{-1} [24]. However,

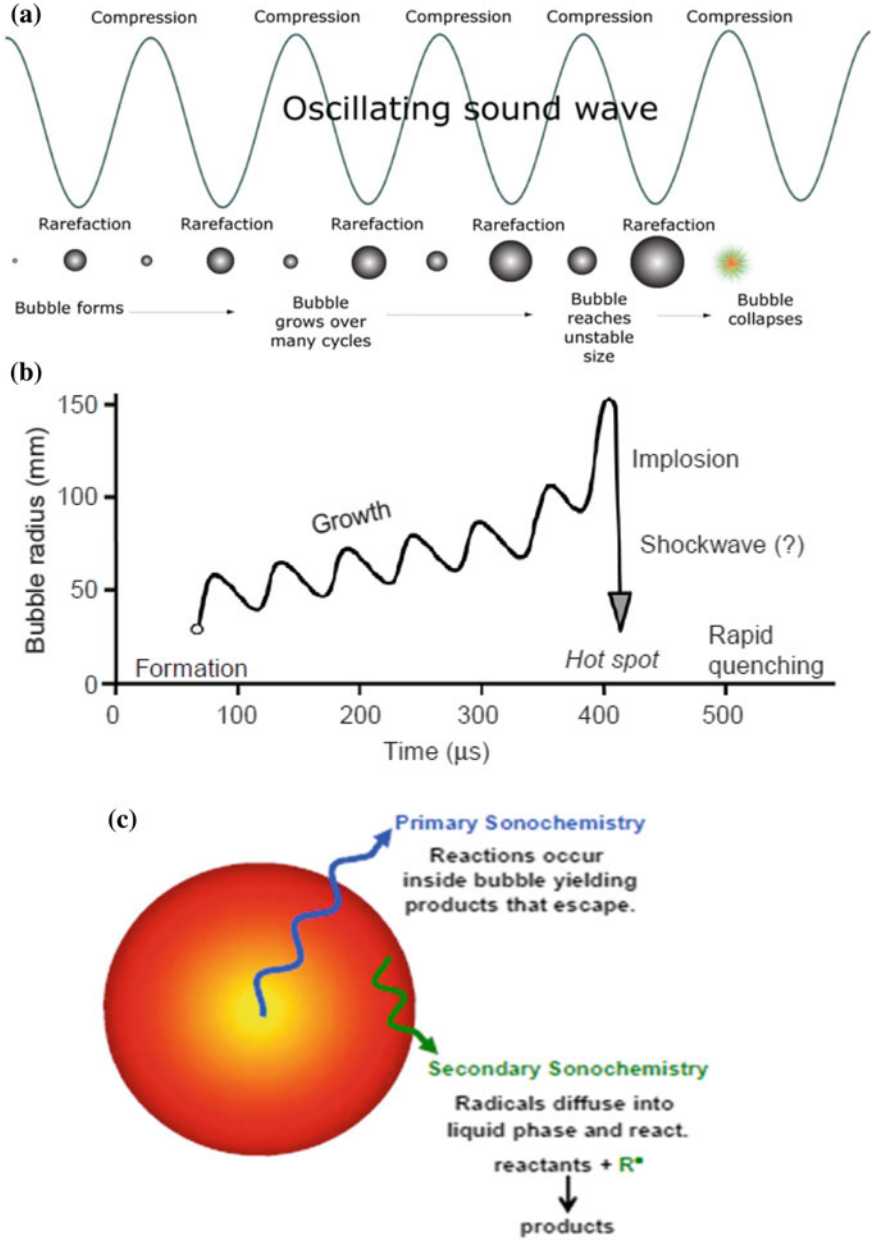

Fig. 1 **a** Schematic representation of ultrasound mediated micro-bubble formation, showing oscillating sound waves propagating—contracting during compression and expanding during rarefactions, during its growth process and ultimately collapsing/imploding after several acoustic cycles [9]. **b** Plot of varying micro-bubble radius in the course of hot spot formation [11]. **c** Types of sonochemistry derived from reactions within the hot spot generated by the collapsing bubble [12]. Reproduced on permission

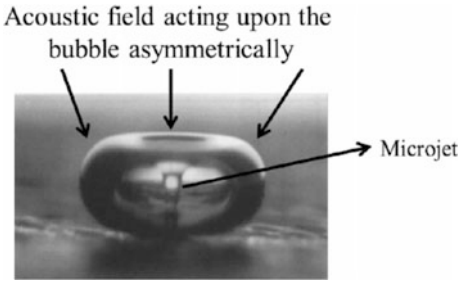

Fig. 2 Microjet formation when a bubble collapses near a solid surface [2]. Reproduced on copyright permission

if there exists an interface in the vicinity (e.g., solid, immiscible liquid or gas phase), an asymmetrical collapse results with the formation of a "micro-liquid jet", as shown in Fig. 2, penetrating through the bubble and striking the interface with high pace and pressure [25].

Such a fast and drastic impact of the microjets on the striking point of the matter elevate the localized temperature to reach $>10^9$ Ks^{-1}. Faster cooling rates at this micro-scale regime, initiate significant morphological transformations, variations in intermolecular hydrophobic/hydrophilic interactions, endorse mass transfer and modify interfacial characteristics, promoting controllable colloidal engineering [10, 26]. These cumulative physical effects from the localized environment produces strong mechanical shear forces in the bulk that promote ultrasonic emulsification, extraction, crystallization, surface modification, and sonogelation processes, etc. [27–29].

The general relationship between the bubble resonance radius and ultrasound frequency applied as displayed in Eq. (1), indicates that increase in ultrasound frequency (**f**) leads to decrease in the resonance radius of cavitation bubbles (**R**), resulting in less violent bubble collapse. Thus, it is important to note that the above discussed physical effects become more insignificant with high range ultrasound frequency.

$$\mathrm{f} \times \mathrm{R} \sim \text{constant} \tag{1}$$

The chemical effects of collapsing bubble lead to radical generation, which is the source of chemical reactions in ultrasonic systems i.e. sonochemistry. Such extreme temperature at the time of bubble collapse caused cleavage of O–H bond in water molecules, thereby producing hydrogen and hydroxyl radicals, shown in Reaction (a):

$$\mathrm{H-O-H} \Rightarrow))) (\textit{ultrasound}) \Rightarrow \mathrm{H^{\bullet} + OH^{\bullet}} \tag{a}$$

where, hydrogen radicals and hydroxyl radicals act as the primary reducing and oxidising agents, respectively and "))" represents ultrasound energy respectively.

There exist four theories to explain sonochemical effects: (1) hot-spot theory; (2) "electrical" theory; (3) "plasma discharge" theory, and (4) supercritical theory. The detailed discussions of these theories are at present beyond the scope of this

chapter. However, among them, the hot-spot theory is commonly accepted in explanation of sonochemical reactions especially in environmental field [30]. According to this theory, each micro-bubble is considered as a "micro-reactor" that generates different reactive species and tremendous thermal energy during its collapse/implosion [31].

The rate of sonochemical reactions in aqueous media depend massively on the yield of these primary radicals (H• and OH•) which is again strongly dictated by ultrasound frequency and cavitation intensity. The yield is again dependent on the cumulative influence of bubble radius, collapse temperature, bubble population and their life time, operating parameters (i.e. ultrasound frequency and power input), organic additives present (sources of secondary radicals), nature of gas within the bubble, etc. Maximum yield of radical production has been observed in the frequency range 200–600 kHz, with checked rate around 20 kHz and above 1 MHz respectively [32].

1.1.3 Brief History of Cavitation and Sonochemistry

The development of sonochemistry embraces three types of transducers used for producing ultrasound in the late 19th century, namely, (i) gas-driven transducers that transform high velocity gas flow into ultrasound: Galton Whistle (1883). (ii) liquid-driven transducers (iii) electromechanical transducers converting electrical energy into sound energy based on piezoelectric effect was discovered by the Curies in 1889. The latter one has been modified with years. Meanwhile, Thornycroft and Barnaby carried out pioneer works on "Cavitation" in 1895 when they investigated the cause of pitted and eroded propellers in their submarines. Such process was a consequence of collapsing bubbles formed due to hydrodynamic cavitation that generated intense pressure and temperature gradients in the local vicinity of the propellers. This phenomenon was extrapolated for micro-bubbles. Shortly, Lord Rayleigh in 1917, mathematical modelled a cavitation event in an incompressible fluid. In the same year, Paul Langevin investigated transmission of sound waves in sea water and suggested use of ultrasound for determining the depth of sea. In 1927, Loomis described the first chemical and biological effects of ultrasound, and highlighted the fact that cavitation could be an essential tool in certain chemical processes [33, 34]. One of such premier applications involved cavitation induced degradation of a biological polymer. Besides ultrasound assisted rate enhancement of chemical reactions, oil emulsification, pollutant degradation, etc. have subsequently emerged. The advantage of employing acoustic cavitation for these applications is that it involves milder operating conditions compared to conventional techniques bypassing the requirements of toxic reagents or intensive reaction conditions. In the late 1960s, use of ultrasound in metallurgy was noticed. Biologists started practising cell rupturing process using ultrasound in the 1970s [35]. Subsequently, with the detection of nano-dimensions, different research groups started working on sonochemical synthesis of various nanomaterials, followed by sono-processing, sono-gelation and sono-catalysis procedures emerging

only in recent times [36, 37]. As an example, the recent discovery of a simple sonochemical synthesis of amorphous iron helped settle the long-standing controversy over its magnetic properties [38, 39]. Furthermore, ultrasound has proved extremely useful in the synthesis of a wide range of nanostructured materials, including high-surface-area transition metals, alloys, carbides, oxides, and colloids [40, 41]. Sonochemical decomposition of volatile organometallic precursors in high-boiling solvents produces nanostructured materials in various forms with high catalytic activities. Nanometer colloids; nanoporous high-surface-area aggregates; nanostructured carbides, sulphides, and oxides; and supported heterogeneous catalysts can all be prepared by this general route [42]. The above features developed the idea of sonochemical synthesis of high quality graphene systems that otherwise requires severe conditions, generally not accessible in the conventional synthesis methods [43, 44].

1.1.4 Common Ultrasound Energy Generating Devices

A variety of ultrasonic devices can be employed for carrying out sonochemistry. However, mainly three designs have maximum usage at present in the literature, namely, the ultrasonic cleaning bath, immersion ultrasonic horn, and flow reactors as displayed in Fig. 3a–c. Ultrasound is commonly generated from a piezo-ceramic material which on subjecting to high AC voltage produces the desirable ultrasound frequency ($\sim$15–50 kHz). The vibrating source, depending on the device design, is attached to the wall of a cleaning bath, or to an amplifying horn, or to the outer surfaces of a flow-through tube or diaphragm. Ultrasonic cleaning bath is the cheapest, readily accessible ultrasound source for laboratory usage for executing a variety of sonochemical studies. However, it has limited capability, especially in terms of intensity and frequency generation.

Ultrasonic horns, on the other hand, generate highly intense and serve as consistent ultrasound source of power density (50–500 Wcm^{-2}), which can be employed for various purposes especially under different experimental setups including inert/reactive atmospheres or high/low pressure conditions. These devices are available from several manufacturers at reasonable cost [45].

Ultrasonic Flow reactors enable sonication in a closed system—either in flow-through operation mode or simply enclosed chamber sonication. It is mainly opted for large scale sonochemical applications and for vicious material sonication. Continuous flow ultrasonic system has several merits such as (i) higher processing quality and capacity (ii) high processing uniformity (iii) temperature control (iv) safety, etc. [46, 47].

1.1.5 Sonochemical Synthesis—Uniqueness

Sonochemistry, on the basis of the nature of the cavitation event, can be categorized as: homogeneous sonochemistry of liquids, heterogeneous sonochemistry involving

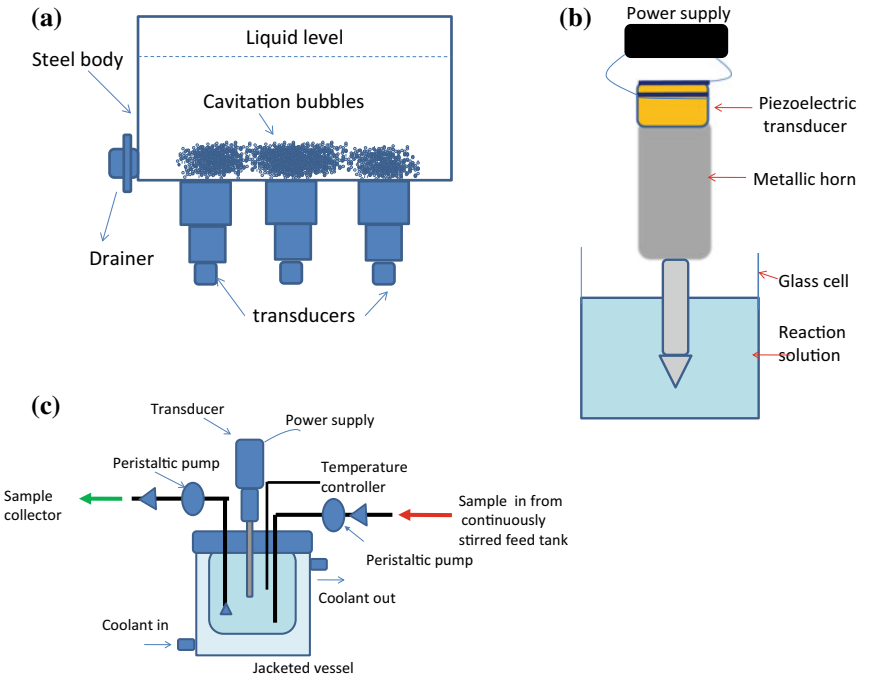

Fig. 3 Diagrams showing various ultrasound generating devices employed for sonochemistry **a** ultrasonic cleaning bath, **b** Immersion ultrasonic horn and **c** flow sono-reactors respectively

biphasic systems such as liquid–liquid or liquid–solid systems, and thirdly, sonocatalysis (embracing the two categories). Ultrasound assisted reactions involving solid or gas systems are rare as cavitation can primarily occur only in liquids. Ultrasonic irradiation varies largely from traditional energy sources such as thermal, light, or ionizing radiation considerably in terms of time interval, pressure, and energy per molecule. The tremendous localized temperatures and pressures conditions with ultrafast heating and cooling rates from collapsing cavitation bubble or at micro-jet points assures unusual mechanistic approach for high-energy chemistry. Similar to photochemical reactions, here, very large amounts of energy are introduced in a short period of time. However, control of sonochemical reaction conditions is subject to the similar limitations to that of thermal process at present, although technological innovations are already in the process to resolve the issue at the earliest. Nonetheless, frequency tuning, is equally more important at least within the range where cavitation can occur (a few hertz to a few megahertz), although there have been few detailed studies regarding its important role in the recent past [48, 49].

Sonochemistry is intimately related with green chemistry [50, 51]. Shortly after the fabrication of the famous twelve principles of green chemistry by Paul T. Anastas and John C. Warner in 1998, Jean-Louis Luche in no time (1999) connected

sonochemistry and green chemistry [52] with the merits of sonochemical approach. He highlighted that: (a) novel selectivity (reduced wastages) in various reactions via sonochemical switching; (b) improved reaction rates (energy savings), and yields; (c) use of nontrivial eco-compatible reagents in aqueous media (considering safety, energy savings) [53]. In recent times, Timothy J. Mason highlighted the "green link" of sonochemistry, fields of environmental protection and process technology at large production scale [54].

2 Ultrasound-Assisted Synthesis of Graphene and Its Derivatives

2.1 Unique Features of Graphene and Its Derivatives

Graphene, monolayer of sp^2 hybridized carbon forming the basis of two-dimensional honeycomb lattice, has been the subject of utmost scientific importance since the last decade [55]. It is considered to be the building block of graphitic materials for all dimensions, starting from wrapped-0D-fullerene, rolled – up-1D nanotube to 2D-nanographites or 3D-stacked graphite as shown in Fig. 4 [56–58].

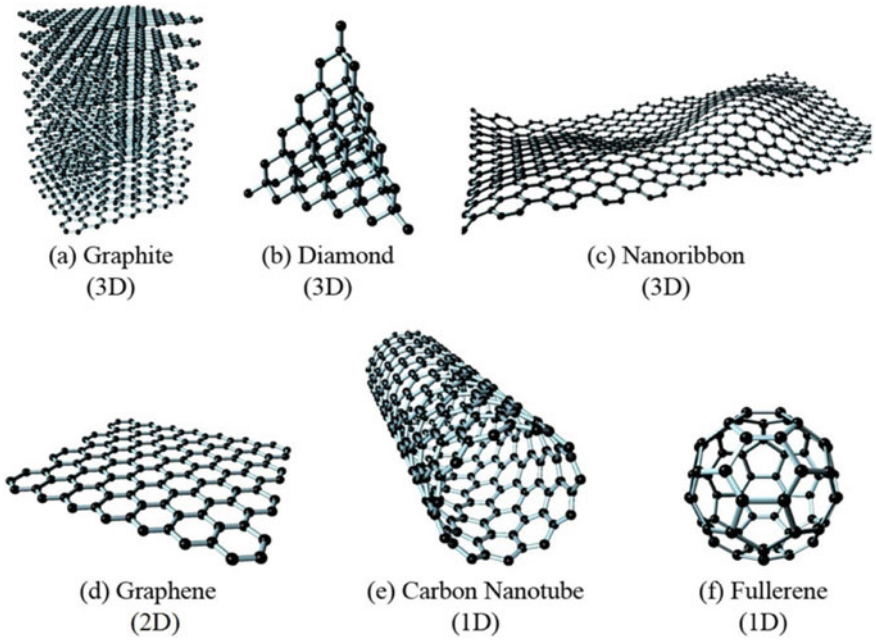

Fig. 4 Carbon-based nanomaterials derived from graphene. Ref. [58], reproduced on permission

The unique structural features befits graphene with versatile and superior properties, such as excellent thermal conductivity (5300 $W(mK)^{-1}$), mechanical flexibility (Young's modulus ~1100 GPa), electrical charge transport characteristics (~2000 Scm^{-1}), specific magnetism and large surface area (~2630 m^2g^{-1}) that have dictated its immense potential applications in several technological fields of photovoltaics, transparent electrodes, sensors and catalysts, supercapacitors, batteries, fuel cells and allied energy storages, transistors and in various opto-electronic devices [59–68].

Based on the number of stacked layers, graphenes have been categorized as: mono-layered, few-layered (2–10 layers), and multi-layered systems. It was initially considered that few-layered morphology would be ideal for preserving the distinctive features of the graphene. For example, few-layered graphenes illustrated excellent potential abilities in flexible photovoltaic applications [69]. Nonetheless, some of the beneficial properties can still be retained in thin graphite-form as well [70, 71]. Recently, comparative studies of mono-, few- and multi-layered graphenes for enzyme-immobilization and bio-sensing applications were employed. It was observed that the electrochemical response during the electro-analysis was independent of the number of layers stacked within the graphene [72]. More applications such as electromagnetic shielding/absorbers show impressive results with multilayered graphenes compared to single-sheets [73].

Furthermore, an additional benefit lies in the fact that its chemical functionalization do not significantly alter the basic features such as electronic charge transport which can be tuned accordingly with functionality; rather it enhances its processability for commercialization. The principal method of graphene production involves micromechanical cleavage of graphite layers [74, 75]. However, it is too hard to control and standardize for industrial level. Single-layered graphene has also been synthesized via epitaxial growth on silicon carbide using CVD but requires expensive instrumentations. Further, the so-obtained graphenes are difficult to transfer from the silicon carbide substrate [70]. An alternative, less expensive and more acceptable route is chemical oxidation of graphite to obtain graphene oxide with subsequent reduction to obtain graphene systems [76, 77].

Graphene oxide (GO) is as stated, the commonest form of oxygen-containing functionalized graphenes that include carboxyl, hydroxyl, and epoxide functional moities on the surface of exfoliated graphene layers [78, 43]. It contains both localized sp^3 defects and sp^2-bonded carbon atoms in a hexagonal lattice with two-dimensional planar sheets. Presence of these oxygen functional groups makes GO considerably befitting in fabricating various nanocomposites [79, 80]. Its' admirable aqueous processability, remarkable amphiphilicity, facile surface modification capability have opened up many novel diversified applications [81]. Again functional groups on GO can be proportionately tuned or controlled to reduced graphene oxide or graphene employing various chemical, photochemical, photo-thermal, and sonochemical reduction methods[58, 82, 83] (Fig. 5).

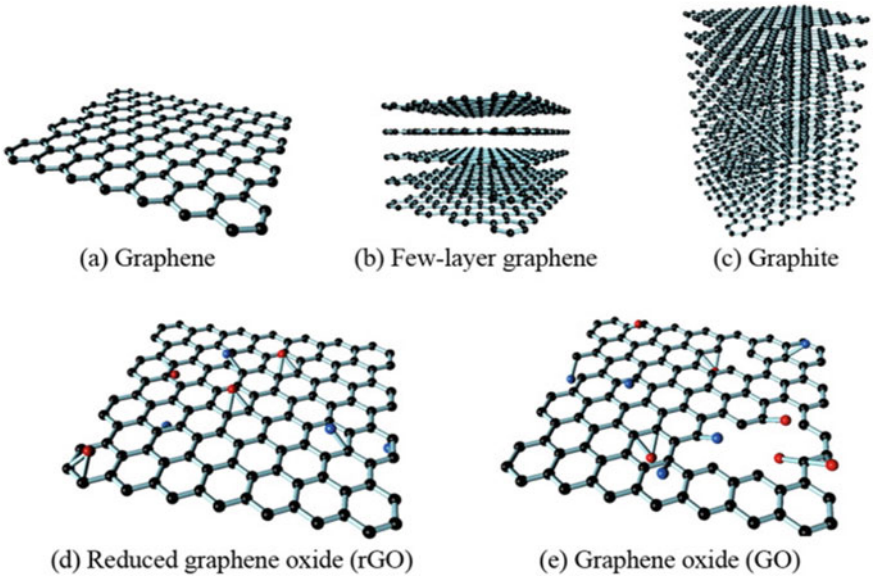

Fig. 5 Structures of various graphene family nanosystems Ref. [58], reproduced on permission

2.2 Why Sonochemical Synthesis of Graphene?

Sonochemistry has achieved immense attention in the preparation of graphene systems. Sonochemical intervention has eliminated the requirement of elevated temperature, high pressure, long reaction tenures and laborious reaction steps of conventional chemical techniques, thus making the synthetic methodology more environment-friendly and cost-effective. Exfoliation of the layered-graphitic materials as well as its functionalisation including oxidation, reduction, dispersion and modification with various chemical functional groups are sonochemically feasible [84]. Even covalent functionalisation has been found to be successful employing short exposure to ultrasonication using the aids of sono-derived 'hot spots'/"high velocity liquid microjets" that generate excited state species or even meta-stable molecular ions for successful graphene functionalisation [85, 86]. Besides, these high velocity micro-liquid jets and acoustic vibrations create shock waves that have manifold effects—considerably damage graphene surfaces; causes peeling off the stacked graphenes into monolayer sheets; homogeneous fragmentation to small dimensional sheets resulting in graphene exfoliation [87]. Collectively, this technique makes dispersion and chemical functionalization of graphene—facile, uniform, more effective and much faster in various media using suitable surface-functionalisation species, surfactants or polymers.

Studies on relative stable dispersions of graphenes prepared from other techniques such as thermal, hydrothermal, etc. were carried out with three different types of ultrasound devices: sonication bath (200 W, 35 kHz), ultrasound horn

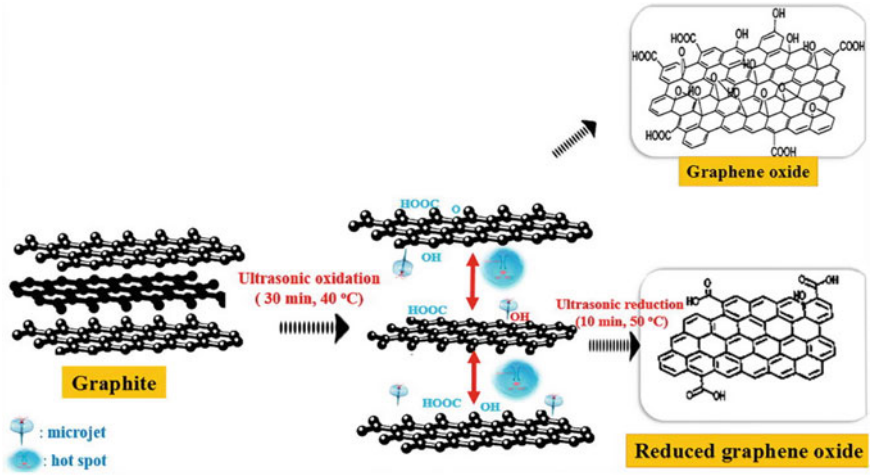

Fig. 6 Production of graphene oxide and reduced graphene oxide from pristine graphite via ultrasonication technique. Reprinted with permission from Ref. [89]

(750 W, 20 kHz) and high-power micro-tip sonication (1000 W, 20 kHz) respectively [88]. Interestingly, horn sonication produced the most stable RGO dispersion that remained unchanged up to 2 years. On the other hand, both high power based micro-tip-horn and sonication-bath failed to yield stable dispersion, owing to failure of supplying the optimum power intensity required for producing stable dispersion.

Ultrasonication also serves an effective tool for obtaining reduced-graphene oxide (rGO) from graphite. Figure 6 delineates the synthetic strategy, highlighting the roles of microjets and hot spots in the process of graphite exfoliation [89]. Even, reduction of GO, to form reduced graphene oxide (rGO), that mainly contains hydroxyl (–OH) functionalities on graphene sheets. The proposed mechanism is based on the theory that demonstrates that the bulk solution containing large GO sheets when subjected to ultrasound irradiation, the resultant large acoustic-generated shearing force and fast streaming solvent jets emanate intense shock waves that promote bond cleavage at the defect sites (originated from functionalisation) and rupture them into smaller moieties, besides functionalizing them too [85, 90, 91]. Various reactions activated by these surface hydroxyl and carboxyl functional groups on graphene under sonocatalysis have been reported in the recent past [92]. Even, ultrasonic can help in modifying the graphene properties too. Few year ago, Saha group fabricated ultrasound assisted-graphene quantum sheets with zigzag edge states that exhibited room temperature ferromagnetism, with outstanding magneto-resistance response, ideally-suited for organic spintronic devices [93]. Similarly, ultrasound assisted graphene quantum dots were obtained for versatile applications [94, 95].

2.3 Controlling Parameters for Sonochemical Synthesis of Graphene Materials

A variety of parameters are involved in sonochemical synthesis of graphene materials. Firstly, the choice of precursor or the starting material is crucial for determining the resulting morphology of produced graphene system. For instance, poorly crystalline and low dimensional artificial graphite leads to single layered graphenes whereas highly-oriented pyrolytic graphite (HOPG), natural flake graphite, Kish graphite and flake graphite powder etc. leads to multilayered large dimensional sheets [96, 97]. The instrumental parameters such as sonication duration, applied ultrasound frequency and power input are essential to tune the resultant sizes of the graphitic materials [98, 99]. Generally, horn (probe)/sonotrode-based ultrasonication are employed for high-power exfoliation of a multi-layered material such as raw graphite while for a mild exfoliation as well as homogenization of a solution sonication baths are very effective. The sonotrode systems are found to generate about 10-fold high power to that of a bath sonicator, yielding a more efficient synthesis within shorter reaction period [100]. Homogeneous stable suspensions of graphenes can be obtained by deploying optimum sonication time and intensity. Reports display that extended graphene nanoribbons (GNRs) formation requires shorter sonication time ($\sim$1 h) while longer sonication, leads to short ribbons [97].

Dual frequency application is often effective especially for proficient reduction as well as dispersion of graphene derivatives. Low frequency sonication generates strong shear forces that tears and fractures the sheets while at high frequency sonication generates large concentration of radicals, initiating redox reactions. Even a range of different graphene shapes like nano-ribbons, nano-scrolls can be achieved using ultrasonic aid [101–108]. In addition, simultaneous low and high frequencies not only enhance the reduction rate of metals but also trigger their higher and homogeneous loading on GO surfaces, especially effective in the synthesis of graphene composites [109]. Again homogeneous size distribution of graphene sheets results on extending sonication time rather than increasing power. Such evidences are obtained when chitosan-GO sonicated for 30 min under 120 W power resulted in wide range of 500–1500 nm sheets while on increasing the sonication time to 1 h at the same power led to homogeneous GO suspension ($\sim$500 nm). This phenomenon is termed as “debris grinding effects”. The effect of ultrasound power that provides necessary reaction activation energy was also effective for amidation of graphene composites [110]. However, increased power to 240 W for 1 h sonication yielded homogeneous but smaller sized chitosan-GO sheets ($\sim$400 nm). Thus, it is evident that tuning of the above parameters is essential for tailoring desired dimensions of graphenes for appropriate applications and undoubtedly, their information ought to be reported.

2.4 Large Scale Production of Graphene and Its Derivatives Applying Sonochemistry

Large scale production of graphene and its derivatives is very crucial especially to bring down the overall materials' production cost for various technological applications. Various ultrasound mediated techniques have been employed for the purpose. Initially, large graphene dispersion to $\sim$1 mg mL^{-1} was achieved by ultrasonication for <40 min through hydrazine reduction of graphene oxide [111]. Again, good-quality flat graphene sheets with $\sim$4 nm thickness and <5 layers were obtained from simple bath sonication at 65 °C that showed stable dispersion for 40 days owing to effective inhibition of intermediates (commonly formed in GO chemical reduction) that accelerate sheets agglomeration during conventional mechanical stirring. Furthermore, repeated sonication coupled with low heating resulted in tunable graphene sheets [112]. Short period ultrasound application within pressurized batch reactor resulted in large graphene sheets as well as its inorganic analogues such as boron nitrides, hexagonal-boron-carbon nitrides, and graphitic-carbon nitrides with uniform thickness in good scalable quantities [113]. Also large quantities of less-defects content few-layered graphenes were produced from graphite exfoliation in aqueous medium mixed with liquid hand soap and PVP as bio-compatible stabilizers, employing high intensity sonication probe [114]. Graphene quantum dots (GQDs) were recently obtained using ultrasonic-assisted liquid-phase exfoliation technique turned out to be an effective, environmental friendly, rapid scalable procedure. The sizes and defects of these GQDs can be tuned using suitable precursors and their optical and luminescence properties can be desirably varied accordingly as shown in Fig. 7 [115].

Again, ultrasound in presence of supercritical fluids (SFs) promotes successful intercalation process and such procedure enhances the exfoliation efficiency considerably as depicted in Fig. 8 [116]. Besides, eco-compatible nature, the free energy barrier in supercritical CO_2 prevents graphene aggregation to large extent. Adjustment of processing parameters assisted in tuning the layer- numbers and lateral dimension of graphene sheets. Graphene sheets of $\sim$0.5–5.0 μm with $\sim$16.7 wt% yield resulted under optimum conditions that could be enhanced to 40–50 wt% by repetitive sediment exfoliations. The resultant pristine graphene films exhibited high electrical conductivity of 2.8×10^7 Sm^{-1} [116]. High-velocity liquid microjets, generated from the collapse of cavitation bubbles continuously strike bulk graphite surface to create gaps and break way the layers during SFs intercalation in between the layers to exfoliate them [117]. Even large scale massive-graphene oxide sheets could be obtained using shearing-ultrasound technique. The shearing force is effective in de-laminating the layers without small fragmentation assisted by the ultrasonic cavitation that promotes their exfoliation [118]. Very recently, biodegradable and renewable solvent "Cyrene" exhibited higher defect-free graphene dispersion compared to other organic solvents within short time period of ultrasonication. Such a time saving procedure would be extremely helpful in industrial scale-up reactions [119].

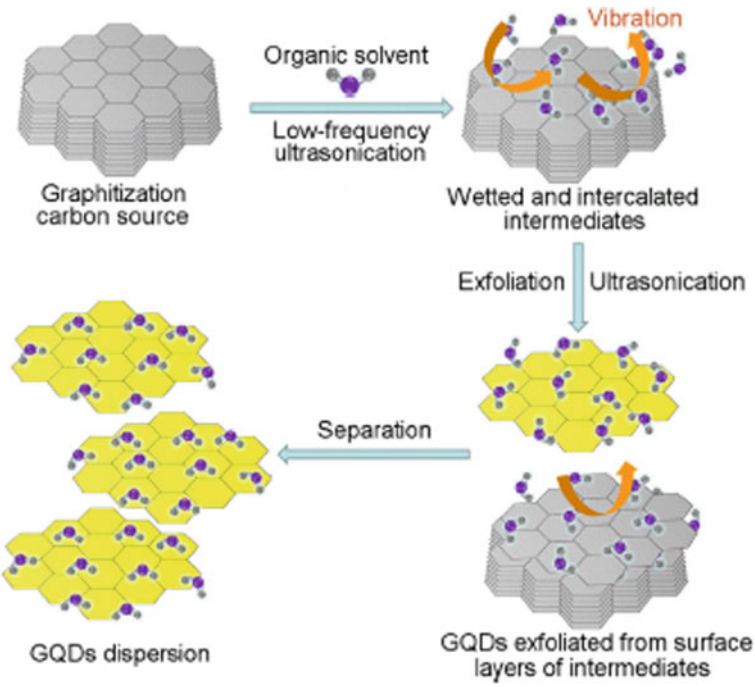

Fig. 7 Outline of ultrasound-assisted preparation of Graphene Quantum dots from graphitic carbon precursors in organic solvents. Ref. [115], reproduced on permission

3 Graphene Exfoliation via Ultrasound Assisted Intercalation Process

Earlier studies revealed that graphene oxide has been the commonest derivative of graphite that has been subsequently reduced to obtain graphene. However, such chemical reduction process remains incomplete simply by adding reductants and therefore, supplementary heating is essentially required for the elimination of all the functionalities to reach graphene [120]. Preliminary works on exfoliation involved functionalisation of graphitic oxide with isocyanate in organic solvents [121]. The foremost successful chemically unmodified, large-sized, conducting graphene ($\sim$28% monolayer yield and rest <6 layers thick) was obtained via ultrasound-based graphite exfoliation in *N*-methyl-2-pyrrolidone (NMP). However, the solubility was low $\sim$0.01 mg mL^{-1} with low reproducibility [122]. Subsequent works on graphite exfoliation in various other solvents by varying the sonication time and intensity such as dimethylformamide (DMF), water, poly (tert-butylacrylate), ortho-dichlorobenzene, pentafluorobenzonitrile, benzylamine, etc. were carried out that yielded different dispersive abilities but agglomeration occurred on standing after few days [123–126]. Thus, more effective methods are in

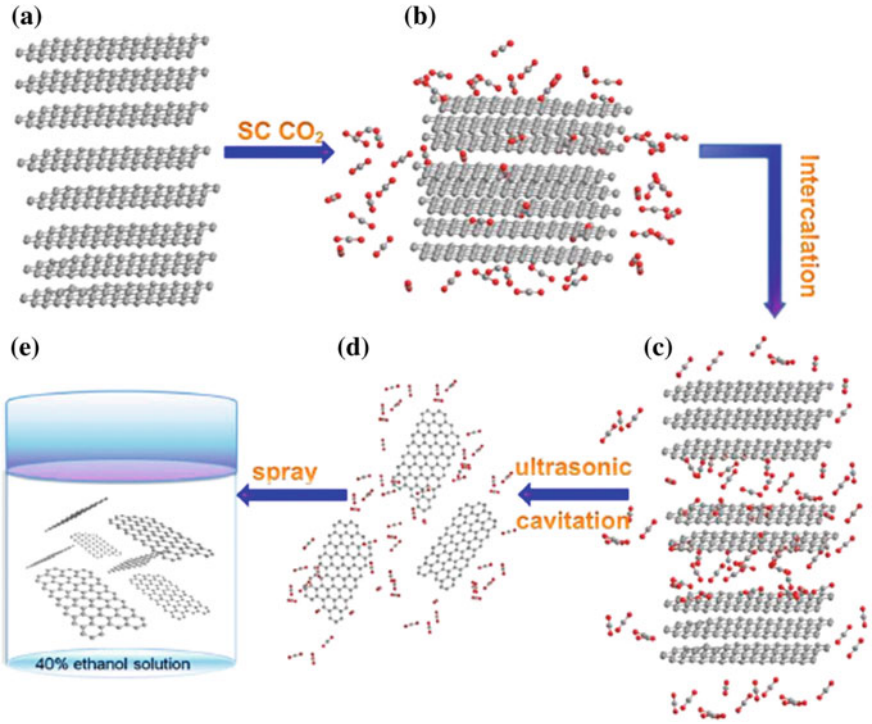

Fig. 8 Schematic illustration of graphene exfoliation using supercritical CO_2 assisted ultrasonication technique: **a** layered graphite **b** layered graphite introduced in supercritical CO_2 fluid **c** Intercalation of CO_2 molecules within graphite interlayers **d** formation of single- or few-layered graphene sheets **e** dispersion of as-obtained graphene sheets in 40% ethanol aqueous medium. Ref. [116], reproduced on permission

continuous search. Again, due to strong interlayer interactions in graphite, direct exfoliation is very difficult and thus it necessitates the use of intercalating agents to facilitate exfoliation [127]. Such a proposition has been outlined in Fig. 9.

Again, hydrophobic graphenes tend to agglomerate in polar solvents and so suitable stabilizing agents are certainly essential for its stability. Lotya and co-workers reported the earliest surfactant based sono-assisted graphite exfoliation in aqueous medium. They employed surfactant sodium dodecyl benzene sulfonate (SDBS) for the purpose, but the dispersion was relatively <0.01 mg mL^{-1} [128]. Additionally, the obtained graphenes were low conducting due to surface adsorption of surfactants. Low power sonication for longer periods slightly improved the results [129]. Various other surfactants including cationic surfactants like cetyltrimethylammonium bromide (CTAB), natural surfactants such as sodium cholate and sodium deoxycholate obtained as bile salts, and a bolaamphiphile that have hydrophilic terminals and long chain hydrophobic chain, etc. have been deployed, some of the performances of which has been illustrated in Fig. 10 [130–135].

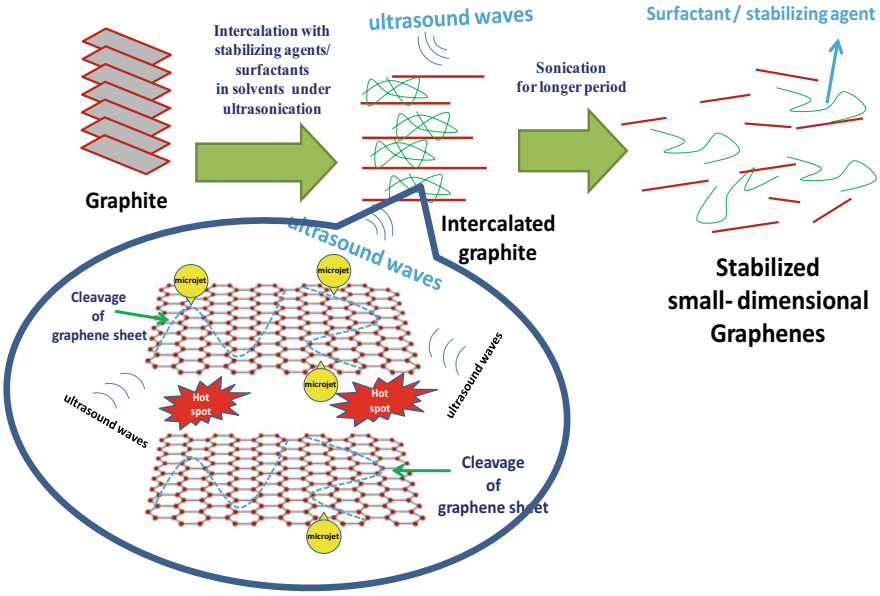

Fig. 9 Schematic representation highlighting intercalation and subsequent exfoliation are common strategy for graphite exfoliation to functionalized graphenes

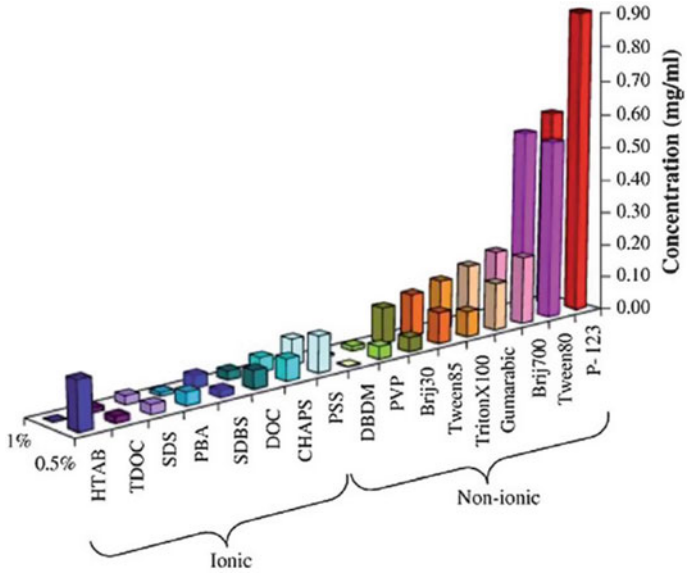

Fig. 10 Comparative study of relative yield of sonochemically obtained graphenes employing various types of surfactants. Ref. [135], reproduced on permission

Detailed investigation sonication-based exfoliation and dispersion of graphene with range of ionic and non-ionic surfactants in aqueous medium was explored [135]. Most of the non-ionic surfactants exhibited better results than their ionic counterparts. The most successful result was observed for triblock copolymer Pluronic® P-123 that dispersed $\sim$1 mg mL^{-1} graphene within two hours of sonication only with considerable improvement in yield $\sim$1.5 mg mL^{-1}, in 5 h sonication. Further, the ionic surfactants get adsorbed on graphene surface making them charged and thus, electrostatic repulsion prevent aggregation of these functionalized-graphenes. Again, the long and bulky hydrophobic tail along with functional moieties of the non-ionic surfactants sterically stabilized graphene segregation [136].

Another class of compounds called Ionic liquids, which are basically semi-organic salts existing as liquids below 100 °C, having comparable surface energies with graphene, emerged as capable solvating agents for ultrasound-based graphite exfoliation. The ionic liquid 1-butyl-3-methylimidazolium bis(trifluoro-methane-sulfonyl)imide provided stable dispersion of $\sim$0.95 mg mL^{-1} with large and thin graphenes only within one hour of sonication [137]. Recently, grinding graphite with 1-hexyl-3-methylimidazolium hexafluorophosphate followed by ultrasonication for 24 h yielded large-sized 4–6 layered graphenes with stable dispersions at $\sim$5.33 mg mL^{-1} [138]. The results till date are acceptable although challenges still remain regarding their production of large scale mono-layered graphenes.

Recently an alternative cost-effective, scalable technique involving bromine intercalation that considerably reduced the cohesive forces between the layers followed by mild sonication that further imposed additive effect resulting in severe delamination of the graphite layers [139]. Often ultrasonication has been used as a hyphenated technique during preparation of exfoliated graphites. For example, tetraethylammonium intercalated graphite prepared by high-power tip-sonication on exposure to microwave irradiation produced highly exfoliated graphite, easily dispersible in various organic solvents on mild sonication [140]. In another approach, oxidants such as CrO_3/H_2O_2 followed by HCl lead to production of di-oxygen gas that intercalates the graphite sheets and later on facilitates their exfoliation on ultrasound exposure. The method is advantageous as it can be carried out under ambient conditions and resultant graphenes have fairly high surface area similar to that of the 3-layered graphenes [141].

In the recent past, efforts for controlling the intercalation of graphite layers were tried out electrochemically with sonochemical assistance that gained significant success in regulating the graphene stacked-layer numbers with minimum surface defects. Ultrasound aid helped in de-intercalation of intercalated graphitic structure obtained via electrochemical Li-ion conversion reaction. The van der Waals forces of adjacent graphene sheets were destroyed by ultrasonication that ultimately led graphene exfoliation [142].

Nonetheless, substantial effort has been devoted for improving the quality and quantity of graphene exfoliation, although scientists are non-stopping seeking out for more effective procedures with higher reproducibility, especially with green and eco-friendly solvents and surfactants/stabilizing agents for the scalable production of varying-layered graphenes.

4 Ultrasound-Assisted Exfoliation and Dispersion of Graphene Composites

Recently, decoration of functionalized graphene surface with various nano-materials have drawn immense interests since this new class of hybrid materials have exhibited superior properties compared to their individual components. The nano-morphology (such as metal nano-structures, metal chalogenides/pnictonides based 0-D, 1-D or 2-D-quantized systems) that when introduced in-between the layers of graphene sheets prevents restacking of graphene sheets and exposes high active surface area by making both sides of these sheets accessible to external reagents. Fabrication of such smart materials is still a great challenge as majority nano-composites obtained from existing preparation methods lack homogeneity and reproducibility. However, such constraints in graphene based nano-composites have been largely overcome in the recent times using sono-chemical or ultrasound assisted synthetic approach, some of which have been highlighted in the discussion in the following sub-sections.

4.1 Metal Nanoparticles Decorated Functionalized Graphenes

Metal nanoparticles decorated graphene composites are very valuable systems with various technological applications especially in the areas of fuel cells, catalysis, energy storages sensors. Different morphologies of metal nano-systems on graphene substrates exhibited active surface areas for catalysis as well as promoted faster electron transfer channels for rapid, sensing responses. However, in situ reduction of metallic salts on preformed graphene sheets or their anchoring onto pre-synthesized graphene sheets and vice versa are very complex and less reproducible. Furthermore, resultant composites are highly susceptible to aggregation and so a one-pot synthetic route for such nanocomposite to obtain well-dispersed materials with high applicability is exceedingly required.

Based on this objective, Sun et al. designed a simple, less expensive environmentally benign ultrasound assisted one-pot synthesis route of Ag nanoparticles/graphene nanocomposites with the use of tannic acid as reductant. The resultant composite with thin-layered, surface-enhanced morphology exhibited excellent SERS activity and also catalyzed peroxide decomposition, and more importantly acted as glucose sensor in blood serum successfully [143].

In the recent past, graphene-Au-nano-hexagons prepared from in situ sonication technique manifested enhanced surface enhanced Raman spectroscopy (SERS) effectively employed for the detection of breast cancer and its stem cells was reported. The chemical mechanism for SERS intensity enhancement is greatly influenced by the number of graphene layers present. It has been reported that few-layered graphenes decorated Au-nanosystems owing to overlapping of surface

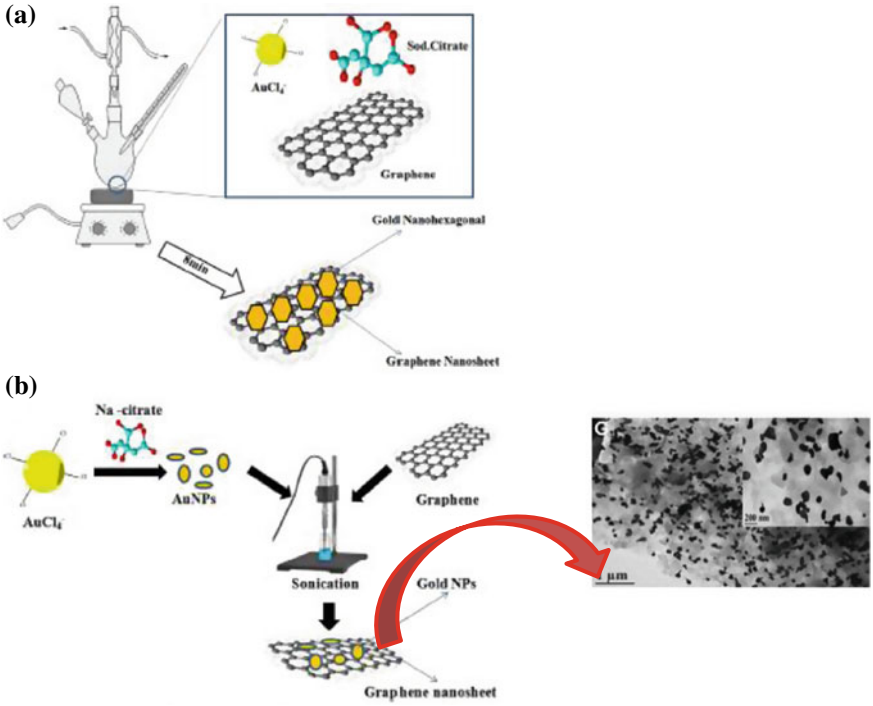

Fig. 11 Schematic representation of two-stepped-in situ ultrasound assisted preparation of graphene-Au-nano-hexagons nanocomposite for enhanced surface enhanced Raman spectroscopy (SERS). Ref. [144], reproduced on permission

plasmon resonance of Au with π-electron clouds of graphene extends lifetime of transitory vibration states of various bonds leading to intensifying SERS signal. Schematic representation of two-stepped-in situ ultrasound assisted preparation of graphene-Au-nano-hexagons nanocomposite has been shown in Fig. 11 [144].

Lately, sonochemically prepared Sn nanoparticles anchored reduced graphene oxide nano-discs in polyol medium were communicated with potential optoelectronic applications. Ultrasound played crucial role in the formation of these nano-discs. It was presumed that acoustic cavitation produced shear forces that cleaved the nanosheets (functionalized with polyols especially at the edges) into nano-discs to lower surface energy. Further, anchoring of Sn nanoparticles on the graphene impart stability to these nano-discs [145]. Even thermodynamically driven bimetallic alloys formation graphene substrates have been achieved by overcoming the kinetic barriers as a result of aid of ultrasound energy; successfully applied for various biomedical applications [146]. Based on similar strategies, several reports exists on sonochemically synthesized graphene-metal derivatives that have been employed in diversified applications, some of which have been summarized in Table 1 [147].

Table 1 Ultrasound assisted graphene-metal nanocomposite synthesis and their applications

Graphene-metal nanocomposite	Sonication parameters	Applications	Refs.
GO–Au	Horn sonication 20 kHz	Cholesterol sensing	[148]
RGO–Au	Probe sonication 120 min, 20 kHz, 750 W, 80% amplitude, RT	NO detection	[149]
GO–Ag–Au	Bath sonication Ag NPs: 120 min, 42 kHz, Au NPs: 360 min, RT	Anticancer activity	[150]
GO–Au–Ag	Dual frequency, bath and horn sonication 9 min, 213 kHz, 110–125 mW/mL, 20 kHz, 390 mW/mL, 10 mm (dia), 1 min (0.5 s on and 0.5 s off), 3 h, 28 °C	Bimetallic catalyst for the reduction of organic compound	[151]
RGO–Pt–Pd	Dual frequency, bath and horn sonication High: 211 kHz, 110–125 mW/mL, 9 min, 28 °C Low: 20 kHz, 390 mW/mL, 10 mm (tip dia), 1 min (0.5 s on and 0.5 s off)	High electrocatalytic activity for methanol oxidation	[109]
GO decorated with Ag and Au NPs	Bath sonication, high frequency (∼213 kHz) and then horn sonication, low frequency (20 kHz) for 3 h	Catalytic reduction of 4-aminophenol	[152]
Reduced graphene oxide/Pt/Sn	Horn sonicator (20 kHz), ∼3 h under argon atmosphere	Electrocatalytic methanol oxidation	[153]

4.2 Metal Oxide Based Functionalized Graphene-Nanocomposites

Metal oxide based graphene or graphene oxide (GO) nanocomposites have been of immense interest to the scientific community since last decade as these systems display unique physico-chemical features such as optical and electronic properties considerably with tuned particle size and structural modifications. Their anchoring on functionalized graphene oxide sheets prevents both agglomerations of the metal oxide nanosystems as well restacking of graphene layers owing to strong Van der Waals interactions between themselves, thus improving the stability of the individual components [154]. Moreover, the properties of the versatile and tailored quantum dots could be improved on 2D-graphene substrates because of the synergetic effect between them [155]. These nanocomposites have showed great results in different technological fields such as in photovoltaic devices, photo-catalysis as well as in various energy-devices starting from its harvesting, conversion and storage, etc. With this view, huge efforts have been made in assembling a large number of transition metal oxide nanosystems that includes TiO_2, ZnO, SnO_2, MnO_2, Co_3O_4, Fe_3O_4, Fe_2O_3, NiO, CuO etc. fabricating graphene hybrids since last decade [156–158].

Although many synthetic approaches have been adopted to prepare various nanocomposites based on the desired mode of applications, some of the common features that are urged for superior properties include large active-surface area, porosity, utilization of active material, faster charge transport features leading to high conductivity. For this, good exfoliation of the graphene sheets, uniform distribution of the nanomaterials on the sheets, optimum size formation of both the nano-metal oxides as well as the graphene sheets are necessary. Such features are very much obtainable with ultrasound energy assisted synthesis adopting optimum sonochemical parameters. Ultrasonic irradiations improve dispersion procedure and assist in achieving uniform loading of nanoparticles on functionalized graphene nanosheets, increasing the surface properties of the resultant product. Such an improvisation in synthetic methodology provides smarter materials with superior properties. Recently, Majumdar et al. explored two back-to-back hybrid systems—ultrasound-assisted rGO/CuO nanocomposites and MnO_2/hydroxyl-functionalized graphene systems with improved electrochemical energy storage behavior. Better interfacing characteristics were achieved due to in situ formation of nano-metal oxides over functionalized graphene surfaces under the aid of ultrasonication. The outline of synthetic procedure of ultrasound assisted-MnO_2/hydroxy-graphene composite has been displayed in Fig. 12 [159, 160].

Microjets formation due to cavitation effects improves the nanoparticle nucleation rates to obtain uniformly, distributed, oxides nanoparticles and considerably resolves the problem of agglomeration during synthesis to obtain intelligent materials. Sonochemical synthetic approach has been applied for obtaining various metal oxide-graphene composite used for various scientific applications some of

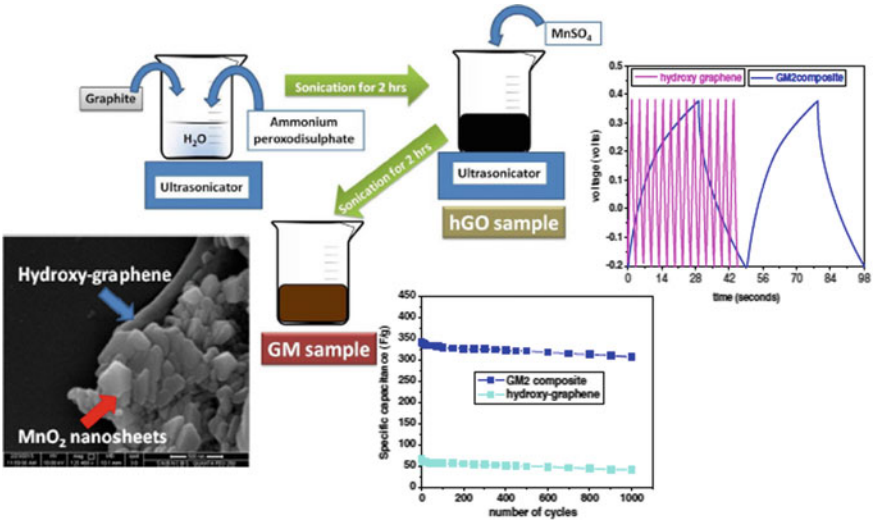

Fig. 12 Outline of synthesis procedure of ultrasound assisted-MnO_2/hydroxy-graphene composite and its supercapacitor characteristics. Ref. [160], reproduced on permission

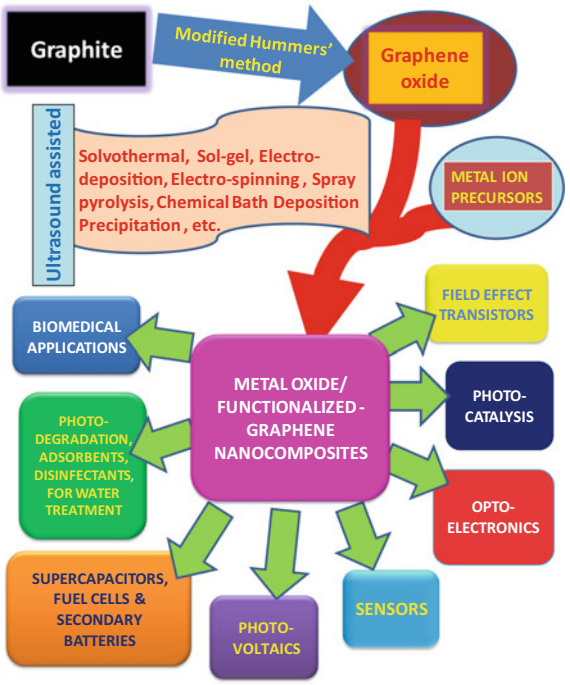

Fig. 13 Metal oxide-graphene nanocomposite obtained via sonochemically assisted syntheses approach for various scientific applications

which are summarized in Fig. 13. Moreover, the sonochemical technique is particularly important for resolving aggregation effects and limiting the size of 2D-graphene systems [161, 162]. Hence, in recent investigations, ultrasound techniques are employed in assisted/hyphenated mode for obtaining desired morphologies such as nanotubes, rods or even 2D plates [163–165]. The ultrasonication aid in these cases is indispensable and play important role in achieving homogeneous dispersion of GO so that maximum extent of the surfaces get exposure to the precursor materials for metal oxide formation can easily nucleate on its surface.

4.3 Polymer Based Functionalized Graphene-Nanocomposites

As discussed earlier, ultrasonic irradiation generates acoustic cavitation that also initiates polymer degradation in addition to morphological alterations. The strategy has been deliberately employed in obtaining various polymer nanostructures too [166]. The polymer chains when exposed to the vicinity of the collapsing bubbles experience high-gradient shear field that results in their segregation as well as lead to breakage of macromolecular C–C bonds. Such effects result in the formation of long chain radicals as detected for poly(methyl methacrylate), polystyrene, and poly

(vinyl alcohol) (PVA) by means of ESR spectroscopy [167, 168]. The approach has been applied to obtain a larger number of polymer functionalized graphene systems for different practical utilities. For instance, polystyrene functionalized graphenes obtained by mixing styrene with natural graphite flakes using horn sonication-probe of 20 kHz frequency, power density 50 Wcm^{-2} at 0 °C for 2 h under Argon atmosphere yielded the polystyrene-functionalized graphenes. 3D graphene-foam was obtained by initially functionalizing GO with polystyrene followed by its removal. These materials easily get dispersed in different common organic solvents and formed stable dispersions in them, which promotes their easy processibility for various applications [169]. Similarly, Poly(vinylalcohol)-functionalized graphene was prepared using sonochemical technique yielded the composite with higher tensile strength and improvement Young's modulus values for various potential uses [170]. Copolymer-based graphene nanoplatelets using ultrasound assisted synthesis showed unique characteristics with less agglomeration rate with good processibility in wide range of polar and non-polar solvents [171]. In many cases, the viscous nature of polymers are reduced by segregation of polymer chains by applying ultrasound frequency of 10–50 kHz and this pre-treatment is essential for integration and graphene dispersion in polymer [172]. Such reports were made by Bian group and Ma group while fabricating poly(propylene carbonate)/modified graphite oxide nanocomposites and elastomeric composites respectively using solution intercalation technique [173–175].

The ultrasound assisted graphene oxide/PVA composites were found to exhibit highly sensitivity to ultrasound exposure (or energy input). Ultrasonication for short time period leads to poor exfoliation of GO sheets and thus a partial strengthening effect is achieved. However, long time ultrasonication often causes reduction in GO sheet sizes, obstructing the mechanical improvement. Thus, an optimized ultrasound energy input $\sim$15 W hL^{-1} is ideal for the preparation of such composites [176]. Lately, graphene oxide was used as epoxy curing agents where cross-linking in epoxy resinwas induced by GO. Combination of covalent and π–π interactions promoted excellent dispersibility of the GO within polymeric matrix. The material with excellent adhesion and structural flexibility displayed potential capabilities to resist corrosion on a steel surface [177].

Ultrasound-synthesized graphene based-polymer nanocomposites have wide range of potential applications. Majumdar and co-researchers also fabricated single crystalline, epitaxial polyaniline (PANI) films on graphene sheets using sonochemical- assisted in situ polymerization technique with high quality P–N junction displaying excellent diode-like characteristics. The local cavitation energy supplied necessary activation for homolytic cleavage of the strained epoxy groups on GO sheets for in situ oxidation of aniline to polyaniline as depicted in Fig. 14 [178].

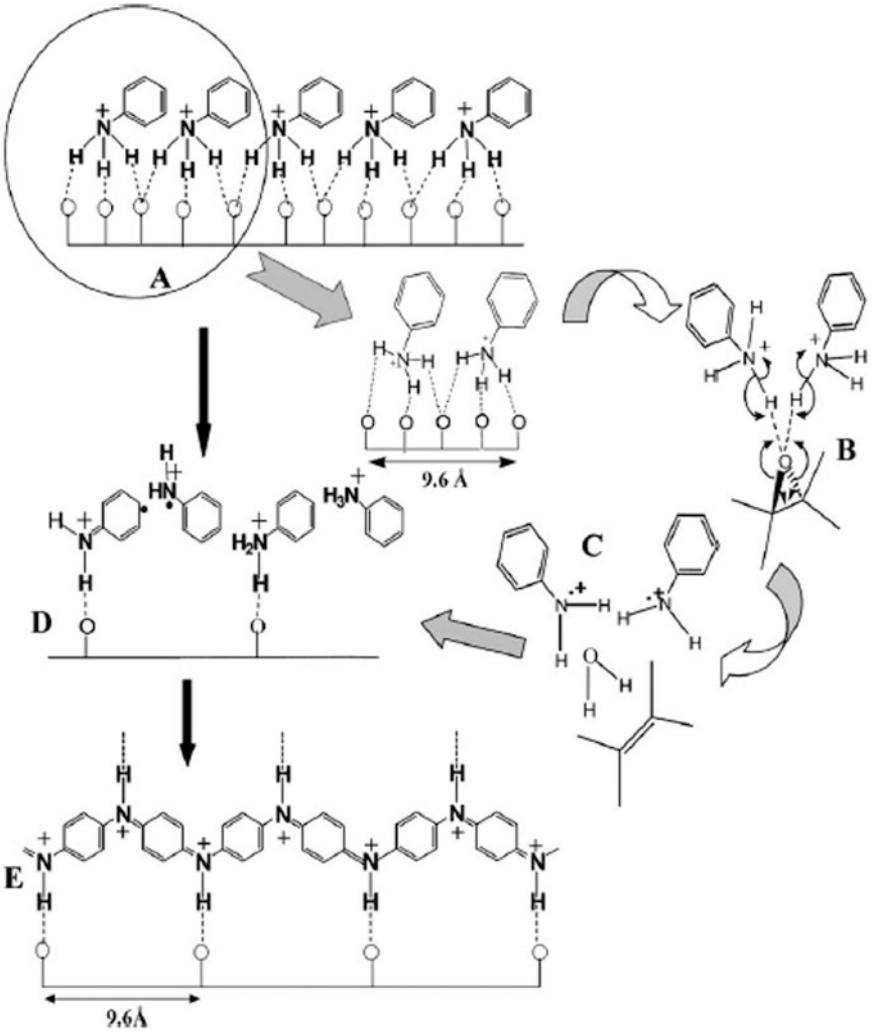

Fig. 14 Mechanism of oxidation-reduction process and preferential growth of PANI-chains on r-GO super-lattice in aid of ultrasound energy. Ref. [178], reproduced on permission

4.4 Other Graphene/Nano-Carbon Based Derivatives

Nano-porous carbons based on CNTs, Carbon nanofibers, etc. offer huge opportunity of straightforward tuning of their texture and surface chemistry thereby introducing novel effects derived from confinement, doping effects, and electron transfer features. Blending of these nano carbons with graphene and its derivatives reinforce each of the components shortcomings leading to reformed characteristics. The aid of ultrasound lead to intimate blending instigated by synergism, many such

instances are available in the literature. For example, ultrasound-mediated preparation of electrospun carbon nanofiber/graphene nanocomposite was employed for energy storage applications [179]. The resultant composite electrode showed improved conductivity, reduced agglomeration effects. Its novel structure and synergism of the components contributed to a specific capacitance of 183 Fg^{-1} much higher than pristine nanofibers, with good rate capability and galvanostatic charging/discharging cycle efficiency. Graphene-carbon nanotube hybrids designed for facilitating direct electron transfer of glucose oxidase and promoting glucose bio-sensing were achieved by sonochemical route. The well-dispersed, large area-based, highly conducting composite with interconnected network channels assist faster electron transport for sensing applications [180]. Ultrasound—assisted physical blending of pristine-graphene and pristine-fullerenes were employed for various applications that include solar cells, catalysis, bio-sensing, etc. [181–187]. Even, ultrasound-assisted pulse electrodeposition technique was successfully used to fabricate the GO-hydroxyapatite composite with better mechanical properties. Hydroxyapatite (calcium phosphate) which is analogous to similar to the human hard tissues in morphology and composition, blending with GO sheets have increased its hardness to large extent. Studies revealed that during sonolysis of water, the auto-generated, highly reactive hydroxy radicals along with GO had a constructive influence on the mineralization of the hydroxyapatite phase. The resultant material has high implication in biomedical fields [188, 189].

5 Sonochemically Synthesized Graphene Ternary Composites

A ternary composite is aimed to utilize the full benefits of each of the three components to yield a smarter material with improved characteristics in comparison to the binary composites. Ternary hybrids assist in resolving technological hurdles associated with agglomeration, interfacial chemistry, electronic, chemical and mechanical stability and flexibility issues. Various scientific landmarks have been achieved through usage of ternary composites especially in the fields of energy storage, photo-catalysis, metal ion detoxification water treatment, etc. [190–192].

Ultrasound assisted fabrication of ternary composites are rapidly emerging in the recent past. Scalable, homogeneous and densely dispersed core-double–shell cobalt/graphene//polystyrene high magnetization nanocomposites were designed by “in situ-sonochemical polymerization” technique that exhibited higher thermal stability with significant increase in glass transition temperature compared to pristine-polymer. The technique offered opportunity to produce covalent bonding between polymer and the graphene shell, using by two surface reactions: “grafting from” as the pre-immobilized monomer on graphene surface grows to polymer, while the “grafting to” occurs when pre-synthesized polymer is immobilized on graphene surface respectively [193]. Few years ago, ternary self-assembled

free-standing and flexible alternating layers of metal oxide andgraphene nanocomposites electrodes with graphene as fundamental building blocks designed for Li-ion batteries should high charge storage capacity with minimum charge/discharge loss. The surfactants in aid with ultrasound energy uniformly intercalated into graphene and homogenously distributed the nucleation sites for metal oxide formation with desired morphology on the graphene surface via solvothermal method [194]. Lately, ternary composites based on Pd nanoparticles immobilized on Fe_3O_4/amine-functionalized GO using sonochemical method without additional reducing agents that exhibited improved catalytic efficiency in Sonogashira cross-coupling reactions. Adoption of sonochemical reduction strategy generated mono-dispersed Pd nanoparticles on the binary composite surface that favoured cross-coupling reaction with high turnover frequency [195]. Similarly, ultrasonic assisted uniformly dispersed nano-sized Co_2SnO_4/graphene for electrochemical hydrogen storage application was reported shortly. The group studied different parameters such as duration of ultrasonic irradiation, solvent nature and basic reagent required to attain optimum size and morphology conditions [196]. Very recently, sonochemical strategy as adopted to prepare $CoSe_2$/Graphene/TiO_2 ternary nanocomposites exhibited appreciable photo-catalytic degradation of water soluble dye. Here also, the ultrasound technique promotes uniform dispersion strong anchoring as well as effective active mass utilization of the photo-catalyst on graphene surface [197].

6 Toxicity Issues

Rapid progress in graphenes applications has triggered spontaneous risks of inadvertent occupational and environmental exposures [198]. Comprehensive studies and their reviews highlighting their exclusive biocompatible properties for potential biomedical applications including drug encapsulation and release, gene delivery, biosensors, tissue engineering, neurosurgery, etc. are available in the literature [199–204]. Even they have been applied for water purification and treatments too. However, acute and chronic effects of different graphene systems obtained from different techniques including sonochemistry, should be taken into account from the point of environmental issues. For innumerous occasions, sonochemical methods of preparation of graphenes have been adopted for obtaining their optimal dimensions for the aforesaid versatile implications. As sonochemical technique is extremely handful in minimizing dimensions and functionalizing graphenes for desired morphology, while working with such strategy, strict safety measures should be availed so as to avoid the probable toxicities induced by graphenes. Besides, toxicity of the various nano-composites so obtained from ultrasound-assisted techniques should also be carefully looked into and studied in detail, in view of overall well-being and safety of the entire ecosystem.

Very recently, investigation on graphene exposure showed that its occupational contact have probable toxicity to the workers and researchers [205]. Besides, the

graphene impact on the air, soil and water environments were explored too [206, 207]. These nanomaterials get introduced into living bodies by intra-tracheal instillation, oral administration, intra-venous/intra-peritoneal/subcutaneous injection procedures [208], etc. Both acute and chronic tissue injuries through blood contamination can cause their accumulation within the vital organs. For instance, graphene aerosols on inhalation get substantially deposited in the human respiratory tract through the trachea-bronchial and lower lung airways resulting in the subsequent formation of granulomas, lung fibrosis and other possible adverse health effects on exposure. In vivo and in vitro studies on toxicity of graphenes and derivatives, their entry-paths, mechanism of toxicities were explored too on mice to simulate the impact on humans [209, 210].

Low doses of graphene systems contamination are less risky but on exposure to large concentrations leads to deposition of the same in vital internal organs such as lungs, spleen, liver, kidney, etc. High GO concentrations percolate cell membranes to invade lysosomes, mitochondria, endoplasm, even cell nucleus [211]. Several records inform that rGO caused apoptosis (a genetically controlled cell self-destruction process) mediated cell death even at a lower dose but that necrosis (disease induced cell death) was common with the increasing dose/duration of exposure. Even, the lateral dimension of graphene is crucial as the diameter between 100 and 500 nm may promote severe toxicity, while smaller diameters <40 nm are assigned to be comparatively safe. Besides, surface charge, functionalisation, composite components, etc. are important factors that should be taken into compulsory consideration during fabrication of graphene systems.

Thus, the author narrates here this section especially bearing in mind the fact that the present chapter would definitely increase the awareness of the beginners to this field of research in the near future, which may largely assist in their scientific planning.

7 Conclusion and Upcoming Perspectives

The present chapter emphasizes on the fundamentals aspects of ultrasound energy employed for sonochemical synthesis of graphenes and its derivatives. The parametric studies and subsequent challenges depicted during the sonochemical preparation of graphenes and its composites have been delineated here. Rigorous studies reveal that ultrasound assisted synthesis easily resolves the frequently-faced issues such as rapid agglomeration and non-uniform, irregular morphology-based graphene sheets, experienced on mechanical stirring commonly adopted during wet-chemical synthesis of graphene. The ultrasound- assisted exfoliation of graphene minimizes the reaction time considerably, thereby lowering the production cost as well as allows fabrication of more homogeneously sized graphene sheets with the flexibility of tuning the dimension and morphology according to technological demands. It has been observed that high power ultrasound generally yields thin and single-layered graphene sheets whereas low-power ultrasound such as bath

sonication leads to multi-layered, less damaged sheets with roughened surfaces and edges. Hence, as per requirement of graphene sheet morphology, ultrasonication probe (such as ultrasonic bath, horn, microtip, etc.) are employed with optimized sonication time. The ultrasound intensity, power and frequency are crucial for tuning the sizes of the formed graphenes. In addition to this, ultrasound also initiates functionalisation of graphene sheets by the chemical activation of surface functional group such as carboxyl, epoxy and hydroxyl groups with suitable components such as metal ions/organic monomers to form various graphene-metal or graphene-metal oxide nanocomposites or graphene-bio-molecule compounds respectively. Even ternary composites are also effective with suitable choice of components for achieving smarter materials. The ultrasound generated local hot spots and microjets provide such an intensive environment that makes sonochemical reactions spontaneously viable without the need of external catalyst or promoters. In a nutshell, sonochemistry provides a scalable, greener, cost-effective and proficient approach for advanced exploration of graphene.

In recent times, ultrasonication treatment supplements other preparation methods such as solvothermal, sol-gel, precipitation, etc. to obtain desired morphology based nanocomposites. Further, recent investigations urge bulk exfoliation of graphite to graphene for many applications that necessities large scale production of functionalized graphenes with controlled properties. Such requirements are well addressed by sonochemical synthesis of graphenes. Extensive efforts have been dedicated using ultrasound for improving the yield and degree of exfoliation of graphenes, taking into count the bio-compatibility of solvents, and intercalating/stabilizing agents but the adequate yield of single-layered graphene still remains a great challenge. A better understanding of graphene colloidal dispersion of graphene in various solvents with higher concentrations urges further explorations.

It is important to note that mechanical exfoliation of both graphite oxide and graphite has become one of the major techniques for the preparation of desired graphene-based composites for various technological applications. However, systematic studies on tuning of several controlling factors including heat intensity control by acoustic cavitation, physical parameters such as thermal conductivity of dissolved gases, solvent vapour pressure within micro-bubbles, ambient pressure, nature of dissolved impurities within solvents, etc. needs further detailed exploration for achieving better sonochemical yield of graphenes with better properties. Such challenges are certainly opening up vast and novel prospects on sonochemical synthesis of graphenes and related composites for the near-future technologies. It is no far way when sonochemical synthetic approach would become the pioneering mode for scalable graphene production for commercial applications.

Acknowledgements DM acknowledges Indian Association for the Cultivation of Science, Jadavpur, Kolkata, WB, India and Department of Chemistry (Physical Chemistry Section), Jadavpur University, Kolkata-700032, WB, India for Library facilities. DM also acknowledges Department of Chemistry, Chandernagore College, Hooghly, Pin-712136, WB, India for providing permission to do honorary research.

References

1. Pilli, S., Bhunia, P., Yan, S., LeBlanc, R.J., Tyagi, R.D.: Ultrasonic pretreament of sludge: a review. Ultrason. Sonochem. **18**, 1–18 (2011)
2. Suslick, K.S.: The chemical effects of ultrasound. Sci. Am. **260**, 80–86 (1989)
3. Bhangu, S.K., Ashokkumar, M.: Theory of sonochemistry. Top. Curr. Chem. **374**, 56 (2016)
4. Baillon, F., Espitalier, F., Cogné, C., Peczalski, R., Louisnard, O.: Crystallization and freezing processes assisted by power ultrasound. Power Ultrason. Appl. High-Intensity Ultrasound **28**, 845–874 (2015)
5. Neis, U.: The use of power ultrasound for wastewater and biomass treatment. Power Ultrason. Appl. High-Intensity Ultrasound **32**, 973–996 (2015)
6. Gaete-Garretón, L.: The use of power ultrasound in mining power ultrasonics applications of high-intensity. Ultrasound **35**, 1059–1094 (2015)
7. Yeong, W.T., Guo, N., Yang, T.C., Xiao, W.H.J.: Theory and fundamentals of ultrasound. In: Advances in Ultrasound Technology for Environmental Remediation. Springer Briefs in Green Chemistry for Sustainability. https://doi.org/10.1007/978-94-007-5533-8_2 (2013)
8. Prajapati, J.V., Agrawal, Y.K.: Synthesis, characterization and application of microbubbles: a review. IJPSR **3**(6), 1532–1543 (2012)
9. Leong, T., Ashokkumar, M., Kentish, S.: The fundamentals of power ultrasound—a review. Acoust Aust **39**(2), 54–63 (2011)
10. Thompson, L.H., Doraiswamy, L.K.: Sonochemistry: science and engineering. Ind. Eng. Chem. Res. **38**(4), 1215–1249 (1999)
11. Suslick, K.S.: Applications of ultrasound to materials chemistry. MRS Bull. **20**, 29–34 (1995)
12. Suslick, K.S.: Mechanochemistry and sonochemistry: concluding remarks. Faraday Discuss. **170**, 411–422 (2014)
13. Flint, E.B., Suslick, K.S.: The temperature of cavitation. Science **253**(5026), 1397–1399 (1991)
14. Duckhouse, H., Mason, T.J., Phull, S.S., Lorimer, J.P.: The effect of sonication on microbial disinfection using hypochlorite. Ultrason. Sonochem. **11**(3–4), 173–176 (2004)
15. Chemat, F., HumaZ, Khan M.K.: Applications of ultrasound in food technology: processing, preservation and extraction. Ultrason. Sonochem. **18**(4), 813–835 (2011)
16. Goldberg, B.B., Liu, J.B., Forsberg, F.: Ultrasound contrast agents: a review. Ultrasound Med. Biol. **20**(4), 319–333 (1994)
17. Ferrara, K., Pollard, R., Borden, M.: Ultrasound microbubble contrast agents: fundamentals and application to gene and drug delivery. Annu. Rev. Biomed. Eng. **9**(1), 415–447 (2007)
18. Li, W., Leong, T.S., Ashokkumar, M., Martin, G.J.: A study of the effectiveness and energy efficiency of ultrasonic emulsification. Phys. Chem. Chem. Phys. **20**, 86–96 (2018)
19. Cavalieri, F., Ashokkumar, M., Grieser, F., Caruso, F.: Ultrasonic synthesis of stable, functional lysozyme microbubbles. Langmuir **24**, 10078–10083 (2008)
20. Neppolian, B., Bruno, A., Bianchi, C.L., Ashokkumar, M.: Graphene oxide based Pt–TiO_2 photocatalyst: ultrasound assisted synthesis, characterization and catalytic efficiency. Ultrason. Sonochem. **19**, 9–15 (2012)
21. Madhavan, J., Grieser, F., Ashokkumar, M.: Degradation of Orange-G by advanced oxidation processes. Ultrason. Sonochem. **17**, 338–343 (2010)
22. Ashokkumar, M.: Theoretical and Experimental Sonochemistry Involving Inorganic Systems. Springer Science & Business Media (2010)
23. Kiss, A.A., Geertman, R., Wierschem, M., Skiborowski, M., Gielen, B., Jordens, J., John, J. J., Van Gerven, T.: Ultrasound-assisted emerging technologies for chemical processes. J. Chem. Technol. Biotechnol. **93**(5), 1219–1227 (2018)
24. Liu, B., Cai, J., Huai, X., Li, F.: Cavitation bubble collapse near a heated wall and its effect on the heat transfer. J. Heat Transfer **136**, 022901 (2014)
25. Caupin, F., Herbert, E.: Cavitation in water: a review. C. R. Phys. **7**, 1000–1017 (2006)

26. Bang, J.H., Suslick, K.S.: Applications of ultrasound to the synthesis of nanostructured materials. Adv. Mater. **22**, 1039 (2010)
27. Bardelang, D.: Ultrasound induced gelation: a paradigm shift. Soft Matter **5**, 1969 (2009)
28. Naota, T., Koori, H.: Molecules that assemble by sound: an application to the instant gelation of stable organic fluids. J. Am. Chem. Soc. **127**, 9324 (2005)
29. Pollet, B.G.: The use of ultrasound for the fabrication of fuel cell materials. Int. J. Hydrogen Energy **35**, 11986 (2010)
30. Adewuyi, Y.G.: Sonochemistry: environmental science and engineering applications. Ind. Eng. Chem. Res. **40**, 4681–4715 (2001)
31. Vajnhandl, S., Marechal, A.M.L.: Ultrasound in textile dyeing and the decolourization/ mineralization of textile dyes. Dyes Pigm. **65**, 89–101 (2005)
32. Johansson, L., Singh, T., Leong, T., Mawson, R., McArthur, S., Manasseh, R., Juliano, P.: Cavitation and non-cavitation regime for large-scale ultrasonic standing wave particle separation systems—in situ gentle cavitation threshold determination and free radical related oxidation. Ultrason. Sonochem. **28**, 356 (2016)
33. Henglein, A.: Sonochemistry: historical developments and modern aspects. Ultrasonics **25** (1), 6–16 (1987)
34. Alhelfi, A., Sunden, B.: The cavitation phenomenon: a literature survey. Adv. Comput. Methods Exp. Heat Transf. **XIII**, 351, WIT Trans. Eng. Sci. **83.** https://doi.org/10.2495/ht140311 (2014)
35. Mason, T.J., Lorimer, J.P.: An introduction to sonochemistry. Endeavour **13**(3), 123–128 (1989)
36. Suslick, K.S., Price, G.: Applications of ultrasound to materials chemistry. Annu. Rev. Mater. Sci. **29**, 295–326 (1999)
37. Pokhrel, N., Vabbina, P.K., Pala, N.: Sonochemistry: science and engineering. Ultrason. Sonochem **29**, 104–128 (2016)
38. Suslick, K.S., Choe, S.B., Cichowlas, A.A., Grinstaff, M.W.: Sonochemical synthesis of amorphous iron. Nature **353**, 414–416 (1991)
39. Grinstaff, M.W., Salamon, M.B., Suslick, K.S.: Magnetic properties of amorphous iron. Phys. Rev. B **48**, 269–273 (1993)
40. Hyeon, T., Fang, M., Suslick, K.S.: Nanostructured molybdenum carbide: sonochemical synthesis and catalytic properties. J. Am. Chem. Soc. **118**, 5492–5493 (1996)
41. Cao, X., Prozorov, R., Koltypin, Y., Kataby, G., Felner, I., Gedanken, A.: Synthesis of pure amorphous Fe2O3. J. Mater. Res. **12**(2), 402–406 (1997)
42. Shafi, K.V.P.M., Koltypin, Y., Gedanken, A., Prozorov, R., Balogh, J., Lendvai, J., Felner, I.: Sonochemical preparation of nanosized amorphous $NiFe_2O_4$ particles. J. Phys. Chem. B. **101**, 6409–6414 (1997)
43. Zhu, Y., Murali, S., Cai, W., Li, X., Suk, J.W., Potts, J.R., Ruoff, R.S.: Graphene and graphene oxide: synthesis, properties, and applications. Adv. Mater. **22**, 3906–3924 (2010)
44. Esmaeili, A., Entezari, M.H.: Facile and fast synthesis of graphene oxide nanosheets via bath ultrasonic irradiation. J. Colloid Interface Sci. **432**, 19–25 (2014)
45. Suslick, K.S.: Sonochemistry, comprehensive coordination chemistry. II ISBN (set): 0-08-0437486 **1**, 731–739. ISBN 0-08-0443230
46. Guilane, S., Hamdaoui, O.: Desorption of 4-chlorophenol from spent granular activated carbon in continuous flow ultrasonic reactor. Desalin. Water Treat **57**(27), 12708–12716 (2016)
47. Suslick, K.S., Hyeon, T., Fang, M.: Nanostructured materials generated by high intensity ultrasound. Chem. Mater. **8**, 2172–2179 (1996)
48. Brotchie, A., Grieser, F., Ashokkumar, M.: Effect of power and frequency on bubble-size distributions in acoustic cavitation. Phys. Rev. Lett. **102**, 084302 (2009)
49. Okitsu, K., Ashokkumar, M., Grieser, F.: Sonochemical synthesis of gold nanoparticles: effects of ultrasound frequency. J. Phys. Chem. B **109**(44), 20673–20675 (2005)
50. Chatel, G.: How sonochemistry contributes to green chemistry? Ultrason. Sonochem. **40**, 117–122 (2018)

51. Cintas, P.: Ultrasound and green chemistry–further comments. Ultrason. Sonochem. **28**, 257–258 (2016)
52. Anastas, P.T., Warner, J.C.: Green chemistry: Theory and Practice, pp. 11–54. Oxford University Press, Oxford (1998)
53. Cintas, P., Luche, J.-L.: Green chemistry, the sonochemical approach. Green Chem. **1**, 115–125 (1999)
54. Mason, T.J.: Sonochemistry and the environment—providing a "green" link between chemistry, physics and engineering. Ultrason. Sonochem. **14**, 476–483 (2007)
55. Allen, M.J., Tung, V.C., Kaner, R.B.: Honeycomb carbon: a review of graphene. Chem. Rev. **110**(1), 132–145 (2010)
56. Geim, A.K., Novoselov, K.S.: The rise of graphene. Nat. Mater. **6**, 183–191 (2007)
57. Sur, U.K.: Graphene: a rising star on the horizon of materials science. Int. J. Electrochem. Article ID 237689, 12. https://doi.org/10.1155/2012/237689 (2012)
58. Kiew, S.F., Kiew, L.V., Lee, H.B., Imae, T., Chung, L.Y.: Assessing biocompatibility of graphene oxide-based nanocarriers: a review. J. Controlled Release **226**, 217–228 (2016)
59. Bharech, S., Kumar, R.: A review on the properties and applications of graphene. J. Mater. Sci. Mech. Eng. (JMSME) **2**, 70–73 (2015)
60. Almazan, A.: Graphene an excellent conductor of electricity and potential component of future electronics. Cosmos 8, 1–18 (2012)
61. Liu, Z.K., Li, J.H., Sun, Z.H., Tai, G.A., Lau, S.P., Yan, F.: Package-free flexible organic solar cells with graphene top electrodes the application of highly doped single-layer graphene as the top electrodes of semitransparent organic solar cells. ACS Nano **6**, 810–818 (2012)
62. Ang, P.K., Chen, W., Thye, A., Wee, S., Loh, K.P.: Solution-gated epitaxial graphene as pH sensor. J. Am. Chem. Soc. **130**, 14392–14395 (2008)
63. Li, X., Zhao, T., Chen, Q., Li, P., Wang, K., Zhong, M., Wei, J., Wu, D., Wei, B., Zhu, H.: Flexible all solid-state supercapacitors based on chemical vapor deposition derived graphene fibers. Phys. Chem. Chem. Phys. **15**, 17752–17757 (2013)
64. Zhao, L., Zhao, L., Xu, Y., Qiu, T., Zhi, L., Shia, G.: Polyaniline electrochromic devices with transparent graphene electrodes. Electrochim. Acta **55**, 491–497 (2009)
65. Tong, X., Wang, H., Wang, G., Wan, L., Ren, Z., Bai, J., Bai, J.: Controllable synthesis of graphene sheets with different numbers of layers and effect of the number of graphene layers on the specific capacity of anode material in lithium-ion batteries. J. Solid State Chem. **184**, 982–989 (2011)
66. Zhuo, Q., Ma, Y., Gao, J., Zhang, P., Xia, Y., Tian, Y., Sun, X., Zhong, J., Sun, X.: Facile synthesis of graphene/metal nanoparticle composites via self-catalysis reduction at room temperature. Inorg. Chem. **52**, 3141–3147 (2013)
67. Zheng, L., Ye, D., Xiong, L., Xu, J., Tao, K., Zou, Z., Huang, D., Kang, X., Yang, S., Xia, J.: Preparation of cobalt-tetraphenylporphyrin/reduced graphene oxide nanocomposite and its application on hydrogen peroxide biosensor. Anal. Chim. Acta **768**, 69–75 (2013)
68. Xiang, Q., Yu, J., Jaroniec, M.: Graphene-based semiconductor photocatalysts. Chem. Soc. Rev. **41**, 782–796 (2012)
69. Kuila, T., Bose, S., Mishra, A.K., Khanra, P., Kim, N.H., Lee, J.H.: Chemical functionalization of graphene and its applications. Prog. Mater. Sci. **57**, 1061–1105 (2012)
70. Berger, C., Song, Z., Li, T., Li, X., Ogbazghi, A.Y., Feng, R., Dai, Z., Marchenkov, A.N., Conrad, E.H., First, P.N., de Heer, W.A.: Ultrathin epitaxial graphite: 2D electron gas properties and a route toward graphene-based nanoelectronics. J. Phys. Chem. B **108**(52), 19912–19916 (2004)
71. Lacatus, E.: Modeling a multilayered graphene biosensing structure. Mater. Today Proc. **3** (8), 2635–2645 (2016)
72. Alwarappan, S., Boyapalle, S., Kumar, A., Li, C.-Z., Mohapatra, S.: Comparative study of single-, few-, and multilayered graphene toward enzyme conjugation and electrochemical response. J. Phys. Chem. C **116**, 6556–6559 (2012)

73. Krajewska, A., Pasternak, I., Sobon, G., Sotor, J., Przewloka, A., Ciuk, T., Sobieski, J., Grzonka, J., Abramski, K.M., Strupinski, W.: Fabrication and applications of multi-layer graphene stack on transparent polymer. Appl. Phys. Lett. **110**, 041901 (2017)
74. Novoselov, K.S., Geim, A.K., Morozov, S.V., Jiang, D., Zhang, Y., Dubonos, S.V., Grigorieva, I.V., Firsov, A.A.: Electric field effect in atomically thin carbon films. Science **306**, 666–669 (2004)
75. Novoselov, K.S., Jiang, D., Schedin, F., Booth, T.J., Khotkevich, V.V., Morozov, S.V., Geim, A.K.: Two-dimensional atomic crystals. P. Natl Acad. Sci. USA **102**, 10451–10453 (2005)
76. Li, D., Muller, M.B., Gilje, S., Kaner, R.B., Wallace, G.G.: Processable aqueous dispersions of graphene nanosheets. Nat. Nanotechnol. **3**(2), 101–105 (2008)
77. Skákalová, V., Kotrusz, P., Jergel, M., Susi, T., Mittelberger, A., Vretenár, V., Šiffalovič, P., Kotakoski, J., Meyer, J.C., Hulman, M.: Chemical oxidation of graphite: evolution of the structure and properties. J. Phys. Chem. C, **122**(1), 929–935 (2018)
78. Eda, G., Chhowalla, M.: Chemically derived graphene oxide: towards large-area thin-film electronics and optoelectronics. Adv. Mater. **22**, 2392–2415 (2010)
79. Stankovich, S., Dikin, D., Dommett, G.H.B., Kohlhaas, M.K., Zimney, E., Stach, E., Piner, R.D., Nguyen, S., Ruoff, R.: Graphene-based composite materials. Nature **442**, 282–286 (2006)
80. Devasena, S.: Review on graphene oxide composites. Int. J. Nanomater. Nanostruct. **2**, 24–30 (2016)
81. Chung, C., Kim, Y.K., Shin, D., Ryoo, S.R., Hong, B.H., Min, D.H.: Biomedical applications of graphene and graphene oxide. Acc. Chem. Res. **46**(10), 2211–2224 (2013)
82. Bhuyan, M., Uddin, M., Bipasha, F.A., Islam, M.M., Hossain, S.S.: A Review of Functionalized Graphene properties and its application. Int. J. Innov. Sci. Res. **1**, 303–315 (2015)
83. Akinwande, D., Brennan, C.J., Bunch, J.S., Egberts, P., Felts, J.R., Gao, H., Huang, R., Kim, J.-S., Li, T., Li, Y., Liechti, K.M., Lu, N., Park, H.S., Reed, E.J., Boris, P.W., Yakobson, I., Zhang, T., Zhang, Y.-W., Zhu, Y.: A review on mechanics and mechanical properties of 2D materials—graphene and beyond. Extreme Mech. Lett. **13**, 42–77 (2017)
84. Xu, H., Suslick, K.S.: sonochemical preparation of functionalized graphenes. J. Am. Chem. Soc. **133**(24), 9148–9151 (2011)
85. Suslick, K.S., Price, G.J.: Applications of ultrasound to materials chemistry. Annu. Rev. Mater. Sci. **29**, 295–326 (1999)
86. Shen, J., Shi, M., Ma, H., Yan, B., Li, N., Hu, Y., Ye, M.: Synthesis of hydrophilic and organophilic chemically modified graphene oxide sheets. J. Colloid Interface Sci. **352**, 366–370 (2010)
87. Muthoosamya, K., Manickam, S.: State of the art and recent advances in the ultrasound-assisted synthesis, exfoliation and functionalization of graphene derivatives. Ultrason. Sonochem. **39**, 478–493 (2017)
88. Bai, R.G., Muthoosamy, K., Shipton, F.N., Manickam, S.: Acoustic cavitation induced generation of stabilizer-free, extremely stable reduced graphene oxide nanodispersion for efficient delivery of paclitaxel in cancer cells. Ultrason. Sonochem. **36**, 129–138 (2017)
89. Soltani, T., Kyu, L.B.: A benign ultrasonic route to reduced graphene oxide from pristine graphite. J. Colloid Interface Sci. **486**, 337–343 (2017)
90. Rae, J., Ashokkumar, M., Eulaerts, O., von Sonntag, C., Reisse, J., Grieser, F.: Estimation of ultrasound induced cavitation bubble temperatures in aqueous solutions. Ultrason. Sonochem. **12**, 325–329 (2005)
91. Ciawi, E., Rae, J., Ashokkumar, M., Grieser, F.: Determination of temperatures within acoustically generated bubbles in aqueous solutions at different ultrasound frequencies. J. Phys. Chem. B **110**, 13656–13660 (2006)
92. Hashim, N., Muda, Z., Hussein, M.Z., Isa, I.M., Mohamed, A., Kamari, A., Abu Bakar, A., Mamat, M., Mohamad Jaafar, A.: A brief review on recent graphene oxide-based material nanocomposites: synthesis and applications. J. Mater. Environ. Sci. **7**(9), 3225–3243 (2016)

93. Saha, S.K., Baskey, M., Majumdar, D.: Graphene quantum sheets: a new material for spintronic applications. Adv. Mater. **22**, 5531–5536 (2010)
94. Zhuo, S., Shao, M., Lee, S.-T.: Upconversion and downconversion fluorescent graphene quantum dots: ultrasonic preparation and photocatalysis. ACS Nano **6**(2), 1059–1064 (2012)
95. Zeng, Z., Chen, S., Tan, T.T.Y., Xiao, F.-X.: Graphene quantum dots (GQDs) and its derivatives for multifarious photocatalysis and photoelectrocatalysis. Catal. Today **315**, 171–183 (2018)
96. Li, X., Wang, X., Zhang, L., Lee, S., Dai, H.: Chemically derived, ultrasmooth graphene nanoribbon semiconductors. Science **319**, 1229–1232 (2008)
97. Wu, Z.S., Ren, W., Gao, L., Liu, B., Zhao, J., Cheng, H.M.: Efficient synthesis of graphene nanoribbons sonochemically cut from graphene sheets. Nano Res. **3**, 16–22 (2010)
98. Wood, R.J., Lee, J., Bussemake, M.J.: A parametric review of sonochemistry: control and augmentation of sonochemical activity in aqueous solutions. Ultrason. Sonochem, **38**, 351–370 (2017)
99. Durge, R., Kshirsagar, R.V., Tambe, P.: Effect of sonication energy on the yield of graphene nanosheets by liquid-phase exfoliation of graphite. Procedia Eng. **97**, 1457–1465 (2014)
100. Vinodgopal, K., Neppolian, B., Salleh, N., Lightcap, I.V., Grieser, F., Ashokkumar, M., Ding, T.T., Kamat, P.V.: Dual-frequency ultrasound for designing two dimensional catalyst surface: reduced graphene oxide–Pt composite. Colloids Surf., A **409**, 81–87 (2012)
101. Wang, M., Yuan, W.: Modeling bubble dynamics and radical kinetics in ultrasound induced microalgal cell disruption. Ultrason. Sonochem. **28**, 7–14 (2016)
102. Tuncay, A., Dustman, J.A., Fisher, G., Tuncay, C.I., Suslick, K.S.: Ultrasound promoted hypervalent iodine reactions: α-Tosyloxylation of Ketones. Tetrahedron Lett. **33**, 7647–7650 (1992)
103. Neppolian, B., Bruno, A., Bianchi, C.L., Ashokkumar, M.: Pt–TiO2 photocatalyst: ultrasound assisted synthesis, characterization and catalytic efficiency. Ultrason. Sonochem. **19**(2012), 9–15 (2012)
104. Neppolian, B., Celik, E., Anpo, M., Choi, H.: Ultrasonic-assisted pH swing method forthe synthesis of highly efficient TiO2 nano-size photocatalysts. Catal. Lett. **125**, 183–191 (2008)
105. Maitra, U., Matte, H.S.S.R., Kumar, P., Rao, C.N.R.: Strategies for the synthesis of graphene, graphene nanoribbons, nanoscrolls and related materials. Chimia **66**, 941–948 (2012)
106. Neppolian, B., Doronila, A., Grieser, F., Ashokkumar, M.: Simple and efficient sonochemical method for the oxidation of arsenic(III) to arsenic(V). Environ. Sci. Tech. **43**, 6793–6798 (2009)
107. Kanthale, P., Ashokkumar, M., Grieser, F.: Sonoluminescence, sonochemistry (H_2O_2yield) and bubble dynamics: frequency and power effects. Ultrason. Sonochem. **15**, 143–150 (2008)
108. Neppolian, B., Doronila, A., Ashokkumar, M.: Sonochemical oxidation of arsenic(III) to arsenic(V) using potassium peroxydisulfate as an oxidizing agent. Water Res. **44**, 3687–3695 (2010)
109. Neppolian, B., Sáez, V., González-García, J., Grieser, F., Gómez, R., Ashokkumar, M.: Sonochemical synthesis of graphene oxide supported Pt–Pd alloy nanocrystals as efficient electrocatalysts for methanol oxidation. J. Solid State Electrochem. **18**, 3163–3171 (2014)
110. Jia, J., Gai, Y., Wang, W., Zhao, Y.: Green synthesis of biocompatiable chitosan–graphene oxide hybrid nanosheet by ultrasonication method. Ultrason. Sonochem. **32**, 300–306 (2016)
111. Zhang, W., He, W., Jing, X.: Preparation of a stable graphene dispersion with high concentration by ultrasound. J. Phys. Chem. B **114**, 10368–10373 (2010)
112. Tung, V.C., Allen, M.J., Yang, Y., Kaner, R.B.: High-throughput solution processing of large-scale graphene. Nat. Nano **4**, 25–29 (2009)
113. Štengl, V., Henych, J., Slušná, M., Ecorchard, P.: Ultrasound exfoliation of inorganic analogues of graphene. Nanoscale Res. Lett. **9**, 167 (2014)

114. Noroozi, M., Zakaria, A., Radiman, S., Abdul Wahab, Z.: Environmental synthesis of few layers graphene sheets using ultrasonic exfoliation with enhanced electrical and thermal properties. PLoS ONE **11**(4), e0152699 (2016)
115. Lu, L., Zhu, Y., Shi, C., Pei, Y.T.: Large-scale synthesis of defect-selective graphene quantum dots by ultrasonic-assisted liquid-phase exfoliation. Carbon **109**, 373–383 (2016)
116. Gao, Y., Shi, W., Wang, W., Wang, Y., Zhao, Y., Lei, Z., Miao, R.: Ultrasonic-assisted production of graphene with high yield in supercritical CO_2 and its high electrical conductivity film. Ind. Eng. Chem. Res. **53**, 2839–2845 (2014)
117. Gao, H., Zhu, K., Hu, G., Xue, C.: Large-scale graphene production by ultrasound-assisted exfoliation of natural graphite in supercritical CO_2/H_2O medium. Chem. Eng. J. **308**, 872–879 (2017)
118. Cai, C., Sang, N., Shen, Z., Zhao, X.: Facile and size-controllable preparation of graphene oxide nanosheets using high shear method and ultrasonic method. J. Exp. Nanosci. **12**(1), 247–262 (2017)
119. Salavagione, H.J., Sherwood, J., De bruyn, M., Budarin, V.L., Ellis, G.J., Clark, J.H., Shuttleworth, P.S.: Identification of high performance solvents for the sustainable processing of graphene. Green Chem. **19**, 2550–2560 (2017)
120. Gao, X., Jang, J., Nagase, S.: Hydrazine and thermal reduction of graphene oxide: reaction mechanisms, product structures, and reaction design. J. Phys. Chem. C **114**(2), 832–842 (2010)
121. Stankovich, S., Piner, R.D., Nguyen, S.T., Ruoff, R.S.: Synthesis and exfoliation of isocyanate-treated graphene oxide nanoplatelets. Carbon **44**, 3342–3347 (2006)
122. Hernandez, Y., Nicolosi, V., Lotya, M., Blighe, F.M., Sun, Z.Y., De, S., McGovern, I.T., Holland, B., Byrne, M., Gun'ko, Y.K., Boland, J.J., Niraj, P., Duesberg, G., Krishnamurthy, S., Goodhue, R., Hutchison, J., Scardaci, V., Ferrari, A.C., Coleman, J.N.: High-yield production of graphene by liquid-phase exfoliation of graphite Nat. Nanotechnol. **3**, 563–568 (2008)
123. (a) Li, G.L., Liu, G., Li, M., Wan, D., Neoh, K.G., Kang, E.T.: Organo- and water-dispersible graphene oxide−polymer nanosheets for organic electronic memory and gold nanocomposites. J. Phys. Chem. C **114,** 12742–12748 (2010). (b) Hill, C.M., Zhu, Y., Pan, S.: Fluorescence and electroluminescence quenching evidence of interfacial charge transfer in Poly (3-hexylthiophene): graphene oxide bulk heterojunction photovoltaic devices. ACS Nano **5**, 942–951 (2011)
124. Hamilton, C.E., Lomeda, J.R., Sun, Z., Tour, J.M., Barron, A.R.: High-yield organic dispersions of unfunctionalized graphene. Nano Lett. **9**, 3460–3462 (2009)
125. Economopoulos, S.P., Rotas, G., Miyata, Y., Shinohara, H., Tagmatarchis, N.: Exfoliation and chemical modification using microwave irradiation affording highly functionalized graphene. ACS Nano **4**, 7499–7507 (2010)
126. Khan, U., O'Neill, A., Lotya, M., De, S., Coleman, J.N.: High-concentration solvent exfoliation of graphene Small **6**, 864–871 (2010)
127. Cai, M., Thorpe, D., Adamson, D.H., Schniepp, H.C.: Methods of graphite exfoliation. J. Mater. Chem. **22**, 24992–25002 (2012)
128. Lotya, M., Hernandez, Y., King, P.J., Smith, R.J., Nicolosi, V., Karlsson, L.S., Blighe, F.M., De, S., Wang, Z., McGovern, I.T.: Liquid phase production of graphene by exfoliation of graphite in surfactant/water solutions. J. Am. Chem. Soc. **131**, 3611–3620 (2009)
129. Lotya, M., King, P., Khan, U., De, S., Coleman, J.N.: High-concentration, surfactant-stabilized graphene dispersions. ACS Nano **4**, 3155–3162 (2010)
130. Vadukumpully, S., Paul, J., Valiyaveettil, S.: Cationic surfactant mediated exfoliation of graphite into graphene flakes. Carbon **47**, 3288–3294 (2009)
131. Hasan, T., Torrisi, F., Sun, Z., Popa, D., Nicolosi, V., Privitera, G., Bonaccorso, F., Ferrari, A.C.: Solution-phase exfoliation of graphite for ultrafast photonics. Phys. Status Solidi B, **247**, 2953–2957 (2010)
132. Green, A.A., Hersam, M.C.: Solution phase production of graphene with controlled thickness via density differentiation. Nano Lett. **9**, 4031–4036 (2009)

133. De, S., King, P.J., Lotya, M., O'Neill, A., Doherty, E.M., Hernandez, Y., Duesberg, G.S.: Coleman JN Flexible, transparent, conducting films of randomly stacked graphene from surfactant-stabilized, oxide-free graphene dispersions. Small **6**, 458–464 (2010)
134. Englert, J.M., Rohrl, J., Schmidt, C.D., Graupner, R., Hundhausen, M., Hauke, F., Hirsch, A.: Soluble graphene: generation of aqueous graphene solutions aided by a perylenebisimide-based bolaamphiphile. Adv. Mater. **21**, 4265–4269 (2009)
135. Guardia, L., Fernandez-Merino, M.J., Paredes, J.I., Solis-Fernandez, P., Villar-Rodil, S., Martinez-Alonso, A., Tascon, J.M.D.: High-throughput production of pristine graphene in an aqueous dispersion assisted by non-ionic surfactants. Carbon **49**, 1653–1662 (2011)
136. Smith, R.J., Lotya, M., Coleman, J.N.: The importance of repulsive potential barriers for the dispersion of graphene using surfactants. New J. Phys. **12**, 125008 (2010)
137. Wang, X.Q., Fulvio, P.F., Baker, G.A., Veith, G.M., Unocic, R.R., Mahurin, S.M., Chi, M. F., Dai, S.: Direct exfoliation of natural graphite into micrometre size few layers graphene sheets using ionic liquids. Chem. Commun. **46**, 4487–4489 (2010)
138. Nuvoli, D., Valentini, L., Alzari, V., Scognamillo, S., Bon, S.B., Piccinini, M., Illescas, J., Mariani, A.: High concentration few-layer graphene sheets obtained by liquid phase exfoliation of graphite in ionic liquid. J. Mater. Chem. **21**, 3428–3431 (2011)
139. Widenkvist, E., Boukhvalov, D., Rubino, S., Akhtar, S., Lu, J., Quinlan, R., Katsnelson, M., Leifer, K., Grennberg, H., Jansson, U.: Mild sonochemical exfoliation of bromine-intercalated graphite: a new route towards graphene. J. Phys. D Appl. Phys. **42**, 112003 (2009)
140. Zhou, M., Tian, T., Li, X., Sun, X., Zhang, J., Cui, P., Tang, J., Qin, L.-C.: Production of graphene by liquid-phase exfoliation of intercalated graphite. Int. J. Electrochem. Sci. **9**, 810–820 (2014)
141. Lin, S., Dong, L., Zhang, J., Lu, H.: Room-temperature intercalation and $\sim$ 1000-fold chemical expansion for scalable preparation of high-quality graphene. Chem. Mater. **28**, 2138–2146 (2016)
142. Wang, F., Chen, G., Li, W., Wang, Y., Wang, C., Zhang, Y., Xia, Y.: Layer controllable graphene using graphite intercalation compounds with different stage numbers through li conversion reaction. Adv. Mater. Interfaces **3**(1–5), 1500496 (2016)
143. Zhang, Y., Liu, S., Wang, L., Qin, X., Tian, J., Lu, W., Chang, G., Sun, X.: One-pot green synthesis of Ag nanoparticles-graphene nanocomposites and their applications in SERS, H_2O_2, and glucose sensing. RSC Adv. **2**, 538–545 (2012)
144. Manikandan, M., Nasser Abdelhamid, H., Talib, A., Wu, H.-F.: Facile synthesis of gold nanohexagons on graphene templates in Raman spectroscopy for biosensing cancer and cancer stem cells. Biosens. Bioelectron. **55**, 180–186 (2014)
145. Anandan, S., Asiri, A.M., Ashokkumar, M.: Ultrasound assisted synthesis of Sn nanoparticles-stabilized reduced graphene oxide nanodiscs. Ultrason. Sonochem. **21**, 920–923 (2014)
146. Mondal, M.K., Banerjee, P.P., Saha, S.K., Chowdhury, P., Sengupta, A., Bandyopadhyay, A., Bhattacharya, S., Chattopadhyay, A.: Selective reduction technique (SRT): a robust method to synthesize bioactive Ag/Au doped graphene oxide. Mater. Des. **102**, 186–195 (2016)
147. Anandan, S., Manivel, A., Ashokkumar, M.: One-step sonochemical synthesis of reduced graphene oxide/Pt/Sn hybrid materials and their electrochemical properties. Fuel Cells **12**(6), 956–962 (2012)
148. Nandini, S., Nalini, S., Reddy, M.B.M., Suresh, G.S., Melo, J.S., Niranjana, P., Sanetuntikul, J., Shanmugam, S.: Synthesis of one-dimensional gold nanostructures and the electrochemical application of the nanohybrid containing functionalizedgraphene oxide for cholesterol biosensing. Bioelectrochemistry **110**, 79–90 (2016)
149. Bai, R.G., Muthoosamy, K., Zhou, M., Ashokkumar, M., Huang, N.M., Manickam, S.: Sonochemical and sustainable synthesis of graphene-gold (G-Au)nanocomposites for enzymeless and selective electrochemical detection of nitric oxide. Biosens. Bioelectron. **87**, 622–629 (2017)

150. Mondal, M.K., Banerjee, P.P., Saha, S.K., Chowdhury, P., Sengupta, A., Bandyopadhyay, A., Bhattacharya, S., Chattopadhyay, A.: Selective reduction technique (SRT): a robust method to synthesize bioactive Ag/Au doped grapheneoxide. Mater. Des. **102**, 186–195 (2016)
151. Neppolian, B., Wang, C., Ashokkumar, M.: Sonochemically synthesized mono and bimetallic Au–Ag reduced graphene oxide based nanocomposites with enhanced catalytic activity. Ultrason. Sonochem. **21**, 1948–1953 (2014)
152. Anandan, S., Grieser, F., Ashokkumar, M.: Sonochemical synthesis of Au–Ag core–shell bimetallic nanoparticles. J. Phys. Chem. C **112**, 15102–15105 (2008)
153. Okitsu, K., Cavalieri, F.: Synthesis of metal nanomaterials with chemical and physical effects of ultrasound and acoustic cavitation. In: Sonochemical Production of Nanomaterials. SpringerBriefs in Molecular Science. Springer, Cham (2018)
154. Zhao, G., Kui, L., Wang, X.: A brief review of graphene-based material synthesis and its application in environmental pollution management. Chin. Sci. Bull. **57**, 1223–1234 (2012)
155. Tong, L., Qiu, F., Zeng, T., Long, J., Yang, J., Wang, R., Zhang, J., Wang, C., Sun, T., Yang, Y.: Recent progress in the preparation and application of quantum dots/graphene composite materials RSC Adv. **7**, 47999–48018 (2017)
156. Upadhyay, R.K., Soin, N., Roy, S.S.: Role of graphene/metal oxide composites as photocatalysts, adsorbents and disinfectants in water treatment: a review. RSC Adv. **4**, 3823–3851 (2014)
157. Jeong, G.H., Baek, S., Lee, S., Kim, S.-W.: Metal oxide/graphene composites for supercapacitive electrode materials. Chem. Asian J. **11**, 949 (2016)
158. Hu, C., Lu, T., Chen, F., Zhang, R.: A brief review of graphene–metal oxide composites synthesis and applications in photocatalysis. J. Chin. Adv. Mater. Soc. **1**(1), 21–39 (2013)
159. Majumdar, D., Baugh, N., Bhattacharya, S.K.: Ultrasound assisted formation of reduced graphene oxide-copper (II) oxide nanocomposite for energy storage applications. Colloids Surf. A **512**, 158–170 (2017)
160. Majumdar, D., Bhattacharya, S.K.: Sonochemically synthesized hydroxy-functionalized graphene–MnO_2 nanocomposite for supercapacitor applications. J. Appl. Electrochem. **47** (7), 789–801 (2017)
161. Bonaccorso, F., Lombardo, A., Hasan, T., Sun, Z., Colombo, L., Ferrari, A.C.: Production and processing of graphene and 2d crystals. Mater. Today **15**(12), 564–589 (2012)
162. Khan, M., Tahir, M.N., Adil, S.F., Khan, H.U., Rafiq, M., Siddiqui, H., Al-warthan, A.A., Tremel, W.: Graphene based metal and metal oxide nanocomposites: synthesis, properties and their applications. J. Mater. Chem. A **3**, 18753–18808 (2015)
163. Khedekar, V.V., Zaeem, M.S., Das, S.: Graphene-metal oxide nanocomposites for supercapacitors: a perspective review. Adv. Mater. Lett. **9**, 02–19 (2018)
164. Xia, Y., Li, R., Chen, R., Wang, J., Xiang, L.: (2018) 3D architectured graphene/metal oxide hybrids for gas sensors: a review. Sensors (Basel) **18**(5), 1456 (2018)
165. Dhand, V., Rhee, K.Y., Kim, H.J., Jung, D.H.: A comprehensive review of graphene nanocomposites: research status and trends. J. Nanomater. Article ID 763953, 14. https://doi.org/10.1155/2013/763953 (2013)
166. Majumdar, D., Maiti, R.P., Basu, S., Saha, S.K.: Mechanism of ultrasonic energy-assisted formation of V-, Y-shaped nano-structures in conjugated polymers. J. Nanosci. Nanotechnol. **9**, 6896–6901 (2009)
167. Tabata, M., Miyazawa, T., Kobayashi, O., Sohma, J.: Direct evidence of main-chain scissions induced by ultrasonic irradiation of benzene solutions of polymers. Chem. Phys. Lett. **73**, 178–180 (1980)
168. Gronroos, A., Pirkonen, P., Heikkinen, J., Ihalainen, J., Mursunen, H., Sekki, H.: Ultrasonic depolymerization of aqueous polyvinyl alcohol. Ultrason. Sonochem. **8**, 259–264 (2001)
169. (a) Xu, H., Suslick, K.S.: Sonochemical preparation of functionalized graphenes. J. Am. Chem. Soc. **133**, 9148–9151 (2011). (b) Lee, K.G., Jeong, J.M., Lee, S.J., Yeom, B., Lee, M.K., Choi, B.G.: Sonochemical assisted synthesis of 3D graphene/nanoparticle foams and their application in supercapacitor. Ultrason. Sonochem. **22**, 422–428 (2015)

170. Shen, B., Zhai, W., Lu, D., Wang, J., Zheng, W.: Ultrasonication-assisted direct functionalization of graphene with macromolecules. RSC Adv. **2**, 4713–4719 (2012)
171. Shen, J., Hu, Y., Li, C., Qin, C., Ye, M.: Synthesis of amphiphilic graphene nanoplatelets. Small **5**(1), 82–85 (2009)
172. Li, M., Gao, C., Hu, H., Zhao, Z.: Electrical conductivity of thermally reduced graphene oxide/polymer composites with a segregated structure. Carbon **65**, 371–373 (2013)
173. Araby, S., Meng, Q., Zhang, L., Kang, H., Majewski, P., Tang, Y., Ma, J.: Electrically and thermally conductive elastomer/graphene nanocomposites by solution mixing. Polymer **55**, 201–210 (2014)
174. Bian, J., Wei, X.W., Lin, H.L., Gong, S.J., Zhang, H., Guan, Z.P.: Preparation and characterization of modified graphite oxide/poly(propylene carbonate) composites by solution intercalation. Polym. Degrad. Stab. **96**, 1833–1840 (2011)
175. Fawaz, J., Mittal, V.: Synthesis of polymer nanocomposites: review of various techniques in the book synthesis techniques for polymer nanocomposites, 1st edn. In: Mittal, V. (ed.) © 2015Wiley-VCH Verlag GmbH & Co. KGaA. Published by Wiley-VCH Verlag GmbH & Co. KGaA (2015)
176. Li, Y., Umer, R., Samad, Y.A., Zheng, L., Liao, K.: The effect of the ultrasonication pre-treatment of graphene oxide (GO) on the mechanical properties of GO/polyvinyl alcohol composites. Carbon **55**, 321–327 (2013)
177. Patil, V., Dennis, R.V., Rout, T.K., Banerjee, S., Yadav, G.D.: Graphene oxide and functionalized multi walled carbon nanotubes as epoxy curing agents: a novel synthetic approach to nanocomposites containing active nanostructured fillers. RSC Adv. **4**, 49264 (2014)
178. Majumdar, D., Baskey, M., Saha, S.K.: Epitaxial growth of crystalline polyaniline on reduced graphene oxide. Macromol. Rapid Commun. **32**, 1277–1283 (2011)
179. Dong, Q., Wang, G., Hu, H., Yang, J., Qian, B., Ling, Z., Qiu, J.: Ultrasound-assisted preparation of electrospun carbon nanofiber/graphene composite electrode for supercapacitors. J. Power Sources **243**, 350–353 (2013)
180. Chen, J., Zheng, X., Miao, F., Zhang, J., Cui, X., Zheng, W.: Engineering graphene/carbon nanotube hybrid for direct electron transfer of glucose oxidase and glucose biosensor. J. Appl. Electrochem. **42**(10), 875–888 (2012)
181. Tung, V.C., Huang, J.H., Tevis, I., Kim, F., Kim, J., Chu, C.W., Stupp, S.I., Huang, J.: Surfactant-free water-processable photoconductive all-carbon composite. J. Am. Chem. Soc. **133**, 4940–4947 (2011)
182. (a) Gan, T., Hu, C., Sun, Z., Hu, S.: Facile synthesis of water-soluble fullerene–graphene oxide composites for electrodeposition of phosphotungstic acid-based electrocatalysts. Electrochim. Acta **111**, 738–745 (2013). (b) Gan, T., Hu, C., Hu, S.: Preparation of graphene oxide–fullerene/phosphotungstic acid films and their application as sensor for the determination of cis-jasmone Anal. Methods **6**, 9220–9227 (2014)
183. Zhang, H., Lv, X., Li, Y., Wang, Y., Li, J.: P25-graphene composite as a high performance photocatalyst. ACS Nano **4**(1), 380–386 (2010)
184. Thirumalraj, B., Palanisamy, S., Chen, S.M., Yang, C.Y., Periakaruppan, P., Lou, B.S.: Direct electrochemistry of glucose oxidase and sensing of glucose at a glassy carbon electrode modified with a reduced graphene oxide/fullerene-C60 composite. RSC Adv. **5**, 77651–77657 (2015)
185. Thirumalraj, B., Palanisamy, S., Chen, S.M., Lou, B.S.: Preparation of highly stable fullerene C60 decorated graphene oxide nanocomposite and its sensitive electrochemical detection of dopamine in rat brain and pharmaceutical samples. J. Colloid Interface Sci. **462**, 375 (2016)
186. Garrido, M., Calbo, J., Pérez, L.R., Arago, J., Ort, E., Herranz, M., Martın, N.: Non-covalent graphene nanobuds from mono- and tripodal binding motifs. Chem. Commun. **53**, 12402 (2017)

187. Song, P., Liu, L., Huang, G.B., Yu, Y.M., Guo, Q.P.: Largely enhanced thermal and mechanical properties of polymer nanocomposites via incorporating C60@graphene nanocarbon hybrid. Nanotechnology **24**, 505706 (2013)
188. Fathyunes, L., Khalil-Allafi, J.: Characterization and corrosion behavior of graphene oxide-hydroxyapatite composite coating applied by ultrasound-assisted pulse electrodeposition. Ceram. Int. **43**(16), 13885–13894 (2017)
189. Fathyunes, L., Khalil-Allafi, J., Sheykholeslami, S.O.R., Moosavifar, M.: Biocompatibility assessment of graphene oxidehydroxyapatite coating applied on TiO_2 nanotubes by ultrasound-assisted pulse electrodeposition. Mater. Sci. Eng., C **87**, 10–21 (2018)
190. Mungondori, H.H., Mtetwa, S., Tichagwa, L., Katwire, D.M., Nyamukamba, P.: Synthesis and application of a ternary composite of clay, saw-dust and peanut husks in heavy metal adsorption. Water Sci. Technol. **75**(10), 2443–2453 (2017)
191. Azman, N.H.N., Mamat@Mat Nazir, M.S., Ngee, L.H., Sulaiman, Y.: Graphene-based ternary composites for supercapacitors. Int. J. Energy Res. **42**, 2104–2116 (2018)
192. Chen, Y., Sun, H., Peng, W.: 2D transition metal dichalcogenides and graphene-based ternary composites for photocatalytic hydrogen evolution and pollutants degradation. Nanomaterials **7**, 62 (2017)
193. Hermán, V., Takacs, H., Duclairoir, F., Renault, O., Tortai, J.H., Viala, B.: Core double–shell cobalt/graphene/polystyrene magnetic nanocomposites synthesized by in situ sonochemical polymerization. RSC Adv. **5**, 51371–51381 (2015)
194. Wang, D., Kou, R., Choi, D., Yang, Z., Nie, Z., Li, J., Saraf, L.V., Hu, D., Zhang, J., Graff, G.L., Liu, J., Pope, M.A., Aksay, I.A.: Ternary self-assembly of ordered metal oxidegraphene nanocomposites for electrochemical energy storage. ACS Nano **4**(3), 1587–1595 (2010)
195. Kim, M., Kang, H., Park, K.H.: Pd nanoparticles supported on Fe_3O_4@amine-functionalized graphene composite and catalytic performance in Sonogashira cross-coupling reactions. Catal. Commun. **72**, 150–155 (2015)
196. Masjedi-Arani, M., Salavati-Niasari, M.: Ultrasonic assisted synthesis of a nano-sized Co_2SnO_4/graphene: a potential material for electrochemical hydrogen storage application. Int. J. Hydrogen Energy **43**(9), 4381–4392 (2018)
197. Ali, A., Oh W.-C.: Ultrasonic synthesis of $CoSe_2$-Graphene-TiO_2 ternary composites for high photocatalytic degradation performance. J. Korean Ceram. Soc. **54**(3), 205–210 (2017)
198. Arvidsson, R., Molander, S., Sandén, B.A.: Review of potential environmental and health risks of the nanomaterial graphene. Hum. Ecol. Risk Assess. **19**(4), 873–887 (2013)
199. Zheng, X.T., Ananthanarayanan, A., Luo, K.Q., Chen, P.: Glowing graphene quantum dots and carbon dots: properties, syntheses, and biological applications. Small **11**(1613–6829 (Electronic)), 1620–1636 (2015)
200. Caffo, M., Merlo, L., Marino, D., Caruso, G.: Graphene in neurosurgery: the beginning of a new era. Nanomed. **10**, 615–625 (2015)
201. Wu, S.Y., An, S.S., Hulme, J.: Current applications of graphene oxide in nanomedicine. Int. J. Nanomed. **10**(Spec Iss), 9–24 (2015)
202. Tonelli, F.M., Goulart, V.A., Gomes, K.N., Ladeira, M.S., Santos, A.K., Lorencon, E., Lo, Ladeira, Resende, R.R.: Graphene-based nanomaterials: biological and medical applications and toxicity. Nanomedicine **10**(15), 2423–2450 (2015)
203. Zhou, R., Gao, H.: Cytotoxicity of graphene: recent advances and future perspective. Wiley Interdiscip. Rev. Nanomed. Nanobiotechnol. **6**(5), 452–474 (2014)
204. Ema, M., Hougaard, K.S., Kishimoto, A., Honda, K.: Reproductive and developmental toxicity of carbon-based nanomaterials: a literature review. Nanotoxicology **10**, 391–412 (2015)
205. Sanchez, V.C., Jachak, A., Hurt, R.H., Kane, A.B.: Biological interactions of graphene-family nanomaterials: an interdisciplinary review. Chem. Res. Toxicol. **25**(1), 15–34 (2012)

206. Lee, J.H., Han, J.H., Kim, J.H., Kim, B., Bello, D., Kim, J.K., Lee, G.H., Sohn, E.K., Lee, K., Ahn, K., Faustman, E.M., Yu, I.J.: Exposure monitoring of graphene nanoplatelets manufacturing workplaces. Inhal. Toxicol. **28**(6), 281–291 (2016)
207. Maynard, R.L.: Nano-technology and nano-toxicology. Emerg. Health Threats J. **5**. https://doi.org/10.3402/ehtj.v5i0.17508 (2012)
208. Ou, L., Song, B., Liang, H., Liu, J., Feng, X., Deng, B., Sun, T., Shao, L.: Toxicity of graphene-family nanoparticles: a general review of the origins and mechanisms. Part. Fibre Toxicol. **13**, 57 (2016)
209. Yang, K., Gong, H., Shi, X., Wan, J., Zhang, Y., Liu, Z.: In vivo biodistribution and toxicology of functionalized nano-graphene oxide in mice after oral and intraperitoneal administration. Biomaterials **34**(11), 2787–2795 (2013)
210. Ding, Z., Zhang, Z., Ma, H., Chen, Y.: In vitro hemocompatibility and toxic mechanism of graphene oxide on human peripheral blood T lymphocytes and serum albumin. ACS Appl. Mater. Interf. **6**(22), 19797–19807 (2014)
211. Chang, Y., Yang, S.T., Liu, J.H., Dong, E., Wang, Y., Cao, A., Liu, Y., Wang, H.: Invitro toxicity evaluation of graphene oxide on A549 cells. Toxicol. Lett. **200**(3), 201–210 (2011)

Sonochemically Covalent Functionalized Graphene Oxide Towards Photoluminescence and Nanocytotoxicity Activities

Gopal Avashthi, Shrikant S. Maktedar and Man Singh

Abstract The greener mechanistic cavitation method has been applied for synthesis of graphene oxide (GrO) based functionalized materials. The GrO functionalization with various amine substituted heterocyclic moieties (ASHM) have an emerging technology towards biomedical processing of graphene. Hence, an ultrasound energy has been applied for GrO functionalization with 2-Amino-1,3,4-thidiazole (ATDZ) to synthesize Covalent functionalized product f-(ATDZ) GrO. Structural investigations have confirmed the covalent functionalization (CF) of GrO to synthesize f-(ATDZ)GrO. The structure of f-(ATDZ)GrO has confirmed with Fourier-transform infrared spectroscopy (FTIR), ultraviolet–visible spectroscopy (UV), RAMAN, X-ray diffraction (XRD), thermogravimetric analysis (TGA)/differential thermal analysis (DTA)/Differential thermal Gravimetry (DTG), Dynamic Light Scattering (DLS), high-resolution transmission electron microscopy (HRTEM), selected area electron diffraction (SAED), atomic force microscopy (AFM), scanning electron microscopy (SEM). The structural insights provide a mechanistic understanding of functional expression, through the contribution of atomic domains (CAD). TGA of f-(ATDZ)GrO validates total percentage weight loss of 95.5% at 198.17 °C. Thermal stability of f-(ATDZ)GrO as temperature aspects also certified an exothermic curve obtained with DTA. The calculated PL band gap of 3.87 eV in noncompatible f-(ATDZ)GrO is indicating towards biosensing applications. In extension of functionalization series of GrO with heterocyclic derivative, the cytotoxicity of f-(ATDZ)GrO has evaluated with Sulforhodamine B (SRB) assay to living cells, HaCaT and Vero cell lines. The average estimated cell viabilities have observed ~91.575% with HaCaT cell lines over a wide concentration range of 10–80 μg mL^{-1}. The high cytocompatibility of f-(ATDZ)GrO has further extent with Vero cell lines of ~36.825%

G. Avashthi · S. S. Maktedar · M. Singh (✉)
School of Chemical Sciences, Central University of Gujarat, Gandhinagar 382030, India
e-mail: mansingh50@hotmail.com

G. Avashthi
e-mail: gopalavashthi@gmail.com

S. S. Maktedar
e-mail: shrikantmaktedar@gmail.com

A. Khan et al. (eds.), *Graphene Functionalization Strategies*,
Carbon Nanostructures, https://doi.org/10.1007/978-981-32-9057-0_4

biocompatibility. However, the morphological effect on HaCaT cell line and some extinct significant with Vero have evidently confirmed that higher cytocompatibility of f-(ATDZ)GrO can be explore for the cytocompatibility as Nanotoxicity aspects. Therefore, f-(ATDZ)GrO appeared as an advanced material which can be further used for development of various biomedical applications.

Keywords Graphene oxide · Covalent functionalization · 2-Amino-1,3,4-thidiazole · HaCaT and vero · Cytocompatibility · Photoluminescence activity

1 Introduction

Recently, the processability of GrO based materials are a challenge in biological field due to its solubility and stability. But the unique properties of 21st century materials, have been opened the door for designing functional nanomaterials for biomedical applications. Several potential properties like high surface area, light weight, thinnest material, high mechanical strength [1–7] graphene is not easy to apply for biomedical applications due to its high thermal stability and poor processability. Therefore, development of GrO based advanced functional material has emerged as a decisive solution for biomedical applications of graphene [8–21]. Although, there are lot of parameters like degree of oxidation, electronic constituents of functionalized GrO, dosage, size and time of exposure consider for the nanotoxicity of the graphene-based materials [22–24]. The flexibility of the graphene and graphene oxide are expected to rise and develop in various form of its derivatives and can be explore in biomedical tissue engineering field in future. In previous few years the Scientific community proves the strength of graphene in biomedical applications but lot of studies are necessary to reach at much more efficient level [25–27]. The enhanced dispersibility of functional graphene materials facilitates its smooth processability in various organic solvents. However, water assisted formulation of the graphene-based nanomaterials enhance the physiological stability, solubility and to act as an efficient chemotherapeutic agent [28]. Therefore, surface modification of graphene is essentially required for biomedical applications [29–36]. Even, the electrochemical based synthesized highly featured oxygen and nitrogen doped graphene quantum dots explored for the various potential applications for the cytotoxicity investigation [37]. The hetero atomic domains like oxygen and nitrogen over graphene surface, cause mechanistic structural changes of the cells and revealing its potency in biological applications and thermally stable nanocomposite synthesis [38–41].

The conventional wet functionalization of graphene has been extensively known for enhancing functionality of graphene-based materials [42–44]. A cost-effective graphite (Gt) has been used as starting material for chemical twisting of graphene edges, with same problem of stability and solvent processability. Therefore, Gt is chemically modified into graphite oxide (GtO) and then an ultrasound irradiation

facilitates the process of exfoliation for the preparation of GrO. The surplus oxygen containing functionalities confirms the suitability of GrO for chemical functionalization and used as a precursor for graphene functionalization [45–47]. The surface functionalization of GrO completely avoided the use of the hazardous acylating and coupling reagents. However, several efforts have been effectively known for biological applications of GrO based materials including in vitro cytotoxicity [48–55]. Therefore, the present studies have successfully reported the formation of f-(ATDZ) GrO through robust sonochemical approach. The as-prepared f-(ATDZ)GrO was further evaluated towards biomedical applications through cytotoxicity profile at nano level. The higher cell viabilities have confirmed the lower toxicity and hence an excellent cytocompatibility of f-(ATDZ)GrO. The thermal studies have confirmed, stability of f-(ATDZ)GrO w.r.t. to temperature (T) as compared to GrO, due to the presence of a surplus oxygen containing functionalities and destabilizing structural electronic domains. However, f-(ATDZ)GrO has shown an enhanced thermal stability w.r.t to T due to covalent attachment of ATDZ over GrO surface. Therefore, the suitability of f-(ATDZ)GrO has confirmed for thermally stable biocompatible coatings. The synergistic impact of various functionalities over f-(ATDZ)GrO surface, have mechanistically confirmed through the contribution of atomic domains (CAD). Hence, f-(ATDZ)GrO is truly emerging as an advanced functional material for biomedical applications.

2 Experimental Section

2.1 Materials

Graphite (Gt) flakes, conc. sulphuric acid (97%), phosphoric acid (>85 wt% in H_2O), concentrated hydrogen chloride, 2-Amino-1,3,4-thidiazole (97%), were purchased from Sigma-Aldrich Co. 30% hydrogen peroxide was procured from S.D Fine chemicals. Analytical grade potassium permanganate was purchased from Rankem. Absolute alcohol was procured from Scvuksmandli Ltd. India. All chemicals were used without further purification.

2.2 Synthesis of GrO

The GtO has been efficiently prepared with certain modifications by improved oxidation process [45]. Gt flakes have oxidized by using mixture of concentrated H_2SO_4/H_3PO_4 in 9:1 ratio (180:20 mL), was poured into 500 mL RB flask containing a mixture of graphite flakes (1.5 g) and $KMnO_4$ (9.0 g), producing a slight exotherm to up to 40 °C. The exotherm heat was controlled and cooled to RT. The oil bath setup was heated to 50 °C on magnetic hot plate stirrer. The reaction was

performed by keeping the RB flask with reaction mixture, inside oil bath and heated and reflux at 50 °C with constantly 12 h stirring. After completion of the reaction, the reaction mixture was cooled to RT and mixed onto ice water (~ 200 mL) with H_2O_2 (1.5 mL). The washing of reaction mixture was performed for removal of impurities by centrifugation at 8000 rpm for 15 min each. Stepwise washing, to separate solid sediments of reacted materials and supernatant possess inorganic salts, were decanted away from the sediment. The complete washing of solid sediment is accomplished by repeating two times and each wash is completed by successively with 200 mL of distilled water to remove the water-soluble component, 150 mL HCl to remove the minerals, and 100 mL ethanol to remove the organic soluble components. The sediments were centrifuged at 8000 rpm for 15 min for each wash and supernatant was decanted away. Hence, complete washed materials were obtained after multiple washing. The solid cake like brownish purified material was coagulated in 100 mL of ether and poured in Petri dish and vacuum-dried for 12 h at 50 °C. The synthesized brown colored solid GtO is generally known for precursor of well-oxidized exfoliated GrO [45–47] 180 min intense ultrasound irradiation has been applied for the exfoliation of GtO into GrO. Hence, the homogeneously dispersed GrO solution was directly used as a precursor for chemical functionalization with ATDZ under ultrasound irradiation.

2.3 Synthesis of f-(ATDZ)GrO

In continuation of synthesizing series of f-GrO with metal free ASHM, and further these were explored for the cytocompatibility study [53, 54]. The as-prepared GrO is directly used for chemical functionalization. The kinetically active homogeneous dispersion of GrO facilitates the enhance kinetic energy to lowered the activation energy in process of direct chemical functionalization through physical and chemical effects of an ultrasound irradiation. To obtain homogenous dispersion of GrO, 1 mg/mL conc. in ethanol is used for exfoliation. The 0.04 g GtO in 40 mL ethanol was subjected to intense ultrasonic treatment with Oscar ultrasonic (Microclean-103) for 3 h. The ultrasound energy reinforces the dispersion of GtO into homogenize GrO. The mechanochemical energy enhances the chemical reactivity of GrO and develops light brown colored dispersion. The 0.2 g ATDZ is added directly to the reaction mixture, which are set under the ultrasound bath. The reaction takes place in 15 min. After addition of ATDZ to GrO indicates a formation of the dark brown colored agglomerate. The f-(ATDZ)GrO was washed batch wise thrice with 20 mL of ethanol and centrifuged at 8000 rpm for 15 min. for each wash. The obtained functionalized material was dried at 50 °C under vacuum for 24 h. The structural investigations have confirmed the covalent attachment of ATDZ over GrO surface.

2.4 Nanocytotoxicity Evaluation

Nanocytotoxicity evaluation was completed with cell line study by growing in RPMI 1640 medium with fetal bovine serum (10%) and L-glutamine (2 mM). For initial screening, the inoculated cells into 96 microtiter plates of 100 μL coating densities were studied, as contingent on repetition of distinct cell lines. After cell inoculation, the microtiter plates were incubated at 37 °C, 5% CO_2, 95% air and 100% comparative humidity for 24 h before to addition of experimental drugs. Experimental drugs were initially solubilized in dimethyl Sulfoxide (DMSO) at 100 mg/ml and diluted to 1 mg/mL using water and kept ice-covered prior to practice. During drug addition, an aliquot of ice-freeze concentrate (1 mg/mL) was liquified and diluted up to 100, 200, 400 and 800 μg/mL in whole medium, containing test sample. The microtiter wells were added by a portion of 10 μL of dissimilar drug dilutions which, already containing 90 μL in medium, resulting in the required final drug concentrations i.e. 10, 20, 40 and 80 μg/mL. After the addition of compound, plates were incubated at normal lab condition for 48 h and the assay was terminated by the addition of cold trichloroacetic acid (TCA). Cells were secure in situ by the moderate addition of 50 μL of cold 30% (w/v) TCA (final conc., 10% TCA) and incubated for 1 h at 4 °C. The supernatant was decanted away and plates were cleaned several times with water, followed by air drying. Sulforhodamine B (SRB) solution (50 μL) at 0.4% (w/v) in 1% acetic acid has supplied to each well, and plates were incubated for 20 min. at room temperature. After completion of staining, unstained dye was isolated and the residual dye was removed by washing five times with 1% acetic acid. Further, the plates were air dried. 10 mM trizma base was used to eluate the bound stain successively and absorbance (A) was distinguished on a plate scale at 540 nm with 690 nm reference wavelength. Percent growth (PG) was analyzed on a plate-by-plate serial basis for wells testing relative to control wells. PG was stated as the proportion of average A of test well to the average A of control wells *100. Using six A measurements [control growth (CG), test growth (TG) and time zero (TZ) in occurrence of article drug at four concentration dose (Ti)], the PG was observed at each drug concentration levels. The PG inhibition was calculated as:

$$[\mathrm{Ti}/\mathrm{C}] \times 100\%$$

2.5 Characterization Techniques

The synthesis of GrO and f-(ATDZ)GrO were carried out with REMI 1MLH magnetic stirrer with a hot plate and Oscar ultrasonic sonicator (Microclean-103). The purification was carried with Eltek centrifuge, MP 400. The various functional groups over GrO and f-(ATDZ)GrO were identified with Perkin Elmer Spectrum 65 FTIR. The surface morphology and electronic diffraction pattern was observed with

HRTEM (FEI Model Tecnai G2 S Twin) and SAED patterns which is supported by UV/Vis spectrophotometer (Spectro 2060 plus model). The Raman spectra of samples were recorded with Horiba HR 800 instrument with 480 nm Ar laser. The thermal properties were carried out under N_2 ambient, measured with EXSTAR TG/DTA 7300 analyzer. The X-ray diffraction spectra were recorded in the range of 5°–80° on D8 Advance instrument. The topographical analyses were carried out with AFM in non-contact mode. The SEM analysis was performed on Carl-Zeiss Evo-18 instrument. The particle size and homogenous dispersion were investigated by Dynamic Light Scattering (DLS, Microtrac, Zetatrac, U2771). The all characteristics investigations were carried out with reference to GrO [39].

3 Results and Discussion

The ultrasound assisted functionalization of GrO is explored to develop advanced materials in various challenging technological field. Hence, the amine substituted organic moieties have many advantage in biological field. The functionalization of GrO with ASHM can be explore for the enhance their activity due to synergistic impact by involvement of extra electronic domains as a whole. The amide bond formation is stabilized the carboxyl functionality over GrO surface after functionalization, and functionalized product is more stabilized as whole, which is more applicable to show their activity against the thermophile organism. But sometimes, the electronic strain of organic frame also plays a contrary role as a stabilization perspective. In this contest, ultrasound energy is used a greener route to functionalize GrO with ATDZ into f-(ATDZ)GrO. The f-(ATDZ)GrO possesses amide bond in functionalization with GrO through in situ ester mechanism (Scheme 1), which is further explored for their structural investigation, thermal stability behavior than GrO and their biological activity.

3.1 Structural Investigation

The covalent attachment of ATDZ on GrO surface has been confirmed with FTIR spectroscopy (Fig. 1). The FTIR spectra of f-(ATDZ)GrO comprises with a characteristic peak for amide at $\sim$1640 cm^{-1} with $\sim$80% transmittance, which is absent in GrO [39], confirms the formation of covalent functionalized amide bond on GrO surface. However, FTIR spectrum of f-(ATDZ)GrO shows multifunctional groups besides the amide bond. The characteristic peaks for these functionalities are observed at 3352 cm^{-1} (–OH), 1072 cm^{-1} (C–O–C), and 1736 cm^{-1} (C = O).

The UV-Vis absorbance spectrum of ATDZ and f-(ATDZ)GrO is shown in Fig. 2. The spectrum of GrO shows two types of transitions, a sharp transition peak at 230 nm, was attributed to $\pi \rightarrow \pi^*$ transition of C=C bond. The second broad peak at 300 nm corresponds to $n \rightarrow \pi^*$ transition of C=O bond [39]. These

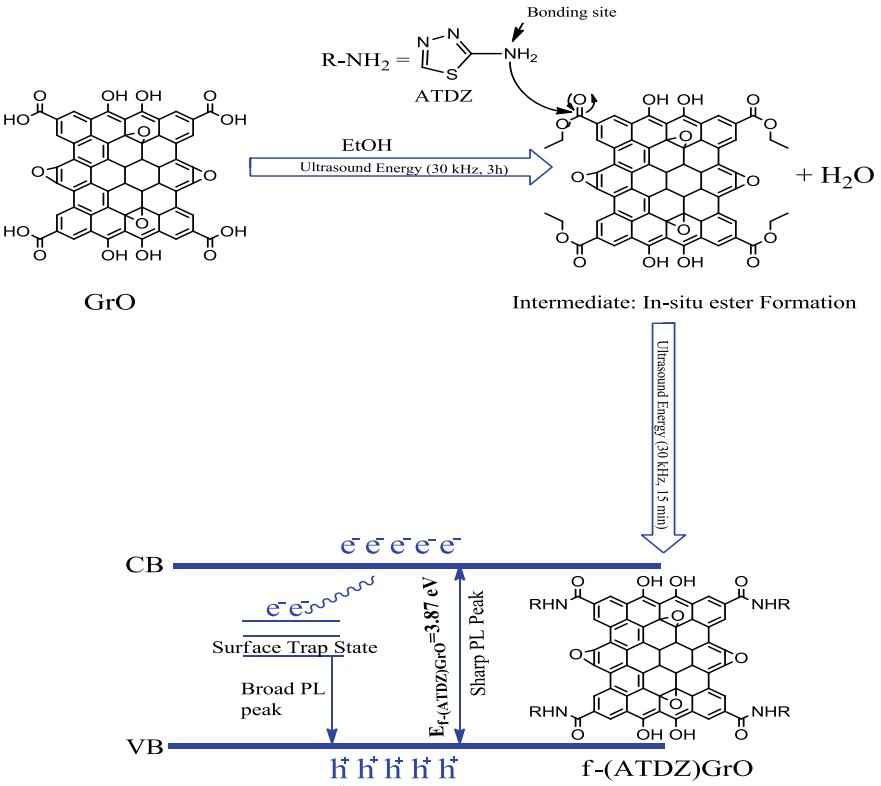

Scheme 1 Functionalization of GrO with ATDZ through in-situ esterification mechanism

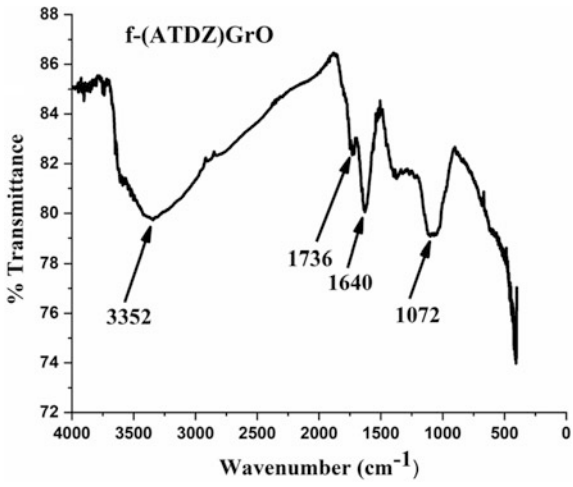

Fig. 1 FTIR spectrum of f-(ATDZ)GrO

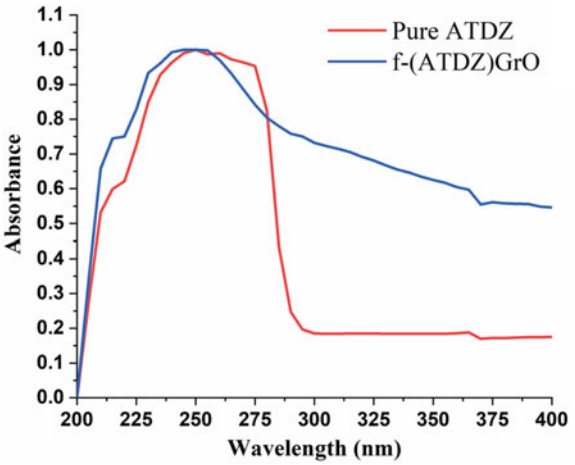

Fig. 2 Comparative spectrum of pure ATDZ and f-(ATDZ)GrO

investigations suggest the higher degree of oxidation and presence of oxygen functionality over the graphene surface. Further, UV-Vis absorbance spectrum of f-(ATDZ)GrO is observed broad peak at 245 nm, which has similarity like pure ATDZ and another broad hump like peak at 295 nm. The bathochromic shift at 245 nm confirms the enhancing the conjugation and restoration of π electron due to covalent functionalization of GrO with ATDZ. Therefore, UV-Vis spectrum of f-(ATDZ)GrO has confirmed the covalent bond formation of ATDZ onto the surface of GrO via amide bond.

Structural defects of GrO and f-(ATDZ)GrO were analyzed with Raman spectroscopy. The characteristic D and G peaks in Raman spectra of GrO is observed at 1359 and 1596 Cm^{-1} respectively with D/G ratio 0.85, which confirms the larger defects in crystal lattice [39]. The distinctive D peak is observed for sp^3 hybridized carbon, which agrees to A_{1g} symmetry and G peak corresponds to the graphitic carbon of E_{2g} symmetry. The D and G peak in f-(ATDZ)GrO is observed at 1367 and 1581 Cm^{-1} respectively (Fig. 3). The calculated D/G ratio is equal to 0.86, which shows more defects in f-(ATDZ)GrO than GrO. Hence, the presence of wider peak and larger defects in D peak at 1367 is supported for the covalent functionalization of ATDZ with GrO into a defective f-(ATDZ)GrO. To break up the thermal stability of the f-(ATDZ)GrO must have low enthalpy and it was confirmed by DTA as an exothermic reaction.

The powder XRD were examined with Cu Kα radiations λ = 1.54 A° run with 40 kV voltage and 30 mA cathodic current. The spectra have taken in range of 5°–80° at 0.01 degree/s scan rate. The hexagonal Gt flakes PDF 00-025-0284 is used as precursor for the synthesis of GrO followed by its functionalization with ATDZ. A sharp 2θ peak at 26.28 corresponding to (002) plane having interlayer spacing 3.38 A° is observed. The Powder XRD pattern of GrO is observed of (002) plane at 2θ of 10.54 A° with interlayer spacing 8.38 A° [39]. The XRD of f-(ATDZ)GrO (Fig. 4) validates two diffraction peak at 10.1132 and 24.0075 with their relative

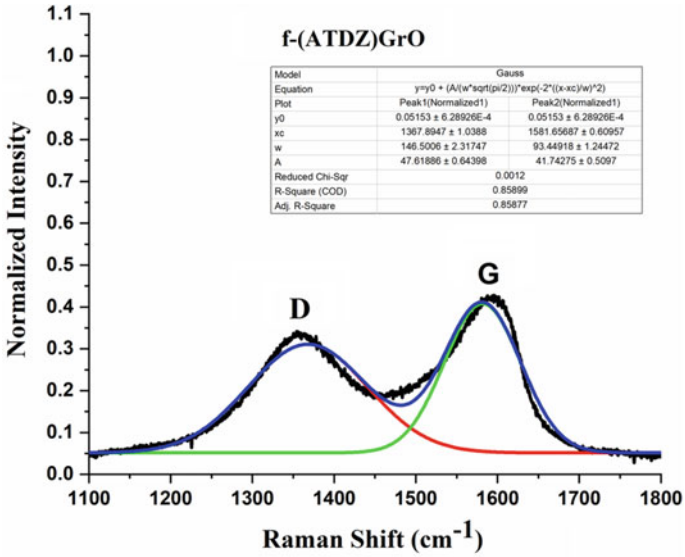

Fig. 3 Raman spectrum of f-(ATDZ)GrO

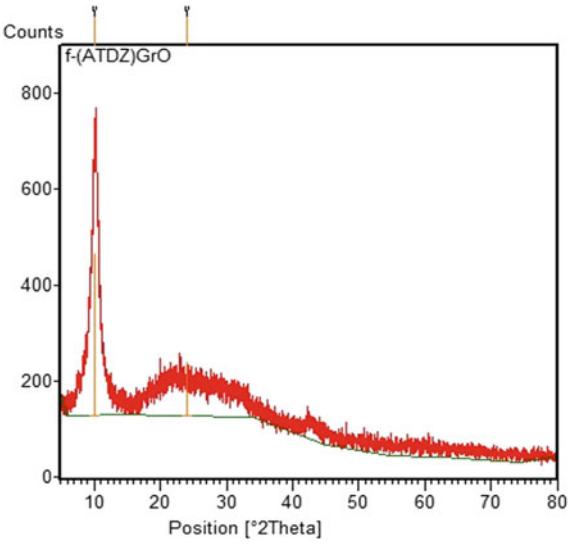

Fig. 4 Powder XRD of f-(ATDZ)GrO

intensity 100 and 34.02% respectively (Table 1). A diffraction peak at 10.1132 in XRD pattern of f-(ATDZ)GrO is observed due to reflection from (002) plane. The shift in the position of diffraction peak as compared to starting materials infers the formation of f-(ATDZ)GrO. However, the d-spacing of f-(ATDZ)GrO is found to be 8.73949 and 3.70379 A° for both peak respectively. The enhanced value of

Table 1 XRD analysis of f-(ATDZ)GrO

Sample	No. of peak	Position ($2\theta°$)	d-spacing (A°)	Relative intensity (%)	FWHM ($2\theta°$)	Area (cts. **$2\theta°$)	Height (cts.)
f-(ATDZ) GrO	1	10.1132	8.73949	100.00	3.5255	1001.66	336.64
	2	24.0075	3.70379	34.02	4.0000	385.80	114.51

d-spacing as compared to GrO infers the covalent functionalization of ATDZ on GrO surface. The FWHM of f-(ATDZ)GrO was 3.5255 and 4.0000 for both peaks respectively. Therefore, the formation of f-(ATDZ)GrO has confirmed with XRD.

The thermal profile of f-(ATDZ)GrO has been studied with TGA, DTA and DTG. The investigations of mass loss as a function of temperature infers the thermal decomposition and its stability. Nitrogen (Industrial grade) at a 100 mL/min has been used for the measurements with a slow ramp of 10 °C/min in range of 50–600 °C. TGA comparison of f-(ATDZ)GrO is depicted in Fig. 5a. Almost a complete single stage mass loss ∼95.50% has been observed at near 198.17 °C for f-(ATDZ)GrO. While GrO shows single stage decomposition 88.51% at 197.7 °C with significant mass loss due to labile oxygen functionality over the GrO surface [39]. TGA curve specifies rapid mass loss start just above room temperature (RT). The effective mass loss for f-(ATDZ)GrO was found near 198.17 °C and total % wt. loss was ∼95.50%, due to the elimination of thermally labile oxygen containing groups along with the highly strained amine substituted heterocyclic based organic based moieties functionalized with the GrO. 95.5% wt. loss of f-(ATDZ)GrO infers its little significant higher thermal stability at 198.17 °C than GrO at 197.7 °C. The higher mass loss of f-(ATDZ)GrO at 198.17 °C with generation of highly strain and destabilized electronic environment of functionalized product as a whole. The DTA curve at 198.17 °C confirms the exothermic behavior of the f-(ATDZ)GrO and it support for the thermodynamically feasibility for the decomposition of the highly strained f-(SA)GrO at 198.17 °C (Fig. 5b). Hence, f-(ATDZ)GrO shows an intense exothermic peak at 198.17 °C. The lack of endothermic peak in f-(ATDZ)GrO infers nonspontaneous reaction. The DTA describes exothermic performance with higher heat holding the capacity of f-(ATDZ)GrO and hence its thermal stability. The exothermic behavior indicates greater heat holding capacity (q) of f-(ATDZ)GrO and hence its thermal stability. The DTG peaks shows the 95.50% single decomposition of f-(ATDZ)GrO at 198.17 °C (Fig. 5c).

The average size and Polydispersity Index (PDI) of GrO, ATDZ and f-(ATDZ)GrO was analyzed with DLS (Fig. 6). The dispersed GrO in EtOH with average diameter size of 3380 nm and PDI 0.10 is observed (Fig. 6a), while the pure ATDZ is measured with average diameter size of 547 nm and PDI 0.26 (Fig. 6b). But dispersed f-(ATDZ)GrO with PDI 0.19 is reduced the average diameter size of 12.18 nm (Fig. 6c). The reduction in size f-(ATDZ)GrO is confirms involvement of electronic covalent bonding and conjugation in new functionalities of substituted moieties with GrO which after functionalization leads to strong effective

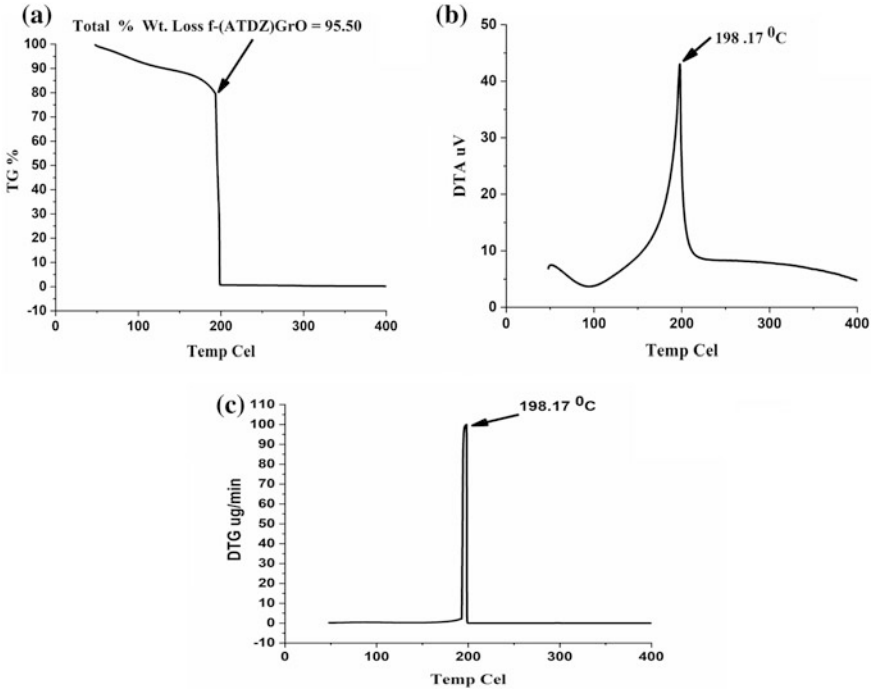

Fig. 5 Thermal analysis of f-(ATDZ)GrO, **a** TGA, **b** DTA, **c** DTG

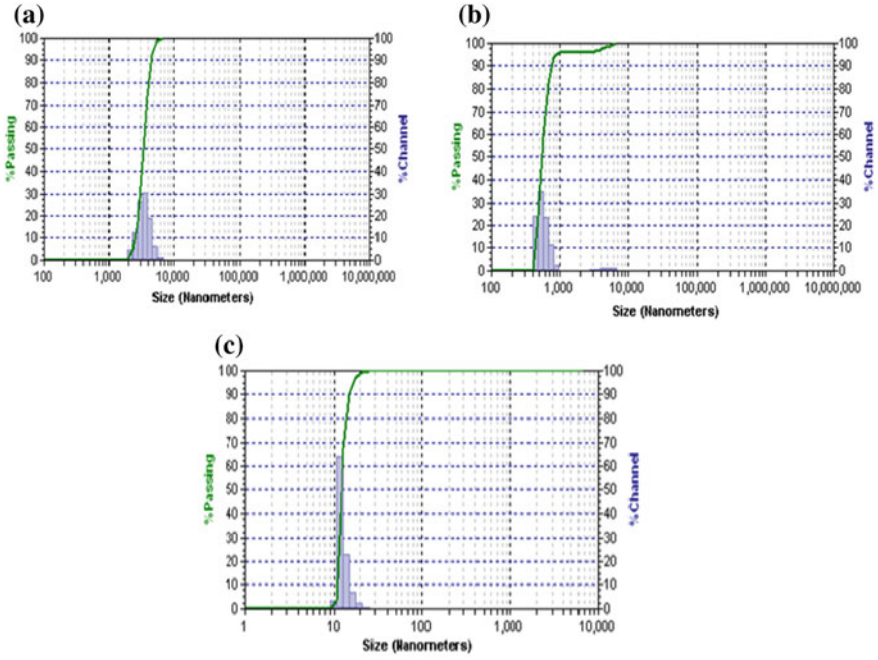

Fig. 6 DLS analysis of **a** GrO, **b** pure ATDZ, **c** f-(ATDZ)GrO

confinement effect subjected for development of nanomaterials. The PDI less than 1, confirms that functionalized product uniformly dispersed of same size in medium. The lower PDI of f-(ATDZ)GrO implies the higher kinetically active domains towards the functionality due to the hydrophilicities and higher intramolecular entropies, which confirms the functionalization. Hence, the nano-functionalization of GrO into f-(ATDZ)GrO is confirmed with reduction of size and their uniform polydispersity index.

The TEM morphological investigation and their high-resolution images were collected by Tecnai G2 S Twin gun operated at 200 kV. Samples were dispersed in ethanol and sonicated for 1 h. The 5 μL of GrO and f-(ATDZ)GrO were uniformly dispersed over 200 mesh holey carbon-coated copper grid with syringe and desiccated in a packed petri dish for 6 h to avoid the contamination from dust particles. The TEM, high resolution phase contrast images and SAED patterns of f-(ATDZ)GrO are compared with GrO. The images of GrO is confirmed sheet like morphology [39] but after bonding of ATDZ onto GrO surface, the highly dense sheet like morphology with some appearance of tunnel edges, confirms the more electronic density which is also confirmed by the broad peak in UV-vis spectrophotometer at 245 and 295 nm. The phase contrast images of f-(ATDZ)GrO shows a regular physical uniformity of lattice fringes (Fig. 7b). The crystalline morphology of GrO and f-(ATDZ)GrO have further investigated from the corresponding SAED patterns (Fig. 7c). The crystalline pattern of GrO confirms its ordered arrangement. The well-resolved hexagonal concentric rings and intense spots in SAED pattern of GrO clearly confirms the formation of crystalline GrO multiple layers [39]. The hexagonal pattern in diffraction of GrO is corresponds with its consistent lattice ($a = b \neq c$, $\alpha = \beta = 90°$ and $\gamma = 120°$), confirms the restoration of ordered graphitic AB stacking in lattice even after the higher degree of oxidation. The interlayer spacing (1/R nm) for first ring is 0.20 nm, which corresponds to more intense hexagonal spot in GrO due to restoration of the ordered Gt lattice. The second less intense spots of GrO with interlayer spacing 0.12 nm infers the disordered domains due to generate the oxygen functionality over GrO surface. Thus, the GrO surface consists of sp^2 and sp^3 hybridized carbon atoms [39].

The SAED pattern of f-(ATDZ)GrO shows the dispersed dark spot along with interlayer spacing 0.196 and 0.116 nm for first and second electronic diffraction ring respectively (Fig. 7c). The change in the interlayer spacing of the SAED patterns confirms covalent attachment of ATDZ on GrO surface. On moving towards the successive rings, fading of hexagonal spots observed which validates for the capturing of the intense activated domains by ATDZ. Therefore, the presence of thick and dispersed crystalline spots of electronic domains in f-(ATDZ)GrO clearly reveals the covalent bonding of ATDZ on GrO surface.

The AFM data (Fig. 8) was collected in non-contact mode. Before analysis, the samples were mounted on freshly cleaved mica sheet. The dispersions of as-prepared f-(ATDZ)GrO were filtered with 0.45 μm PTFE membranes. The collected filtrate was again sonicated for 90 min and by using micropipette a dispersed solution was mounted over the mica sheet and small clumps were cleaned

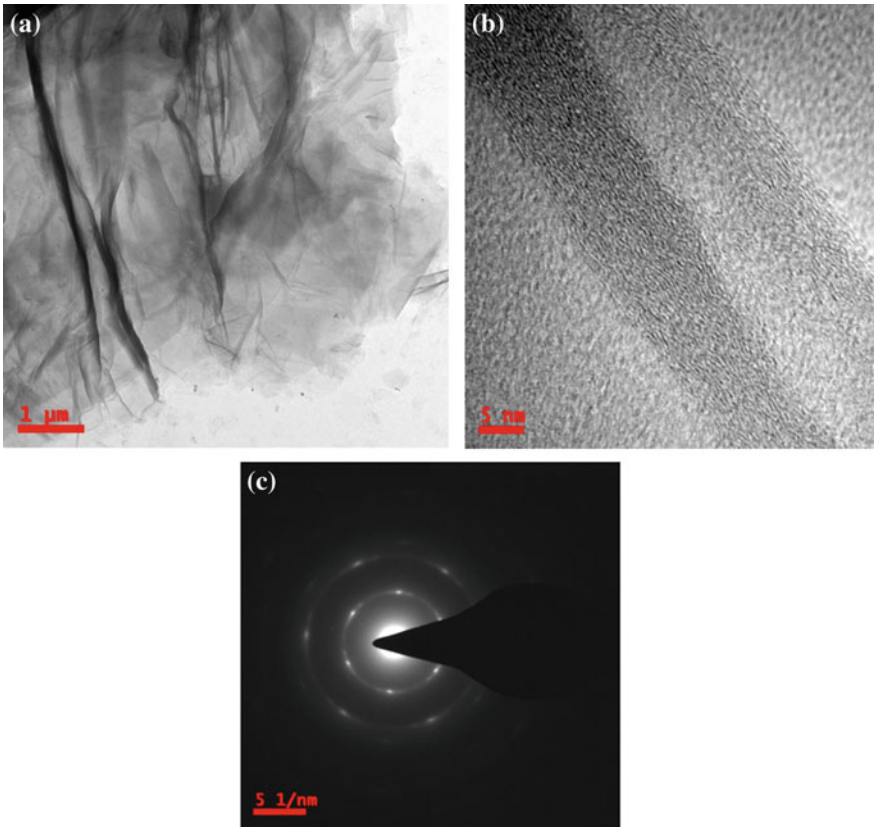

Fig. 7 TEM of f-(ATDZ)GrO **a** morphological Investigation, **b** high resolution analysis, **c** SAED pattern

with ethanol. The ethanol was evaporated at RT and sample was dried by using a hair drier. The same procedure is repeated for the second sample. The 6.0 × 6.0 μm^2 area was scanned to view 2D and 3D topography of GrO sheet. The total region surface roughness is 10.898 nm of GrO validates by 2D and 3D topography view [39]. The 3-D image of GrO surface confirmed the more surface roughness than f-(ATDZ)GrO. Moreover, a 4.2 × 4.2 μm^2 area was scanned to generate a 2D and 3D topographical view of f-(ATDZ)GrO (Fig. 8a, b). The 3-D image of f-(ATDZ)GrO has confirmed the surface roughness of 2.958 nm with larger peak valley values (Table 2). The sheet like topography in 2D topography view and more smoothened surface in 3D view were observed. The histogram shows in scanning area 4.2 × 4.2 μm^2, the maximum numbers of frequent atomic domains nearly 700 (Fig. 8c) are in evaluated range of size 225.4 nm (Fig. 8a). The distance between maximum point height to the lowest point of peak is observed as Rt of 9.244 nm. The root mean square of average height of peak (Rq) at in marked

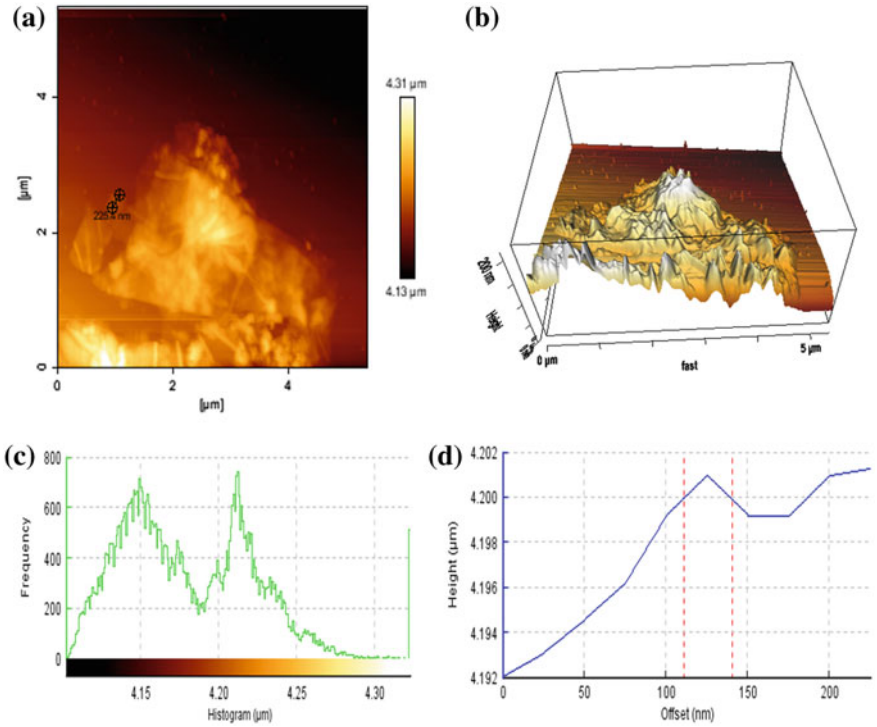

Fig. 8 AFM investigation of f-(ATDZ)GrO **a** 2D view, **b** 3D view, **c** histogram, **d** height measurement

Table 2 AFM analysis of f-(ATDZ)GrO

Sample	X (µm)	Y (µm)	Rt (nm)	Rq (nm)	Ra (nm)
f-(ATDZ)GrO	4.2	4.2	9.244	3.263	2.958

length of 225.4 nm, is observed of 3.263 nm. The offset height graph is shown in Fig. 8d. Hence, the more smoothness of functionalized product with the increasing the numbers of electronic domains in evaluated length scale, confirms the involvement of the ATDZ with GrO into f-(ATDZ)GrO formation.

The morphological investigations were conducted with SEM (Fig. 9). The stub is used for sample preparation, covered with carbon tape. The powdered samples were adhered on carbon tape, which is mounted on stub, exposed for plasma sputtering inside the coater chamber for purpose of gold and palladium surface coating in 80:20 ratios. After coating, 7 kV beam voltage was applied to provide an energy to excite secondary electrons from GrO and f-(ATDZ)GrO surface. The

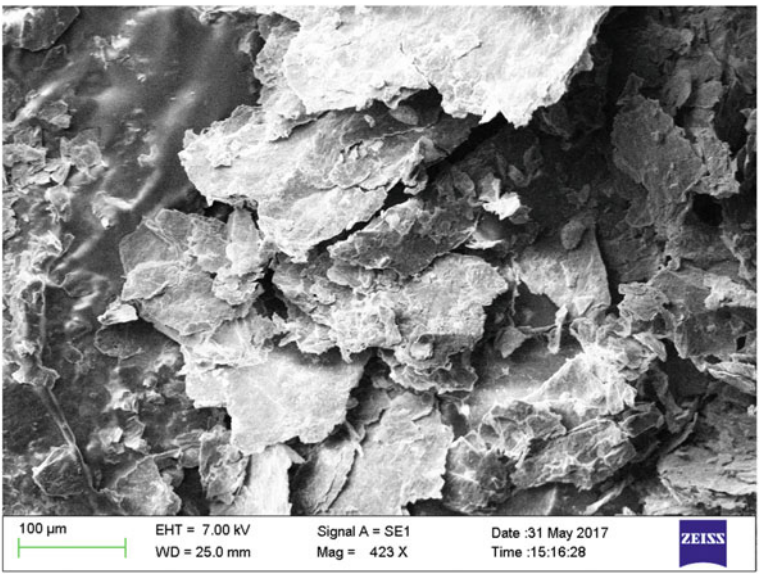

Fig. 9 SEM morphological analysis of f-(ATDZ)GrO

20 µm area is selected for SEM images of GrO [39]. The morphological images of GrO and f-(ATDZ)GrO display a very close resemblance to roughness data, obtained from atomic force microscopy.

The 100 µm SEM micrograph of the f-(ATDZ)GrO is examined with more d spacing further increased due to functionalization of ATDZ with GrO through amide bond, which is also supported by the XRD (Fig. 4) and HRTEM (Fig. 7). The SEM Image of f-(ATDZ)GrO shows flake-like morphology with the enhanced the thickness, agglomeration and crumpled on edge of GrO sheet. The number of smaller sheet like structure on the surface of functionalized graphene oxide materials evidences of ATDZ occurrence on the GrO sheets. Hence, morphological characterization indicates the formation of the rough surface of GrO than f-(ATDZ) GrO.

3.2 Photoluminescence Activity of f-(ATDZ)GrO

The extensive structural investigation with various techniques confirms the involvement of amine substituted heteroatomic domains as a covalent bond formation with GrO via amide bond. The two N and one S atoms in ring of ATDZ play an important role to electronic stabilization of functionalized product and enhanced the electronic transition from the conduction band (CB) to valence band (VB) (Scheme 1). The more electronegative oxygen atoms of carboxyl group of

GrO inhibits the electronic transiton as contray to role of N in fucntionalization through amide bond. The small organic moities as an substituents, creates strain which reinforce destabilization of f-(ATDZ)GrO, but the functionalization leads to strengthen electronic conjugation in f-(ATDZ)GrO through amide bond and as resultant the whole systems little be stabilized (Fig. 5). The Photoluminescence emission spectra of f-(ATDZ)GrO shows two peaks (Fig. 10), one sharp peak at 320.93 and another broad peak at 617.96 nm at exciton 280 nm. One spikes is seen due to instrumentation error. The strong photoluminescence emission peak at 320.93 nm is defined the electronic transition between two fixed energy well due to quantum structural confinement. Besides these, the generation of defects by Raman spectrum in the f-(ATDZ)GrO also validates for broadening of emission peak at 617.96 nm due to convolution of multiple electronic transition at various energy levels of surface. However, the calculated band gap energy of f-(ATDZ)GrO is 3.87 eV (Scheme 1). Hence, the f-(ATDZ)GrO also can be explored for energetics materials instead of biomedical applications and also for the biosensing applications.

3.3 *Cytotoxicity Behavior*

The previous documented cytotoxicity study of O-doped graphene [39], and functionalized graphene oxide with ASHM had investigated on MCF-7 and Vero cell lines as a highly cytocompatibility of materials [39]. In this contest, also *In vitro* cytotoxicity have been screened on human skin keratinocytes HaCaT and monkey kidney cell lines i.e. Vero for f-(ATDZ)GrO (Fig. 10a, b). The SRB assay has been used for an estimation of cell growth. Adriamycin (ADR) is used as a positive control in experiments in range of 10–80 μg mL^{-1} of doses in DMSO. The

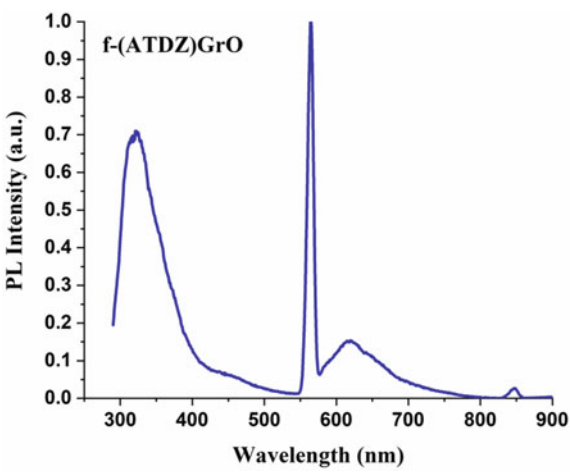

Fig. 10 PL Spectra of f-(ATDZ)GrO

repetition of experiment nearly thrice and data mean is measured to plot evaluation growth curve between % control growth (CG) versus conc. The GI50 (conc. of drug that produces 50% inhibition of the cells), TGI (conc. of drug that produces the total inhibition of cells) and LC50 (conc. of drug that kills 50% of cells) have been screened from a mean growth curve. The f-(ATDZ)GrO (Fig. 10a) is identified against cell line HaCaT. The ∼91.575% GI50 value, is confirmed the least cytotoxicity and extraordinary cytocompatibility. Hence, the observed least cytotoxicity of f-(ATDZ)GrO is explored to investigate its healthy impact on the cellular morphology.

In continuation of studied with next cell lines, f-(ATDZ)GrO further is examined against Vero cell line of monkey ∼36.825% GI50 (Fig. 10b). The f-(ATDZ)GrO shows the higher cytocompatibility on Vero at lower conc. 10 and 20 μg mL^{-1} (Fig. 10b), but from higher conc. i.e. 40 μg mL^{-1} nearly equal toxicity with reference ADR. Therefore, f-(ATDZ)GrO has been exposed as excellent cytocompatible material for HaCaT and some extent significant with Vero at lower conc. The morphological effect on HaCaT and Vero cell lines are designated the cytocompatibility of f-(ATDZ)GrO (Fig. 11). The Fig. 11a is shown restoration of maximum tubular morphology of HaCaT, while Fig. 11b showed some tubular morphology has been damage of Vero cells by applying testing sample. The maximum cells are restored their morphology appearance on of f-(ATDZ)GrO. So, the cellular morphological impact obviously has established a cytocompatibility of f-(ATDZ)GrO. The GrO is showed more cytocompatibility for Vero [39] than f-(ATDZ)GrO, due to the presence of more reactive oxygen species (ROS). But because of thermal instability, the GrO has less applicability. However, f-(ATDZ)GrO has revealed as an excellent cytocompatible material due to least toxicity and enhanced thermal stability. Therefore, f-(ATDZ)GrO can be used as biomaterial development in thermally stable tissue engineering and heat resistant biocompatible coating. Also, due to, large surface area, thermal stability and cytocompatibility of f-(ATDZ)GrO, it may be suitable for other biomedical applications (Fig. 12).

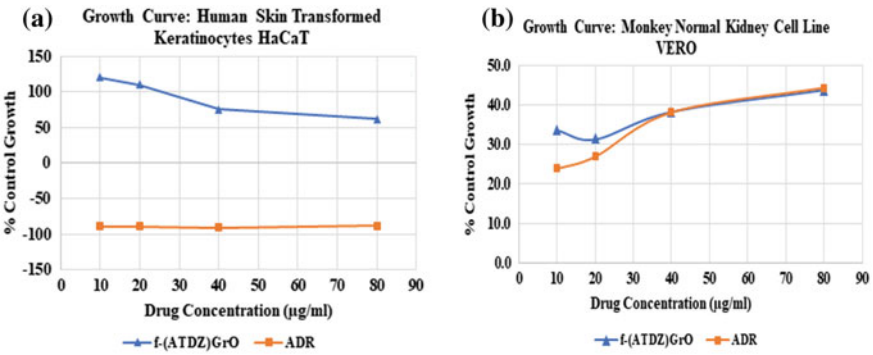

Fig. 11 In vitro SRB assay for the cytotoxicity evaluation on **a** HaCaT, **b** vero cell lines

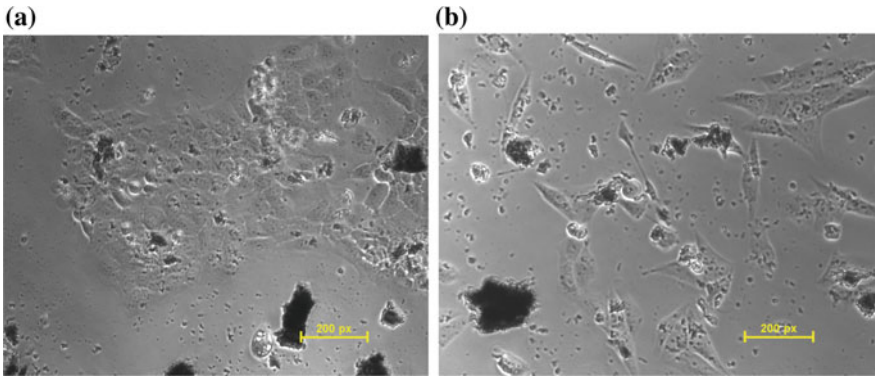

Fig. 12 Morphological impact of f-(ATDZ)GrO on at magnification 20 X **a** HaCaT, **b** vero cell lines

3.4 Contribution of Hetero Atomic Domains (CAD)

The different states of carbon, oxygen nitrogen and sulphur have synergistically played role towards the cytocompatibility behaviour of f-(ATDZ)GrO. The CF of GrO is accountable for the formation of thermally stable f-(ATDZ)GrO w.r.t to T. An enhanced thermal stability of f-(ATDZ)GrO as compared to GrO has confirmed the contribution of various atomic domains in form of electronic functionalities. Therefore, f-(ATDZ)GrO has practically advanced towards thermally stable biocompatible coatings as compared to GrO. The impact of various hetero atoms in different states has confirmed the significance of f-(ATDZ)GrO towards biomedical applications. The FTIR have confirmed the presence of characteristics functionalities like alcohol, carbonyl, carboxyl, amide and epoxy in f-(ATDZ)GrO. The synergistic impact of these different states of various electronic domains has significantly contributed towards biomedical applications of graphene and show their activity against the thermophile microorganism. In vitro cytocompatibility profile on HaCaT $\sim$91.575% and on Vero cell lines $\sim$36.825% cell viabilities is confirmed. The enhanced cytocompatibility with HaCaT and Vero cell lines at lower conc. have confirmed the reduced cytotoxicity and excellent cytocompatibility. Therefore, the involvement of hetero atoms like N and S are play an important role for identifying the Nanocytotoxicity performance of f-(ATDZ)GrO.

4 Conclusions

The greener sonochemical methods for synthesis of covalent functionalized GrO has been developed. This protocol is helpful to make the healthy environment by avoiding hazardous chemicals during functionalization of GrO. The cost effective

and healthy methods have been completely avoided the use of harmful reactive reagents and reduced the time of reaction within to 15 min. The newly prepared material has been characterized with high-end analytical techniques to ensure a formation of f-(ATDZ)GrO. The crystalline behaviour has been analysed with XRD spectrum to show 2θ peak at 10.1132 and 24.0075 with d-spacing 8.73949 and 3.70379 respectively, which is differ as reference with GrO. The defects in crystalline lattice of f-(ATDZ)GrO has been calculated with Raman spectrum value of 0.86 D/G ratio. The reduced size of f-(ATDZ)GrO has been analysed with DLS in support for Nano-functionalization. SAED pattern with the less interlayer spacing with 0.196 and 0.116 for first and second diffraction ring respectively, confirms the f-(ATDZ)GrO formation. The more smoothened topography view as compared to GrO is confirmed a bonding of ATDZ with GrO surface. The f-(ATDZ)GrO is also explored for the energetics application by calculating the band gap value of 3.87 eV with PL. The influence of f-(ATDZ)GrO is explored with thermal and cytotoxicity profile as a cytotoxicity. The total % wt. loss of f-(ATDZ)GrO is 95.5% at 198.17 ° C that inferred its higher decomposition w.r.t. T than GrO. The f-(ATDZ)GrO is showed ~91.575% GI50 value for HaCaT and ~36.825 Vero cell line which confirmed a excellent cytocompatibility with HaCaT and some extent significant cytocompatibility with Vero at lower conc., which can be further optimized. The results have cross confirmed with morphological effect. Thus, f-(ATDZ)GrO can be developed as a precursor in thermal resistant tissue engineering field efficiently.

Acknowledgements Authors are thankful to Central University of Gujarat, India for support. Dr. Vasant Sathe, UGC-DAE CSR Indore, India is acknowledged for providing Raman facility. Dr. Jyoti A. Kode, ACTREC, Tata Memorial Centre, Mumbai, India is acknowledged for providing in vitro cytotoxicity screening facility.

References

1. Geim, A.K., Novoselov, K.S.: The rise of graphene. Nat. Mate. **6**, 183–191 (2007)
2. Georgakilas, V., Otyepka, M., Bourlinos, A.B., Chandra, V., Kim, N., Kemp, K.C.P., Zboril, R., Kim, K.S.: Functionalization of graphene: covalent and non-covalent approaches, derivatives and applications. Chem. Rev. **112**, 6156–6214 (2012)
3. Dai, L.: Functionalization of graphene for efficient energy conversion and storage. Acc. Chem. Res. **1**, 31–42 (2013)
4. Park, J., Yan, M.: Covalent functionalization of graphene with reactive intermediates. Acc. Chem. Res. **46**, 181–189 (2013)
5. Chng, E.L.K., Pumera, M.: The toxicity of graphene oxides: dependence on the oxidative methods used. Chem. Eur. J. **19**, 8227–8235 (2013)
6. Chng, E.L.K., Sofer, Z., Pumera, M.: Cytotoxicity profile of highly hydrogenated graphene. Chem. Eur. J. **20**, 6366–6373 (2014)
7. Pinto, A.M., Gonçalves, C., Sousa, D.M., Ferreira, A.R., Moreira, J.A., Gonçalves, I.C., Magalhaes, F.D.: Smaller particle size and higher oxidation improves biocompatibility of graphene-based materials. Carbon **99**, 318–329 (2016)

8. Kumar, A.M., Suresh, B., Ramakrishna, S., Kim, K.S.: Biocompatible responsive polypyrrole/GO nanocomposite coatings for biomedical applications. RSC Adv. **5**, 99866–99874 (2015)
9. Hasanzadeh, M., Mokhtari, F., Shadjou, N., Eftekhari, A., Mokhtarzadeh, A., Jouyban-Gharamaleki, V., Soltanali, M.: Poly arginine-graphene quantum dots as a biocompatible and non-toxic nanocomposite: layer-by-layer electrochemical preparation, characterization and non-invasive malondialdehyde sensory application in exhaled breath condensate. J. Mater. Sci. Eng. C **75**, 247–258 (2017)
10. Barua, S., Chattopadhyay, P., Phukan, M.M., Konwar, B.K., Islam, J., Karak, N.: Biocompatible hyperbranched epoxy/silver–reduced graphene oxide–curcumin nanocomposite as an advanced antimicrobial material. RSC Adv. **4**, 47797–47805 (2014)
11. Barahuiea, F., Saifullaha, B., Dorniania, D., Fakurazid, S., Karthivashand, G., Husseina, M. Z., Elfghi, F.M.: Graphene oxide as a nanocarrier for controlled release and targeted delivery of an anticancer active agent, chlorogenic acid. J. Mater. Sci. Eng. C **74**, 177–185 (2017)
12. Zhang, H., Grüner, G., Zhao, Y.: Recent advancements of graphene in biomedicine. J. Mater. Chem. B **1**, 2542 (2013)
13. Shi, S., Chen, F., Ehlerding, E.B., Cai, W.: Surface engineering of graphene-based nanomaterials for biomedical applications. Bioconjugate Chem. **25**, 1609–1619 (2014)
14. Pattnaik, S., Swain, K., Lin, Z.: Graphene and graphene-based nanocomposites: biomedical applications and biosafety. J. Mater. Chem. B **4**, 7813–7831 (2016)
15. Yousefi, M., Dadashpour, M., Hejazi, M., Hasanzadeh, M., Behnam, B., de la Guardia, M., Shadjou, N., Mokhtarzadeh, A.: Anti-bacterial activity of graphene oxide as a new weapon nanomaterial to combat multidrug-resistance bacteria. J. Mater. Sci. Eng. C **74**, 568–581 (2017)
16. Barua, S., Thakur, S., Aidew, L., Buragohain, A.K., Chattopadhyay, P., Karak, N.: One step preparation of a biocompatible, antimicrobial reduced graphene oxide–silver nanohybrid as a topical antimicrobial agent. RSC Adv. **4**, 9777–9783 (2014)
17. Kostarelos, K., Novoselov, K.S.: Materials science. exploring the interface of graphene and biology. Science **344**, 261–263 (2014)
18. An, J., Gou, Y., Yang, C., Hu, F., Wang, C.: Synthesis of a biocompatible gelatin functionalized graphene nanosheets and its application for drug delivery. J. Mater. Sci. Eng. C **33**, 2827–2837 (2013)
19. Mitra, T., Manna, P.J., Raja, S.T.K., Gnanamani, A., Kundu, P.P.: Curcumin loaded nano graphene oxide reinforced fish scale collagen—a 3D scaffold biomaterial for wound healing applications. RSC Adv. **5**, 98653–98665 (2015)
20. Zhou, L., Wang, W., Tang, J., Zhou, J.-H., Jiang, H.-J., Shen, J.: Graphene oxide noncovalent photosensitizer and its anticancer activity in vitro. Chem. Eur. J. **17**, 12084–12091 (2011)
21. Yang, Y., Zhang, Y.-M., Chen, Y., Zhao, D., Chen, J.-T., Liu, Y.: Construction of a graphene oxide based noncovalent multiple nanosupramolecular assembly as a scaffold for drug delivery. Chem. Eur. J. **18**, 4208–4215 (2012)
22. Gies, V., Zou, S.: Systematic toxicity investigation of graphene oxide: evaluation of assay selection, cell type, exposure period and flake size. Toxicol. Res. **7**, 93–101 (2018)
23. Pelin, M., Fusco, L., León, V., Martín, C., Criado, A., Sosa, S., Vázquez, E., Tubaro, A., Prato, M.: Differential cytotoxic effects of graphene and graphene oxide on skin Keratinocytes. Sci. Rep. **7**, 40572-12 (2016)
24. Liao, K.-H., Lin, Y.-S., Macosko, C.W., Haynes, C.L.: Cytotoxicity of graphene oxide and graphene in human erythrocytes and skin fibroblasts. ACS Appl. Mater. Interfaces. **3**, 2607–2615 (2011)
25. Seabra, A.B., Paula, A.J., de Lima, R., Alves, O.L., Duran, N.: Nanotoxicity of graphene and graphene oxide. Chem. Res. Toxicol. **27**, 159–168 (2014)
26. Guo, X., Mei, N.: Assessment of the toxic potential of graphene family nanomaterials. J. Food Drug Anal. **22**, 105–115 (2014)
27. Kumar, S., Modak, D.M., Paik, P.: Graphene oxide for biomedical applications. J. Nanomed. Res. **5**(6), 00136 (2017)

28. Dubey, P., Dr. Gopinath, P.: Functionalized graphene oxide based nanocarrier for tumor-targeted combination therapy to elicit enhanced cytotoxicity against breast cancer cells in vitro. Chem. Select. **1**, 4845–4855 (2016)
29. Li, Y., Feng, L., Shi, X., Wang, X., Yang, Y., Yang, K., Liu, T., Yang, G., Liu, Z.: Surface coating-dependent cytotoxicity and degradation of graphene derivatives: towards the design of non-toxic, degradable nano-graphene. Small **10**, 1544–1554 (2014)
30. Yang, K., Li, Y., Tan, X., Peng, R., Liu, Z.: Behavior and toxicity of graphene and its functionalized derivatives in biological systems. Small **9**, 1492–1503 (2013)
31. Peña-Bahamondea, J., Miguela, V.S., Nguyenb, H.N., Ozisikc, R., Rodrigues, D.F.: Functionalization of reduced graphene oxide with polysulfone brushes enhance antibacterial properties and reduce human cytotoxicity. Carbon **111**, 258–268 (2017)
32. Dong, H., Li, Y., Yu, J., Song, Y., Cai, X., Liu, J., Zhang, J., Ewing, R.C., Shi, D.: A versatile multicomponent assembly via β-cyclodextrin Host-guest chemistry on graphene for biomedical applications. Small **9**, 446–456 (2013)
33. Chena, J., Shia, X., Rena, L., Wanga, Y.: Graphene oxide/PVA inorganic/organic interpenetrating hydrogels with excellent mechanical properties and biocompatibility. Carbon **111**, 18–27 (2017)
34. Liu, Y., Zhang, Y., Zhang, T., Jiang, Y., Liu, X.: Synthesis, characterization and cytotoxicity of phosphorylcholine oligomer grafted graphene oxide. Carbon **71**, 166–175 (2014)
35. Bao, H., Pan, Y., Ping, Y., Sahoo, N.G., Wu, T., Li, L., Li, J., Gan, L.H.: Chitosan-functionalized graphene oxide as a nanocarrier for drug and gene delivery. Small **7**, 1569–1578 (2011)
36. Sayyar, S., Murray, E., Thompson, B.C., Gambhir, S., Officer, D.L., Wallace, G.G.: Covalently linked biocompatible graphene/polycaprolactone composites for tissue engineering. Carbon **52**, 296–304 (2013)
37. Yan, R., Wu, H., Zheng, Q., Wang, J., Huang, J., Ding, K., Guo, Q., Wang, J.: Graphene quantum dots cut from graphene flakes: high electrocatalytic activity for oxygen reduction and low cytotoxicity. RSC Adv. **4**, 23097–23106 (2014)
38. Maktedar, S.S., Mehetre, S.S., Singh, M., Kale, R.K.: Ultrasound irradiation: a robust approach for direct functionalization of graphene oxide with thermal and antimicrobial aspects. Ultrason. Sonochem. **21**, 1407–1416 (2014)
39. Maktedar, S.S., Avashthi, G., Singh, M.: Understanding the significance of O-doped graphene towards biomedical applications. RSC Adv. **6**, 114264–114275 (2016)
40. Mehetre, S.S., Maktedar, S.S., Singh, M.: Understanding the mechanism of surface modification through enhanced thermal and electrochemical stabilities of N-doped graphene oxide. Appl. Surf. Sci. **366**, 514–522 (2016)
41. Wang, T., Zhu, S., Jiang, X.: Toxicity mechanism of graphene oxide and nitrogen- doped graphene quantum dots in RBCs revealed by surface-enhanced infrared absorption spectroscopy. Toxicol. Res. **4**, 885–894 (2015)
42. Hirsch, A., Englert, J.M., Hauke, F.: Wet chemical functionalization of graphene. Acc. Chem. Res. **46**, 87–96 (2013)
43. James, E.J., Hersam, M.C.: Atomic covalent functionalization of graphene. Acc. Chem. Res. **46**, 77–86 (2013)
44. Hangxun, X., Kenneth, S.S.: Sonochemical preparation of functionalized graphenes. J. Am. Chem. Soc. **133**, 9148–9151 (2011)
45. Marcano, D.C., Kosynkin, D.V., Berlin, J.M., Sinitskii, A., Sun, Z., Slesarev, A., Alemany, L. B., Lu, W., Tour, J.M.: Improved synthesis of graphene oxide. ACS Nano **4**, 4806–4814 (2010)
46. Clauss, A., Plass, R., Boehm, H.P., Hofmann, U.: Untersuchungen zur structur des Graphitoxyds. Anorg. Allergy. Chem. **291**, 205–220 (1957)
47. Scholz, W., Boehm, H.P.: Untersuchungen am Graphitoxid. VI. Betrachtungen zur Struktur des Graphitoxids. Anorg. Allg. Chem. **369**, 327–340 (1969)
48. Kenry, T., Lim, C.T.: Biocompatibility and nanotoxicity of layered two-dimensional nanomaterials. Chem. Nano. Mat. **3**, 5–16 (2017)

49. Majeeda, W., Bourdoa, S., Petiboneb, D.M., Sainia, V., Vanga, K.B., Nimaa, Z.A., Darriguesa, E., Ghosha, A., Watanabea, F., Cascianoa, D., Alid, S.F., Birisa, A.S.: The role of surface chemistry in the cytotoxicity profile of graphene. J. Appl. Toxicol. **37**, 462–470 (2017)
50. Crisana, L., Crisanb, B., Soritauc, O., Baciutb, M., Radu, Birisd A., Baciuta, G., Lucaciu, O.: In vitro study of biocompatibility of a graphene composite with gold nanoparticles and hydroxyapatite on human osteoblasts. J. Appl. Toxicol. **35**, 1200–1210 (2015)
51. Bitounis, D., Ali-Boucetta, H., Hong, B.H., Min, D.-H., Kostarelos, K.: Prospects and challenges of graphene in biomedical applications. Adv. Mater. **25**, 2258–2268 (2013)
52. Farshid, B., Lalwani, G., Sitharaman, B.: In vitro cytocompatibility of one-dimensional and two-dimensional nanostructure-reinforced biodegradable polymeric nanocomposites. J. Biomed. Mater. Res. A **103**, 2309–2321 (2015)
53. Maktedar, S.S., Mehetre, S.S., Avashthi, G., Singh, M.: In situ sonochemical reduction and direct functionalization of graphene oxide: a robust approach with thermal and biomedical applications. Ultrason. Sonochem. **34**, 67–77 (2017)
54. Maktedar, S.S., Avashthi, G., Singh, M.: Ultrasound assisted simultaneous reduction and direct functionalization of graphene oxide with thermal and cytotoxicity profile. Ultrason. Sonochem. **34**, 856–864 (2017)
55. Maktedar, S.S., Malik, P., Avashthi, G., Singh, M.: Dispersion enhancing effect of sonochemically functionalized graphene oxide for catalysing antioxidant efficacy of curcumin. Ultrason. Sonochem. **39**, 208–217 (2017)

Functionalized Graphene/Polymer Nanofiber Composites and Their Functional Applications

Hanan Abdali and Abdellah Ajji

Abstract Nanofiber composites materials produced by electrospinning may have a very high specific surface area owing to their small diameters, and nanofiber mats can be highly porous with excellent pore interconnection. However, applications using nanofiber composites also require specific properties such as good electrical conductivity, are flame retardant, anti-static and anti-radiative as well. Over the past few decades, the carbon nanomaterial, graphene has been researched widely owing to its intrinsic properties such as large surface area, excellent thermal, electrical, and optical properties in addition to superior chemical and mechanical characteristics needed in specific applications. The chemical functionalization of graphene nanosheet improved its dispersibility in common organic solvents, which is important when developing novel graphene-based nanocomposites. Moreover, graphene may also be functionalized in order to modify its intrinsic characteristics, for example, its electronic properties can be modified to control the conductivity and band gap in nano-electronic devices. Functionalized graphene-based polymer nanofiber composites exhibit a variety of improved, or even new properties such as adsorption performance, anti-bacterial, hydrophobicity and conductivity valued across a wide range of applications in sensors, biosensors, transparent conductive films, high-frequency circuits, toxic material removal, capacitors, spintronic devices, fuel cells, touch screens, flexible electronics and batteries. This book chapter summarizes the recent progress in functionalized graphene-based polymer nanofibers composites, with an emphasis on their applications.

Keywords Functionalized graphene · Nanofibers · Nanocomposite · Electrospinning · Electrospun polymers · Applications

H. Abdali · A. Ajji (✉)
Department of Chemical Engineering, CREPEC, Polytechnique Montréal, Station Centre-Ville, P.O. Box 6079, H3C 3A7 Montreal, QC, Canada
e-mail: abdellah.ajji@polymtl.ca

H. Abdali
e-mail: hanan.abdali@polymtl.ca

H. Abdali
Ministry of Education, P.O. Box 225085, 11153 Riyadh, Saudi Arabia

A. Khan et al. (eds.), *Graphene Functionalization Strategies*,
Carbon Nanostructures, https://doi.org/10.1007/978-981-32-9057-0_5

1 Introduction

Materials with nanoscale dimensions, occur in zero, one, two or three dimensions. One dimensional (1D) fibrous nanostructures can be fabricated by various methods such as self-assembly [1, 2], template synthesis [3], phase separation [4], and electrospinning [5–7] (see Fig. 1). Among these methods, electrospinning is a cost-effective, user-friendly and extremely versatile technique, allowing the manufacture of macro/nanofibers in a continuous process and at longer-length scales. There are three phases in the electrospinning process: jet initiation, jet elongation with or without branching, and/or splitting, followed by the solidification of the jet solution into nanofibers [6–8]. Hitherto, more than 100 polymers and numerous inorganic materials haven been electrospun into nanofibers. The flexible nature of the electrospinning process allows for easily modifying hierarchical features such as; nonwoven, aligned or patterned fibers, nanoribbons, nanorods, random three-dimensional structures, sub-micron spring and convoluted fibers with controlled diameters when preparing complex nanostructures by changing the solution and processing parameters [6–9] and/or set-up geometries [10–12]. Moreover,

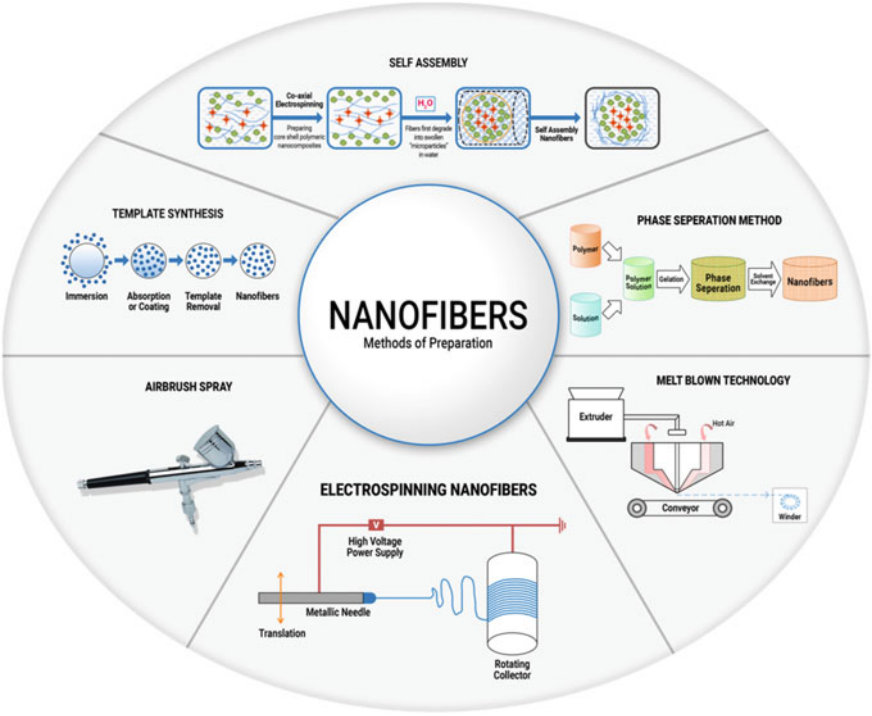

Fig. 1 Various methods for preparation of nanofibers. With permission from [6]. Copyright © 2017, Elsevier B.V. All rights reserved

electrospinning nanofibers of mixed polymers and carbon particles enhance the mechanical properties of the resultant nanofiber mats and presents structural advantages as it constitutes a nonwoven mesh characterized by large surface area, unit mass and interconnected porosity [13–15]. In particular, graphene is composed of single layers of aromatic carbons and is considered a suitable prospect in the production of functionalized electrospun fibers owing to its remarkable physical and chemical properties, including high fracture strength (∼125 GPa), high Young's modulus (∼1100 thermal conductivity (∼5000 W/mK), rapid mobility of charge carriers (∼200,000 cm^2/Vs GPa), excellent electrical (∼10^6 S/cm) and large specific surface area (theoretically calculated value, 2630 m^2/g) [13–16]. The unique features of graphene surfaces enable easy suspension and mixture with the polymers in powder form for electrospinning solutions. These composites are suitable for producing architectured, nanofiber materials for tissue engineering, drug release, sensors, biosensors, batteries and supercapacitors, dye-sensitised solar cells, fuel cells, catalysts, filters, memory devices, and in food applications [14–17]. However, graphene's low dispersibility in common organic and inorganic solutions necessary in such applications, poses a significant challenge that needs to be addressed. In particular, a proficient dispersion of graphene in common solvents is key toward forming homogeneous nanocomposites. Therefore, modifying graphene by tailoring its solubility remains crucial in a multitude of commercial applications. Covalent and noncovalent methods are usually used to modify the surface of graphene. Often, these modification techniques were commonly performed to enhance the dispersion of graphene in a polymer matrix to attain the greatest impact on the fiber materials and correlate the introduced graphene properties to enrich the performance of fibers [13, 18].

In this chapter, the preparation of nanofibers with functionalized graphene and the corresponding effects on the nanofiber composites, while exploring recent research in relevant applications is also discussed. The strategies to functionalize graphene surfaces are also briefly highlighted.

2 Chemical Functionalization of Graphene

Graphene, consisting of a single-layer sp^2-hybridized carbon atom network, is the most intensively studied material in nanotechnology owing to its properties and features. This single-atom-thick sheet of carbon atoms arranged in a honeycomb pattern is the world's thinnest, strongest, and stiffest material, also boasts excellent conductivity, thus graphene is being studied in almost all fields of science, medicine and engineering [19–21]. Despite its potential in various applications, it is also noteworthy that graphene itself possesses a zero band gap including inertness to reaction, that weakens its competitiveness in the field of semiconductors and sensors. Consequently, this remains a significant reason for research in this material paying special attention to its functionalization, reaction with organic and inorganic

substances, as well as the chemical modifications of graphene surfaces including the intensity of covalent and noncovalent interactions with graphene [18–23].

As, the most current and lucrative method for large scale production of graphene-based materials is centered around the oxidation of graphite to graphene oxide (GO) and then reducing the GO to graphene by either thermal, chemical, or electrochemical methods [18, 20] (see Fig. 2). The GO surfaces are highly oxygenated, and carboxyl, diol, ketone, epoxide, and hydroxyl functional groups can alter the van der Waals interactions significantly and enable greater solubility in water and some organic solvents. Yet, owing to the presence of the oxygen functional groups in its structure, GO is electronically insulating and thermally unstable as it undergoes pyrolysis at elevated temperatures [19–21]. Therefore, reducing GO removes most but not all of the hydroxyl, carboxylic acid and epoxy functional groups [19–21].

Usually variations on the Staudenmaier [24] or Hummers [25] methods are used to obtain GO in which graphite is oxidized using strong oxidants such as $KMnO_4$, $KClO_3$, and $NaNO_2$ in the presence of nitric acid or its mixture with sulfuric acid

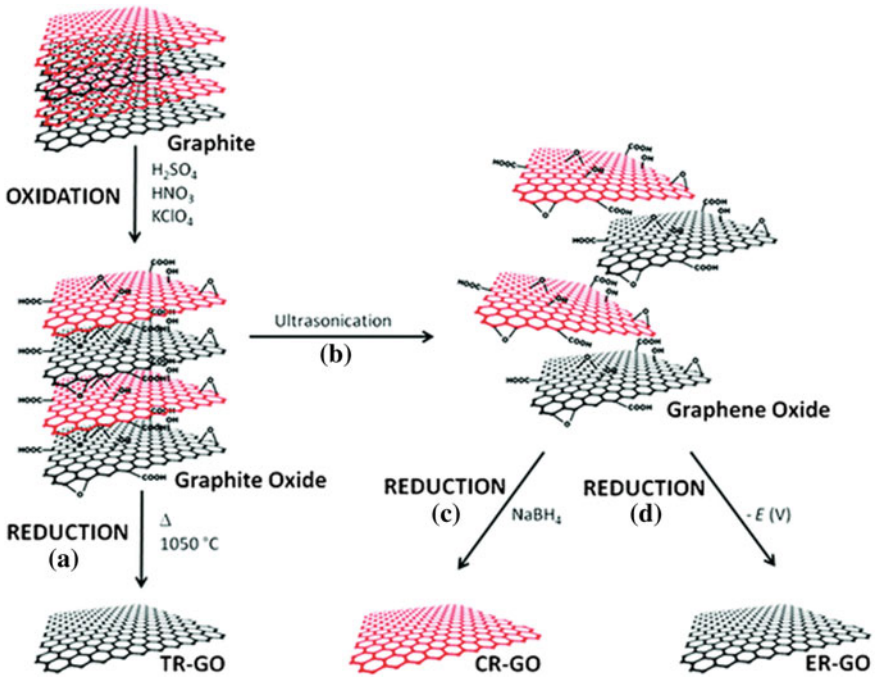

Fig. 2 Schematic of the production of CMGs from graphite. Graphite was first oxidized to graphite oxide. Thermal reduction and exfoliation (a) of graphite oxide led directly to TR-GO. Graphite oxide was ultrasonicated (b) to generate graphene oxide, following which the chemical reduction (c) of graphene oxide yielded CR-GO. Alternatively, graphene oxide was electrochemically reduced (d) to afford ER-GO. With permission from [20]. Copyright © 2012, Royal Society of Chemistry

[25]. Gao et al. [26] used a K_2FeO_4-based oxidation approach instead of $KMnO_4$ to obtained a single-layer GO at room temperature. Recently, using the Hummers method, Yu et al. [27] have obtained GO that is free of $NaNO_3$ by partly replacing $KMnO_4$ with K_2FeO_4 and controlling the amount of concentrated sulfuric acid. The chemical reduction of GO by using reducing agents for example; hydrazine [28, 29], sodium borohydride followed by hydrazine [30], hydroquinone [31], dimethylhydrazine [32], and ascorbic acid [33], etc., provides a streamlined technique for the production of graphene, nevertheless, the cost and hazardous nature of these chemicals utilized during the reduction may limit its application [34]. Conversely, thermally reducing graphene oxide (RGO) is produced by heating dry GO under inert gas and high temperature [34–37], for instance, heating GO in an inert environment at 1000 °C for 30 s results in the reduction and exfoliation of GO generating RGO layers. As such, the thermal reduction produces chemically modified graphene layers without the need for dispersion in a solvent compared with other chemical reduction methods [34]. Accordingly, to obtain functionalized graphene, the chemical modification of graphene oxide followed by reduction was used. It has been demonstrated that both modification techniques are excellent for the preparation of processable graphene, preventing agglomeration and enabling the formation of stable dispersions and was utilized for the fabrication of polymer nanofiber composites in numerous applications [13, 18, 37].

2.1 Non-covalent Functionalization

The non-covalent functionalization, which relies on the van der Waals force, electrostatic interaction or π-π stacking [38, 39], is easier to undertake without changing the chemical structure of the graphene sheets. Consequently, this is the most effective way of customizing the electronic/optical property and solubility of the nanosheets [40], because, without affecting the electronic network, it offers the possibility of attaching functional groups to graphene [41, 42]. Noncovalent modification is attained by the interaction with polymers, such as poly (3-hexylthiophene) (P3HT), porphyrin, pyren, cellulose derivatives, polyaniline (PANi), poly(sodium 4-styrenesulfonate) (PSS), and porphyrins or biomolecules such as deoxyribonucleic acid (DNA) and peptides, as well as adsorption of surfactants or small aromatic molecules. The first example of non-covalent functionalization of graphene nanosheets using PSS was published by Stankovich et al. [39]. It was found that exfoliation and in situ reduction of GO in the presence of PSS could form non-covalently-functionalized graphitic nanosheets that were extremely stable and dispersible in water (1 mg/ml). It is possible to achieve a stable dispersion of reduced graphene in different organic solvents with amine-terminated polymers through non-covalent functionalization [43]. In this technique, the reduction of GO is first undertaken in an aqueous medium using an ammonia-hydrazine mixture, this is then followed by washing and the removal of aggregated graphene sheets. The amine-terminated polymer is dissolved in organic

solvents for non-covalent functionalization of RGO. Next, the aqueous dispersion of RGO is added to the organic polymer solution. The phial including phase-separated organic and aqueous phases then undergoes a 5 h sonication for the non-covalent functionalization of graphene. Here, the functionalized graphene can easily be dispersed in a variety of solvents and is shown to exhibit electrical conductivity [43]. Liu et al. [44] have successfully functionalized the graphene surfaces with a pyrene-terminated positive charged polymer, poly(2-N,N′-(dimethyl amino ethyl acrylate)) (PDMAEA), and a negatively charged polymer, polyacrylic acid (PAA) via π-π stacking. The functionalized graphene polymer composites indicated that the phase transfer behavior between aqueous and organic media occurs at different pH values. The remarkable electrical conductivity of graphene with an extremely high surface area (theoretically 2630 m^2/g), is combined with the graphene nanosheets is used to construct nanodevices specifically when developing high capacity cathode materials for Li-ion batteries [44]. In other research, gold nanoparticles were deposited on DNA-functionalized graphene presented by Liu et al. [45] (see Fig. 3), where thiolated DNA oligonucleotides were prepared to adsorb on to the GO nanosheets resulting in the DNA-coated GO being reduced by hydrazine to DNA-RGO. Gold nanoparticles were then mixed in aqueous solutions of DNA-RGO and DNA-GO composites respectively. These gold-arrayed DNA-functionalized graphene nanosheets have considerable potential not only in the field of bio detection but also for use in optoelectronics, battery materials, magnetism catalysis, field effect devices [45]. In a subsequent study, Choi et al. [46] have described the functionalization of graphene through self-assembly of a hydrophobic backbone of Nafion (see Fig. 4). The result indicated that the graphene nanosheets were easily dispersible and presented with biosensing properties of good conductivity and electrochemical characteristics for organophosphates.

Functionalization can be used to maximally retain the natural structure of graphene, yet, it must be also be noted that interactions between functionalities and graphene surfaces remain weak and therefore unsuitable applications requiring strong interactions.

2.2 *Covalent Functionalization*

Reaction between the functional groups of the molecules and the oxygenated groups on GO or reduced GO (RGO) surfaces is the foundation for covalent functionalization of graphene [47, 48], for example, carboxyls on the edges with epoxides and hydroxyls on their basal planes [49]. The abundant surface chemistry of GO/RGO enables a myriad of possibilities during the covalent functionalization of graphene-based sheets when compared with non-covalent functionalization. Covalent techniques are employed to generate composites that have strong interactions between graphene and the modifier [49]. GO or RGO can be grafted onto polymeric chains that have reactive groups like hydroxyls and amines, such as, poly (ethylene glycol), polylysine, polyallylamine, and poly(vinyl alcohol). These

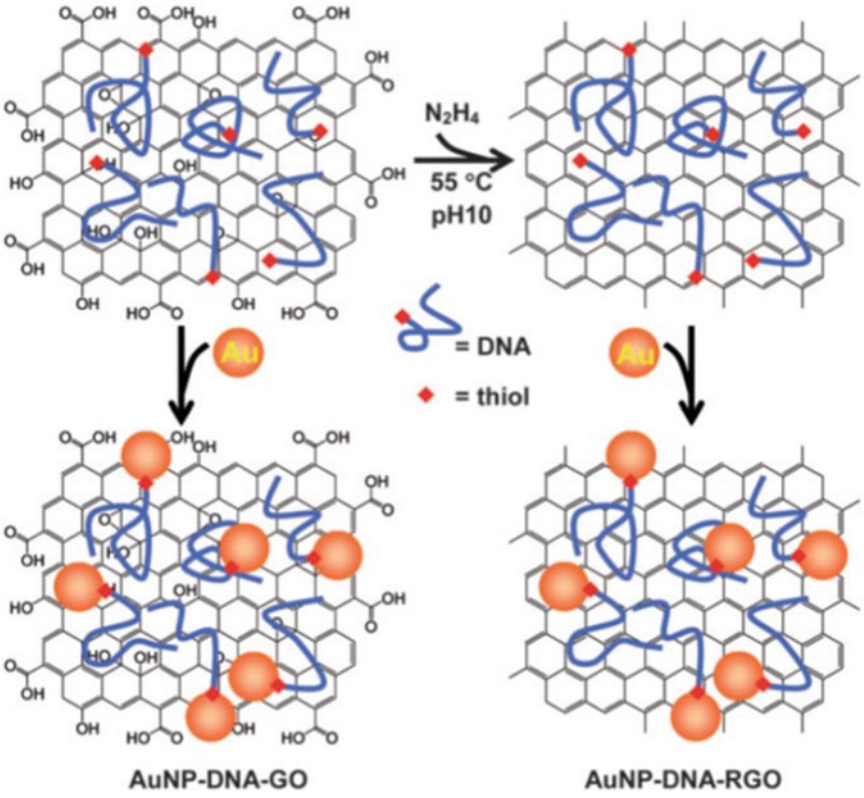

Fig. 3 DNA coating and aqueous dispersion of GO and RGO, which were then used as two-dimensional bio-nano-interfaces for homogeneous assembly of metal carbon heteronanostructures. With permission from [45]. Copyright © 2010, Royal Society Chemistry

materials are combined together and promise the desired properties of their individual parts, for example; the polymeric part offers dispersibility in certain solvents, mechanical strengthening, and many morphological properties, while the graphene nanosheets exhibits characteristics such as chemical reactivity, electrical conductivity, and reinforcement of the mechanical properties. The poly-L-lysine (PLL) was covalently grafted to RGO through the reaction of epoxy groups on graphene oxides and amino groups on PLL in the presence of potassium hydroxide (KOH) [50] (see Fig. 5). PLL-functionalized graphene is water-soluble and biocompatible, which makes it a novel material promising in biological applications. In an analogous approach, Salavagione et al. [47] successfully prepared the PVA covalently grafted onto GO nanosheets via ester bonds between the carboxylic groups of GO and the hydroxyl groups of PVA. These chemical bonds can be created either by direct formation or after the transformation of carboxylates to the more reactive acyl chlorides. It was shown that the PVA/RGO composite was

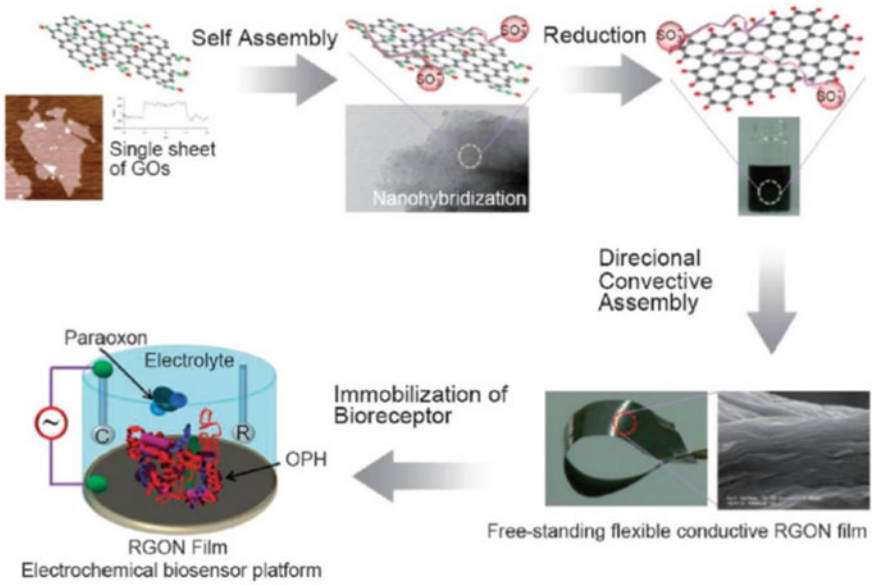

Fig. 4 Illustration of a procedure to design RGON hybrids and the RGON platform used as an electrochemical biosensor. With permission from [46]. Copyright © 2010, American Chemical Society

generated after partial reduction by hydrazine [47]. Lee et al. [51] have also presented an easily obtained method for covalent attachment of polymer brushes to GO surface utilizing initiated atom transfer radical polymerization (ATRP). The hydroxyl groups formed on the surface of GO were initially functionalized with a common ATRP initiator (a-bromoisobutyryl bromide), and next polymers of styrene, butyl acrylate, or methyl methacrylate were grown directly through a surface-initiated polymerization (SIP).

Moreover, Lee et al. [51] presented two primary conclusions in their investigation of polystyrene (PS). First, it was suggested that by altering the ratio of initiator modified GO and monomer it was possible to adjust the polymer chain length. Second, it was discovered that the monomer loading changes the molecular weight of the grafted PS, this was produced by gel permeation chromatography (GPC) after detaching by saponification, and it was noted that the polydispersity was low. As such, the authors suggest that the polymerization proceeded in a controlled way. Furthermore, the PS-functionalized GO was shown to increase the solubility in N,N-dimethylformamide (DMF), toluene, chloroform, and dichloromethane significantly, further enhancing the processing capacity of PS-functionalized GO for applications in polymer-based composites [51]. It was found that heating a diazonium salt, resulted in an extremely reactive free radical, which attacks the sp^2 carbon atoms of graphene forming a covalent bond. This reaction has been applied by Niyogi et al. [52] the covalent attachment of

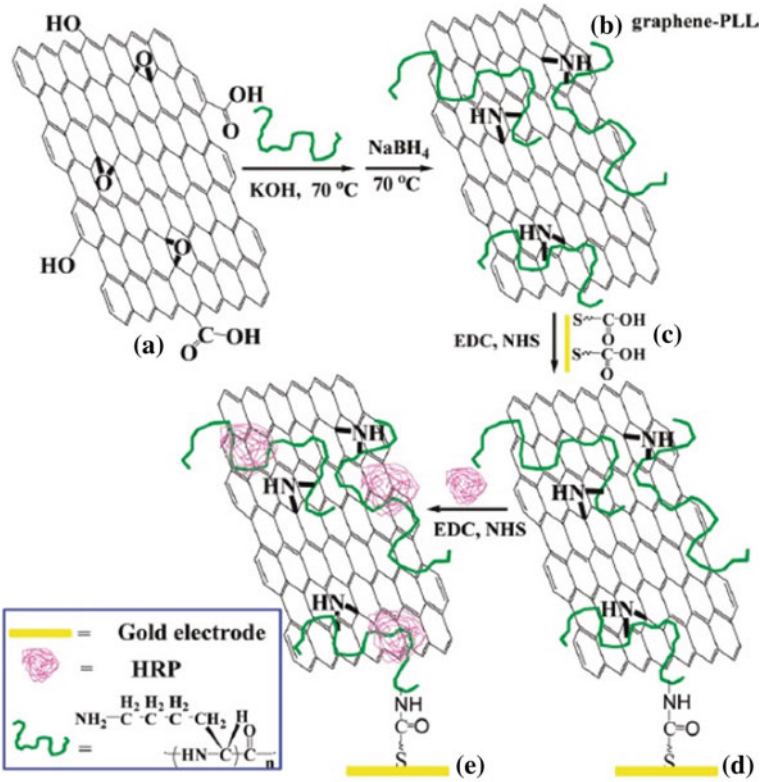

Fig. 5 Schematic diagram of graphene-PLL synthesis and assembly process of graphene-PLL and HRP at a gold electrode. With permission from [50]. Copyright © 2009, American Chemical Society

nitrophenyls to graphene sheets introduces a band gap, which can be controlled, making the functionalized graphene potentially useful as semiconducting nanomaterials. Furthermore, the addition of an alternative free radical includes the reaction of benzoyl peroxide with graphene sheets [53]. In another study, Vadukumpully et al. [54] developed a basic yet flexible method for the covalent functionalization of graphene with alkylazides, where the alkyl chains incorporated various functional groups such as hydroxylundecanyl, dodecyl, hexyl and carboxy-undecanyl resulting in improved dispersibility that helped facilitate composite fabrication. This strategy provides a useful platform for the synthesis of functional graphene nanocomposites using gold nanoparticles (the carboxyl groups can trap and immobilize the gold nanoparticles in a selective manner). Moreover, GO could be used as a support for enzyme immobilization in the preparation of biosensing devices. The immobilization of glucose oxidase (GOx) onto GO nanosheets was attained via amide bonding [55].

3 Preparation of Functionalized Graphene Based Polymer

3.1 Nanofiber Composites

Graphene's unique electronic, mechanical and thermal properties [14, 15] ensure its role as a promising filling agent for nanofibers composite applications [14]. Graphene has the ability to function as a nanofiller that can potentially enhance the characteristics of polymer-based nanofiber composites at a very low loading. However, several factors can control the characteristics and uses of graphene/polymer nanofiber composites such as the type of graphene utilized, its inherent properties, the manner of dispersion of graphene in the polymeric matrix, its interfacial interaction, the state of wrinkling in the graphene, and the structure of its network in the matrix [13, 56]. Therefore, the functionalization of graphene by covalent and non-covalent modifications promotes the dispersion of graphene in various organic solvents, and this aqueous dispersibility is greatly beneficial for producing graphene sheets, films, fibers composites, etc. Hence, many studies have shown that the chemical modification of graphene alters the graphene microstructure, producing graphene with various functional groups, electrical conductivity, carbon to oxygen atomic ratio (C/O ratio), and solubility in solvents, etc. [13, 43, 57–59]. He and Gao reported a simple and efficient strategy for grafting different functional groups or polymeric chains onto graphene nanosheets using nitrene cycloaddition. This method produced single-layered, functionalized graphene with a variety of functional groups (e.g., hydroxyl, carboxyl, amino, bromine, long alkyl chain, etc.) or polymers (e.g., poly(ethylene glycol), polystyrene) to covalently attach onto the graphene, in a one-step reaction (see Fig. 6) [58]. The modified graphene nanosheets produced are electrically conductive, and have good dispersibility and processability in organic solvents, which advocates their properties as potential contenders not only in future modifications but also in various applications of polymer nanofiber composites. Similarly, Moayeri and Ajji [60] have successfully fabricated a conductive polymer nanofiber composite of 1-pyrenebutanoic acid, succinimidyl ester functionalized graphene/polyaniline/poly (ethylene oxide) (G-PBASE/PANi/PEO). This unique nanostructured composite of PANi/PEO/G-PBASE with small loading of G-PBASE (5 wt% relative to PANi) exhibited increased improvement in the electrical conductivity and good thermal stability in comparison to PANi/PEO nanofibers owing to the homogenous distribution of the functionalized graphene in the polymeric matrix [60]. Moreover, Rafiee et al. [61] have reported that the modified graphene nanosheets are notably effective at intensifying the energy, fracture toughness, fatigue resistance, strength, and stiffness of epoxy polymers at significantly lower loading fractions upon comparison with other additives such as nanoclay, carbon nanotubes (CNTs), and nanoparticles additives. At 0.125% weight of functionalized graphene sheets was remarked to have improved the fracture toughness ≈65% and the fracture energy by ≈115% [61].

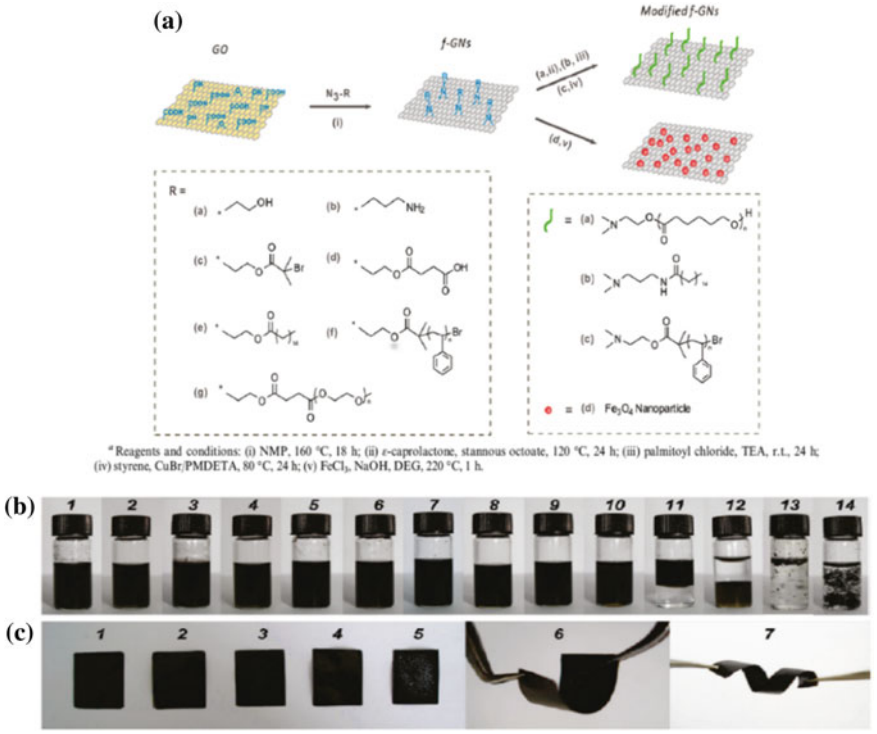

[a] Reagents and conditions: (i) NMP, 160 °C, 18 h; (ii) ε-caprolactone, stannous octoate, 120 °C, 24 h; (iii) palmitoyl chloride, TEA, r.t., 24 h; (iv) styrene, CuBr/PMDETA, 80 °C, 24 h; (v) $FeCl_3$, NaOH, DEG, 220 °C, 1 h.

Fig. 6 **a** General strategy for the preparation of functionalized Graphene Nanosheets (f-GNs) by Nitrene Chemistry and the further chemical modifications[a]. **b** Photographs of f-GNs dispersion in solvents after sonication: G–N–OH in water (1) and DMF (2), G–N–COOH in water (3) and DMF (4), G–N–PEG1900 in water (5) and DMF (6), G–N–C16 in chloroform (7) and toluene (8), G–N–PS in chloroform (9) and toluene (10), G–N–NH_2 in water/chloroform (11), G–N–NH_2-g-C16 in water/chloroform (12), GO in chloroform (13), and reduced GO in DMF (14). **c** Photographs of 10 wt% f-GNs/polyurethane composites: (1) G–N–OH, (2) G–N–COOH, (3) G–N–NH_2, (4) G–N–Br, (5) reduced GO, (6) G–N–OH, and (7) G–N–COOH. With permission from [58]. Copyright © 2010, American Chemical Society

The composite fibers are prepared using the two main processes of mixing and spinning. The modified graphene sheets can be dispersed and incorporated in the mixing process in three different ways: melt blending, in situ polymerization, or solution mixing (see Fig. 7). Moreover, other research has coated functionalized graphene onto the fiber surface after spinning [13, 56].

Melt blending uses a twin-screw extruder to produce fibers via melt-spinning under specific conditions after the direct addition of the functionalized graphene into the melted polymer in a Brabender mixing chamber, for example; screw speed, temperature and time. This method is commercially preferred to the two others due to its versatility, environmentally friendly nature, economic suitability in mass production [14]. However, in melt processing, dispersing the graphene in the

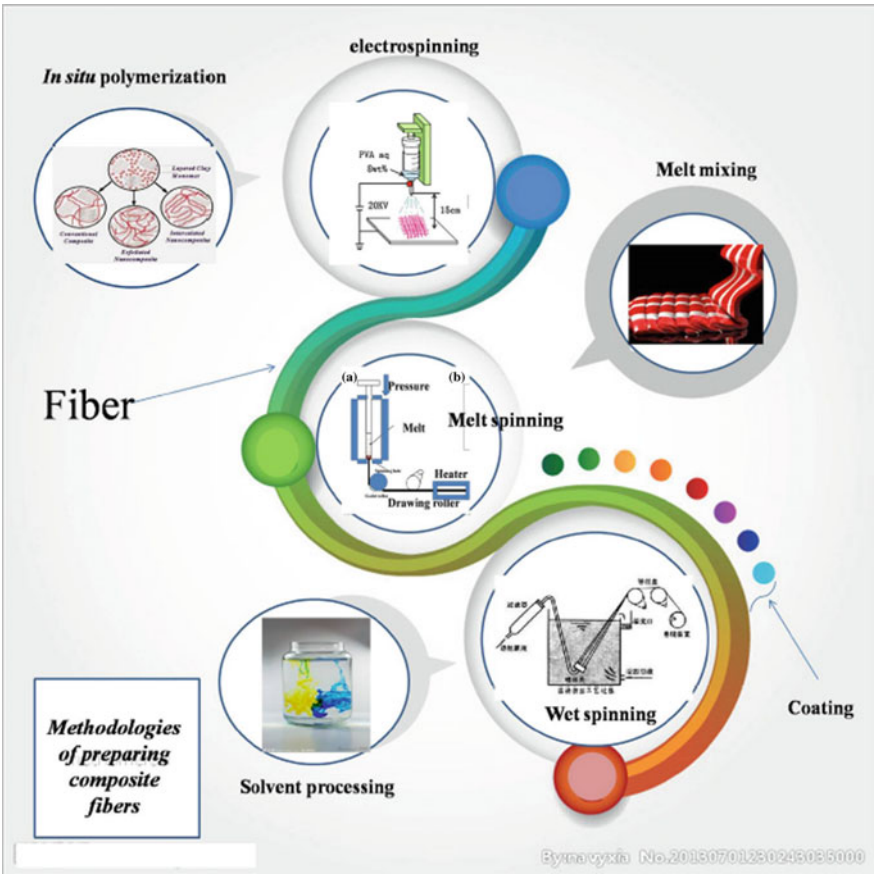

Fig. 7 Schematic illustration of the methods for preparation of fiber composite materials. With permission from [13]. Copyright © 2016, Elsevier Ltd. All rights reserved

polymer matrix remains a considerable challenge as it does in both in situ polymerization and solvent processing [62]. Chatterjee et al. [63] have studied the influence of graphene nanosheets on the structure and mechanical properties of polyamide 12 (PA12) fibers. The PA12 and graphene composite fibers that were fabricated via melt processing were found to help in breaking the agglomerates present in the PA12 and graphene composite fibers during the melt compounding in the micro extruder due to the shear high forces. Although the composite fibers exhibited improved elasticity, yield and tensile strength, the melt spinning process also revealed that there is a high risk of agglomeration [63].

In situ polymerization provides strong interaction between the functionalized graphene and the polymeric matrix and enables an outstanding, homogeneous dispersion. Generally, functionalized graphene is mixed with prepolymers or

monomers where heat or radiation is then used to initiate the polymerization process [64]. As functionalized graphene can be further functionalized by grafting polymer chains through atom transfer radical polymerization (ATRP) resulting in covalent bonding. Generally, for in situ polymerized nanocomposites, melt spinning which is conducted in a piston spinning machine and hot-roller drawing machine, is commonly used. The research on in situ polymerization of nanocomposites studies not only the effect of the nanofillers on the morphology of the polymer matrix and its final characteristics but also includes the polymerization reaction. Hou et al. [65] successfully prepared nanocomposites of functionalized graphene grafted by polyamide 6 (PA6) by in situ polycondensation of caprolactam (CPL), using the melt spinning and drawing process to produce the nanocomposite fibers. It was established that due to the good distribution of functionalized graphene (0.1 wt%) in the PA6 matrix, the tensile strength of the fibers increased dramatically. Yet, when the functionalized graphene is 0.5 wt% or higher, the graphene agglomerates in the nanocomposite fibers resulting in a reduced tensile strength (see Fig. 8) [65].

Solution processing is widely used to produce polymer nanofiber composites with uniform graphene dispersion effectively. In this method, functionalized graphene is mixed with a polymer solution after first dispersing in a solvent by using techniques such as magnetic agitation, mechanical mixing, or high-energy sonication [56]. Next, by vaporizing the solvent a composite is produced. Many types of polymer nanofibers have been reinforced by graphene, for instance poly(vinyl alcohol) (PVA) [66–68], polystyrene (PS) [32], Polyethylene (PE) [69], polyvinyl fluoride (PVF) [70], polymethyl methacrylate (PMMA) [57, 60, 71], nylon 6 [72], and chitosan [73–75], etc. However, the specific surface area of the 2D fillers could decrease considerably due to the re-stacking, aggregation and folding techniques of the graphene-based nanosheets. As such, surface functionalization of graphene-based fillers before solution mixing is undertaken to overcome this problem.

Usually, there are three types of spinning techniques to fabricate modified graphene-based polymer nanofiber composites: melt-spinning, wet-spinning and electrospinning. We mainly discuss below the electrospinning technique to fabricate functionalized graphene-based polymer nanofiber composites.

4 Principle of Electrospinning

Recently, interest in nanoscale properties and technologies have increased the use of electrospinning technology, owing to its efficient, relatively simple and cost-effective process for producing ultrafine nanofibers or fibrous structures of many polymers with a range of diameters from sub-microns to nanometers [7, 76, 77]. The nanofibers structures obtained using this process result in unique advantages for example, the flexible porosity of the electrospun structure, high surface to volume ration and the ability to spin into different shapes and sizes. These

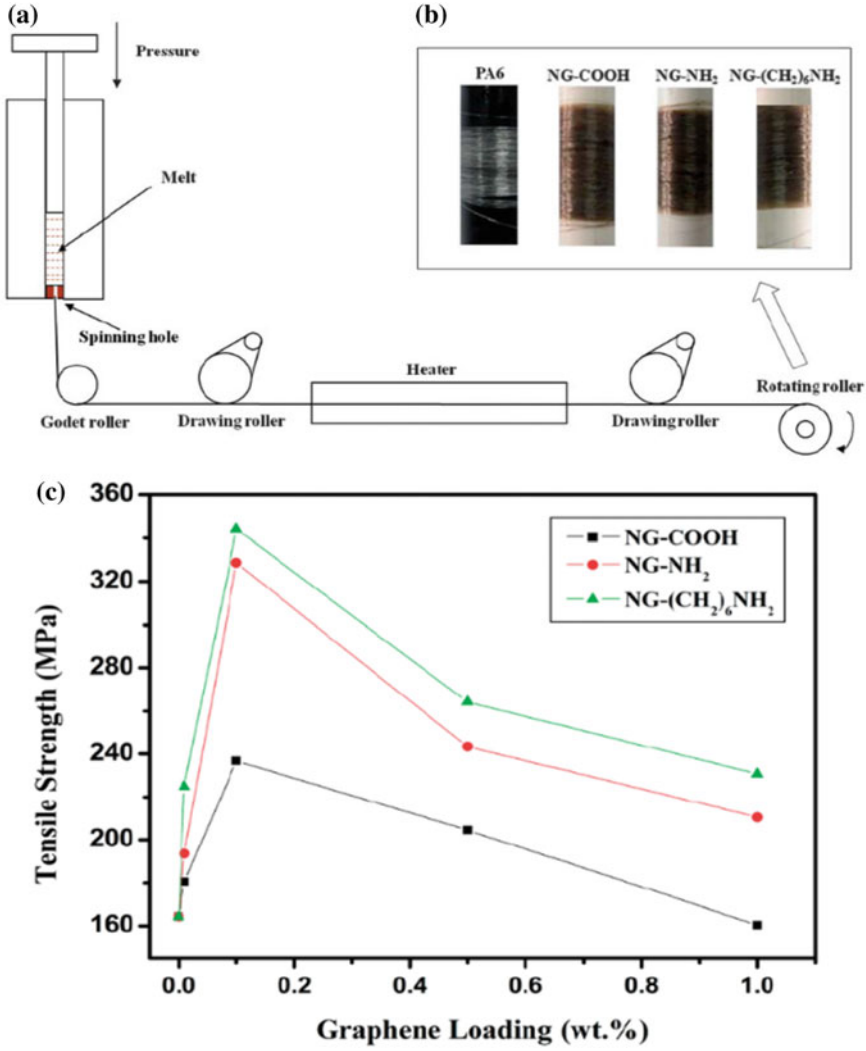

Fig. 8 **a** Melt spinning apparatus used for preparing nanocomposite fibers. **b** Photographs of neat PA6 and 0.1 NG fibers. **c** Tensile strength of NG nanocomposite fibers with different loadings of graphene. With permission from [65]. Copyright © 2014, The Royal Society of Chemistry

characteristics exemplified by the nanofibers qualifies their candidacy for applications in filtrations, tissue engineering scaffolds, wound healing, energy storage, sensors, catalyst and enzyme carriers [7]. Technically, electrospinning is a method that employs a strong electric field to draw liquid polymer into fine filaments [12, 78, 79]. The simple electrospinning apparatus made up of a micro-syringe with a needle of small diameter, a nozzle, a high voltage supplier, and an electrode collector, (see Fig. 9) The collector can be fashioned into any shape according to

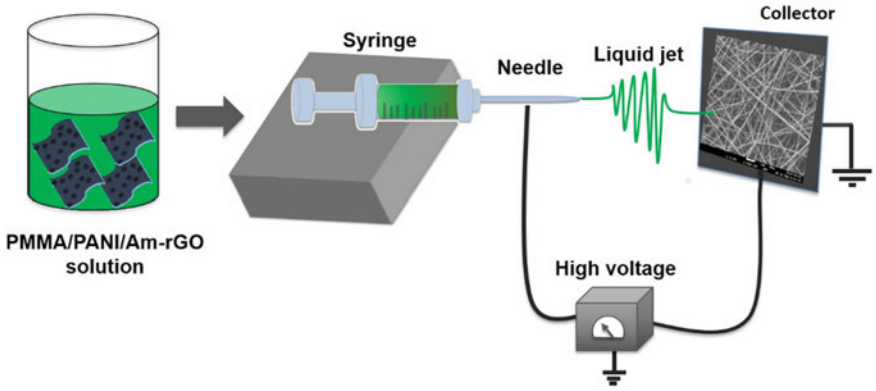

Fig. 9 Schematic illustration of the electrospinning setup. With permission from [57]. Copyright © 2017, Polymers

the specified product requirements for example; a flat plate, rotating drum, or patterned collector. In most cases, the collector is simply grounded. When a high voltage solution is charged, and the repulsive force within the charged solution is larger than its surface tension and a jet erupts from the tip of the spinneret. This electrified jet then moves counterclockwise towards the electrode, forming a long and thin thread. Subsequently, as the liquid jet is continuously elongated and the solvent is evaporated, randomly oriented, nonwoven mat nanofibers with small diameters (micro to nanometers) are deposited on the collector [12, 78, 79].

Electrospinning deals with several conditions that can influence the transformation of polymer solutions into nanofibers through its process. These include; (i) the intrinsic properties of the solution, such as viscosity, elasticity, conductivity, and surface tension, (ii) the processing parameters for example; the electric potential at the needle, the feeding rate for the polymer solution, and the distance between the syringe and the collector screen [78, 79], (iii) ambient conditions such as temperature, humidity and air velocity in the electrospinning chamber [78, 79]. Proper control of these parameters can be tailored to fiber morphologies and diameters of the electrospun fibers. However, researchers usually elect to keep ambient conditions constant in their research.

Zong et al. [80] studied the effects of varying the processing parameters and solution properties on the structure and morphology of the electrospun fibers. It was discovered that the effect of solution conductivity on the fiber diameter are inversely related, for example, the lower solution conductivity resulted in a larger fiber diameter. Zong et al. reported that the addition of different salts to the polymer spinning solutions, resulted in a higher charge density on the surface of the ejected jet exhibiting more electric charges carried by the jet [80]. The results also demonstrated that salts with smaller ionic radii formed fibers with smaller diameters and vice versa. Mainly, it indicated that greater charge densities led to greater mobility of ions with smaller radii which generated increased elongation forces

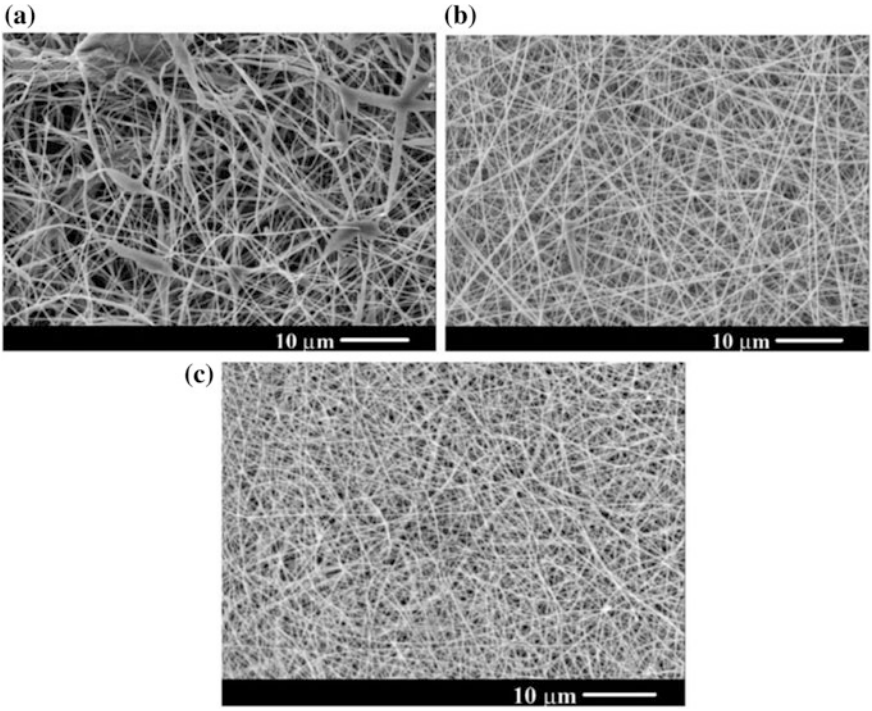

Fig. 10 SEM images of PDLA membranes fabricated by electrospinning of a 30 wt% solution at voltage of 20 kV, feeding rate of 20 ml/min and with 1 wt% of **a** KH_2PO_4; **b** NaH_2PO_4 and **c** NaCl. With permission from [80]. Copyright © 2002 Elsevier Science Ltd. All rights reserved

exerted on the polymer jet creating a smaller fiber (see Fig. 10) [80]. Moreover, they reported that different fiber morphologies can also be obtained by altering the solution feed rate at a given electric field. They concluded that the droplet suspension at the end of the spinneret is larger with a higher feed rate so the jet of the solution could carry the fluid away at faster velocity. Therefore, this can lead to large beaded fibers as the polymer is not completely dry upon reaching the collector (see Fig. 11) [80]. Additionally, it was demonstrated that higher concentrations and the corresponding higher charge densities of the solution produced uniform fibers with no bead-like textures.

In another study, Ramazani and Karimi investigated the presence of varying amounts of graphene oxide (GO) with different oxidation levels on the morphological appearance, fiber diameter, and structure of poly(ε-caprolactone) (PCL) nanofibers fabricated by the electrospinning method [81]. It was observed that parameters such as GO dispersibility, charge relaxation time, polarity and wettability all of which are used to measure the fiber diameter, improves with oxidation. The surface tension of PCL solution is unchangeable in the presence of GO with different loading and level of oxidation, resulting in diameter variations in

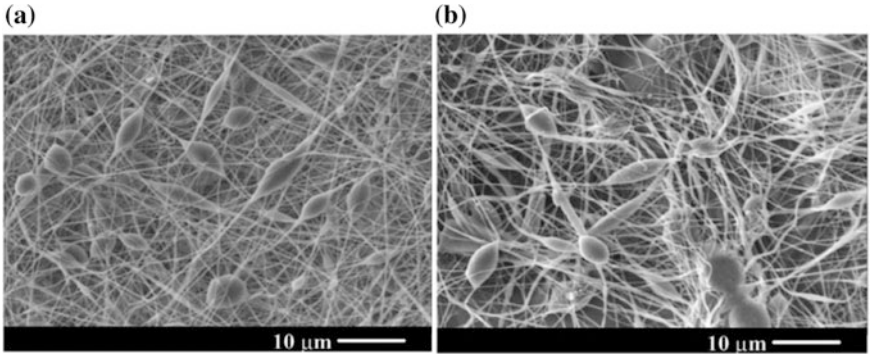

Fig. 11 SEM images showing the variation of beaded fibers at different feeding rates: **a** 20 ml/min; **b** 75 ml/min. The applied voltage was 20 kV and concentration was 25 wt% with 1 wt% KH_2PO_4. With permission from [80]. Copyright © 2002 Elsevier Science Ltd. All rights reserved

the electrospun fibers. Moreover, they reported that the average fiber diameter decreases in the presence of GO with different loading, owing to the reduction of solution viscosity and increase in the conductivity [81]. Accordingly, researchers have also shown that after GO surfaces were functionalized with poly(ethylene glycol) (PEG), the poly(lactic acid) (PLA)/GO-g-PEG nanocomposite nanofibers exhibited a decrease in diameters when comparing with pure PLA [82]. The plasticizing effect of the grafted PEG molecules on the surface of GO attributed to the decrease in viscosity for PLA/GO-g-PEG electrospinning suspensions, indicating strong interfacial adhesion between GO-g-PEG and PLA and was responsible for the reduction in the average diameter from PLA to PLA/GO-g-PEG [82]. Das et al. [83] indicated that the addition of non-covalently functionalized graphene to the PVA fibers increased the effective fluid charge density, therefore it was necessary to change the flow rate from 0.3 to 15 ml/h. It was shown that a reduction in bead formation resulted with an increase in applied voltage from 10 to 15 kV. An increase in voltage is necessary as the conductivity of the graphene increases the surface charge of the fiber, perpetuating natural bead formation. Furthermore, a higher voltage is required as the elasticity of the jet is increased due to the addition of graphene when compared with the baseline experiment. Increasing the voltage amplifies the repulsive electrostatic force and favors the formation of fibers with smaller diameters [83].

Overall, it was considered that preparing an optimized suspension of functionalized graphene in the solution improved the applicability of the resulting nanofibers. Therefore, many experiments are still needed to produce electrospun functionalized graphene/polymer nanofibers for morphological modification, necessary to meet specific requirements for applications.

5 Properties of Functionalized Graphene Based Polymer

5.1 Nanofibers Composite

Surface functionalization of graphene showed significant improvement in dispersibility/processability in solvents, as well as in polymer matrices [49, 56, 84]. These in turn, exhibit excellent enhancement in mechanical, electrical, optical and thermal properties of host polymers at very low loading levels. Numerous studies on the properties of functionalized graphene based polymer nanofiber composites have been reported [14, 56, 84]. For instance, Young's modulus, tensile strength, thermal stability, conductivity, and hydrophobicity. Hsiao et al. [85] advocated a basic yet effective method to decorate silver nanoparticles (AgNPs) and RGO on the surface of polyurethane (PU) fibers to fabricate AgNP@RGO/PU fiber composites. This technique provided an effective way of producing lightweight, highly flexible electronic products that have excellent electrical properties. The surface of PU fiber mat was decorated with GO by dipping the PU fiber mats into the GO aqueous solution (GO/PU) and then the GO/PU fiber composite was reduced in hydriodic acid (HI). After that, the AgNPs were deposited on RGO/PU to fabricate AgNP@RGO/PU fiber composites (see Fig. 12a) [85]. They found that the decorated AgNP@RGO restricts the PU fiber mat from thermal decomposition resulting in a notable improvement in thermal stability of composite (see Fig. 7b). Moreover, the AgNP@RGO/PU fiber composites showed superior improvement in electrical properties (<10 U/sq), because the deposited m-AgNPs effectively facilitate the charge transfer ability of RGO [85].

Chee et al. [86] reported a new, non-covalent surface functionalization technique of GO via a UV-sensitive initiator embedded via π-π interactions on the graphene nanosheets, followed by the polymerization of hydrophobic polymeric chains along the surface of the graphene. Thereafter, the functionalized GO/Polyacrylonitrile (PAN) nanofibers were produced by the electrospinning technique and then the nanofibers underwent thermal treatments that converted the polymeric chains into a CNF structure as shown in Fig. 13a. The results revealed that functionalized GO was readily dispersed in different solvents, and in the hydrophobic polymeric solution. Furthermore, the functionalized GO-reinforced CNF (CNF/fGO) exhibited an extraordinary ability by showing a specific capacitance of 140.10 F/g, approximately three times higher than that of neat CNF, coupled with a high stability capacitance retention of 96.2% after 1000 times of charge/discharge cycles at 1 A/g (see Fig. 13b and c) [86]. In a further study, Moayeri and Ajji [87, 44] have produced core-shell structured CNF embedded with non-covalently modified graphene by single-nozzle electrospinning setup utilizing phase separated solutions of PAN and polyvinylpyrrolidone (PVP) in DMF solution, followed by the calcination and carbonization processes. Electrochemical assessment of CNF/graphene (G) nanofibers revealed a maximum specific capacitance of 265 F/g after addition of 10 wt% graphene nanosheets. Furthermore, based on the Brunauer-Emmett-Teller (BET) results, the specific surface area and pore volume were increased, directly proportional from

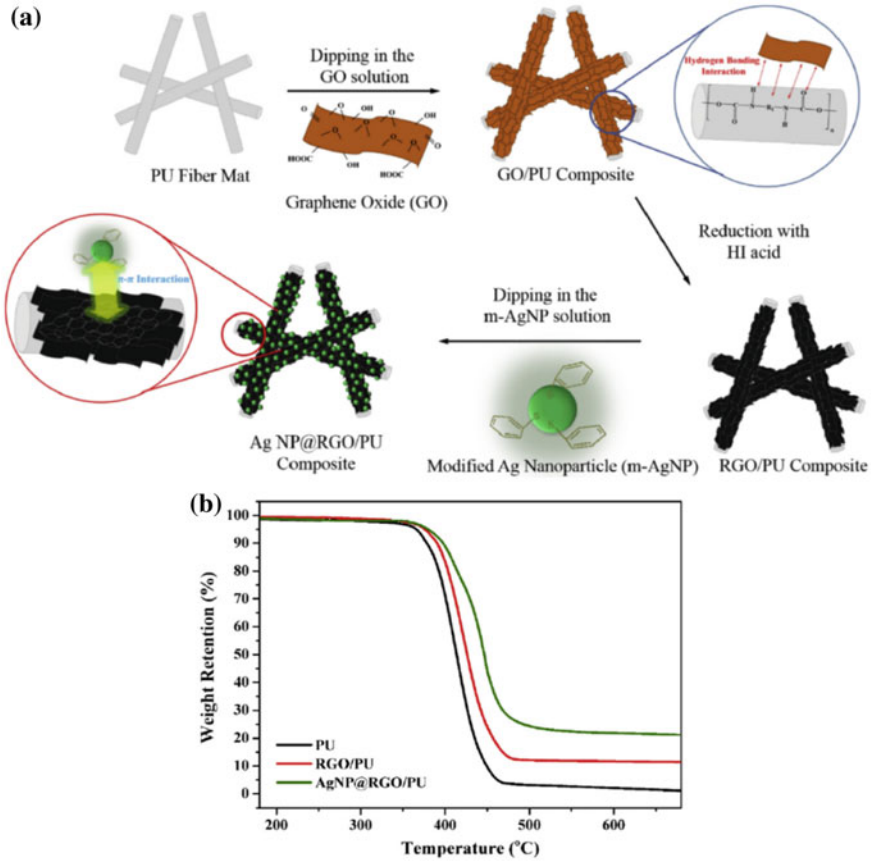

Fig. 12 **a** Schematic representation of the procedure for preparing the AgNP@RGO/WPU composites; **b** The TGA curves for PU, RGO/PU and AgNP@RGO/PU. With permission from [85]. Copyright © 2015, Elsevier Ltd. All rights reserved

CNF/G0 to CNF/G10 samples and then showed a decreased amount for CNF/G15 sample, which further supports the outcomes generated from the electrochemical tests. The larger pore volume and surface area can be attributed for affecting ion diffusion with high speed at high loading current density and allows for more efficient utilization of specific surface area [87].

Scaffaro et al. [88] investigated the reaction of GO-g-PEG on the mechanical and wettability characteristics of polycaprolactone (PCL) electrospun scaffolds. The contact water angle measurements of PCL/GO-g-PEG composite nanofiber showed better performance with lower water contact angles. The Young moduli of the composite nanofiber mats were significantly improved by adding a low concentration of GO-g-PEG, owing to the grafted PEG chains, which enhanced the filler dispersion. Additionally, the primary proliferation rate results were studied, to

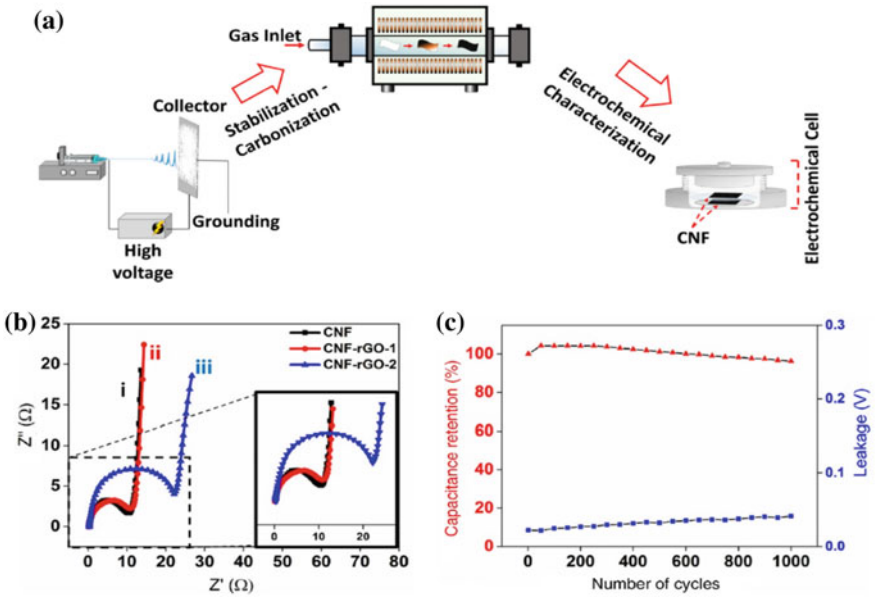

Fig. 13 **a** Schematic diagram illustrates the synthesis of functionalized CNF/fGO for electrochemical measurement in a two-electrode configuration; **b** Nyquist plots of pure (i) CNF, (ii) CNF/fGO-1, and (iii) CNF/fGO-2. The inset magnified the high frequency region of the spectra; **c** capacitance retention and voltage drop of CNF/fGO-2 as the function of continuous charge/discharge cycles. With permission from [86]. Copyright © 2017, Science Press and Dalian Institute of Chemical Physics, Chinese Academy of Sciences. Published by Elsevier B.V. and Science Press. All rights reserved

examine the capability of MC3T3-E1 osteoblastic cells to proliferate on the surfaces of PCL and PCL/GO-g-PEG nanocomposite scaffolds. The preliminary biological assay indicated that PCL/GO-g-PEG improved the ability of cell growth and attachment, owing to the increased hydrophilicity and the resulting degree of cell affinity for the substrate, when compared with the electrospun PCL scaffold [88]. Other research showed significant improvements in thermal, mechanical, and wettability properties of PLA electrospun nanofibers upon addition of GO-g-PEG was published [82]. These studies found that the PLA/GO-g-PEG demonstrated better wettability with lower water contact angles than PLA and PLA/GO as well as the TGA results, that exhibited the GO-g-PEG had a prominent influence than GO in enhancing the thermal stability of PLA electrospun nanofibers. Besides, a significant enhancement of tensile strength of PLA/GO-g-PEG composite nanofibers was reported [82]. In addition, the initial tests of cytocompatibility with Swiss mouse NIH 3T3 cells of PLA, PLA/GO, and PLA/GO-g-PEG nanofibers, were examined. The results indicated the PLA/GO and PLA/GO-g-PEG composite nanofiber scaffolds were non-toxic to NIH 3T3 cells and able to support cell attachment and growth [82, 88].

It can be generally regarded that these electrospun functionalized graphene/polymer nanofibers are capable of supporting various applications in different fields such as sensors, biosensors, electrodes, energy storage or conversion (supercapacitors, fuel cells, solar cells, and batteries), conductive wires, and biomedical materials.

6 Application of Functionalized Graphene-Based Polymer

6.1 Nanofiber Composites

Various applications can be designed using functionalized graphene/polymer composite nanofibers. For instance, the produced polymer/GO-g-PEG composite nanofiber scaffolds have good cytocompatibility, noncytotoxicity characteristics, superior mechanical, thermal, and electrical properties, which have broad applications in tissue engineering [82, 88]. It was observed that a small amount of GO-g-PEG did not prevent the proliferation and viability of cells, which indicates the high cell affinity of GO-g-PEG. It is expected that the cells will spread on the composite scaffolds and in some cases improve cell growth by having similar rate of cell proliferation to that of tissue culture plates [82, 88].

Advances in sensor technology are in constant demand because of their wide use in various industries, environmental monitoring, space exploration, biomedicine, and pharmaceutics. Therefore, improving Gas/chemical sensors and biosensors with faster response times, higher accuracies, increased sensitivities and other properties is an important area of research.

The desired features of sensors include small sizes, quicker response times, small sample volumes, selectivity or specificity, stability, longevity, and low costs. Therefore, owing to the unique electronic structures, remarkable mechanical, optical, electrochemical, thermal, magnetic properties, and ease of functionalization with antibodies and other bioreceptors, functionalized graphene has been extensively used in ultrasensitive sensors and biosensor applications [89, 90]. Abideen et al. [91] examined the gas sensing characteristics of gold (Au) or palladium (Pd) functionalized RGO-loaded ZnO nanofibers. The gas sensing tests were carried out at varying temperatures and in the presence of varying concentrations of specific gases (see Fig. 14). It was found that the Au-functionalized RGO-loaded ZnO nanofibers showed higher sensitivity toward 1 ppm of carbon monoxide (CO) gas in the air, while the Pd-functionalized sensors exhibited good performance for 1 ppm of benzene (C_6H_6) gas. The high sensing properties of the Au or Pd functionalized RGO loaded ZnO nanofibers was attributed to the RGO/ZnO heterointerfaces, the catalytic effect of Au and Pd nanoparticles, and the large surface area of nanofibers [91]. Li et al. [92] developed a sensor of N-doped, graphene quantum dots decorated with N-doped, carbon nanofibers (NGQDs@NCNFs) composites. The electrochemical sensors for the detection of nitrites found in sausage, pickle, lake water and

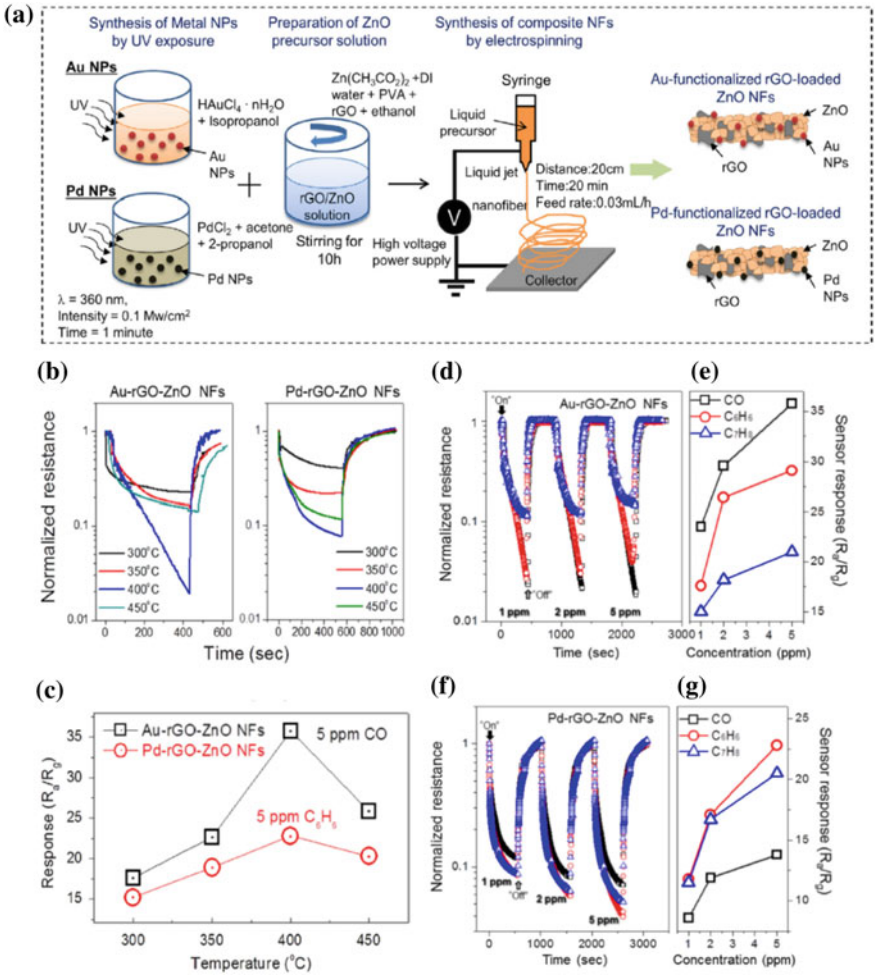

Fig. 14 **a** Schematic illustration of the synthesis procedure for Au- or Pd-functionalized rGO-loaded ZnO NF; **b** Dynamic normalized resistances of the Au-functionalized rGO-loaded ZnO NFs sensor to 5 ppm CO gas at different temperatures and dynamic normalized resistances of the Pd-functionalized rGO-loaded ZnO NFs sensor to 5 ppm C_6H_6 gas at different temperatures; **c** Temperature dependence of the response of the Au-functionalized rGO-loaded ZnO NF sensor and the Pd-functionalized rGO-loaded ZnO NFs sensor to CO and C_6H_6 gases; **d** Dynamic normalized resistances of the Au-functionalized rGO-loaded ZnO NFs sensor to different concentrations of CO, C_6H_6 and C_7H_8 gases; **e** Corresponding calibration curves; **f** Dynamic normalized resistances of the Pd-functionalized rGO-loaded ZnO NFs sensor to different concentrations of CO, C_6H_6 and C_7H_8 gases; **g** Corresponding calibration curves. With permission from [91].

tap water showed wide linear ranges (5–300 μM, $R^2 = 0.999$; 400–3000 μM, $R^2 = 0.997$), low detection limit (3 μM), superior reproducibility and selectivity, and good testing recoveries. In another work, Ali et al. [93] reported the fabrication of a microfluidic electrochemical sensor for the detection and immunodiagnosis of breast cancer biomarkers using a new three-dimensional (3D) immunoelectrodes produced by hierarchical graphene foam (GF) functionalized with electrospun carbon-doped titanium dioxide nanofibers ($nTiO_2$) and anti-ErbB2 molecules (see Fig. 15). Blending GF with functional $nTiO_2$ yields high charge transfer resistance, high surface area, and absorption to the sensor's surface by the analyte, resulting in sensor with remarkable detection of breast cancer biomarkers.

Moreover, functionalized graphene nanosheets are a promising material for flexible, transparent, conductive, thin films, and electronic devices, such as transistors [94], solar cells [95], and field emission displays [96], due to their remarkable, mechanical strength and flexibility. Huang et al. [97] presented a simple yet effective technique to synthesize large silver nanoparticles (AgNps)-graphene nanosheet (GNS) films onto a polyethylene terephthalate (PET), a flexible substrate, by decorating AgNps on GNS surface and enhancing self-assembly of AgNps-GNSs onto the surface of PU nanofibers. They found that the AgNp-GNS (5:1)/PU thin film revealed a considerable rising in transmittance after melting, resulting in a thin film with surface resistance of 150 Ω/sq and transmittance of 85% at 550 nm [97]. It has been also reported that the decoration of TiO_2 with metals such as Pd, Nickel (Ni) and Au with graphene, improve the catalytic and photocatalytic characteristics of TiO_2 [98–100]. The fabrication of Pd-functionalized graphene nanoparticles merged with TiO_2 composite nanofibers displayed good photocatalysis to methylene blue [101].

Graphene quantum dots (GQDs) have extraordinary electrical conductivity, good dispersion in various solvents, tunable photoluminescence, high specific surface area, and exhibit low toxicity and good biocompatibility, thus having contributed to energy storage devices applications [102]. For example, the electropolymerization of poly(3,4-ethylenedioxythiophene) (PEDOT) onto polyvinyl alcohol-graphene quantum dot-cobalt oxide (PVA-GQD-Co_3O_4), (PVA-GQD-Co_3O_4/PEDOT) nanofiber composite showed a specific capacitance of 361.97 F/g, low equivalent series resistance (ESR) and good stability with retention of 96% after 1000 cycles. The results also inducted a high specific energy and exceptional power ranging from 16.51 to 19.98 W/kg and 496.10 to 2396.99 W/kg, as the current density increased from 1.0 to 5.0 A/g [102]. In another example, GQD/PANi (GQDP) nanofiber exhibited an excellent specific capacitance value of $\sim$1044 F/g at a current density of 1 A/g as well as moderate cyclic stability with a retention of life time of 80.1% after 3000 cycles [103].

Contaminants such as dyes that contribute to water pollution crisis that has affected agriculture, industries and inevitably economic growth has generated interest in solving this problem. Consequently, the process of adsorption is a commonly used technique owing to its relative easy operation, good performance and cost effectiveness when compared with other approaches. Water-dispersible amine-functionalized graphene (G-NH_2) nanosheets, were blended directly into the

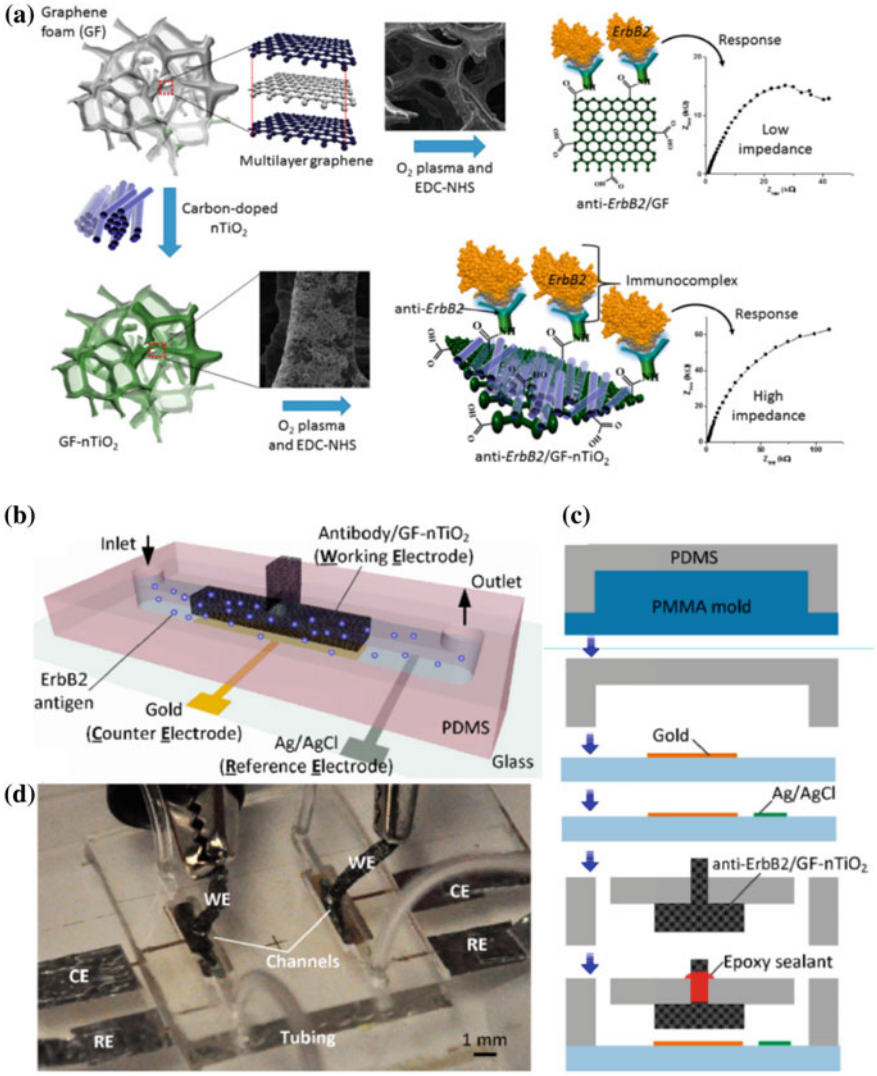

Fig. 15 **a** Functionalization of anti-ErbB2 molecules on the surface of GF and GF − $nTiO_2$ electrodes using EDC-NHS chemistry followed by oxygen plasma treatment; **b** Schematic of the microfluidic immunosensor with 3D porous GF electrode modified with carbon-doped TiO_2 nanofibers for the detection of breast cancer biomarkers; **c** Schematic representation of the fabrication of the microfluidic sensor; **d** Photo of two microfluidic immunosensors. With permission from [93]. Copyright © 2016, American Chemical Society

PVA/glutaraldehyde (GA) aqueous solution for crystal violet (CV) adsorption, deemed hazardous to cells and tissues of living organisms and could possibly be cancer-causing upon prolonged exposure in concentrated amounts [68]. The study indicated that the G-NH_2 is a desirable reinforcing filler to promote higher adsorption sites for the PVA fibers, and by that means an greater adsorption of the CV dye from water in composite mats (removal efficiency of 80.85% compared to 66.24% for crosslinked PVA/GA mats) [68].

Additionally, several other studies have concentrated on the application in areas such as antimicrobial agents in food applications, dentistry, drug release, catalysts, recovery of metal ions, medical implants and enzyme carriers [72, 104–106]. Current research and focus on functionalized graphene/polymer nanofiber composites seem to indicate that their use in a variety of industries will be proliferate and long lasting.

7 Conclusions and Future Scope

The functionalization of graphene by covalent and non-covalent methods has been discussed briefly in this chapter. The electrospinning process to prepare modified, graphene based polymer nanofiber composites, their properties and applications were also discussed. It has been proven that these modification techniques are extremely successful when preparing processable graphene. However, it must be remarked that a suitable technique for mass producing functionalized graphene has not yet been discovered. In conclusion, it is important that future research in this field concentrate on realizing grand-scale production of functionalized graphene if science and technology in this area remain relevant when concerning environmental safety and security standards, health, and energy production. Numerous researchers have indicated that the functionalized graphene is a suitable and desirable choice as multifunctional nanofiller, which will encourage many industry developments and forge our steps into a new energy and material world. The use of electrospinning to develop functionalized graphene polymer nanofiber composites is an effective choice when obtaining high specific surface area and fibers at a nanoscale level. Moreover, this method offers appreciable improvements in maximizing specific properties out of the electrospun composites. However, research towards commercializing functionalized graphene polymer electrospun nanofibers in applications as well as the refinement of electrospinning machines needs to be further investigated, so that their advantages can be fully realized to a greater extent. Finally, further investigation on fundamental issues such as the homogeneous distribution of individual functionalized graphene nanofillers, their orientation, connectivity, and interface bonding with the polymer matrix are required.

Acknowledgements The authors would like to thank the NSERC (Natural Science and Engineering Research Council of Canada), and ProAmpac, for their support. We are also sincerely grateful to the Saudi Ministry of Education for their financial support to Hanan Abdali.

References

1. Hassan, M.A., et al.: Fabrication of nanofiber meltblown membranes and their filtration properties. J. Membr. Sci. **427**, 336–344 (2013)
2. Ma, P.X., Zhang, R.: Synthetic nano-scale fibrous extracellular matrix. J. Biomed. Mater. Res. **46**(1), 60–72 (1999)
3. Martin, C.R.: Membrane-based synthesis of nanomaterials. Chem. Mater. **8**(8), 1739–1746 (1996)
4. Nakata, K., et al.: Poly (ethylene terephthalate) nanofibers made by Sea–Island-type conjugated melt spinning and laser-heated flow drawing. Macromol. Rapid Commun. **28**(6), 792–795 (2007)
5. Drosou, C., Krokida, M., Biliaderis, C.G.: Composite pullulan-whey protein nanofibers made by electrospinning: impact of process parameters on fiber morphology and physical properties. Food Hydrocoll. **77**, 726–735 (2018)
6. Kamble, P., et al.: Nanofiber based drug delivery systems for skin: a promising therapeutic approach. J. Drug Deliv. Sci. Technol. **41**, 124–133 (2017)
7. Garg, K., Bowlin, G.L.: Electrospinning jets and nanofibrous structures. Biomicrofluidics **5** (1), 013403 (2011)
8. Theron, S., Zussman, E., Yarin, A.: Experimental investigation of the governing parameters in the electrospinning of polymer solutions. Polymer **45**(6), 2017–2030 (2004)
9. Bhardwaj, N., Kundu, S.C.: Electrospinning: a fascinating fiber fabrication technique. Biotechnol. Adv. **28**(3), 325–347 (2010)
10. Teo, W.E., Ramakrishna, S.: A review on electrospinning design and nanofibre assemblies. Nanotechnology **17**(14), R89 (2006)
11. Cavaliere, S., et al.: Electrospinning: designed architectures for energy conversion and storage devices. Energy Environ. Sci. **4**(12), 4761–4785 (2011)
12. Reneker, D.H., Chun, I.: Nanometre diameter fibres of polymer, produced by electrospinning. Nanotechnology **7**(3), 216 (1996)
13. Ji, X., et al.: Review of functionalization, structure and properties of graphene/polymer composite fibers. Compos. A Appl. Sci. Manuf. **87**, 29–45 (2016)
14. Kuilla, T., et al.: Recent advances in graphene based polymer composites. Prog. Polym. Sci. **35**(11), 1350–1375 (2010)
15. Geim, A.K., Novoselov, K.S.: The rise of graphene. In: Nanoscience and Technology: A Collection of Reviews from Nature Journals, pp. 11–19. World Scientific (2010)
16. Service, R.F.: Materials science. Carbon sheets an atom thick give rise to graphene dreams. Science (New York, NY) **324**(5929), 875 (2009)
17. Pan, Y., Sahoo, N.G., Li, L.: The application of graphene oxide in drug delivery. Expert Opin. Drug Deliv. **9**(11), 1365–1376 (2012)
18. Kuila, T., et al.: Chemical functionalization of graphene and its applications. Prog. Mater. Sci. **57**(7), 1061–1105 (2012)
19. Gao, W.: The chemistry of graphene oxide. In: Graphene Oxide, (pp. 61–95). Springer, Berlin (2015)
20. Wong, C.H.A., Pumera, M.: Stripping voltammetry at chemically modified graphenes. RSC Adv. **2**(14), 6068–6072 (2012)
21. Szabó, T., et al.: Evolution of surface functional groups in a series of progressively oxidized graphite oxides. Chem. Mater. **18**(11), 2740–2749 (2006)
22. Nethravathi, C., et al.: Graphite oxide-intercalated anionic clay and its decomposition to graphene–inorganic material nanocomposites. Langmuir **24**(15), 8240–8244 (2008)
23. Tung, V.C., et al.: High-throughput solution processing of large-scale graphene. Nat. Nanotechnol. **4**(1), 25 (2009)
24. Staudenmaier, L.: Verfahren zur darstellung der graphitsäure. Ber. Dtsch. Chem. Ges. **31**(2), 1481–1487 (1898)

25. Hummers Jr., W.S., Offeman, R.E.: Preparation of graphitic oxide. J. Am. Chem. Soc. **80**(6), 1339–1339 (1958)
26. Gao, C., et al.: A green method to fast prepare single-layer graphene oxide. China patent CN104310385A, 28 Jan 2015 (in Chinese)
27. Yu, H., et al.: High-efficient synthesis of graphene oxide based on improved hummers method. Sci. Rep. **6**, 36143 (2016)
28. Stankovich, S., et al.: Synthesis of graphene-based nanosheets via chemical reduction of exfoliated graphite oxide. Carbon **45**(7), 1558–1565 (2007)
29. Wang, H., et al.: Solvothermal reduction of chemically exfoliated graphene sheets. J. Am. Chem. Soc. **131**(29), 9910–9911 (2009)
30. Si, Y., Samulski, E.T.: Synthesis of water soluble graphene. Nano Lett. **8**(6), 1679–1682 (2008)
31. Wang, G., et al.: Facile synthesis and characterization of graphene nanosheets. J. Phys. Chem. C **112**(22), 8192–8195 (2008)
32. Stankovich, S., et al.: Graphene-based composite materials. Nature **442**(7100), 282 (2006)
33. Zhang, J., et al.: Reduction of graphene oxide via L-ascorbic acid. Chem. Commun. **46**(7), 1112–1114 (2010)
34. Kim, H., Abdala, A.A., Macosko, C.W.: Graphene/polymer nanocomposites. Macromolecules **43**(16), 6515–6530 (2010)
35. Schniepp, H.C., et al.: Functionalized single graphene sheets derived from splitting graphite oxide. J. Phys. Chem. B **110**(17), 8535–8539 (2006)
36. McAllister, M.J., et al.: Single sheet functionalized graphene by oxidation and thermal expansion of graphite. Chem. Mater. **19**(18), 4396–4404 (2007)
37. Steurer, P., et al.: Functionalized graphenes and thermoplastic nanocomposites based upon expanded graphite oxide. Macromol. Rapid Commun. **30**(4–5), 316–327 (2009)
38. Shen, B., et al.: Melt blending in situ enhances the interaction between polystyrene and graphene through π–π stacking. ACS Appl. Mater. Interfaces **3**(8), 3103–3109 (2011)
39. Stankovich, S., et al.: Stable aqueous dispersions of graphitic nanoplatelets via the reduction of exfoliated graphite oxide in the presence of poly (sodium 4-styrenesulfonate). J. Mater. Chem. **16**(2), 155–158 (2006)
40. Huang, X., et al.: Graphene-based composites. Chem. Soc. Rev. **41**(2), 666–686 (2012)
41. Karousis, N., Tagmatarchis, N., Tasis, D.: Current progress on the chemical modification of carbon nanotubes. Chem. Rev. **110**(9), 5366–5397 (2010)
42. Tasis, D., et al.: Chemistry of carbon nanotubes. Chem. Rev. **106**(3), 1105–1136 (2006)
43. Choi, E.-Y., et al.: Noncovalent functionalization of graphene with end-functional polymers. J. Mater. Chem. **20**(10), 1907–1912 (2010)
44. Liu, J., et al.: Synthesis, characterization, and multilayer assembly of pH sensitive graphene–polymer nanocomposites. Langmuir **26**(12), 10068–10075 (2010)
45. Liu, J., et al.: Noncovalent DNA decorations of graphene oxide and reduced graphene oxide toward water-soluble metal–carbon hybrid nanostructures via self-assembly. J. Mater. Chem. **20**(5), 900–906 (2010)
46. Choi, B.G., et al.: Solution chemistry of self-assembled graphene nanohybrids for high-performance flexible biosensors. ACS Nano **4**(5), 2910–2918 (2010)
47. Salavagione, H.J., Gomez, M.A., Martinez, G.: Polymeric modification of graphene through esterification of graphite oxide and poly (vinyl alcohol). Macromolecules **42**(17), 6331–6334 (2009)
48. Liu, Z., et al.: PEGylated nanographene oxide for delivery of water-insoluble cancer drugs. J. Am. Chem. Soc. **130**(33), 10876–10877 (2008)
49. Park, S., Ruoff, R.S.: Chemical methods for the production of graphenes. Nat. Nanotechnol. **4**(4), 217 (2009)
50. Shan, C., et al.: Water-soluble graphene covalently functionalized by biocompatible poly-L-lysine. Langmuir **25**(20), 12030–12033 (2009)

51. Lee, S.H., et al.: Polymer brushes via controlled, surface-initiated atom transfer radical polymerization (ATRP) from graphene oxide. Macromol. Rapid Commun. **31**(3), 281–288 (2010)
52. Niyogi, S., et al.: Spectroscopy of covalently functionalized graphene. Nano Lett. **10**(10), 4061–4066 (2010)
53. Liu, H., et al.: Photochemical reactivity of graphene. J. Am. Chem. Soc. **131**(47), 17099–17101 (2009)
54. Vadukumpully, S., et al.: Functionalization of surfactant wrapped graphene nanosheets with alkylazides for enhanced dispersibility. Nanoscale **3**(1), 303–308 (2011)
55. Liu, Y., et al.: Biocompatible graphene oxide-based glucose biosensors. Langmuir **26**(9), 6158–6160 (2010)
56. Du, J., Cheng, H.M.: The fabrication, properties, and uses of graphene/polymer composites. Macromol. Chem. Phys. **213**(10–11), 1060–1077 (2012)
57. Abdali, H., Ajji, A.: Preparation of electrospun nanocomposite nanofibers of polyaniline/poly(methyl methacrylate) with amino-functionalized graphene. Polymers **9**(9), 453 (2017)
58. He, H., Gao, C.: General approach to individually dispersed, highly soluble, and conductive graphene nanosheets functionalized by nitrene chemistry. Chem. Mater. **22**(17), 5054–5064 (2010)
59. Jia, L., Liu, J., Wang, H.: Preparation of poly (diallyldimethylammonium chloride)-functionalized graphene and its applications for H_2O_2 and glucose sensing. Electrochim. Acta **111**, 411–418 (2013)
60. Moayeri, A., Ajji, A.: Fabrication of polyaniline/poly (ethylene oxide)/non-covalently functionalized graphene nanofibers via electrospinning. Synth. Met. **200**, 7–15 (2015)
61. Rafiee, M.A., et al.: Fracture and fatigue in graphene nanocomposites. Small **6**(2), 179–183 (2010)
62. Dasari, A., Yu, Z.-Z., Mai, Y.-W.: Electrically conductive and super-tough polyamide-based nanocomposites. Polymer **50**(16), 4112–4121 (2009)
63. Chatterjee, S., Nüesch, F., Chu, B.: Crystalline and tensile properties of carbon nanotube and graphene reinforced polyamide 12 fibers. Chem. Phys. Lett. **557**, 92–96 (2013)
64. Zheng, W., Lu, X., Wong, S.C.: Electrical and mechanical properties of expanded graphite-reinforced high-density polyethylene. J. Appl. Polym. Sci. **91**(5), 2781–2788 (2004)
65. Hou, W., et al.: Preparation and physico-mechanical properties of amine-functionalized graphene/polyamide 6 nanocomposite fiber as a high performance material. RSC Adv. **4**(10), 4848–4855 (2014)
66. Jiang, L., et al.: Preparation and characterization of graphene/poly (vinyl alcohol) nanocomposites. J. Appl. Polym. Sci. **118**(1), 275–279 (2010)
67. Liang, J., et al.: Molecular-level dispersion of graphene into poly (vinyl alcohol) and effective reinforcement of their nanocomposites. Adv. Func. Mater. **19**(14), 2297–2302 (2009)
68. Chailek, N., et al.: Crosslinking assisted fabrication of ultrafine poly (vinyl alcohol)/functionalized graphene electrospun nanofibers for crystal violet adsorption. J. Appl. Polym. Sci. **135**(22), 46318 (2018)
69. Chen, Y., et al.: Preparation, mechanical properties and biocompatibility of graphene oxide/ultrahigh molecular weight polyethylene composites. Eur. Polymer J. **48**(6), 1026–1033 (2012)
70. Yu, J., et al.: Permittivity, thermal conductivity and thermal stability of poly (vinylidene fluoride)/graphene nanocomposites. IEEE Trans. Dielectr. Electr. Insul. **18**(2), 478–484 (2011)
71. Zhang, H.-B., et al.: The effect of surface chemistry of graphene on rheological and electrical properties of polymethylmethacrylate composites. Carbon **50**(14), 5117–5125 (2012)
72. Leyva-Porras, C., et al.: EELS analysis of Nylon 6 nanofibers reinforced with nitroxide-functionalized graphene oxide. Carbon **70**, 164–172 (2014)

73. Cao, L., et al.: Fabrication of chitosan/graphene oxide polymer nanofiber and its biocompatibility for cartilage tissue engineering. Mater. Sci. Eng. C **79**, 697–701 (2017)
74. Hong-Pei, L., et al.: Electrospinning gelatin/chitosan/hydroxyapatite/graphene oxide composite nanofibers with antibacterial properties. J. Inorg. Mater. **30**(5), 516–522 (2015)
75. Ardeshirzadeh, B., et al.: Controlled release of doxorubicin from electrospun PEO/chitosan/graphene oxide nanocomposite nanofibrous scaffolds. Mater. Sci. Eng. C **48**, 384–390 (2015)
76. Bao, Q., et al.: Graphene–polymer nanofiber membrane for ultrafast photonics. Adv. Func. Mater. **20**(5), 782–791 (2010)
77. Ding, B., et al.: Gas sensors based on electrospun nanofibers. Sensors **9**(3), 1609–1624 (2009)
78. Doshi, J., Reneker, D.H.: Electrospinning process and applications of electrospun fibers. J. Electrostat. **35**(2–3), 151–160 (1995)
79. Feng, L., Xie, N., Zhong, J.: Carbon nanofibers and their composites: a review of synthesizing, properties and applications. Materials **7**(5), 3919–3945 (2014)
80. Zong, X., et al.: Structure and process relationship of electrospun bioabsorbable nanofiber membranes. Polymer **43**(16), 4403–4412 (2002)
81. Ramazani, S., Karimi, M.: Electrospinning of poly (ε-caprolactone) solutions containing graphene oxide: effects of graphene oxide content and oxidation level. Polym. Compos. **37**(1), 131–140 (2016)
82. Zhang, C., et al.: The surface grafting of graphene oxide with poly (ethylene glycol) as a reinforcement for poly (lactic acid) nanocomposite scaffolds for potential tissue engineering applications. J. Mech. Behav. Biomed. Mater. **53**, 403–413 (2016)
83. Das, S., et al.: Electrospinning of polymer nanofibers loaded with noncovalently functionalized graphene. J. Appl. Polym. Sci. **128**(6), 4040–4046 (2013)
84. Georgakilas, V., et al.: Noncovalent functionalization of graphene and graphene oxide for energy materials, biosensing, catalytic, and biomedical applications. Chem. Rev. **116**(9), 5464–5519 (2016)
85. Hsiao, S.-T., et al.: Preparation and characterization of silver nanoparticle-reduced graphene oxide decorated electrospun polyurethane fiber composites with an improved electrical property. Compos. Sci. Technol. **118**, 171–177 (2015)
86. Chee, W., et al.: Functionalized graphene oxide-reinforced electrospun carbon nanofibers as ultrathin supercapacitor electrode. J. Energy Chem. **26**(4), 790–798 (2017)
87. Moayeri, A., Ajji, A.: High capacitance carbon nanofibers from poly (acrylonitrile) and poly (vinylpyrrolidone)-functionalized graphene by electrospinning. J. Nanosci. Nanotechnol. **17**(3), 1820–1829 (2017)
88. Scaffaro, R., et al.: Electrospun PCL/GO-g-PEG structures: processing-morphology-properties relationships. Compos. A Appl. Sci. Manuf. **92**, 97–107 (2017)
89. Latif, U., Dickert, F.L.: Graphene hybrid materials in gas sensing applications. Sensors **15**(12), 30504–30524 (2015)
90. Llobet, E.: Gas sensors using carbon nanomaterials: a review. Sens. Actuators B Chem. **179**, 32–45 (2013)
91. Abideen, Z.U., et al.: Sensing behavior to ppm-level gases and synergistic sensing mechanism in metal-functionalized rGO-loaded ZnO nanofibers. Sens. Actuators B Chem. **255**, 1884–1896 (2018)
92. Li, L., et al.: Quantitative detection of nitrite with N-doped graphene quantum dots decorated N-doped carbon nanofibers composite-based electrochemical sensor. Sens. Actuators B Chem. **252**, 17–23 (2017)
93. Ali, M.A., et al.: Microfluidic immuno-biochip for detection of breast cancer biomarkers using hierarchical composite of porous graphene and titanium dioxide nanofibers. ACS Appl. Mater. Interfaces **8**(32), 20570–20582 (2016)
94. Sun, Q., et al.: Characteristics of a pentacene thin film transistor with periodic groove patterned poly (methylmethacrylate) dielectrics. Appl. Phys. Lett. **96**(10), 41 (2010)

95. Ratcliff, E.L., Lee, P.A., Armstrong, N.R.: Work function control of hole-selective polymer/ITO anode contacts: an electrochemical doping study. J. Mater. Chem. **20**(13), 2672–2679 (2010)
96. Yoon, B.-J., et al.: Fabrication of flexible carbon nanotube field emitter arrays by direct microwave irradiation on organic polymer substrate. J. Am. Chem. Soc. **127**(23), 8234–8235 (2005)
97. Huang, Y.-L., et al.: Self-assembly of silver–graphene hybrid on electrospun polyurethane nanofibers as flexible transparent conductive thin films. Carbon **50**(10), 3473–3481 (2012)
98. Zhang, L., et al.: Electrospun titania nanofibers segregated by graphene oxide for improved visible light photocatalysis. Appl. Catal. B **201**, 470–478 (2017)
99. Zhang, H., et al.: P25-graphene composite as a high performance photocatalyst. ACS Nano **4**(1), 380–386 (2010)
100. Wu, M.-C., et al.: Enhanced photocatalytic activity of TiO2 nanofibers and their flexible composite films: decomposition of organic dyes and efficient H2 generation from ethanol-water mixtures. Nano Res. **4**(4), 360–369 (2011)
101. Lee, H.-G., et al.: Facile synthesis of functionalized graphene-palladium nanoparticle incorporated multicomponent TiO2 composite nanofibers. Mater. Chem. Phys. **154**, 125–136 (2015)
102. Abidin, S.N.J.S.Z., et al.: Electropolymerization of poly (3, 4-ethylenedioxythiophene) onto polyvinyl alcohol-graphene quantum dot-cobalt oxide nanofiber composite for high-performance supercapacitor. Electrochim. Acta (2017)
103. Mondal, S., Rana, U., Malik, S.: Graphene quantum dot-doped polyaniline nanofiber as high performance supercapacitor electrode materials. Chem. Commun. **51**(62), 12365–12368 (2015)
104. De Faria, A.F., et al.: Antimicrobial electrospun biopolymer nanofiber mats functionalized with graphene oxide–silver nanocomposites. ACS Appl. Mater. Interfaces **7**(23), 12751–12759 (2015)
105. Ding, X., et al.: Spinning fabrication of graphene/polypyrrole composite fibers for all-solid-state, flexible fibriform supercapacitors. J. Mater. Chem. A **2**(31), 12355–12360 (2014)
106. Li, S., et al.: One-step synthesis of graphene/polypyrrole nanofiber composites as cathode material for a biocompatible zinc/polymer battery. ACS Appl. Mater. Interfaces **6**(19), 16679–16686 (2014)

Graphene Functionalization and Nanopolymers

Martin Kássio Leme Silva and Ivana Cesarino

Abstract This chapter focuses on the functionalization of graphene, mainly in graphene oxide (GO) and reduced graphene oxide (rGO). In this sense the main syntheses for obtaining GO and rGO, as well as their characterizations and applications, were described. To evaluate the electrochemical, spectrophotometric and morphological properties of functionalized graphene, the GO obtained commercially and the rGO synthesized by the chemical method using sodium borohydride were characterized by scanning electron microscopy, Raman, UV-vis, cyclic voltammetry and electrochemical impedance spectroscopy. Through these characterizations it is possible to comprehend the differences between GO and rGO. After that, the importance of the graphene functionalized in the development of electrochemical biosensors and sensors are presented.

Keywords Graphene oxide · Reduced graphene oxide · Characterization · Electroanalysis

1 Introduction

Carbon based materials comprises a large variety of applications in electroanalysis. The physical properties of these materials have drawn the attention of many researchers in the field of sensors for monitoring applications. Graphene is a 2D allotrope of carbon, which normally forms an atomic monolayer sheet. Linus Pauling proposed the first structure of graphene in 1972, but only in 2004, Novoselov and co-works presented a new approach for graphene due to its interesting optical, mechanical, thermal and electronic properties. Graphene usually refers to a single layer of sp^2 bonded carbon atoms, also known as pristine graphene. IUPAC describes graphene as *a single carbon layer of the graphite structure, describing its nature by analogy to a polycyclic aromatic hydrocarbon of*

M. K. L. Silva · I. Cesarino (✉)
School of Agriculture, Sao Paulo State University (UNESP), Botucatu, SP, Brazil
e-mail: ivana.cesarino@unesp.br

A. Khan et al. (eds.), *Graphene Functionalization Strategies*,
Carbon Nanostructures, https://doi.org/10.1007/978-981-32-9057-0_6

quasi-infinite size [1]. However, the high cost of fabrication and the deficiency of manufacturing in large scale makes graphene a complicated material for application in electroanalytical sensors. Therefore, another forms of graphene, such as graphene oxide (GO) and reduced graphene oxide (rGO) are employed instead [2, 3].

Graphene oxide is another form of graphene, also known as chemically modified graphene, which is prepared by oxidation and exfoliation of graphite oxide. These processes lead to an extensive modification of the basal plane of graphene. Another singularity of GO is the oxygen content, usually characterized by a C/O ratio less than 3:1 and typically closer to 2:1 [3]. GO can also be characterized as a single monomolecular layer of graphite with various oxygen containing functionalities such as epoxide, carbonyl, carboxyl and hydroxyl groups [2].

The reduction of GO forms a new material known as reduced graphene oxide (rGO). This reduced form of GO (rGO) sheets are usually considered as one kind of chemically derived graphene. The main goal of GO reduction is to produce a graphene-like material, with the same structure and properties of pristine graphene. There are several protocols for GO reduction, such as, hydrothermal, chemical, microwave and thermal [4]. Those methodologies will further be investigated in the next section. The reduction processes from GO to rGO diminishes the oxygen content in the material and cause several structural defects on rGO surface. The C/O ratio is not zero like pristine graphene, however the reduced amount of functional groups based on C–O bonds influences on the electroanalytical response for several analytical targets [5, 6].

GO and rGO have come to the forefront of electroanalytical applications in past few years. Versatility, easy manipulation, modification and good stability make these materials gain great attention in the field of electroanalysis. The modification of working electrodes such as glassy carbon (GC), boron-doped diamond (BDD), and screen-printed electrodes is the common approach for GO and rGO for sensing applications [7].

Enzymatic biosensors, immunosensors and modification with metallic nanoparticles for contaminants determination are some examples of GO and rGO applications. In biosensing, these functionalized graphene proved to be promising materials for immobilizing enzymes and enhance detection of different targets by the effect of enzyme activity [8–10]. The main applications in biosensors include detection of glucose, cholesterol, phenol, catechol, neurotransmitters and carbaryl [11].

In the field of immunosensing, the measuring of the antibody-antigen specific conjugation is the target of this type of electroanalytical sensors. Hence, GO and rGO are interesting platforms for antibody or antigen immobilization. Several protocols for these biomolecules have been extensively investigated. The use of nanopolymers, bioconjugation agents, metallic nanoparticles are some successful examples in this field [12, 13].

As highlighted above, GO and rGO hold interesting properties and applications of great interest in electroanalysis. However, the main point of this chapter will be focused on the fabrication and functionalization of GO and rGO nanomaterials for different sensing applications. Firstly, we will discuss the various methodologies for fabrication of these materials and the proper characterization by electrochemical,

morphological and spectroscopy techniques. Then, recent strategies and functionalization methodologies will be covered in the next section. Finally, the recent applications for targeting hazardous pollutants using graphene modified with metallic nanoparticles (MNPs) will be covered in the last section.

2 Synthesis

The techniques for synthesis of graphene are compressed in several methodologies. In literature, the most applied methods consists in mechanical or chemical exfoliation of graphite, unrolling of carbon nanotubes (CNTs), chemical vapor deposition (CVD) or epitaxial growth, reduction of GO and several others organic synthetic protocols [14, 15]. However, in this chapter we will focus on the synthesis of GO and rGO materials and its applications.

2.1 Synthesis of Graphene Oxide

The main objective of graphite oxidation to obtain GO was actually to prepare graphene at large-scale. Therefore, several methodologies for production of GO in large-scale starting from graphite was intensively reviewed and optimized through years. Brodie developed the first methodology for obtaining GO in 1860. Precisely, graphite is oxidized to graphite oxide using fumaric nitric acid and potassium chlorate under controlled temperature, and then the material obtained is reduced to graphene oxide by thermal exfoliation/reduction processes [16]. Staudenmaier in 1898, Hofmann in 1937, Hummers in 1958 and the novel tour method in 2010 are some examples of improvement of GO fabrication [17]. All methodologies cited above make use of strong oxidants and consequent thermal exfoliation and reduction by thermal shock to produce GO [18].

The most common methodology for synthesis of GO is based on the work presented by Hummers and Offeman in 1958. Briefly, the graphite is oxidized to graphite oxide by treatment with a solution containing sulfuric acid, potassium permanganate and sodium nitrate (water-free solution) [4, 19].

However, GO itself has several functional groups and a high oxigen content. Hence, another step of reduction of the material is required for obtaining a graphene-like material.

2.2 Synthesis of Reduced Graphene Oxide

The reduced form of GO produces a graphene-like material, known as rGO. The common techniques for production of rGO are chemical, thermal and

Table 1 Comparison of different reductant agents in rGO synthesis

Reductant agent	Application	Conductivity σ (S/cm)	C/O ratio	References
$NaBH_4$/SDS	Detection of estriol	–	–	[26]
$NaBH_4$ only	Electrical conductance	0.045	8.6	[59]
Hydrazine hydrate		10.3	2	[60]
Glucose sugar	Detection of catecholamine	–	–	[20]
Ascorbic acid (AA)	Various applications	980	5.15	[61]
Shewanella	Bioremediation of bacteria	–	–	[62]
Yeast	–	43	5.9	[63]
hydrohalic acids	–	298	>14.9	[64]

electrochemical reduction. Variations and modifications will also be covered in the subsequent topics.

2.2.1 Chemical Reduction

Chemical reduction of GO to rGO does not require expensive equipment and the environment is not as critical as other synthesis routes. These characteristics make chemical reduction the most common methodology for reduction of GO. Through years, several reducing agents have been applied for synthesis of rGO. Hydrazine hydrate, sodium borohydride ($NaBH_4$) accompanied or not with dodecyl sodium phosphate (SDS), vitamin C, pyrogallol and potassium hydroxide (KOH) are some of the most common reductant agents for rGO synthesis. However, some reagents, such as, hydrazine and its by-products are environmentally hazardous and can affect human health. The search for greener reducing agents is the main goal in rGO synthesis. Organic acids, microorganisms, sugars, extract from plants, protein and amino acids, antioxidants are some examples of green reductants used for synthesis of rGO. Table 1 summarizes the most common reductant agents for rGO synthesis.

2.2.2 Thermal Reduction

The reduction of GO by thermal methodology is composed mainly in two techniques: Thermal annealing and microwave/photo reduction. Briefly, thermal annealing is the rapid heating of GO. Usually, thermal annealing uses thermal irradiation for reducing GO. Several authors reports thermal annealing a two-hand technique. In one side the C/O ratio of rGO is close to graphene, in the other hand this procedure is found only to produce small size and wrinkled graphene sheets. In addition the electrical conductivity is much lower than pristine graphene.

Another route for thermal reduction of GO can accomplished using electromagnetic irradiation; the mainly two approaches are microwave and photo reduction. Using microwave irradiation, which heats substances uniformly and rapidly,

rGO can be produced up to 1 min using graphite powders and a commercial microwave system [20, 21]. Using photo reduction, the sample is irradiated by a laser beam for instance. Zhang et al. reported an obtained rGO films with an electrical conductivity of 256 S/cm, proving that a laser-based reduction is efficient.

2.2.3 Electrochemical Reduction

Electrochemical removal of oxygen functionalities of GO sheets to produce rGO is a promise method holding easy preparation and application. Normally carried in 3-electrode conventional cell the reduction of GO takes place on the surface of the working electrode (WE) as shown in Fig. 1. A thin film of GO is casted o the surface of the WE (GC, ITO, etc.).

Unnikrishnan et al. reported the reduction of GO to rGO by performing continuous cyclic voltammetry (15 cycles) ranging from 0 to −1.5 V at a scan rate of 50 mV s^{-1} in a phosphate buffer solution [22]. Several combinations of electrolytes (KNO_3, PBS, aqueous electrolyte, etc.) and electrochemical techniques (cyclic, electrophoretic deposition, chronoamperometry, etc.) have been reported in this methodology.

2.2.4 Microwave-Assisted Hydrothermal Reduction

The microwave-assisted hydrothermal (MAH), also known as microwave-solvothermal, is a methodology for synthesis rGO using unique properties of

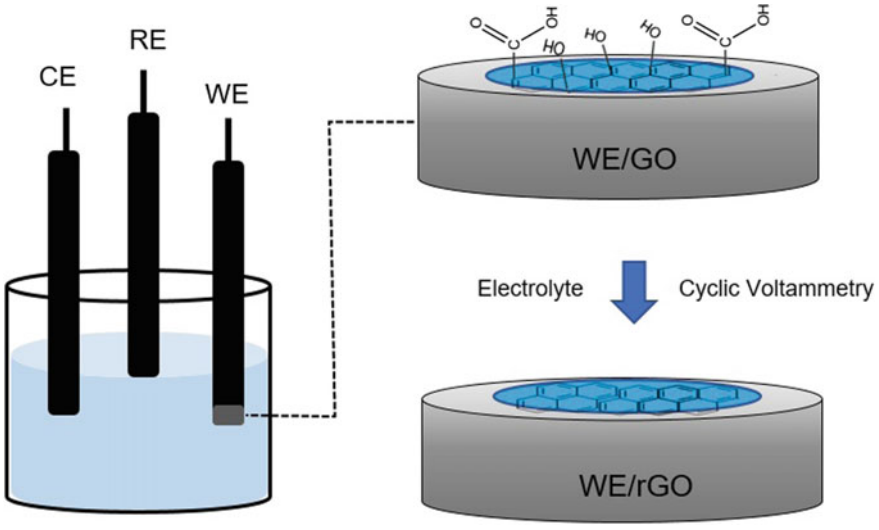

Fig. 1 Electrochemical reduction of rGO

Table 2 Comparison of properties of rGO by different methods

Reduction method	Application	Conductivity σ (S/cm)	C/O ratio	References
Chemical	Various applications	980	5.15	[61]
Thermal annealing	Synthesis	2000	15–18	[65]
Photo reduction	Synthesis	256	–	[40, 41]
Electrochemical reduction	Detection of catecholamine	85	23.9	[66]
MHA	Determination of sulfamethazine	–	–	[24]

solvents under hydrothermal conditions, which can change drastically properties of vapor pressure, surface tension, viscosity and density of the solvent. Combined with application of microwave, which is an electromagnetic wave with a frequency between 300 MHz and 300 GHz and the wavelength ranging from 1 m to 1 mm, gives the MAH methodology. The advantages of MAH method lies on the preparation of nanoscale materials, also energy saving conditions and eco-friendly advantages make this technique an interesting route for rGO and rGO-MNPs synthesis [23]. MAH applications varies from metal oxides and hydroxides, gas sensor, catalytic, electrochemical, solar cells and optical applications.

In electroanalysis, [24] reported the synthesis of rGO-gold nanoparticles (rGO-AuNPs) composite for the detection of sulfamethazine antibiotic [24]. The obtained composite showed nanoparticles ranging from 5 to 30 nm. [25] reported another interesting application of graphene-wrapped with copper oxide synthesized using MAH methodology for lithium ion batteries [25].

As described above, there are several methodologies for reducing GO into rGO. Table 2 summarizes the electrochemical conductivity of the obtained materials in correlation with the corresponding methodology. In the next section, we will cover the characterization of GO and rGO composites by electrochemical, spectroscopy and spectrophotometric techniques.

3 Characterization of Functionalized Graphene: GO and RGO

To evaluate the electrochemical, spectroscopic and morphological properties of GO and rGO, the materials were characterized by scanning electron microscopy, Raman, UV-vis, cyclic voltammetry (CV) and electrochemical impedance spectroscopy (EIS). For this purpose, the GO obtained from Sigma-Aldrich (4 mg/mL) and the rGO synthesized from GO by sodium borohydride chemical method were studied. Figure 2 presented the SEM micrographs of the GO and rGO. Figure 2a displays typical images of GO where the material consists of a mixture of single

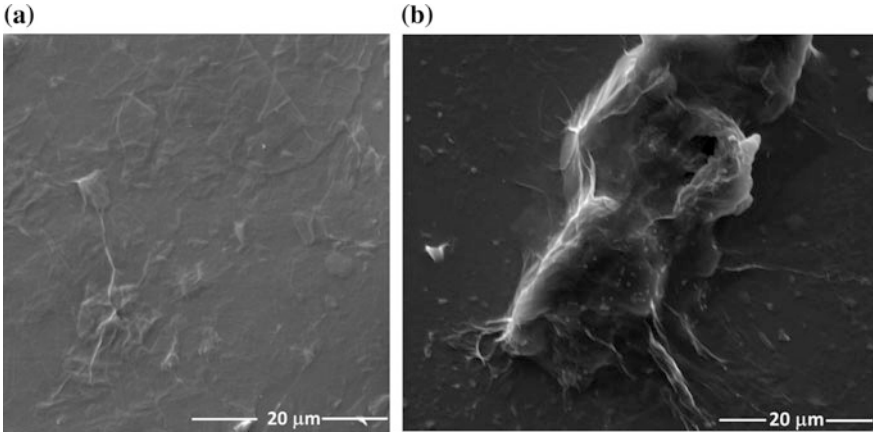

Fig. 2 SEM micrographs for: **a** GO and **b** rGO

layers and multi-layer graphene sheets. Figure 2b presents the images of functionalized GO, in which the graphitic material displayed a typical wrinkled structure with plenty of corrugations. The reduction of GO causes the unstacking of sheets and, consequently, the unblocking of active sites [8, 26]. This profile was also observed in other studies, in which the GO was chemically synthesized from Natural Flake Graphite (NFG) or via the Hummers and Offeman [19] method and the reduction was performed using hydrazine [27, 28].

Raman spectroscopy is considered to be a popular technique for characterization of the structural and electronic properties of graphene, including disorder and defect structures [20, 21]. Thus, the spectroscopic characterizations of the materials were performed by Raman and UV-vis as shown in Fig. 3. Figure 3a presents Raman spectra for the GO and the chemical functionalized GO. It was observed that the

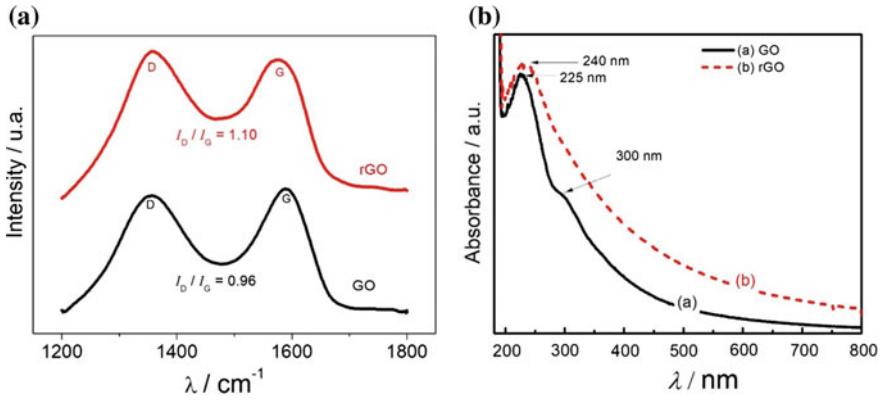

Fig. 3 Spectroscopic characterizations of the functionalized graphene: **a** Raman spectra and **b** UV-vis for the GO and rGO

synthesized GO and rGO presented two characteristic absorption bands in its Raman spectrum: the G band at around 1585 cm^{-1} and the D band at 1355 cm^{-1}. The G band corresponds to bond stretching of sp^2 carbon pairs. The D band is associated with the breathing mode of aromatic rings with dangling bond in-plane terminations [26]. The relationship between the intensity of the D band (I_D) and G band (I_G) is usually employed to evaluate the size of the in-plane sp^2 domains for carbon materials. The obtained values for the I_D/I_G ratio was 0.96 and 1.10 for GO and rGO, respectively. The higher magnitude of the D band for the functionalized GO suggests the increase in disorder and confirms the occurrence of reduced graphene oxide. Also, the increase of the ratio from GO to rGO indicated that during the reduction of GO, most of oxygenated functional groups were removed, resulting in a decrease in the average size of the sp^2 domains [29]. This same behaviour was observed in several works of the literature, in which GO and functionalized GO were obtained by different methodologies [30–33]. The characterization of the materials by UV-vis spectroscopy is shown in Fig. 3b. As observed in others works [30, 34, 35] the UV-vis spectrum of GO showed 2 maximum bands at 225 and 300 nm, which are due to the $\pi \rightarrow \pi^*$ transition of aromatic C–C bonds and $n \rightarrow \pi^*$ transition of C=O. However, rGO presented only one maximum band at 240 nm. This results were expected since rGO has a higher C/O coefficient due to removal of oxygen functionalities and establishment of C=C conjugated graphene structures as observed by Raman spectroscopy.

The electrochemical characterizations of the materials were performed by CV and EIS as presents in Fig. 4. For this purpose, the GO and rGO was dispersed in ultrapure water at a concentration of 0.3 mg/mL. After that, 10 μL of these suspensions were dropped in the cleaned GC electrodes. Figure 4a showed the cyclic voltammograms of the GC/GO and GC/rGO electrodes in 0.2 mol L^{-1} phosphate buffer solution (PBS) pH 7.4, 0.1 mol L^{-1} KCl containing 5.0 mmol L^{-1} of the redox couple $[Fe(CN_6)]^{3-/4-}$ with a scan rate of 50 mV s^{-1}. The voltammetric

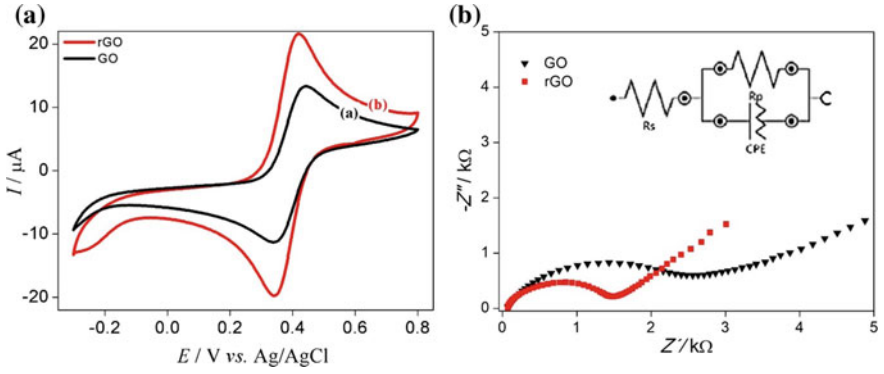

Fig. 4 Electrochemical characterizations of the functionalized graphene: **a** Cyclic voltammograms and **b** Nyquist diagram for GC/GO and GC/rGO electrodes. Inset: electrical equivalent circuit

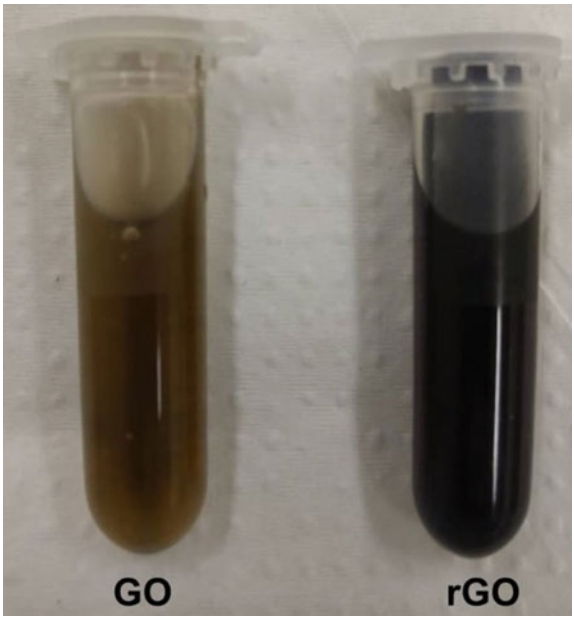

Fig. 5 Image of the functionalized graphene

profiles show well-defined oxidation and reduction peaks for the GC/GO and GC/rGO electrodes due to the Fe^{3+}/Fe^{2+} redox couple in identical potentials of approximately +0.40 and +0.35 V versus Ag/AgCl/KCl (3 mol L^{-1}), respectively. However, the GC/rGO electrode (curve b) showed a 1.6-fold increase in the peak current compared to the GC/GO electrode (curve a). This increase is due to the presence of defects introduced in its structure, as well less oxygen atoms increase the electron transport [8]. The electrochemical properties of GO and rGO were also analyzed using EIS in order to quantify the charge transfer resistance values for the GC/GO and GC/rGO electrodes as presented in Fig. 4b. Nyquist plots were used to analyze EIS data and presented with the equivalent circuit inset, as shown in Fig. 4b. The EIS plots exhibited R_s for GC/GO about 49.3 Ω, which was larger than GC/rGO (46.9 Ω). The fitted value of R_{ct} obtained for GC/GO and GC/rGO was 1.52 and 2.84 Ω, respectively. The lower value of R_{ct} for rGO was also observed in recent publications [36, 37], indicating the improvement in electron transfer of this material. This behaviour is in agreement with CV experiments that rGO has a higher peak current response for the redox couple.

A visual characterization of the GO and rGO is presented in Fig. 5. Different colours can be seen for the GO and functionalized GO suspensions. The characteristic colour of GO suspension is yellowish, while after reduction the GO presents a darker colour. This is a way of differentiating GO from rGO.

4 Functionalization of Graphene for Electroanalytical Applications

Electrochemical biosensors hold the interesting properties of specific biological recognition processes with the analytical versatility of electrochemical techniques. The main goal of biosensors is to produce a correlation between the concentration of the analyte target and an electrochemical measurement. Usually, the biological component (enzymes, DNA probes, cells and antibodies) is immobilized on the surface of the WE, also known as the transduction component. The electrode converts the biochemical reactions within into quantitative or semi-quantitative electroanalytical response. The immobilization strategy on the electrode is extremely vital for success. The use of nanopolymers, metallic nanoparticles and the functionalities of GO and rGO themselves are some common approaches for biologic component immobilization. In the subsequent topics, we will discuss recent strategies for construction of biosensors. For better understanding purposes, the biosensors will be separated by recognition component.

4.1 Functionalized Graphene for Enzymatic Biosensors

Enzymatic biosensors make use of enzymes, which are proteins that catalyze biochemical reactions in living organisms. Enzymes proved to be very efficient recognition elements and easy handling. A simple scheme of an electrochemical biosensor and the recognition of the electron transfer between enzyme and electrode surface is shown in Fig. 6.

For the last 20 years intensive studies have been made on the immobilization of enzymes on the sensors surfaces, due to the difficulty of this immobilization on the

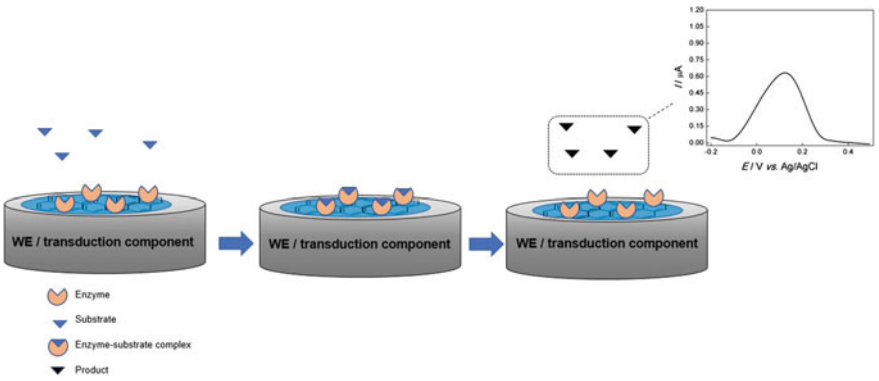

Fig. 6 Enzymatic biosensor based on direct electron transfer between enzyme and electrode surface

bare electrodes surfaces. Enzymes usually have short life times and lose their activities at bare electrodes. Also, there are mass transport problems associated with long paths between the sites of enzyme and the electrode. To overcome such limitations, studies have been focused on different strategies for enzymes immobilization on the electrode surface [38, 39]. There are two categories of immobilization procedures, namely, reversible and irreversible immobilization. The reversible immobilization methods include metal chelation, disulfide bounds formation and adsorption, while the irreversible immobilization methods comprise covalent bonding, cross-linking, entrapment and encapsulation. The covalent bonding represents one of the most frequently used methods for enzyme immobilization, due the stable nature of the bonds formed between functional groups of the enzyme and functional groups present on the support. In these sense, the functionalized graphene, GO and rGO, are presented as an excellent support to be used in the covalent immobilization of enzymes.

Carbonyl groups of GO can immobilize enzymes by a simple binding reaction with free amino groups of enzymes through covalent linkage, as reported by Unnikrishnan et al. In the work of Zhang et al. [40, 41] the GO prepared by the modified Hummers method was investigated as a matrix for enzyme immobilization, using horseradish peroxidase and lysozyme, as model enzymes. The immobilization of the enzymes in the GO was observed using AFM and the authors observed that the catalytic performance of the immobilized enzymes is determined by the interaction of enzyme molecules with the functional groups of the GO, but the enzyme specific activity is not influenced by the enzyme loading as far as the substrate surface was not fully covered by the enzyme. The use of chemical linkers are also very common in biosensor manufacturing. Cysteamine and 6-mercaptohexanoic acid (6-MHA) can be used to produce NH_2-functionalites on MoS_2 nanoparticles, and therefore immobilize enzymes by electrostatic bonding [42].

Using rGO as platform for enzymes immobilization, two different effects are highlighted for biosensors construction. Structural defects and residual oxygen functional groups in rGO surface can contribute for enzyme immobilization. Ting et al. [43] used the electrochemically reduced graphene oxide in the immobilization of the catalase enzyme for detection of H_2O_2. The fabricated biosensor exhibited quick response (5 s), excellent electrocatalytic activity towards H_2O_2 in the linear concentration range from 0.05 to 1.91 mM with a sensitivity of 7.76 μA mM^{-1} cm^{-2}.

Vijayaraj et al. [44] proposed a glucose biosensor based on rGO and glucose oxidase (GOx) modified a pencil graphite electrode. The efficient immobilization of GOx on rGO surface was confirmed by electrochemical, spectroscopic and morphological measurements. The determination of glucose was performed indirectly by O_2 reduction, which showed high sensitivity, selectivity, reproducibility and stability without a redox mediator. The sensor exhibited a linear current response for a wide range of glucose concentrations between 1.0×10^{-5} and 1.0×10^{-3} M with a detection limit of 5.8 μM.

When the immobilization of enzyme is performed using functionalized graphene as support none bi-functional groups or spacers such as glutaraldehyde and aminopropyltriethoxysilanes is necessary. This constitutes a real contribution from

the biocomposite surface to the efficiency of the biosensor since the cross-linking agents frequently bond themselves to the active sites of enzymes, thus inhibiting their activity.

Some studies compare the properties of the functionalized graphene in the immobilization of enzymes for the construction of electrochemical biosensors. The work developed by Kohori et al. evaluated the GO and rGO in the immobilization of laccase enzyme and its application in the determination of dopamine. The authors observed that the structural defects of rGO facilitate the immobilization of the laccase as a covalent attachment. On the other hand, the laccase is immobilized in the GO by physical adsorption by the interactions of π–π stacking between the rings of GO and those of any aromatic amino acids exposed on the surface of the protein. This immobilization relies on weak physical forces, which can affect the stability of the enzyme. When the rGO-laccase biosensor is compared with the GO-laccase biosensor in the determination of dopamine, the second biosensor showed a lowest cathodic current for the dopamine reduction. This is due to the absence of structural defects on GO sheets which can interfere in the laccase efficiently immobilization. Also, GO has more oxygen atoms than rGO and actually has more functional groups that decrease the electron transport. Thus, the authors concluded that rGO was more efficient in the immobilization of the laccase enzyme.

Modification of rGO with nanopolymers are another example of physical entrapment. Enzymes are adsorbed into the new composite, and the synergistic effect of rGO associated with the thermal stability of nanopolymers provides a stable environment for enzyme encapsulation [45–47].

Reports on enzyme immobilization based rGO-MNPs and rGO-polymer-MNPs electrodes, generally needs a cross-linking agent such as glutaraldehyde for functional groups linking bond [48–51]. Table 3 summarizes the most common approaches for enzyme immobilization on GO and rGO composites.

4.2 Functionalized Graphene for Immunosensors Construction

Electrochemical immunosensors are affinity biosensors with high selectiveness for the target analyte. In recent years, the field of electrochemical immunosensors has grown tremendously. These affinity sensors have a large variety of applications: food safety, quality control, and biomedicine, blood testing, environmental and agricultural. The correct immobilization of antibodies is the most important step for immunosensors. An antibody molecule is usually composed by two main structures: the Fab-fragment, antigen binding and Fc-fragment parts, as simplified shown in Fig. 7.

The antibody immobilization can happen by random and site-directed techniques. The random immobilization is the easiest way to immobilize an antibody; it does not require bioconjugation agents or other materials to create functional

Table 3 Functionalized graphene and its modifications for enzyme immobilization

Functionalization	Sensor	Enzyme/protein	Target analyte	References
GO-NPs	MoS_2/GO/Mb	Myoglobin	Nitric oxide	[42]
	ChOx/ZnO/Ag/GO	Cholesterol oxidase	Cholesterol	[46]
rGO only	Lac/rGO	Laccase	Dopamine	[8]
	AChE/rGO	Acetylcholinesterase	Carbaryl	[9, 10]
	GOX/rGO	Glucose oxidase	Glucose	[22]
	TRGO/FDH	D-fructose dehydrogenase	D-fructose	[67]
rGO-polymer	ChOx/PSS/PILs–GP	Cholesterol oxidase	Cholesterol	[46]
	rGO/PPy/NR	Nitrate reductase	Nitrate	[45]
rGO-NPs	HRP/CeO2-rGO	horseradish peroxidase	H_2O_2	[51]
	Lac-rGO/RhNPs	Laccase	17β-estradiol	[50]
	Lac/rGO/Sb2O5	Laccase	Estriol	[48]
rGO-polymer-NPs	NA/Ag@rGO-NH2/AChE	Acetylcholinesterase	Pesticides	[49]

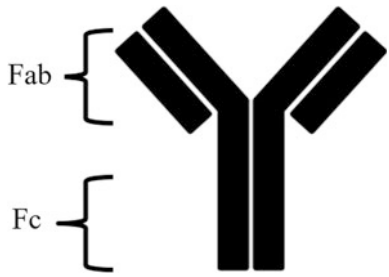

Fig. 7 General structure of an antibody

groups on the sensor surface. However, denaturation of proteins, low specificity and random orientation are some examples of this technique disadvantages.

In the other hand, site-direct immobilization is more efficient. The focus of this methodology is to immobilize the Fc segment of antibody on the sensor and leave the Fab segment free for antigen binding. The Fc segment is rich in carboxylic groups, therefore can bind to the electrode surface modified with an amine group.

Hu and co-workers reported the functionalization of GO with an amino-terminated perylene derivative ($PTCNH_2$) for the detection of tumor necrosis factor-alpha (TNF-α). Giving the NH_2 functionalized surface, the anti-TNF- α was successfully immobilized. The linear region for the analyte target ranging from 10 pg/mL to 100 ng/mL with a detection limit of 3.33 pg/mL. The sensor is promising for application in clinical diagnosis [52].

Table 4 Functionalized graphene for immunosensors construction

Functionalization	Sensor	Antibody	Target Analyte	References
GO-bioconjugation agent	GO/PTCNH$_2$	anti-TNF-α	TNF-α	[52]
GO-NPs-functionalized	Au@APTES-GS	Anti-CEA	Carcinoembryonic antigen (CEA)	[68]
rGO-bioconjugation agent	rGO-EDC/NHS	Anti-H1N1	H1N1 viruses	[69]
	rGO-TEPA-PTC-NH$_2$	Anti-Vangl1	human vang-like protein (Vangl1)	[70]
	rGO-EDC/NHS	Anti-HCT	SKBR-3 breast cancer cell	[77]
rGO-NPs	Ag/MoS$_2$/rGO	Anti-CEA	carcinoembryonic antigen (CEA)	[68]
	rGO-AuNPS	anti-PCT	Procalcitonin (PCT)	[71]
rGO-polymer-NPs	AuNPs-PEDOT/PB-rGO	Anti-AFP	α-fetoprotein	[55]
	AuNPs/Cs/Gr	Anti-BoNT/A	botulinum neurotoxin serotype A	[54]

Gold nanoparticles (AuNPs) also hold interesting properties for antibody immobilization. Gold electrodes have been extensively applied in immunosensors fabrication due to self-assembled monolayers (SAM) technique. AuNPs can be functionalized with amine groups by different reagents, such as cystamine, 4-Aminothiophenol and lipoic acid. The thiol part of these reagents binds spontaneously with the AuNPs due to Au-S affinity [53]. In that way, modification of graphene-based materials with terminal amino groups is the main route for antibody conjugation. Table 4 shows some examples of functionalized graphene for immunosensor preparation and Fig. 8 summarizes some bioconjugation routes of antibody for immunosensing application.

4.3 Functionalized Graphene Using Nanopolymers

Functionalization of graphene using conducting nanostructured polymers have several applications, as highlighted above. Poly (3,4-ethylene-dioxythiophene) (PEDOT), polypyrrole (PPy), chitosan (Cs), nafion (NA) and poly(sodium-p-styrenesulfonate) (PSS) are common polymers applied in electroanalysis due to their high conductivity, high biocompatibility and thermal stability [45–47, 49, 54, 55].

Afkhami and co-workers prepared a chitosan/graphene nanostructure by continues stirring for 2 h of a Cs solution (0.50 wt%) and 5.0 mg of graphene to obtain a Cs-graphene nanocomposite for immunosensing.

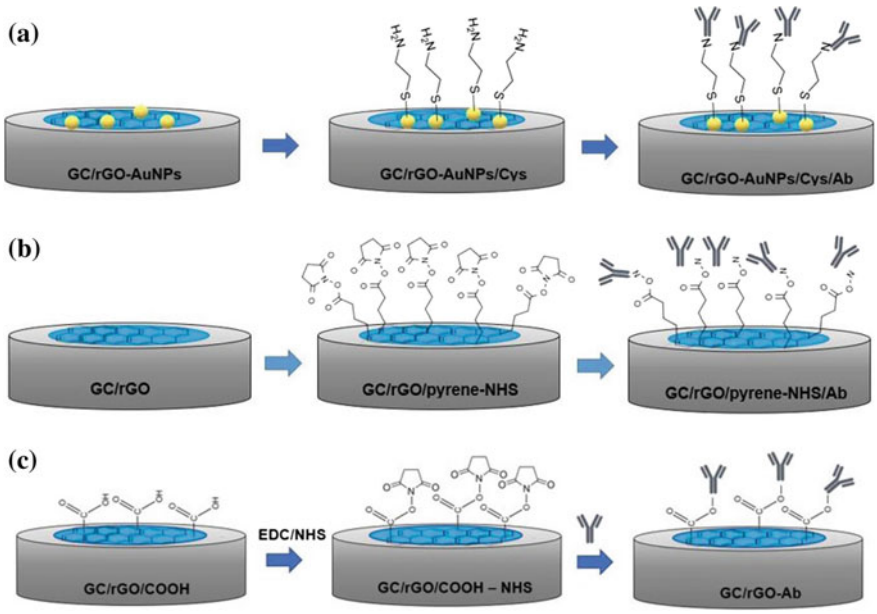

Fig. 8 Common approaches for antibody conjugation in electrodes for immunosensing

Besides the preparation of polymers-graphene composites, another approach can be used for modifying the WE with nanopolymers. The electropolymerization procedure involves the formation of polymeric products by electrochemical oxidation of their monomers, which is a versatile technique for synthesizing hybrid conduction polymers. Bo et al. [56] electropolymerized polyaniline (PANI) nanowires on graphene using a three-step electrochemical deposition procedure for construction of a DNA biosensor. The DNA sensor showed a sensitive and selective DNA detection with a detection limit of 3.25 mol L^{-1} of the complementary oligonucleotide. Huang et al. [57] performed cyclic voltammetry experiments (15 cycles) in an acetate buffer solution (0.1 mol L^{-1}, pH = 6.0) for direct electropolymerization of poly (thionine) on a modified graphene-Au nanorods electrode for DNA sensing of papillomavirus (HPV). Table 5 summarizes the different monomers and electropolymerization approaches for graphene modification and their applications. Electropolymerization offers some advantages in comparison with other synthesis approaches, such as: directly deposition of the nanopolymers, formation of thin films and possibility of thickness and conductivity control. In the other hand, it is an expensive method and only films can be formed [58]. As highlighted above, cyclic voltammetry (CV) is the most common electrochemical technique for monomers polymerization on electrodes surface, and it is essential for the characterization of the electrochemical properties of conducting nanopolymers. As theCV is performed, the thickness of the PPy film increases and so does current response. Figure 9 shows a typical CV experiment of

Table 5 Functionalized graphene with nanopolymers

Nanopolymers/ composite	Application	Synthesis	Conditions	References
PANI-graphene	DNA sensor	Three-step electropolymerization	–	[56]
Poly (thionine)–Graphene–Au nanorods	DNA sensor	Cyclic voltammetry (15 cycles)	acetate buffer (pH = 6.0)	[57]
PANI-rGO				
PANI-graphene	–	Chronoamperometry (0.75 V)	0.5 M H_2SO_4	[72]
Polycarbazole-graphene	Detection of 4-nitropenol	Cyclic voltammetry (8 cycles)	BFEE solution	[73]
PEDOT-graphene	Supercapacitor	Chronoamperometry (1.8 V)	EDOT water solution	[74]

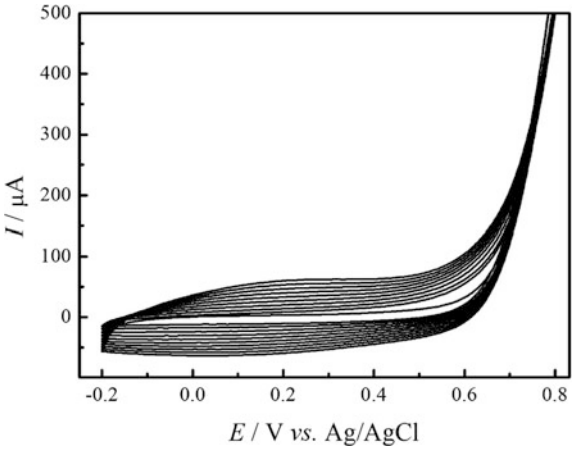

Fig. 9 Typical experiment of polypyrrole electropolymerization by cyclic voltammetry

polypyrrole deposition on a WE. The CV ranged from −0.2 to 0.8 V in a 0.1 mol L^{-1} NaCl solution.

5 Functionalized Graphene with Metallic Nanoparticles for Electrochemical Sensors

Reduced graphene oxide plays an important role in electroanalysis nowadays. Due to its easy fabrication and low cost, rGO is frequently used in electrochemical sensors and other associated applications [3]. Silva et al. [9, 10] compared the performance of rGO modified with antimony (Sb) and copper (Cu) nanoparticles

Table 6 rGO modified with metallic nanoparticles for emergent contaminant detection

Electrode	Analytical target	Limit of detection	References
rGO-AgNPs	Estriol	21.0 nmol L^{-1}	[78]
rGO-CuNPs	Levofloxacin	1.73×10^{-8} mol L^{-1}	[17]
rGO-SbNPs	Levofloxacin	4.13×10^{-8} mol L^{-1}	[17]
rGO-SbNPs	Estriol	0.5 nmol L^{-1}	[26]
rGO-$BiVO_4$	Sodium diclofenac	4.2×10^{-9} mol L^{-1}	[75]
rGO-PdNPs	Desipramine	1.04 nmol L^{-1}	[76]

for electrochemical detection of levofloxacin. The rGO-CuNPs composite showed a detection limit of 1.73×10^{-8} mol L^{-1} in levofloxacin detection and the proposed composite was applied for drug pharmaceutical detection with promising results. In recent years, rGO has been modified with various metallic nanoparticles. Silver, gold, antimony, copper, bismuth and palladium are some examples of metallic nanoparticles for modification of rGO towards pollutants detection as presented in Table 6.

6 Conclusion

An overview of the functionalization of graphene in GO and rGO has been presented in this chapter. The main syntheses to obtain GO and rGO were reported and for a better understanding of their properties, these materials were characterized morphologically, structurally and electrochemically. It was possible to observe that the C/O ratio varies from GO to rGO, generating structural defects in the sheet and different electronic properties for the two materials since less oxygen atoms increase the electron transport in the rGO. The applications of the functionalized graphene were highlighted in the electrochemical area. Thus, the use of GO and rGO as platforms for the construction of a wide range of electrochemical biosensors and sensors was showed which presented an improvement of the analytical behavior.

Acknowledgements The authors would like to acknowledge the financial support of FAPESP (grant 2015/02136-2).

References

1. Fitzer, E., Kochling, K.-H., Boehm, H.-P., Marsh, H.: Recommended terminology for the description of carbon as a solid (IUPAC Recommendations 1995). Pure Appl. Chem. **67**, 473–506 (1995)
2. Dreyer, D.R., Park, S., Bielawski, C.W., Ruoff, R.S.: The chemistry of graphene oxide. Chem. Soc. Rev. **39**, 228–240 (2010)

3. Rowley-Neale, S.J., Randviir, E.P., Dena, A.S.A., Banks, C.E.: An overview of recent applications of reduced graphene oxide as a basis of electroanalytical sensing platforms. Appl. Mater. Today **10**, 218–226 (2018)
4. Pei, S., Cheng, H.-M.: The reduction of graphene oxide. Carbon **50**, 3210–3228 (2011)
5. Brownson, D.A.C., Varey, S.A., Hussain, F., Haigh, S.J., Banks, C.E.: Electrochemical properties of CVD grown pristine graphene: monolayer- versus quasi-graphene. Nanoscale **6**, 1607–1621 (2014)
6. Randviir, E.P., Brownson, D.A.C., Banks, C.E.: A decade of graphene research: production, applications and outlook. Mater. Today **17**, 426–432 (2014)
7. Brownson, D.A.C., Banks, C.E.: The Handbook of Graphene Electrochemistry. Springer, London Ltd (2014)
8. Kohori, N.A., da Silva, M.K.L., Cesarino, I.: Evaluation of graphene oxide and reduced graphene oxide in the immobilization of laccase enzyme and its application in the determination of dopamine. J. Solid State Electrochem. **22**, 141–148 (2018)
9. da Silva, M.K.L., Vanzela, H.C., Defavari, L.M., Cesarino, I.: Determination of carbamate pesticide in food using a biosensor based on reduced graphene oxide and acetylcholinesterase enzyme. Sens. Actuators B **277**, 555–561 (2018)
10. da Silva, M.K.L., Plana Simões, R., Cesarino, I.: Evaluation of reduced graphene oxide modified with antimony and copper nanoparticles for levofloxacin oxidation. Electroanalysis **30**, 2066–2076 (2018)
11. Zheng, D., Hu, H., Liu, X., Hu, S.: Application of graphene in electrochemical sensing. Curr. Opin. Colloid Interface Sci. **20**, 383–405 (2015)
12. Song, Y., Luo, Y., Zhu, C., Li, H., Du, D., Lin, Y.: Recent advances in electrochemical biosensors based on graphene two-dimensional nanomaterials. Biosens. Bioelectron. **76**, 195–212 (2016)
13. Wang, J.: Electrochemical biosensors: towards point-of-care cancer diagnostics. Biosens. Bioelectron. **21**, 1887–1892 (2006)
14. Brownson, D.A.C., Banks, C.E.: Graphene electrochemistry: an overview of potential applications. Analyst **135**, 2768–2778 (2010)
15. Park, S., Ruoff, R.S.: Chemical methods for the production of graphenes. Nat. Nanotechnol. **4**, 217–224 (2009)
16. Brodie, B.C.: Hydration behavior and dynamics of water molecules in graphite oxide. Annales Chimie et de Physique **59**, 466–472 (1860)
17. De Silva, K.K.H., Huang, H.-H., Joshi, R.K., Yoshimura, M.: Chemical reduction of graphene oxide using green reductants. Carbon **119**, 190–199 (2017)
18. Poh, H.L., Sanek, F., Ambrosi, A., Zhao, G., Sofer, Z., Pumera, M.: Graphenes prepared by Staudenmaier, Hofmann and Hummers methods with consequent thermal exfoliation exhibit very different electrochemical properties. Nanoscale **4**, 3515–3522 (2012)
19. Hummers, W.S., Offeman, R.E.: Preparation of graphitic oxide. J. Am. Chem. Soc. **80**, 1339 (1958)
20. Zhu, C., Guo, S., Fang, Y., Dong, S.: Reducing sugar: new functional molecules for the green synthesis of graphene nanosheets. ACS Nano **4**, 2429–2437 (2010)
21. Zhu, Y., Murali, S., Stoller, M.D., Velamakanni, A., Piner, R.D., Ruoff, R.S.: Microwave assisted exfoliation and reduction of graphite oxide for ultracapacitors. Carbon N. Y. **48**, 2118–2122 (2010)
22. Unnikrishnan, B., Palanisamy, S., Chen, S.-M.: A simple electrochemical approach to fabricate a glucose biosensor based on graphene–glucose oxidase biocomposite. Biosens. Bioelectron. **39**, 70–75 (2013)
23. Meng, L.-Y., Wang, B., Ma, M.-G., Lin, K.-L.: The progress of microwave-assisted hydrothermal method in the synthesis of functional nanomaterials. Mater. Today Chem. **1–2**, 63–83 (2016)
24. Cesarino, I., Simões, R.P., Lavarda, F.C., Batagin-Neto, A.: Electrochemical oxidation of sulfamethazine on a glassy carbon electrode modified with graphene and gold nanoparticles. Electrochim. Acta **192**, 8–14 (2016)

25. Zhou, W., Zhang, F., Liu, S., Wang, J., Du, X., Yin, D., Wang, L.: Microwave-assisted hydrothermal synthesis of graphene-wrapped CuO hybrids for lithium ion batteries. RSC Adv. **4**, 51362–51365 (2014)
26. Cesarino, I., Cincotto, F.H., Machado, S.A.S.: A synergistic combination of reduced graphene oxide and antimony nanoparticles for estriol hormone detection. Sens. Actuators B Chem. **210**, 453–459 (2015)
27. Aldosari, M.A., Othman, A.A., Alsharaeh, E.H.: Synthesis and characterization of the in situ bulk polymerization of PMMA containing graphene sheets using microwave irradiation. Molecules **18**, 3152–3167 (2013)
28. Eluyemi, M.S., Eleruja, M.A., Adedeji, A.V., Olofinjana, B., Fasakin, O., Akinwunmi, O.O., Ilori, O.O., Famojuro, A.T., Ayinde, S.A., Ajayi, E.O.B.: Synthesis and characterization of graphene oxide and reduced graphene oxide thin films deposited by spray pyrolysis method. Graphene **5**, 143–154 (2016)
29. He, D., Shen, L., Zhang, X., Wang, Y., Bao, N., Kung, H.H.: An efficient and eco-friendly solution-chemical route for preparation of ultrastable reduced graphene oxide suspensions. Am. Inst. Chem. Eng. J. **60**, 2757–2764 (2014)
30. Gurunathan, S., Han, J.W., Dayem, A.A., Eppakayala, V., Kim, J.H.: Oxidative stress-mediated antibacterial activity of graphene oxide and reduced graphene oxide in *Pseudomonas aeruginosa*. Int. J. Nanomed. **7**, 5901–5914 (2012)
31. How, G.T.S., Pandikumar, A., Ming, H.N., Ngee, L.H.: Highly exposed 001 facets of titanium dioxide modified with reduced graphene oxide for dopamine sensing. Sci. R. **4**, 5044 (2014). https://doi.org/10.1038/srep05044
32. Khan, Q.A., Shaur, A., Khan, T.A., Joya, Y.F., Awan, M.S.: Characterization of reduced graphene oxide produced through a modified Hoffman method. Cogent Chem. **3**, 1298980 (2017)
33. Xu, C., Shi, L., Ji, A., Shi, X., Wang, X., Wang, X.: Synthesis and characterization of reduced graphene oxide with D-fructose and D-galactose as reductants. J. Nanosci. Nanotechnol. **16**, 9914–9918 (2016)
34. Emiru, T.F., Ayele, D.W.: Controlled synthesis, characterization and reduction of graphene oxide: a convenient method for large scale production. Egypt. J. Basic Appl. Sci. **4**, 74–79 (2017)
35. Rokmana, A.W., Asriani, A., Suhendar, H., Triyana, K., Kusumaatmaja, A., Santoso, I.: The optical properties of thin film reduced graphene oxide/poly (3,4 ethylenedioxtriophene):poly (styrene sulfonate)(pedot:pss) fabricated by spin coating. IOP Conf. Ser. J. Phys. **1011**, 012007 (2018). https://doi.org/10.1088/1742-6596/1011/1/012007
36. Casero, E., Parra-Alfambra, A.M., Petit-Domínguez, M.D., Pariente, F., Lorenzo, E., Alonso, C.: Differentiation between graphene oxide and reduced graphene by electrochemical impedance spectroscopy (EIS). Electrochem. Commun. **20**, 63–66 (2012)
37. Gong, Y., Li, D., Fu, Q., Pan, C.: Influence of graphene microstructures on electrochemical performance for supercapacitors. Prog. Nat. Sci. **25**, 379–385 (2015)
38. Barton, S.C., Gallaway, J., Atanassov, P.: Enzymatic biofuel cells for implantable and microscale devices. Chem. Rev. **104**, 4867–4886 (2004)
39. Takahashi, H., Li, B., Sasaki, T., Miyazaki, C., Kajino, T., Inagaki, S.: Catalytic activity in organic solvents and stability of immobilized enzymes depend on the pore size and surface characteristics of mesoporous silica. Chem. Mater. **12**, 3301–3305 (2000)
40. Zhang, Y., Guo, L., Wei, S., He, Y., Xia, H., Chen, Q., Sun, H.-B., Xiao, F.-S.: Direct imprinting of microcircuits on graphene oxides film by femtosecond laser reduction. Nanotoday **5**, 15–20 (2010)
41. Zhang, J., Zhang, F., Yang, H., Huang, X., Liu, H., Zhang, J., Guo, S.: Graphene oxide as a matrix for enzyme immobilization. Langmuir **26**, 6083–6085 (2010)
42. Yoon, J., Shin, J.-W., Lim, J., Mohammadniaei, M., Bharate Bapurao, G., Lee, T., Choi, J.-W.: Electrochemical nitric oxide biosensor based on amine-modified MoS2/graphene oxide/myoglobin hybrid. Colloids Surf. B Biointerfaces **159**, 729–736 (2017)

43. Ting, S.W., Periasamy, A.P., Chen, S.M., Saraswathi, R.: Direct electrochemistry of catalase immobilized at electrochemically reduced graphene oxide modified electrode for amperometric H_2O_2 biosensor. Int. J. Electrochem. Sci. **6**, 4438–4453 (2011)
44. Vijayaraj, K., Hong, S.W., Jin, S.H., Chang, S.C., Park, D.S.: Fabrication of a novel disposable glucose biosensor using an electrochemically reduced graphene oxide–glucose oxidase biocomposite. Anal. Methods **8**, 6974–6981 (2016)
45. Umar, M.F., Nasar, A.: Reduced graphene oxide/polypyrrole/nitrate reductase deposited glassy carbon electrode (GCE/RGO/PPy/NR): biosensor for the detection of nitrate in wastewater. Appl. Water Sci. **8**, 211 (2018)
46. Wu, Q., Hou, Y., Zhang, M., Hou, X., Xu, L., Wang, N., Wang, J., Huang, W.: Amperometric cholesterol biosensor based on zinc oxide films on a silver nanowire–graphene oxide modified electrode. Anal. Methods **8**, 1806–1812 (2016)
47. Wu, S., Wang, Y., Mao, H., Wang, C., Xia, L., Zhang, Y., Ge, H., Song, X.-M.: Direct electrochemistry of cholesterol oxidase and biosensing of cholesterol based on PSS/polymeric ionic liquid–graphene nanocomposite. RSC Adv. **6**, 59487–59496 (2016)
48. Cincotto, F.H., Canevari, T.C., Machado, S.A.S., Sánchez, A., Barrio, M.A.R., Villalonga, R., Pingarrón, J.M.: Reduced graphene oxide-Sb_2O_5 hybrid nanomaterial for the design of a laccase-based amperometric biosensor for estriol. Electrochim. Acta **174**, 332–339 (2015)
49. Guler, M., Turkoglu, V., Basi, Z.: Determination of malation, methidathion, and chlorpyrifos ethyl pesticides using acetylcholinesterase biosensor based on Nafion/Ag@rGO-NH2 nanocomposites. Electrochim. Acta **240**, 129–135 (2017)
50. Povedano, E., Cincotto, F.H., Parrado, C., Díez, P., Sánchez, A., Canevari, T.C., Machado, S. A.S., Pingarrón, J.M., Villalonga, R.: Decoration of reduced graphene oxide with rhodium nanoparticles for the design of a sensitive electrochemical enzyme biosensor for 17β-estradiol. Biosens. Bioelectron. **89**, 343–351 (2017)
51. Radhakrishnan, S., Kim, S.J.: An enzymatic biosensor for hydrogen peroxide based on one-pot preparation of CeO_2 -reduced graphene oxide nanocomposite. RSC Adv. **5**, 12937–12943 (2015)
52. Hu, H., Pan, D., Xue, H., Zhang, M., Zhang, Y., Shen, Y.: A photoelectrochemical immunoassay for tumor necrosis factor-α using a GO-PTCNH2 nanohybrid as a probe. J. Electroanal. Chem. **824**, 195–200 (2018)
53. Asav, E., Akyilmaz, E.: Preparation and optimization of a bienzymic biosensor based on self-assembled monolayer modified gold electrode for alcohol and glucose detection. Biosens. Bioelectron. **25**, 1014–1018 (2010)
54. Afkhami, A., Hashemi, P., Bagheri, H., Salimian, J., Ahmadi, A., Madrakian, T.: Impedimetric immunosensor for the label-free and direct detection of botulinum neurotoxin serotype A using Au nanoparticles/graphene-chitosan composite. Biosens. Bioelectron. **93**, 124–131 (2017)
55. Yang, T., Jia, H., Liu, Z., Qiu, X., Gao, Y., Xu, J., Lu, L., Yu, Y.: Label-free electrochemical immunoassay for α-fetoprotein based on a redox matrix of Prussian blue-reduced graphene oxide/gold nanoparticles-poly(3,4-ethylenedioxythiophene) composite. J. Electroanal. Chem. **799**, 625–633 (2017)
56. Bo, Y., Yang, H., Hu, Y., Yao, T., Huang, S.: A novel electrochemical DNA biosensor based on graphene and polyaniline nanowires. Electrochim. Acta **56**, 2676–2681 (2011)
57. Huang, H., Bai, W., Dong, C., Guo, R., Liu, Z.: An ultrasensitive electrochemical DNA biosensor based on graphene/Au nanorod/polythionine for human papillomavirus DNA detection. Biosens. Bioelectron. **68**, 442–446 (2015)
58. Iqbal, S., Ahmad, S.: Recent development in hybrid conducting polymers: synthesis, applications and future prospects. J. Ind. Eng. Chem. **60**, 53–84 (2018)
59. Shi, H.-J., Kim, K.K., Yoon, S.M., Park, H.K., Jung, I.S., Jin, M.H., Jeong, H.K., Kim, J.M., Choi, J.Y., Lee, Y.H.: Efficient reduction of graphite oxide by sodium borohydride and its effect on electrical conductance. Adv. Func. Mater. **19**, 1987–1992 (2009)

60. Stankovicha, S., Dikin, D.A., Piner, R.D., Kohlhaas, K.A., Kleinhammes, A., Jia, Y., Wu, Y., Nguyen, S.T., Ruoff, R.S.: Synthesis of graphene-based nanosheets via chemical reduction of exfoliated graphite oxide. Carbon **45**, 1558–1565 (2007)
61. Xu, C., Shi, X., Ki, A., Zhou, C., Cui, Y.: Fabrication and characteristics of reduced graphene oxide produced with different green reductants. PLoS ONE **10**, 1–15 (2015)
62. Salas, E.C., Sun, Z., Lu, A., Tour, J.M.: Reduction of graphene oxide via bacterial respiration. ACS Nano **4**, 4852–4856 (2010)
63. Khanra, P., Kuila, T., Kim, N.H., Bae, S.H., Yu, S.D., Lee, J.H.: Simultaneous bio-functionalization and reduction of graphene oxide by baker's yeast. Chem. Eng. J. **183**, 526–533 (2012)
64. Pei, S., Zhao, J., Du, J., Ren, W., Cheng, H.-M.: Direct reduction of graphene oxide films into highly conductive and flexible graphene films by hydrohalic acids. Carbon **48**, 4466–4474 (2010)
65. Wu, Z.-S., Ren, W., Gao, L., Zhao, J., Chen, Z., Liu, B., Tang, D., Yu, B., Jiang, C., Cheng, H.-M.: Synthesis of graphene sheets with high electrical conductivity and good thermal stability by hydrogen arc discharge exfoliation. ACS Nano **3**, 411–417 (2009)
66. Zhou, M., Wang, Y., Zhai, Y., Zhai, J., Ren, W., Wang, F., Dong, S.: Controlled synthesis of large-area and patterned electrochemically reduced graphene oxide films. Chem. Eur. J. **15**, 6116–6120 (2009)
67. Šakinytė, I., Barkauskas, J., Gaidukevič, J., Razumienė, J.: Thermally reduced graphene oxide: the study and use for reagentless amperometric d-fructose biosensors. Talanta **144**, 1096–1103 (2015)
68. Wang, Y., Wang, Y., Wu, D., Ma, H., Zhang, Y., Fan, D., Pang, X., Du, B., Wei, Q.: Label-free electrochemical immunosensor based on flower-like Ag/MoS_2/rGO nanocomposites for ultrasensitive detection of carcinoembryonic antigen. Sens. Actuators B Chem. **255**, 125–132 (2018)
69. Singh, R., Hong, S., Jang, J.: Label-free detection of influenza viruses using a reduced graphene oxide-based electrochemical immunosensor integrated with a microfluidic platform. Sci. R. **7**, 42771 (2017)
70. Chen, Q., Yu, C., Gao, R., Gao, L., Li, Q., Yuan, G., He, J.: A novel electrochemical immunosensor based on the rGO-TEPA-PTC-NH2 and AuPt modified C60 bimetallic nanoclusters for the detection of Vangl1, a potential biomarker for dysontogenesis. Biosens. Bioelectron. **79**, 364–370 (2016)
71. Liu, P., Li, C., Zhang, R., Tang, Q., Wei, J., Lu, Y., Shen, P., (2018). An ultrasensitive electrochemical immunosensor for procalcitonin detection based on the gold nanoparticles-enhanced tyramide signal amplification strategy. In: Biosensors and Bioelectronics, In press
72. Wang, D.-W., Li, F., Zhao, J., Ren, W., Chen, Z.-G., Tan, J., Wu, Z.-S., Gentle, I., Lu, G.Q., Cheng, H.-M.: Fabrication of graphene/polyaniline composite paper via in situ anodic electropolymerization for high-performance flexible electrode. ACS Nano **3**, 1745–1752 (2009)
73. Zhang, Y., Wu, L., Lei, W., Xia, X., Xia, M., Hao, Q.: Electrochemical determination of 4-nitrophenol at polycarbazole/N-doped graphene modified glassy carbon electrode. Electrochim. Acta **146**, 568–576 (2014)
74. Jacob, D., Mini, P.A., Balakrishnan, A., Nair, S.V., Subramanian, K.R.V.: Electrochemical behaviour of graphene–poly (3,4-ethylenedioxythiophene) (PEDOT) composite electrodes for supercapacitor applications. Bull. Mater. Sci. **37**, 61–69 (2014)
75. do Prado, T.M., Cincotto, F.H., Fatibello-Filho, O., de Moraes, F.C.: Bismuth vanadate/reduced graphene oxide nanocomposite electrode for photoelectrochemical determination of diclofenac in urine. Electroanalysis **30**, 2704–2711 (2018)
76. Cincotto, F.H., Golinelli, D.L.C., Machado, S.A.S., Moraes, F.C.: Electrochemical sensor based on reduced graphene oxide modified with palladium nanoparticles for determination of desipramine in urine samples. Sens. Actuators B Chem. **239**, 488–493 (2017)

77. Tabrizi, M.A., Shamsipur, M., Saber, R., Sarkar, S., Zolfaghari, N.: An ultrasensitive sandwich-type electrochemical immunosensor for the determination of SKBR-3 breast cancer cell using rGO-TPA/FeHCFnano labeled Anti-HCT as a signal tag. Sens. Actuators B Chem. **243**, 823–830 (2017)
78. Donini, C.A., da Silva, M.K.L., Simões, R.P., Cesarino, I.: Reduced graphene oxide modified with silver nanoparticles for the electrochemical detection of estriol. J. Electroanal. Chem. **809**, 67–73 (2018)

Electrochemical Detection of Dopamine in the Presence of Uric Acid Using Graphene Oxide Modified Electrode as Highly Sensitive and Selective Sensors

Buse Demirkan, Hasan Ay, Sümeyye Karakuş, Gülseren Uzun, Anish Khan and Fatih Şen

Abstract Graphene is a very advantageous material with its excellent electronic properties as well as its physical properties. The use of graphene and its derivatives in addition to polymers is very suitable for applications such as flexible devices, functional nanocomposites, and sensors. Graphene with a 2D network has been an important material due to its excellent physicochemical values (excellent conductivity, functionalization, mass production ease, high surface area, and high mechanical strength). In this study, graphene oxide based glassy carbon electrode (GO/GCE) was used for the simultaneous detection of dopamine (DA) and uric acid (UA) in the presence of chemically synthesized the graphene oxide (GO). To define the uric acid (UA) and dopamine (DA) levels simultaneously and separately, measurements were obtained by cyclic voltammetry (CV). Accordingly, it has been found that dopamine and uric acid can be measured simultaneously with these sensors in biological samples and are hoped to be used in future applications.

Keywords Dopamine · Electrode · Graphene oxide · Sensors · Uric acid

1 Introduction

Dopamine (DA), one of the essential neurotransmitters, plays a vital role in the function of the central nervous, kidney, hormonal, and cardiovascular system [1]. Abnormal DA levels may result in Parkinsonism, Schizophrenia, Huntington, HIV,

B. Demirkan · H. Ay · S. Karakuş · G. Uzun · F. Şen (✉)
Sen Research Group, Biochemistry Department, Dumlupinar University, 43100 Kütahya, Turkey
e-mail: fatihsen1980@gmail.com

A. Khan
Chemistry Department, Faculty of Science, King Abdulaziz University, P.O. Box 80203, Jeddah 21589, Saudi Arabia

A. Khan
Center of Excellence for Advanced Materials Research, King Abdulaziz University, P.O. Box 80203, Jeddah 21589, Saudi Arabia

A. Khan et al. (eds.), *Graphene Functionalization Strategies*, Carbon Nanostructures, https://doi.org/10.1007/978-981-32-9057-0_7

and similar diseases [2]. For these types of problems, research in the field of neurotransmitters like dopamine electrochemistry has been very important at understanding the functions within and within the human body [3]. Recently, too many electrochemical systems have been designed and implemented for the analysis of dopamine in real body fluid. Modification and development of voltammetric sensors for the detection of many components in the extracellular fluid in the living body have recently attracted much attention [4–6]. Another common biological molecule with higher concentrations of DA in biological samples is uric acid. Ascorbic acid (AA) is widely used as an antioxidant in food, animal feed, pharmaceutical formulations, and cosmetic applications and is usually found in biological samples with DA. It is also essential that ascorbic acid has a biologically important task in many processes, such as collecting radicals in the system, strengthening the immune system, reducing the possibility of cancer, and preventing diseases such as AIDS [7–9]. Unfortunately, AA is always present in organisms with DA and shares a similar oxidation potential in electrochemical detection. The electrochemical techniques for the detection of these biomolecules in the extracellular fluid have attracted considerable attention in recent years. The most significant obstacle for electrochemical detection of dopamine is that it is dominant due to the presence of uric acid in the same environment. In addition to this problem, the product resulting from the oxidation of dopamine can catalyze the oxidation of the uric acid by causing the electrode to be contaminated by low discrimination and repetition of measurements [10–15]. Therefore, the relative importance of Dopamine in the presence of uric acid has been the most critical problem and aim of the research in this area. In the metabolism of uric acid, which is one of the leading products in the metabolic system, gut, hyperuricemia, pneumonia, and Lesch Nyan syndrome occur depending upon its concentration [16–22]. Therefore, the identification of these molecules is not only crucial in the field of biomedical chemistry and neurochemistry, but also in diagnostic and pathological research. Over the last decade, more and more methods have been explored and developed for the analysis and measurement of these molecules. Various methods have been developed for the determination of DA and UA, such as chemiluminescence, high-performance liquid chromatography, electrochemical process, ultraviolet spectroscopy, and capillary electrophoresis.

Among these methods, the electrochemical method has attracted considerable interest because of its ease of use, fast, high precision, excellent stability, and low cost to determine electrochemical behaviour of DA and UA components [23, 24]. For this reason, it is essential to modify the sensors that work very sensitive and relative to the simultaneous detection of UA and DA in the analytical and diagnostic studies of applications [25]. Accordingly, in the case of relevant and sensitive analysis of dopamine and uric acid is still experiencing problems in its biological analysis. To eliminate this problem, experiments were carried out by experimenting with many materials, such as monolayer, carbon-based nanotubes, and other similar components which were spontaneously incorporated into the system as the nanoparticle [26–36], and the agents to reduce the organic bonds [23, 25, 37, 38]. On the other hand, they were used as a modification added to develop a relative and

sensitive dopamine biosensor. The development of electrodes arranged by the use of so many different materials sheds light on a huge future in the field of biosensors and electroanalytical chemistry. Accordingly, the results of the studies with unmodified electrodes are not satisfactory, as the electrochemical reactions in the detection of the components are not reproducible, and the products resulting from the oxidation of the surfaces of the measuring electrodes contaminate them [18]. For this reason, cyclic voltammetry was used to investigate the electrochemical behavior of UA and DA. A precise and relative method for simultaneous detection of UA and DA in the body fluid was achieved. To improve the detection of DA and UA, glassy carbon (GC) electrodes were used. Porous structural materials were also investigated. Due to the presence of uniaxial (1D) carbon-based nano-sized tubes, these materials have been put into use as supporting materials for sensors in dopamine and uric acid analysis due to their excellent electronic properties and conductivity. Graphene, a two-dimensional single layer of graphite, has attracted considerable attention recently due to its extraordinary features. The application of graphene in the sensor field is also critical. It has perfect properties like graphite, such as good electrical conductivity and rapid non-uniform electron transfer for applications in electrochemical devices. Huge specific surface and better biocompatibility ratio at the edges of the graphene layer and basal plane defect areas are also other desirable properties.

Graphene structured carbon based electrode, surface film modified electrode and micro/nanoelectrodes were investigated to analyze various types of glucose, dopamine, UA, DNA, hydrogen peroxide, and nicotinamide adenine dinucleotide. For this purpose, various carbon materials [39–46] were used as electrode components, including carbon nanotubes [12], boron-reinforced diamonds [10], graphite [15], and nanofibers [11]. To this end, various materials, such as organic reducing media additives, polymers, nanoparticles, self-integrating monolayers, and carbon nanotubes have been used in the development of electrodes. Graphene, having a 2D structure and having a single layer structure with a tight structure of carbon atoms, similar to a honeycomb, has recently become popular in many applications in the scientific field. Thanks to its very ideal electronic properties due to the fact that electrons are collected in a large area depending on their structure in two dimensions, it has the potential to apply in different fields such as electromechanical resonators, field effect transistors, and gas sensors and has a significant advantage in this regard. GO is more ideal than graphene for biosensor studies because of its excellent surface-to-surface properties and unique interaction with biological components. Graphene is already a widely used material in many sectors and areas due to its wide surface area, rapid heterogeneous electron transfer, high electrical conductivity, and excellent mechanical properties. We produce graphene modified electrodes in the current communication and report their applications for dopamine detection. The electrochemical changes of UA and DA with this electrode were investigated, and it was seen that the reduction signal of dopamine was found to be better in GO layer electrodes. The graphene oxide used in this study was obtained by hummers method which is one of the well-known techniques. Electrochemical analysis of the glassy carbon electrode developed by GO was measured using (CV) cycle voltammetry.

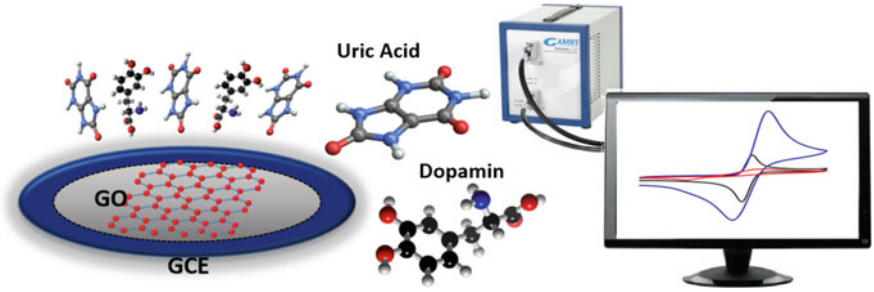

Scheme 1 Illustration of preparations of GO sensors for simultaneous determination of DA, and UA

Based on this behavior, the fixed electrode was applied as an excellent biosensor to detect dopamine in the presence of uric acid. The results show that the electrochemical responses of graphene to the target molecules originate from the planar geometric structure and the special electronic character of the graphene. For this reason, graphene is considered to be a good candidate for advanced electrode materials with forward-looking applications in electrochemistry [47–51]. The study of graphene is expected to provide a fundamental perspective to all carbon materials [30, 32, 35, 52–57]. Compared to carbon nanotubes, graphene offers potential advantages regarding low cost, high surface area, ease of operation, and safety. Graphene is expected to compete gradually with carbon nanotubes in many applications [47, 50]. As a summary, the resulting GO/GCE electrode was applied to the simultaneous determination of DA and UA. In addition, they exhibited low detection limits for DA and UA. The resulting GO/GCE electrode was applied to the simultaneous determination of DA and UA. Furthermore, the electrochemical data of dopamine with the GO/GCE and the reaction modified sensors were analyzed in detail in this study. Compared to the dopamine biosensors of chemically GO-based materials, the modified sensor shows better relative separation and precision with a much simpler system [13, 58] (Scheme 1).

2 Experimental Sections

2.1 Material and Method

Graphite powder (<20 μm), hydrogen peroxide (H_2O_2), and sulfuric acid (H_2SO_4) were obtained from Sigma Aldrich; sodium nitrate ($NaNO_3$) and potassium permanganate ($KMnO_4$) were obtained from Merck. The transparent structures of GO are defined by SEM images. Based on the results of the SEM analysis, it was found that the carbon ratio was about 90%. As a result of FT-IR analysis, graphene oxide was found to be suitable for epoxy, hydroxyl, alkoxy, and carbonyl bonds.

2.2 Synthesis of Graphene Oxide

In the first stage of the synthesis process, 2.5 g of graphite powder, 1.25 g of sodium nitrate ($NaNO_3$), and 57.5 mL of 96.4% sulfuric acid (H_2SO_4) in ice bath were added and stirred for 1 h. 8 g of potassium permanganate ($KMnO_4$) was added slowly to the mixture in the prepared bath. During this process, the temperature was below 5 °C. The mixture was removed from the ice bath and stirred for 2 h while the mixture temperature was in the range of 30–40 °C [59, 60]. In the second stage of the synthesis process, 500 mL of deionized water was added slowly to the mixture, and stirring continued for 1 h. 6 mL hydrogen peroxide (35.7%), was added to the mixture, the mixture temperature was not above 40 °C, and stirred for 2 h. At this step, the color of the mixture changed from black to brown. The mixture was then washed with deionized water to pH = 7 and filtered. After the filtration, the remaining material was dried at 50 °C for 24 h in the oven and GO in powder form [25].

3 Results and Discussion

3.1 Characterization of Graphene Oxide

After GO synthesis, FTIR, Raman, XRD, and XPS were characterized using various analytical techniques. In order to determine the functional groups within the GO structure, Perkin Elmer Spectrum 2 device was used for FT-IR analysis in the range of 500–4000 cm^{-1}. Raman spectroscopy analysis was performed using Raman microprobe (Renishaw Instruments) with 514 nm laser stimulation to examine the regular and irregular structures in the transition from graphite structure to GO structure. Ultima-theta-theta high-resolution goniometer and X-ray generator (Cu K radiation, $\lambda = 1.54056$) with working conditions in mA were obtained using a Panalytical Empyrean diffractometer. XPS measurements were performed with a Specs spectrometer using the K lines Mg (1253.6 eV, 10 mA). The reference point was determined as C 1 s line at 284.6 eV, and the insertion of XPS peaks was performed using a Gaussian function.

3.2 Fourier Transform Infrared Spectroscopy (FTIR) Spectra of Prepared Material

FTIR spectra were obtained on a Perkin Elmer Spectrum 2. FT-IR spectra of the GO sample and the hydroxyl bond (OH^-) was at 3116 cm^{-1} in accordance with the literature, the carbonyl bond was at 1713 cm^{-1} (C=O), the aromatic bond was at 1613 cm^{-1}, Epoxy bond (CO) was at 1215 cm^{-1}, and alkoxy bond (CO) was at

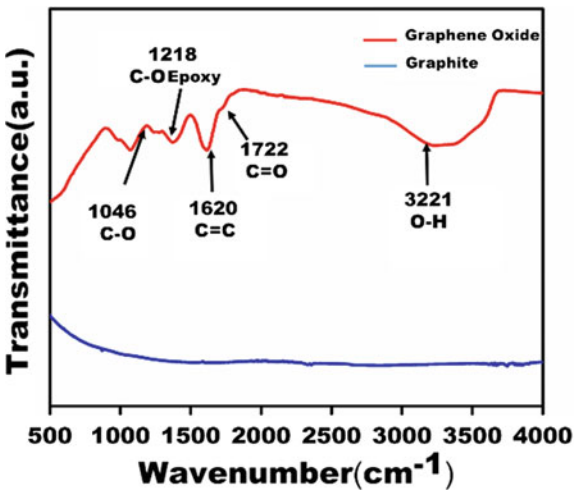

Fig. 1 FT-IR spectra of graphite and GO

1042 cm^{-1} [60–63] as illustrated in Fig. 1. In the FT-IR analysis, the stresses of 3427 cm^{-1} (OH^{-}) and 1624 cm^{-1} (C=C) are seen in the GO structure, and the functional groups and bond structures of GO are not recognized. It is understood that the bond structures in the GO structure are degraded by the reduction reactions and the (OH^{-}) and (O^{2-}) groups are removed. Compared with those of pristine graphite, these new peaks suggested that graphite had been successfully oxidized to generate GO [64, 65].

3.3 SEM Analysis of Prepared Materials

Images of GO were obtained with the SEM device (Fig. 2). From the SEM images, it is understood that the GO structure is ideally synthesized as a result of the Hummers method [64, 66, 67]; Images of GO show thin layers with crumpled surfaces similar to each other.

3.4 Raman Analysis of Prepared Materials

Raman spectroscopy is the technique used to detect and analyze crystal morphology and electronic properties of carbon-based materials. Raman spectra of GO are given in Fig. 3.

Generally, graphene oxide was synthesized by a modified Hummers method for Raman spectroscopy. In the Raman spectrum, the G (sp^2) band expresses the regular/aromatic structures while the D (sp^3) band shows the irregularities,

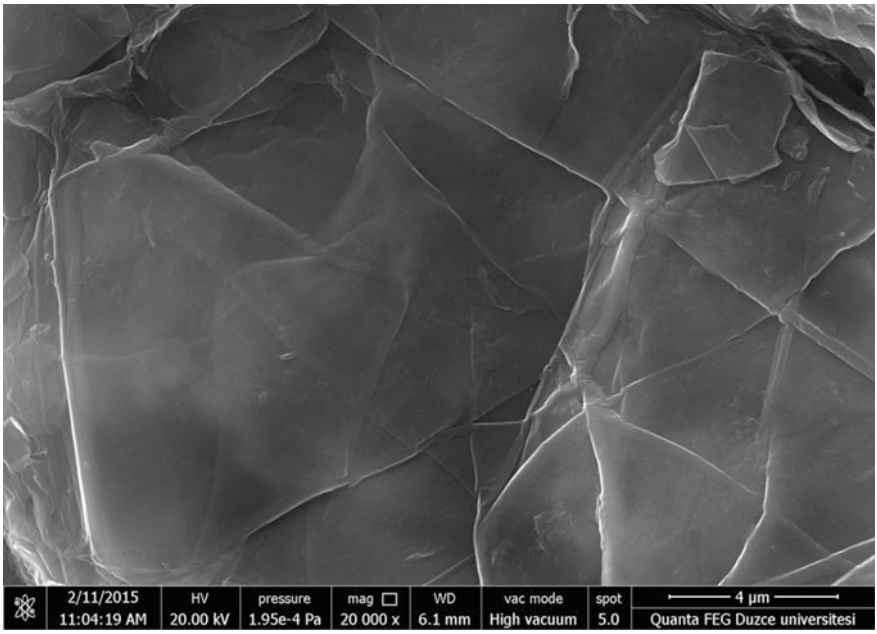

Fig. 2 SEM images of GO

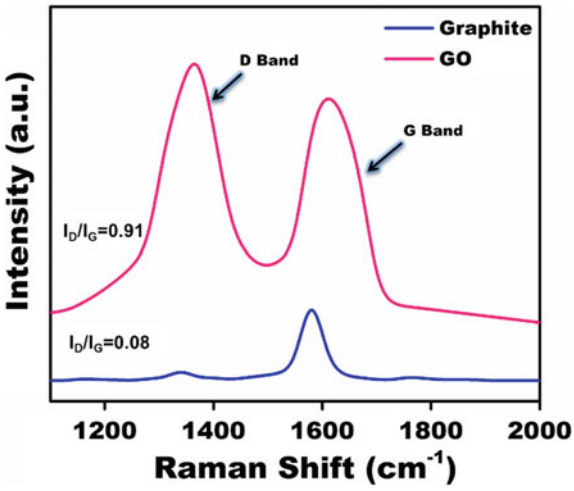

Fig. 3 Raman spectra for graphite and GO

amorphous structures, and structures that deteriorate as a result of oxidation [62, 63, 68]. In the Raman spectrum, the D (sp^3) peak of GO was 1330 cm^{-1} and G (sp^2) peak was 1601 cm^{-1}, respectively, consistent with the literature [67, 69]. The ID/IG ratio of the graphite structure was 0.08, and the ID/IG ratio of the GO structure was determined as 0.91 [48, 63].

3.5 XRD Analysis of Prepared Materials

In XRD analysis, the prepared GO were analyzed in detail. As a result of XRD spectroscopy analysis, $2\theta = 10.5524°$ peak was determined for GO [70–72]. In XRD analysis, the crystalline structures in prepared materials were found in the plane of (002) [13, 63, 73–75] (Fig. 4).

3.6 Electrochemical Activity of the Fabricated GO/GCE

In the determination of DA and UA, the CVs were examined in a solution of 0.1 M PBS (pH = 7.0). The potential range was set to −0.2 to 0.8 V and cyclic voltammetry measurements were obtained. In Fig. 5, a concentration study in pH of 7 for DA and UA was carried out in PBS. Here, the concentrations of the DA and UA biomolecules were increased in a certain range. Then, the sensing potential of the prepared material was monitored. A significant anodic peak current of DA can be observed in Fig. 5a, showing the outstanding electrochemical activity of GO/GCE. Besides, the oxidation peak current in the GO/GCE reaches 757.1 μA in Fig. 5b for UA. The results show that the GO catalyst has a very good electrocatalytic activity to determine the DA and UA. Further, the CVs with the simultaneous addition of DA and UA are shown in Fig. 5c. From these figures, it can be concluded that both simultaneous and separate detection of DA and UA were performed with the help of prepared nanosensor. In general, the GO modified electrode provided excellent electrocatalytic activity for the determination of DA and UA. These results can be attributed to the increasing electron transfer with the help of GO.

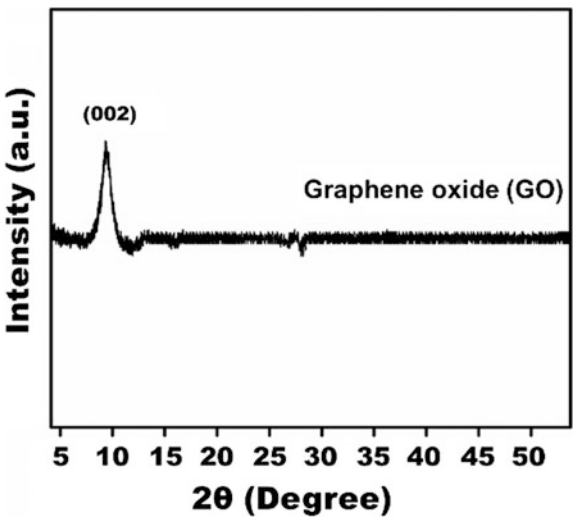

Fig. 4 XRD of GO

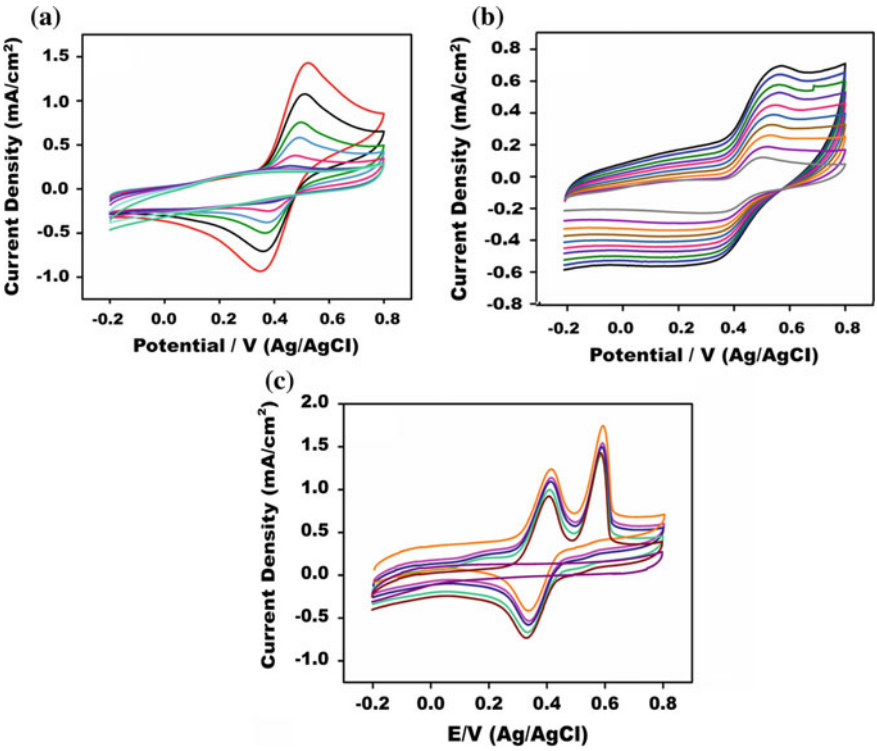

Fig. 5 Cyclic voltammetry measurements of GO/GCE in 0.1 M PBS (pH = 7.0) containing **a** dopamine (0.1–1.0 mM) and **b** uric acid (0.2–1.2 mM) **c** (0.1–1.0 mM) DA + (0.2–1.2 mM) UA, scan rate: 50 mV/s

4 Conclusions

In this study, the graphene oxide electrodes was obtained by a covalently bonded and modified interface to the glassy carbon electrode for the detection of both dopamine and uric acid. The electrochemical experiments and the obtained data showed that dopamine and uric acid had a different effect on a graphene oxide film. According to the measurements made with graphene oxide electrodes, better signals and peaks were obtained. Also, based on the results of dopamine and uric acid with a modified electrode, it was applied as a biosensor to detect dopamine in the presence of uric acid. The results showed that the presence of uric acid in the environment did not affect the detection of dopamine. This allows the modified electrode to be able to analyze and measure these components simultaneously without interfering of each other. To date, many electrode studies have been reported with graphene and its composites [9, 13, 21, 76, 77], but the modified electrode mentioned here is a very quickly prepared, environmentally compatible, much better sensitive biosensor compared to the others.

References

1. Zhang, R., Di, Jin G., Chen, D., Hu, X.Y.: Simultaneous electrochemical determination of dopamine, ascorbic acid and uric acid using poly(acid chrome blue K) modified glassy carbon electrode. Sens. Actuat. B Chem. **138**, 174–181 (2009). https://doi.org/10.1016/j.snb.2008.12.043
2. Reyes, S., Fu, Y., Double, K.L., et al.: Trophic factors differentiate dopamine neurons vulnerable to Parkinson's disease. Neurobiol. Aging **34**, 873–886 (2013). https://doi.org/10.1016/j.neurobiolaging.2012.07.019
3. Zen, J.M., Chen, P.J.: A selective voltammetric method for uric acid and dopamine detection using clay-modified electrodes. Anal. Chem. **69**, 5087–5093 (1997). https://doi.org/10.1021/ac9703562
4. Alwarappan, S., Butcher, K.S.A., Wong, D.K.Y.: Evaluation of hydrogenated physically small carbon electrodes in resisting fouling during voltammetric detection of dopamine. Sens. Actuat. B Chem. **128**, 299–305 (2007). https://doi.org/10.1016/j.snb.2007.06.016
5. Mao, Y., Bao, Y., Gan, S., et al.: Electrochemical sensor for dopamine based on a novel graphene-molecular imprinted polymers composite recognition element. Biosens. Bioelectron. **28**, 291–297 (2011). https://doi.org/10.1016/j.bios.2011.07.034
6. Sun, C.L., Lee, H.H., Yang, J.M., Wu, C.C.: The simultaneous electrochemical detection of ascorbic acid, dopamine, and uric acid using graphene/size-selected Pt nanocomposites. Biosens. Bioelectron. **26**, 3450–3455 (2011). https://doi.org/10.1016/j.bios.2011.01.023
7. Habibi, B., Jahanbakhshi, M., Pournaghi-Azar, M.H.: Differential pulse voltammetric simultaneous determination of acetaminophen and ascorbic acid using single-walled carbon nanotube-modified carbon-ceramic electrode. Anal. Biochem. (2011). https://doi.org/10.1016/j.ab.2011.01.005
8. Raoof, J.B., Kiani, A., Ojani, R., et al.: Simultaneous voltammetric determination of ascorbic acid and dopamine at the surface of electrodes modified with self-assembled gold nanoparticle films. J. Solid State Electrochem. **14**, 1171–1176 (2010). https://doi.org/10.1007/s10008-009-0917-z
9. Zhou, C., Li, S., Zhu, W., et al.: A sensor of a polyoxometalate and Au–Pd alloy for simultaneously detection of dopamine and ascorbic acid. Electrochim. Acta **113**, 454–463 (2013). https://doi.org/10.1016/J.ELECTACTA.2013.09.109
10. Fujishima, A., Rao, T.N., Popa, E., et al.: Electroanalysis of dopamine and NADH at conductive diamond electrodes. J. Electroanal. Chem. **473**, 179–185 (1999). https://doi.org/10.1016/S0022-0728(99)00106-0
11. Heien, M.L.A.V., Phillips, P.E.M., Stuber, G.D., et al.: Overoxidation of carbon-fiber microelectrodes enhances dopamine adsorption and increases sensitivity. Analyst **128**, 1413–1419 (2003). https://doi.org/10.1039/b307024g
12. Jiang, L., Liu, C., Jiang, L., et al.: A chitosan-multiwall carbon nanotube modified electrode for simultaneous detection of dopamine and ascorbic acid. Anal. Sci. **20**, 1055–1059 (2004). https://doi.org/10.2116/analsci.20.1055
13. Kim, Y.-R., Bong, S., Kang, Y.-J., et al.: Electrochemical detection of dopamine in the presence of ascorbic acid using graphene modified electrodes. Biosens. Bioelectron. **25**, 2366–2369 (2010). https://doi.org/10.1016/J.BIOS.2010.02.031
14. Li, J., Yang, J., Yang, Z., et al.: Graphene–Au nanoparticles nanocomposite film for selective electrochemical determination of dopamine. Anal. Methods **4**, 1725 (2012). https://doi.org/10.1039/c2ay05926f
15. Ramesh, P., Suresh, G.S., Sampath, S.: Selective determination of dopamine using unmodified, exfoliated graphite electrodes. J. Electroanal. Chem. **561**, 173–180 (2004). https://doi.org/10.1016/j.jelechem.2003.08.002
16. Ahn, M., Kim, J.: Electrochemical behavior of dopamine and ascorbic acid at dendritic Au rod surfaces: selective detection of dopamine in the presence of high concentration of ascorbic acid. J. Electroanal. Chem. **683**, 75–79 (2012). https://doi.org/10.1016/j.jelechem.2012.08.012

17. Cai, W., Lai, T., Du, H., Ye, J.: Electrochemical determination of ascorbic acid, dopamine and uric acid based on an exfoliated graphite paper electrode: a high performance flexible sensor. Sens. Actuat. B Chem. **193**, 492–500 (2014). https://doi.org/10.1016/J.SNB.2013.12.004
18. Deng, C., Chen, J., Wang, M., et al.: A novel and simple strategy for selective and sensitive determination of dopamine based on the boron-doped carbon nanotubes modified electrode. Biosens. Bioelectron. **24**, 2091–2094 (2009). https://doi.org/10.1016/j.bios.2008.10.022
19. Popa, E., Kubota, Y, Tryk, D.A., Fujishima, A.: Selective voltammetric and amperometric detection of uric acid with oxidized diamond film electrodes (2000). https://doi.org/10.1021/ac990862m
20. Niu, L.M., Lian, K.Q., Shi, H.M., et al.: Characterization of an ultrasensitive biosensor based on a nano-Au/DNA/nano-Au/poly(SFR) composite and its application in the simultaneous determination of dopamine, uric acid, guanine, and adenine. Sens. Actuat. B Chem. **178**, 10–18 (2013). https://doi.org/10.1016/j.snb.2012.12.015
21. Raoof, J.B., Ojani, R., Baghayeri, M.: A selective sensor based on a glassy carbon electrode modified with carbon nanotubes and ruthenium oxide/hexacyanoferrate film for simultaneous determination of ascorbic acid, epinephrine and uric acid. Anal. Methods **3**, 2367 (2011). https://doi.org/10.1039/c1ay05305a
22. Wang, C., Yuan, R., Chai, Y., et al.: Simultaneous determination of ascorbic acid, dopamine, uric acid and tryptophan on gold nanoparticles/overoxidized-polyimidazole composite modified glassy carbon electrode. Anal. Chim. Acta **741**, 15–20 (2012). https://doi.org/10.1016/j.aca.2012.06.045
23. Alwarappan, S., Erdem, A., Liu, C., Li, C.-Z.: Probing the electrochemical properties of graphene nanosheets for biosensing applications. J. Phys. Chem. C **113**, 8853–8857 (2009). https://doi.org/10.1021/jp9010313
24. Zhang, Y., Pan, Y., Su, S., et al.: A novel functionalized single-wall carbon nanotube modified electrode and its application in determination of dopamine and uric acid in the presence of high concentrations of ascorbic acid. Electroanalysis **19**, 1695–1701 (2007). https://doi.org/10.1002/elan.200703901
25. Liu, M., Chen, Q., Lai, C., et al.: A double signal amplification platform for ultrasensitive and simultaneous detection of ascorbic acid, dopamine, uric acid and acetaminophen based on a nanocomposite of ferrocene thiolate stabilized Fe3O4@Au nanoparticles with graphene sheet. Biosens. Bioelectron. **48**, 75–81 (2013). https://doi.org/10.1016/J.BIOS.2013.03.070
26. Çelik, B., Başkaya, G., Sert, H., et al.: Monodisperse Pt(0)/DPA@GO nanoparticles as highly active catalysts for alcohol oxidation and dehydrogenation of DMAB. Int. J. Hydrogen Energy **41**, 5661–5669 (2016). https://doi.org/10.1016/j.ijhydene.2016.02.061
27. Erken, E., Yıldız, Y., Kilbaş, B., Şen, F.: Synthesis and characterization of nearly monodisperse Pt nanoparticles for C_1 to C_3 alcohol oxidation and dehydrogenation of dimethylamine-borane (DMAB). J. Nanosci. Nanotechnol. (2016). https://doi.org/10.1166/jnn.2016.11683
28. Goksu, H., Zengin, N., Karaosman, A., Sen, F.: Highly active and reusable Pd/AlO(OH) nanoparticles for the suzuki cross-coupling reaction. Curr. Organocatalysis **5**, 34–41 (2018). https://doi.org/10.2174/2213337205666180614114550
29. Şahin, B., Aygün, A., Gündüz, H., et al.: Cytotoxic effects of platinum nanoparticles obtained from pomegranate extract by the green synthesis method on the MCF-7 cell line. Colloids Surf. B **163**, 119–124 (2018). https://doi.org/10.1016/j.colsurfb.2017.12.042
30. Şen, B., Aygün, A., Okyay, T.O., et al.: Monodisperse palladium nanoparticles assembled on graphene oxide with the high catalytic activity and reusability in the dehydrogenation of dimethylamine-borane. Int. J. Hydrogen Energy **2**, 2–9 (2018). https://doi.org/10.1016/j.ijhydene.2018.03.175
31. Şen, B., Aygün, A., Şavk, A., et al.: Bimetallic palladium–iridium alloy nanoparticles as highly efficient and stable catalyst for the hydrogen evolution reaction. Int. J. Hydrogen Energy **43**, 20183–20191 (2018). https://doi.org/10.1016/j.ijhydene.2018.07.081

32. Sen, B., Kuzu, S., Demir, E., et al.: Polymer-graphene hybride decorated Pt nanoparticles as highly efficient and reusable catalyst for the dehydrogenation of dimethylamine–borane at room temperature. Int. J. Hydrogen Energy **42**, 23284–23291 (2017). https://doi.org/10.1016/j.ijhydene.2017.05.112
33. Sen, B., Şavk, A., Sen, F.: Highly efficient monodisperse Pt nanoparticles confined in the carbon black hybrid material for hydrogen liberation. J. Colloid Interface Sci. **520**, 112–118 (2018). https://doi.org/10.1016/j.jcis.2018.03.004
34. Şen, F., Gökağaç, G.: Different sized platinum nanoparticles supported on carbon: an XPS study on these methanol oxidation catalysts. J. Phys. Chem. C **111**, 5715–5720 (2007). https://doi.org/10.1021/jp068381b
35. Yıldız, Y., Erken, E., Pamuk, H., et al.: Monodisperse Pt nanoparticles assembled on reduced graphene oxide: highly efficient and reusable catalyst for methanol oxidation and dehydrocoupling of dimethylamine-borane (DMAB). J. Nanosci. Nanotechnol. **16**, 5951–5958 (2016). https://doi.org/10.1166/jnn.2016.11710
36. Yıldız, Y., Kuzu, S., Sen, B., et al.: Different ligand based monodispersed Pt nanoparticles decorated with rGO as highly active and reusable catalysts for the methanol oxidation. Int. J. Hydrogen Energy **42**, 13061–13069 (2017). https://doi.org/10.1016/j.ijhydene.2017.03.230
37. Chen, J., Zhang, J., Lin, X., et al.: Electrocatalytic oxidation and determination of dopamine in the presence of ascorbic acid and uric acid at a poly (4-(2-Pyridylazo)-Resorcinol) modified glassy carbon electrode. Electroanalysis **19**, 612–615 (2007). https://doi.org/10.1002/elan.200603755
38. Li, F., Chai, J., Yang, H., et al.: Synthesis of Pt/ionic liquid/graphene nanocomposite and its simultaneous determination of ascorbic acid and dopamine. Talanta **81**, 1063–1068 (2010). https://doi.org/10.1016/j.talanta.2010.01.061
39. Ayranci, R., Başkaya, G., Güzel, M., et al.: Carbon based nanomaterials for high performance optoelectrochemical systems. ChemistrySelect **2**, 1548–1555 (2017). https://doi.org/10.1002/slct.201601632
40. Çelik, B., Kuzu, S., Erken, E., et al.: Nearly monodisperse carbon nanotube furnished nanocatalysts as highly efficient and reusable catalyst for dehydrocoupling of DMAB and C1 to C3 alcohol oxidation. Int. J. Hydrogen Energy **41**, 3093–3101 (2016). https://doi.org/10.1016/j.ijhydene.2015.12.138
41. Eris, S., Daşdelen, Z., Sen, F.: Investigation of electrocatalytic activity and stability of Pt@f-VC catalyst prepared by in-situ synthesis for methanol electrooxidation. Int. J. Hydrogen Energy **43**, 385–390 (2018). https://doi.org/10.1016/j.ijhydene.2017.11.063
42. Göksu, H., Çelik, B., Yıldız, Y., et al.: Superior monodisperse CNT-supported CoPd (CoPd@CNT) nanoparticles for selective reduction of nitro compounds to primary amines with NaBH4 in aqueous medium. ChemistrySelect **1**, 2366–2372 (2016). https://doi.org/10.1002/slct.201600509
43. Günbatar, S., Aygun, A., Karataş, Y., et al.: Carbon-nanotube-based rhodium nanoparticles as highly-active catalyst for hydrolytic dehydrogenation of dimethylamineborane at room temperature. J. Colloid Interface Sci. **530**, 321–327 (2018). https://doi.org/10.1016/j.jcis.2018.06.100
44. Li, G., Yi, Q., Yang, X., et al.: Ni-Co-N doped honeycomb carbon nano-composites as cathodic catalysts of membrane-less direct alcohol fuel cell. Carbon N Y **140**, 557–568 (2018). https://doi.org/10.1016/J.CARBON.2018.08.037
45. Sert, H., Yıldız, Y., Okyay, T.O., et al.: Monodisperse Mw-Pt NPs@VC as highly efficient and reusable adsorbents for methylene blue removal. J. Clust. Sci. **27**, 1953–1962 (2016). https://doi.org/10.1007/s10876-016-1054-3
46. Sert, H., Yıldız, Y., Onal Okyay, T., et al.: Activated carbon furnished monodisperse Pt nanocomposites as a superior adsorbent for methylene blue removal from aqueous solutions. J. Nanosci. Nanotechnol. **17**, 1–6 (2017). https://doi.org/10.1166/jnn.2017.13776
47. Banks, C.E., Crossley, A., Salter, C., et al.: Carbon nanotubes contain metal impurities which are responsible for the "electrocatalysis" seen at some nanotube-modified electrodes. Angew. Chem. Int. Ed. **45**, 2533–2537 (2006). https://doi.org/10.1002/anie.200600033

48. Chen, D., Tang, L., Li, J.: Graphene-based materials in electrochemistry. Chem. Soc. Rev. **39**, 3157–3180 (2010). https://doi.org/10.1039/b923596e
49. Li, D., Müller, M.B., Gilje, S., et al.: Processable aqueous dispersions of graphene nanosheets. Nat. Nanotechnol. **3**, 101–105 (2008). https://doi.org/10.1038/nnano.2007.451
50. Segal, M.: Selling graphene by the ton. Nat. Nanotechnol. **2009**, 410 (2009)
51. Wang, C., Jiang, F., Yue, R., et al.: Enhanced photo-electrocatalytic performance of Pt/RGO/TiO2 on carbon fiber towards methanol oxidation in alkaline media. J. Solid State Electrochem. **18**, 515–522 (2014). https://doi.org/10.1007/s10008-013-2282-1
52. Demir, E., Savk, A., Sen, B., Sen, F.: A novel monodisperse metal nanoparticles anchored graphene oxide as counter electrode for dye-sensitized solar cells. Nano-Struct. Nano-Objects (2017). https://doi.org/10.1016/j.nanoso.2017.08.018
53. Eris, S., Daşdelen, Z., Yıldız, Y., Sen, F.: Nanostructured polyaniline-rGO decorated platinum catalyst with enhanced activity and durability for methanol oxidation. Int. J. Hydrogen Energy **43**, 1337–1343 (2018). https://doi.org/10.1016/j.ijhydene.2017.11.051
54. Esirden, I., Erken, E., Kaya, M., Sen, F.: Monodisperse Pt NPs@rGO as highly efficient and reusable heterogeneous catalysts for the synthesis of 5-substituted 1H-tetrazole derivatives. Catal. Sci. Technol. **5**, 4452–4457 (2015). https://doi.org/10.1039/c5cy00864f
55. Gezer, B., Sert, H., Onal Okyay, T., et al.: Reduced graphene oxide (rGO) as highly effective material for the ultrasound assisted boric acid extraction from ulexite ore. Chem. Eng. Res. Des. **117**, 542–548 (2017). https://doi.org/10.1016/j.cherd.2016.11.007
56. Şen, B., Akdere, E.H., Şavk, A., et al.: A novel thiocarbamide functionalized graphene oxide supported bimetallic monodisperse Rh-Pt nanoparticles (RhPt/TC@GO NPs) for Knoevenagel condensation of aryl aldehydes together with malononitrile. Appl. Catal. B Environ. **225**, 148–153 (2018). https://doi.org/10.1016/j.apcatb.2017.11.067
57. Şen, B., Lolak, N., Paralı, Ö., et al.: Bimetallic PdRu/graphene oxide based catalysts for one-pot three-component synthesis of 2-amino-4H-chromene derivatives. Nano-Struct. Nano-Objects **12**, 33–40 (2017). https://doi.org/10.1016/j.nanoso.2017.08.013
58. Liu, Q., Zhu, X., Huo, Z., et al.: Electrochemical detection of dopamine in the presence of ascorbic acid using PVP/graphene modified electrodes. Talanta **97**, 557–562 (2012). https://doi.org/10.1016/j.talanta.2012.05.013
59. Sun, L., Fugetsu, B.: Mass production of graphene oxide from expanded graphite. Mater. Lett. **109**, 207–210 (2013). https://doi.org/10.1016/J.MATLET.2013.07.072
60. Tan, J.L., De Jesus, A.M., Chua, S.L., et al.: Preparation and characterization of palladium-nickel on graphene oxide support as anode catalyst for alkaline direct ethanol fuel cell. Appl. Catal. A Gen. **531**, 29–35 (2017). https://doi.org/10.1016/j.apcata.2016.11.034
61. Karteri, İ., Karataş, Ş., Yakuphanoğlu, F.: Electrical characterization of graphene oxide and organic dielectric layers based on thin film transistor. Appl. Surf. Sci. **318**, 74–78 (2014). https://doi.org/10.1016/J.APSUSC.2014.01.013
62. Ryu, S.H., Shanmugharaj, A.M.: Influence of long-chain alkylamine-modified graphene oxide on the crystallization, mechanical and electrical properties of isotactic polypropylene nanoc omposites. Chem. Eng. J. **244**, 552–560 (2014). https://doi.org/10.1016/J.CEJ.2014.01.101
63. Zhou, Y., Bao, Q., Tang, L.A.L., et al.: Hydrothermal dehydration for the "green" reduction of exfoliated graphene oxide to graphene and demonstration of tunable optical limiting properties. Chem. Mater. **21**, 2950–2956 (2009). https://doi.org/10.1021/cm9006603
64. Arbuzov, A.A., Muradyan, V.E., Tarasov, B.P.: Synthesis of few-layer graphene sheets via chemical and thermal reduction of graphite oxide. Proc. Int. Conf. Nanomater. Appl. Prop. **1**, 1–07 (2012)
65. Chen, W., Yan, L., Bangal, P.R.: Chemical reduction of graphene oxide to graphene by sulfur-containing compounds. J. Phys. Chem. C **114**, 19885–19890 (2010). https://doi.org/10.1021/jp107131v
66. Allen, M.J., Tung, V.C., Kaner, R.B.: Honeycomb carbon: a review of graphene. Chem. Rev. **110**, 132–145 (2010). https://doi.org/10.1021/cr900070d

67. Loryuenyong, V., Totepvimarn, K., Eimburanapravat, P., et al.: Preparation and characterization of reduced graphene oxide sheets via water-based exfoliation and reduction methods. Adv. Mater. Sci. Eng. **2013**, 1–5 (2013). https://doi.org/10.1155/2013/923403
68. Shahriary, L., Athawale, A.A.: Graphene oxide synthesized by using modified hummers approach (2014)
69. Gao, Y., Ma, D., Wang, C., et al.: Reduced graphene oxide as a catalyst for hydrogenation of nitrobenzene at room temperature. Chem. Commun. **47**, 2432–2434 (2011). https://doi.org/10.1039/C0CC04420B
70. Hanifah, M.F.R., Jaafar, J., Aziz, M., et al.: Synthesis of graphene oxide nanosheets via modified hummers' method and its physicochemical properties. J. Teknol. **74** (2015). https://doi.org/10.11113/jt.v74.3555
71. Karteri, İ., Karataş, Ş., Al-Ghamdi, A.A., Yakuphanoğlu, F.: The electrical characteristics of thin film transistors with graphene oxide and organic insulators. Synth. Met. **199**, 241–245 (2015). https://doi.org/10.1016/J.SYNTHMET.2014.11.036
72. Liao, K.-H., Mittal, A., Bose, S., et al.: Aqueous only route toward graphene from graphite oxide. ACS Nano **5**, 1253–1258 (2011). https://doi.org/10.1021/nn1028967
73. Bajaj, P., Sreekumar, T.V., Sen, K.: Structure development during dry-jet-wet spinning of acrylonitrile/vinyl acids and acrylonitrile/methyl acrylate copolymers. J. Appl. Polym. Sci. **86**, 773–787 (2002). https://doi.org/10.1002/app.10973
74. Ma, X., Chao, M., Wang, Z.: Electrochemical detection of dopamine in the presence of epinephrine, uric acid and ascorbic acid using a graphene-modified electrode. Anal. Methods **4**, 1687 (2012). https://doi.org/10.1039/c2ay25040c
75. Schniepp, H.C., Li, J.-L., McAllister, M.J., et al.: Functionalized single graphene sheets derived from splitting graphite oxide. J. Phys. Chem. B **110**, 8535–8539 (2006). https://doi.org/10.1021/jp060936f
76. Alwarappan, S., Boyapalle, S., Kumar, A., et al.: Comparative study of single-, few-, and multilayered graphene toward enzyme conjugation and electrochemical response. J. Phys. Chem. C **116**, 6556–6559 (2012). https://doi.org/10.1021/jp211201b
77. Alwarappan, S., Joshi, R.K., Ram, M.K., Kumar, A.: Electron transfer mechanism of cytochrome c at graphene electrode. Appl. Phys. Lett. **96**, 263702 (2010). https://doi.org/10.1063/1.3458698

Cyclodextrin Functionalized Graphene and Its Applications

Li Fu

Abstract Cyclodextrin (CD) is the general name for a series of cyclic oligosaccharides produced via glucotransferase by Bacillus. The inner cavity of cyclodextrin is hydrophobic, while the outer cavity is hydrophilic, which enables interactions with many organic or inorganic molecules through van der Waals forces and hydrophobic interactions. In this chapter, we summarized the incorporation of graphene with CD through different strategies and the resulting applications. Surface functionalization processes, including covalent interactions and noncovalent interactions, were discussed in detail. Then, the applications of surface-CD-functionalized graphene in drug delivery, chiral recognition, electrochemical sensing, and pollutant removal were summarized.

Keywords Cyclodextrin · Graphene · Surface functionalization · Electrochemical sensor · Drug delivery

1 Introduction

Graphene is considered the most promising substitute for silicon in electronic components. Since its discovery in 2004, due to its excellent electrochemical, thermal and mechanical properties, it has been destined to encompass a class of "star materials" and has attracted a great deal of attention [16, 26]. As a structure made of carbon, graphene is very thin while having a very high strength, and like copper, it has a good electrical conductivity, which is better than those of all other known materials in the field of heat conduction [30, 60, 72, 73]. In addition, graphene is almost completely transparent, but its atoms are tightly arranged; even helium molecules cannot penetrate it. Graphene is also known as "single-layer graphite", but because of its π-π stacking tends to accumulate via self-assembly,

L. Fu (✉)
College of Materials and Environmental Engineering, Hangzhou Dianzi University, Hangzhou 310018, People's Republic of China
e-mail: fuli@hdu.edu.cn

A. Khan et al. (eds.), *Graphene Functionalization Strategies*, Carbon Nanostructures, https://doi.org/10.1007/978-981-32-9057-0_8

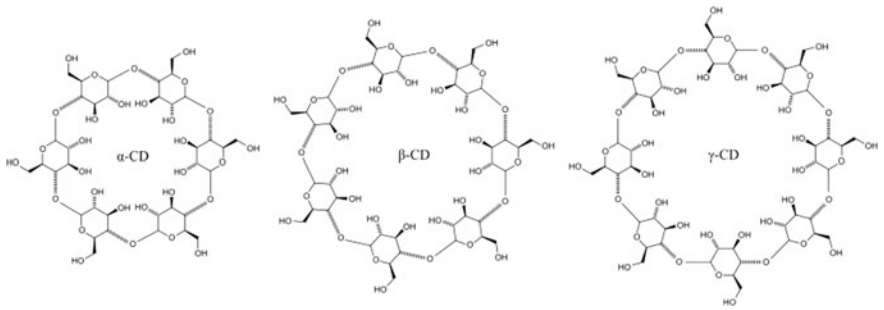

Fig. 1 Chemical structures of α-CD, β-CD and γ-CD

many excellent properties of graphene can only be displayed in a single layer with two-dimensional structure, which makes it important to prevent the aggregation of graphene [27, 55, 80].

Cyclodextrins (CDs) are a family of compounds made of sugar molecules bound together in a ring [2, 23, 61]. CDs are composed of 5 or more α-D-glucopyranoside units linked 1 → 4, as in amylose. Figure 1 shows the chemical structures of α-CD, β-CD and γ-CD. CD is a typical "bottomless" cone-like molecule. Because of their unique structure, CDs can identify and bind a number of substrates in aqueous solution [22, 31]. CD is made of glucose units, making it an important principal molecule in supramolecular chemistry that is cheap and easy to obtain and has good biocompatibility. It is widely used in the fields of catalysis, self-assembly, molecular recognition and drug transportation [17, 54, 91]. If CDs and graphene are combined, the excellent molecular properties of the CDs can enhance the water solubility of graphene and prevent its aggregation. In this chapter, the surface functionalization of graphene and its derivatives is introduced first. Then, the applications of CD-functionalized graphene are examined.

2 Functionalization of Graphene and Its Derivatives by CD

Covalently bonded CD-graphene supramolecular systems have strong chemical stability and a relatively straightforward chemical composition. The main approach of CD-graphene supramolecular-system synthesis is covalent-bond coupling between graphene oxide and modified CDs.

Graphene itself is a high-surface-area and flexible two-dimensional material that has the potential to construct gel systems. In addition to improving water solubility, it is possible to expand the application scope by using two-dimensional graphene as a gel to build a three-dimensional grid system. For example, Liu and coworkers demonstrated that graphene sheets could serve as a desirable inorganic constituent in constructing hybrid polymeric hydrogels via supramolecular routes [35]. More

specifically, as shown in Fig. 2, graphene oxide (GO) nanosheets were modified by grafting β-CD first, leading to chemically converted graphene, and then noncovalently functionalized by the block copolymer AZO-PDMA-b-PNIPAM via inclusion complexation. The oxygen-containing functional groups on the GO surface could covalently bond CD by a simple mixing process. To accelerate this process, a microwave catalytic approach can be introduced. Xu and coworkers prepared hydroxypropyl-β-CD-modified graphene nanosheets using a facile and rapid method assisted by microwave irradiation in water [77]. In this system, β-CD and graphene are connected through ester bonds. The obtained supramolecular system has a high specific surface area and molecular recognition ability.

Noncovalent interactions between CD and graphene can also be used for synthesizing supramolecular systems. For example, a CD-graphene supramolecular system was fabricated through noncovalent interactions using a folic acid-modified β-CD acting as a target unit, an adamantanyl porphyrin acting as a linker unit, and GO acting as a carrier unit [81]. Ogoshi et al. [47] reported a per-6-amino-β-CD-functionalized GO using the ionic interaction between the GO carboxylic acid and β-CD amino moieties. This ionic interaction is a very simple approach but may affect the electrochemical properties of graphene. An indirect modification process was proposed to overcome this problem [94]. Triblock copolymers (PEO-b-PPOb-PEO) were employed as the solubilizing agent for chemically exfoliated graphite oxide, and graphene was formed through in situ reduction by hydrazine. The formation of the stable aqueous copolymer-coated graphene solution was due to the noncovalent interaction between the hydrophobic PPO segments

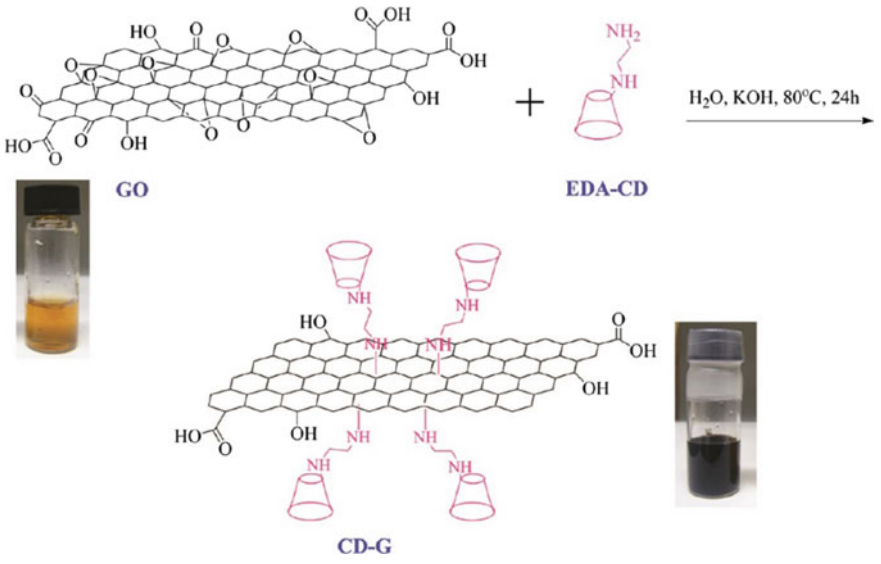

Fig. 2 Synthetic route of CD-G and the corresponding photos of aqueous solutions of GO and CD-G. Reprinted from Ref. [18], Copyright 2018 with permission from ACS Publications

of the triblock copolymer and the hydrophobic graphene surface, whereas the hydrophilic PEO chains extended into the water. Then, a supramolecular hydrogel with α-CD was formed through the penetration of PEO chains into the CD cavities. A more universal method was proposed by Guo et al. [20] using a simple wet-chemical strategy for the preparation of CD-graphene organic–inorganic hybrid nanosheets (Fig. 3). In a typical synthesis of a CD-graphene hybrid nanosheet, the homogeneous GO dispersion was mixed with CD aqueous solution, ammonia, and hydrazine solution. After the mixture was stirred for a few minutes and kept at 60 °C in a water bath for more than 3.5 h, a stable black dispersion of CD-graphene was obtained.

In addition to wet chemical synthesis methods, electrochemically based methods have been successfully used for CD-graphene supramolecular-system preparation. Wu et al. [76] reported the preparation of a CD-graphene supramolecular system on a glassy carbon electrode by electrochemical reduction. More specifically, under ultrasonic conditions, GO and β-CD were dispersed into the water system and then dropped onto the glassy carbon electrode. Electrochemical reduction was carried out

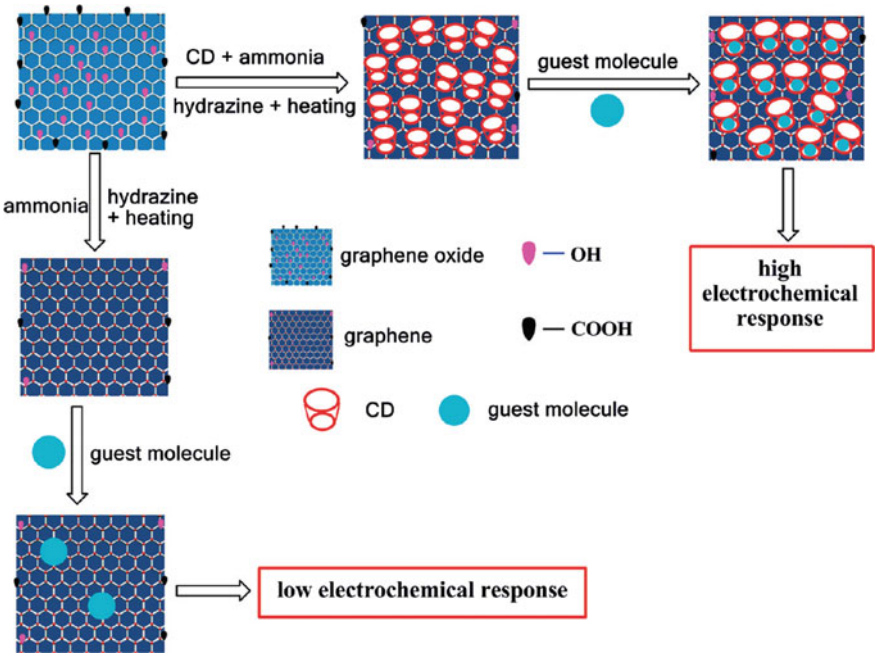

Fig. 3 Illustration of the procedure for preparing CD-graphene organic–inorganic hybrid nanosheets and GNs, and sensing the guest molecules by an electrochemical strategy. Reprinted from Ref. [18], Copyright 2018 with permission from ACS Publications

in a pH = 7.0 PBS buffer solution with a potential of −1.2 to +1.2 V and a scanning rate of 100 mV/s. The glassy carbon electrode was modified by CD, and the graphene supramolecular system was obtained after washing and drying with N_2.

3 Cyclodextrin-Functionalized Graphene for Drug Delivery

Drug delivery is a way to transport medicine molecules through a carrier to a specific part of the body or animal to maximize their specific efficacy. A nano-drug-loading system is a drug-carrier-complex system that is loaded on a nanomaterial carrier by physical or chemical methods to form a drug carrier system between 10 and 1000 nm. Many studies have confirmed that CD or its derivatives can transport drugs by forming physical complexes or bonds with drug molecules (including therapeutic genes) and can significantly improve the solubility and stability of the drugs and enhance their bioactivity [4, 5, 21, 46, 51]. In addition, CDs can also be used to reduce the irritation of drugs to the body and improve the dosage of drugs. The application of CDs in the field of drug delivery can be traced back to the 1980s [62]. In recent years, with the rapid development of medicine, polymers, materials and nanotechnology, nanomaterials containing CDs have been widely used in controlled drug delivery and gene therapy.

Graphene-based nanocarriers for drug transportation were first reported in 2008. Dai et al. [39] reported a PEG-modified GO and used it for carrying SN38 molecules. SN38 is a derivative of camptothecin, a water-soluble aromatic drug molecule, which blocks the growth of cells by blocking the synthesis of topoisomerase I. SN38 can be adsorbed on the PEG GO surface by π-π stacking interactions. Although SN38 is not water soluble, the GO-PEG/SN38 complex is not only soluble in water but can also be dispersed in physiological solution after loading on the surface of GO. Compared with water-insoluble SN38, GO-PEG/SN38 has stronger toxicity against human colon cancer HCTll6 cells. Since then, many graphene-based carriers have been reported to transport other drug molecules.

In recent years, studies on the preparation of nanosized drug carriers by graphene or graphene oxide with CDs have been published. For example, Dong et al. [8] synthesized CD-functionalized graphene nanosheets. The material is highly stable in the biological environment and can selectively load various biological and functional agents. He et al. [24] reported gelatin- and HP-β-CD-functionalized GO nanospheres prepared via an electrospray technology. The interaction of HP-β-CD and the carboxyl group on the GO surface was used for the transport of Taxol. Similar work has been reported using HP-β-CD-modified carboxylated GO (Fig. 4) to incorporate the anticancer drug paclitaxel [63]. Table 1 summarizes the recently reported CD-graphene supermolecular systems for drug transportation applications.

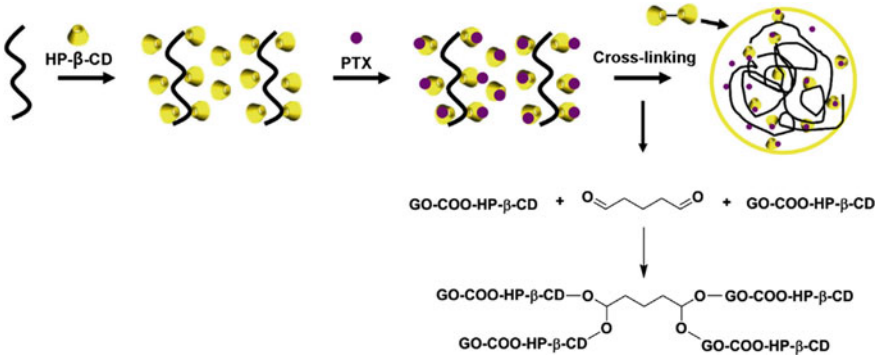

Fig. 4 Schematic illustration of drug-loaded GO-COO-HP-β-CD nanosphere formation. Reprinted from Ref. [34], Copyright 2018 with permission from Elsevier

Table 1 Recent reported works regard to the drug delivery based on CDs-graphene supermolecular system

CDs-graphene based carrier	Drug molecules	References
β-CD-graphene-dendrimer	Doxorubicin, camptothecin, photosensitizer	Siriviriyanun et al. [56]
HP-β-CD-GO-COOH	Paclitaxel	Tan et al. [63]
β-CD-graphene-MGC nanocomposite	Doxorubicin	Wang et al. [67]
C_6H_4-CO-NH-PEI-NH-CO-CD-Biotin	Doxorubicin	Wei et al. [74]
PEO-PPO-PEO-graphene-α-CD	Fluorescein	Quinn et al. [50]
CD-GO-Fe_3O_4	SN38	Einafshar et al. [10]
β-CD/GO	Camptothecin	Zhang et al. [88]

4 Cyclodextrin Functionalized Graphene for Chiral Recognition

In stereochemistry, the characteristic that a substance cannot be superimposed upon its mirror image is called chirality. Chirality is ubiquitous in nature. It is one of the most basic characteristics of life processes. Most drugs used by humans are also composed of chiral molecules. The mirror images of a chiral molecule are called enantiomers. Most of the organic compounds that constitute the living body, such as proteins, polysaccharides and nucleic acids, are chiral molecules. Among them, the basic unit amino acids that constitute proteins are L-amino acids, except for glycine, and the ribose in polysaccharides and nucleic acids is D-monosaccharide. When there are two enantiomers of chiral drugs, often only one of them has a therapeutic effect, and the other may be ineffective or even have toxic side effects.

Enantiomers can be identified only in a chiral environment. Chiral selectors form unstable stereoisomeric complexes by stereospecific interaction with enantiomers. When the equilibrium constants of the formation and dissociation of these two stereoisomeric complexes do not reach the recognition effect at the same time, the interaction is called chiral recognition.

Chiral recognition is the most basic process in nature and is also very important to life. Chiral recognition is of great value in many fields, such as medicine, life science, food science and material science. At present, there are many methods of chiral recognition that have been developed and have achieved certain results; these approaches are mainly divided into spectroscopic, chromatographic and sensor-based methods. With the development of chromatographic technology, enantiomeric separation methods based on CDs have become standardized. In high-performance liquid chromatography, CDs have good optical purity and do not interfere with detection, so they can be directly added to the mobile phase or anchored to a suitable carrier for the preparation of a chiral stationary phase [34, 53, 82, 92]. Compared with high-performance liquid chromatography, the application of CDs in capillary-zone electrophoresis is concerned with the type and structure of chiral agents [43, 44, 52]. The applications of natural CDs are limited due to poor water solubility, so various neutral and ionic derivatives have been developed.

Chiral recognition can be achieved by using a combination of chiral chromatography and chiral spectrometry. However, the specific operating process still retains disadvantages, such as a long detection time, sample damage or pollution resulting from the test itself, and the high price of the instruments and equipment. The use of various chemical organic reagents also pollutes the environment. Therefore, developing new chiral recognition methods is of great practical significance. Sensors are widely used in compound recognition because of their advantages, such as simplicity and speed. Chiral sensors are mainly divided into fluorescent chiral sensors and electrochemical chiral sensors. Fluorescent chiral sensors are based on the formation of different complexes of chiral selectors and enantiomers, causing different changes in the fluorescence of chiral selectors. Electrochemical chiral sensors are based on the differences among the effects of chiral selectors and enantiomers (such as hydrogen bonds, dipole interactions, charge transfer effects, coordination effects, and hydrophobic interactions), and these differences can be identified by conversion of the redox probe into electrical signals.

Graphene has a high surface area, high intrinsic mobility and good electrical conductivity and has been applied to the detection of biomolecules. The combination of CD and graphene is a new type of sensor for chiral recognition. Feng et al. [13] reported a simple β-CD-graphene-modified glassy carbon electrode for the chiral recognition of tryptophan in the presence of Cu(II). Ou et al. [48] reported a graphene quantum dot (GQD)/β-CD nanocomposite. The GQD/β-CD nanocomposites combine the advantages of GQDs (highly negatively charged) and β-CD (chiral microenvironment). They found that although tapered hydrophobic cavities in β-CD that are capable of including various guest molecules exist, the enantiorecognition efficiency of pure β-CD-modified GCE was dramatically inferior to

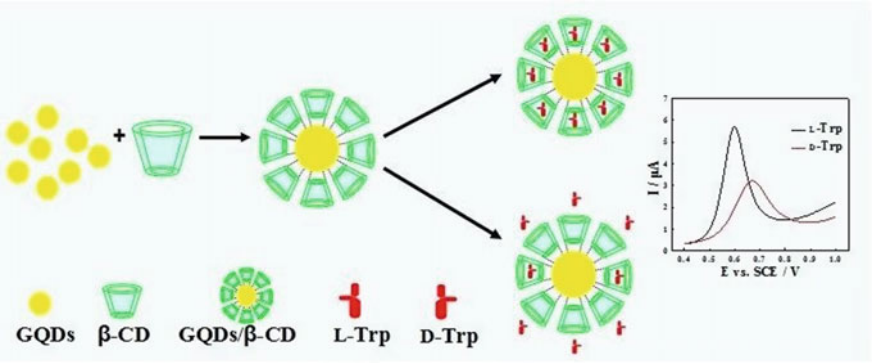

Fig. 5 Schematic illustrating the preparation of GQDs/β-CD and the recognition of Trp isomers by the nanocomposites. Reprinted from Ref. [49], Copyright 2018 with permission from Elsevier

Table 2 Recent reported works regard to the chiral recognition based on CDs-graphene supermplecular system

CDs-graphene based composite	Enantiomers	References
β-CD-Pt NPsNPs/graphene	Tryptophan	Xu et al. [78]
GQDs/β-CD	Tryptophan	Ou et al. [48]
β-CD/Cu(II)/graphene	Tryptophan	Feng et al. [13]
β-CD/graphene	Moxifloxacin hydrochloride	Upadhyay et al. [66]
β-CD/RGO	Phenylalanine	Zaidi [85]
β-CD/graphene	DOPA	Ates et al. [3]
β-CDs-GQDs	Tyrosine	Dong et al. [9]
rGO/β-CD	Cystine	Zor et al. [93]
Amino-modified β-CD/graphene	Tryptophan	Song et al. [57]

that of GQD/β-CD-modified GCE (Fig. 5). Table 2 summarizes the recently reported CD-graphene supermolecular systems for chiral recognition applications.

5 Cyclodextrin-Functionalized Graphene for Electrochemical Detection

5.1 Drug Molecule Detection

With the development of modern medicine, chemical composition analysis technology is playing an increasingly important role in research, production and clinical use. Electrochemical analysis has the advantages of a low loss of equipment, reduced sample quantity, rapid operation and low detection limit. Graphene nanosheets have a larger specific surface area than other commonly used

nanomaterials and can form strong π-π conjugation interactions with many drug molecules. Therefore, graphene nanomaterials are ideal candidates for fabricating electrochemical biosensors to detect drugs. This area has become an important research direction in the field of biomedicine. If graphene is modified by β-CD, the unique properties of both graphene and β-CD can be improved, and consequently, these materials may be applied to the fields of sensors and electrocatalysis. The author and coworkers reported a β-CD/RGO formed using a simple wet chemical method (Fig. 6) [15]. The β-CD/RGO nanohybrid-modified GCE was employed for the sensitive electrochemical determination of paracetamol. Cyclic voltammetry measurements indicated that β-CD could significantly enhance the electrochemical response of paracetamol due to the outstanding electronic properties of RGO sheets and the high supramolecular recognition and enrichment capability of β-CD. Under optimized conditions, the amperometric oxidation currents of paracetamol were linearly proportional to concentrations in the range of 0.01–0.8 mM, with a detection limit of 2.3 μM.

Molecularly imprinted polymer is a synthetic artificial receptor that has a cavity that matches the shape of the substrate and has a specific functional group that can be identified by the substrate molecules. The prominent feature of molecularly

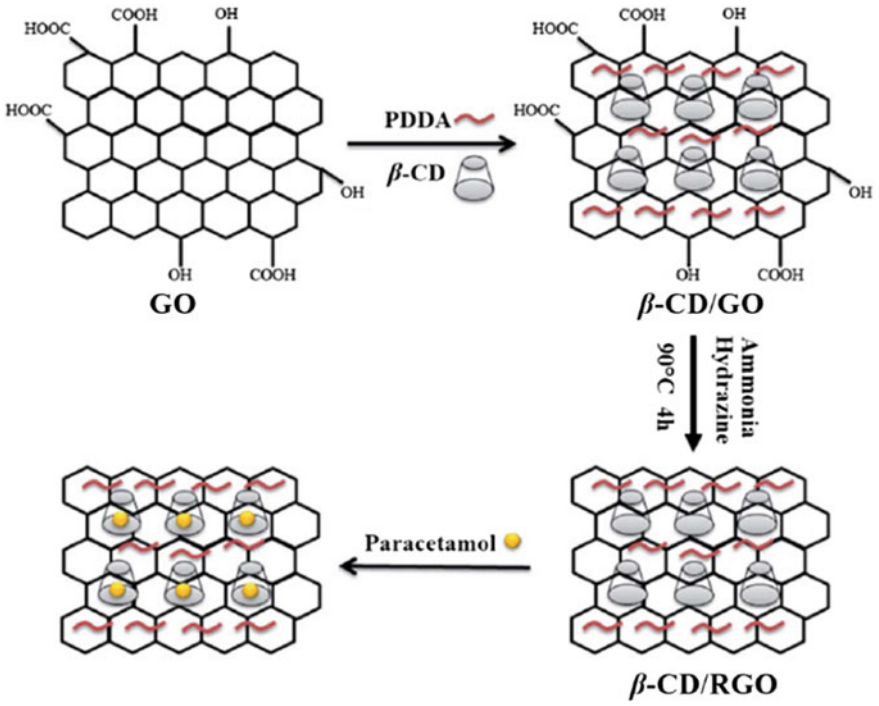

Fig. 6 Schematic diagram of the formation of β-CD/RGO which was used for sensing paracetamol molecules via host–guest interaction. Reprinted from Ref. [57], Copyright 2018 with permission from Royal Society of Chemistry

imprinted polymer is its high selectivity for the target analyte compared with that obtained using the conventional and traditional separation and analysis approach. Wang and coworkers reported a molecularly imprinted electrochemical sensor based on magnetic GO/β-CD@Au NPs for chrysoidine analysis [71]. After the MGO/β-CD@AuNPs were modified on the surface of the GCE and dried at room temperature, the modified GCE was placed into a mixed solution containing chrysoidine, pyrrole and KCl. Then, the electrodes were swept for fifteen cycles of CV to form molecularly imprinted polymer films. Table 3 summarizes the recently reported CD-graphene electrochemical sensors for drug-molecule detection.

5.2 *Biomolecule Detection*

Using sensor technology to acquire biological information is very important for bioinformatics development. Electrochemical biosensors mainly consist of two parts: biomolecular recognition and information conversion. When the analyte is specifically combined with the molecular recognition element, the generated complex produces a signal that can be output through a signal converter, thus achieving the purpose of analysis and detection. Electrochemical biosensors can be divided into enzyme sensors, microbiological sensors, immune sensors and DNA sensors.

In 2010, Tan and coworkers demonstrated a simple β-CD-functionalized graphene sheet for dopamine detection [64]. Since then, many β-CD/graphene composites have been used for biomolecule detection. Tian et al. [65] reported the simultaneous determination of L-ascorbic acid, dopamine and uric acid based on a Au NP–β-CD–graphene-modified electrode. Zhang et al. [89] further incorporated multiwalled carbon nanotubes into a β-CD–graphene composite and applied the material in the simultaneous voltammetric determination of ascorbic acid, dopamine and NO_2^-.

Table 3 Recent reported works regard to the drug molecule detection based on CDs-graphene constructed sensors

Sensor	Analyte	LDR	LOD	References
β-CD@RGO/ Nafion	Rutin	6 nM–10 μM	2 nM	Liu et al. [37]
β-CD/RGO	Diethylstilbestrol	0.01–13 μM	4 nM	Lu et al. [41]
β-CD/RGO	Doxorubicin, methotrexate	10 nM–0.2 μM and 0.1–1.0 μM	0.1 and 20 nM	Guo et al. [18]
β-CD/RGO	Quercetin	0.005–20 μM	0.001 μM	Zhang et al. [90]
DM-β-CD/ RGO	Isoquercitrin, baicalin	10 nM–3.0 μM and 0.04–3.0 μM	4 and 10 nM	Liu et al. [40]
MGO/ β-CD@AuNPs	Chrysoidine	50 nM–5 μM	17 nM	Wang et al. [71]

β-CD/graphene composites

Electrochemical immunosensors are an important application in the field of electroanalysis. β-CD/graphene composites can be used in the design of electrochemical immunosensors due to their outstanding electrochemical properties. Gao and coworkers prepared a β-CD/graphene-Cu@Ag core-shell NP composite for carcinoembryonic antigen (CEA) detection.

Aptamers, synthetic oligonucleotides also known as "artificial antibodies", offer great potential as a bio-recognition element in biosensors. Xue et al. [79] demonstrated an electrochemical thrombin aptasensor based on SH-β-CD-graphene/AuNPs. The proposed biosensor exhibits a wide linear range for thrombin and a very low limit of detection.

In addition to the electrochemical approach, β-CD/graphene composites have also been applied for the fluorescent detection of biomolecules. Mondai and Jana reported a β-cyclodextrin-functionalized graphene for the fluorescent detection of cholesterol [45]. The β-CD component offers detection selectivity via selective host-guest interactions, and graphene efficiently translates this interaction into an optical signal, which allows the sensor to detect cholesterol in the nanomolar range. Table 4 summarizes the recently reported CD-graphene electrochemical sensors for biomolecule detection.

5.3 Pollutant Detection

Environmental disputes are becoming a key focus of political and scientific attention because of the growing global population; intensification of agricultural and industrial activities; contamination of air, soils and aquatic ecosystems; and global climate change. Therefore, the detection of environmental pollutants has aroused widespread concern around the world and has received increasing attention from various environmental protection departments. Graphene is an ideal candidate for pollutant detection due to its high surface area and excellent conductivity. The incorporation of graphene with CD could further enhance its dispersibility and adsorption properties.

The author and coworkers reported a β-CD/RGO electrochemical sensor for the sensitive measurement of carbendazim [49], which is one of the effective benzimidazole fungicides commonly used in agriculture. The β-CD-RGO nanocomposites were synthesized using hydrazine as the reducing agent at room temperature (Fig. 7). The nanocomposites, with a combination of the physicochemical properties of RGO and the high molecular-recognition capability of β-CD, were used to modify the surface of a glassy carbon electrode for the electrochemical determination of the drug carbendazim using cyclic voltammetry and differential pulse voltammetry (DPV). DPV is a highly sensitive electrochemical technique that has been applied to determine trace amounts of carbendazim under optimum conditions. Figure 8 shows the DPV responses of different concentrations of carbendazim with

Table 4 Recent reported works regard to the biomolecules detection based on CDs-graphene constructed sensors

Sensor	Analyte	LDR	LOD	References
β-CD/graphene	Dopamine	0.9–200 μM	–	Tan et al. [64]
Au NPs–β-CD–graphene	Ascorbic acid/dopamine/uric acid	30–2000 μM, 0.5–150 μM and 0.5–60 μM	10, 0.15 and 0.21 μM	Tian et al. [65]
Graphene/poly-CD/MWCNTs	Ascorbic acid/dopamine/NO_2^-	5 μM–0.48 mM, 0.15–21.65 μM and 5 μM–6.75 mM	1.65, 0.05 and 1.65 μM	Zhang et al. [89]
β-CD/graphene	Cholesterol	–	–	Mondal and Jana [45]
β-CD/graphene-Cu@Ag core–shell NPs	CEA	0.0001–20 ng/mL	20 fg/mL	Gao et al. [17]
β-CD-PDDA-graphene	Sunset yellow, tartrazine	50 nM–20 μM	12.5 and 14.3 nM	Ye et al. [83]
β-CD/graphene	Cholesterol	0.001–0.1 mM	–	Agnihotri et al. [1]
SH-β-CD-graphene/AuNPs	Thrombin	0.016–8 fM	5.2 aM	Xue et al. [79]
Pt-MSC/β-CD-graphene	Alpha-fetoprotein	2.0 pg/mL–10.0 ng/mL	1.5 pg/mL	Zeng et al. [86]
Py-CD/RGO	Dopamine	–	–	Fritea et al. [14]

β-CD–RGO/GCE at an incubation time of 10 min. The peak current response increased when the concentration of carbendazim changed from 100 nM to 40 μM. The detection limit using DPV was measured to be 18.6 nM. Similar work has been reported by Guo and coworkers [19].

Xu et al. [77] synthesized HP-β-CD-modified graphene nanosheets via microwave irradiation in water. The as-prepared HP-β-CD-RGO nanocomposites possessed the unique properties of a high surface area and host–guest recognition and were thus applied in the electrochemical determination of several phenolic organic pollutants, including *o*-nitrophenol, 2,4,6-trichlorophenol, *o*-aminophenol, catechol, *o*-cresol and *o*-chlorophenol. An acetylcholinesterase biosensor was fabricated using a RGO-Au NPs-β-CD/Prussian blue-chitosan nanocomposite [91]. Based on the inhibition of organophosphorus pesticides as detected by acetylcholinesterase activity, the sensor is highly sensitive towards malathion and carbaryl. Table 5 summarizes the recently reported CD-graphene electrochemical sensors for pollutant detection.

Table 5 summarized the recently reported CDs-graphene electrochemical sensors for pollutants detection.

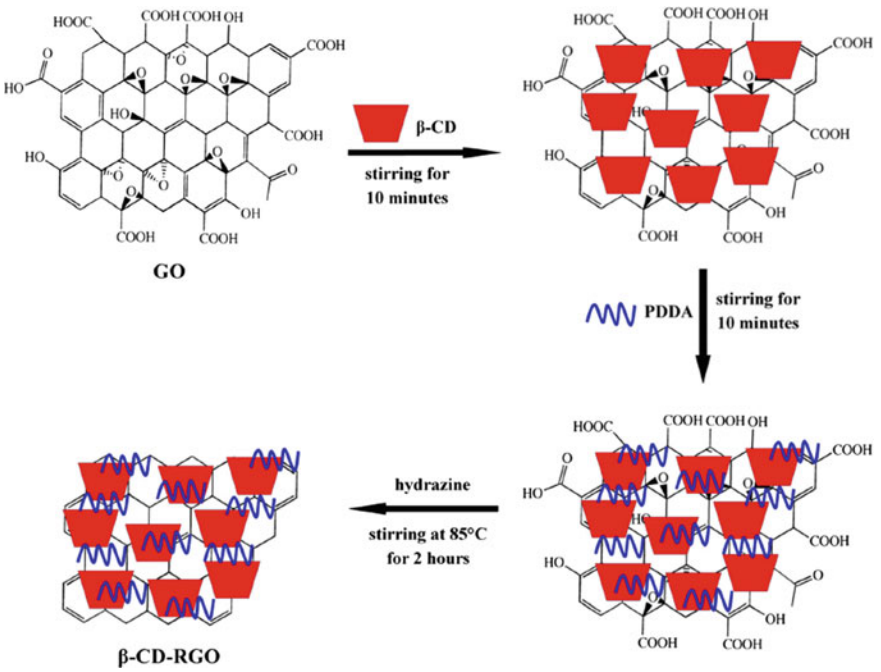

Fig. 7 The schematic diagram of β-CD–RGO nanocomposite fabrication process. Reprinted from Ref. [74], Copyright 2018 with permission from Springer Nature

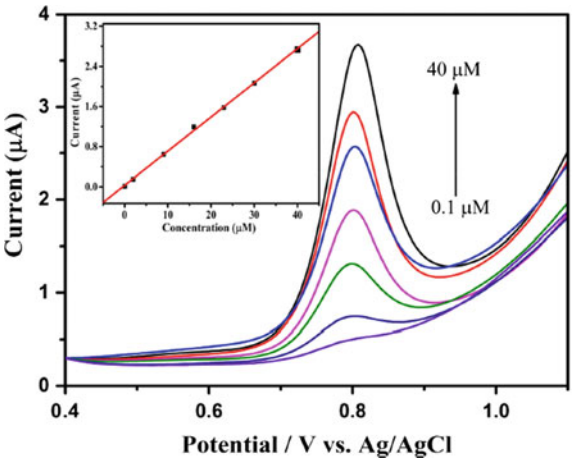

Fig. 8 The DPV responses of the different concentrations of carbendazim (0.1, 2, 9, 16, 23, 30, 40 μM) in pH 7.0 PBS at β-CD–RGO/GCE. The pulse period 0.2 s, amplitude 50 mV, incubation time 10 min. Inset: the calibration curve of carbendazim. Reprinted from Ref. [74], Copyright 2018 with permission from Springer Nature

Table 5 Recent reported works regard to the pollutants detection based on CDs-graphene constructed sensors

Sensor	Analyte	LDR	LOD	References
β-CD–RGO	Carbendazim	100 nM–40 μM	18.6 nM	Pham et al. [49]
RGO-Au NPs-β-CD/Prussian blue-chitosan	Malathion, carbaryl	7.98–2.00 × 10^3 pg/mL and 4.3–1.00 × 10^3 pg/mL	4.14 and 1.15 pg/mL	Zhao et al. [91]
β-CD–RGO	Imidacloprid	1–150 μM	0.1 μM	Chen et al. [6]
HP-β-CD–RGO	lead(II), cadmium(II)	0.1–1 nM and 0.5–9 nM	0.0942 nM and 0.0673	Lv et al. [42]
poly-β-CD–RGO	Bisphenol A	1–6000 nM	52 pM	Zhang et al. [87]
β-CD–RGO	2-chlorophenol, 3-chlorophenol	0.5–40 μM and 0.4–77 μM	0.2 and 0.09 μM	Wei et al. [75]
poly(L-arginine)-β-CD–CNT-RGO	2-aminophenol, 4-aminophenol	25–1300 nM	6.2 and 3.5 nM	Yi et al. [84]
β-CD/graphene/Ag	4-nitrophenol	10–100 nM	0.89 nM	Liu et al. [38]

6 Other Applications

6.1 Pollutant Removal

Graphene has a high specific surface area, which makes it an excellent absorbent material for water-pollution treatment. Li et al. [28] reported a magnetic β-CD–chitosan/GO composite for Cr(VI) adsorption. The results indicate that the proposed magnetic β-CD–chitosan/GO composite has an excellent adsorption capacity and chemical stability for the adsorption of metal ions. Similar work has been reported by Fan and coworkers [11, 12]. They reported a β-CD–chitosan/GO composite for dye and Cr(VI) removal. Wang et al. [68] reported a similar composite for malachite green removal. Other targets of pollutant removal include uranium, Cu(II), Co(II), *p*-phenylenediamine, Hg(II), methylene blue, hydroquinone, safranine T, and humic acid [7, 25, 36, 58, 59, 69, 70].

6.2 Stationary Phase

Enantioselective open-tubular capillary electrochromatography (OT-CEC), in which the chiral selector is coated onto the inner wall of the capillary as a stationary phase, has been used in many studies to achieve enantioseparation using various enantioselective OT columns. Liang and coworkers reported a β-CD-functionalized GO-magnetic nanocomposite as a tunable stationary phase with excellent solubility and high dispersibility [29, 33].

6.3 Methanol Oxidation

Direct methanol fuel cells (DMFCs) are a class of proton-exchange membrane fuel cells (PEMFCs). The direct use of methanol-water solution or steam methanol is the source of fuel, instead of using hydrogen production from methanol, gasoline and natural gas for power generation. Graphene is the most promising candidate as a support material to load catalysts. β-CD has been used for surface functionalization in order to prevent irreversible aggregation. Li and coworkers reported a β-CD–graphene as a supporting material to construct nanodendritic hydrangea-like Pt NPs [32]. β-CD on graphene surfaces has been used to guide the final morphology of Pt NPs without additional capping agents and seeds. The Pt/graphene-CD hybrid exhibited much higher catalytic activity and stability than Pt/graphene and Pt/Vulcan X72R towards methanol oxidation.

7 Conclusion

Recent advances in CD-functionalized graphene were reviewed in the present chapter. CDs can be covalently and noncovalently formed on the graphene surface. Graphene oxide has been widely used as a precursor for composite formation and then reduced via chemical means. In addition to wet chemical synthesis methods, electrochemically based methods have been successfully used for the preparation of CD-graphene supramolecular systems. This chapter also summarized the applications of the prepared CD-graphene, including drug delivery, chiral recognition, electrochemical sensing, pollutant removal, stationary phases and methanol oxidation.

References

1. Agnihotri, N., Chowdhury, A.D., De, A.: Non-enzymatic electrochemical detection of cholesterol using β-cyclodextrin functionalized graphene. Biosens. Bioelectron. **63**, 212–217 (2015)
2. Alsbaiee, A., Smith, B.J., Xiao, L., Ling, Y., Helbling, D.E., Dichtel, W.R.: Rapid removal of organic micropollutants from water by a porous β-cyclodextrin polymer. Nature **529**, 190 (2016)
3. Ates, S., Zor, E., Akin, I., Bingol, H., Alpaydin, S., Akgemci, E.G.: Discriminative sensing of DOPA enantiomers by cyclodextrin anchored graphene nanohybrids. Anal. Chim. Acta **970**, 30–37 (2017)
4. Bonnet, V., Gervaise, C., Djedaïni-Pilard, F., Furlan, A., Sarazin, C.: Cyclodextrin nanoassemblies: a promising tool for drug delivery. Drug Discov. Today **20**, 1120–1126 (2015)
5. Challa, R., Ahuja, A., Ali, J., Khar, R.: Cyclodextrins in drug delivery: an updated review. AAPS PharmSciTech **6**, E329–E357 (2005)
6. Chen, M., Meng, Y., Zhang, W., Zhou, J., Xie, J., Diao, G.: β-cyclodextrin polymer functionalized reduced-graphene oxide: application for electrochemical determination imidacloprid. Electrochim. Acta **108**, 1–9 (2013)
7. Cui, L., Wang, Y., Gao, L., Hu, L., Wei, Q., Du, B.: Removal of Hg (II) from aqueous solution by resin loaded magnetic β-cyclodextrin bead and graphene oxide sheet: synthesis, adsorption mechanism and separation properties. J. Colloid Interface Sci. **456**, 42–49 (2015)
8. Dong, H., Li, Y., Yu, J., Song, Y., Cai, X., Liu, J., Zhang, J., Ewing, R.C., Shi, D.: A versatile multicomponent assembly via β-cyclodextrin host–guest chemistry on graphene for biomedical applications. Small **9**, 446–456 (2013)
9. Dong, S., Bi, Q., Qiao, C., Sun, Y., Zhang, X., Lu, X., Zhao, L.: Electrochemical sensor for discrimination tyrosine enantiomers using graphene quantum dots and β-cyclodextrins composites. Talanta **173**, 94–100 (2017)
10. Einafshar, E., Asl, A.H., Nia, A.H., Mohammadi, M., Malekzadeh, A., Ramezani, M.: New cyclodextrin-based nanocarriers for drug delivery and phototherapy using an irinotecan metabolite. Carbohydr. Polym. **194**, 103–110 (2018)
11. Fan, L., Luo, C., Sun, M., Qiu, H.: Synthesis of graphene oxide decorated with magnetic cyclodextrin for fast chromium removal. J. Mater. Chem. **22**, 24577–24583 (2012)
12. Fan, L., Luo, C., Sun, M., Qiu, H., Li, X.: Synthesis of magnetic β-cyclodextrin–chitosan/graphene oxide as nanoadsorbent and its application in dye adsorption and removal. Colloids Surf. B **103**, 601–607 (2013)

13. Feng, W., Liu, C., Lu, S., Zhang, C., Zhu, X., Liang, Y., Nan, J.: Electrochemical chiral recognition of tryptophan using a glassy carbon electrode modified with β-cyclodextrin and graphene. Microchim. Acta **181**, 501–509 (2014)
14. Fritea, L., le Goff, A., Putaux, J.-L., Tertis, M., Cristea, C., Săndulescu, R., Cosnier, S.: Design of a reduced-graphene-oxide composite electrode from an electropolymerizable graphene aqueous dispersion using a cyclodextrin-pyrrole monomer. Application to dopamine biosensing. Electrochim. Acta **178**, 108–112 (2015)
15. Fu, L., Lai, G., Yu, A.: Preparation of β-cyclodextrin functionalized reduced graphene oxide: application for electrochemical determination of paracetamol. RSC Adv. **5**, 76973–76978 (2015)
16. Gandhi, M.R., Vasudevan, S., Shibayama, A., Yamada, M.: Graphene and graphene-based composites: a rising star in water purification—a comprehensive overview. ChemistrySelect **1**, 4358–4385 (2016)
17. Gao, J., Guo, Z., Su, F., Gao, L., Pang, X., Cao, W., Du, B., Wei, Q.: Ultrasensitive electrochemical immunoassay for CEA through host–guest interaction of β-cyclodextrin functionalized graphene and Cu@Ag core–shell nanoparticles with adamantine-modified antibody. Biosens. Bioelectron. **63**, 465–471 (2015)
18. Guo, Y., Chen, Y., Zhao, Q., Shuang, S., Dong, C.: Electrochemical sensor for ultrasensitive determination of doxorubicin and methotrexate based on cyclodextrin-graphene hybrid nanosheets. Electroanalysis **23**, 2400–2407 (2011)
19. Guo, Y., Guo, S., Li, J., Wang, E., Dong, S.: Cyclodextrin–graphene hybrid nanosheets as enhanced sensing platform for ultrasensitive determination of carbendazim. Talanta **84**, 60–64 (2011)
20. Guo, Y., Guo, S., Ren, J., Zhai, Y., Dong, S., Wang, E.: Cyclodextrin functionalized graphene nanosheets with high supramolecular recognition capability: synthesis and host–guest inclusion for enhanced electrochemical performance. ACS Nano **4**, 4001–4010 (2010)
21. Halpern, J.M., Gormley, C.A., Keech, M.A., von Recum, H.A.: Thermomechanical properties, antibiotic release, and bioactivity of a sterilized cyclodextrin drug delivery system. J. Mater. Chem. B **2**, 2764–2772 (2014)
22. Harada, A., Hashidzume, A.: Cyclodextrin-based chemo- and pH-responsive polymer systems for pharmaceutical and biomedical applications. In: Chemoresponsive Materials (2015)
23. Harada, A., Takashima, Y., Nakahata, M.: Supramolecular polymeric materials via cyclodextrin–guest interactions. Acc. Chem. Res. **47**, 2128–2140 (2014)
24. He, Y., Chen, D., Xiao, G.: Hydroxypropyl-β-cyclodextrin functionalized graphene oxide nanospheres as unmodified paclitaxel carriers. Asian J. Chem. **26**, 4232 (2014)
25. Hu, X.-J., Liu, Y.-G., Wang, H., Zeng, G.-M., Hu, X., Guo, Y.-M., Li, T.-T., Chen, A.-W., Jiang, L.-H., Guo, F.-Y.: Adsorption of copper by magnetic graphene oxide-supported β-cyclodextrin: effects of pH, ionic strength, background electrolytes, and citric acid. Chem. Eng. Res. Des. **93**, 675–683 (2015)
26. Huang, H., Ying, Y., Peng, X.: Graphene oxide nanosheet: an emerging star material for novel separation membranes. J. Mater. Chem. A **2**, 13772–13782 (2014)
27. Jin, Z., Nackashi, D., Lu, W., Kittrell, C., Tour, J.M.: Decoration, migration, and aggregation of palladium nanoparticles on graphene sheets. Chem. Mater. **22**, 5695–5699 (2010)
28. Li, L., Fan, L., Sun, M., Qiu, H., Li, X., Duan, H., Luo, C.: Adsorbent for chromium removal based on graphene oxide functionalized with magnetic cyclodextrin–chitosan. Colloids Surf., B **107**, 76–83 (2013)
29. Li, L., Fan, L., Sun, M., Qiu, H., Li, X., Duan, H., Luo, C.: Adsorbent for hydroquinone removal based on graphene oxide functionalized with magnetic cyclodextrin–chitosan. Int. J. Biol. Macromol. **58**, 169–175 (2013)
30. Li, Z.-Y., Akhtar, M.S., Kuk, J.H., Kong, B.-S., Yang, O.-B.: Graphene application as a counter electrode material for dye-sensitized solar cell. Mater. Lett. **86**, 96–99 (2012)
31. Li, Z., Chen, J., Yang, J., Su, Y., Fan, X., Wu, Y., Yu, C., Wang, Z.L.: β-cyclodextrin enhanced triboelectrification for self-powered phenol detection and electrochemical degradation. Energy Environ. Sci. **8**, 887–896 (2015)

32. Li, Z., Zhang, L., Huang, X., Ye, L., Lin, S.: Shape-controlled synthesis of Pt nanoparticles via integration of graphene and β-cyclodextrin and using as a noval electrocatalyst for methanol oxidation. Electrochim. Acta **121**, 215–222 (2014)
33. Liang, R.-P., Liu, C.-M., Meng, X.-Y., Wang, J.-W., Qiu, J.-D.: A novel open-tubular capillary electrochromatography using β-cyclodextrin functionalized graphene oxide-magnetic nanocomposites as tunable stationary phase. J. Chromatogr. A **1266**, 95–102 (2012)
34. Lin, Y., Zhou, J., Tang, J., Tang, W.: Cyclodextrin clicked chiral stationary phases with functionalities-tuned enantioseparations in high performance liquid chromatography. J. Chromatogr. A **1406**, 342–346 (2015)
35. Liu, J., Chen, G., Jiang, M.: Supramolecular hybrid hydrogels from noncovalently functionalized graphene with block copolymers. Macromolecules **44**, 7682–7691 (2011)
36. Liu, J., Liu, G., Liu, W.: Preparation of water-soluble β-cyclodextrin/poly (acrylic acid)/graphene oxide nanocomposites as new adsorbents to remove cationic dyes from aqueous solutions. Chem. Eng. J. **257**, 299–308 (2014)
37. Liu, K., Wei, J., Wang, C.: Sensitive detection of rutin based on β-cyclodextrin@chemically reduced graphene/Nafion composite film. Electrochim. Acta **56**, 5189–5194 (2011)
38. Liu, W., Li, C., Gu, Y., Tang, L., Zhang, Z., Yang, M.: One-step synthesis of β-cyclodextrin functionalized graphene/Ag nanocomposite and its application in sensitive determination of 4-nitrophenol. Electroanalysis **25**, 2367–2376 (2013)
39. Liu, Z., Robinson, J.T., Sun, X., Dai, H.: PEGylated nanographene oxide for delivery of water-insoluble cancer drugs. J. Am. Chem. Soc. **130**, 10876–10877 (2008)
40. Liu, Z., Zhang, A., Guo, Y., Dong, C.: Electrochemical sensor for ultrasensitive determination of isoquercitrin and baicalin based on DM-β-cyclodextrin functionalized graphene nanosheets. Biosens. Bioelectron. **58**, 242–248 (2014)
41. Lu, D., Lin, S., Wang, L., Shi, X., Wang, C., Zhang, Y.: Synthesis of cyclodextrin-reduced graphene oxide hybrid nanosheets for sensitivity enhanced electrochemical determination of diethylstilbestrol. Electrochim. Acta **85**, 131–138 (2012)
42. Lv, M., Wang, X., Li, J., Yang, X., Zhang, C.A., Yang, J., Hu, H.: Cyclodextrin-reduced graphene oxide hybrid nanosheets for the simultaneous determination of lead(II) and cadmium(II) using square wave anodic stripping voltammetry. Electrochim. Acta **108**, 412–420 (2013)
43. Menestrina, F., Ronco, N.R., Romero, L.M., Castells, C.B.: Enantioseparation of polar pesticides on chiral capillary columns based on permethyl-β-cyclodextrin in matrices of different polarities. Microchem. J. **140**, 52–59 (2018)
44. Mikuma, T., Iwata, Y.T., Miyaguchi, H., Kuwayama, K., Tsujikawa, K., Kanamori, T., Kanazawa, H., Inoue, H.: Approaching over 10 000-fold sensitivity increase in chiral capillary electrophoresis: cation-selective exhaustive injection and sweeping cyclodextrin-modified micellar electrokinetic chromatography. Electrophoresis **37**, 2970–2976 (2016)
45. Mondal, A., Jana, N.R.: Fluorescent detection of cholesterol using [small beta]-cyclodextrin functionalized graphene. Chem. Commun. **48**, 7316–7318 (2012)
46. Ntoutoume, G.M.N., Granet, R., Mbakidi, J.P., Brégier, F., Léger, D.Y., Fidanzi-Dugas, C., Lequart, V., Joly, N., Liagre, B., Chaleix, V.: Development of curcumin–cyclodextrin/cellulose nanocrystals complexes: new anticancer drug delivery systems. Bioorg. Med. Chem. Lett. **26**, 941–945 (2016)
47. Ogoshi, T., Ichihara, Y., Yamagishi, T.-A., Nakamoto, Y.: Supramolecular polymer networks from hybrid between graphene oxide and per-6-amino-β-cyclodextrin. Chem. Commun. **46**, 6087–6089 (2010)
48. Ou, J., Zhu, Y., Kong, Y., Ma, J.: Graphene quantum dots/β-cyclodextrin nanocomposites: a novel electrochemical chiral interface for tryptophan isomer recognition. Electrochem. Commun. **60**, 60–63 (2015)
49. Pham, T.S.H., Fu, L., Mahon, P., Lai, G., Yu, A.: Fabrication of β-cyclodextrin-functionalized reduced graphene oxide and its application for electrocatalytic detection of carbendazim. Electrocatalysis **7**, 411–419 (2016)

50. Quinn, M.D.J., Wang, T., Al Kobaisi, M., Craig, V.S.J., Notley, S.M.: PEO-PPO-PEO surfactant exfoliated graphene cyclodextrin drug carriers for photoresponsive release. Mater. Chem. Phys. **205**, 154–163 (2018)
51. Réti-Nagy, K., Malanga, M., Fenyvesi, É., Szente, L., Vámosi, G., Váradi, J., Bácskay, I., Fehér, P., Ujhelyi, Z., Róka, E.: Endocytosis of fluorescent cyclodextrins by intestinal Caco-2 cells and its role in paclitaxel drug delivery. Int. J. Pharm. **496**, 509–517 (2015)
52. Řezanka, P., Navrátilová, K., Řezanka, M., Král, V., Sýkora, D.: Application of cyclodextrins in chiral capillary electrophoresis. Electrophoresis **35**, 2701–2721 (2014)
53. Schmarr, H.-G., Mathes, M., Wall, K., Metzner, F., Fraefel, M.: Enantiodifferentiation of whisky and cognac lactones using gas chromatography with different cyclodextrin chiral stationary phases. J. Chromatogr. A **1516**, 135–141 (2017)
54. Schmidt, B.V., Hetzer, M., Ritter, H., Barner-Kowollik, C.: Complex macromolecular architecture design via cyclodextrin host/guest complexes. Prog. Polym. Sci. **39**, 235–249 (2014)
55. Shih, C.-J., Lin, S., Strano, M.S., Blankschtein, D.: Understanding the stabilization of liquid-phase-exfoliated graphene in polar solvents: molecular dynamics simulations and kinetic theory of colloid aggregation. J. Am. Chem. Soc. **132**, 14638–14648 (2010)
56. Siriviriyanun, A., Tsai, Y.-J., Voon, S.H., Kiew, S.F., Imae, T., Kiew, L.V., Looi, C.Y., Wong, W.F., Lee, H.B., Chung, L.Y.: Cyclodextrin- and dendrimer-conjugated graphene oxide as a nanocarrier for the delivery of selected chemotherapeutic and photosensitizing agents. Mater. Sci. Eng., C **89**, 307–315 (2018)
57. Song, J., Yang, C., Ma, J., Han, Q., Ran, P., Fu, Y.: Voltammetric chiral discrimination of tryptophan using a multilayer nanocomposite with implemented amino-modified β-cyclodextrin as recognition element. Microchim. Acta **185**, 230 (2018)
58. Song, W., Hu, J., Zhao, Y., Shao, D., Li, J.: Efficient removal of cobalt from aqueous solution using β-cyclodextrin modified graphene oxide. RSC Adv. **3**, 9514–9521 (2013)
59. Song, W., Shao, D., Lu, S., Wang, X.: Simultaneous removal of uranium and humic acid by cyclodextrin modified graphene oxide nanosheets. Sci. China Chem. **57**, 1291–1299 (2014)
60. Song, Y., Qu, K., Zhao, C., Ren, J., Qu, X.: Graphene oxide: intrinsic peroxidase catalytic activity and its application to glucose detection. Adv. Mater. **22**, 2206–2210 (2010)
61. Szejtli, J.: Introduction and general overview of cyclodextrin chemistry. Chem. Rev. **98**, 1743–1754 (1998)
62. Szeman, J., Fenyvesi, E., Szejtli, J., Ueda, H., Machida, Y., Nagai, T.: Water soluble cyclodextrin polymers: their interaction with drugs. J. Incl. Phenom. **5**, 427–431 (1987)
63. Tan, J., Meng, N., Fan, Y., Su, Y., Zhang, M., Xiao, Y., Zhou, N.: Hydroxypropyl-β-cyclodextrin–graphene oxide conjugates: carriers for anti-cancer drugs. Mater. Sci. Eng. C **61**, 681–687 (2016)
64. Tan, L., Zhou, K.-G., Zhang, Y.-H., Wang, H.-X., Wang, X.-D., Guo, Y.-F., Zhang, H.-L.: Nanomolar detection of dopamine in the presence of ascorbic acid at β-cyclodextrin/graphene nanocomposite platform. Electrochem. Commun. **12**, 557–560 (2010)
65. Tian, X., Cheng, C., Yuan, H., Du, J., Xiao, D., Xie, S., Choi, M.M.F.: Simultaneous determination of L-ascorbic acid, dopamine and uric acid with gold nanoparticles–β-cyclodextrin–graphene-modified electrode by square wave voltammetry. Talanta **93**, 79–85 (2012)
66. Upadhyay, S.S., Kalambate, P.K., Srivastava, A.K.: Enantioselective analysis of moxifloxacin hydrochloride enantiomers with graphene-β-cyclodextrin-nanocomposite modified carbon paste electrode using adsorptive stripping differential pulse voltammetry. Electrochim. Acta **248**, 258–269 (2017)
67. Wang, C., Li, B., Niu, W., Hong, S., Saif, B., Wang, S., Dong, C., Shuang, S.: β-Cyclodextrin modified graphene oxide–magnetic nanocomposite for targeted delivery and pH-sensitive release of stereoisomeric anti-cancer drugs. RSC Adv. **5**, 89299–89308 (2015)
68. Wang, D., Liu, L., Jiang, X., Yu, J., Chen, X.: Adsorption and removal of malachite green from aqueous solution using magnetic β-cyclodextrin-graphene oxide nanocomposites as adsorbents. Colloids Surf. A **466**, 166–173 (2015)

69. Wang, D., Liu, L., Jiang, X., Yu, J., Chen, X., Chen, X.: Adsorbent for *p*-phenylenediamine adsorption and removal based on graphene oxide functionalized with magnetic cyclodextrin. Appl. Surf. Sci. **329**, 197–205 (2015)
70. Wang, H., Liu, Y.-G., Zeng, G.-M., Hu, X.-J., Hu, X., Li, T.-T., Li, H.-Y., Wang, Y.-Q., Jiang, L.-H.: Grafting of β-cyclodextrin to magnetic graphene oxide via ethylenediamine and application for Cr(VI) removal. Carbohydr. Polym. **113**, 166–173 (2014)
71. Wang, X., Li, X., Luo, C., Sun, M., Li, L., Duan, H.: Ultrasensitive molecularly imprinted electrochemical sensor based on magnetism graphene oxide/β-cyclodextrin/Au nanoparticles composites for chrysoidine analysis. Electrochim. Acta **130**, 519–525 (2014)
72. Wang, Y., Li, Y., Tang, L., Lu, J., Li, J.: Application of graphene-modified electrode for selective detection of dopamine. Electrochem. Commun. **11**, 889–892 (2009)
73. Wang, Y., Shao, Y., Matson, D.W., Li, J., Lin, Y.: Nitrogen-doped graphene and its application in electrochemical biosensing. ACS Nano **4**, 1790–1798 (2010)
74. Wei, G., Dong, R., Wang, D., Feng, L., Dong, S., Song, A., Hao, J.: Functional materials from the covalent modification of reduced graphene oxide and β-cyclodextrin as a drug delivery carrier. New J. Chem. **38**, 140–145 (2014)
75. Wei, M., Tian, D., Liu, S., Zheng, X., Duan, S., Zhou, C.: β-Cyclodextrin functionalized graphene material: a novel electrochemical sensor for simultaneous determination of 2-chlorophenol and 3-chlorophenol. Sens. Actuators B Chem. **195**, 452–458 (2014)
76. Wu, S., Lan, X., Cui, L., Zhang, L., Tao, S., Wang, H., Han, M., Liu, Z., Meng, C.: Application of graphene for preconcentration and highly sensitive stripping voltammetric analysis of organophosphate pesticide. Anal. Chim. Acta **699**, 170–176 (2011)
77. Xu, C., Wang, J., Wan, L., Lin, J., Wang, X.: Microwave-assisted covalent modification of graphene nanosheets with hydroxypropyl-β-cyclodextrin and its electrochemical detection of phenolic organic pollutants. J. Mater. Chem. **21**, 10463–10471 (2011)
78. Xu, J., Wang, Q., Xuan, C., Xia, Q., Lin, X., Fu, Y.: Chiral recognition of tryptophan enantiomers based on β-cyclodextrin-platinum nanoparticles/graphene nanohybrids modified electrode. Electroanalysis **28**, 868–873 (2016)
79. Xue, Q., Liu, Z., Guo, Y., Guo, S.: Cyclodextrin functionalized graphene–gold nanoparticle hybrids with strong supramolecular capability for electrochemical thrombin aptasensor. Biosens. Bioelectron. **68**, 429–436 (2015)
80. Yang, S.-T., Chang, Y., Wang, H., Liu, G., Chen, S., Wang, Y., Liu, Y., Cao, A.: Folding/aggregation of graphene oxide and its application in Cu^{2+} removal. J. Colloid Interface Sci. **351**, 122–127 (2010)
81. Yang, Y., Zhang, Y.M., Chen, Y., Zhao, D., Chen, J.T., Liu, Y.: Construction of a graphene oxide based noncovalent multiple nanosupramolecular assembly as a scaffold for drug delivery. Chem. A Eur. J. **18**, 4208–4215 (2012)
82. Yao, X., Tan, T.T.Y., Wang, Y.: Thiol–ene click chemistry derived cationic cyclodextrin chiral stationary phase and its enhanced separation performance in liquid chromatography. J. Chromatogr. A **1326**, 80–88 (2014)
83. Ye, X., Du, Y., Lu, D., Wang, C.: Fabrication of β-cyclodextrin-coated poly (diallyldimethylammonium chloride)-functionalized graphene composite film modified glassy carbon-rotating disk electrode and its application for simultaneous electrochemical determination colorants of sunset yellow and tartrazine. Anal. Chim. Acta **779**, 22–34 (2013)
84. Yi, Y., Zhu, G., Wu, X., Wang, K.: Highly sensitive and simultaneous electrochemical determination of 2-aminophenol and 4-aminophenol based on poly(L-arginine)-β-cyclodextrin/carbon nanotubes@graphene nanoribbons modified electrode. Biosens. Bioelectron. **77**, 353–358 (2016)
85. Zaidi, S.A.: Facile and efficient electrochemical enantiomer recognition of phenylalanine using β-cyclodextrin immobilized on reduced graphene oxide. Biosens. Bioelectron. **94**, 714–718 (2017)
86. Zeng, L., Li, Q., Tang, D., Chen, G., Wei, M.: Metal platinum-wrapped mesoporous carbon for sensitive electrochemical immunosensing based on cyclodextrin functionalized graphene nanosheets. Electrochim. Acta **68**, 158–165 (2012)

87. Zhang, X., Wu, L., Zhou, J., Zhang, X., Chen, J.: A new ratiometric electrochemical sensor for sensitive detection of bisphenol A based on poly-β-cyclodextrin/electroreduced graphene modified glassy carbon electrode. J. Electroanal. Chem. **742**, 97–103 (2015)
88. Zhang, Y.-M., Cao, Y., Yang, Y., Chen, J.-T., Liu, Y.: A small-sized graphene oxide supramolecular assembly for targeted delivery of camptothecin. Chem. Commun. **50**, 13066–13069 (2014)
89. Zhang, Y., Yuan, R., Chai, Y., Li, W., Zhong, X., Zhong, H.: Simultaneous voltammetric determination for DA, AA and NO_2^- based on graphene/poly-cyclodextrin/MWCNTs nanocomposite platform. Biosens. Bioelectron. **26**, 3977–3980 (2011)
90. Zhang, Z., Gu, S., Ding, Y., Shen, M., Jiang, L.: Mild and novel electrochemical preparation of β-cyclodextrin/graphene nanocomposite film for super-sensitive sensing of quercetin. Biosens. Bioelectron. **57**, 239–244 (2014)
91. Zhao, H., Ji, X., Wang, B., Wang, N., Li, X., Ni, R., Ren, J.: An ultra-sensitive acetylcholinesterase biosensor based on reduced graphene oxide-Au nanoparticles-β-cyclodextrin/Prussian blue-chitosan nanocomposites for organophosphorus pesticides detection. Biosens. Bioelectron. **65**, 23–30 (2015)
92. Zhou, J., Yang, B., Tang, J., Tang, W.: Cationic cyclodextrin clicked chiral stationary phase for versatile enantioseparations in high-performance liquid chromatography. J. Chromatogr. A **1467**, 169–177 (2016)
93. Zor, E., Bingol, H., Ramanaviciene, A., Ramanavicius, A., Ersoz, M.: An electrochemical and computational study for discrimination of D- and L-cystine by reduced graphene oxide/β-cyclodextrin. Analyst **140**, 313–321 (2015)
94. Zu, S.-Z., Han, B.-H.: Aqueous dispersion of graphene sheets stabilized by pluronic copolymers: formation of supramolecular hydrogel. J. Phys. Chem. C **113**, 13651–13657 (2009)

Simulation Paths of Anticancer Drugs on a Graphene Oxide Surface

Miroslava Nedyalkova, Julia Romanova, Joanna Stoycheva and Sergio Madurga

Abstract Graphene derivatives have occurred as central materials in the development of anticancer drug delivery systems. Graphene, graphene oxide and graphene quantum dots have been used for the effective delivery of different anticancer drugs. Graphene oxide (GO) nanomaterials have drew wide attention due to their surface properties. The oxygen-containing functional groups on the surface provide it modification by functionalization with molecules with focus to enlarge the range of biological applications with the impact on reduce toxicity effect. In this chapter, the properties of GO as a nanocarrier to load drug molecules and improve the solubility of carrier-drug systems effectively when functionalized with various hydrophilic molecules or polymers, implying potential applications in clinical treatments is performed in the frame of density functional theory (DFT) and molecular dynamics (MD) calculations.

Keywords Graphene · Molecular dynamic · DFT · Graphene oxide

Recently, more and more researchers have marked that to treatment of the illnesses such as cancer is an interdisciplinary approach. The role of mathematical models and computer simulations allow deeply to evaluate the experimental and statistical data accumulation and to attain supplementary qualitative and quantitative data.

The implementation in clinical practice various effective hydrophobic molecules, the majority of which are aromatic, is often hampered by low their water solubility and unfortunately the same trend for the biocompatibility. Drug carriers based on nanomaterial have become in a last years an important division of research and the interface between nanotechnology and biomedicine. The ability capacity of the nanocarriers for loadings, targeted delivery, and controlled release of drugs. Graphene has occurred as a two-dimensional (2D) honeycomb lattice with physical properties since it was synthesized in 2004 [1]. Graphite oxide, also known as graphene oxide (GO), has a similar structure to graphite, but the formed plane by

M. Nedyalkova (✉) · J. Romanova · J. Stoycheva · S. Madurga
Univeristy of Sofia, St. Kliment Ohrydski, Sofia, Bulgaria
e-mail: mici345@yahoo.com

A. Khan et al. (eds.), *Graphene Functionalization Strategies*,
Carbon Nanostructures, https://doi.org/10.1007/978-981-32-9057-0_9

carbon atoms in graphite oxide is covered by oxygen-containing groups; such as the hydroxyl (–OH) and epoxide (–O–) groups on the basal plane, and carboxyl (–COOH), carboxylic anhydride, lactones, phenols, lactols, pyrones and ketones groups at the sheet edges [2–4]. The reactive oxygen functional groups of GO can help GO exfoliated in various solvents to produce homogeneous colloidal suspensions. The basal plane of GO encloses free π electrons localized on the surface from unchanged areas of Graphene, which are hydrophobic and accomplished of π–π interactions for drug loading and functionalization based on non-covalent interactions [5–7].

The biocompatibility and low toxicity make GO as a hopeful material for drug carrier substances [8–11]. Based on the information in several reports [12, 13] about in vivo toxicity of GO, no obvious toxicity was observed after the exposure to multiple-low-dose small size GO. In the macrophage nodules GO accumulates, by the use of Raman mapping this behavior was verified. These findings will benefit the applications of GO in the future, especially in biomedical fields and anti-cancer therapies. Graphene nanocomposites have occurred as a promising tool to address these drawbacks.

Liang et al. [14] evaluated the potential cytotoxicity of different size graphene quantum dots by molecular dynamics simulations of their translocation through a lipid membrane composed by palmitoyl-2-oleoyl-phosphatidylcholine (POPC). Graphene quantum dots with 0.375 nm (GQDs7), 0.618 nm (GQDs19), 1.08 nm (GQDs61), 1.65 nm (GQDs151) and 2.05 nm radius were considered (GQDs275). The CHARMM27 and TIP3 force fields were applied for the membrane-graphene systems and water, respectively. In order to study the effect of the concentration, the ratio quantum dots: POPC molecules was varied as 1:256 (GQDs7), 12:256 (GQDs7-H1), 24:256 (GQDs7-H2), 26:256 (GQDs7-H3) and 12:256 (GQDs7-H4). Based on these results the authors concluded that the size of the quantum dot does not affect the absorption time but has a great effect on the permeation process—the bigger the quantum dot, the bigger the damage of the lipid membrane. The calculations demonstrated (Fig. 1) that graphene quantum dots with radius up to 1.08 nm can penetrate the membrane, while absorption is observed for the dots with larger radius. It was shown that at high concentration the GQDs7 molecules aggregate quickly in water and disaggregate in a mono-dispersed manner when entering the membrane interior. In addition, the simulations revealed that the high

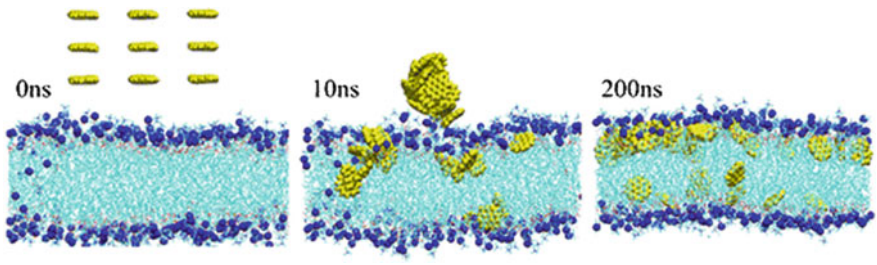

Fig. 1 GQDs permeation into the lipid membrane in a vertical way

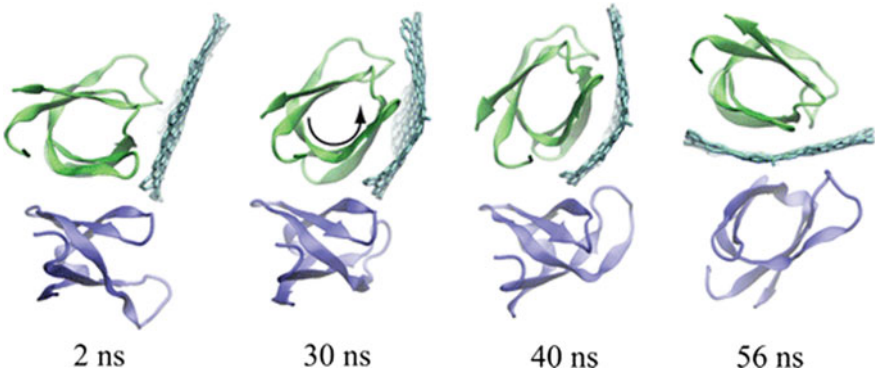

Fig. 2 Dynamic of the insertion of a graphene sheets into the dimer

concentration of GQDs7 molecules has influence on the lipid bilayer properties and an impact on the structure and diffusion properties of the membrane, which suggest also their effect on the cell signal transduction. Although, the mechanical damage of the membrane by the small size GQDs7 molecules was not observed. The final conclusion of the work is that graphene quantum dots with small size are the best candidates for the design of biomedical materials.

By using large-scale all-atom molecular dynamics simulations Luan et al. [15] explored the potential toxicity of graphene to cell functions. In particular, the authors investigated the C-terminal DNA-binding domain of human immunovirus-1 integrase that can form a dimer in solution with a well-defined hydrophobic interface. The simulations were performed with the CHARMM force field for the protein, the standard force field for NaCl, the TIP3P model for water and the force field for graphene was taken from the literature. The theoretical results demonstrated that the graphene nanosheet can interrupt the hydrophobic protein-protein interaction responsible for the biological functions. It was observed that the graphene nanosheet enters preferably in the hydrophobic interface between two contacting functional proteins, such as dimer (Fig. 2). As a result of such forced protein-protein separation negative impact on the cell's metabolism and even cell's mortality can be expected.

By using coarse-grained molecular dynamics approach and dissipative particle dynamics, Guo et al. [16] investigated the translocation of a graphene nanosheet across a lipid bilayer membrane. The study also explored the role of size and edge (square and circular) of the graphene nanosheet. It was found that small graphene nanosheets can enter cells through direct penetration, while for the larger ones the translocation undergoes vesiculation process with the formation of hemisphere lipid vesicles. The simulations indicated that such formation of vesicles disturbs the local bilayer structure and the larger the nanosheet size, the higher the cytotoxicity relationship is predicted. It was demonstrated that the smooth circular graphene nanosheet edge facilitates the translocation process, as well as that the graphene nanosheets with square and circular edge have similar translocation mechanism.

Tu et al. [17] reported theoretical and experimental investigation on graphene's antibacterial activity towards *Escherichia coli*. The experimental approach comprises transmission electron microscopy (TEM). The molecular dynamics approach and the Berger lipid force field were applied for the theoretical modeling of the problem. The outer membrane of the Gram-negative bacteria (*Escherichia coli*) was modelled by pure palmitoyloleoylphosphati-dylethanolamine and the inner membrane by a mixture of palmitoyloleoylphosphati-dylethanolamine and palmitoylo-leoylphosphatidylglycerol phospholipids in 3:1 ratio. It was found that the graphene-induced cytotoxicity toward *Escherichia coli* results from strong dispersion interactions and occurs by two type of mechanisms. One of the mechanisms is severe insertion and cutting, while the other represents destructive extraction of lipid molecules from the cell membrane. This graphene-induced cytotoxicity between graphene and lipid molecules. TEM images confirmed the molecular dynamics observations of a direct extraction of phospholipids from lipid membranes. It was demonstrated that both severe insertion and destructive lipid extraction can lead to a loss of cell membrane integrity and significantly reduce bacteria viability. In addition, it was observed that the antibacterial activity increases with increasing graphene lateral size and concentration. The evidence for a destructive extraction of phospholipids by graphene is reported for the first time in the work of Tu et al. Due to the detection of bacterial killing mechanism by 'physical damage', the authors envisioned that graphene may represent a new type of 'green' antibacterial material with little bacterial resistance.

The work of Chong et al. [18] aimed to clarify the interaction mechanisms between serum proteins and graphene-based nanomaterials (Fig. 3). Such interactions are important because blood is one of the first biological environments that these nanomaterials meet when entering the living organism. In particular, the authors investigated the adsorption of four blood proteins (bovine fibrinogen, BFG; immunoglobulin, Ig; transferrin, Tf; and bovine serum albumin, BSA) onto graphene oxide and reduced graphene oxide. The adsorption process is explored theoretically by applying the molecular dynamics approach with the TIP3P model for water and the CHARMM27 force field. The systems were also characterized experimentally by using the atomic forced microscopy, fluorescence spectroscopy and surface plasmon resonance affinity measurements. The molecular dynamics results predicted that the binding affinities follow the rank order BFG > Ig > Tf > BSA and this finding was in agreement with the experimental measurements. The calculations indicated that the hydrophobic interactions and in particular the π–π stacking interactions with the aromatic residues are responsible for the strong protein adsorption on the graphene oxide surface. It was shown that the graphene oxide possesses higher adsorption capacity for proteins than single wall carbon nanotubes. Moreover, it was observed that the coating of the graphene oxide with proteins decreases substantially the cytotoxicity with respect to pristine and protein coated single wall carbon nanotubes. Finally, due to its planarity and therefore highly accessible surface for π–π stacking interactions, the graphene oxide was suggested as a promising material for biomedical applications.

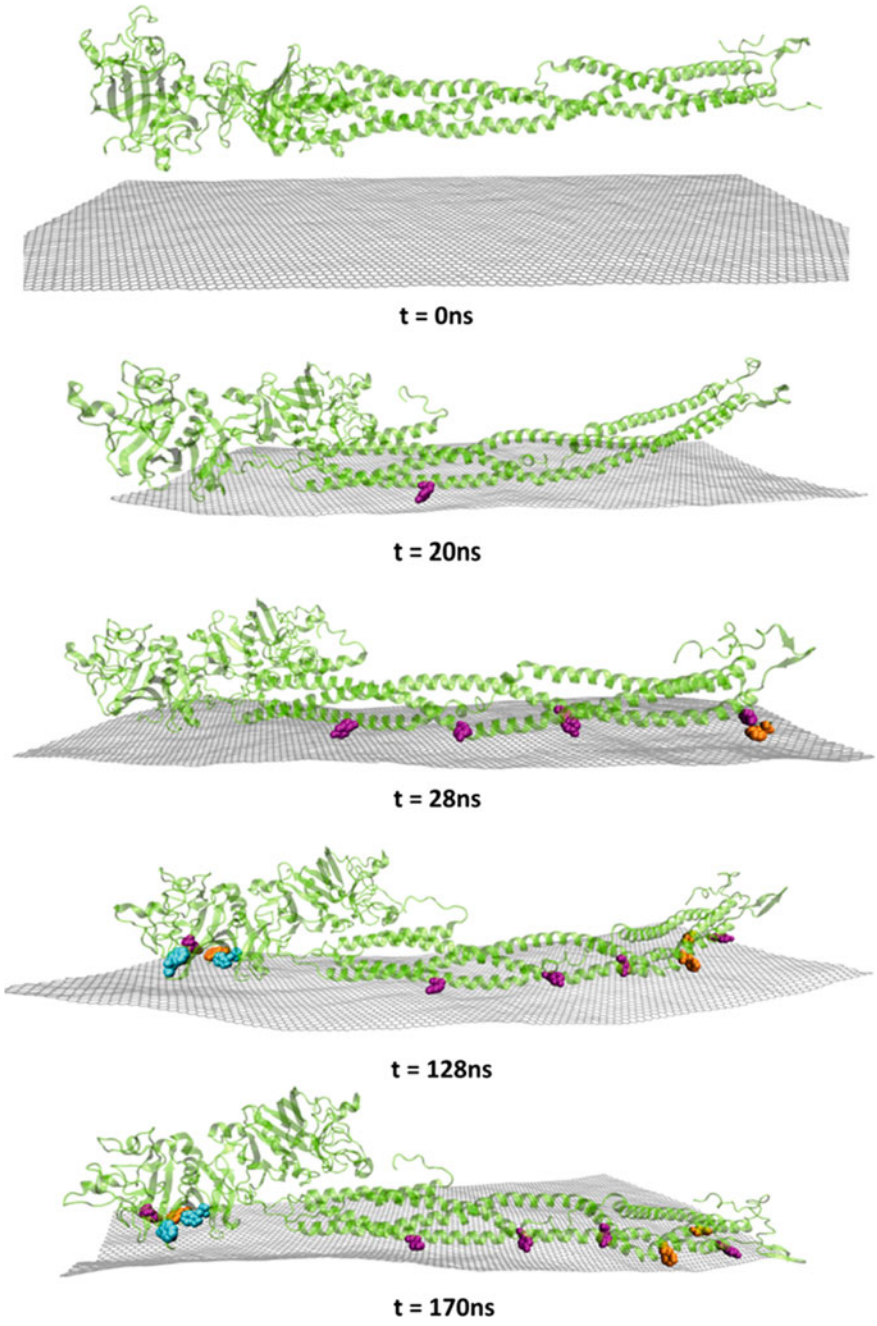

Fig. 3 Molecular dynamics snapshots of the absorption of BFG onto the graphene surface. Cartoon representations of the full protein are depicted in yellow, and hydrophobic Tyr (purple), Phe (orange), and Trp (blue) within 0.5 nm distance of the graphene surface are represented as vdW spheres. Atoms corresponding to the graphene sheet are colored in gray

Mao et al. [19] performed large-scale computer simulations in order to study the interaction of graphene nanosheets with different size and oxidization degree with lipid bilayer membrane. Such interaction is directly related to the cytotoxicity and antibacterial activity of these nanomaterials. The translocation of graphene-based materials across a $56 \times 56\ nm^2$ membrane were simulated by using the coarse-grained approach and dissipative particle dynamics. The theoretical results are discussed with respect to experimental observations reported previously in the literature. As a function of the degree of oxidation four typical states of graphene-membrane interactions were predicted theoretically: graphene-sandwiched superstructure, graphene adhering to the membrane, graphene lying across the membrane and hemisphere vesicle structures. The evidences for the existence of the four states can be found among the already published experimental results. Based on the theoretical results the authors presented a two-dimensional phase diagram explaining the interrelated effects of graphene size and oxidization degree on the equilibrium states of the graphene nanosheets interacting with the lipid bilayer membrane. It was found that the graphene nanosheets with a higher oxidization degree causes stronger perturbation in the membrane and destroy its integrity. In addition, it was shown that the perturbation degree increases in line with the edge length of nanosheet. The theoretical analysis revealed that the cellular endocytosis is more likely to occur for the hemisphere vesicle structures and less likely to occur in the case of graphene-sandwiched superstructures.

The modified GO were used as nanocarriers to load two types of anticancer drugs (DOX and SN38) for targeted drug delivery. Other groups have used a series of macromolecular polymers to modify graphene oxide by covalent chemical reactions, including polyethyleneimine (PEI), chitosan (CS), poval (PVA), poly(*N*-isopropyl acrylamide) (PNIPAM), and amine-modified dextran (DEX). These researches demonstrate that graphene can be used as a nanocarrier to load drug molecules and improve the solubility of carrier-drug systems effectively when functionalized with various hydrophilic molecules or polymers, implying potential applications in clinical treatments. The theoretical works on such a topic comprise the study of the interactions between biomolecules and graphene: Qin et al. [20] by performed density functional theory (DFT) and molecular dynamics (MD) calculations to explore the interaction between graphene and L-leucine, showing that van der Waals interactions between the L-leucine and graphene play a central role in the absorption process. By the use of molecular dynamics method to study the interaction between graphene and drug molecules focusing on the various sizes of graphene sheets as well as the types, numbers, and loading modes of drugs. Four types of anticancer drug molecules (CE6, DOX, MTX, and SN38) absorbed onto graphene sheets with various sizes (10, 20, 30, 40, and 50 Å finite and periodic graphene sheets) and graphene oxide functionalized with amine-modified polyethylene glycol (GO-PEG) [21].

MD Simulations scheme was used to investigate the dynamic process of drug molecules on the graphene. On the basis of the geometry optimization first was to carry out the simulations at the constant volume and constant temperature (NVT) ensembles. A total computation time of 1 ns and a time step of 1 fs were used to integrate Newton's equation of motion. The focus in the research article is

on the influences of the size of graphene sheets, the number and types of drug molecules, and the loading modes. The simulations find outs shows that the binding strength of graphene-drug complex is mainly determined by the deformation of sheets. When the areas that drug molecules occupy have comparable sizes as graphene sheets, the distortion of graphene sheets is reduced, and the graphene-drug bindings are the strongest. The average binding strength per molecule fluctuates between 10 and 70 kcal/mol that is not sensitive to the number and kind of drug molecule as well as their loading modes. If the density of drug coverage is low and graphene sheets are relatively large, the binding strength is mainly determined by the interaction of graphene-drug. The limited sizes of graphene sheets restrict the movement of drug molecules. Multiple drug molecules may form clusters that slow down the diffusion on graphene sheets. Diffusion in the double-side loading mode is often slower than that in the single-side loading mode. Compared with pristine graphene sheets, graphene oxide functionalized with PEG chains has stronger bindings with drug molecules so that the drug molecules are essentially immobilized. These results give physical insights into the stability and dynamics of graphene-drug complexes, helpful for designing novel graphene-based drug delivery systems.

In the work of Safdari et al. [22] the central point is focused on interaction of 5-fluorouracil (5-FU) anticancer drug with graphene oxide nanosheet (GONS) using density functional theory and molecular dynamics simulation. The molecular dynamics simulation based on the interaction between drug molecules and the surface of GO have been studied at four various temperatures. Four simulation boxes have been defined. The GO has been located in the center of boxes; then, ten drug molecules have been added. Next, the temperature of the system increased from 250, 300, 350 and 400 K in order of from the first to fourth boxes, respectively. Before running the molecular dynamics for relaxing solvent molecules, all systems have been equilibrated with position restraints on the drug molecules and GONS. The TIP3P water model has been used. The charge of the system is zero and its dynamics is simulated for 5000 ps. All MD simulations are performed using Gromacs package with CHARRM27 force field. The MD calculations are analyzed to provide insights into the drug adsorption behavior on the GONS. The set of properties are investigated and summarized for 5-FU adsorption on the GONS are performed using the DFT computations. The results obtained MD results elucidate that the rise of simulation temperature up to 400 K promotes the formation of hydrogen bonds including functional groups on GO and 5-FU molecules.

In a very recent paper, Shariatinia and Mazloom-Jalali [23] investigated nanocomposites between chitosan and graphene-based nanoparticles as delivery systems of the anticancer drug ifosfamide. The nanocomposites were modeled by means of molecular dynamics simulations and COMPASS force field. The drug delivery model systems consist of one graphene based nanoparticle as a filler, five chitosan chains (each having twenty repeating units) representing the polymer matrix and three ifosfamide molecules. Three types of graphene based nanoparticles were studied (pure graphene, N-doped graphene and P-doped graphene) in order to investigate the effect of the filler on the capacity of the nanocomposite to deliver the

drug molecules. The temperature effects were also taken into account by running simulations at 298.15, 308.15, 318.15 and 328.15 K. As criteria for the drug delivery capacity, the authors estimated the free volume, fractional free volume and diffusion coefficient for the nanocomposites. It was concluded that the free volume and fractional free volume increase by raising the temperature. The drug delivery system containing N-doped graphene filler showed greatest free volume and fractional free volume values, followed by P-doped graphene and pure graphene nanoparticles. The simulations at 328.15 K revealed that the interchain distances are smallest for the nanocomposite with the N-doped graphene filler. This was explained by the formation of hydrogen bonds network and strong intermolecular interaction among ifosfamide, N-doped graphene nanoparticle and chitosan chains. The lowest diffusion coefficient was observed for the case with the N-doped graphene filler, followed by P-doped and pure graphene analogues. This result demonstrates that in the drug delivery system containing N-doped graphene the diffusion of ifosfamide molecules occurs in a most controlled manner. Finally, it was concluded that the most efficient ifosfamide delivery is expected for the nanocomposite containing chitosan and N-doped graphene filler.

The interaction between ellipticine anticancer drug and graphene oxide nanosheet (Fig. 4) was investigated by Hasanzade and Raissi [24] By using DFT the authors studied the effect of the solvent on the molecular and electronic structure of the ellipticine drug. The DFT calculations were performed with the wB97XD functional and 6-31G** basis set. The solvent effects were taken into account by using polarizable continuum model (PCM) and three different polar solvents—water, dimethyl sulfoxide and ethanol. The DFT results demonstrated that the adsorption of ellipticine on graphene oxide nanosheet is an exothermic process and that the non-covalent interactions, as well as the highly polar aqueous environment stabilize the intermolecular complex. In addition to the DFT calculations, MD simulations were performed in order to explore the pH effect on the loading and release of ellipticine molecules on graphene oxide nanosheet. The model system

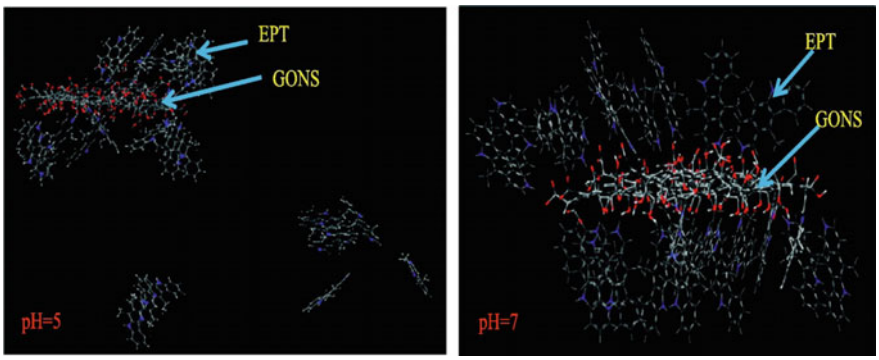

Fig. 4 Density functional theory calculations and molecular dynamics simulations of the adsorption of ellipticine anticancer drug on graphene oxide surface in aqueous medium as well as under controlled pH conditions

was composed by 24 drug molecules, graphene oxide nanosheet with dimensions of 20×20 Å^2, TIP3P water molecules and Na^+ ions for charge neutralization. The MD results indicated that the ellipticine molecules load on the graphene oxide nanosheet at pH = 7 (blood environment) and release at pH = 5 (cancerous tumor environment). The graphene oxide was suggested as a promising candidate for pH controlled drug delivery system for anticancer applications.

The same authors, Hasanzade and Raissi [25] reported DFT and MD study on the adsorption of the anticancer drug thioguanine on graphene oxide surface. The focus of this investigation was the solvent/co-solvent effect on the electronic structure and adsorption mechanism. Three different solvents are taken into account —water, ethanol and nicotine. The DFT calculations were performed with two different functionals—M06-2X and wB97X-D, 6-31G** basis set and PCM model for the solvent effect. The results from the quantum-chemical simulations revealed that the adsorption is governed by hydrogen bonds formation between the thioguanine and graphene oxide surface. The MD calculations were performed with the CHARRM27 force field and TIP3P water molecules. The nanosheet is modeled by graphene oxide with dimensions of 4.67×1.97 nm. The results of RDF patterns and the van der Waals energy calculations showed that in aqueous environment the interaction between graphene oxide and thioguanine is strongest compared to other solvents. In addition, it was demonstrated that the addition of nicotine and ethanol hinder the drug adsorption. It was concluded that in aqueous solution graphene oxide can be used as a delivery system of the thioguanine anticancer drug.

Mahdavi et al. [26] investigated the interaction between doxorubicin anticancer drug and graphene-based nanocarriers in an aqueous environment as a function of pH. Several types of drug delivery systems were investigated, namely, pristine graphene and graphene oxide with different surface oxygen densities. The calculations were performed by using molecular dynamics and the COMPASS II force field. The size of the noncarrier was 20×20 Å^2 and 44×41 Å^2 in the model systems with one and multiple drug molecules, respectively. It was found that the interaction between the doxorubicin drug and nanocarrier become stronger when the surface oxygen density increases. The results for the model systems with one drug molecule demonstrated that pH has negligible effect on the doxorubicin absorption on the graphene oxide nanocarrier at pH = 7 (blood environment) and pH (tumor environment) levels. It was shown that the interaction with one drug molecule decreases in the order: graphene oxide with low O/C ratio 1:6, pristine graphene and graphene oxide with high O/C ratio 1:3. This result was explained by preferential adsorption of doxorubicin on the edges of the nanosheets with 1:3 O/C ratio, while adsorption on the surface was observed for the cases of pristine graphene and nanosheet with 1/6 O/C ratio. The simulations for the model systems with 24 doxorubicin molecules and graphene oxide with low 1:6 O/C ratio confirmed that the drug load at neutral pH and release at pH = 5. The results indicated that at pH = 7 the number of the H-bonds between the doxorubicin molecules is higher and that they tend to aggregate around the edges of the nanosheet. At pH = 5 the number of H-bonds between the drug molecules and the nanocarrier increased, the interaction among the doxorubicin molecules weakened and they are more

adsorbed more evenly on the graphene oxide surface. This investigation shade light on the mechanism of the doxorubicin adsorption on graphene-based nanocarriers, which is of primary importance for the design of better drug delivery systems for targeting applications.

Saika and Deka [27] reported DFT and molecular docking investigation on the non-covalent interaction between the anticancer camptothecin drug and different graphene based nanocarriers. In particular, boron nitride nanosheets, BN-graphene hybrid nanomaterials and graphene oxide were considered as nanocarriers. Two types of DFT methods have been applied - PBE functional with double numerical basis set with polarization functions and wB97XD with 6–31G(d,p) basis set and dispersion correction. It was demonstrated that in the case of boron nitride nanosheets and BN-graphene hybrid nanomaterials the drug interact via π–π stacking, while in the case of graphene oxide the H-bonding dominates in the adsorption process. The molecular docking results indicated that the camptothecin-graphene and camptothecin-graphene oxide systems bind topoisomerase I trough π–π stacking interaction of the drug with the adenine and cytosine bases of DNA. In addition, it was shown that the DNA bases preferentially gets bound to the basal plane of graphene and GO rather than the edges. The results reported by Saika et al. are another proof for the high potential of graphene based nanocarriers in cancer therapy.

In their recent work, Mirhosseini et al. [28] studied the interaction between the doxorubicin anticancer drug and functionalized graphene by using molecular dynamics simulations. The COMPASS force field was applied. Several types of chemical groups for graphene functionalization were explored—hydroxyl, carboxyl, methyl and amine. Among all the most effective adsorption was reported for the case of graphene functionalized with COOH groups. It was observed that in all cases of functionalized graphene the drug adsorption is realized via H-bonds formation. Therefore, it was concluded for functionalized graphenes the hydrogen bonding plays a significant role in the doxorubicin loading process. The authors investigated also the effect of the temperature and porosity. The results indicated that the optimal temperature for doxorubicin adsorption on COOH-graphene is 35 °C. In addition, good adsorption behavior is observed when the nanoporous graphene surface is with pore diameter nearly the diameter of the drug molecule.

Tonel et al. [29] reported DFT and ab initio molecular dynamics results on the structural and electronic properties of pristine graphene interacting with doxorubicin. In order to model the graphene-drug interaction, the authors applied periodic boundary conditions, PBE functional and double-ζ plus polarization function basis set. The physical sorption of the drug was confirmed by relatively low bonding energy and minor changes in the band structures of the pristine graphene due to the doxorubicin loading. Moreover, the ab initio molecular dynamics simulations revealed that an increase in the temperature weaken the interaction between the graphene and the anticancer drug, which suggest the possibility for temperature control of the drug releasing process.

Using both experimental and theoretical approaches Vovusha et al. [30] studied the adsorption of doxorubicin on graphene monolayer and graphene oxide. The

experimental characterization was done by fluorescence, Raman and X-ray photoelectron spectroscopy, as well as by scanning electron microscopy. The theoretical modeling was carried out in the DFT framework by using the projector augmented wave method, plane wave basis set and the PBE functional with D2 dispersion correction. The calculations showed that the doxorubicin-graphene interactions are with π–π and CH-π origin, while hydrogen bonding and π–π intermolecular contacts are present in the doxorubicin-graphene oxide system. The theoretical simulations revealed that the binding of doxorubicin to graphene is more favored than to graphene oxide due to the domination of π–π interactions. This result is in agreement with the fluorescence spectroscopy measurements.

Duverger et al. [30] proposed to use a graphene nanoflake as a carrier of phtalocyanine (ZnPc) in order to increase the targeting in the photodynamic therapy treatment. The proposition is based on promising results obtained by DFT/TD-DFT and molecular dynamics simulations. The DFT calculations were performed with the projector augmented wave method, PBE functional and D3 dispersion correction. The TD-DFT modeling of the optical properties was done in vacuum, as well as in water environment by using the PCM method. The molecular dynamics simulations were conducted with the CHARMM36 force field and by building a the ZnPc molecular force field. The MD model system was composed by ZnPc, graphene nanoflakes, NaCl, water molecules and 656 1-palmitoyl-2-oleoyl-sn-glycero-3-phosphocholine (POPC) lipid molecules representing the membrane cell (Fig. 5). The TD-DFT calculations demonstrated that the noncovalent interaction with the graphene nanoflake does not cause a change in the optical properties of ZnPc, which indicates that the photodynamic response is not perturbed by the carrier. The molecular dynamics simulations revealed that the use of graphene as a

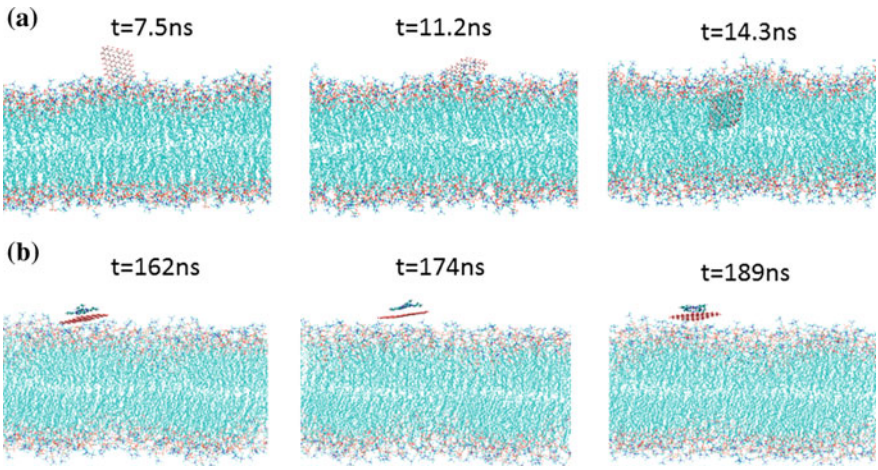

Fig. 5 Snapshots of the MD simulations of **a** a graphene nanoflake and **b** a ZnPc/graphene nanoflake near a POPC membrane in a biological solution from t = 0 to 200 ns. Water is not shown for convenience

carrier improves the stability of the ZnPc-nanoflake system at the proximity of the cell membrane, which was not possible when using ZnPc alone. These results are very promising and indicates that one can obtain a higher PDT yield near the cell membrane with less ZnPc molecules. Moreover, it was suggested that the graphene nanoflake carrier may be combined with other promising photosensitizers in photodynamic therapy, such as SiPc or naphthalocyanine molecules. The work of Duverger et al. is a good example how the multiscale molecular modelling approach can be applied for improvement of the anticancer treatment and in particular of the photodynamic therapy.

The theoretical work of Armaković et al. [31] demonstrates that the graphene nanosheet represents a promising candidate for detection, delivery or removal of ephedrine from the environment. The ephedrine was chosen as the most frequently used active component in sport supplements and one of the overused pharmaceutical contaminants in the environment. In order to study the adsorption of the ephedrine on graphene nanosheets, a variety of computational approaches were applied—DFT [B3LYP-D3/6-31G(d)], TD-DFT [CAM-B3LYP/6-31G(d,p)], DFT with periodic boundary conditions (dispersion corrected PBE with ultrasoft pseudopotentials) and molecular dynamics (OPLS3 force field). The results for the density of states and charge distribution revealed that the ephedrine loading process has physisorption nature. The IR frequency calculations showed that several new normal modes in the 750 cm^{-1} regions arise from of ephedrine-graphene interaction. Three characteristic normal modes of ephedrine (including the OH stretching at 3600 cm^{-1}) change their intensity and/or frequency as a result of the drug loading process. The simulated UV-vis spectra indicated small effect of the drug adsorption on the optical properties of graphene sheet.

Wu et al. made a revision of computer simulation studies related to the generation of graphene nanostructures by particle beam irradiation. Using atomistic computer simulations based on analytical potentials and density-functional theory were able to identify the mechanism of doping, joining and nanopore formation of graphene structures under particle beam irradiation. From these studies, four different phenomena could be described during ion bombardment: ion beam transmission, ion beam reflection, ion beam embedded within graphene and ion beam adsorption on graphene surface. There different cases could be differentiated depending on the energy of the incident beam. At low energy, incident ions will tend to adsorb on the surface of graphene. In the range of several tens of eV to several hundred of eV, some carbon atoms are ejected from the surface. The incident ions could replace the ejected atoms (substitution doping), or remain adsorbed on the surface, or cross the graphene surface. At higher incident energy, all carbon atoms are ejected. And at a very high incident energy, ions will cross through the graphene surface without inducing any elimination of surface carbon atoms. If an electron beam is also applied to the system, the irradiation process is usually described in the simulations by the Primary Knock-On Atoms (PKAs) methodology [32].

Acknowledgements The authors Miroslava Nedyalkova and Sergio Madurga are gratefully acknowledged financial support from the "Materials Networking" project, Horizon 2020 research and innovation programme under grant agreement No. 692146. Author M. Nedyalkova is grateful to the National Scientific Program ICT in SES, financed by the Ministry of Education and Science. The author M. Nedyalkova is gratefully acknowledged to the L'Oréal Program for Woman in Science. Financial support from Generalitat de Catalunya (Grant 2017SGR1033) and Spanish Structures of Excellence María de Maeztu program through grant MDM- 2017–0767 is fully acknowledged.

References

1. Geim, A.K., Novoselov, K.S.: The rise of graphene. Nat. Mater. https://doi.org/10.1038/nmat1849 (2007)
2. Cai, W., Piner, R.D., Stadermann, F.J., Park, S., Shaibat, M.A., Ishii, Y., Yang, D., Velamakanni, A., An, S.J., Stoller, M., An, J., Chen, D., Ruoff, R.S.: Synthesis and solid-state NMR structural characterization of 13C-labeled graphite oxide. Science. https://doi.org/10.1126/science.1162369 (2008)
3. He, H., Klinowski, J., Forster, M., Lerf, A.: A new structural model for graphite oxide. Chem. Phys. Lett. https://doi.org/10.1016/S0009-2614(98)00144-4 (1998)
4. Lerf, A., He, H., Forster, M., Klinowski, J.: Structure of graphite oxide revisited. J. Phys. Chem. B. https://doi.org/10.1021/jp9731821 (1998)
5. Zhu, Y., Stoller, M.D., Cai, W., Velamakanni, A., Piner, R.D., Chen, D., Ruoff, R.S.: Exfoliation of graphite oxide in propylene carbonate and thermal reduction of the resulting graphene oxide platelets. ACS Nano. https://doi.org/10.1021/nn901689k (2010)
6. Lee, S.H., Dreyer, D.R., An, J., Velamakanni, A., Piner, R.D., Park, S., Zhu, Y., Kim, S.O., Bielawski, C.W., Ruoff, R.S.: Polymer brushes via controlled, surface-initiated atom transfer radical polymerization (ATRP) from graphene oxide. Macromol. Rapid Commun. https://doi.org/10.1002/marc.200900641 (2010)
7. Chunder, A., Liu, J., Zhai, L.: Reduced graphene oxide/poly(3-hexylthiophene) supramolecular composites. Macromol. Rapid Commun. https://doi.org/10.1002/marc.200900626 (2010)
8. Sun, X., Liu, Z., Welsher, K., Robinson, J.T., Goodwin, A., Zaric, S., Dai, H.: Nano-graphene oxide for cellular imaging and drug delivery. Nano Res. https://doi.org/10.1007/s12274-008-8021-8 (2008)
9. Liu, Z., Robinson, J.T., Sun, X., Dai, H.: PEGylated nanographene oxide for delivery of water-insoluble cancer drugs. J Am. Chem. Soc. https://doi.org/10.1021/ja803688x (2008)
10. Zhang, R., Hummelgård, M., Lv, G., Olin, H.: Real time monitoring of the drug release of rhodamine B on graphene oxide. Carbon. https://doi.org/10.1016/j.carbon.2010.11.026 (2011)
11. Zhang, L., Xia, J., Zhao, Q., Liu, L., Zhang, Z.: Functional graphene oxide as a nanocarrier for controlled loading and targeted delivery of mixed anticancer drugs. Small. https://doi.org/10.1002/smll.200901680 (2010)
12. Chen, L., Hu, P., Zhang, L., Huang, S., Luo, L., Huang, C.: Toxicity of graphene oxide and multi-walled carbon nanotubes against human cells and zebrafish. Sci. China Chem. https://doi.org/10.1007/s11426-012-4620-z (2012)
13. Manjunatha, B., Park, S.H., Kim, K., Kundapur, R.R., Lee, S.J.: In vivo toxicity evaluation of pristine graphene in developing zebrafish (*Danio rerio*) embryos. Environ. Sci. Pollut. Res. https://doi.org/10.1007/s11356-018-1420-9 (2018)
14. Liang, L., Kong, Z., Kang, Z., Wang, H., Zhang, L., Shen, J.-W.: Theoretical evaluation on potential cytotoxicity of graphene quantum dots. ACS Biomater. Sci. Eng. https://doi.org/10.1021/acsbiomaterials.6b00390 (2016)
15. Luan, B., Huynh, T., Zhao, L., Zhou, R.: Potential toxicity of graphene to cell functions via disrupting protein–protein interactions. ACS Nano. https://doi.org/10.1021/nn506011j (2015)

16. Guo, R., Mao, J., Yan, L.-T.: Computer simulation of cell entry of graphene nanosheet. Biomaterials. https://doi.org/10.1016/j.biomaterials.2013.02.047 (2013)
17. Tu, Y., Lv, M., Xiu, P., Huynh, T., Zhang, M., Castelli, M., Liu, Z., Huang, Q., Fan, C., Fang, H., Zhou, R.: Destructive extraction of phospholipids from *Escherichia coli* membranes by graphene nanosheets. Nat. Nanotechnol. https://doi.org/10.1038/nnano.2013.125 (2013)
18. Chong, Y., Ge, C., Yang, Z., Garate, J.A., Gu, Z., Weber, J.K., Liu, J., Zhou, R.: Reduced cytotoxicity of graphene nanosheets mediated by blood-protein coating. ACS Nano. https://doi.org/10.1021/nn5066606 (2015)
19. Mao, J., Guo, R., Yan, L.-T.: Simulation and analysis of cellular internalization pathways and membrane perturbation for graphene nanosheets. Biomaterials. https://doi.org/10.1016/j.biomaterials.2014.03.087 (2014)
20. Qin, W., Li, X., Bian, W.-W., Fan, X.-J., Qi, J.-Y.: Density functional theory calculations and molecular dynamics simulations of the adsorption of biomolecules on graphene surfaces. Biomaterials. https://doi.org/10.1016/j.biomaterials.2009.10.013 (2010)
21. Wang, X., Liu, Y., Xu, J., Li, S., Zhang, F., Ye, Q., Zhai, X., Zhao, X.: Molecular dynamics study of stability and diffusion of graphene-based drug delivery systems. J. Nanomater. https://doi.org/10.1155/2015/872079 (2015)
22. Safdari, F., Raissi, H., Shahabi, M., Zaboli, M.: DFT calculations and molecular dynamics simulation study on the adsorption of 5-fluorouracil anticancer drug on graphene oxide nanosheet as a drug delivery vehicle. J. Inorg. Organomet. Polym. Mater. https://doi.org/10.1007/s10904-017-0525-9 (2017)
23. Shariatinia, Z., Mazloom-Jalali, A.: Chitosan nanocomposite drug delivery systems designed for the ifosfamide anticancer drug using molecular dynamics simulations. J. Mol. Liq. https://doi.org/10.1016/j.molliq.2018.10.047 (2019)
24. Hasanzade, Z., Raissi, H.: Density functional theory calculations and molecular dynamics simulations of the adsorption of ellipticine anticancer drug on graphene oxide surface in aqueous medium as well as under controlled pH conditions. J. Mol. Liq. https://doi.org/10.1016/j.molliq.2018.01.159 (2018)
25. Hasanzade, Z., Raissi, H.: Solvent/co-solvent effects on the electronic properties and adsorption mechanism of anticancer drug thioguanine on graphene oxide surface as a nanocarrier: density functional theory investigation and a molecular dynamics. Appl. Surf. Sci. https://doi.org/10.1016/j.apsusc.2017.05.245 (2017)
26. Mahdavi, M., Rahmani, F., Nouranian, S.: Molecular simulation of pH-dependent diffusion, loading, and release of doxorubicin in graphene and graphene oxide drug delivery systems. J. Mater. Chem. B. https://doi.org/10.1039/C6TB00746E (2016)
27. Saikia, N., Deka, R.C.: Ab initio study on the noncovalent adsorption of camptothecin anticancer drug onto graphene, defect modified graphene and graphene oxide. J. Comput. Aided Mol. Des. https://doi.org/10.1007/s10822-013-9681-3 (2013)
28. Mirhosseini, M.M., Rahmati, M., Zargarian, S.S., Khordad, R.: Molecular dynamics simulation of functionalized graphene surface for high efficient loading of doxorubicin. J. Mol. Struct. https://doi.org/10.1016/j.molstruc.2017.04.007 (2017)
29. Tonel, M.Z., Martins, M.O., Zanella, I., Pontes, R.B., Fagan, S.B.: A first-principles study of the interaction of doxorubicin with graphene. Comput. Theor. Chem. https://doi.org/10.1016/j.comptc.2017.07.004 (2017)
30. Vovusha, H., Banerjee, D., Yadav, M.K., Perrozzi, F., Ottaviano, L., Sanyal, S., Sanyal, B.: Binding characteristics of anticancer drug doxorubicin with two-dimensional graphene and grapheneoxide: insights from density functional theory calculations and fluorescence spectroscopy. J. Phys. Chem. C. https://doi.org/10.1021/acs.jpcc.8b04496 (2018)
31. Armaković, S., Armaković, S.J., Tomić, B.T., Pillai, R.R., Panicker, C.Y.: Adsorption properties of graphene towards the ephedrine—a frequently used molecule in sport. Comput. Theor. Chem. https://doi.org/10.1016/j.comptc.2017.12.009 (2018)
32. Xin, W., Fengwen, M., Yinghui, W., Haiyan, Z.: Application of atomic simulation methods on the study of graphene nanostructure fabrication by particle beam irradiation: a review. Comput. Mat. Sci. https://doi.org/10.1016/j.commatsci.2018.03.022 (2018)

Graphene-Based Nanomaterials for Hydrogen Storage

Ayşenur Aygün, Esra Atalay, Shukria Yassin, Anish Khan and Fatih Şen

Abstract Graphene, which was discovered in the last ten years, has attracted considerable attention in the field of material science and has been one of the most important materials. Graphene has a two-dimensional structure, and this structure gives the structural, electronic, and optical properties characteristic of the graphene. Thanks to these characteristics, many graphene-based materials have been synthesized for use in many potential applications, such as electronics, energy storage, catalysis, gas absorption, separation, and detection. The function, surface area and porosity, adjustable for energy-based materials and stable graphene are of great importance to these applications. The most important feature that makes the graphene a very useful nanoparticle is its electronic feature. Also, graphene is used as an electrode in solar cells with unprecedented transparency and conductivity. Moreover, a certain amount of graphene can store energy. In this chapter, we outline the structure, properties of graphene, and developments in energy storage systems, and graphene-based hydrogen storage systems.

Keywords Graphene · Graphene oxide · Synthesis · Hydrogen storage · Gas storage

1 Introduction

Today, the studies on production, storage, and consumption of renewable energy are of great importance. Because in the near future there is a danger of the depletion of fossil fuels that the scientist currently are seeking new sources for energy pro-

A. Aygün · E. Atalay · S. Yassin · F. Şen (✉)
Sen Research Group, Department of Biochemistry, Dumlupınar University, 43100 Kütahya, Turkey
e-mail: fatih.sen@dpu.edu.tr; fatihsen1980@gmail.com

A. Khan
Chemistry Department, Faculty of Science, King Abdulaziz University, P.O. Box 80203, Jeddah 21589, Saudi Arabia

Center of Excellence for Advanced Materials Research, King Abdulaziz University, P.O. Box 80203, Jeddah 21589, Saudi Arabia

A. Khan et al. (eds.), *Graphene Functionalization Strategies*, Carbon Nanostructures, https://doi.org/10.1007/978-981-32-9057-0_10

duction. The aim of these studies is to find recyclable and sustainable energy sources and to use the energy efficiently in the required fields. There are many types of materials for energy storage [1–167]. But, when we calculate the ratio of energy/weight and material cost into consideration, the range of material selection becomes narrower. Carbon is the lightest element used in energy storage, which can be configured in diversified forms to provide elevated surface field and energy. In recent years, carbon nanotubes (CNTs) have attracted great attention in the materials produced for the storage of energy [78, 144]. Carbon nanotubes are lightweight and have many advantages. Specifically, single-walled carbon nanotubes with a large surface area (up to 1315 m^2/g) can be produced in large quantities [138]. However, carbon nanotubes exhibit some of the disadvantageous, such as remaining toxic metal dirtiness, which is hard to remove [92, 93], and high production costs. Graphene, another carbon derivative, has attracted attention as an alternative energy storage material due to its superior properties [92, 93]. Graphene is a carbon sheet attached to a two-dimensional (2D) sp^2 orbital with hexagonal honeycomb shape [33, 38, 85, 91]. In other words, graphene is a two-dimensional (2D) material composed of stacked graphite layers. Graphite layers forming the graphene are bound by weak van der Waals forces (vdW). Graphene is also unique in that it has properties such as a thin membrane, a high coefficient, and a strong thermal and electrical conductivity [1, 85, 100]. Graphene also has a large surface area of approximately 2600 m^2/g^{-1} and created a wealthy platform for surface chemistry [29–31, 52, 62, 64, 73, 136, 145]. Physical and chemical properties of graphene led to intensive research in the fields of nanoparticles, superconductors, photovoltaic cells, fuel cells, catalysis, batteries, gas absorption, separation, storage, and detection [17, 19, 32, 62–64, 70, 81, 82, 99, 131, 132, 146, 148, 151, 163, 164]. There are so many methods for the preparation of these types of materials that can be listed as: (a) the thermal decomposition of the graphite oxide and subsequent reduction of the graphene oxide to the graphene [22, 161] (b) Chemical vapor deposition technique [130]; (c) mechanical separation of graphite (original Scotch-tape method) [86]; (d) removal of carbon nanotubes [67, 72], and (e) electrochemical separation of graphite. The properties of graphene may vary depending on the structural state and number of layers [85, 134, 166]. Therefore, in order to benefit from the majority of proposed applications, the pathways and conditions of installation are important in modifying the structure and properties of graphene. Many studies have been performed in the literature in order to use the optical and electronic properties of graphene in the field of photomicrography and electrochemical applications [12, 13, 29–31, 41, 80, 83, 95, 139, 141, 162, 167]. However, their significant molecular interactions (e.g. molecular adsorption and storage) have not been taken into account [50]. Graphene is also one of the most essential nanomaterials since it has excellent physical and chemical properties [39, 130]. Table 1 shows some features of graphite. Figure 1 also shows hexagonal honeycomb graphene.

Table 1 Some of the graphite properties [150]

Physical properties	Value
Young's modulus	1.0 TPa [20, 75]
C–C bond length	1.42 Å [84, 96, 133]
Thermal conductivity	5300 W mK^{-1} [14]
Specific surface	2600 m^2 g^{-1} [28]
Electron mobility	15,000 cm^2 V^{-1} s^{-1} at 300 K [51]
Fermi velocity, v_F	10^6 m s^{-1} [66, 84, 87, 96, 135]
Lattice constant	2046 Å [74, 101]
Specific capacitance	100 F g^{-1} [137]
Intrinsic mobility	2000 cm^2 V^{-1} s^{-1} [18, 40]

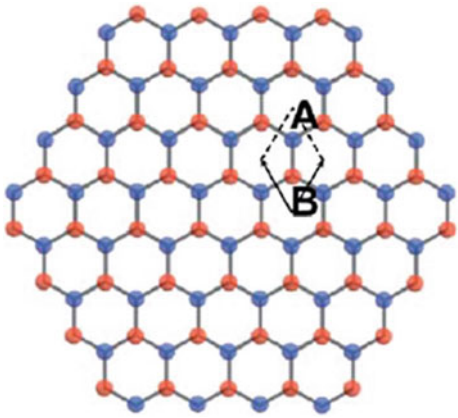

Fig. 1 Hexagonal honeycomb graphene [150]

2 Gas Adsorption and Storage

The absorption, separation, and storage of carbon-structured materials depend on physical adsorption on surfaces. Primarily, it depends on electrostatic reactions and dispersion (e.g., VdW). The stability of the reaction is determined without limiting the properties of the carbon-structure materials and the target absorption molecules. The size and shape of adhesion molecules, in addition to polarity, magnetic susceptibility, and bipolar hardness, also affect the strength of the reaction [50]. Many gaseous or vapor adsorbents did not give the physical parameters associated with adsorption. Table 2 shows the parameters of N_2, H_2, SO_2, CO, H_2S, NH_3, CO_2, and CH_4 [76].

For instance, the adsorbent having a specific surface area is a suitable nominee for absorbing a high polar but non-polar molecule. Adsorbents with high polarity surfaces are characterized by high torque adsorption particles. Typically, the linking or adsorption power with a carbon nanostructure is comparatively low in order to H_2 and N_2; Intermediate for CO_2, CO, and CH_4; and H_2S are comparatively loud

Table 2 Some physical adsorption parameters of selected gases [50]

Adsorbate	Normal BP (EC)	T_c (K)	V_c (cm^3/mol)	P_c (bar)	Kinetic diameter (nm)	Polarizability $\times 10^{25}$ (cm^3)	Dipole moment $\times 10^{18}$ (esu cm)	Quadrupole moment $\times 10^{26}$ (esu cm^2)
He	4.30	5.19	57.30	2.27	0.2551	2.04956	0	0
H_2	20.27	32.98	64.20	12.93	0.2827–0.289	8.042	0	0.662
N_2	77.35	126.20	90.10	33.98	0.364–0.380	17.403	0	1.52
O_2	90.17	154.58	73.37	50.43	0.3467	15.813	0	0.39
CO	81.66	132. 85	93.10	34.94	0.3690	19.5	0.1098	2.50
CO_2	216.55	304.12	94.07	73.74	0.33	29.11	0	4.30
NO_2	302.22	431.01	–	101.00	–	30.2	0.316	–
SO_2	263.13	430.80	122.00	78.84	0.4112	37.2–42.8	1.633	–
H_2S	212.84	373.40	98.00	89.63	0.3623	37.82–39.5	0.9783	–
NH_3	239.82	405.40	72.47	113.53	0.2900	21.0–28.1	1.4718	–
H_2O	373.15	647.14	55.95	220.64	0.2641	14.5	1.8546	–
CH_4	111.66	190.56	98.60	45.99	0.3758	25.93	0	0

for NH_3 and H_2O. Hence, surface modifications, like vaccination, functions, the development of pore structure and surface field specific to nanoparticles, are essential for increasing gas adsorption. In order to this aim, graphene provides a large area for carbon-specific adsorbents [50].

3 Electrochemical Storage of Hydrogen

Hydrogen is one of the best remarkable energy sources among these clean fuels. The hydrogen may be stored under pressure on a fluid, pressurized gas or a substrate (absorbent material). Research on the storage of hydrogen in liquid form has been studied under NASA's Apollo program for many years. Unfortunately, the technology developed as a result of these studies is not suitable for use in daily life. The US Department of Energy's (DOE) goal of using hydrogen to store energy in mobile applications, according to the Office of Fuel Cell Technologies, is 6.5% of the hydrogen in a dense sorbent of 62 kg H_2/m^3 at ambient temperature. Given that the stoichiometric C–H rate has a hydrogen weight of 7.7%, this high capacity is difficult to obtain. In order to store the hydrogen, storage of molecular hydrogen or atomic hydrogen deposition methods based on hydrogen emissions can be used.

3.1 Storage of Hydrogen in the Form of Molecular Hydrogen

Hydrogen is a non-polar molecule, and its connections with graphene-content agents are based on induced dipole-dipole called London dispersion forces. There are many theoretical studies in the literature aiming to explain the mechanism of H_2 adsorption of graphene-based materials and advance to further the experiments on H_2 adsorption [89]. In the H_2-graphene system at room temperature, there is a slightly attractive force of -1.2 kJ mol^{-1} [90]. This force corresponds to the equilibrium constant of the free energy of the physical adsorption, which means that a single graphene layer at room temperature only raises the amount of hydrogen by about 60%. Theoretical studies show that for a graphene layer separated by a distance of 6 Å, a single H_2 layer can be placed in the integrated structure (2–3% by weight of storage at 5 MPa). This storage capacity is quite good, however nevertheless under the target of DOE. For storing the two-layer hydrogen molecule in a single graphene-graphene intermediate layer; two graphene layers separated by 8 must be obtained, and this leads to the gravimetric storage capacity of 5.0–6.5% H_2 which can be obtained under technologically acceptable conditions (Fig. 2). The interaction between the H_2 molecules and the transition metal and metal nanoparticles are powerful enough to obtained important capacity [160]. Also, metal nanoparticles themselves form clusters, thus reducing their accessibility [69]. The

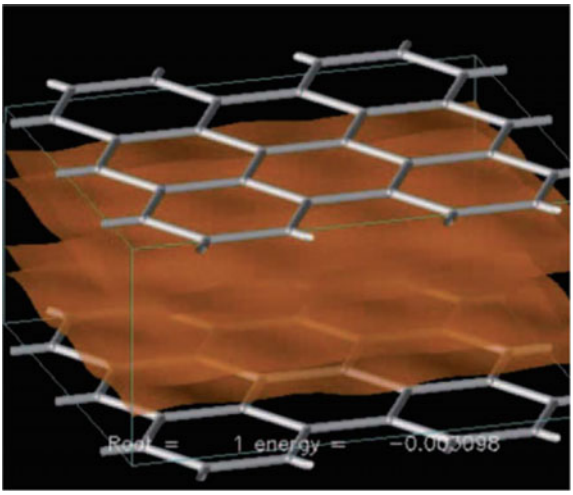

Fig. 2 Use of graphene-containing nanomaterials in hydrogen storage [94]

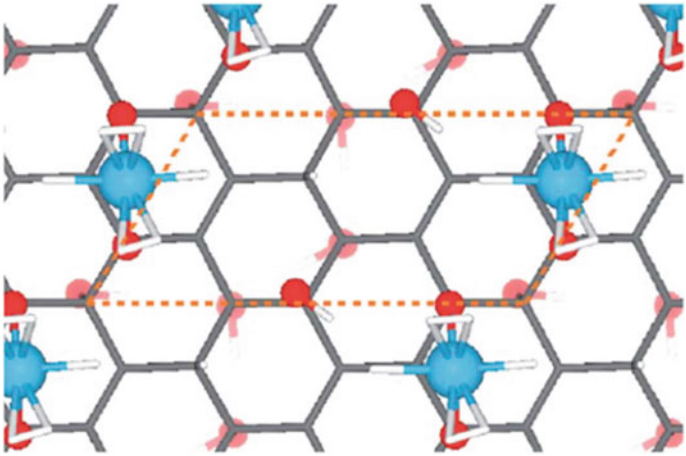

Fig. 3 Location of H_2 between graphene layers with a rational range [94]

use of graphene oxide with functional groups to stabilize metals is very functional. For example, in Fig. 3 it is shown that the titanium metal is firmly bonded to the oxygen groups of the graphene oxide layers [142]. Since each Ti atom can be associated with several H_2 molecules, the theoretical capacity of this light-metal-graphene is 4.9% by weight and 64 g by L^{-1}. Several theoretical studies have shown that the doped graphene, in particular, boron [165] or aluminum [8], demonstrates a significantly improved bonding capacity for adsorption of H_2. Calcium-enriched graphene has a storage capacity of 5% by weight [11]. Ca

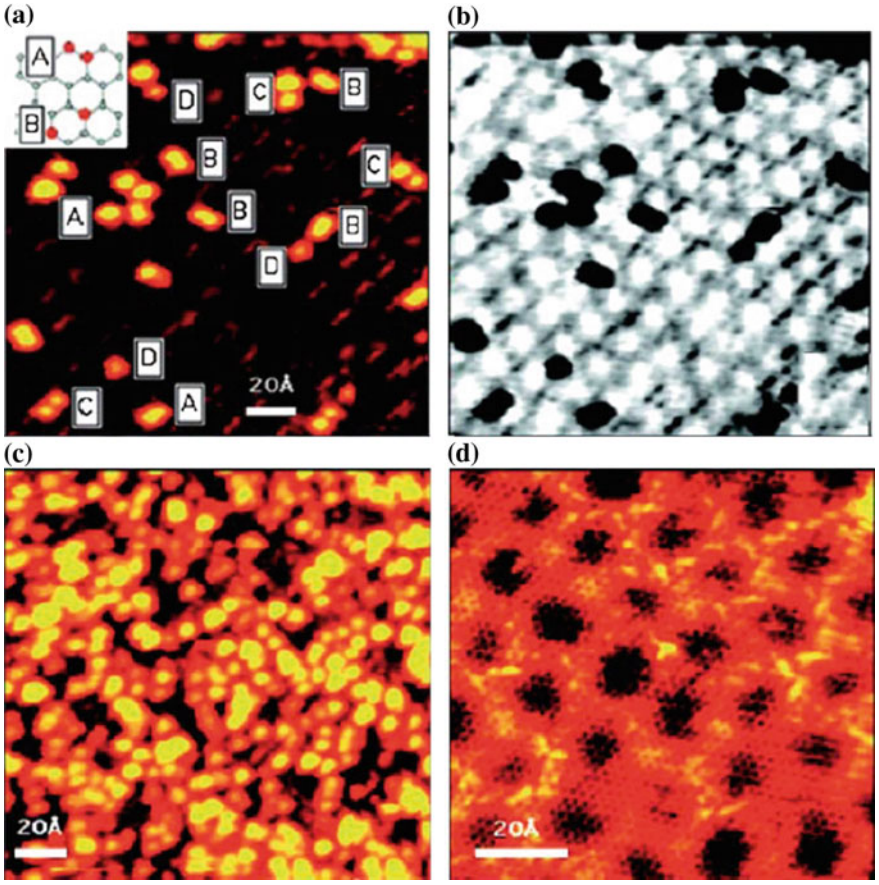

Fig. 4 **a** Scanning tunneling microscopy image of the hydrogenated graphene. (A) Ortho-dimers, (B) para-dimers, (C) elongated dimers, as shown in the image, belong to atomic hydrogen adsorbate structures, defined as D-monomers. The (A) image indicates **a** ortho- and **b** para-dimer configuration on the graphical lattice. **b** It is the same as the image in (**a**) by an inverse color scheme, giving importance to preferential hydrogen adsorption. **c** STM image of the graphene surface after expansion with hydrogen exposure. Bright projections in the image are defined as clusters of atomic hydrogen. **d** Image of the vast graphene region recovered from hydrogenation by annealing to 800 °C [94]

preferably adsorbed at the 10 Ca–Ca distance on the distorted edge of the graphene; each Ca atom may adsorb the 6 H_2 molecules. Hornekaer described the structure-adsorbed hydrogen on graphene with STM [11]. It has been found that in the low coverage area, preferably hydrogen dimers are formed on the specific regions (Fig. 4). It is necessary to have an excellent technique to investigate the surface area and hydrogen storage capacity of nanostructured carbon materials [7]. Characterization of carbon-containing materials such as graphene and carbon nanotube can be performed by Nuclear Magnetic Resonance (NMR) technique etc.

Characterization results by NMR indicate that hydrogen can be stored in porous nanotubes and then produced by carbon crystallization [79].

3.2 Hydrogen Storage in 3D Graphene-Based Materials (GBMs)

The demand for renewable and sustainable energy sources is increasing due to the depletion of fossil fuels used for energy production and the harm to the environment [149]. Hydrogen is an alternative source of fuel because of the lack of environmental pollution, clean combustion, and fantastic energy intensity [61, 143, 147]. However, the use of hydrogen energy in daily life is limited due to the complicated production and storage of hydrogen [147]. Thanks to its large surface area and pore volume, high chemical stability and specially designed pores, porous carbon materials have attracted considerable attention in the storage of hydrogen [23]. The 3D network nanostructured GBMs have been certified to have excellent hydrogen storage capacity based on theoretical estimates and test consequences [6, 61, 147]. The hydrogen molecule has an nonpolar structure, and its interactions with graphene-based materials are formed by induced dipole-dipole forces. Micro and mesoporous metallomacrocycle-graphene frameworks (MGFs) were gradually formed using two separate structure blocks: GO and metallomacrocyclics. This hybrid showed an adsorption capacity of 1 bar at 77 K and 1.54% by weight and a significant delay. MGF's storage capacity was increased by three factors with significantly reduced GO's pores, (i) high-value of mineral centres (ii) open as strong acidic regions of Lewis (iii) the microporous nature of the MGFs may be particularly suitable for H_2 absorption [140]. Graphene Oxide (GO) and Carbon Nanotubes were brought together, and the product with the 3D structure was obtained. The obtained hydrogen content of this material at room temperature was found to be higher than the GO, multi-walled carbon nanotubes (MWCNTs), reduced graphene oxide-MWCNT (rGO-MWCNT) used in hydrogen storage [6]. The GO structure with structurally less error and proportional intermediate layer spacing may have higher hydrogen storage capacity. Furthermore, they examined molecular hydrogen adsorption on a 3D column grouping in various environments [61]. While the large gap between low temperatures, high pressure, and graphene layers increases the hydrogen absorption capacity, only a slight improvement is achieved by increasing the CNT diameter. One of the other methods for storing hydrogen is the storage of atomic hydrogen. Here the hydrogen emission is caused by the chemical decomposition of hydrogen on metal nanoparticles. The hydrogen or H atom produced from the activator is then transported to the material by surface diffusion: 3-dimensional graphene-supported nickel (0.83% by weight) and boron (1.09% by weight) metal combination having shown hydrogen storage capacity of 4.4 at 77 K and 106 kPa. This value is higher than previously tested graphene and all carbon-based materials [143]. The Ni–B metal alloy in 3-D graphite showed a

critical effect in the chemical decomposition of hydrogen molecules by diffusion. The presence of this Ni–B metal alloy provides a high hydrogen storage capacity. By the Ni–B alloy in nanoscale, the hydrogen molecules are separated into hydrogen atoms and then spread to the graphene regions to form a C–H bond [140].

4 Conclusions

Briefly, high temperature and chemical stability, adjustable surface area/pore structure, porous molecular structure of the graphene-based materials have been used in many sectors. High capacity energy storage with graphene relates to the fact that separate graphene layers have appropriately aligned error-free and comparable properties. Hence, hydrogen storage with graphene-containing materials can be a promising research subject, even though it is a complicated process.

References

1. Abergel, D.S.L., Apalkov, V., Berashevich, J., et al.: Properties of graphene: a theoretical perspective. Adv. Phys. **59**, 261–482 (2010)
2. Abrahamson, J.T., Sen, F., Sempere, B., et al.: Excess thermopower and the theory of thermopower waves. ACS Nano **7**(8), 6533–6544 (2013)
3. Aday, B., Pamuk, H., Kaya, M., et al.: Graphene oxide as highly effective and readily recyclable catalyst using for the one-pot synthesis of 1,8-dioxoacridine derivatives. J. Nanosci. Nanotechnol. **16**, 6498–6504 (2016)
4. Aday, B., Yildiz, Y., Ulus, R., et al.: One-pot, efficient and green synthesis of acridinedione derivatives using highly monodisperse platinum nanoparticles supported with reduced graphene oxide. New J. Chem. **40**, 748–754 (2016)
5. Akocak, S., Sen, B., Lolak, N., et al.: One-pot three-component synthesis of 2-amino-4H-chromene derivatives by using monodisperse Pd nanomaterials anchored graphene oxide as highly efficient and recyclable catalyst. Nano-Struct. Nano-Objects **11**, 25–31 (2017)
6. Alizadeh, T., Zare, M., Ganjali, M.R., et al.: A new molecularly imprinted polymer (MIP)-based electrochemical sensor for monitoring 2,4,6-trinitrotoluene (TNT) in natural waters and soil samples. Biosens. Bioelectron. **25**, 1166–1172 (2010)
7. Anderson, R., McNicholas, T.P., Kleinhammes, A., et al.: NMR methods for characterizing the pore structures and hydrogen storage properties of microporous carbons. J. Am. Chem. Soc. **132**, 8618 (2010)
8. Ao, Z.M., Jiang, Q., Zhang, R.Q., et al.: Al doped graphene: a promising material for hydrogen storage at room temperature. J. Appl. Phys. **105**, 074307 (2009)
9. Ayranci, R., Baskaya, G., Guzel, M., et al.: Enhanced optical and electrical properties of PEDOT via nanostructured carbon materials: a comparative investigation. Nano-Struct. Nano-Objects **11**, 13–19 (2017)
10. Ayranci, R., Baskaya, G., Guzel, M., et al.: Carbon-based nanomaterials for high-performance optoelectrochemical systems. ChemistrySelect **2**(4), 1548–1555 (2017)
11. Balog, R., Jorgensen, B., Wells, J., et al.: Atomic hydrogen adsorbate structures on graphene. J. Am. Chem. Soc. **131**, 8744–8745 (2009)

12. Bai, H., Li, C., Shi, G.: Functional composite materials based on chemically converted graphene. Adv. Mater. **23**, 1089–1115 (2011)
13. Bai, S., Shen, X.: Graphene-inorganic nanocomposites. RSC Adv. **2**, 64–98 (2012)
14. Balandin, A.A., Ghosh, S., Bao, W., et al.: Superior thermal conductivity of single-layer graphene. Nano Lett. **8**, 902–907 (2008)
15. Baskaya, G., Esirden, I., Erken, E., et al.: Synthesis of 5-substituted-1H-tetrazole derivatives using monodisperse carbon black decorated Pt nanoparticles as heterogeneous nanocatalysts. J. Nanosci. Nanotechnol. **17**, 1992–1999 (2017)
16. Baskaya, G., Yıldız, Y., Savk, A., et al.: Rapid, sensitive, and reusable detection of glucose by highly monodisperse nickel nanoparticles decorated functionalized multi-walled carbon nanotubes. Biosens. Bioelectron. **91**, 728–733 (2017)
17. Basu, S., Bhattacharyya, P.: Recent developments on graphene and graphene oxide based solid state gas sensors. Sens. Actuators B **173**, 1–21 (2012)
18. Bolotin, K.I., Sikes, K.J., Jiang, Z., et al.: Ultrahigh electron mobility in suspended graphene. Solid State Commun. **146**, 351–355 (2008)
19. Bonaccorso, F., Sun, Z., Hasan, T., et al.: Graphene photonics and optoelectronics. Nat. Photon. **4**, 611–622 (2010)
20. Booth, T.J., Blake, P., Nair, R.R., et al.: Macroscopic graphene membranes and their extraordinary stiffness. Nano Lett. **8**, 2442–2446 (2008)
21. Bozkurt, S., Tosun, B., Sen, B., et al.: A hydrogen peroxide sensor based on TNM functionalized reduced graphene oxide grafted with highly monodisperse Pd nanoparticles. Anal. Chim. Acta **989C**, 88–94 (2017)
22. Brodie, B.C.: On the atomic weight of graphite. Philos. Trans. R Soc. **149**, 249–259 (1859)
23. Burress, J.W., Gadipelli, S., Ford, J., et al.: Graphene oxide framework materials: theoretical predictions and experimental results. Angew. Chem. Int. Ed. **49**, 8902 (2010)
24. Celik, B., Baskaya, G., Karatepe, O., et al.: Monodisperse Pt(0)/DPA@GO nanoparticles as highly active catalysts for alcohol oxidation and dehydrogenation of DMAB. Int. J. Hydrogen Energy **41**, 5661–5669 (2016)
25. Celik, B., Erken, E., Eris, S., et al.: Highly monodisperse Pt(0)@AC NPs as highly efficient and reusable catalysts: the effect of the surfactant on their catalytic activities in room temperature dehydrocoupling of DMAB. Catal. Sci. Technol. **6**, 1685–1692 (2016)
26. Celik, B., Kuzu, S., Erken, E., et al.: Nearly monodisperse carbon nanotube furnished nanocatalysts as highly efficient and reusable catalyst for dehydrocoupling of DMAB and C_1 to C_3 alcohol oxidation. Int. J. Hydrogen Energy **41**, 3093–3101 (2016)
27. Celik, B., Yildiz, Y., Erken, E., et al.: Monodisperse palladium-cobalt alloy nanoparticles assembled on poly (*N*-vinyl-pyrrolidone) (PVP) as highly effective catalyst for the dimethylamine borane (DMAB) dehydrocoupling. RSC Adv. **6**, 24097–24102 (2016)
28. Chae, H.K., Siberio-Perez, D.Y., Kim, J., et al.: A route to high surface area, porosity and inclusion of large molecules in crystals. Nature **427**, 523–527 (2004)
29. Chen, D., Feng, H., Li, J.: Graphene oxide: preparation, functionalization, and electrochemical applications. Chem. Rev. **112**, 6027–6053 (2012)
30. Chen, L., Hernandez, Y., Feng, X., et al.: From nanographene and graphene nanoribbons to graphene sheets: chemical synthesis. Angew. Chem. Int. Ed. **51**, 7640–7654 (2012)
31. Chen, Y., Zhang, B., Liu, G., et al.: Graphene and its derivatives: switching ON and OFF. Chem. Soc. Rev. **41**, 4688–4707 (2012)
32. Choi, H.J., Jung, S.M., Seo, J.M., et al.: Graphene for energy conversion and storage in fuel cells and supercapacitors. Nano Energy **1**, 534–551 (2012)
33. Dai, L., Chang, D.W., Baek, J.B., et al.: Carbon nanomaterials for advanced energy conversion and storage. Small **8**, 1130–1166 (2012)
34. Dasdelen, Z., Yıldız, Y., Eris, S., et al.: Enhanced electrocatalytic activity and durability of Pt nanoparticles decorated on GO-PVP hybrid material for methanol oxidation reaction. Appl. Catal. B **219C**, 511–516 (2017)
35. Demirci, T., Celik, B., Yıldız, Y., et al.: One-pot synthesis of Hantzsch dihydropyridines using highly efficient and stable PdRuNi@GO catalyst. RSC Adv. **6**, 76948–76956 (2016)

36. Demir, E., Savk, A., Sen, B., et al.: A novel monodisperse metal nanoparticles anchored graphene oxide as counter electrode for dye-sensitized solar cells. Nano-Struct. Nano-Objects **12**, 41–45 (2017)
37. Demir, E., Sen, B., Sen, F.: Highly efficient nanoparticles and f-MWCNT nanocomposites based counter electrodes for dye-sensitized solar cells. Nano-Struct. Nano-Objects **11**, 39–45 (2017)
38. Dreyer, D.R., Ruoff, R.S., Bielawski, C.W.: From conception to realization: an historial account of graphene and some perspectives for its future. Angew. Chem. Int. Ed. **51**, 7640–7654 (2012)
39. Dong, L.X., Chen, Q.: Properties, synthesis, and characterization of graphene. Front. Mater. Sci. China **4**, 45–51 (2010)
40. Du, X., Skachko, I., Barker, A., et al.: Approaching ballistic transport in suspended graphene. Nat. Nanotechnol. **3**, 491–495 (2008)
41. Eda, G., Chhowalla, M.: Chemically derived graphene oxide: towards large-area thin-film electronics and optoelectronics. Adv. Mater. **22**, 2392–2415 (2010)
42. Erken, E., Esirden, I., Kaya, M., et al.: A rapid and novel method for the synthesis of 5-substituted 1H-tetrazole catalyzed by exceptional reusable monodisperse Pt NPs@AC under the microwave irradiation. RSC Adv. **5**, 68558–68564 (2015)
43. Erken, E., Pamuk, H., Karatepe, O., et al.: New Pt(0) nanoparticles as highly active and reusable catalysts in the C_1–C_3 alcohol oxidation and the room temperature dehydrocoupling of dimethylamine-borane (DMAB). J. Cluster Sci. **27**, 9–23 (2016)
44. Erken, E., Yildiz, Y., Kilbas, B., et al.: Synthesis and characterization of nearly monodisperse Pt nanoparticles for C_1 to C_3 alcohol oxidation and dehydrogenation of dimethylamine-borane (DMAB). J. Nanosci. Nanotechnol. **16**, 5944–5950 (2016)
45. Eris, S., Dasdelen, Z., Sen, F., et al.: Investigation of electrocatalytic activity and stability of Pt@f-VC catalyst prepared by in-situ synthesis for Methanol electrooxidation. Int. J. Hydrogen Energy **43**(1), 385–390 (2018)
46. Eris, S., Dasdelen, Z., Sen, F.: Enhanced electrocatalytic activity and stability of monodisperse Pt nanocomposites for direct methanol fuel cells. J. Colloid Interface Sci. **513**, 767–773 (2018)
47. Eris, S., Dasdelen, Z., Yildiz, Y., et al.: Nanostructured polyaniline-rGO decorated platinum catalyst with enhanced activity and durability for methanol oxidation. Int. J. Hydrogen Energy **43**(3), 1337–1343 (2018)
48. Esirden, I., Erken, E., Kaya, M., et al.: Monodisperse Pt NPs@rGO as highly efficient and reusable heterogeneous catalysts for the synthesis of 5-substituted 1H-tetrazole derivatives. Catal. Sci. Technol. **5**, 4452–4457 (2015)
49. Fuel Cell Technologies Office Department of Energy: A Multiyear Plan for the Hydrogen R&D Program. https://www.energy.gov (1999)
50. Gadipelli, S., Guo, Z.X.: Graphene-based materials: synthesis and gas sorption, storage and separation. Prog. Mater. Sci. **69**, 1–60 (2015)
51. Geim, A.K., Novoselov, K.S.: The rise of graphene. Nat. Mater. **6**, 183–191 (2007)
52. Georgakilas, V., Otyepka, M., Bourlinos, A.B., et al.: Functionalization of graphene: covalent and non-covalent approaches, derivatives and applications. Chem. Rev. **112**, 6156–6214 (2012)
53. Giraldo, J.P., Landry, M.P., Faltermeier, S.M., et al.: A nanobionic approach to augment plant photosynthesis and biochemical sensing using targeted nanoparticles. Nat. Mater. **13**, 400–408 (2014)
54. Goksu, H., Celik, B., Yildiz, Y., et al.: Superior monodisperse CNT-supported CoPd (CoPd@CNT) nanoparticles for selective reduction of nitro compounds to primary amines with $NaBH_4$ in an aqueous medium. ChemistrySelect **1**(10), 2366–2372 (2016)
55. Goksu, H., Kilbas, B., Sen, F.: Recent advances in the reduction of nitro compounds by heterogenous catalysts. Curr. Org. Chem. **21**(9), 794–820 (2017)

56. Goksu, H., Yildiz, Y., Celik, B., et al.: Eco-friendly hydrogenation of aromatic aldehyde compounds by tandem dehydrogenation of dimethylamine-borane in the presence of reduced graphene oxide furnished platinum nanocatalyst. Catal. Sci. Technol. **6**, 2318–2324 (2016)
57. Goksu, H., Yildiz, Y., Celik, B., et al.: Highly efficient and monodisperse graphene oxide furnished Ru/Pd nanoparticles for the dehalogenation of aryl halides via ammonia borane. ChemistrySelect **1**(5), 953–958 (2016)
58. Goksu, H., Zengin, N., Karaosman, N., et al.: Highly active and reusable Pd/AlO(OH) nanoparticles for the Suzuki cross-coupling reaction. Curr. Organocatal. **5**, 1–8 (2018)
59. Gulcin, I., Taslimi, P., Aygün, A., et al.: Antidiabetic and antiparasitic potentials: inhibition effects of some natural antioxidant compounds on α-glycosidase, α-amylase and human glutathione S-transferase enzymes. Int. J. Biol. Macromol. **119**, 741–746 (2018)
60. Gunbatar, S., Aygun, A., Karataş, Y., et al.: Carbon-nanotube-based rhodium nanoparticles as highly-active catalyst for hydrolytic dehydrogenation of dimethylamineborane at room temperature. J. Colloid Interface Sci. (2018). https://doi.org/10.1016/j.jcis.2018.06.100
61. Hou, J., Yang, C., Cheng, H., et al.: Ternary 3D architectures of CdS QDs/graphene/$ZnIn_2S_4$ heterostructures for efficient photocatalytic H_2 production. Phys. Chem. Chem. Phys. **15**, 15660 (2013)
62. Huang, X., Qi, X., Boey, F., et al.: Graphene-based composites. Chem. Soc. Rev. **41**, 666–686 (2012)
63. Huang, X., Yin, Z., Wu, S., et al.: Graphene-based materials: synthesis, characterization, properties, and applications. Small **7**, 1876–1902 (2011)
64. Huang, X., Zeng, Z., Fan, Z., et al.: Graphene-based electrodes. Adv. Mater. **24**, 5979–6004 (2012)
65. Iverson, N.M., Barone, P.W., Sen, F., et al.: In vivo biosensing via tissue-localizable near-infrared-fluorescent single-walled carbon nanotubes. Nat. Nanotechnol. **11**, 873–880 (2013)
66. Jiang, Z., Henriksen, E., Tung, L., et al.: Infrared spectroscopy of Landau levels of graphene. Phys. Rev. Lett. **98**, 197403 (2007)
67. Jiao, L., Zhang, L., Wang, X., et al.: Narrow graphene nanoribbons from carbon nanotubes. Nature **458**, 877–880 (2009)
68. Karatepe, O., Yildiz, Y., Pamuk, H., et al.: Enhanced electrocatalytic activity and durability of highly monodisperse Pt@PPy-PANI nanocomposites as a novel catalyst for electro-oxidation of methanol. RSC Adv. **6**, 50851–50857 (2016)
69. Kim, G., Jhi, S.H., Park, N., et al.: Optimization of metal dispersion in doped graphitic materials for hydrogen storage. Phys. Rev. B: Condens. Matter **78**, 085408 (2008)
70. Kim, K., Choi, J.Y., Kim, T., et al.: A role for graphene in silicon-based semiconductor devices. Nature **479**, 338–344 (2011)
71. Koskun, Y., Şavk, A., Şen, B., et al.: Highly sensitive glucose sensor based on monodisperse palladium nickel/activated carbon nanocomposites. Anal. Chim. Acta **1010**, 37–43 (2018)
72. Kosynkin, D.V., Higginbotham, A.L., Sinitskii, A., et al.: Longitudinal unzipping of carbon nanotubes to form graphene nanoribbons. Nature **458**, 872–876 (2009)
73. Kuila, T., Bose, S., Mishra, A.K., et al.: Chemical functionalization of graphene and its applications. Prog. Mater. Sci. **57**, 1061–1105 (2012)
74. Kwon, S.Y., Ciobanu, C.V., Petrova, V., et al.: Growth of semiconducting graphene on palladium. Nano Lett. **9**, 3985–3990 (2009)
75. Lee, C., Wei, X., Kysar, J.W., Hone, J.: Measurement of the elastic properties and intrinsic strength of monolayer graphene. Science **321**, 385–388 (2008)
76. Li, J.R., Kuppler, R.J., Zhou, H.C.: Selective gas adsorption and separation in metal-organic frameworks. Chem. Soc. Rev. **38**, 1477–1504 (2009)
77. Liu, J., Cao, G., Yang, Z., et al.: Oriented nanostructures for energy conversion and storage. Chemsuschem **1**, 676–697 (2008)
78. Liu, C., Li, F., Ma, L.P., Cheng, H.M.: Advanced materials for energy storage. Adv. Mater. **22**, E28–E62 (2010)

79. Lueking, A.D., Gutierrez, H.R., Fenseca, D.A., et al.: Combined hydrogen production and storage with subsequent carbon crystallization. J. Am. Chem. Soc. **128**, 7758 (2006)
80. Luo, B., Liu, S., Zhi, L.: Chemical approaches toward graphene-based nanomaterials and their applications in energy-related areas. Small **8**, 630–646 (2012)
81. Machado, B.F., Serp, P.: Graphene-based materials for catalysis. Catal. Sci. Technol. **2**, 54–75 (2012)
82. Malig, J., Jux, N., Guldi, D.M.: Toward multifunctional wet chemically functionalized graphene-integration of oligomeric, molecular, and particulate building blocks that reveal photoactivity and redox activity. Acc. Chem. Res. **46**, 53–64 (2013)
83. Mao, S., Pu, H., Chen, J.: Graphene oxide and its reduction: modeling and experimental progress. RSC Adv. **2**, 2643–2662 (2012)
84. Neto, A.H.C., Guinea, F., Peres, N., et al.: The electronic properties of graphene. Rev. Mod. Phys. **81**, 109 (2009)
85. Novoselov, K.S., Falko, V.I., Colombo, L., et al.: A roadmap for graphene. Nature **490**, 192–200 (2012)
86. Novoselov, K.S., Geim, A.K., Morozov, S.V., et al.: Electric field effect in atomically thin carbon films. Science **306**, 666–669 (2004)
87. Novoselov, K.S., Geim, A., Morozov, S.V., et al.: Two-dimensional gas of massless Dirac fermions in graphene. Nature **438**, 197–200 (2005)
88. Pamuk, H., Aday, B., Kaya, M., et al.: Pt Nps@GO as highly efficient and reusable catalyst for one-pot synthesis of acridinedione derivatives. RSC Adv. **5**, 49295–49300 (2015)
89. Park, C., Anderson, P.E., Chambers, A., et al.: Further studies of the interaction of hydrogen with graphite nanofibers. J. Phys. Chem. B **103**, 10572–10581 (1999)
90. Patchkovskii, S., Tse, J.S., Yurchenko, S.N., et al.: Graphene nanostructures as tunable storage media for molecular hydrogen. Proc. Natl. Acad. Sci. USA **102**, 10439–10444 (2005)
91. Pierson, H.O.: Handbook of Carbon, Graphite, Diamond and Fullerenes. New Jersey (1993)
92. Pumera, M.: Carbon nanotubes contain residual metal catalyst nanoparticles even after washing with nitric acid at elevated temperature because these metal nanoparticles are sheathed by several graphene sheets. Langmuir **23**, 6453–6458 (2007)
93. Pumera, M.: The electrochemistry of carbon nanotubes: fundamentals and applications. Chem. Eur. J. **15**, 4970–4978 (2009)
94. Pumera, M.: Graphene-based nanomaterials for energy storage. Energy Environ. Sci. **4**, 668–674 (2011)
95. Rao, C.N.R., Sood, A.K., Subrahmanyam, K.S.: Graphene: the new two-dimensional nanomaterial. Angew. Chem. Int. Ed. **48**, 7752–7757 (2009)
96. Rozhkov, A.V., Giavaras, G., Bliokh, Y.P., et al.: Electronic properties of mesoscopic graphene structures: charge confinement and control of spin and charge transport. Phys. Rep. **503**, 77–114 (2011)
97. Sahin, B., Aygun, A., Gunduz, H., et al.: Cytotoxic effects of platinum nanoparticles obtained from pomegranate extract by the green synthesis method on the MCF-7 cell line. Colloids Surf. B **163**, 119–124 (2018)
98. Sahin, B., Demir, E., Aygun, A., et al.: Investigation of the effect of pomegranate extract and monodisperse silver nanoparticle combination on MCF-7 cell line. J. Biotechnol. **260C**, 79–83 (2017)
99. Sahoo, N.G., Pan, Y., Li, L., et al.: Graphene-based materials for energy conversion. Adv. Mater. **24**, 4203–4210 (2012)
100. Sarma, S.D., Adam, S., Hwang, E.H., et al.: Electronic transport in two-dimensional graphene. Rev. Mod. Phys. **83**, 407–470 (2011)
101. Schwierz, F.: Graphene transistors. Nat. Nanotechnol. **5**, 487–496 (2010)
102. Sen, B., Akdere, E.H., Savk, A., et al.: A novel thiocarbamide functionalized graphene oxide supported bimetallic monodisperse Rh-Pt nanoparticles (RhPt/TC@GO NPs) for Knoevenagel condensation of aryl aldehydes together with malononitrile. Appl. Catal. B **225**(5), 148–153 (2018)

103. Sen, B., Aygün, A., Onal Okyay, T., et al.: Monodisperse palladium nanoparticles assembled on graphene oxide with the high catalytic activity and reusability in the dehydrogenation of dimethylamine-borane. Int. J. Hydrogen Energy (2018). https://doi.org/10.1016/j.ijhydene.2018.03.175
104. Sen, B., Demirkan, B., Levent, M., et al.: Silica-based monodisperse PdCo nanohybrids as highly efficient and stable nanocatalyst for hydrogen evolution reaction. Int. J. Hydrogen Energy (2018). https://doi.org/10.1016/j.ijhydene.2018.07.080
105. Sen, B., Demirkan, B., Savk, A., et al.: Trimetallic PdRuNi nanocomposites decorated on graphene oxide: a superior catalyst for the hydrogen evolution reaction. Int. J. Hydrogen Energy **43**, 17984–17992 (2018)
106. Sen, B., Demirkan, B., Simsek, B., et al.: Monodisperse palladium nanocatalysts for dehydrocoupling of dimethylamineborane. Nano-Struct. Nano-Objects **16**, 209–214 (2018)
107. Sen, B., Kuyuldar, E., Demirkan, B., et al.: Highly efficient polymer supported monodisperse ruthenium-nickel nanocomposites for dehydrocoupling of dimethylamine borane. J. Colloid Interface Sci. **526**, 480–486 (2018)
108. Sen, B., Kuzu, S., Demir, E., et al.: Highly efficient catalytic dehydrogenation of dimethyl ammonia borane via monodisperse palladium-nickel alloy nanoparticles assembled on PEDOT. Int. J. Hydrogen Energy **42**(36), 23307–23314 (2017)
109. Sen, B., Kuzu, S., Demir, E., et al.: Highly monodisperse RuCo nanoparticles decorated on functionalized multiwalled carbon nanotube with the highest observed catalytic activity in the dehydrogenation of dimethylamine borane. Int. J. Hydrogen Energy **42**(36), 23292–23298 (2017)
110. Sen, B., Kuzu, S., Demir, E., et al.: Hydrogen liberation from the dehydrocoupling of dimethylamine-borane at room temperature by using novel and highly monodispersed RuPtNi nanocatalysts decorated with graphene oxide. Int. J. Hydrogen Energy **42**(36), 23299–23306 (2017)
111. Sen, B., Kuzu, S., Demir, E., et al.: Monodisperse palladium-nickel alloy nanoparticles assembled on graphene oxide with the high catalytic activity and reusability in the dehydrogenation of dimethylamine-borane. Int. J. Hydrogen Energy **42**(36), 23276–23283 (2017)
112. Sen, B., Kuzu, S., Demir, E., et al.: Polymer-graphene hybrid decorated Pt nanoparticles as highly efficient and reusable catalyst for the dehydrogenation of dimethylamine-borane at room temperature. Int. J. Hydrogen Energy **42**(36), 23284–23291 (2017)
113. Sen, B., Lolak, N., Paralı, O., et al.: Bimetallic PdRu/graphene oxide based catalysts for the one-pot three-component synthesis of 2-amino-4H-chromene derivatives. Nano-Struct. Nano-Objects **12**, 33–40 (2017)
114. Sen, B., Savk, A., Kuyuldar, E., et al.: Hydrogen liberation from the hydrolytic dehydrogenation of hydrazine borane in acidic media. Int. J. Hydrogen Energy **43**, 17978–17983 (2018)
115. Sen, B., Savk, A., Sen, F.: Highly efficient monodisperse nanoparticles confined in the carbon black hybrid material for hydrogen liberation. J. Colloid Interface Sci. **520**, 112–118 (2018)
116. Sen, F., Boghossian, A.A., Sen, S., et al.: Observation of oscillatory surface reactions of riboflavin, trolox, and singlet oxygen using single carbon nanotube fluorescence spectroscopy. ACS Nano **6**(12), 10632–10645 (2012)
117. Sen, F., Boghossian, A.A., Sen, S., et al.: Application of nanoparticle antioxidants to enable hyperstable chloroplasts for solar energy harvesting. Adv. Energy Mater. **3**(7), 881–893 (2013)
118. Sen, F., Gokagac, G.: Different sized platinum nanoparticles supported on carbon: an XPS study on these methanol oxidation catalysts. J. Phys. Chem. C **111**, 5715–5720 (2007)
119. Sen, F., Gokagac, G., et al.: The activity of carbon supported platinum nanoparticles towards methanol oxidation reaction—the role of the metal precursor and a new surfactant, tert-octanethiol. J. Phys. Chem. C **111**, 1467–1473 (2007)

120. Sen, F., Gokagac, G.: Improving catalytic efficiency in the methanol oxidation reaction by inserting Ru in face-centered cubic Pt nanoparticles prepared by a new surfactant, tert-octanethiol. Energy Fuels **22**(3), 1858–1864 (2008)
121. Sen, F., Gokagac, G.: Pt nanoparticles synthesized with new surfactants: improvement in C_1–C_3 alcohol oxidation catalytic activity. J. Appl. Electrochem. **44**(1), 199–207 (2014)
122. Sen, F., Ertan, S., Sen, S., et al.: Platinum nanocatalysts prepared with different surfactants for C_1 to C_3 alcohol oxidations and their surface morphologies by AFM. J. Nanopart. Res. **14**, 922–926 (2012)
123. Sen, F., Karatas, Y., Gülcan, M., et al.: Amylamine stabilized platinum (0) nanoparticles: active and reusable nanocatalyst in the room temperature dehydrogenation of dimethylamine-borane. RSC Adv. **4**(4), 1526–1531 (2014)
124. Sen, F., Ozturk, Z., Sen, S., et al.: The preparation and characterization of nano-sized Pt-Pd alloy catalysts and comparison of their superior catalytic activities for methanol and ethanol oxidation. J. Mater. Sci. **47**, 8134–8144 (2012)
125. Sen, S., Sen, F., Boghossian, A.A., et al.: The effect of reductive dithiothreitol and trolox on nitric oxide quenching of single-walled carbon nanotubes. J. Phys. Chem. C **117**(1), 593–602 (2013)
126. Sen, F., Sen, S., Gokagac, G., et al.: Efficiency enhancement in the methanol/ethanol oxidation reactions on Pt nanoparticles prepared by a new surfactant, 1,1-dimethyl heptanethiol, and surface morphology by AFM. Phys. Chem. Chem. Phys. **13**, 1676–1684 (2011)
127. Sen, S., Sen, F., Gokagac, G.: Preparation and characterization of nano-sized Pt–Ru/C catalysts and their superior catalytic activities for methanol and ethanol oxidation. Phys. Chem. Chem. Phys. **13**, 6784–6792 (2011)
128. Sen, F., Sen, S., Gokagac, G.: High-performance Pt nanoparticles prepared by new surfactants for C_1 to C_3 alcohol oxidation reactions. J. Nanopart. Res. **15**, 1979 (2013)
129. Sen, F., Ulissi, Z.W., Gong, X., et al.: Spatiotemporal intracellular nitric oxide signaling captured using internalized, near-infrared fluorescent carbon nanotube nanosensors. Nano Lett. **14**(8), 4887–4894 (2014)
130. Shang, N.G., Papakonstantinou, P., McMullan, M., et al.: Catalyst-free efficient growth, orientation and biosensing properties of multilayer graphene nanoflake films with sharp edge planes. Adv. Funct. Mater. **18**, 3506–3514 (2008)
131. Shao, Y., Wang, J., Wu, H., et al.: Graphene based electrochemical sensors and biosensors: a review. Electroanalysis **22**, 1027–1036 (2010)
132. Singh, V., Joung, D., Zhai, L., et al.: Graphene based materials: past, present and future. Prog. Mater Sci. **56**, 1178–1271 (2011)
133. Slonczewski, J.C., Weiss, P.R.: Band structure of graphite. Phys. Rev. **109**, 272 (1958)
134. Soldano, C., Mahmood, A., Dujardin, E.: Production, properties and potential of graphene. Carbon **48**, 2127–2150 (2010)
135. Soodchomshom, B.: Switching effect in a gapped graphene d-wave superconductor structure. Phys. B **405**, 1383–1387 (2010)
136. Sun, Z., James, D.K., Tour, J.M.: Graphene chemistry: synthesis and manipulation. J. Phys. Chem. Lett. **2**, 2425–2432 (2011)
137. Stoller, M.D., Park, S., Zhu, Y., et al.: Graphene-based ultracapacitors. Nano Lett. **8**, 3498–3502 (2008)
138. Thayer, A.M.: Anticipating new commercial applications, producers increase capacity. Chem. Eng. News **85**, 29–35 (2007)
139. Terrones, M., Botello-Mendez, A.R., Campos-Delgado, J., et al.: Graphene and graphite nanoribbons: morphology, properties, synthesis, defects and applications. Nano Today **5**, 351–372 (2010)
140. Wang, H., et al.: Three dimensional graphene based materials: synthesis and applications from energy storage and conversion to electrochemical sensor and environmental remediation. Adv. Colloid Interface. Sci. **221**, 41–59 (2015)

141. Wang, H., Maiyalagan, T., Wang, X.: Review on recent progress in nitrogen-doped graphene: synthesis, characterization, and its potential applications. ACS Catal. **2**, 781–794 (2012)
142. Wang, L., Lee, K., Sun, Y.Y., et al.: Graphene oxide as an ideal substrate for hydrogen storage. ACS Nano **3**, 2995–3000 (2009)
143. Wang, Y., Wang, K., Guan, C., et al.: Surface functionalization-enhanced spillover effect on hydrogen storage of Ni–B nanoalloy-doped activated carbon. Int. J. Hydrogen Energy **36**, 13663–13668 (2011)
144. Wei, D., Liu, Y.: Controllable synthesis of graphene and its applications. Adv. Mater. **22**, 3225–3241 (2010)
145. Wei, W., Qu, X.: Extraordinary physical properties of functionalized graphene. Small **8**, 2138–2151 (2012)
146. Weiss, N.O., Zhou, H., Liao, L., et al.: Graphene: an emerging electronic material. Adv. Mater. **24**, 5782–5825 (2012)
147. Wu, C.D., Fang, T.H., Lo, J.Y.: Effects of pressure, temperature, and geometric structure of pillared graphene on hydrogen storage capacity. Int. J. Hydrogen Energy **37**, 14211–14216 (2012)
148. Xiang, Q., Yu, J., Jaroniec, M.: Graphene-based semiconductor photocatalysts. Chem. Soc. Rev. **41**, 782–796 (2012)
149. Xu, C., Xu, B., Gu, Y., et al.: Graphene-based electrodes for electrochemical energy storage. Energy Environ. Sci. **6**, 1388 (2013)
150. Yao, J., Sun, Y., Yang, M., Duan, Y.: Chemistry, physics and biology of graphene-based nanomaterials: new horizons for sensing, imaging and medicine. J. Mater. Chem. **22**, 14313–14329 (2012)
151. Yavari, F., Koratkar, N.: Graphene-based chemical sensors. J. Phys. Chem. Lett. **3**, 1746–1753 (2012)
152. Yildiz, Y., Erken, E., Pamuk, H., et al.: Monodisperse Pt nanoparticles assembled on reduced graphene oxide: highly efficient and reusable catalyst for methanol oxidation and dehydrocoupling of dimethylamine-borane (DMAB). J. Nanosci. Nanotechnol. **16**, 5951–5958 (2016)
153. Yildiz, Y., Esirden, I., Erken, E., et al.: Microwave (Mw)-assisted synthesis of 5-substituted 1H-tetrazoles via [3 + 2] cycloaddition catalyzed by Mw-Pd/Co nanoparticles decorated on multi-walled carbon nanotubes. ChemistrySelect **1**(8), 1695–1701 (2016)
154. Yildiz, Y., Kuzu, S., Sen, B., et al.: Different ligand based monodispersed metal nanoparticles decorated with rGO as highly active and reusable catalysts for the methanol oxidation. Int. J. Hydrogen Energy **42**(18), 13061–13069 (2017)
155. Yildiz, Y., Okyay, T.O., Gezer, B., et al.: Monodisperse Mw-Pt NPs@VC as highly efficient and reusable adsorbents for methylene blue removal. J. Cluster Sci. **27**, 1953–1962 (2016)
156. Yildiz, Y., Okyay, T.O., Sen, B., et al.: Activated carbon furnished monodisperse Pt nanocomposites as a superior adsorbent for methylene blue removal from aqueous solutions. J. Nanosci. Nanotechnol. **17**, 4799–4804 (2017)
157. Yildiz, Y., Okyay, T.O., Sen, B., et al.: Highly monodisperse Pt/Rh nanoparticles confined in the graphene oxide for highly efficient and reusable sorbents for methylene blue removal from aqueous solutions. ChemistrySelect **2**(2), 697–701 (2017)
158. Yildiz, Y., Pamuk, H., Karatepe, O., et al.: Carbon black hybrid material furnished monodisperse platinum nanoparticles as highly efficient and reusable electrocatalysts for formic acid electro-oxidation. RSC Adv. **6**, 32858–32862 (2016)
159. Yildiz, Y., Ulus, R., Eris, S., et al.: Functionalized multi-walled carbon nanotubes (f-MWCNT) as highly efficient and reusable heterogeneous catalysts for the synthesis of acridinedione derivatives. ChemistrySelect **1**(13), 3861–3865 (2016)
160. Yildirim, T., Ciraci, S.: Titanium-decorated carbon nanotubes as a potential high-capacity hydrogen storage medium. Phys. Rev. Lett. **94**, 175501 (2005)
161. Yu, A., Ramesh, P., Itkis, M.E., et al.: Graphite nanoplatelet–epoxy composite thermal interface materials. J. Phys. Chem. C **111**, 7565–7569 (2007)

162. Zhang, Y., Zhang, L., Zhou, C.: Review of chemical vapor deposition of graphene and related applications. Acc. Chem. Res. **46**, 2329–2339 (2013)
163. Zhang, N., Zhang, Y., Xu, Y.J.: Recent progress on graphene-based photocatalysts: current status and future perspectives. Nanoscale **4**, 5792–5813 (2012)
164. Zhao, G., Wen, T., Chen, C., et al.: Synthesis of graphene-based nanomaterials and their application in energy related and environmental-related areas. RSC Adv. **2**, 9286–9303 (2012)
165. Zhou, Y.G., Zu, X.T., Gao, F., et al.: Adsorption of hydrogen on boron-doped graphene: a first-principles prediction. J. Appl. Phys. **105**, 014309 (2009)
166. Zhu, Y., Murali, S., Cai, W., et al.: Graphene and graphene oxide: synthesis, properties, and applications. Adv. Mater. **22**, 3906–3924 (2010)
167. Zhu, Y., James, D.K., Tour, J.M.: New routes to graphene, graphene oxide and their related applications. Adv. Mater. **24**, 4924–4955 (2012)

Functionalized Graphene for Drug Delivery Applications

T. K. Henna, K. P. Nivitha, V. R. Raphey, Chinnu Sabu and K. Pramod

Abstract The unique characteristics of functionalized graphene make it a multi-faceted molecule having crucial therapeutic as well as medical significance. Different aspects of functionalized graphene are being discussed here. Functionalization of graphene could even scale up its importance. Functionalization can be done by different methods namely covalent functionalization, covalent functionalization with reaction intermediates, functionalization with nanoparticles, multi-functionalization, substitutional doping. These functionalization strategies mainly aim at reducing the in vivo and in vitro toxicity and agglomeration, moreover the main goal of functionalization is to disperse or solubilize it in different solvents. An Improvised drug and gene targeting nanocarrier system with unique properties have become possible with this graphene functionalization. The anticancer and antibacterial effect and several other applications of functionalized graphene are also being discussed.

Keywords Graphene · Graphene oxide · Functionalization · Covalent and non covalent functionalization · Drug delivery

T. K. Henna · K. P. Nivitha · V. R. Raphey · C. Sabu · K. Pramod (✉)
College of Pharmaceutical Sciences, Government Medical College, Kozhikode 673008, Kerala, India
e-mail: pramodkphd@yahoo.com

T. K. Henna
e-mail: hennatk13@gmail.com

K. P. Nivitha
e-mail: nivitha.kp@gmail.com

V. R. Raphey
e-mail: riyaraphey@gmail.com

C. Sabu
e-mail: chinnu824@gmail.com

A. Khan et al. (eds.), *Graphene Functionalization Strategies*, Carbon Nanostructures, https://doi.org/10.1007/978-981-32-9057-0_11

1 Introduction

Graphene is a crystalline two-dimensional allotropic form of carbon, consisting of a single layer of sp^2 hybridized carbon atoms and they are arranged in a hexagonal lattice. Even though they are of single atom scale thickness, they are the hardest material ever known. Thus, they can be processed into thin sheets. They draw attention due to their unique features like high surface area, high strength, high thermal conductivity, electrical conductivity, the excellent transmittance of light, lower toxicity, and low cost [1]. Graphene family of nanomaterials includes single-layer graphene, bilayer graphene, multilayer graphene, Graphene oxide, reduced graphene, and chemically modified graphene. This classification is based on a number of layers, oxygen content, surface chemistry, purity, and their composition. Since graphene doesn't contain any oxygen groups, it possesses high electrical and optical conductivity [2]. Graphene forms stable colloid in various solvents [3]. But graphene oxide have oxygen-containing functional groups, thus they have relatively poor electrical and optical conductivity. Graphene is hydrophobic and poorly dispersible in water. Thus, its biomedical application is limited. It is overcome by converting graphene to graphene oxide. Graphene oxide is hydrophilic in nature, but it is toxic [2]. Functionalization with biocompatible polymers such as PEG reduces the in vivo and in vitro toxicity of graphene oxide [4]. To improve the electrical conductivity of functionalized graphene oxide, it is converted to functionalized graphene by reduction. Hydrazine monohydrate, sodium borohydride, p-phenylenediamine, hydroquinone, and sodium hydrosulfite are used as reducing agents. Since they are hazardous, some other reducing agents are also employed. Acetic acid and HCl act as good reducing agents and they are used as an alternative to hydrazine monohydrate [4].

Reduced graphene possess high conductivity than GO, but less than graphene. And reduced graphene oxide also exhibits high solubility than graphene, but less than graphene oxide. The oxygen-containing functional group is higher in graphene oxide than reduced graphene oxide. The differences in their physicochemical properties are represented in Fig. 1. Crystal structure of reduced graphene oxide is better than graphene oxide [2].

2 Structure

Graphene is a unique single-layered carbon foil having two-dimensional structures. The term graphene originates as a coalition of graphite and the suffix-ene [5]. Usually, graphene consists of six atoms which look like one atom thickness honeycomb network with sp^2 hybridization. The C–C bond length is 1.42 A and bond angle 120°. The structure of graphene is somewhat similar to that of benzene especially the bonding arrangement. Hence graphene can be considered as an enormous polycyclic aromatic hydrocarbon (PAH) [6]. When considering the

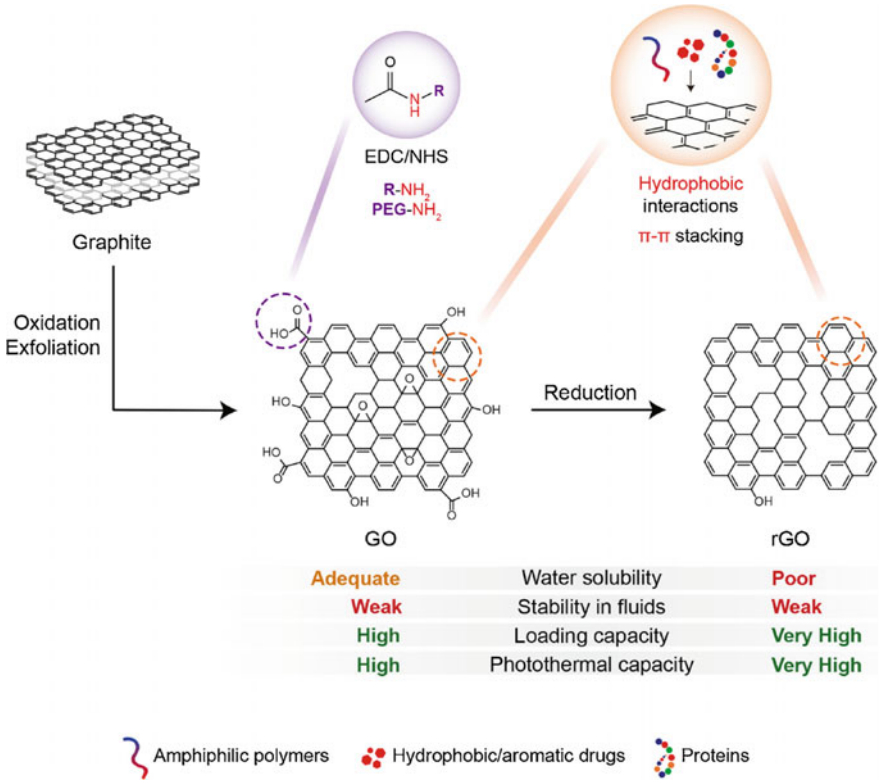

Fig. 1 Schematic representation of the synthesis and physicochemical properties of graphene oxide and reduced graphene oxide. Reprinted from [32], © 2018, with permission from Elsevier

microscopical structure of graphene flakes; one edge is highly dominated by the zig-zag edges and the other side has armchair orientation. It has several functional groups on the surface, such as epoxy, carboxyl, and hydroxyl. The peripheral carboxylate group is responsible for colloidal stability and pH-dependent negative surface charge. Epoxide and hydroxyl groups are uncharged but polar. Thus it allows weak interactions, hydrogen bonding and other surface reactions [7].

3 Synthesis

Pristine graphene is hydrophobic, and its biomedical applications are comparatively limited. Thus an alternative graphene form is discovered [8]. For the synthesis of processable graphene, graphene oxide (GO) has been commonly used as starting material. There are plenty of methods proposed by several researchers about the preparation of reduced graphene oxide (RGO). Graphene can be produced from

graphite and non-graphite sources. The synthesis of graphene can be done by two methods namely top-down and bottom-up. The top-down methods include mechanical cleavage, redox method, and arc discharge. While the bottom-up method includes chemical vapor deposition and organic synthesis [6].

Graphene was first exfoliated mechanically from graphite in 2004 [9]. In redox method, graphite is first treated with an oxidizing agent to change the crystalline shape and structure of graphite and then treated with strong acid to form graphene oxide. This GO is reduced to graphene [6]. In 1859, the first chemical exfoliation of graphite was performed by extensive oxidation of graphite by exposing to a mixture of fuming nitric acid, potassium chlorate for few days [10]. In 1898, this method is modified by exchanging 2/3rd of fuming nitric acid to sulphuric acid and used multiple aliquots of potassium chlorate. This addition of potassium chlorate leads to explosion [11]. Thus, this is again modified in 1958 by reacting graphite powder (100 g) with a mixture of sodium nitrate (50 g), sulphuric acid (2.3 L) and potassium permanganate (300 g) [12]. Hummer's method is the most commonly used method for graphene oxide synthesis in laboratory scale. The drawback of this method is that it produces toxic gases like NO_2 and N_2O_4 and can't be synthesized in large scale [13]. Arc discharge method was used in large-scale preparation, in this method electric current is passed between two electrodes made of graphite at a particular pressure. During this process, the anode will be consumed and the product graphene is obtained on the cathode. Graphene obtained by this method exhibits better electrical conductivity, high crystallization, and thermal stability [6]. Chemical vapour deposition method is the most promising method. It is also known as surface segregation method on a solid surface. The principle involved is that, when hydrocarbon (usually methane CH_4) exposed to heated metal surfaces like nickel and copper under vacuum, a carbon film with single crystal size was formed. The metal leads to the loss of hydrogen and dissolves the carbon to form a metal carbide layer. As the temperature decreases, saturation of metal carbide surface layer occurs which leads to precipitation of graphite carbon from carbide sol [14]. Diluted methane gas (CH_4) is used as a carbon precursor and produced a single-layered graphene. Copper can control the layer formation because of its lowest carbon solubility, thus it is used to prepare large sheet (75 cm) of single-layered graphene. Nickel can't control the number of layers, but the alloy form of nickel gives a better result. Cu–Ni alloy can be used to prepare single-layered graphene [15]. The thickness and width of graphene nanoribbon can be adjusted by changing annealing temperature, time of exposure and nature of substrate metal [16].

4 Functionalization

Since graphene is hydrophobic, it aggregates in an aqueous medium such as proteins, salts, buffer or cell medium, which may be lead to toxicity. This is due to the electrostatic interactions and non-specific interactions between charged graphene

and proteins. So the surface of graphene should be functionalized or modified chemically [2]. Suitable chemical functionalization protects graphene from agglomeration and maintains its inherent properties. Graphene oxide exhibits toxicity. Functionalization with biocompatible polymers such as PEG reduces in vivo and in vitro toxicity. The main purpose of functionalization is to dissolve or solubilize them in a variety of solvents such as water, DMF, chloroform, THF etc. [4]. Graphene can be functionalized via covalent and non-covalent methods by using poly ethylene glycol (PEG), poly ethylene imine, gelatin, chitosan or sulfonic acid groups. When GO is functionalized with polar polymers such as chitosan, polyethylene glycol and polyethyleneimine (PEI), their half-life in systemic circulation is increased and identification by the reticuloendothelial system may be decreased [17]. Functionalization can be performed by two methods, covalent and non-covalent modifications.

4.1 Covalent Modification

To improve the stability of graphene oxide or reduced graphene oxide in a physiological medium, some organic molecules are covalently attached to their surface. Biocompatible PEG was the first molecule attached covalently [2]. Covalent functionalization of graphene solves the issue of poor dispersibility in certain solvents [18]. The mechanism of covalent bond formation involves, (a) Covalent bond formation between free radicals or compounds that readily reacts with dienes and C=C bonds present in graphene or (b) Formation of a covalent bond between organic functional groups and oxygen groups present in GO [19]. GO can be functionalized with D-mannose using mannosylated ethylenediamine. This reduces toxicity to red cells [20]. The covalent modification can be achieved by four methods, nucleophilic substitution, electrophilic substitution, condensation, and addition.

Nucleophilic substitution

The reactive site for the nucleophilic substitution is mainly epoxide groups on the GO. The modifying agent used is amine terminal groups such as amino acids or alkyl amines. The lone pair electron present on the amine ($-NH_2$) group of modifier attacks the epoxy group of GO. Nucleophilic substitution methods are commonly used functionalization techniques because it is very simple, it can be performed in room temperature. This method is employed as large-scale production of GO.

Amines and amino acids are used for functionalization of graphene. Functionalization by small chain primary amines was carried out at room temperature and long-chain aliphatic amines by heating the reaction mixture and refluxed for 24 h [21].

Electrophilic substitution

In this reaction, the hydrogen atom is displaced by an electrophile. Consider, spontaneous grafting of diazonium salt of p-nitro aniline to graphene surface.

Condensation reaction

In the condensation reaction, two molecules combine together to form a single molecule with a loss of small molecules. Through amide and carbamide ester linkages condensation reaction occurs by agents such as isocyanate, diisocyanate, and amines.

Addition reaction

In an addition reaction, two or more molecules combine to form a large molecule. Maleic anhydride can be added to graphene surface in the presence of free radicals. They are highly soluble in THF and are more stable [4].

4.2 Non-covalent Modification

The non-covalent modification is the physical adsorption of certain molecules on graphene surface through π–π stacking interaction, hydrophobic, van der Waals, and electrostatic forces. It is performed through polymer wrapping, adsorption of surfactant or small aromatic molecules and interaction with porphyrins, DNA or peptides. First non-covalent functionalization of graphene nanosheets was performed by using poly (sodium 4-styrene sulfonate). It is prepared by exfoliation and simultaneous reduction of GO using PSS and the obtained product was found to be highly dispersible in water [22]. Sodium deoxycholate, protein, DNA, tween can also be used for non-covalent modification [2]. Nafion graphene nanocomposite was prepared by dispersing nafion in an aqueous solution of graphene and it is reduced by hydrazine. This exhibits excellent electrical conductivity [23]. Non-covalent functionalization has several advantages such as it minimizes the chemical reaction, reduces purification step and it retains the physical properties of GO. Additionally, non-covalent functionalized graphene oxide can work as both a stabilizer for preventing aggregation and as a targeting agent [24]. But the disadvantage is that non-covalent functionalization is not as strong as covalent and it may undergo some variations in the external environment. It may lead to less stable drug delivery. And the drug loading capacity of non-covalent functionalized graphene oxide is less. It is experimentally proved by using covalent and non-covalent modified PEI-GO. The results show that non-covalent modified PEI-GO was less stable [2].

4.3 Covalent Functionalization with Reaction Intermediates

Free radicals, nitrenes, and carbenes are major reaction intermediates. Free radicals are most commonly used for graphene functionalization and are produced from diazonium salt and benzoyl peroxide. During the reaction, electron transfer occurs from graphene to aryl diazonium ion to form aryl radicals that are added to graphene to form covalent adducts. Nitrenes are another reaction intermediates, used for graphene functionalization, formed by thermal or photochemical activation of organic azides. Carbenes undergo CH insertion and C=C cycloaddition reactions with graphene, but they are less frequently used than nitrenes [25].

4.4 Functionalization with Nanoparticles

Graphene is also functionalized with metal nanoparticles, metal oxide nanoparticles, quantum dots, and some other nanoparticles. Noble metals such as Pt, Au, Rh, Pd are used for the functionalization of graphene. Gold nanoparticles on graphene sheets are synthesized by direct reduction of $AuCl_4$ by $NaBH_4$ in a suspension of GO THF. It is found that Pd has a greater affinity towards graphene than Au; the reason suggested is partial covalent binding between Pd and graphene. Metal oxides such as Tin oxide (SnO_2), manganese oxide (Mn_3O_4), cobalt oxide (Co_3O_4) and titanium oxide (TiO_2) nanocrystals are also deposited on graphene surface and are used as anodes in Li-ion batteries. Graphene quantum dots are formed when quantum dots deposit on graphene surface and they have wide range of applications in drug delivery, biological labelling and can be used solar cells and LED preparation [19].

4.5 Substitutional Doping

sp^2 hybridized carbon atoms of graphene lattice can be substituted by nitrogen or boron atoms. By controlling the degree of doping, the electrical properties of graphene can be adjusted. In nitrogen doping, the lone pair of nitrogen atoms conjugates with π system of graphene. N-doped graphene sheets are electron rich, thus n-type semiconducting behavior is expected. Wang et al. performed N-doping of graphene nanoribbons by using high power electrical joule heating in ammonia gas. They also conducted N-doping and simultaneous reduction of GO during annealing in Ammonia. GO was heated from 300 to 500 °C and small amounts of N-doped GO was produced by this method. The efficiency of N-doping depends upon the number of oxygen groups at the edge sites of GO [19]. Functionalization of graphene is very essential to prevent aggregation, but it reduces the electrical conductivity. But, the separation of the excess chemical modifying agent from the functionalized graphene is difficult [20].

4.6 Multi Functionalization

Graphene can also be functionalized by two or more molecules. PEG and PEI were covalently conjugated to graphene oxide through amide bonds. It gives physiologically stable ultra small size conjugate [26]. Multi-functionalized graphene oxide has several advantages and is extensively used in targeted drug delivery. They are described in the application section of this paper.

5 Properties of Functionalized Graphene

Graphene is a compound possessing honeycomb shaped crystal lattice and is highly bonded to each other via sp^2 bonds. Studies have shown that it is the strongest material that has ever tested i.e. 200 times stronger than steel. Graphene is a semiconductor with zero band gaps. Other dominant characters include high thermal conductivity $\sim(4.84 \pm 0.44) * 10^3$ to $(5.30 \pm 0.48) * 10^3$ Wm K^{-1}. The boundary molecular electrons of different organic molecules interact with the π electrons in the graphene molecule which becomes the main reason of preferring electrophilic substitution over nucleophilic substitution. And other reactions include cyclo-additions, click reactions, carbene-insertion reactions [4]. Focusing on to the mechanical properties, graphene has high Young's modulus. The effect of temperature on mechanical strength was studied, and the research shows that temperature decreases the mechanical strength. They also concluded that functionalization of graphene with certain groups have a negative effect on mechanical strength. Young's modulus decreases by adding certain groups. It is in the order of Y (NH_2) > Y (C_6H_5) > Y (OH) > Y (CH_3). Physicochemical properties such as large specific surface area, unique 2D structure, and π electron cloud make graphene suitable for interaction with a different organic molecule and thereby proving that it has wide application in different drug delivery systems [27].

Another excellent property of Graphene is its optical characteristics. It was found that single-layer graphene transmits 97.7% of the total incident light and also the light absorption capacity increase as the number of layers increases. By using this unique property it has been widely used in different electro-optical devices like tunable IR detectors, modulators and emitters by electrical gating and charge injection. Other optical properties include great light transmittance, photoluminescence, and better charge mobility make graphene a significant biomedical tool and can take part in different imaging techniques like magnetic resonance imaging (MRI) and biomedical imaging [7].

6 Characterization of Functionalized Graphene

Focusing on the characterization of single-layered graphene that exhibits unique features when compared with double or multi-layered graphene is considered more relevant in an application level [4]. Various methods that prevail for the characterization of functionalized graphene are discussed in this section.

X-ray diffraction

Graphene oxide is having a broad peak at 10.9°, whereas the pure graphite powder is exhibiting a peak at 26° [28]. Although X-ray diffraction is informative, these studies are limited in the identification of single-layered graphene. The similar X-ray diffraction pattern is exhibited by single-layered graphene oxide as well as the single-layered graphene [4]. Exfoliation of graphite oxide into single-layer graphene oxide gives a straight line in the X-ray diffraction pattern with no diffraction peak.

UV-visible spectroscopy

UV-visible spectroscopic methods are successful in providing information regarding the number of layers and the graphene formation. An absorption peak at 262 nm is exhibited by 2-dimensional graphene and a peak at 230 nm by single-layered graphene oxide in the UV-visible spectrum. And this peak is due to the π–π* transition of the aromatic C–C bonds. At a wavelength of the 550 nm monolayer, graphene nanosheets are having a transmittance of 97.1% [4].

Transmission electron microscopy

Transmission electron microscopy gives an accurate idea regarding the thickness and the number of layers present in the graphene sample. An analysis of the TEM images (Fig. 2) obtained by keeping the folded graphene sheets parallel to the electron beam will provide information about the number of layers present in graphene. The small area electron diffraction (SAED) ensures more accurate data [4].

Raman spectroscopy

Raman spectroscopy is the most effective and fast approachable method for the determination of the quality of exfoliated graphene and serves as a characterization tool for the analysis of graphene-based materials. The method is used to analyze the molecular functionalization, doping effects, oxidation and number of layers on graphene. For this purpose, Raman spectroscopy uses its most significant indicators namely-D, G and 2D modes [29]. The vibration of the sp^2 bonded carbon atoms in the two-dimensional hexagonal lattice a peak at 1576 cm^{-1} is exhibited by chemically reduced graphene. The peak obtained at 1326 cm^{-1} is the result of the defects and disorders chemically reduced graphene. Raman spectroscopy is highly efficient in distinguishing single layered, double layered and other multilayered graphene sheets. A G band and the 2D band are given by graphene at 1580 and 2700 cm^{-1} respectively in the Raman spectra [4].

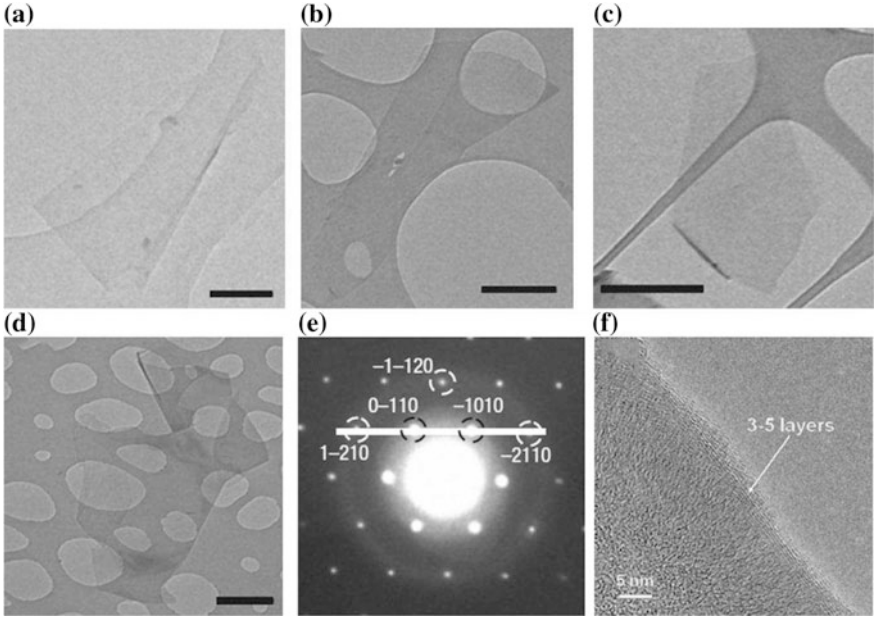

Fig. 2 TEM and HR-TEM of Graphene. Reprinted from [4], © 2012 with permission from Elsevier

Fourier transforms infrared spectroscopy (FTIR)

The Fourier transform infrared spectroscopic method provides all the information regarding the functionalities of graphene oxide. In FTIR spectra of graphene oxide, it exhibits a peak at 3400 and 1620 cm^{-1} because of the stretching vibration of OH groups and the skeletal vibration of graphene oxide sheets respectively [30].

7 Applications

7.1 Functionalized Graphene in Drug Delivery

The two dimensional sp^2 hybridized carbon network of graphene has a tremendous range of applications in drug delivery, biosensors, nanoelectronics, and polymer nanocomposites. Aggregation and processing problems of pure graphene can be overcome by using functionalized graphene which will pay a huge path in the research field as well as in the therapeutic field. Graphene oxide is the derivative of graphene-based materials, which have the good biocompatibility, hypotoxicity, so many functional groups on the surface (epoxide, hydroxyl and carboxyl groups), high strength, surface area, electrical and thermal conductivity, flexibility,

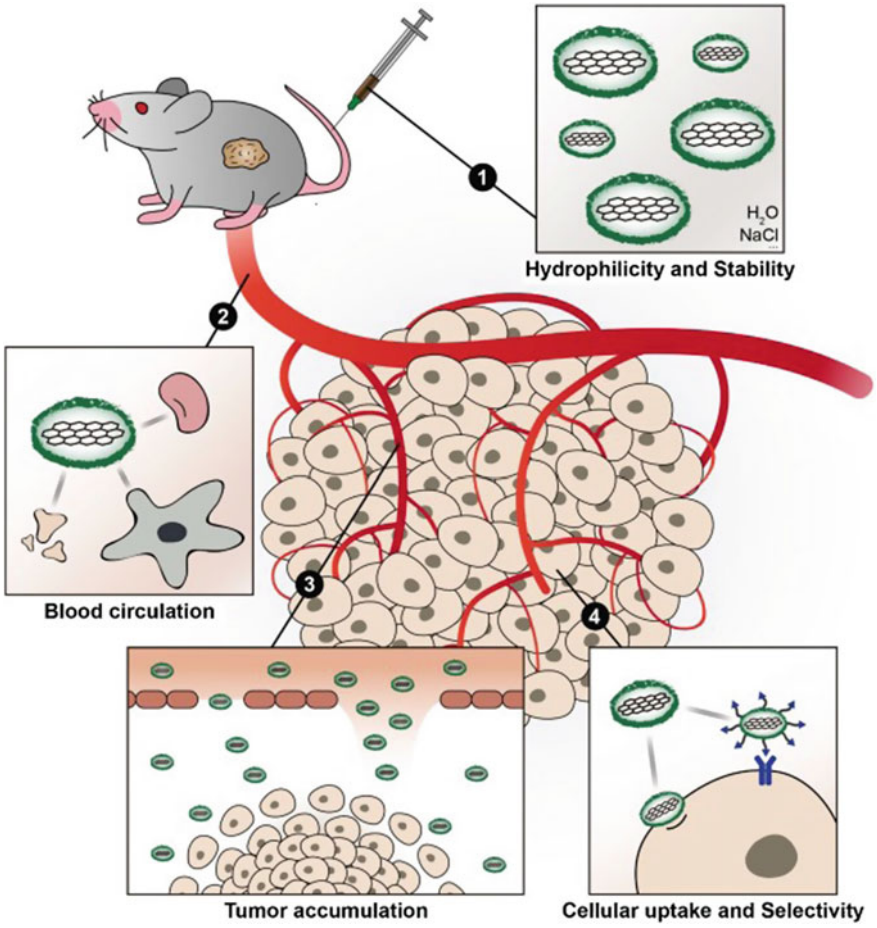

Fig. 3 Schematic representation of the different barriers and barrier crossing by functionalized graphene in order to accumulate in the tumor cells and internalized by cancer cells. Reprinted from [32], © 2018, with permission from Elsevier

transparency and low cost [31]. Functionalization of graphene facilitate easy delivery of different drug molecules and other nanomaterial's and help to cross different biological barriers which enable an efficient and site-specific accumulation at tumor cells as shown in Fig. 3 [32].

Moreover the toxicity studies of pristine graphene and carboxylated graphene (COOH–GO) in monkey kidney cell. It is noticed that pristine graphene was accumulated in the cell membrane and leads to destabilization of F-actin alignment and COOH–GO internalized by the cells and accumulated in the perinuclear region without causing any membrane destabilization even at higher concentration [33]. Pristine graphene generates intracellular reactive oxygen species and it causes damage to DNA and protein and finally leads to cell death via apoptosis or necrosis.

Sharp edges of graphene may cause membrane destabilization and loss of cell integrity when they become direct contact with the cell surface. *A*dsorption of GO on the surface of RBC causes loss of cell membrane and leads to hemolysis [34]. Immunotoxicity study of GO and PVP functionalized GO against human immune cells such as T-lymphocyte, dendritic cell and macrophages were performed. The result shows that PVP functionalized GO have lower immunogenicity than pristine graphene oxide [35]. These studies reveal that functionalization reduces the toxicity of graphene. For the researchers in the pharmaceutical field, graphene opens a new world of drug delivery. Their high dispensability in polar solvents, ability to undergo chemical modifications and excellent loading ability for aromatic drugs, functionalized graphene is recognized as the ideal candidate for drug delivery [36].

Recently, the graphene oxide based targeted drug delivery has become a great interest of topic for many researchers. Drug or gene can be loaded to modified graphene-based nanomaterials by hydrophobic interactions, π–π stacking, and electrostatic interactions. Carriers are made to respond to internal stimuli such as body temperature, pH, specific chemical reaction or external stimuli such as light, field, and ultrasound. The pH of a tumor micro environment, intracellular lysosomes and endosomes are acidic. Thus, pH responsive graphene-based nanocarriers are developed for cancer therapy. For achieving targeted therapy, targeting molecules like folic acid, antibody, carbohydrate, peptide, protein, and aptamers are coupled on the surface of graphene oxide. The Photosensitizer can be loaded on the graphene-based material surface to use in photodynamic therapy. Chemotherapic agent, 1,3-bis (2-chloroethyl)-1-nitrosourea was loaded into PAA-GO via ester linkage for malignant brain tumor therapy. It improves the thermal stability and half-life of the loaded drug. The drug release is controlled by the hydrolysis of ester linkage [2]. Studies on aptamer-conjugated magnetic graphene oxide nanocarriers for specifically targeting the tumor cells loaded with an anticancer agent has provided an entrapment efficiency of 95.75% and good release percentage also [37].

A novel advancement in graphene-based drug delivery is the approach to develop a dual faced graphene oxide by simultaneous grafting of different polymers with different hydro-affinity. This dual drug loaded graphene-based system is a promising approach for combination therapy, that could completely circumvent chemotherapeutic drug resistance in cancer therapy [38]. With the idea of developing a pH sensitive drug carrier, carboxy methylcellulose modified graphene oxide has been developed that could provide a controlled and sustained drug release with small side effects and improved drug bioavailability [39]. In order to overcome the compromised biocompatibility of graphene oxide hyperbranched polyglycerol conjugated graphene oxide has been synthesized. The chemotherapeutic effect was evaluated after loading an antitumor drug to the surface modified graphene oxide, the carrier [40]. Rivastigmine loaded hydrogel beads based on ion-crosslinked gum tragacanth and graphene oxide was prepared. In this preparation, the use of GO increased swelling capacity, entrapment efficiency and controlled release [41]. Since fluorinated graphene is hydrophobic, a nanosized water-soluble fluorinated graphene oxide (FGO) sheets were developed, which shows bright fluorescence used for controlled and targeted drug delivery. FGO can be modified with folic acid

for targeted cancer therapy. The small size enables them to easily endocytosed into cells. They also possess photothermal effects, thus doxorubicin loaded FGO shows synergistic chemo-photo thermal effects in cancer therapy. Their study concluded that FGO can be used as a drug carrier and photothermal agent and it can overcome the systemic drug-related toxicity [42]. Graphene can be surface functionalized by different functionalizing agents like hydroxyl (OH), carboxyl (COOH), methyl (CH_3) and amine (NH_2) groups. A comparison study reveals that G–COOH is considered as strongest. The study was conducted by using doxorubicin as a drug model and the studies have shown that G–COOH adsorbs DOX more effectively because of its high surface binding energy [43]. Zwitter ion modified graphene oxide was developed by using a kind of zwitterion based saline, 3-(dimethyl(3-(trimethoxysilyl)propyl)-amino)propane-1-sulfonate (SBS). They exhibit more stability in both sera free and serum containing solution. Drug-loaded SBS-GO shows thermosensitivity and sustained release nature. Doxorubicin-loaded SBS-GO can be easily internalized by HepG2 cells and exhibits remarkable cytotoxicity [44]. Functionalization of graphene with sulfonate groups and grafting with polyurethane yields polymer with improved properties. It shows high corrosion resistance and is used as filler. It releases cancer drug in a sustained manner [45].

Graphene oxide–galic acid nano-delivery system can release anticancer agent galic acid in a sustained manner. It is effective against liver cancer cells (HepG2) [46]. Dopamine (DA) functionalized graphene oxide nanocarriers are developed and loaded anticancer methotrexate. This is effective against DA receptor-positive human breast cancer adenocarcinoma cell line. Since it is dopamine functionalized, it can be easily targeted to the cell [47]. Considering the high potential of graphene oxide, especially when conjugated with polyethyleneimine for stem cell-induced osteogenesis during fracture healing and tissue engineering also the ability of graphene oxide for promoting the efficient loading and controlled release of aspirin from titanium implants, the surface modification of titanium with graphene oxide could lead a path for the improved success rate of titanium implants in patients [48].

A synergistic anticancer activity was developed by combining the therapeutic actions of curcumin and graphene oxide. The curcumin uptake was found to be improved with the number of oxygen functional groups [49]. Another highly potent nanocomposite of curcumin, paclitaxel and graphene oxide of size 140 nm was synthesized to get synergistic action towards lung and breast carcinoma cells. The higher curcumin load was an advantage of using graphene oxide as the nanocarrier it also can improve the bioavailability of the curcumin-paclitaxel drug complex. The reduced graphene oxide carrier was further improvised with an amphiphilic polymer P-127 [50]. The protein delivery in various genetic and refractory diseases has been compromised due to the proteolytic cleavage resulting in short half-life and instability. A new protein nanocarrier was developed combining graphene oxide with chitosan that could avoid the proteolytic cleavage. Studies were conducted by loading the novel protein nanocarrier with bovine serum albumin and this could provide protection against proteolytic cleavage. Thus this chitosan modified graphene oxide nanocarrier was proven as the effective platform for protein delivery [51]. A new hypothesis has been improvised for targeting the lung carcinoma cells

by synthesizing the molybdenum disulfide conjugated graphene oxide. This molybdenum disulfide-graphene oxide nanocomposite is exhibiting an excellent tumor targeting action along with a high drug loading capability. Additional advantages of good biocompatibility and aqueous dispersibility have been obtained with these nanocarriers [52]. Sodium alginate was covalently linked to graphene oxide with the help of adipic acid dihydride, and doxorubicin was loaded to this. pH responsive release of DOX is achieved at a faster rate. It has a cytotoxic effect against HeLa cells. This nanocarrier enters into the cell by receptor-mediated endocytosis [53].

Graphene functionalization for the development of stimuli-responsive nanocarriers in order to achieve the goal of nuclei based targeted drug delivery is one of the most researched areas. Extensive studies have been conducted by utilizing acidic pH, high intracellular levels of glutathione and near-infrared for the cytosolic delivery of DOX. Doxorubicin-loaded graphene oxide has been developed as a solution for the cancer drug resistance in DOX-resistant MCF-7/ADR cells. And this strategy of DOX delivery by graphene oxide surface loading could satisfactorily improve the cytotoxic effect. The surface functionalization of graphene with natural biopolymers like gelatin and chitosan is useful in reducing the toxic effects of graphene and enhancing the drug loading capacity of graphene. Studies on the development of DOX-loaded GO-folic acid β-cyclodextrin complex, the co-delivery of multiple drugs using graphene oxide and enabling the controlled release of various kinds of drugs from chitosan-GO complex itself explains the significance of graphene as a drug delivery system or the drug carrier [7].

Numerous studies are still going on in the cancer treatment. The great challenge existing is, to target the drug to the affected tissues or cells specifically and to protect normal cells from the damage. The study of the anticancer activity of graphene nanosheets was done by exfoliating graphene sheets by using polyvinyl pyrrolidone which is having an average particle size of 42 nm. The study was performed on various cells like HCT-116, HeLa, SCC-9, NIH-3T, and HEK-293. Researchers have shown that the combination of graphene–polyvinyl pyrrolidone nanoparticle have anticancer activity and act as a pH-sensitive drug carrier for certain anticancer drugs like doxorubicin, as shown in Fig. 4. The graphene-PVP complex loaded with drug by tip ultrasonication thereby forming a stable complex.

Doxorubicin release from the complex in a sustained fashion about 2–3 days in normal as well as in acidic pH It has been found that an anticancer drug-loaded graphene-PVP complex is found to be a most innovative method to treat cancer even though long-term exposure (48–72 h) to graphene-PVP cause mitochondrial toxicity in normal cells. Exfoliated graphene nanosheets based drug carriers will make a revolution in the field of future oncology studies and other drug delivery systems [54]. A schematic representation of the mechanism of graphene-PVP-NP induced cytotoxicity in cancer cells is shown in Fig. 5.

In an earlier study, it was shown that β-cyclodextrin is not considered as a suitable carrier for the poorly water-soluble anticancer drug. But it can be combined with a magnetic compound to produce β-cyclodextrin (β-CD) grafted magnetic graphene oxide nanocarrier and used for the delivery of both hydrophilic and

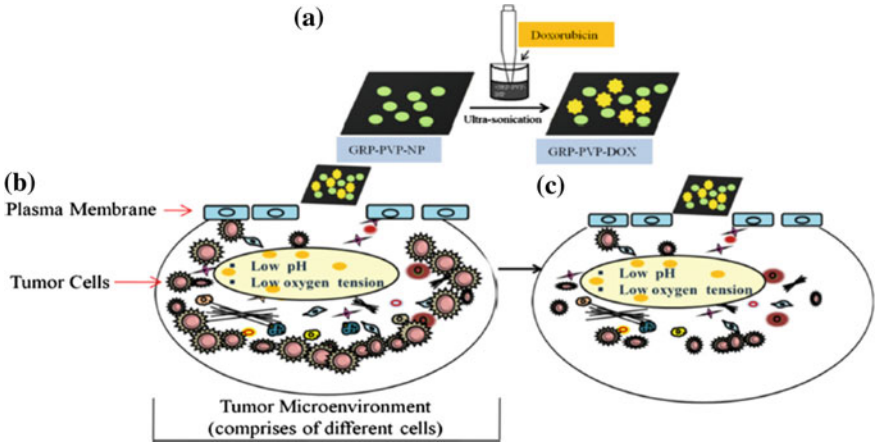

Fig. 4 **a** Loading of doxorubicin in the graphene-PVP complex; **b** release of drug from the complex at low pH and low oxygen concentration which is corresponding to the environment in tumor cells; **c** reduction in the cancer cell growth. Reprinted from [54], © 2017, with permission from Elsevier

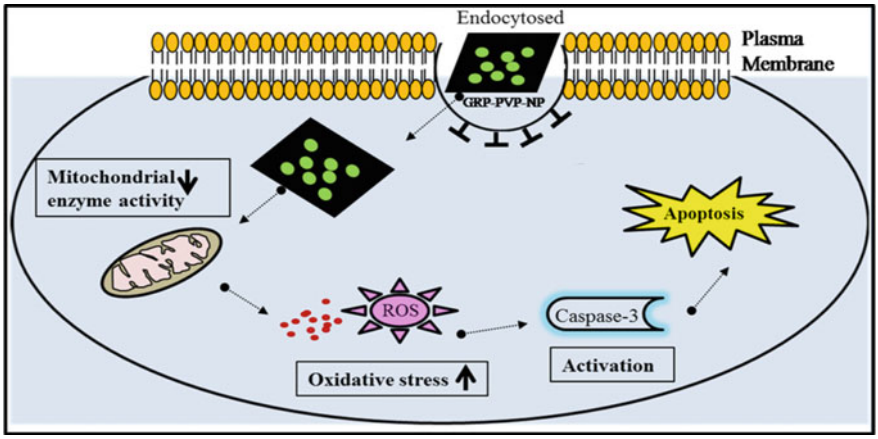

Fig. 5 Schematic representation of the mechanism of graphene-PVP-NP induced cytotoxicity in cancer cells. Reprinted from [54], © 2017, with permission from Elsevier

hydrophobic drugs. MG can be prepared by inverse chemical co-precipitation iron on GO [55]. Chemical co-precipitation of Fe_3O_4 magnetic particles on the surface of GO nanoplatelet leads to the formation of magnetic graphene oxide (MGO). It is then modified with chitosan and MPEG via a covalent linkage to form MgoC-PEG. The anticancer Irinotecan or doxorubicin can be successfully loaded to this magnetic carrier system and are effectively targeted magnetically to U87 cells. PEG enhances the circulation time and decreases the reticuloendothelial system uptake

[56]. Similarly, another magnetic nanocarrier was developed by mounting supra magnetic iron oxide nanoparticle on graphene oxide and then coating PVA. To this carrier system, 5-fluoro uracil was loaded, which releases the drug in controlled release at acidic pH 5.8. PVA increases the circulation time of the drug. This system acts as both imaging and drug delivery system.

Change in pH is a marker of tumor environment, thus a pH sensitive PAA functionalized graphene oxide is used to carry gemcitabine, an analog of deoxycytidine nucleoside for the treatment of ovarian and metastatic breast cancer [57]. Hypericin, a natural photosensitizer, isolated from *Hypericum perforatum* can act as a ligand to target mitochondria. It can penetrate the mitochondrial double membrane. Hypericin-functionalized graphene oxide loaded with doxorubicin gives synergistic anti-tumor effect [58]. Similarly, synergistic chemo and phototherapy by formulating polylysine functionalized graphene were also demonstrated. The photosensitizing agent Zn (II)-phthalocyanine and chemotherapeutic agent doxorubicin was loaded to biocompatible poly-L-lysin functionalized graphene. This nano complex shows high solubility and stability in biological solutions [59]. Pirfenidone is a drug used for the treatment of subarachnoid hemorrhage. It prevents secondary bleeding and cerebral infarction. This activity of Pirfenidone can be improved by loading into a functionalized graphene. Graphene oxide is first treated with transcription activator peptide (Tat) and then functionalized with methoxy Polyethylene glycol and then Pirfenidone was loaded. This carrier system can easily penetrate the blood-brain barrier (BBB) due to the presence of transcription activator peptide. It has a good loading capacity and a fast release at lower pH. Pirfenidone loaded to functionalized graphene oxide shows better activity than single pirfenidone [60].

Aptamer coated dextran functionalized graphene oxide was developed for the targeted drug delivery in cancer therapy. Dextran (DEX) was covalently bonded to graphene oxide nanosheet surface. Then AS1411 aptamer was linked to the hydroxyl group of dextran. To this nanocarrier system, curcumin (CUR), a hydrophobic natural anticancer agent was loaded by π–π stacking interactions. The AS1411 aptamer is a nucleolin recognizer. Thus GO-DEX-Apt-CUR nanosystem having less than 200 nm size can effectively enter into 4T1 and MCF-7 nucleolin overexpressed cancer cells [61].

Doxorubicin acts only after reaching to the nucleus of the cell. pH-responsive charge reversed polyelectrolyte and integrin $\alpha_v\beta_3$ monoantibody functionalized graphene oxide was used to deliver anticancer doxorubicin. DOX released to the cytoplasm of the cancer cell and then moves to the nucleus [62]. Carboxymethyl chitosan functionalized graphene conjugated with hyaluronic acid (HA) and then fluorescein isothiocyanate (FI) can be used to load doxorubicin. The drug encapsulation efficiency was found to be 95%. It can target HeLa cells overexpressing CD44 receptors and suppress their growth. GO-CMC-FI-HA-DOX can release the drug in controlled rate in lower pH tumor cell microenvironment [63]. Graphene functionalized with a polyoxyethylene bi amine and is used to carry silver nanoparticles to form GO-PEG-AgNPs. It is active against *E. coli* and *Staphylococcus aureus*. And it is more effective than silver nanoparticles alone [64]. Carboxylated GO functionalized with β-cyclodextrin by covalent bonds via

esterification. This is used as a drug carrier due to its higher dispersibility in water and is stable for 12 months [65]. Antibodies can be used as targeting ligands. *A* targeting system was developed by the conjugating monoclonal antibody on graphene, which acts against the follicle stimulating hormone receptor. This system is a best tumor targeting agent because of its higher stability, specificity towards FSHR and rapid tumor uptake. Since graphene has a large surface area, they are used for multifunctional drug delivery system. Chemo-photothermal targeted therapy of glioma cells are successfully developed by using IL-13 as targeting ligand, since IL-13 is overexpressed in malignant tumors. And GO is used to absorb NIR lasers because of its good heat transfer for photothermal therapy. It gives a higher effect than single chemotherapy [6]. Certain drugs and polymers have the ability to respond to specific pH of the tumor microenvironment. These drugs or polymers are conjugated to graphene to form a pH targeted system. *G*elatine functionalized graphene nanosheets are loaded with methotrexate, which shows pH-dependent release. The drug is released in acidic pH than neutral [66].

Multifunctional targeted drug delivery system can be developed by using a bio-targeting ligand and a superparamagnetic iron oxide for magnetic targeted delivery. Lactoferrin functionalized graphene oxide iron oxide is effective for glioma targeting. Here, lactoferrin is the bio-targeting material; it is an iron transporting serum glycoprotein, which binds to receptors overexpressed at glioma cell surface and brain tumor. When doxorubicin loaded to this system, it effectively delivers the drug to the tumor cells [67].

Graphene was functionalized with heparin (Hep) via a linker, adipic dihydrazide (ADH). It is then loaded with doxorubicin to form GO-ADH-Hep-DOX nanocomposite; it provides pH sensitive sustained release. It is non-toxic, stable, blood compatible and biocompatible [68]. The hybrid molecule obtained when the thiolated graphene covalently functionalized with luminescent, subnanometer clusters of silver protected by glutathione is having a wide possibility in targeted drug delivery [69]. Biocompatible polymer poly(2-diethylaminoethyl) methacrylate is conjugated with graphene oxide via in situ atom transfer radical polymerization reaction and then loaded camptothecin, which is noncytotoxic and good biocompatible [70].

7.2 Multi Functionalized Graphene in Drug Delivery

A Novel method of cancer treatment using graphene oxide nanoparticle functionalized with polyethylene glycol and folic acid using camptothecin as an anticancer drug. According to the study, functionalizing the Drug-GO-NP complex with PEG and folic acid will markedly increase the uptake of the drug by cancer cells. The development of nanoparticle with folic acid is a good candidate for an effective drug delivery system for cancer therapy. The drug-loaded complex could deliver the drug in a sustained fashion and also have an advantage of reduced dosing frequency when considering the therapeutic viewpoint [71]. Another study shows the loading

capability, drug release and cytotoxic effect of poor water-soluble drug (e.g. camptothecin) loaded GO-PVP/β-cyclodextrin complex. Among the two complexes (GO-PVP and GO-β CD), poorly water-soluble drug loaded GO-PVP was found to be the most guaranteed system for drug delivery and have wide therapeutic applications mainly in the field of oncology [72]. Hydroxypropyl-β-cyclodextrin (HP-β-CD) GO conjugates are also used as carriers. Later this carrier was used for Paclitaxel delivery for ovarian, breast and lung cancer. HP-β-CD chemically bonded onto –COOH group of GO. The paclitaxel-loaded HP-β-CD nanospheres exhibit excellent stability and sustained release of ant cancer agents [73]. Even though graphene oxide based drug delivery for cancer therapy found to beneficial but its action can be modified even more i.e. natural peptide protamine sulfate and sodium alginate can be used; these are adsorbed on to the GO which will give high dispensability and stability to the complex [74]. Functionalized graphene oxide is used as a nanocarrier of new copper (II) complexes for targeted therapy in nasopharyngeal carcinoma. Folic acid and poly ethylenimine (PEI) functionalized GO (FA-PEI-GO) used as a carrier for two new copper complexes to folate receptor-positive nasopharyngeal carcinoma. Folic acid is the ligand interacting with the folate receptor, which can be easily conjugated with GO. Copper complexes have broad-spectrum anti-cancer activity by cell apoptosis mechanism. Thus, this FA-PEI-GO therapy with copper complexes is an efficient carrier for targeted drug delivery [75]. Folic acid—bovine serum albumin (BSA) conjugated GO nanocomposite is used for the delivery of doxorubicin. Here, FA-BSA acts as both stabilizing agent and targeting agent. Doxorubicin is targeted to the folate receptor-rich MCF-7 cell. The clear concept is shown below in Fig. 6. This system reduces the toxicity of GO, increases stability and biocompatibility in physiological fluids [24].

In HER 2 overexpressed breast cancer, nuclear accumulation of drug is achieved by anti-HER 2 antibodies conjugated poly-L-lysine functionalized reduced graphene oxide. Anti HER 2 antibody was bonded to the amino group of poly-L-lysine via glutaraldehyde bifunctional linkage. It is reported that this method of drug delivery shows 7 folds benefit than reduced graphene oxide-PLL nanocarrier delivery.

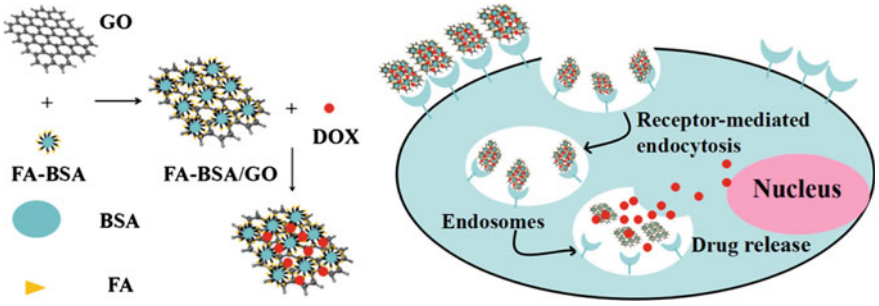

Fig. 6 Schematic representation of Doxorubicin targeted delivery by FA-BSA-GO carrier. Reprinted from [24], © 2016, with permission from Elsevier

It delivers drug rapidly to the nucleus within 4 h by energy-dependent macropinocytic internalization [76]. Phospholipid and PEG-modified graphene nanoribbon loaded with Doxorubicin are active against U87 glioma cells. This activity is 6–7 times higher than free doxorubicin [77]. A detailed study on the functionalization of graphene oxide (GO), by using lactobionic acid (LA) and carboxymethyl chitosan (CMC) was conducted to achieve targeted drug delivery. Here LA acts as a carrier for targeting GO on cancer cells mainly on liver cells (SMMC-7721) and can induce cell death when loaded with drugs like Doxorubicin. In FGO-LA-CMC-DOX complex, LA allows the selective uptake of cancer cells without disturbing normal cell system [78].

Dual-functionalized graphene oxide is used for better siRNA delivery to breast cancer cells. Here reduced graphene oxide (rGO) based nanocarrier was dual functionalized by a phospholipid-based amphiphilic polymer and R8 cell penetrating peptide (CPPs) i.e., for improved hydrocolloid stability and better siRNA transfection ability towards MCF-7 breast cancer cells. By incorporating R8-CPP, it will provide a high positive surface charge which will facilitate easy loading and condensation of siRNA, as well as helps in penetration [79].

7.3 Functionalized Graphene; a Vector for Gene Delivery

The utility of graphene in gene delivery is another field that has to be explored more. Since DNA/RNA are negatively charged, a cationic polymer is used as a vector. The capacity to deliver the gene effectively and the ability to facilitate the gene uptake with high transfection efficiency make graphene a satisfactory vector for the gene delivery and gene-drug co-delivery. The polyethyleneimine, a cationic polymer functionalized GO-based gene delivery thus enables the gene delivery with high transfection efficiency and provide reduced toxic effects associated with polyethylenimine. Graphene oxide surface conjugated with chitosan is another complex carrier widely accepted for the gene delivery and the gene-drug co-delivery [7]. The cell penetrating peptide (CPP) has received immense attraction when conjugated with graphene oxide to generate the CPP-GO complex as the nanocarrier exhibiting excellent intracellular delivery for genes [80].

Oxidized graphenes are efficient nonviral vectors for genetic materials. They are easily uptake by HeLa cells and HUVEC cell and released into the cytoplasm and enter into the nucleus. Graphene oxide functionalized with polyamidoamine (PAMAM) dendrimer and Oleic acid is used as a biocompatible gene vector. It is developed by chemical adsorption of oleic acid and covalent linkage of PAMAM to graphene oxide. GO functionalized with both PAMAM and oleic acid shows higher transfection capacity than GO functionalized with PAMAM only [2]. PEG functionalized graphene oxide is used to deliver molecular beacon (MB), as a model oligonucleotide directed to HeLa cells to detect targeted mRNA. PEG also protects MB from enzymatic cleavage and are less cytotoxic [80].

7.4 Dual Gene/Drug Delivery by Graphene Nanocarriers

The therapeutic efficiency can be enhanced to a higher extent by co-delivery of nucleotide-based therapeutic agent and chemical-based drug simultaneously. Since graphene has a large surface area, both agents are easily loaded to graphene-based nanocarriers by physical or chemical interactions [80]. Since the drug resistance is a major challenge in chemotherapy, an effective strategy of co-delivery of the gene, small interfering RNA(siRNA) along with the drug Doxorubicin using functionalized graphene as the dual nanocarrier has been developed. This could silence the expression of efflux transporters and can be a remedy for the drug resistance during chemotherapy. The folic acid (FA)-conjugated polyethyleneimine-modified PEGylated nanographene exhibited a high DOX and siRNA loading capability along with effective intracellular DOX delivery and gene silencing effect [81]. PAMAM dendrimer functionalized graphene oxide is used for co-delivery of MMP-9 shRNA plasmid and doxorubicin. It increases the efficiency of breast cancer therapy [82]. A complex of PEI and poly-sodium-4-styrene sulfonate (PSS) functionalized GO (PPG) is used for co-delivery of doxorubicin and miR-21 targeted siRNA for the treatment of cancer. Here, first doxorubicin is loaded on PPG by physical mixing and then anti-miRR-21 by electrical adsorption. This system gives synergistic effect by gene silencing of miR-21 and accumulation of doxorubicin in tumor cell [83]. PEI grafted graphene oxide nanocarriers are developed for co-delivery of Bcl2 targeted SiRNA and doxorubicin. It reduces the cytotoxicity and enhances anticancer effect [80].

7.5 Anticancer Activity of Functionalized Graphene

Functionalized graphene is not only a drug carrier but also exhibits anticancer activity itself by exerting inhibitory effects on tumor cells [84]. Resveratrol functionalized graphene oxide induces membrane leakage and oxidative stress in ovarian cancer cells and induces apoptosis [85]. PEG functionalized GO inhibits breast cancer cell metastasis by downregulating the expression of multiple mitochondrial OXPHOS-related proteins and ATP production in cancer cells selectively [86]. Experiments are conducted with graphene to prove its anticancer effects by using glioblastoma multiform tumor cells as a model. But pure graphene is known to have agglomeration and processing problems. In order to increase the anticancer activity and to overcome the disadvantages, the graphene is functionalized with arginine. Studies were made on both normal cells and tumor tissues. After the study, they concluded that both graphenes have anticancer activity and functionalized graphene shown to have more distributed in tumor cells without any agglomeration and arginine suppress the tumor invasiveness. Hence, graphene in its reduced form i.e. rGO-arginine complex is proved to have beneficial against glioblastoma multiform tumor cells [87].

The strategy of functionalization of graphene surface with amino acids for enhancing the surface charge and facilitating the easy uptake by the tumor cells as these cells are negatively charged could synergize anticancer action of graphene. The anticancer activity of ginsenoside Rh2–treated graphene oxide (GO-Rh2), lysine-functionalized highly porous graphene (Gr-Lys), arginine-functionalized graphene (Gr-Arg), Rh2–treated Gr-Lys (Gr-Lys-Rh2) and Rh2–treated Gr-Arg (Gr-Arg-Rh2) were subjected to various cytotoxic assays and these nanostructures were found to be exhibiting satisfactory antitumor activity also these nanostructures is having effect on blood coagulation system [88]. Silver decorated reduced graphene oxide nanocomposites have apoptosis-inducing ability in A549 lung cancer. This is prepared by using *Pulicaria glutinosa* extract (PGE) as reducing agent. The anticancer activity of PGE-HRG-Ag-2 was studied in 5 human cancer cell lines, MCF-7 (breast), A549 (lung), HeLa (cervical), DU-145 (prostate) and HepG2 (liver) and tamoxifen were used as standard reference drug. The results show that PGE-HRG-Ag-2 possesses higher activity than reference tamoxifen against human lung cancer cell line, A549 [89]. *A* unique field of therapeutics i.e. photothermal therapy (PTT) based cancer treatment was developed by using functionalized graphene as a suitable vehicle. The PTT will produce ablations in the cancer cells, eventually tumor growth inhibition and cell death. Graphene oxide (GO), reduced graphene oxide (rGO) and GO-nanocomposites are mainly used. Large specific surface area, abundant functional groups which are available for bioconjugation, drug loading, and targeting make them suitable candidates for PTT. There were a number of comprehensive researches on PTT, and many of them were succeeded and later concluded that it is a great tool for cancer treatment. The main mechanism behind PTT is that they utilize an optical absorbing agent along with electromagnetic radiation for treatment of cancer moreover they induce apoptosis rather than necrosis so there will not be any inflammatory response [90].

7.6 Antibacterial Activity of Functionalized Graphene

The research works has been shown that graphene possess a broad spectrum of antibacterial activity and functionalization of graphene with different organic molecules especially with amine/amide groups which itself having anti-inflammatory activity are found to be tremendously effective against different disease-causing bacteria like Gram-positive (*E. coli*, *Pseudomonas aeruginosa*) and gram-positive (*Staphylococcus aureus*) [91]. *A*ntibacterial activity was found in graphene oxide functionalized with guanidine polymer i.e. with polyethylene glycol (PEG) and polyhexamethylene guanidine hydrochloride (PHGC). Here we get a dual functionalized graphene-GO-PEG-PHGC complex. The complex is incubated with both Gram-positive and Gram-negative bacteria. The results reveal that the complex interact with the cell contents and other nanoparticles present in the bacteria causing greater damage to them leads to cell death. The complex is found to effective against both gram-positive and gram-negative bacteria. The GO-PEG-PHGC can be used as

a disinfectant which is capable of inhibiting the bacterial growth and propagation [92]. Functionalized graphene possesses toxicity against bacterial cell. Thus, they can be used as effective antibacterial agents. Polyethyleneimine functionalized reduced GO coated with silver nanoparticles (PEI-rGO-AgNPs) show antibacterial activity against *Escherichia coli* and *Staphylococcus aureus.* It shows >90% reduction in cell viability. The mechanism involved is that the sharp blade like edges of GO interacts with bacterial cell wall and is damaged. And then, silver ions interact with intracellular components. This leads to bacterial death [93]. A similar investigation was conducted by replacing polyethyleneimine with L-cysteine (L-Cys) and decorating with silver nanoparticles. The GO-Ag-L-Cys complex has high bactericidal activity especially against gram-negative bacteria by disrupting the cell wall integrity while bacteriostatic effect against gram-negative bacteria by inhibiting their cell division. They are active even at low concentration [94]. Thin film and solution of poly (*N*-vinyl carbazole) graphene (PVK-G) have activity against *E. coli* and *Bacillus subtilis* at 1 mg/mL concentration. This shows 80% reduction in bacterial growth [95]. rGO functionalized with polysulfone (PSU) have activity against *Bacillus subtilis and Escherichia coli.* The investigation reveals that this complex has high antibacterial activity because of the production of reacting oxygen species. Another advantage is that the presence of shorter polymer chain which allows greater contact with the bacteria on the surface of graphene [96]. Chlorophyllin and zinc functionalized graphene oxide also exhibit antimicrobial activity. The incubation of bacteria with this functionalized graphene oxide causes loss of cellular integrity and cell death [97].

Amino acid arginine functionalized mono-layer graphene shows excellent antibacterial activity, and it can overcome the silver nanoparticle-induced toxicity [98]. Effect of the size of graphene sheets in its antibacterial effect was studied, and graphene sheets with smaller size show higher antibacterial activity [99]. Noncovalent functionalization of graphene with surfactants shows antibacterial activity. *A* study was conducted by using different surfactants such as tween 80, cetrimide, sodium dodecyl sulfate and reported that cetrimide functionalized graphene possess antibacterial activity. Antibacterial activity of cetrimide functionalized graphene against *S. aureus h*as improved 16 and 65 folds against *P. aeroginosa* than cetrimide alone [100].

7.7 Other Applications

Graphene-based non-materials have a wide variety of biomedical applications which is represented in Fig. 7. By bio-functionalization of graphene-based nonmaterial with various biomolecules, other cells open great field biomedical applications such as bio-imaging, electronic devices, biological sensing, drug/gene delivery, a biocompatible scaffold for cell culture; stem cell differentiation e.g. functionalized graphene is adsorbed with fluorescent-tagged DNA. Both single-stranded (ss) DNA and double-stranded (ds) DNA are adsorbed. If ssDNA having

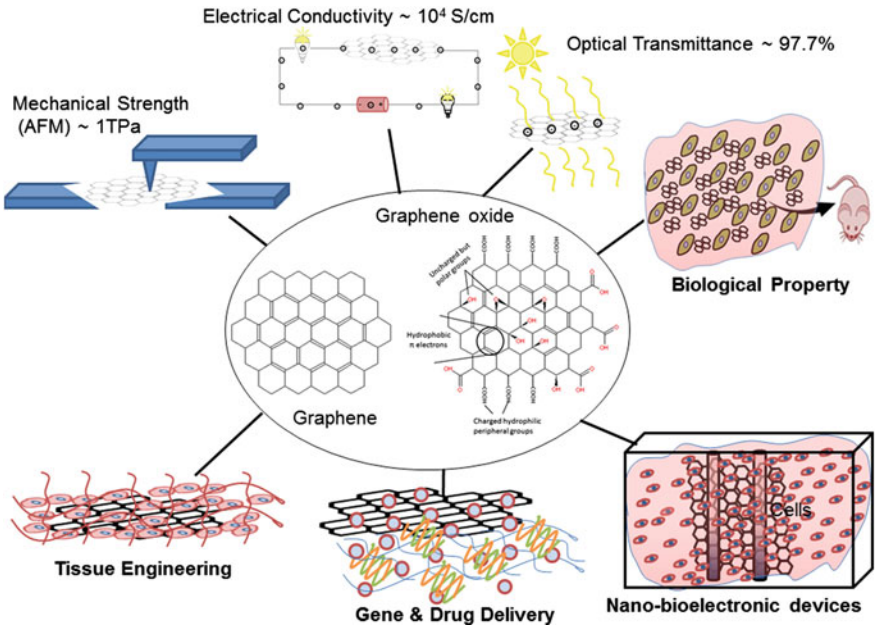

Fig. 7 Schematic representation of applications of graphene. Reprinted from [7], © 2013 with permission from Elsevier

stronger interaction against dsDNA, the fluorescence on the ssDNA darkens more, thus indicating the bio-sensing capability [101]. Graphene can be made luminescent, and it is the best candidate for bioimaging. Fluorescein functionalized pegylated graphene oxide is used in intracellular imaging. Here PEG is used to prevent GO-induced quenching of conjugated fluorescein. Laser irradiation in the presence of nanographene oxide (NGO) creates micro bubbling, which causes immediate cell damage at the specific site, thus it offers localized therapy [19]. Functionalized graphene enhances the properties of the polymer-based nanocomposite. These nanocomposites are used in electronics and sensors in industries and pressure sensors in the biomedical field. Incorporation of poly (vinylidene fluoride-chlorotrifluoroethylene) nanocomposite to hyper branched poly ethylene-graft-poly (trifluoroethyl methacrylate) copolymer functionalized graphene shows increased dielectric property and high energy density. Thus, it can be used in electronic devices, sensors and biomedical applications [102]. The functionalization graphene can be done with different polymers. The polymer functionalized graphene may have advantages in different aspects like it improve mechanical, electronic, optical, thermal and magnetic properties significantly if used appropriate polymer. Polyaniline, polypyrrole called as conducting polymers when used to functionalize graphene, the resultant complex can be used as supercapacitors which have a high capacitance of about 424 F g^{-1} [103].

Graphene has been used for wound healing, regenerative medicine, stem cell, and tissue engineering. A chitosan-PVA nanofibrous scaffolds containing graphene is used for wound healing and is proved in mice and rabbit. Functionalization of graphene with proteins and peptides is used for tissue engineering applications. Graphene materials have the ability to absorb DNA/proteins due to their large surface area, thus it is used in many therapeutic applications [7]. Graphene oxide nanocomposites were developed by functionalizing lactobionic acid and carboxy methyl chitosan and they are used for doxorubicin delivery. It readily releases at lower pH cancer cell environment than at general physiological pH. Cancer cells uptake them and minimal uptake by the non-cancerous cell [78]. A sensing array system in order to differentiate the cancer cells, circulating tumor cells and different cell types based on the functionalized graphene elements electrochemical mechanism has been developed. This innovative approach can be considered as a new pavement in future clinical cancer diagnosis [104]. Encapsulating the MCM-48, mesoporous molecular sieves with either reduced graphene oxide or graphene oxide can be used in remediation of caffeine and phenacetin from aqueous solution [105]. A conductive biodegradable scaffold has been generated by modifying the graphene oxide-gold nanosheets with the natural polymer chitosan. This innovation was sufficient enough to overcome the abnormal conduction and electrical impulse propagation in the heart after myocardial infarction [106]. Circulating tumor cells (CTC) are the main reason for widespread cancer cells. The researchers have demonstrated the isolation of CTC using functionalized graphene oxide nanosheets molded in gold plates. This discovery very effective in therapeutically, i.e. early detection of rare CTC in blood hence spreading of cancer [107]. The chemical functionalization graphene will cause the destruction of sp^2 network and to get converted to sp^3 hybridization. During this conversion the metallic graphene changes to an insulator. Specifically, graphene on appropriate surface modification can be converted to a semiconductor which will lead to new novel nanoelectronic and nanophotonic applications of graphene [4]. Capacitor developed by modifying 3D self-assembled graphene hydrogel by using multi redox anthraquinone derivative alizarine via noncovalent functionalization [108]. Oxygen functionalized graphene shows higher specific capacitance (up to 189 F g^{-1}) than graphene (165 F g^{-1}). This is due to additional pseudo capacitance effect of oxygen-containing functional group, mainly carbonyl and hydroxyl groups. They show large pseudocapacitance and less aggregation. Heteroatom doping alters the physical or chemical characteristics of graphene. Nitrogen doping increases the energy density of graphene supercapacitor in both aqueous and electrolyte solution [109]. Single or multi hetero atom functionalized graphene is used as charge extraction materials to improve solar cell performance [110]. Carboxylated graphene is used as a sensitive electrochemical biosensor [111]. Reduced graphene functionalized with 1,6-diaminohexane and loaded with silver nanoparticles. This is effective against bacterial coliform infection and thus it is used for water disinfection [112].

8 Conclusion

This chapter mainly emphasizes graphene functionalization and the application of functionalized graphene in drug delivery. Chemical modification on graphene helps in enabling additional properties of dispersibility in different solvents, reduced toxicity of graphene and also prevents agglomeration. Covalent and noncovalent modification methods of functionalization along with multi-functionalization, substitutional doping, and nanoparticle functionalization has been described. Functionalization with multi molecules makes graphene an efficient candidate for targeted drug delivery. A wide range of applications of functionalized graphene as carrier for the drug in targeted therapy has been highlighted in this chapter. The tremendous cell targeting ability and the high drug loading capacity opens a wide range of application possibilities as a drug carrier for functionalized graphene. Along with that, the capability of functionalized graphene for gene delivery and for the co-delivery of both drug and gene, the anticancer effect and antibacterial effect has also been pointed up.

References

1. Borandeh, S., Abdolmaleki, A., Abolmaali, S.S., Tamaddon, A.M.: Synthesis, structural and in-vitro characterization of β-cyclodextrin grafted L-phenylalanine functionalized graphene oxide nanocomposite: a versatile nanocarrier for pH-sensitive doxorubicin delivery. Carbohydr. Polym. **201**, 151–161 (2018). https://doi.org/10.1016/j.carbpol.2018.08.064
2. Zhang, B., Wang, Y., Zhai, G.: Biomedical applications of the graphene-based materials. Mater. Sci. Eng.C **61**, 953–964 (2016). https://doi.org/10.1016/j.msec.2015.12.073
3. Li, D., Müller, M.B., Gilje, S., Kaner, R.B., Wallace, G.G.: Processable aqueous dispersions of graphene nanosheets. Nat. Nanotechnol. **3**, 101 (2008). https://doi.org/10.1038/nnano.2007.451
4. Kuila, T., Bose, S., Kumar, A., Khanra, P.: Chemical functionalization of graphene and its applications. Prog. Mater. Sci. **57**, 1061–1105 (2012). https://doi.org/10.1016/j.pmatsci.2012.03.002
5. Ji, X., Xu, Y., Zhang, W., Cui, L., Liu, J.: Review of functionalization, structure and properties of graphene/polymer composite fibers. Compos. Part A Appl. Sci. Manuf. **87**, 29–45 (2016). https://doi.org/10.1016/j.compositesa.2016.04.011
6. Zhang, Q., Wu, Z., Li, N., Pu, Y., Wang, B., Zhang, T., Tao, J.: Advanced review of graphene-based nanomaterials in drug delivery systems: synthesis, modification, toxicity and application. Mater. Sci. Eng. C **77**, 1363–1375 (2017). https://doi.org/10.1016/j.msec.2017.03.196
7. Goenka, S., Sant, V., Sant, S.: Graphene-based nanomaterials for drug delivery and tissue engineering. J. Control. Release. **173**, 75–88 (2014). https://doi.org/10.1016/j.jconrel.2013.10.017
8. Mccallion, C., Burthem, J., Rees-unwin, K., Golovanov, A., Pluen, A.: Graphene in therapeutics delivery: problems, solutions and future opportunities. Eur. J. Pharm. Biopharm. **104**, 235–250 (2016). https://doi.org/10.1016/j.ejpb.2016.04.015
9. Novoselov, K.S., Geim, A.K., Morozov, S.V., Jiang, D.: Electric field effect in atomically thin carbon films. Science **306**, 666–669 (2004)

10. Brodie, B.C.: On the atomic weight of graphite. Philos. Trans. R. Soc. Lond. **149**, 249–259 (1859). https://doi.org/10.1098/rstl.1859.0013
11. Staudenmaier, L.: Darstellung der Graphitslure. Ger. Chem. Soc. **31**, 1481–1487 (1898). https://doi.org/10.1002/cber.18980310237
12. Hummers, W.S., Offeman, R.E.: Preparation of graphitic oxide. J. Am. Chem. Soc. **80**, 1339 (1958). https://doi.org/10.1021/ja01539a017
13. Zaaba, N.I., Foo, K.L., Hashim, U., Tan, S.J., Liu, W.W., Voon, C.H.: Synthesis of graphene oxide using modified hummers method: solvent influence. Procedia Eng. **184**, 469–477 (2017). https://doi.org/10.1016/j.proeng.2017.04.118
14. Guermoune, A., Chari, T., Popescu, F., Sabri, S.S.: Chemical vapor deposition synthesis of graphene on copper with methanol, ethanol, and propanol precursors. Carbon **49**, 4204–4210 (2011). https://doi.org/10.1016/j.carbon.2011.05.054
15. Lee, H.C., Liu, W.-W., Chai, S.-P., Mohamed, A.R., Lai, C.W., Khe, C.-S., Voon, C.H., Hashim, U., Hidayah, N.M.S.: Synthesis of single-layer graphene: a review of recent development. Procedia Chem. **19**, 916–921 (2016). https://doi.org/10.1016/j.proche.2016.03.135
16. Whitener, K.E., Sheehan, P.E.: Graphene synthesis. Diam. Relat. Mater. **46**, 25–34 (2014). https://doi.org/10.1016/j.diamond.2014.04.006
17. Chen, D., Feng, H., Li, J.: Graphene oxide: preparation, functionalization, and electrochemical applications. Chem. Rev. **112**, 6027–6053 (2012). https://doi.org/10.1021/cr300115g
18. Ejigu, A., Kinloch, I.A., Dryfe, R.A.W.: Single stage simultaneous electrochemical exfoliation and functionalization of graphene. ACS Appl. Mater. Interfaces. **9**, 710–721 (2017). https://doi.org/10.1021/acsami.6b12868
19. Georgakilas, V., Otyepka, M., Bourlinos, A.B., Chandra, V., Kim, N., Kemp, K.C., Hobza, P., Zboril, R., Kim, K.S.: Functionalization of graphene: covalent and non-covalent approaches, derivatives and applications. Chem. Rev. **112**(11), 6156–6214 (2012). https://doi.org/10.1021/cr3000412
20. de Sousa, M., Augusto, L., Luna, V. De, Fonseca, L., Giorgio, S., Alves, O.L.: Folic acid-functionalized graphene oxide nanocarrier: synthetic approaches, characterization, drug delivery study and anti-tumor screening folic acid-functionalized graphene oxide nanocarrier : synthetic approaches, characterization, drug delivery St. Appl. Nano Mater. 1–43 (2018). https://doi.org/10.1021/acsanm.7b00324
21. Bourlinos, A.B., Gournis, D., Petridis, D., Szabó, T., Szeri, A., Dékány, I.: Graphite oxide: chemical reduction to graphite and surface modification with primary aliphatic amines and amino acids. Langmuir **19**, 6050–6055 (2003). https://doi.org/10.1021/la026525h
22. Stankovich, S., Piner, R.D., Chen, X., Wu, N., Nguyen, S.T., Ruoff, R.S.: Stable aqueous dispersions of graphitic nanoplatelets via the reduction of exfoliated graphite oxide in the presence of poly(sodium 4-styrenesulfonate). J. Mater. Chem. **16**, 155–158 (2006). https://doi.org/10.1039/b512799h
23. Thakare, S.R., Fendarkar, D.A., Bidkar, C., Yadav, J., Gedam, S.D.: Chemical functionalization of graphene and graphene oxide-a review. Int. J. Adv. Chem. Sci. Appl. **5**, 19–23 (2017)
24. Ma, N., Liu, J., He, W., Li, Z., Luan, Y., Song, Y., Garg, S.: Folic acid-grafted bovine serum albumin decorated graphene oxide: an efficient drug carrier for targeted cancer therapy. J. Colloid Interface Sci. **490**, 598–607 (2017). https://doi.org/10.1016/j.jcis.2016.11.097
25. Park, J., Yan, M.: Covalent functionalization of graphene with reactive intermediates. Acc. Chem. Res. **46**, 181–189 (2013). https://doi.org/10.1021/ar300172h
26. Feng, L., Yang, X., Shi, X., Tan, X., Peng, R., Wang, J., Liu, Z.: Polyethylene glycol and polyethylenimine dual-functionalized nano-graphene oxide for photothermally enhanced gene delivery. Small **9**, 1989–1997 (2013). https://doi.org/10.1002/smll.201202538

27. Zaminpayma, E., Nayebi, P.: Mechanical and electrical properties of functionalized graphene nanoribbon: a study of reactive molecular dynamic simulation and density functional tight-binding theory. Phys. B **459**, 29–35 (2015). https://doi.org/10.1016/j.physb.2014.11.015
28. El-shafai, N.M., El-khouly, M.E., El-kemary, M.: Chemistry fabrication and characterization of graphene oxide—titanium dioxide nanocomposite for degradation of some toxic insecticides. J. Ind. Eng. Chem. (2018). https://doi.org/10.1016/j.jiec.2018.09.045
29. Vecera, P., Chacón-Torres, J.C., Pichler, T., Reich, S., Soni, H.R., Görling, A., Edelthalhammer, K., Peterlik, H., Hauke, F., Hirsch, A.: The: precise determination of graphene functionalization by in situ raman spectroscopy. Nat. Commun. 1–9 (2017). https://doi.org/10.1038/ncomms15192
30. Rattana, T., Chaiyakun, S., Witit-Anun, N., Nuntawong, N., Chindaudom, P., Oaew, S., Kedkeaw, C., Limsuwan, P.: Preparation and characterization of graphene oxide nanosheets. Procedia Eng. **32**, 759–764 (2012). https://doi.org/10.1016/j.proeng.2012.02.009
31. Huang, C., Wu, J., Jiang, W., Liu, R., Li, Z., Luan, Y.: Amphiphilic prodrug-decorated graphene oxide as a multi-functional drug delivery system for efficient cancer therapy. Mater. Sci. Eng. C **89**, 15–24 (2018). https://doi.org/10.1016/j.msec.2018.03.017
32. Melo-diogo, D.De, Lima-sousa, R., Alves, C.G., Costa, E.C., Louro, R.O.: Functionalization of graphene family nanomaterials for application in cancer therapy. Colloids Surf. B Biointerfaces **171**, 260–275 (2018). https://doi.org/10.1016/j.colsurfb.2018.07.030
33. Sasidharan, A., Panchakarla, L.S., Chandran, P., Menon, D., Nair, S., Rao, C.N.R., Koyakutty, M.: Differential nano-bio interactions and toxicity effects of pristine versus functionalized graphene. Nanoscale **3**, 2461–2464 (2011). https://doi.org/10.1039/C1NR10172B
34. Lalwani, G., Agati, M.D., Mahmud, A., Sitharaman, B.: Toxicology of graphene-based nanomaterials. Adv. Drug Deliv. Rev. **105**, 109–144 (2016). https://doi.org/10.1016/j.addr.2016.04.028
35. Zhi, X., Fang, H., Bao, C., Shen, G., Zhang, J., Wang, K., Guo, S., Wan, T., Cui, D.: The immunotoxicity of graphene oxides and the effect of PVP-coating. Biomaterials **34**, 5254–5261 (2013). https://doi.org/10.1016/j.biomaterials.2013.03.024
36. Pooresmaeil, M., Namazi, H.: Biointerfaces Surface modification of graphene oxide with stimuli-responsive polymer brush containing β-cyclodextrin as a pendant group: preparation, characterization, and evaluation as controlled drug delivery agent. Colloids Surf. B Biointerfaces **172**, 17–25 (2018). https://doi.org/10.1016/j.colsurfb.2018.08.017
37. Hussien, N.A., Işıklan, N., Türk, M.: Aptamer-functionalized magnetic graphene oxide nanocarrier for targeted drug delivery of paclitaxel. Mater. Chem. Phys. **211**, 479–488 (2018). https://doi.org/10.1016/j.matchemphys.2018.03.015
38. Khoee, S., Karimi, M.R.: Dual-drug loaded Janus graphene oxide-based thermoresponsive nanoparticles for targeted therapy. Polymer **142**, 80–98 (2018). https://doi.org/10.1016/j.polymer.2018.03.022
39. Rao, Z., Ge, H., Liu, L., Zhu, C., Min, L., Liu, M., Fan, L., Li, D.: Carboxymethyl cellulose modified graphene oxide as pH-sensitive drug delivery system. Int. J. Biol. Macromol. **107**, 1184–1192 (2018). https://doi.org/10.1016/j.ijbiomac.2017.09.096
40. Mu, S., Li, G., Liang, Y., Wu, T., Ma, D.: Hyperbranched polyglycerol-modified graphene oxide as an efficient drug carrier with good biocompatibility. Mater. Sci. Eng. C. **78**, 639–646 (2017). https://doi.org/10.1016/j.msec.2017.04.145
41. Zeinab, R., Sahraei, R., Ghaemy, M.: Preparation of spherical porous hydrogel beads based on ion-crosslinked gum tragacanth and graphene oxide: study of drug delivery behavior. Carbohydr. Polym. **194**, 34–42 (2018). https://doi.org/10.1016/j.carbpol.2018.04.022
42. Gong, P., Ji, S., Wang, J., Dai, D., Wang, F., Tian, M., Zhang, L., Guo, F., Liu, Z.: Fluorescence-switchable ultrasmall fluorinated graphene oxide with high near-infrared absorption for controlled and targeted drug delivery. Chem. Eng. J. **348**, 438–446 (2018). https://doi.org/10.1016/j.cej.2018.04.193

43. Masoud, M., Rahmati, M., Shahrooz, S., Khordad, R.: Molecular dynamics simulation of functionalized graphene surface for high efficient loading of doxorubicin. J. Mol. Struct. **1141**, 441–450 (2017). https://doi.org/10.1016/j.molstruc.2017.04.007
44. Zhang, J., Chen, L., Chen, J., Zhang, Q., Feng, J.: Stability, cellular uptake, and in vivo tracking of zwitterion modified graphene oxide as a drug carrier. 1–19 (2018). https://doi.org/10.1021/acs.langmuir.8b01995
45. Patel, D.K., Senapati, S., Mourya, P., Singh, M., Aswal, V.K., Ray, B., Maiti, P.: Functionalized graphene tagged polyurethanes for corrosion inhibitor and sustained drug delivery functionalized graphene tagged polyurethanes for corrosion inhibitor and sustained drug delivery School of Materials Science and Technology, Indian Institute. Biomater. Sci. Eng. 1–44 (2017). https://doi.org/10.1021/acsbiomaterials.7b00342
46. Dorniani, D., Saifullah, B., Barahuie, F., Arulselvan, P., Hussein, M.Z. Bin, Fakurazi, S., Twyman, L.J.: Graphene oxide-gallic acid nanodelivery system for cancer therapy. Nanoscale Res. Lett. **11**, 491 (2016). https://doi.org/10.1186/s11671-016-1712-2
47. Masoudipour, E., Kashanian, S., Maleki, N.: A targeted drug delivery system based on dopamine functionalized nano graphene oxide. Chem. Phys. Lett. **668**, 56–63 (2017). https://doi.org/10.1016/j.cplett.2016.12.019
48. Liping, R., Shuang, P., Haiqing, L., Yanping, L., He, L., Shuang, Z., Che, J.: Effects of aspirin-loaded graphene oxide coating of a titanium surface on proliferation and osteogenic differentiation of MC3T3-E1 cells. Nat. Publ. Gr. **8**, 1–13 (2018). https://doi.org/10.1038/s41598-018-33353-7
49. Some, S., Gwon, A.R., Hwang, E., Bahn, G.H., Yoon, Y., Kim, Y.: Cancer therapy using ultrahigh hydrophobic drug-loaded graphene derivatives. Nat. Publ. Gr. **4**, 1–9 (2014). https://doi.org/10.1038/srep06314
50. Muthoosamy, K., Abubakar, I.B., Bai, R.G., Loh, H.: Exceedingly higher co-loading of curcumin and paclitaxel onto polymer-functionalized reduced graphene oxide for highly potent synergistic anticancer treatment. Nat. Publ. Gr. 1–14 (2016). https://doi.org/10.1038/srep32808
51. Emadi, F., Amini, A., Gholami, A., Ghasemi, Y.: Functionalized graphene oxide with chitosan for protein nanocarriers to protect against enzymatic cleavage and retain collagenase activity. Nat. Publ. Gr. 1–13 (2017). https://doi.org/10.1038/srep42258
52. Liu, Y., Peng, J., Wang, S., Xu, M., Gao, M., Xia, T., Weng, J., Xu, A., Liu, S.: Molybdenum disulfide/graphene oxide nanocomposites show favorable lung targeting and enhanced drug loading/tumor-killing efficacy with improved biocompatibility. Asia Mater. **10**, 1–15 (2018). https://doi.org/10.1038/am.2017.225
53. Fan, L., Ge, H., Zou, S., Xiao, Y., Wen, H., Li, Y., Feng, H., Nie, M.: Sodium alginate conjugated graphene oxide as a new carrier for drug delivery system. Int. J. Biol. Macromol. **93**, 582–590 (2016). https://doi.org/10.1016/j.ijbiomac.2016.09.026
54. Tyagi, N., Attia, N.F., Geckeler, K.E.: Exfoliated graphene nanosheets: pH-sensitive drug carrier and anti-cancer activity. J. Colloid Interface Sci. **498**, 364–377 (2017). https://doi.org/10.1016/j.jcis.2017.03.057
55. Pooresmaeil, M., Namazi, H.: β-cyclodextrin grafted magnetic graphene oxide applicable as cancer drug delivery agent: synthesis and characterization. Mater. Chem. Phys. **218**, 62–69 (2018). https://doi.org/10.1016/j.matchemphys.2018.07.022
56. Huang, Y., Lu, Y., Chen, J.: Magnetic graphene oxide as a carrier for targeted delivery of chemotherapy drugs in cancer therapy. J. Magn. Magn. Mater. **427**, 34–40 (2017). https://doi.org/10.1016/j.jmmm.2016.10.042
57. Sgarlata, C., Urso, L.D., Consiglio, G., Grasso, G., Satriano, C., Forte, G.: pH sensitive functionalized graphene oxide as a carrier for delivering gemcitabine: a computational approach. Comput. Theor. Chem. **1096**, 1–6 (2016). https://doi.org/10.1016/j.comptc.2016.09.026

58. Han, C., Zhang, C., Ma, T., Zhang, C., Luo, J., Xu, X., Zhao, H., Chen, Y., Kong, L.: Hypericin-functionalized graphene oxide for enhanced mitochondria-targeting and synergistic anticancer effect. Acta Biomater. **77**, 268–281 (2018). https://doi.org/10.1016/j.actbio.2018.07.018
59. Wu, C., He, Q., Zhu, A., Li, D., Xu, M., Yang, H., Liu, Y.: Synergistic anticancer activity of photo- and chemoresponsive nanoformulation based on polylysine-functionalized graphene. Appl. Mater. Interfaces **6**, 21615–21623 (2014). https://doi.org/10.1021/am5066128
60. Yang, L., Wang, F., Han, H., Yang, L., Zhang, G., Fan, Z.: Graphene oxide as a drug carrier for loading pirfenidone in treatment of subarachnoid hemorrhage. Colloids Surf. B Biointerfaces **129**, 21–29 (2015). https://doi.org/10.1016/j.colsurfb.2015.03.022
61. Alibolandi, M., Mohammadi, M., Mohammad, S., Ramezani, M., Abnous, K.: Fabrication of aptamer decorated dextran coated nano-graphene oxide for targeted drug delivery. Carbohydr. Polym. **155**, 218–229 (2017). https://doi.org/10.1016/j.carbpol.2016.08.046
62. Zhou, T., Zhou, X., Xing, D.: Biomaterials controlled release of doxorubicin from graphene oxide based charge-reversal nanocarrier. Biomaterials **35**, 4185–4194 (2014). https://doi.org/10.1016/j.biomaterials.2014.01.044
63. Yang, H., Bremner, D.H., Tao, L., Li, H., Hu, J., Zhu, L.: Carboxymethyl chitosan-mediated synthesis of hyaluronic acid-targeted graphene oxide for cancer drug delivery. Carbohydr. Polym. **135**, 72–78 (2016). https://doi.org/10.1016/j.carbpol.2015.08.058
64. Chen, X., Huang, X., Zheng, C., Liu, Y., Xu, T., Liu, J.: Preparation of different sized nano-silver loaded on functionalized graphene oxide with highly effective antibacterial properties. J. Mater. Chem. B. **3**, 7020–7029 (2015). https://doi.org/10.1039/C5TB00280J
65. Meng, N., Su, Y., Zhou, N., Zhang, M., Shao, M.: Carboxylated graphene oxide functionalized with β-cyclodextrin—engineering of a novel nanohybrid drug carrier. Int. J. Biol. Macromol. **93**, 117–122 (2016). https://doi.org/10.1016/j.ijbiomac.2016.08.051
66. An, J., Gou, Y., Yang, C., Hu, F., Wang, C.: Synthesis of a biocompatible gelatin functionalized graphene nanosheets and its application for drug delivery. Mater. Sci. Eng. C **33**, 2827–2837 (2013). https://doi.org/10.1016/j.msec.2013.03.008
67. Song, M., Xu, H., Liang, J., Xiang, H., Liu, R., Shen, Y.: Lactoferrin modified graphene oxide iron oxide nanocomposite for glioma-targeted drug delivery. Mater. Sci. Eng. C. **77**, 904–911 (2017). https://doi.org/10.1016/j.msec.2017.03.309
68. Zhang, B., Yang, X., Wang, Y., Zhai, G.: Heparin modified graphene oxide for pH-sensitive sustained release of doxorubicin hydrochloride. Mater. Sci. Eng. C. **75**, 198–206 (2017). https://doi.org/10.1016/j.msec.2017.02.048
69. Chandrasekar, A., Pradeep, T.: Luminescent silver clusters with covalent functionalization of graphene. J. Phys. Chem. C **116**, 14057–14061 (2012). https://doi.org/10.1021/jp304131v
70. Theodosopoulos, G.V., Bilalis, P., Sakellariou, G.: Polymer functionalized graphene oxide: a versatile nanoplatform for drug/gene delivery. Curr. Org. Chem. **19**, 1828–1837 (2015). https://doi.org/10.2174/1385272819666150526005714
71. Deb, A., Vimala, R.: Camptothecin loaded graphene oxide nanoparticle functionalized with polyethylene glycol and folic acid for anticancer drug delivery. J. Drug Deliv. Sci. Technol. **43**, 333–342 (2018). https://doi.org/10.1016/j.jddst.2017.10.025
72. Karki, N., Tiwari, H., Pal, M., Chaurasia, A., Bal, R., Joshi, P.: Functionalized graphene oxides for drug loading, release and delivery of poorly water soluble anticancer drug: a comparative study. Colloids Surf. B Biointerfaces **169**, 265–272 (2018). https://doi.org/10.1016/j.colsurfb.2018.05.022
73. Tan, J., Meng, N., Fan, Y., Su, Y., Zhang, M.: Hydroxypropyl-β-cyclodextrin—graphene oxide conjugates: carriers for anti-cancer drugs. Mater. Sci. Eng. C **61**, 681–687 (2016). https://doi.org/10.1016/j.msec.2015.12.098
74. Xie, M., Zhang, F., Liu, L., Zhang, Y., Li, Y., Li, H., Xie, J.: Modification of graphene oxide nanosheets by protamine sulfate/sodium alginate for anti-cancer drug delivery application. Appl. Surf. Sci. **440**, 853–860 (2018). https://doi.org/10.1016/j.apsusc.2018.01.175

75. Guo Li, Yang, Y., Zhou, R., Meng, F., Li, X.: Functionalized graphene oxide as a nanocarrier of new copper (II) complexes for targeted therapy on nasopharyngeal carcinoma. Eur. J. Pharm. Sci. **123**, 249–259 (2018). https://doi.org/10.1016/j.ejps.2018.07.006
76. Ting, X., Qing, X., Ming, C.: Highly efficient nuclear delivery of anti-cancer drugs using a bio-functionalized reduced graphene oxide. J. Colloid Interface Sci. **467**, 35–42 (2016). https://doi.org/10.1016/j.jcis.2015.12.052
77. Lu, Y., Lin, C., Yang, H., Lin, K., Wey, S., Sun, C., Wei, K., Yen, T., Lin, C., Ma, C.M., Chen, J.: Biodistribution of PEGylated graphene oxide nanoribbons and their application in cancer chemo-photothermal therapy. Carbon **74**, 83–95 (2014). https://doi.org/10.1016/j.carbon.2014.03.007
78. Pan, Q., Lv, Y., Williams, G.R., Tao, L., Yang, H., Li, H., Zhu, L.: Lactobionic acid and carboxymethyl chitosan functionalized graphene oxide nanocomposites as targeted anticancer drug delivery systems. Carbohydr. Polym. **151**, 812–820 (2016). https://doi.org/10.1016/j.carbpol.2016.06.024
79. Imani, R., Shao, W., Taherkhani, S., Hojjati, S., Prakash, S., Faghihi, S.: Dual-functionalized graphene oxide for enhanced siRNA delivery to breast cancer cells. Colloids Surf. B Biointerfaces **147**, 315–325 (2016). https://doi.org/10.1016/j.colsurfb.2016.08.015
80. Imani, R., Mohabatpour, F., Mostafavi, F.: Graphene-based nano-carrier modifications for gene delivery applications. Carbon **140**, 569–591 (2018). https://doi.org/10.1016/j.carbon.2018.09.019
81. Zeng, Y., Yang, Z., Li, H., Hao, Y., Liu, C., Zhu, L., Liu, J., Lu, B.: Multifunctional nanographene oxide for targeted gene-mediated thermochemotherapy of drug-resistant tumour. Nat. Publ. Gr. 1–10 (2017). https://doi.org/10.1038/srep43506
82. Gu, Y., Guo, Y., Wang, C., Xu, J., Wu, J., Kirk, T.B., Ma, D., Xue, W.: A polyamidoamne dendrimer functionalized graphene oxide for DOX and MMP-9 shRNA plasmid co-delivery. Mater. Sci. Eng. C **70**, 572–585 (2017). https://doi.org/10.1016/j.msec.2016.09.035
83. Yang, H., Huang, C., Lin, C., Liu, H., Huang, C., Liao, S., Chen, P., Lu, Y., Wei, K., Ma, C.M.: Gadolinium-functionalized nanographene oxide for combined drug and microRNA delivery and magnetic resonance imaging. Biomaterials **35**, 6534–6542 (2014). https://doi.org/10.1016/j.biomaterials.2014.04.057
84. Loutfy, S.A., Salaheldin, T.A., Ramadan, M.A., Yehia, K., Abdallah, Z.F., Youssef, T.: Synthesis, characterization and cytotoxic evaluation of graphene oxide nanosheets: in vitro liver cancer model. Asian Pac. J. Cancer Prev. **18**, 955–961 (2017). https://doi.org/10.22034/apjcp.2017.18.4.955
85. Gurunathan, S., Han, J.W., Kim, E.S., Park, J.H., Kim, J.H.: Reduction of graphene oxide by resveratrol: a novel and simple biological method for the synthesis of an effective anticancer nanotherapeutic molecule. Int. J. Nanomed. **10**, 2951–2969 (2015). https://doi.org/10.2147/IJN.S79879
86. Zhou, T., Zhang, B., Wei, P., Du, Y., Zhou, H., Yu, M., Yan, L., Zhang, W., Nie, G., Chen, C., Tu, Y., Wei, T.: Energy metabolism analysis reveals the mechanism of inhibition of breast cancer cell metastasis by PEG-modified graphene oxide nanosheets. Biomaterials **35**, 9833–9843 (2014). https://doi.org/10.1016/j.biomaterials.2014.08.033
87. Sawosz, E., Jaworski, S., Kutwin, M., Vadalasetty, K.P.: Graphene functionalized with arginine decreases the development of glioblastoma multiforme tumor in a gene-dependent manner. Int. J. Mol. Sci. **16**, 25214–25233 (2015). https://doi.org/10.3390/ijms161025214
88. Zare-Zardini, H., Taheri-Kafrani, A., Amiri, A., Bordbar, A.-K.: New generation of drug delivery systems based on ginsenoside Rh2-, Lysine- and Arginine-treated highly porous graphene for improving anticancer activity. Sci. Rep. **8**, 586 (2018). https://doi.org/10.1038/s41598-017-18938-y
89. Khan, M., Khan, M., Al-Marri, A.H., Al-Warthan, A., Alkhathlan, H.Z., Siddiqui, M.R.H., Nayak, V.L., Kamal, A., Adil, S.F.: Apoptosis inducing ability of silver decorated highly reduced graphene oxide nanocomposites in A549 lung cancer. Int. J. Nanomed. **11**, 873–883 (2016)

90. Chen, Y., Su, Y., Hu, S., Chen, S.: Functionalized graphene nanocomposites for enhancing photothermal therapy in tumor treatment. Adv. Drug Deliv. Rev. **105**, 190–204 (2016). https://doi.org/10.1016/j.addr.2016.05.022
91. Zarafu, I., Turcu, I., Culit, D.C., Petrescu, S., Popa, M., Limban, C., Telehoiu, A., Ionit, P.: Antimicrobial features of organic functionalized. Materials (Basel) **11**, 1–10 (2018). https://doi.org/10.3390/ma11091704
92. Li, P., Sun, S., Dong, A., Hao, Y., Shi, S., Sun, Z.: Developing of a novel antibacterial agent by functionalization of graphene oxide with guanidine polymer with enhanced antibacterial activity. Appl. Surf. Sci. **355**, 446–452 (2015). https://doi.org/10.1016/j.apsusc.2015.07.148
93. Cai, X., Lin, M., Tan, S., Mai, W., Zhang, Y., Liang, Z., Lin, Z., Zhang, X.: The use of polyethyleneimine-modified reduced graphene oxide as a substrate for silver nanoparticles to produce a material with lower cytotoxicity and long-term antibacterial activity. Carbon **50**, 3407–3415 (2012). https://doi.org/10.1016/j.carbon.2012.02.002
94. Chandraker, K., Nagwanshi, R., Jadhav, S.K., Ghosh, K.K., Satnami, M.L.: Antibacterial properties of amino acid functionalized silver nanoparticles decorated on graphene oxide sheets. Spectrochim. Acta Part A Mol. Biomol. Spectrosc. **181**, 47–54 (2017). https://doi.org/10.1016/j.saa.2017.03.032
95. Santos, C.M., Mangadlao, J., Ahmed, F., Leon, A., Advincula, R.C., Rodrigues, D.F.: Graphene nanocomposite for biomedical applications: fabrication, antimicrobial and cytotoxic investigations. Nanotechnology **23**, 395101 (2012). https://doi.org/10.1088/0957-4484/23/39/395101
96. Peña-Bahamonde, J., San Miguel, V., Nguyen, H.N., Ozisik, R., Rodrigues, D.F., Cabanelas, J.C.: Functionalization of reduced graphene oxide with polysulfone brushes enhance antibacterial properties and reduce human cytotoxicity. Carbon **111**, 258–268 (2017). https://doi.org/10.1016/j.carbon.2016.10.005
97. Azimi, S., Behin, J., Abiri, R., Rajabi, L., Derakhshan, A.A., Karimnezhad, H.: Synthesis, characterization and antibacterial activity of chlorophyllin functionalized graphene oxide nanostructures. Sci. Adv. Mat. **6**(4), 771–781 (2014). https://doi.org/10.1166/sam.2014.1767
98. Ra, A.R., Bushroa, A.R., Amiri, A., Vadivelu, J.: Antibacterial biocompatible arginine functionalized mono-layer graphene: no more risk of silver toxicity. J. Hazard. Mater. J. **360**, 132–140 (2018). https://doi.org/10.1016/j.jhazmat.2018.07.107
99. Perreault, F., de Faria, A.F., Nejati, S., Elimelech, M.: Antimicrobial properties of graphene oxide nanosheets: why size matters. ACS Nano **9**, 7226–7236 (2015). https://doi.org/10.1021/acsnano.5b02067
100. Taha, A.A., Mousa, A., Al-ott, M., Faroun, M., Assali, M., Gomez, P.R., Thiab, S.: Department: non-covalent functionalization of graphene sheets with surfactants and their antibacterial activity. Palest. Med. Pharm. J. **1**, 65–72 (2016)
101. Banerjee, A.N.: Prospects and challenges of graphene-based nanomaterials in nanomedicine. Glob. J. Nanomed. **1**, 1–9 (2016). https://doi.org/10.19080/gjn.2016.01.555552
102. Ye, H., Zhang, X., Xu, C., Han, B., Xu, L.: Enhanced dielectric property and energy density in poly(vinylidene fluoride-chlorotrifluoroethylene) nanocomposite incorporated with graphene functionalized with hyperbranched polyethylene-graft-poly(trifluoroethyl methacrylate) copolymer. J. Mater. Chem. C. (2018). https://doi.org/10.1039/c8tc04510k
103. Layek, R.K., Nandi, A.K.: Feature article a review on synthesis and properties of polymer functionalized graphene. Polymer (Guildf) **54**, 5087–5103 (2013). https://doi.org/10.1016/j.polymer.2013.06.027
104. Wu, L., Ji, H., Guan, Y., Ran, X., Ren, J., Qu, X.: A graphene-based chemical nose/tongue approach for the identification of normal, cancerous and circulating tumor cells. Asia Mater. **9**, 1–9 (2017). https://doi.org/10.1038/am.2017.11
105. Akpotu, S.O., Moodley, B.: MCM-48 encapsulated with reduced graphene oxide/graphene oxide and as-synthesised MCM-48 application in remediation of pharmaceuticals from aqueous system. J. Mol. Liq. **261**, 540–549 (2018). https://doi.org/10.1016/j.molliq.2018.04.046

106. Saravanan, S., Sareen, N., Abu-el-rub, E., Ashour, H., Salah, S., Sayed, E., Moudgil, M., Vadivelu, J., Dhingra, S.: Graphene oxide-gold nanosheets containing chitosan scaffold improves ventricular contractility and function after implantation into infarcted heart. Nat. Publ. Gr. **8**, 1–13 (2018). https://doi.org/10.1038/s41598-018-33144-0
107. Yoon, H.J., Kim, T.H., Zhang, Z., Azizi, E., Pham, T.M., Paoletti, C., Lin, J., Ramnath, N., Wicha, M.S., Hayes, D.F.: Sensitive capture of circulating tumor cells by functionalized graphene oxide nanosheets. Nat. Nanotechnol. **8**, 735–741 (2014). https://doi.org/10.1038/nnano.2013.194.Sensitive
108. Ke, Q., Wang, J.: Graphene-based materials for supercapacitor electrodes–a review. J Mater. **2**, 37–54 (2016). https://doi.org/10.1016/j.jmat.2016.01.001
109. Yang, W., Ni, M., Ren, X., Tian, Y., Li, N., Su, Y., Zhang, X.: Graphene in supercapacitor applications. Curr. Opin. Colloid Interface Sci. **20**, 416–428 (2015). https://doi.org/10.1016/j.cocis.2015.10.009
110. Hu, C., Liu, D., Xiao, Y., Dai, L.: Functionalization of graphene materials by heteroatom-doping for energy conversion and storage. Prog. Nat. Sci. Mater. Int. **28**, 121–132 (2018). https://doi.org/10.1016/j.pnsc.2018.02.001
111. Chhabra, V.A.: Functionalization of graphene using carboxylation process. Int. J. Sci. Emerg. Technol. **4**, 13–19 (2012)
112. Abdelhalim, A.O., Galal, A., Hussein, M.Z., Sayed, E.I.: Graphene functionalization by 1,6-diaminohexane and silver nanoparticles for water disinfection (2016). https://doi.org/10.1155/2016/1485280

Microwave-Assisted Modification of Graphene and Its Derivatives: Synthesis, Reduction and Exfoliation

Nitika Devi, Rajesh Kumar and Rajesh K. Singh

Abstract Nowadays, microwave heating to graphene derivatives for carbon based materials processing (reduction, exfoliation and modifications) is new approach because strong interaction with microwave radiation, fast and localized heating can be achieved in a very short time. For graphene derivatives, microwave heating method is facile, simple, fast, controllable and energy-saving and provides an effective way to control nanoparticle size distribution on the surfaces. By tuning the microwave irradiation power, time and temperature different graphene based morphologies has been studied. For clear understanding, this chapter has been written basically into two parts. In first part, the literature published on interaction of microwave with grapheme derivatives and their transformations into reduced graphene oxide have been surveyed. The oxygen containing functional groups in different forms on surfaces of graphene derivatives strongly interact with microwave incident photons and easily detached from its surfaces. By microwave heating, graphite oxide/graphene oxide are easily reduced to very less oxygen containing graphene and also exfoliate into high surface containing porous graphene. In second part, graphene derivatives have been modified with different kind of metal/metal oxide for various kinds of applications. It is focused on the latest developments and the current status of graphene-metal oxide research using microwave processing. The high power microwave irradiation on graphene derivatives with metal oxide offers homogenous reaction environment and leads to controlled shape, size distribution of nanoparticles without any agglomeration. Detailed overview has been discussed on the possibilities and achievements of graphene derivatives–metal oxide research using microwave-based heating

N. Devi · R. K. Singh (✉)
School of Physical and Material Sciences, Central University
of Himachal Pradesh (CUHP), Kangra, Dharamshala 176215, Himachal Pradesh, India
e-mail: rksbhu@gmail.com

R. Kumar
Department of Electrical and Electronic Information Engineering,
Toyohashi University of Technology, 1-1 Hibarigaoka, Tempaku-cho, Toyohashi,
Aichi 441-8580, Japan

A. Khan et al. (eds.), *Graphene Functionalization Strategies*,
Carbon Nanostructures, https://doi.org/10.1007/978-981-32-9057-0_12

approaches. Microwave-assisted hydrothermal/solvothermal methods have also been described to synthesize metal oxides loaded graphene derivatives.

Keywords Microwave heating · Graphene derivatives · Metal oxide · Carbon nanomaterials · Microwave irradiation

1 Introduction

Nowadays, research on the synthesis of graphene (including its derivatives) reveals great attention due to the exceptional properties of the graphene and its derivatives. Graphene has exceptional properties like mobility (2.5×10^5 cm^{-1} V^{-1} s^{-1}) [1], carrier density (10^{12} cm^{-2}) [2], half-integer quantum Hall effect [3], thermal conductivity (300 W m^{-1} K^{-1}) [4], tensile strength (130 GPa) [5] and high transmittance (97.7%) [6].

The synthesis of the graphene can be done employing number of techniques such as mechanical exfoliation [7, 8], chemical vapor deposition (CVD) [9–11], liquid exfoliation of graphite [12], epitaxial growth on the SiC substrate [13], chemical reduction [14] etc. But the methods like CVD, physical exfoliation and others are found to have very low yield and CVD, epitaxial growth are also quite expensive methods. In case of the chemical route, the synthesis process involves many toxic chemical and time taking process. Thus there is need to develop other methods which involves simple, fast as well as cost efficient process and provides a scalable yield [15].

In these days microwave heating/irradiations are applied in various synthesis and modifications processes. Microwave radiations are the electromagnetic wave which wavelength appears in the range of 1 m–1 mm and corresponding frequencies in the region of 0.3–300 GHz. The initial use of microwave radiation is in the communication industry and two most suitable frequencies which are in use are 0.915 and 2.54 GHz. The domestic ovens are operated at 2.54 GHz with λ is 12.23 cm. The microwave heating is different from the conventional heating as in this case there is no conduction and convection like the conventional heating. In this case the electromagnetic energy interact with the materials molecules and directly convert it into the thermal energy. Microwave heating depends upon several factors like types of subjected material whether it is a metal, dielectric, insulator or semiconductor, shape and size etc. As shape and size of materials effect the penetration depth of the employed radiations [16]. This unique microwave heating process gives rise to many advantages as fast synthesis, selective heating without interaction with surroundings and cost efficient. These advantages are highly applicable in research and demonstrated the use of microwave heating in the material synthesis processes. There are several reports in which synthesis/reduction process has been carried out by using the microwave heating/radiation [17, 18]. The graphene derivatives such as graphene oxide (GO), reduced graphene oxide (rGO), graphene quantum dots (g-QDs), graphene nanoribbons (GNRs), graphene platelets and others different

types of doped graphene materials has been synthesized/reduced by microwave radiations [55, 62–64, 70–73]. The microwave assisted synthesis/reduced graphene derivatives materials have different applications and specially it has been frequently used for energy storage such supercapacitors and batteries etc. [65–69, 99].

2 Microwave Heating

Microwave heating is possible because of the microwave absorption tendency of the materials. In the microwave oven electromagnetic radiations are obtained by the device called magnetron. There are cavities in magnetron which size decides the frequency of the resulting wave. These waves travel through the wave guide to the chamber of the microwave oven. This enclosed chamber is made up the metal and reflection of the waves as back and forth until it gets absorbed by the material. The electric field interacts with the dipoles of the material and tries to flip the dipoles as fast as the electromagnetic field is changing its phase. The heating mechanisms behind the process is that in the presence of field dipoles of the molecules start rotating with field and try to align themselves in direction of the applied field. That means the microwave heating is the result of the dipolar and ionic polarization and it provides a volumetric type of heating to the materials as it is arising simultaneously in whole part of material. The friction of the flipping dipoles also results into the heat generation. Also it has been found that the microwave assisted synthesis process can be achieved in one step that means it is simple and fast as compared to the conventional synthesis methods [16, 18–20].

2.1 Microwave for Materials Processing

Microwave heating plays important role in the material processing and its interactions depends upon the nature of materials (conducting, dielectric or semiconducting). The microwave interactions occur at the molecular level of the materials and it has been found that polarization plays the crucial role in the heating of the materials. Mainly dipolar and ionic polarizations are involve in dielectric materials [21]. Dielectric properties are mainly defined by using the complex permittivity and loss tangent. Further these properties are dependent on numerous factors including penetration depth. It is well known that the complex permittivity is defined as the sum of the dielectric constant that is real part of permittivity and complex part of permittivity

$$\varepsilon^* = \varepsilon + \mathrm{i}\varepsilon' \tag{1}$$

Here real part of the complex permittivity deals with the absorption of the microwave radiation and imaginary part deals with the losses. Actually the thermal

losses are the main cause of heating but both parts have some optimized value to find desirable results. The other quantity is the loss tangent which defines the dielectric properties.

$$\tan = \varepsilon'/\varepsilon \tag{2}$$

Dipoles of the materials tend to align them self in accordance with the applied field. But at high frequencies, the flipping of the dipoles cannot match with variation in applied field and consequently there is a time lag between field and dipole orientation. This time lag (relaxation) appears as dissipation of energy in form of materials heating. It has been found that penetration of microwaves inside materials decreases its energy. Penetration depth is defined as the distance from the surface of the materials where the value of its energy decreased by 1/e times the starting value.

The expression for the penetration depth is given as

$$\mathrm{d} = \frac{c\varepsilon^{\circ}}{2\pi f\varepsilon'} \tag{3}$$

Here ε° is the dielectric constant of free space, c is the capacitance of the material and f is the frequency of electromagnetic field. It can be clearly seen from Eq. (3) that penetration depth is directly proportional to the capacitance of the material and inversely proportional to the frequency of the microwaves [16–19, 22, 23]. So the uniform heating can only be achieved when the frequency and penetration depth match with the thickness of the materials. If thicknesses of materials are very large and frequency is not enough then only surface of the material got heated (not the entire materials). Figure 1 shows the relation between dielectric loss factor and power absorbed. Also, it can be seen that the materials with high dielectric loss factor have penetration depth value approaches to zero. These kinds of materials are metals which have high conductance but low capacitance (high dielectric loss factor). These types of materials are actually reflectors of the microwave radiations due to approximately zero penetration depth. Also materials which have very low value of the dielectric loss factor have found to be transparent for the microwaves as because of large penetration depth there is very small absorption of energy [24]. So best suited materials for microwave heating are those which have dielectric loss factor are in middle of conductivity range as shown in Fig. 1.

This is the basic assessment of the behavior of some materials because detail analysis of materials processing is quite complex. Because properties like power absorption, dielectric loss factors are further dependent on many factors such as frequency, temp., size of material, mobility of the dipoles etc. so material behavior can be change depending upon these factors. For example SiC has two different loss factors at two different temperature (1.71 and 27.99 at room temp. and 695 °C respectively) subjecting at same frequency 2.45 GHz [25].

In industry the microwave processing is used in many areas such as ceramic, polymer and their composites processing.

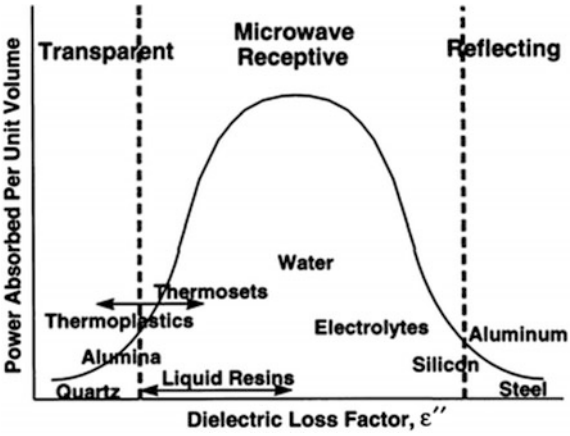

Fig. 1 Relation between power absorption with the dielectric loss factor [16]

2.2 *Microwave for Ceramic Processing*

Microwave processing has extraordinary importance in case of the ceramic processing specially in processing like sintering and chemical vapor infiltration (CVI) because of low thermal conductive nature of these materials. This importance is because of the fact that in case of conventional heating methods the ceramic materials required a high temperature treatment to get sintered and for CVI. Due to this reason, materials have a steep thermal gradient and outcome of this is stress in the materials which is enough to cause a fracture. The thermal gradient sintering process becomes tedious as fracture and stress results decrease in the density as well compactness of the material. But in case of microwave heating, thermal gradient process occurs in the reverse order (as materials are not heated by the surface) and direct heating in entire material takes place due to the radiations [26]. Singh et al. [27] synthesized the CeP_2O_7-phosphate composite using microwave heating in 5 min at 375 °C. There are considerable differences in the morphology as well; microwaves prepared products are found to be more dense and compact. There are other reports in which the microwave sintering results into the significant improvement in the materials properties such as study of the microwave sintering of alumina by Janney and Kimrey [28]. The alumina sintered using microwave heating has a high density value as compared to the conventional heating. This enhanced sintering capacity by microwave heating called as the "microwave effect". It has been found that material like SiC and MgO were also suitable for the microwave heating but there are others ceramic materials which need a critical temperature for absorbing the microwave radiations such as Al_2O_3 and Si_3N_4 [29]. Like sintering, CVI are other processes employed in the ceramic-matrix composites processing in which reactant gases are infiltrates into the preform and these vapors deposited on the solid phase. Solid phase are deposit in the hotter area rapidly as the vapor decomposition takes place easier in high temperature areas. This finding

demonstrates that non-uniform formation of composite can be avoid in CVI by microwave heating [26]. The ceramic materials matrix mostly used to form the composites with help of carbon materials. Morell et al. [30] and Ting et al. [31] suggested microwave capacity to infiltration of the carbon preform and carbon/carbon composites by using the microwave pulse power respectively. Ceramic materials as a matrix element has been used for the sintering the several carbon material. In composites formation, microwave heating is superior as compared to conventional sintering because its contains drawback as non-uniform dispersion, material damage and long duration of the processes [16].

2.3 Microwave for Polymer Processing

Polymer materials have low thermal conductivity so conventional heating cannot provide the sufficient quality of the product. Dielectric behaviors are different in both classes of polymers that are thermosetting and thermoplastic polymers. In case of the thermosets polymers change in the structure cross linking also effect the dielectric properties. It has been found that cross linking in polymer structure results in the increase in viscosity and at the same time decrease in the liquid resins [32, 33]. Due to increase in viscosity, less interaction of microwave radiations appears with the liquid resins affects the movement of dipoles due to decrease in dielectric losses of the polymers. The dielectric behavior of the thermoplastics is slightly similar to the ceramic material in which absorption of the microwave radiations takes place after critical temperature. It has been also described that the thermoplastic polymer materials shows very less dielectric loss if it contains crystallinity $\geq 45\%$ [32–36]. The enhancement in this behavior can be raised by introducing some conducting filler which helps in improving absorption capacity of materials. For composites of glass and aramid fibers the dielectric loss factor is strongly dominated by the matrix material as these fibers have found be very less dielectric losses. But in case of the carbon fiber composites, it was found that the dielectric losses were dominated due to the carbon fiber as it has a good absorption capacity toward microwave radiations [37]. Lee and Springer studied the effect of microwave power on the fiber reinforced composites materials [38, 39].

The effect of microwave radiations in polymer processing are demonstrated by the different research groups [40–42]. The reported studies reveal a conclusion that there is significant decrease in the cure time in the polymer processing using the microwave radiation as compared to the conventional heating. Also there are increases in the mechanical strength of the material with increase in extent in curing when processed with microwave radiations. The observation regarding the elastic properties has been explained by Bai et al. [43] and Jordan et al. [42]. It has been found that carbon fiber can act as aid to form strong resin composite. Due to high microwave absorption tendency of carbon fiber it gets heated more readily than surroundings. Then it can transfer its heat to the resins by conduction which leads to formation of the strong bond

between carbon fiber and resin result into increase in strength of composite material. Microwave heating have great potential for polymer and polymer composites and also reduces other difficulties in conventional heating like thermal degradation, non-uniform cure, stresses induced by process etc. [37, 44, 45].

3 Fundamentals of Microwave-Carbon Interactions

Initially microwave heating of materials was mainly limited to the liquid solutions but now it has been found that electron rich carbon materials have good microwave absorption capacity. This behavior is attributed because of the delocalized π electron from the sp^2 hybridization of the carbon atom. Nowadays, microwave heating is used in the synthesis of the carbon material and their derivatives (carbon nanotubes: CNTs, graphite, graphene, GO etc.) [46]. The mechanism behind the heating of the carbon materials is depends upon the state of the subjected material that whether it is liquid (dispersion in solvent) or solid. When carbon materials are with liquid solvent (DMF, ethanol, water etc.), then dipolar and ionic polarizations are main cause of heating during microwave irradiation. If the carbon materials are in the solid form then mechanism is entirely different from the polar case as there is no dipole's movement which can cause heating of the materials. In case of the solid carbon materials heating is due to delocalized π electrons which give the semiconducting behavior to the most of carbon based materials. When materials have the charged particles then in the presence of the applied field, the charged particles gets the kinetic energy and start moving with the applied field. The moving charge particles have collision and these collision give rise to the heating of the materials. This effect called as joules heating effect [21, 46, 47]. But in addition to this joules heating effect in case of materials such as CNTs, graphene etc. have the delocalized π electron and applied field presence moves the electron in the direction of the applied field. In case of carbon materials, heating is also describes by interfacial polarization which is called as Maxwell–Wagner–Sillar (MWS) [48, 49]. This type of polarization is similar to the formation of the depletion layer in the p-n junction. The separation of charges takes place at interfaces and boundaries of the material and produce loss of energy in form of heat. In some cases, electrons get extra energy and start jumping out of the regular path. Figure 2 shows the complete mechanism of heating and their dependence on frequency. Figure 2a shows the interaction mechanism in solution phase with microwaves and Fig. 2b represents the possible mechanism for solid carbon materials interact with microwaves. Figure 2c shows the total sum of losses as a function of frequency. In Fig. 2c, the red line shows the combined loss due to the ionic and dipolar polarization. From Fig. 2c, it can be seen that this is a type of polarization involves in heating also dependent on frequency of the applied field. At high frequency the losses are mainly due to the dipolar loss and at low frequency the loss is due to ionic mechanism.

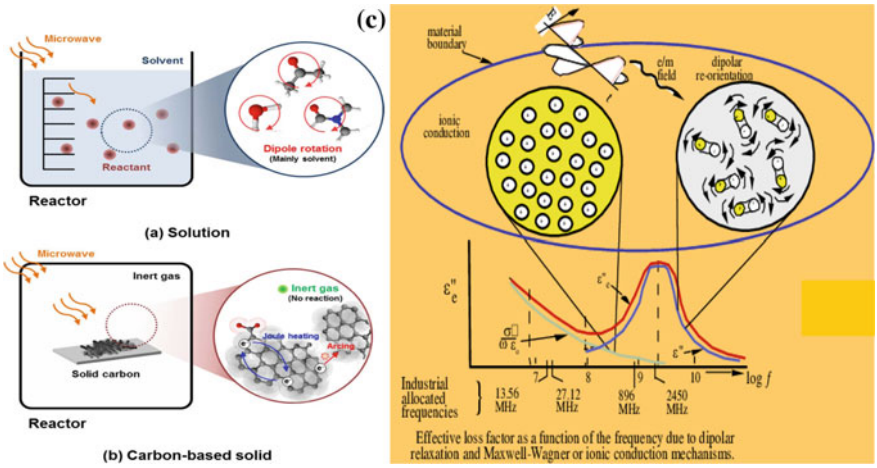

Fig. 2 **a** Mechanism for the interaction of solutions with microwave radiation, **b** mechanism for the microwave heating of solid carbon materials and **c** effective loss factor as a function of the frequency and corresponding involves interaction mechanisms [46, 50]

It has been found that the graphene is good absorber of the microwave radiations due to the presence of the free electrons. There are contradiction for MSW polarization in case of carbon based materials. It was found that the MSW polarization model is typically for the insulating materials and this type of polarization takes place at very low frequencies in comparison to the commercial microwave frequencies.

3.1 Microwave-Assisted Formation of Graphene Derivatives

Graphene is a good absorber of microwave as it has been demonstrated by the several researchers. Microwave assisted synthesis of graphene give additional advantages in comparison to conventional synthesis methods. Irradiation of microwave on graphene derivatives (e.g. GO), removes the oxygen containing function groups and exfoliates into high surface areas. There are many studies on various materials synthesis and modifications for example Kong and Cha [51] reported the microwave induced regeneration of NO_x saturated char. The studied has been performed at an input power of 300 W for 1 min processing time. Menéndez et al. [52] described use of microwave radiation for the restoration of the basic properties of activation carbon by the removal of the oxygen functional groups. These recommend that properties of activated carbon can be changes by adsorbing and removing of the function groups. Carrott et al. [53] explained the

effect of temperature on activated carbon composition and texture above 800 °C. It has been found that there was continuous increase in the carbon content. Dawei et al. [54] suggested the remediation of the crude oil contaminated soil by using the carbon fiber as microwave susceptor. Other microwave assisted synthesis has been used for graphene derivatives such as CNTs, graphite oxide, rGO, g-QDs, graphene nanoplatelets, GNRs other many type of doped graphene [55, 62–64, 70–73].

GO exfoliation using microwave radiations is very popular approach. It is a very fast reduction route from GO to rGO and also very inexpensive method as compared to other possible chemical or physical reduction processes. Zhu et al. [55] used microwave radiations in the synthesis of rGO for the application of the ultra supercapacitor. In this process, authors have treated GO powder in microwave cavity in ambient conditions (700 W for 1 min). Considerable expansion in GO powder has been seen with minimum power required for the synthesis was 280 W and time can be selected upon mass of sample [55]. Yan et al. [56] obtained water-soluble glucose rGO by reacting graphite oxide in an alkaline microwave-assisted environment for several hours. Imholt et al. [57] reported temperature dependence microwave radiations interaction reaction with CNTs. HiPco-generated SWCNTs showed strong microwave absorption at microwave irradiation of 2.45 GHz, 700 W. Lin et al. [58] reported analysis of thermal stability, mechanical property, and electrical property of CNTs which were treated under microwave irradiation for 3 min. The structural properties of CNTs im-proved and it has been confirmed by decreasing the D/G ratio of Raman spectra for CNTs. There are numerous reports which include the microwave irradiations for the graphene and CNTs synthesis. Wang et al. [59] reported microwave assisted synthesis of carbon dots from GO and it was found that microwave assisted synthesis was very suitable as compared to other methods. Table 1 shows the reports on microwaves assisted synthesis of the graphene derivatives.

3.2 *Microwave-Assisted Synthesis: Uniform Formation of Graphene Derivatives*

Due to good microwave absorption capacity of carbon materials [61] researchers are using this approach to synthesized carbon containing composites materials. The rGO is found to be a good matrix element for different composite formations. When rGO are heated with microwaves then due to more microwave absorption its surface gets more heated in comparison to the surroundings. This leads to heterogeneous nucleation and consequently composite materials are uniformly distributed on the surface of rGO [76, 77]. This microwave assisted synthesis method not only gives a uniform formation but also interaction between the matrix and nanoparticles are very strong. It is an advantage of microwave assisted synthesis method over the

Table 1 Microwave assisted synthesis of graphene derivatives

Material type	Polymer/dopant	Morphology and structure of materials	Microwave conditions	Results/applications	References
Graphite oxide	–	GO monolayer sheets with sizes up to micrometers (in width)	250 W for 150 s	High oxygen/carbon ratio graphite oxide prepared	[60, 61]
rGO	–	Worm-like shape of the EG (expandable graphite) with thin layered graphene structures, monolayer structure, few-layer graphene with size 3 μm with a transparent silk-like morphology	800 W for 5–15 s, 100 °C for 4–7 h, 300 W for 1.5 h	High quality graphene layers, antibacterial activity shows potential application in biomedical science, low cost graphene material	[62–64]
rGO	Mesoporous $NiMoO_4$ nanorod, polyethyleneimine/gold nanoparticle, silver (Ag) nanoparticles, (nitrogen, boron), PANI (polyaniline)	Ultrafine $NiMoO_4$ nanorods deposited on rGO nanosheets, AuNPs attached on the PEI wrapped GNS, silver nanoparticle on the rGO sheets, layered structure, paper like structure	200 W, 115 °C for 25 min, 200 W for 2 min, domestic microwave (700 W for 10 min), 700 W for 40 s, 180–300 °C for 5–15 min	High performance supercapacitor, selective electrochemical determination of dopamine, EMI shielding material	[65–69]
Graphene quantum dots	–	Diameter of the GQDs are in range 1–7 nm, high crystalline structure with single or bilayer, diameters of GQDs were mainly distributed in the narrow range of 1.8–2.4 nm, high crystallinity structure with lattice parameter from 0.33 to 0.25 nm	240 W for 1–5 h, 560 W for 10 min	ECL sensor for Cd^{+2}, highly sensitive fluorescent probes for detection of iron ions and pH value	[70, 71]

(continued)

Table 1 (continued)

Material type	Polymer/dopant	Morphology and structure of materials	Microwave conditions	Results/applications	References
Graphene nanoplatelets	Ethylene glycol, ethylene glycol (PEG) and 4-phenylazophenol (Azo)	Wrinkled GNP (graphene nanoplatelets) flakes, wrinkle GNPs flakes	150 °C for 15 min, 700 W for 30 min	Engine coolant, functionalized graphene nanoplatelets	[72, 73]
MWCNT (d: 15 nm [12], l: 300 μm), MWCNT (d: 40 nm, l: 10 μm)	PE (polyethylene), PMMA (polymethylmethacrylate)	Top layer coating sandwich, powder mixture	750 W 5–150 s, 700 W up to 1 min	Bond strength: 9.66 MPa, surface resistance: below 10^3 Ω, microhardness: 0.4 GPa, Young's modulus: 5.6 GPa, electrical resistivity: 11×10^3 Ω	[74, 75]

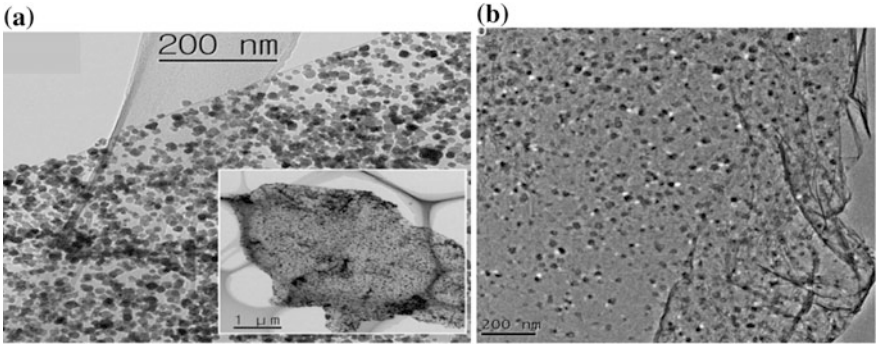

Fig. 3 **a** Uniform distribution of the CO_3O_4 on the surfaces of rGO [76], **b** HRTEM image of NiO nanoparticles distribution on the surface of rGO [78]

conventional synthesis approach in which it is necessary to add a linker chemical agent for the strong interactions. Park et al. investigated synthesis using microwave assisted hydrothermal method and find the uniform distribution of the Co_3O_4 on the surface of rGO as shown in Fig. 3a [76]. Also, Chen et al. [78] synthesized NiO/rGO composite using microwave irradiations. Figure 3b shows the HRTEM image of homogeneous distribution of the NiO nanoparticles on the surface of rGO sheets and the sized of NiO nanoparticles varying from 20 to 50 nm. Authors have explained uniform distribution on the basis of defects on graphene sheets due to thermal treatment of GO for obtaining graphene. These defects can act as a anchoring sites for Ni^{+2} results into the uniform attachment of the NiO on the surface of the graphene sheet [78].

Siamaki et al. [77] reported uniform distribution of the Pd nanoparticles on the graphene sheets using microwave heating. The phenomenon behind the uniform distribution of the Pd nanoparticles is heterogeneous nucleation growth. Liao et al. [79] synthesized uniform distribution of Pt nanoparticles on the rGO sheets. Authors have studied the effect of the timing of microwave irradiations on the size and distribution of the nanoparticles. It was found that 5 min irradiations time was suitable for uniform distribution of the nanoparticles. As the time duration of the irradiation increases, the nanoparticle size increases to average value of 4.56 nm and considerable agglomeration of the nanoparticles occurs. Figure 4 showed the TEM images of Pt/GO at different time duration of microwave heating. It suggest that time duration of irradiation depends upon desired product features. Li et al. [80] synthesized the composite of Pt/rGO formed by the microwave assisted synthesis, which shows uniform distribution of Pt nanoparticles on the graphene sheets.

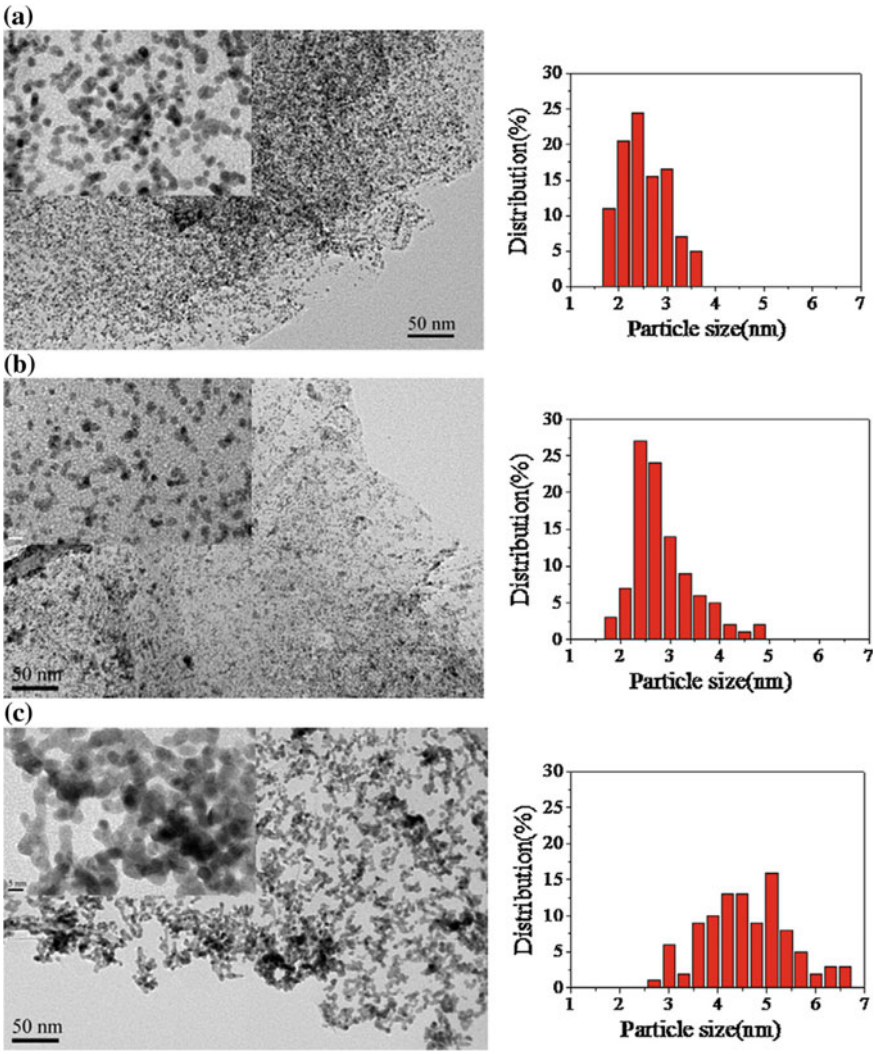

Fig. 4 Effect of irradiation timing on the particle size distribution and particle size of Pt/GO (inserted HRTEM images with 5-nm scale bar); **a** for 5 min, **b** 10 min; **c** 20 min [79]

4 Microwave-Assisted Modification of Graphene Derivatives

4.1 Microwave-Assisted Exfoliation: Highly Porous Structure of Graphene Derivatives

As we know that the graphene derivatives have been used in many application as supercapacitor, Li-ion batteries, sensors [65–69, 81] and for these applications the surface area of the materials are very important to enhance their capacity. Porous structures of the composites have significant contribution to increase the surface area of material. There are countless reports which show that the microwave assisted synthesis approach can give rise to the porous surface area of the products. Amiri et al. [82] fabricated the single or few layer graphene by using microwave heating (700 W for 20 min). In this work they did the functionalization of graphite in the ethylene glycol (EG) and then thermally treat it to get the pure graphene. The BET surface area of the synthesized pure graphene was 1559 m^2/g. It has been found that microwave heating provide the reaction kinetics between the ethylene glycol EG and graphite layers. In the presence of microwave heating the electrophilic reactions can be carried out more prominently which result into the functionalized graphite with no aggregation. It has been found that due to complete removal of functional groups in thermally treated graphene, it has higher adsorption for N_2 which means large surface area. Chemically-assisted Exfoliated graphene (CE-Gr) have less surface area as shown in Fig. 5 [82].

Li et al. [83] developed the sandwich-like porous Al_2O_3/rGO nanosheets anchored with NiO nanoparticles for application of anode materials for lithium-ion batteries. The material was synthesized using microwave heating at 150 °C for 3 min. N_2 adsorption-desorption study showed that the pore nature of material was

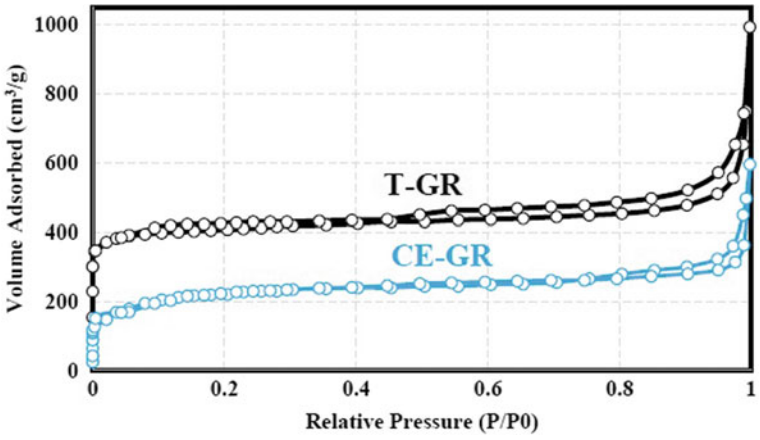

Fig. 5 N_2-adsorption/desorption of the CE-GR and T-GR [83]

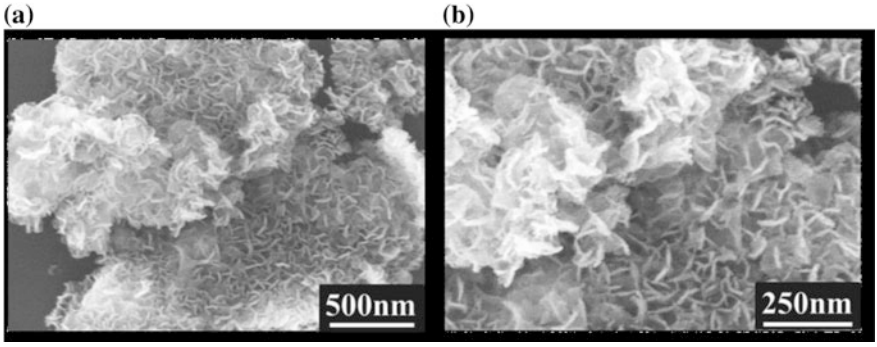

Fig. 6 SEM images of sandwich-like porous NiO-Al_2O_3/rGO nanocomposites [83]

mesoporous with the average diameter of the pores is 3.806 nm. Porous nature of the material can also be signifying by the SEM image of the composite as shown in Fig. 6. Kumar et al. [84] also synthesized palladium nanoparticles intercalated nitrogen doped rGO (NrGO) using microwave method. This treatment gives rise to the partial reduction of GO as well as production of N-doped GO. Then doping of Pd is done by using palladium (II) acetate ($Pd(OAc)_2$). The N-doped rGO and ($Pd(OAc)_2$) was mixed and mixture is again treated at 900 W for 1 min under microwave irradiations. The BET surface area of rGO and Pd-NrGO was 439 and 63 $m^2\ g^{-1}$ respectively. The pore size distribution of the material is in between 2–20 nm for the rGO and 3–90 nm for the Pd/N-rGO hybrid. This material has great affinity for the use of electrocatalytic activity in direct-ethanol fuel cells due to higher active surface area. It suggest that microwave assisted synthesis processes have potential to develop the porous microstructure of the materials [84].

4.2 Microwave-Assisted Reduction: Easily Removal of Oxygen Containing Functional Group from Graphene Derivatives Surfaces

Out of several possible methods of graphene formation the chemical synthesis method is efficient. But disadvantage of this method is that complete removal of the functional group is not possible. Nowadays, microwave irradiations are used for removal of the functional groups from the GO surface. It was found that graphene obtained by using microwave methods are comparatively pure and not contains large amount of functional groups. Microwave radiations are capable for producing the large heat in the layers of the graphite oxide which result into the exfoliation of layers and functional groups are removed in the form of gases. Voiry et al. [85] developed the pure graphene from the GO by using the microwave radiations. In this work GO was synthesized by using the modified Hummer's method and then

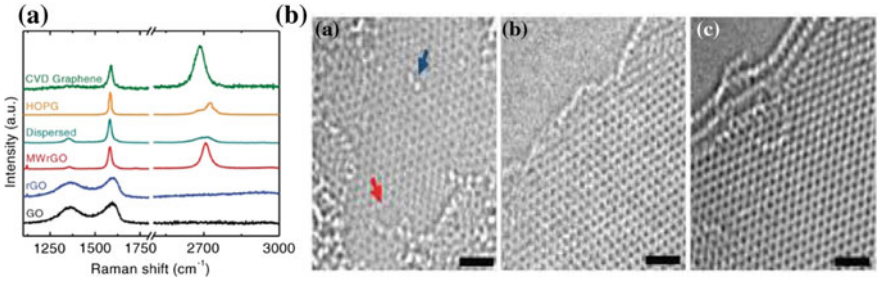

Fig. 7 **a** Raman spectrum of the MW-rGO with other graphene sample. The MW-rGO sample spectrum is showing a close resemblance with the CVD synthesized graphene. **b** High-resolution transmission electron microscopy (HR-TEM) of MW-rGO nanosheets (a) blue arrow is showing presence of oxygen functional group and red arrow is showing presence of hole, (b) trilayer, (c) highly ordered graphene layers

treated with microwave radiations for 1–2 min at 1000 W. Figure 7 shows the Raman spectroscopy and TEM analysis of rGO obtained microwave method Raman spectroscopy results showed the presence of D band is negligible (Fig. 7a). The microstructure of the rGO showed that structure of the graphene layers is highly ordered (Fig. 7b) [85]. There are other reports which shows the successful removal of the oxygen functional groups from the GO surfaces [86, 87].

5 Quality and Functionality of Graphene Derivatives

Quality of the prepared graphene is very important as it affects the properties of material such as mobility of charge carrier, conductivity, transparency etc. The use of low quality graphene shows the degradation of performance in applications. It is well known that there are various methods for the synthesis of graphene but suitable synthesis method is CVD. In CVD, the thermal heating induced the defects in the graphene layers, however microwave heating is found to be suitable to synthesize the good quality graphene with fewer defects as compared to other methods. Leng et al. [88] synthesized graphene using expandable graphite by microwave irradiation. The advantages of this method are the short time process and resulting good quality of graphene. The Raman spectroscopy gives the assurance for the quality of the graphene and the ratio of the intensity of D to G band was about 0.14 which shows good quality of graphene. Also, there are others research work support the strong evidence that the microwave irradiation is an efficient method for producing high quality graphene.

Functionalization of graphene with different functional groups is a challenge due to its low dispersion. It is important to functionalize the graphene for improving its processability and to make its use in various chemical engineering processes. Graphite oxide is found to be a good option for obtaining a functionalized graphene. Melucci et al. [89] carried out the covalent functionalizations of the GO by

employing the microwave irradiations. In this research work, the covalent functionalizations of GO was done with the optically active quaterthiophene molecules (T4) using microwave radiations in microwave oven for 40 min at 80 °C (100 W). It was found that the synthesis method is efficient as the graphite oxide microwave absorption capacity was advantageous for increasing the reaction rates. Sulleiro et al. produced solvent free and less time consuming method for the functionalizations of graphene using microwave approach. This work involved the covalent functionalizations of few layer graphene with arynes by cycloaddition reaction of the arynes with the few layer graphene. The studied shows that effect of microwave radiations for 5 cycle addition of 200 W in each cycle to achieve 250 °C. It was found that 5 cycle method developed the sufficient amount of the functionalized graphene with adequate value of I_D/I_G ratio [90]. Phosphate functionalized GO has been used for the synthesis of DHPM (3,4-dihydropyrimidin-2(1H)-ones) and DAPM (4,6-diarylpyrimidinones) molecules using microwave radiations in a report by Achary et al. [91]. It was found that in comparison to the GO and graphite the phosphate functionalized graphene has a good catalytic activity for the formation of the DHPM and DAPM with a yield of 94%. Supercapacitors electrode materials can be efficiently prepared by using the microwave radiation as reported by Huang et al. [92]. The functionalized graphene on the Ni foam for the supercapacitors electrode material gives high specific capacitance of 265 Fg^{-1} at the current density of 1 Ag^{-1}. The modification of graphene with amido group of the chitosan (CS) by using a microwave irradiation is reported by Hu et al. [93]. It was found that composite of GNS-CS shows good electrorheological (ER) properties.

6 Modification of Graphene Derivatives with Metal/Metal Oxide and Semiconducting Oxide for Formation of Hybrids/Composites

There are many reports on composites formation using graphene and its derivatives with metal/metal oxides. These composites are being used in different research areas such as energy storage (lithium ion batteries, supercapacitors), photocatalytic, sensors and many other applications. Here we have described different composite formation with help of graphene and its derivatives with metal/metal oxide which has been synthesized using microwave irradiations for different application purposes.

6.1 GO/rGO-Co_3O_4 Composite

The synthesis of composite of rGO and Co_3O_4 has been reported by several research groups. Park et al. [76] reported synthesis of Co_3O_4-rGO nanocomposite by microwave assisted hydrothermal synthesis. These composites materials have

been used in Li-ion batteries applications. For the formation of Co_3O_4-GO nanocomposite, authors have used $Co(C_2H_3O_2)_2(H_2O)_4$ as Co_3O_4 precursor and GO was simultaneously reduced in the reaction mixture in the presence of NaOH. The GO and $Co(C_2H_3O_2)_2(H_2O)_4$ were mixed in 2:1 with varying the concentration of the $Co(C_2H_3O_2)_2(H_2O)_4$ in 10 ml of NaOH. Then mixture is kept at 200 °C under microwave irradiation at a power of 1600 W for 30 min. This method is comparatively simple and it was found that large microwave absorption capacity of the carbon materials was also help in the uniform distribution of the nanoparticles on the surface of the rGO. Variation of discharge capacity of the electrode with loading content of the Co_3O_4 nanoparticles has been studied and it shows high potential application in the Li-ion batteries. Yan et al. [94] suggested microwave assisted hydrothermal synthesis of graphene-Co_3O_4 composite for the application of supercapacitors. The synthesized composite materials contain good cyclic life with specific capacitance of 243.2 Fg^{-1} at a scan rate of 10 mVS^{-1}.

6.2 GO/rGO-NiO Composites

Other kinds of composites materials have been also synthesized using rGO with NiO. Chen et al. [78] reported synthesis of rGO-NiO composites for the application of the supercapacitor. The used method for composite formation was rGO mixed with aqueous solution of $Ni(NO_3)_2$, loaded into autoclave and heated at 180 °C for 24 h. The product was dried at 30 °C an irradiated with microwave at 1000 W for 2 min in ambient condition. The synthesized rGO-NiO composite retains specific capacitance of 617 Fg^{-1} at current density of 1 Ag^{-1}. There is another report by Li et al. [83] on same material for the use of anode electrode material in lithium-ion batteries. In this work authors have synthesized sandwich-like porous Al_2O_3/rGO nanosheets anchoring NiO nanocomposite. Zito et al. [95] prepared rGO-NiO composite of different morphology for the use of methanol sensing. The microwave conditions used in this study were 800 W at 140 °C for 1 h. The morphology study shows that hierarchical flower-like NiO structure was preserved after the formation of the assembled composite.

6.3 GO/rGO-CuO Composites

There are many reports on the synthesis of rGO/CuO due to its various applications. The arises interest is because of the low cost of these transition metal oxide like CuO, NiO, Co_3O_4 etc. The main applications of rGO-NiO composite are in the area of Li ion batteries, supercapacitors and sensing. Ragavan et al. [96] reported comparison of two different process that were conventional heating and microwave

heating. Microwave heating shows fast process completed in only 20 min, however conventional heating takes long time (2 h). This is because of the dielectric heating in case of microwave irradiations. This composite shows a good peroxidase activity which results were 12 time increase in the CL (chemiluminescence) signal. Tian et al. [97] synthesized the composite of the CuO/S-doped graphene and process followed for the synthesis was microwave assisted solvothermal synthesis method. In this research work, microwave irradiations also simultaneously used for the reduction and sulfur doping inside. It was found that sulfur doping (2.17 at.%) was significant as comparison to others reported works. Wang et al. [98] reported one pot synthesis of the CuO/rGO composite using microwave assisted hydrothermal synthesis. The strong coupling of CuO with rGO shows good humidity sensing. Several research reports has been published on graphene/rGO-CuO/Cu_2O composites using microwave irradiation which are listed in Table 2.

Table 2 Formation of graphene/rGO-CuO/Cu_2O composites using microwave for different applications

Materials	Composite morphology/ structure	Microwave conditions	Results and applications	References
Graphene-CuO	Quasi-spherical CuO nanoparticles embedded on graphene sheets with 30–50 nm in size	300 W for 20 min	For the detection of Bisphenol-A	[96]
S-doped graphene-CuO	CuO uniformally dispersed on SG (s-doped graphene) sheets	800 W for 15 min for SG, 800 W for 10 min CuO/ SG	Nonenzymatic glucose sensing	[97]
rGO-CuO	Urchinlike CuO with flakes of rGO	150 °C for 30 min	Humidity-sensing	[98]
Graphene-CuO/ Cu_2O	Hollow nanosphere CuO and Cu_2O decorated on the graphene sheet	500 W for 10 min	Anode material for lithium-ion battery	[99]
Graphene-CuO	Leaf like CuO on the graphene sheet	400 W for 10 min at 100 °C	Lithium ion batteries	[81]
rGO-CuO	Rambutan-like 3D CuO on the rGO sheets	130 °C for 10 min with stirring at 1000 ppm	Non-enzymatic glucose detection	[100]
GQDs-CuO nanoneedles	GQDs/CuO nanocomposites has a spindle-shaped structure of 80 ± 10 nm in length and 16 ± 5 nm in width	200 °C for 8 min at 800 W	For the sensing of the H_2O_2 and glucose	[101]

6.4 GO/rGO-Pd Composites

The GO/rGO-Pd composites are mostly used in the applications of electro-oxidation of the methanol, ethanol, formic acid and catalyst in the carbon-carbon cross coupling reactions. Because of these various application areas, researchers are synthesizing these composites by using different methods. Microwave assisted synthesis is a promising method for the development of GO/rGO-Pd composites. Siamaki et al. [77] synthesized Pd nanoparticles supported on graphene surfaces by using microwave irradiations. Microwave irradiation produces uniform and small size of the Pd nanoparticles (7–9 nm) on the graphene sheets. Due to this high degree of dispersion and concentration of Pd nanoparticles on graphene sheets shows high catalyst reactivity toward Suzuki cross coupling. Zhang et al. [102] also employed the microwave irradiations for GO/rGO-Pd composite synthesis and used it for application of the electrocatalytic oxidation of methanol. The loading level and distribution was controlled by using the choice of initial materials and microwave irradiation timing. The experimental observation showed that the conversion of graphite oxide to rGO was possible within 1 min. There are others reports on Pd-graphene composite and demonstrate the use for the oxidation of the different acid and alcohol like formic acid [103], ethanol [104], ethanol glycol [105]. Goswami et al. [106] synthesized rGO decorated by Pt and Pd nanoparticles by using microwave irradiations. These composites are further used for the applications in dehalogenation reactions and reduction of Olefins. The nanoparticles have core shell type of structure for both Pd and Pt nanoparticles. Kumar et al. [84] demonstrated the use of the Pd nanoparticles composites with the nitrogen doped rGO for the electrocatalytic activity in direct ethanol fuel cell. In this work pyridine is used for the nitrogen doping in rGO and structure of the final material was found to be porous which results into the high surface area. The size of Pd nanoparticles is mostly less than <200 nm.

6.5 GO/rGO-Pt Composites

The uses of Pt nanoparticles in composite formations are limited due to high cost of the material. Still there are some research reports on synthesis of Pt composite with rGO. Liao et al. [79] prepared composite of Pt/graphene using polyol as a solvent by microwave irradiation. It has been found that the microwave irradiation give rise to fast growth result and uniform small size distribution of the Pt nanoparticles. This composite offer a high electrocatalytic activity due to large electrochemical active surface area (85.71 $m^2\ g^{-1}$) and Pt inter connecting clusters. Li et al. [80] have also used microwave synthesis method to evaluate the product catalytic activity for the formic acid. The morphological study of the material showed that Pt nano-dendrites were nearly spherical shape with the size of 5–7 nm. The performance of the composite materials also depends upon the concentration of the raw material. There

are other reports which prepared the Pt/rGO composite for the application of the electrocatalyst for the methanol oxidation [107–109].

6.6 GO/rGO-Ag Composites

The microwave irradiation has been also for synthesis of rGO-Ag composites for many applications. Liu et al. [110] synthesized rGO-Ag composite using microwave heating for the detection of H_2O_2 as it has good catalytic activity toward reduction of H_2O_2. In this synthesis process, $AgNO_3$ and GO were sonicated together for two minutes than treated with microwave irradiation (2 min, 750 W). Response time of the material sensor was found to be very fast and it was less than 2 s with a detection limit of 0.5 μM. Li et al. [111] developed microwave assisted synthesis for Ag nanoparticles decorated rGO sheets. The reduction of GO takes place by using the solvent ethanol and morphology study reveals that Ag nanoparticles are uniformly distributed on the rGO sheets with exhibiting strong interactions. It was found that photocatalytic activity of rGO-Ag composite was significantly affected by the microwave cycle time. Hsu et al. [112] reported formation of rGO-Ag composite using microwave heating and L-arginine acting as a reducing agent. It has been found that size of Ag nanoparticle can be changed by varying the number of microwave cycle as it was found to increase with increase in number of cycles. Microwave irradiation cycle was effecting the size of the Ag nanoparticles. Raman intensity was increases by increasing the size of the Ag nanoparticles. Meng et al. [113] developed flower like ZnO/rGO/Ag micro/nano-composite with enhanced photocatalytic properties. The synthesis process was carried using low power microwave heating (120 W) at 100 °C for 30 min. Ag nanoparticles and rGO were deposited on ZnO sheets which were main cause of enhanced catalytic properties because ZnO provide a feasible charge transfer to Ag and rGO. There are some other reports on the microwave assisted synthesis of rGO-Ag composite which are used for different applications such as HT22 neuronal cell [114] and for efficient removal of organic dyes under UV and visible-light irradiation [115].

6.7 GO/rGO-TiO_2 Composites

rGO/TiO_2 composite for the application of photocatalytic reduction of the Cr(VI) is described by Liu et al. [116]. In this work authors have prepared TiO_2 separately using different chemical. And then GO and TiO_2 suspension was prepared in the distilled water and treated with microwave heating (150 W for 10 min). The structure of TiO_2 was spherical nanoparticles and it was decorated on rGO sheets. The morphological study showed that rGO was providing the connection between the TiO_2 nanoparticles. rGO sheets also increases the distance between the two

neighboring nanoparticles by intercalation and which result in increased separation in photogenerated carriers. This separation leads to increase in the photocatalytic activity. There is another report on the photocatalytic application of rGO-TiO_2 composite which is developed by using microwave heating [117]. Kumar et al. [117] reported an in situ process in which reduction of GO and composite formation was taking place at same time. Photocatalytic activity of composite was much greater than the pure TiO_2 due to presence of rGO which makes carrier transfer easy. Liu et al. [118] tried to enhance the photocatalytic property of ZnO/rGO with composite formation of ZnO/TiO_2/rGO. These composites were synthesized by using microwave heating at 150 °C with microwave irradiation power of 150 W for 10 min. The photocatalytic activity of composite was dependent on the content of TiO_2 as its presence increase the light absorption and reduction of photoelectron-hole pair recombination in ZnO. These microwave synthesized TiO_2/rGO composites are also used in the supercapacitor application. Ramadoss et al. [119] synthesized hybrid structure of rGO-TiO_2 composite for electrochemical supercapacitors.

6.8 GO/rGO-ZnO Composites

Microwave facile synthesis process also reported for the formation of GO/rGO-ZnO composites. Lv et al. [120] synthesized ZnO-rGO hybrid composites using microwave method for the application of photocatalytic degradation of the methylene blue. The $Zn(NO_3)_2$ was used for the ZnO source and reduction of GO occurs under 30 min autoclave microwave system at 100 °C. The hexagonal ZnO nanorods were densely distributed on the rGO sheets and synthesized composite contains 88% degradation efficiency with 1.1 wt% of rGO composition [120]. Lv et al. [121] also prepared composite of ZnO/rGO/CNTs for the use of degradation of methylene blue using microwave process and synthesized composite shows 96% degradation efficiency due to presence of CNTs. The CNTs was incorporated in between rGO and ZnO hexagonal nanorods and that was the main cause of increasing efficiency [121]. Herring et al. [122] also synthesized ZnO/rGO composite using microwave radiations with different procedure. The microwave irradiations were incident on zinc acetate and GO suspension in the presence of oleic acid and oleylamine. Work also includes the study of different time duration and powers of microwave irradiation as it was found to affect the morphology of the ZnO nanoparticles. ZnO nanoparticles size increased with increase intime of heating without changing the morphology but power of microwave considerably effects the morphology. At low power irradiation (below 600 W) flower like ZnO nanoparticles were formed and at higher power irradiation (1000 W) stable hexagonal pyramidal shape ZnO nanoparticles were formed. Figure 8 shows the

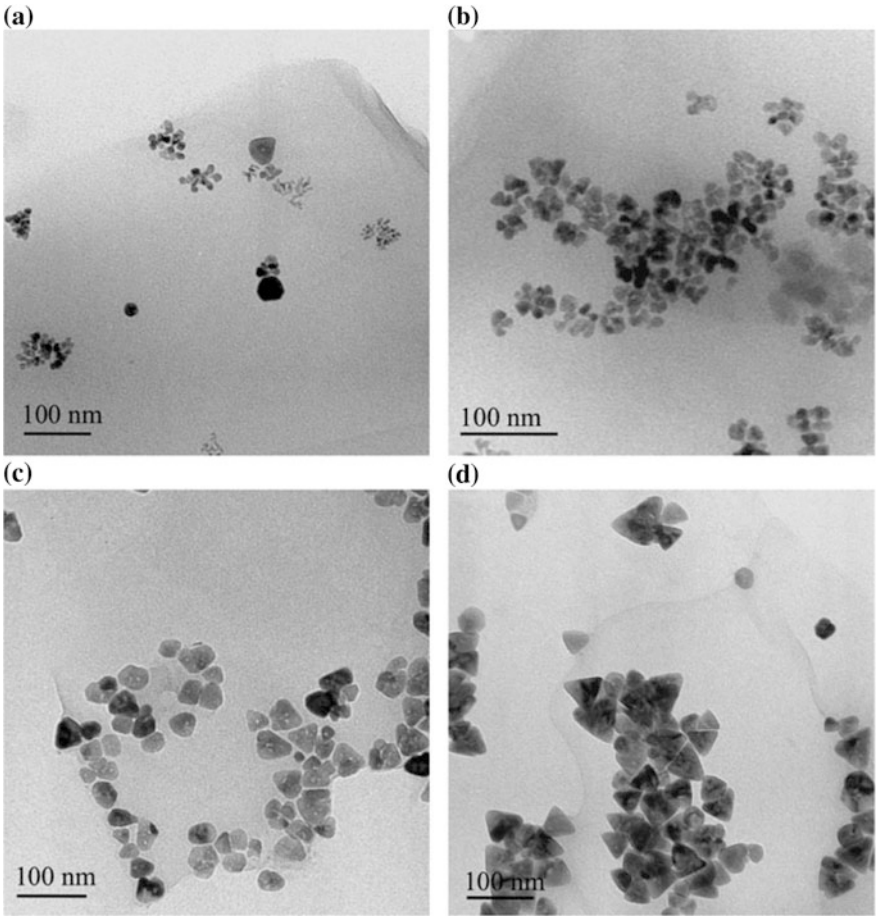

Fig. 8 Effect of microwave power on the structure of the material; **a** 600 W (209 °C), **b** 700 W (220 °C), **c** 800 W (227 °C), and **d** 1000 W (250 °C) [122]

effect of microwave power on the structure of the material. These observations conclude that the degree of heating should be carefully selected for the synthesis.

The enhanced transfer of the photogenerated electrons in the conduction band of ZnO to graphene is the main reason for good photocatalysts activity for the degradation of the MG (malachite green) dye in water [122]. There are other reported works on formation of rGO-ZnO composite using microwave irradiations which are given in Table 3.

Table 3 Formation of rGO-ZnO composites using microwave irradiation for different application

Materials	Composite structure and morphology	Microwave conditions	Results and applications	References
rGO-ZnO	ZnO nanocrystals are anchored onto the wrinkly rGO sheets	300 W for 10 min	Photoactivity for the decolorization of dyes under visible light	[123]
rGO-ZnO	ZnO nanorods apparently originate from a centre forming flower-like morphologies distributed on the surface of rGO	Microwave treatment for 30 min	Adsorption-photocatalysis	[124]
rGO-ZnO	Flower like ZnO nanoparticles are well decked on graphene/GO sheet	120 s at 450 W	Photodegradation of dyes	[125]
rGO-ZnO	Nanowires of ZnO were decorated/anchored on the surface of GO	450 W for 5 min	Photo degradation brilliant blue	[126]

6.9 GO/rGO-MoS_2 Composites

GO/rGO-MoS_2 composite have different applications like battery, photocatalytic degradation, hydro desulfurization etc. [127–131]. Firmiano et al. [127] established a method for crystallization of MoS_2 on the surface on GO. The layered structure of MoS_2 on GO was prepared using modification of sol-gel method. The reduction of GO occurs without using any additional reducing agent and also due to localized heating effect on GO surface give rise to strong interaction between GO and MoS_2. These 2D materials showed a high potential for hydrogen evolution reaction (HER). Firmiano et al. [128] used the microwave fabricated 2D composites for the supercapacitor electrode material. Qin et al. [129] synthesized rGO-MoS_2 composite using microwave heating. The microwave heat treatment was done at 160 °C with microwave irradiation power of 100 W for 10 min. Effect of loading of rGO with MoS_2 on the cycling capacity and performance as an anode material for sodium ion battery has been studied. Composite exhibited high reversible capacity that was after 50 cycles still give a performance of 305 mAh g^{-1} at a current density of 100 mA g^{-1}. Li et al. [130] prepared rGO/MoS_2 composite with same process and used for the application of visible-light photocatalytic degradation of methylene blue. It showed 99% degradation rate under visible light for 60 min with the composition of 5% of rGO. Liu et al. [131] fabricated graphene-MoS_2 composites for application of hydrodesulfurization and it was found that the material has more COS (carbonyl sulfide) hydrogenation capacity than the conventionally synthesized product. It was found that the MoS_2 nanoparticles were uniformly distributed on the sheets of graphene result into the high active surface area for the hydrodesulfurization. This uniform formation was due to the unique microwave absorption of graphene. This reported work showed that graphene can act as good

catalyst for the nanoparticles microwave assisted synthesis. Youn et al. [132] reported synthesis of rGO-MoS_2 composites for the application of anode material in Li-ion batteries.

7 Conclusions and Future Perspectives

It can be concluded from the above discussion that microwave irradiations play an important role in many synthesis processes especially in the case of the carbon based materials. The conclusion of the chapter is that the microwave radiations have a great potential in the carbon based material synthesis processes. Many microwave synthesized materials are further successfully implemented for various applications. The features of the microwave synthesized products are due to its unique heating principles. The implemented applications areas show that the materials have great efficiency for the respected used applications. The microwave radiations gives the advantages like short time processing, uniform heating, simple and solvent free synthesis. The phenomenon of interacting microwave irradiations with carbon materials is different from the other materials which contain the polar molecules. In case of the carbon materials, the π-π electrons are the main cause of heating which give rise to unique heating effect. This unique heating effect is favorable for the material processing and functioning. The microwave heating overcome the many drawbacks of the conventional methods of synthesis such as use of the toxic materials, long processing time and non uniform heating due to heating phenomenon of thermal conduction by the molecules. As in case of the microwave heating the electromagnetic energy is directly converted into the heat give rise to the uniform heating because of volume metric type of heating. In case of the graphene synthesis this process improves the limitations of the other conventional synthesis methods such as CVD. Conventionally CVD synthesis method used for the high quality graphene but it is a high cost process and gives low yield. And other option for large yield of graphene is chemical synthesis route that is from graphite oxide which involves the use of the toxic reduction agent, long duration and low quality. Use of microwave radiations for graphene synthesis play an important role as it is found that microwave assisted synthesis is cost efficient, inexpensive as well as maintain the high quality of the graphene. Using microwave assisted synthesis process, carbon based materials and their composites synthesis can be done in a single step especially conversion from graphite oxide to graphene and their composites preparation. Also the graphene and its composite can be highly porous nature which can give rise to enhancement in many properties specially in the energy storage applications like supercapacitors, Li-ion batteries etc. Using microwave radiations we can functionalize, modified the graphene with different functional groups and dispersed it into different solvents due to special effect of microwave radiations. It is found that functionalities and composite formation with many nanoparticles appears uniform on the graphene sheet. This uniform distribution is because of the unique heterogeneous reaction effect caused by large

microwave absorption capacity of carbon based materials. In future, microwave irradiations assisted synthesis processes must have the prominent role in the development of the material processes due to its unique heating phenomenon. Microwave processes provide an efficient way for the synthesis of graphene which is very favorable for its future applications.

References

1. Mayorov, A.S., Gorbachev, R.V., Morozov, S.V., Britnell, L., Jalil, R., Ponomarenko, L.A., Blake, P., Novoselov, K.S., Watanabe, K., Taniguchi, T., Geim, A.K.: Micrometer-scale ballistic transport in encapsulated graphene at room temperature. Nano Lett. **11**(6), 2396–2399 (2011)
2. Ye, J., Craciun, M.F., Koshino, M., Russo, S., Inoue, S., Yuan, H.: Accessing the transport properties of graphene and its multilayers at high carrier density. Proc. Natl. Acad. Sci. U.S. A. **108**, 13002 (2011)
3. Zhang, Y., Tan, Y.W., Stormer, H.L., Kim, P.: Experimental observation of the quantum Hall effect and Berry's phase in graphene. Nature **438**(7065), 201–204 (2005)
4. Balandin, A.A.: Thermal properties of graphene and nanostructured carbon materials. Nat. Mater. **10**(8), 569–581 (2011)
5. Lee, C., Wei, X., Kysar, J.W., Hone, J.: Measurement of the elastic properties and intrinsic strength of monolayer graphene. Science **321**(5887), 385–388 (2008)
6. Nair, R.R., Blake, P., Grigorenko, A.N., Novoselov, K.S., Booth, T.J., Stauber, T., Peres, N. M.R., Geim, A.K.: Fine structure constant defines visual transparency of graphene. Science **320**(5881), 1308 (2008)
7. Whitener, K.E., Sheehan, P.E.: Graphene synthesis. Diam. Relat. Mater. **46**, 25–34 (2014)
8. Yi, M., Shen, Z.: A review on mechanical exfoliation for the scalable production of graphene. J. Mater. Chem. A **3**(22), 11700–11715 (2015)
9. Muñoz, R., Gómez-Aleixandre, C.: Review of CVD synthesis of graphene. Chem. Vap. Depos. **19**(10–12), 297–322 (2013)
10. Srivastava, A., Galande, C., Ci, L., Song, L., Rai, C., Jariwala, D., Kelly, K.F., Ajayan, P. M.: Novel liquid precursor-based facile synthesis of large-area continuous, single, and few-layer graphene films. Chem. Mater. **22**(11), 3457–3461 (2010)
11. Li, X., Cai, W., An, J., Kim, S., Nah, J., Yang, D., Piner, R., Velamakanni, A., Jung, I., Tutuc, E., Banerjee, S.K., Colombo, L., Ruoff, R.S.: Large area synthesis of high quality and uniform graphene films on copper foils. Science **324**(5932), 1312–1314 (2009)
12. Hernandez, Y., Nicolosi, V., Lotya, M., Blighe, F.M., Sun, Z., De, S., McGovern, I.T., Holland, B., Byrne, M., Gun'ko, Y.K., Boland, J.J., Niraj, P., Duesberg, G., Krishnamurthy, S., Goodhue, R., Hutchison, J., Scardaci, V., Ferrari, A.C., Coleman, J.N.: High-yield production of graphene by liquid-phase exfoliation of graphite. Nat. Nanotechnol. **3**(9), 563–568 (2008)
13. Juang, Z.Y., Wu, C.Y., Lo, C.W., Chen, W.Y., Huang, C.F., Hwang, J.C., Chen, F.R., Leou, K.C., Tsai, C.H.: Synthesis of graphene on silicon carbide substrates at low temperature. Carbon N. Y. **47**(8), 2026–2031 (2009)
14. Abdolhosseinzadeh, S., Asgharzadeh, H., Kim, H.S.: Fast and fully-scalable synthesis of reduced graphene oxide. Sci. Rep. **5**, 1–7 (2015)
15. Krane, N.: Preparation of graphene selected topics in physics: physics of nanoscale carbon. Growth Lakel. **4**(4), 1–5 (1993)
16. Thostenson, E.T., Chou, T.: Microwave processing: fundamentals and applications. Compos. Part A Appl. Sci. Manuf. **30**, 1055–1071 (1999)
17. Hill, M.: Chapter 3. Microwave Theory and Background, pp. 56–79 (1993)

18. Stuerga, D.: Microwave-Material Interactions and Dielectric Properties, Key Ingredients for Mastery of Chemical Microwave Processes, vol. 1 (2008)
19. Sun, J., Wang, W., Yue, Q.: Review on microwave-matter interaction fundamentals and efficient microwave-associated heating strategies. Materials (Basel) **9**(4) (2016)
20. Chandrasekaran, S., Ramanathan, S., Basak, T.: Microwave food processing—a review. Frin **52**(1), 243–261 (2013)
21. Menéndez, J.A., Arenillas, A., Fidalgo, B., Fernández, Y., Zubizarreta, L., Calvo, E.G., Bermúdez, J.M.: Microwave heating processes involving carbon materials. Fuel Process. Technol. J. **91**(1), 1–8 (2010)
22. Stuerga, D.: Fundamental aspects of microwave irradiation in organic chemistry. Microwaves Org. Synth. 1–56 (2012)
23. Suits, B.H.: Nuclear quadrupole resonance spectroscopy (Chapter 2). In: Vij, D.R. (ed.) Handbook of Applied Solid State Spectroscopy, pp. 65–96. Springer US, Boston, MA (2006)
24. Metaxas, A.C.: Microwave heating. Power Eng. J. **5**(5), 237–247 (1991)
25. Sutton, W.: Microwave processing of ceramics - An overview. MRS Proc. **269**, 3–19 (1992)
26. Brandon, J., Samuels, J., Hodgkins, W.: Microwave sintering of oxide ceramics. MRS Proc. **269**, 237–244 (1992)
27. Singh, B., Devi, N., Mathur, L., Singh, R.K., Bhardwaj, A., Song, S.J., Henkensmeier, D.: Fabrication of dense $Ce_{0.9}Mg_{0.1}P_2O_7$-P_mO_n composites by microwave heating for application as electrolyte in intermediate-temperature fuel cells. Ceram. Int. **44**(6), 6170–6175 (2018)
28. Janney, M.A., Kimrey, H.D.: Diffusion-controlled processes in microwave-fired oxide ceramics. MRS Proc. Microw. Process. Mater. II **189**, 215–227 (1991)
29. Agrawal, D.K.: Microwave processing of ceramics. Curr. Opin. Solid State Mater. Sci. **3**(5), 480–485 (1998)
30. Morell, J.I., Economou, D.J., Amundson, N.R.: Pulsed-power volume-heating chemical vapor infiltration. J. Mater. Res. **7**(9), 2447–2457 (1992)
31. Ting, J.M., Lagounov, A.G., Lake, M.L.: Chemical vapour infiltration of diamond into a porous carbon. J. Mater. Sci. Lett. **15**(4), 350–352 (1996)
32. Kranbuehl, D., Delos, S., Yi, E., Mayer, J., Jarvie, T., Winfree, W., Hou, T.: Dynamic dielectric analysis: nondestructive material evaluation and cure cycle monitoring. Polym. Eng. Sci. **26**(5), 338–345 (1986)
33. Mijović, J., Kenny, J.M., Maffezzoli, A., Trivisano, A., Bellucci, F., Nicolais, L.: The principles of dielectric measurements for in situ monitoring of composite processing. Compos. Sci. Technol. **49**(3), 277–290 (1993)
34. Martinelli, M., Rolla, P.A., Tombari, E.: A method for dynamic dielectric measurements at microwave frequencies: applications to polymerization process studies. IEEE Trans. Instrum. Meas. (3), 417–421 (1985)
35. Haran, E.N.: Dielectric properties of an epoxy resin during polymerization. J. Appl. Polym. Sci. **9**(11), 3505–3518 (1965)
36. Chen, M., Siochi, E.J., Ward, T.C., McGrath, J.E.: Basic ideas of microwave processing of polymers. Polym. Eng. Sci. **33**(17), 1092–1109 (1993)
37. Drzal, L.T., Hook, K.J., Agrawal, R.K.: Enhanced chemical bonding at the fibre-matrix interphase in microwave processed composites. MRS Online Proc. Libr. Arch. **189**, 449–454 (1990)
38. Lee, W.I., Springer, G.S.: Interaction of electromagnetic radiation with organic matrix composites. J. Compos. Mater. **18**(4), 357–386 (1984)
39. Lee, W.I., Springer, G.S.: Microwave curing of composites. J. Compos. Mater. **18**(4), 387–409 (1984)
40. Marand, E., Baker, K.R., Graybeal, J.D.: Comparison of reaction mechanisms of epoxy resins undergoing thermal and microwave cure from in situ measurements of microwave dielectric properties and infrared spectroscopy. Macromolecules **25**(8), 2243–2252 (1992)

41. Wei, J., Hawley, M.C., Delong, J.D., Demeuse, M.: Comparison of microwave and thermal cure of epoxy resins. Polym. Eng. Sci. **33**(17), 1132–1140 (1993)
42. Jordan, C., Galy, J., Pascault, J.-P., Moré, C., Delmotte, M., Jullien, H.: Comparison of microwave and thermal cure of an epoxy/amine matrix. Polym. Eng. Sci. **35**(3), 233–239 (1995)
43. Bai, S.L., Djafari, V., Andréani, M., François, D.: A comparative study of the mechanical behaviour of an epoxy resin cured by microwaves with one cured thermally. Eur. Polym. J. **31**(9), 875–884 (1995)
44. Bai, S.L., Djafari, V.: Interfacial properties of microwave cured composites. Compos. Mater. **4361**(July), 645–651 (2014)
45. Adegbite, V., Hawley, M., Decker, D., Sticklen, J.: Automation of microwave processing of graphite/epoxy composite materials using an expert systems technique. MRS Online Proc. Libr. Arch. Microw. Process. Mater. III **269**, 425–430 (1992)
46. Kim, T., Lee, J., Lee, K.-H.: Microwave heating of carbon-based solid materials. Carbon Lett. **15**(1), 15–24 (2014)
47. Bradshaw, S.M., van Wyk, E.J., de Swardt, J.B.: Microwave heating principles and the application to the regeneration of granular activated carbon. J. South. Afr. Inst. Min. Metall. (August), 201–212 (1998)
48. Rogti, F., Ferhat, M.: Maxwell-Wagner polarization and interfacial charge at the multi-layers of thermoplastic polymers. J. Electrostat. **72**(1), 91–97 (2014)
49. Vu, T.T.N., Teyssedre, G., Roy, S.L., Laurent, C.: Maxwell-Wagner effect in multi-layered dielectrics: interfacial charge measurement and modelling. Technologies **5**(2), 27 (2017)
50. Gude, V.G., Patil, P., Martinez-Guerra, E., Deng, S.: Microwave energy potential for biodiesel production. Sustain. Chem. Process. **1**, 1–31 (2013)
51. Kong, Y., Cha, C.Y.: Microwave-induced regeneration of NO_x-saturated char. Energy Fuels **10**(6), 1245–1249 (1996)
52. Menéndez, J.A., Menéndez, E.M., García, A., Parra, J.B., Pis, J.J.: Thermal treatment of active carbons: a comparison between microwave and electrical heating. J. Microw. Power Electromagn. Energy **34**(3), 137–143 (1999)
53. Carrott, P.J., Nabais, J.M., Ribeiro Carrott, M.M., Menéndez, J.: Thermal treatments of activated carbon fibres using a microwave furnace. Microporous Mesoporous Mater. **47**(2), 243–252 (2001)
54. Dawei, L., Zhang, Y., Xie, Q., Yazhi, Z.: Microwave thermal remediation of crude oil contaminated soil enhanced by carbon fiber. J. Environ. Sci. **21**(9), 1290–1295 (2009)
55. Zhu, Y., Murali, S., Stoller, M.D., Velamakanni, A., Piner, R.D., Ruoff, R.S.: Microwave assisted exfoliation and reduction of graphite oxide for ultracapacitors. Carbon N. Y. **48**(7), 2118–2122 (2010)
56. Yan, Q., Liu, Q., Wang, J.: A simple and fast microwave assisted approach for the reduction of graphene oxide. Ceram. Int. **42**(2), 3007–3013 (2016)
57. Imholt, T.J., Dyke, C.A., Hasslacher, B., Perez, J.M., Price, D.W., Roberts, J.A., Scott, J.B., Wadhawan, A., Ye, Z., Tour, J.M.: Nanotubes in microwave fields: light emission, intense heat, outgassing, and reconstruction. Chem. Mater. **15**(21), 3969–3970 (2003)
58. Lin, W., Moon, K., Zhang, S., Ding, Y., Shang, J., Chen, M., Wong, C.: Microwave makes carbon nanotubes less defective. ACS Nano **4**(3), 1716–1722 (2010)
59. Wang, Q., Zheng, H., Long, Y., Zhang, L., Gao, M., Bai, W.: Microwave-hydrothermal synthesis of fluorescent carbon dots from graphite oxide. Carbon N. Y. **49**(9), 3134–3140 (2011)
60. Wang, X., Tang, H., Huang, S., Zhu, L.: Fast and facile microwave-assisted synthesis of graphene oxide nanosheets. RSC Adv. **4**(104), 60102–60105 (2014)
61. Hu, H., Zhao, Z., Zhou, Q., Gogotsi, Y., Qiu, J.: The role of microwave absorption on formation of graphene from graphite oxide. Carbon N. Y. **50**(9), 3267–3273 (2012)
62. Jiang, F., Yu, Y., Wang, Y., Feng, A., Song, L.: A novel synthesis route of graphene via microwave assisted intercalation-exfoliation of graphite. Mater. Lett. **200**, 39–42 (2017)

63. Morales, G.M., Schifani, P., Ellis, G., Ballesteros, C., Martínez, G., Barbero, C., Salavagione, H.J.: High-quality few layer graphene produced by electrochemical intercalation and microwave-assisted expansion of graphite. Carbon N. Y. **49**(8), 2809–2816 (2011)
64. Kumar, D., Raghavan, C.M., Sridhar, C., Shin, J.-H., Ryu, S.H., Jang, K., Shin, D.-S.: Microwave-assisted synthesis, characterization of reduced graphene oxide, and its antibacterial activity. Bull. Korean Chem. Soc. **36**(8), 2034–2038 (2015)
65. Liu, T., Chai, H., Jia, D., Su, Y., Wang, T., Zhou, W.: Rapid microwave-assisted synthesis of mesoporous $NiMoO_4$ nanorod/reduced graphene oxide composites for high-performance supercapacitors. Electrochim. Acta **180**, 998–1006 (2015)
66. Ponnusamy, V.K., Mani, V., Chen, S.M., Huang, W.T., Jen, J.F.: Rapid microwave assisted synthesis of graphene nanosheets/polyethyleneimine/gold nanoparticle composite and its application to the selective electrochemical determination of dopamine. Talanta **120**, 148–157 (2014)
67. Wang, C., Guo, R., Lan, J., Jiang, S., Zhang, Z.: Microwave-assisted synthesis of silver/reduced graphene oxide on cotton fabric. Cellulose **24**(9), 4045–4055 (2017)
68. Umrao, S., Gupta, T.K., Kumar, S., Singh, V.K., Sultania, M.K., Jung, J.H., Oh, I.K., Srivastava, A.: Microwave-assisted synthesis of boron and nitrogen co-doped reduced graphene oxide for the protection of electromagnetic radiation in Ku-band. ACS Appl. Mater. Interfaces **7**(35), 19831–19842 (2015)
69. Murugan, A.V., Muraliganth, T., Manthiram, A.: Rapid, facile microwave-solvothermal synthesis of graphene nanosheets and their polyaniline nanocomposites for energy storage. Chem. Mater. **22**(8), 2692 (2010)
70. Li, L.L., Ji, J., Fei, R., Wang, C.Z., Lu, Q., Zhang, J.R., Jiang, L.P., Zhu, J.J.: A facile microwave avenue to electrochemiluminescent two-color graphene quantum dots. Adv. Funct. Mater. **22**(14), 2971–2979 (2012)
71. Zhang, C., Cui, Y., Song, L., Liu, X., Hu, Z.: Microwave assisted one-pot synthesis of graphene quantum dots as highly sensitive fluorescent probes for detection of iron ions and pH value. Talanta **150**, 54–60 (2016)
72. Amiri, A., Sadri, R., Shanbedi, M., Ahmadi, G., Kazi, S.N., Chew, B.T., Zubir, M.N.M.: Synthesis of ethylene glycol-treated graphene nanoplatelets with one-pot, microwave-assisted functionalization for use as a high performance engine coolant. Energy Convers. Manag. **101**, 767–777 (2015)
73. Amiri, A., Shanbedi, M., Ahmadi, G., Eshghi, H., Chew, B.T., Kazi, S.N.: Microwave-assisted direct coupling of graphene nanoplatelets with poly ethylene glycol and 4-phenylazophenol molecules for preparing stable-colloidal system. Colloids Surf. A Physicochem. Eng. Asp. **487**, 131–141 (2015)
74. Xie, R., Wang, J., Yang, Y., Jiang, K., Li, Q., Fan, S.: Aligned carbon nanotube coating on polyethylene surface formed by microwave radiation. Compos. Sci. Technol. **72**(1), 85–90 (2011)
75. Wang, H., Feng, J., Hu, X., Ng, K.M.: The formation of hollow poly(methyl methacrylate)/multiwalled carbon nanotube nanocomposite cylinders by microwave irradiation. Nanotechnology **20**(9) (2009)
76. Park, S.-H., Kim, H.-K., Roh, K.C., Kim, K.-B.: Co_3O_4-reduced graphene oxide nanocomposite synthesized by microwave-assisted hydrothermal process for Li-ion batteries. Electron. Mater. Lett. **11**(2), 282–287 (2015)
77. Siamaki, A.R., Khder, A.E.R.S., Abdelsayed, V., El-Shall, M.S., Gupton, B.F.: Microwave-assisted synthesis of palladium nanoparticles supported on graphene: a highly active and recyclable catalyst for carbon-carbon cross-coupling reactions. J. Catal. **279**(1), 1–11 (2011)
78. Chen, Y., Huang, Z., Zhang, H., Chen, Y., Cheng, Z., Zhong, Y., Ye, Y., Lei, X.: Synthesis of the graphene/nickel oxide composite and its electrochemical performance for supercapacitors. Int. J. Hydrogen Energy **39**(28), 16171–16178 (2014)

79. Liao, C.S., Liao, C.T., Tso, C.Y., Shy, H.J.: Microwave-polyol synthesis and electrocatalytic performance of Pt/graphene nanocomposites. Mater. Chem. Phys. **130**(1–2), 270–274 (2011)
80. Li, N., Tang, S., Pan, Y., Meng, X.: One-step and rapid synthesis of reduced graphene oxide supported Pt nanodendrites by a microwave-assisted simultaneous reduction. Mater. Res. Bull. **49**(1), 119–125 (2014)
81. Zhou, X., Zhang, J., Su, Q., Shi, J., Liu, Y., Du, G.: Nanoleaf-on-sheet CuO/graphene composites: microwave-assisted assemble and excellent electrochemical performances for lithium ion batteries. Electrochim. Acta **125**, 615–621 (2014)
82. Amiri, A., Shanbedi, M., Ahmadi, G., Eshghi, H., Kazi, S.N., Chew, B.T., Savari, M., Zubir, M.N.M.: Mass production of highly-porous graphene for high-performance supercapacitors. Sci. Rep. **6**(Sept), 1–11 (2016)
83. Li, Q., Yi, Z., Cheng, Y., Wang, X.X., Yin, D., Wang, L.: Microwave-assisted synthesis of the sandwich-like porous Al_2O_3/rGO nanosheets anchoring NiO nanocomposite as anode materials for lithium-ion batteries. Appl. Surf. Sci. **427**, 354–362 (2018)
84. Kumar, R., da Silva, E.T.S.G., Singh, R.K., Savu, R., Alaferdov, A.V., Fonseca, L.C., Carossi, L.C., Singh, A., Khandka, S., Kar, K.K., Alves, O.L., Kubota, L.T., Moshkalev, S. A.: Microwave-assisted synthesis of palladium nanoparticles intercalated nitrogen doped reduced graphene oxide and their electrocatalytic activity for direct-ethanol fuel cells. J. Colloid Interface Sci. **515**, 160–171 (2018)
85. Voiry, D., Yang, J., Kupferberg, J., Fullon, R., Lee, C., Jeong, H.Y., Shin, H.S., Chhowalla, M.: High-quality graphene via microwave reduction of solution-exfoliated graphene oxide. Science **353**(6306), 1413–1416 (2016)
86. Chen, W., Yan, L., Bangal, P.R.: Preparation of graphene by the rapid and mild thermal reduction of graphene oxide induced by microwaves. Carbon N. Y. **48**(4), 1146–1152 (2010)
87. Yuan, X., Wu, Z., Zhong, H., Wang, H., Chen, X., Leng, L., Jiang, L., Xiao, Z., Zeng, G.: Fast removal of tetracycline from wastewater by reduced graphene oxide prepared via microwave-assisted ethylenediamine–N, N′–disuccinic acid induction method. Environ. Sci. Pollut. Res. **23**(18), 18657–18671 (2016)
88. Leng, X., Xiong, X., Zou, J.P.: Rapid microwave irradiation fast preparation and characterization of few-layer graphenes. Trans. Nonferrous Met. Soc. China **24**(1), 177–183 (2014)
89. Melucci, M., Treossi, E., Ortolani, L., Giambastiani, G., Morandi, V., Klar, P., Casiraghi, C., Samorì, P., Palermo, V.: Facile covalent functionalization of graphene oxide using microwaves: bottom-up development of functional graphitic materials. J. Mater. Chem. **20** (41), 9052–9060 (2010)
90. Sulleiro, M.V., Quiroga, S., Peña, D., Pérez, D., Guitián, E., Criado, A., Prato, M.: Microwave-induced covalent functionalization of few-layer graphene with arynes under solvent-free conditions. Chem. Commun. **54**(17), 2086–2089 (2018)
91. Achary, L.S.K., Kumar, A., Rout, L., Kunapuli, S.V.S., Dhaka, R.S., Dash, P.: Phosphate functionalized graphene oxide with enhanced catalytic activity for Biginelli type reaction under microwave condition. Chem. Eng. J. **2018**(331), 300–310 (2017)
92. Huang, Z., Zhang, H., Chen, Y., Wang, W., Chen, Y., Zhong, Y.: Microwave-assisted synthesis of functionalized graphene on Ni foam as electrodes for supercapacitor application. Electrochim. Acta **108**, 421–428 (2013)
93. Hu, H., Wang, X., Wang, J., Liu, F., Zhang, M., Xu, C.: Microwave-assisted covalent modification of graphene nanosheets with chitosan and its electrorheological characteristics. Appl. Surf. Sci. **257**(7), 2637–2642 (2011)
94. Yan, J., Wei, T., Qiao, W., Shao, B., Zhao, Q., Zhang, L., Fan, Z.: Rapid microwave-assisted synthesis of graphene nanosheet/Co_3O_4 composite for supercapacitors. Electrochim. Acta **55** (23), 6973–6978 (2010)
95. Zito, C.A., Perfecto, T.M., Fonseca, C.S., Volanti, D.P.: Effective reduced graphene oxide sheets/hierarchical flower-like NiO composites for methanol sensing under high humidity. New J. Chem. **42**(11), 8638–8645 (2018)

96. Ragavan, K.V., Rastogi, N.K.: Graphene-copper oxide nanocomposite with intrinsic peroxidase activity for enhancement of chemiluminescence signals and its application for detection of Bisphenol-A. Sens. Actuators, B Chem. **229**, 570–580 (2016)
97. Tian, Y., Liu, Y., Wang, W.P., Zhang, X., Peng, W.: CuO nanoparticles on sulfur-doped graphene for nonenzymatic glucose sensing. Electrochim. Acta **156**, 244–251 (2015)
98. Wang, Z., Xiao, Y., Cui, X., Cheng, P., Wang, B., Gao, Y., Li, X., Yang, T., Zhang, T., Lu, G.: Humidity-sensing properties of urchinlike CuO nanostructures modified by reduced graphene oxide. ACS Appl. Mater. Interfaces **6**(6), 3888–3895 (2014)
99. Zhou, X., Shi, J., Liu, Y., Su, Q., Zhang, J., Du, G.: Microwave-assisted synthesis of hollow CuO-Cu_2O nanosphere/graphene composite as anode for lithium-ion battery. J. Alloys Compd. **615**, 390–394 (2014)
100. Zheng, J., Zhang, W., Lin, Z., Wei, C., Yang, W., Dong, P., Yan, Y., Hu, S.: Microwave synthesis of 3D rambutan-like CuO and CuO/reduced graphene oxide modified electrodes for non-enzymatic glucose detection. J. Mater. Chem. B **4**(7), 1247–1253 (2016)
101. Zhang, L., Hai, X., Xia, C., Chen, X.W., Wang, J.H.: Growth of CuO nanoneedles on graphene quantum dots as peroxidase mimics for sensitive colorimetric detection of hydrogen peroxide and glucose. Sens. Actuators, B Chem. **248**, 374–384 (2017)
102. Zhang, Y., Chang, G., Liu, S., Tian, J., Wang, L., Lu, W., Qin, X., Sun, X.: Microwave-assisted, environmentally friendly, one-pot preparation of Pd nanoparticles/graphene nanocomposites and their application in electrocatalytic oxidation of methanol. Catal. Sci. Technol. **1**(9), 1636–1640 (2011)
103. Shi, M., Liu, W., Zhao, D., Chu, Y., Ma, C.: Synthesis of palladium nanoparticles supported on reduced graphene oxide-tungsten carbide composite and the investigation of its performance for electrooxidation of formic acid. J. Solid State Electrochem. **18**(7), 1923–1932 (2014)
104. Zhang, J.X., Yang, X.L., Shao, H.F., Tseng, C.C., Wang, D.S., Tian, S.S., Hu, W.J., Jing, C., Tian, J.N., Zhao, Y.C.: Microwave-assisted synthesis of Pd oxide-rich Pd particles on nitrogen/sulfur Co-doped graphene with remarkably enhanced ethanol electrooxidation. Fuel Cells **17**(1), 115–122 (2017)
105. Ju, K.J., Liu, L., Feng, J.J., Zhang, Q.L., Wei, J., Wang, A.J.: Bio-directed one-pot synthesis of Pt-Pd alloyed nanoflowers supported on reduced graphene oxide with enhanced catalytic activity for ethylene glycol oxidation. Electrochim. Acta **188**, 696–703 (2016)
106. Goswami, A., Rathi, A.K., Aparicio, C., Tomanec, O., Petr, M., Pocklanova, R., Gawande, M.B., Varma, R.S., Zboril, R.: In situ generation of Pd-Pt core-shell nanoparticles on reduced graphene oxide (Pd@ Pt/rGO) using microwaves: applications in dehalogenation reactions and reduction of olefins. ACS Appl. Mater. Interfaces **9**(3), 2815–2824 (2017)
107. Sharma, S., Ganguly, A., Papakonstantinou, P., Miao, X., Li, M., Hutchison, J.L., Delichatsios, M., Ukleja, S.: Rapid microwave synthesis of CO tolerant reduced graphene oxide-supported platinum electrocatalysts for oxidation of methanol. J. Phys. Chem. C **114**(45), 19459–19466 (2010)
108. Chu, Y.-Q., Liu, W.-M., Ma, C.-A., Shi, M.-Q., Zhao, D.: Special microwave-assisted one-pot synthesis of low loading Pt–Ru alloy nanoparticles on reduced graphene oxide for methanol oxidation. Micro Nano Lett. **9**(1), 50–54 (2014)
109. Xie, J.: Microwave synthesis of reduced graphene oxide-supported platinum nanocomposite with high electrocatalytic activity for methanol oxidation. Int. J. Electrochem. Sci. **12**, 466–474 (2017)
110. Liu, S., Tian, J., Wang, L., Sun, X.: Microwave-assisted rapid synthesis of Ag nanoparticles/graphene nanosheet composites and their application for hydrogen peroxide detection. J. Nanopart. Res. **13**(10), 4539–4548 (2011)
111. Li, Q., Hai, P.: Rapid microwave-assisted synthesis of silver decorated-reduced graphene oxide nanoparticles with enhanced photocatalytic activity under visible light. Mater. Sci. Semicond. Process. **22**(1), 16–20 (2014)

112. Hsu, K., Chen, D.: Microwave-assisted green synthesis of Ag/reduced graphene oxide nanocomposite as a surface-enhanced Raman scattering substrate with high uniformity. Nanoscale Res. Lett. **9**, 193 (2014)
113. Meng, A., Shao, J., Fan, X., Wang, J., Li, Z.: Rapid synthesis of a flower-like ZnO/rGO/Ag micro/nano-composite with enhanced photocatalytic performance by a one-step microwave method. RSC Adv. **4**(104), 60300–60305 (2014)
114. Li, Y., Fan, B., Han, F., Yang, J., Zhang, R.: Microwave-assisted synthesis of Ag/rGO composites and their cytotoxicity for HT22 neuronal cell. Mater. Res. Innov. **21**(4), 257–261 (2017)
115. Mady, A.H., Baynosa, M.L., Tuma, D., Shim, J.J.: Facile microwave-assisted green synthesis of Ag-$ZnFe_2O_4$@ rGO nanocomposites for efficient removal of organic dyes under UV- and visible-light irradiation. Appl. Catal. B Environ. **203**, 416–427 (2017)
116. Liu, X., Pan, L., Lv, T., Zhu, G., Lu, T., Sun, Z., Sun, C.: Microwave-assisted synthesis of TiO_2-reduced graphene oxide composites for the photocatalytic reduction of Cr(VI). RSC Adv. **1**(7), 1245–1249 (2011)
117. Kumar, K.D., Kumar, G.P., Reddy, K.S.: Rapid microwave synthesis of reduced graphene oxide-supported TiO_2 nanostructures as high performance photocatalyst. Mater. Today Proc. **2**(4–5), 3736–3742 (2015)
118. Liu, X., Pan, L., Lv, T., Sun, Z.: Investigation of photocatalytic activities over ZnO-TiO_2-reduced graphene oxide composites synthesized via microwave-assisted reaction. J. Colloid Interface Sci. **394**(1), 441–444 (2013)
119. Ramadoss, A., Kim, S.J.: Improved activity of a graphene-TiO_2 hybrid electrode in an electrochemical supercapacitor. Carbon N. Y. **63**, 434–445 (2013)
120. Lv, T., Pan, L., Liu, X., Lu, T., Zhu, G., Sun, Z.: Enhanced photocatalytic degradation of methylene blue by ZnO-reduced graphene oxide composite synthesized via microwave-assisted reaction. J. Alloys Compd. **509**(41), 10086–10091 (2011)
121. Lv, T., Pan, L., Liu, X., Sun, Z.: Enhanced photocatalytic degradation of methylene blue by ZnO-reduced graphene oxide-carbon nanotube composites synthesized via microwave-assisted reaction. Catal. Sci. Technol. **2**(11), 2297–2301 (2012)
122. Herring, N.P., Almahoudi, S.H., Olson, C.R., El-Shall, M.S.: Enhanced photocatalytic activity of ZnO-graphene nanocomposites prepared by microwave synthesis. J. Nanopart. Res. **14**(12) (2012)
123. Liu, Y., Hu, Y., Zhou, M., Qian, H., Hu, X.: Microwave-assisted non-aqueous route to deposit well-dispersed ZnO nanocrystals on reduced graphene oxide sheets with improved photoactivity for the decolorization of dyes under visible light. Appl. Catal. B Environ. **125**, 425–431 (2012)
124. Omar, F.S., Ming, H.N., Hafiz, S.M., Ngee, L.H.: Microwave synthesis of zinc oxide/reduced graphene oxide hybrid for adsorption-photocatalysis application. Int. J. Photoenergy **2014** (2014)
125. Kashinath, L., Namratha, K., Byrappa, K.: Microwave assisted facile hydrothermal synthesis and characterization of zinc oxide flower grown on graphene oxide sheets for enhanced photodegradation of dyes. Appl. Surf. Sci. **357**, 1849–1856 (2015)
126. Lellala, K., Namratha, K., Byrappa, K.: Microwave assisted synthesis and characterization of nanostructure zinc oxide-graphene oxide and photo degradation of brilliant blue. Mater. Today Proc. **3**(1), 74–83 (2016)
127. Firmiano, E.G.S., Cordeiro, M.A.L., Rabelo, A.C., Dalmaschio, C.J., Pinheiro, A.N., Pereira, E.C., Leite, E.R.: Graphene oxide as a highly selective substrate to synthesize a layered MoS_2 hybrid electrocatalyst. Chem. Commun. **48**(62), 7687–7689 (2012)
128. Da Silveira Firmiano, E.G., Rabelo, A.C., Dalmaschio, C.J., Pinheiro, A.N., Pereira, E.C., Schreiner, W.H., Leite, E.R.: Supercapacitor electrodes obtained by directly bonding 2D MoS_2 on reduced graphene oxide. Adv. Energy Mater. **4**(6), 1–8 (2014)
129. Qin, W., Chen, T., Pan, L., Niu, L., Hu, B., Li, D., Li, J., Sun, Z.: MoS_2-reduced graphene oxide composites via microwave assisted synthesis for sodium ion battery anode with improved capacity and cycling performance. Electrochim. Acta **153**, 55–61 (2015)

130. Li, J., Liu, X., Pan, L., Qin, W., Chen, T., Sun, Z.: MoS_2-reduced graphene oxide composites synthesized via a microwave-assisted method for visible-light photocatalytic degradation of methylene blue. RSC Adv. **4**(19), 9647–9651 (2014)
131. Liu, N., Wang, X., Xu, W., Hu, H., Liang, J., Qiu, J.: Microwave-assisted synthesis of MoS_2/graphene nanocomposites for efficient hydrodesulfurization. Fuel **119**, 163–169 (2014)
132. Youn, D.H., Jo, C., Kim, J.Y., Lee, J., Lee, J.S.: Ultrafast synthesis of MoS_2 or WS_2-reduced graphene oxide composites via hybrid microwave annealing for anode materials of lithium ion batteries. J. Power Sources **295**, 228–234 (2015)

Graphene Functionalizations on Copper by Spectroscopic Techniques

Mehmet Gülcan, Ayşenur Aygün, Fatıma Almousa, Hakan Burhan, Anish Khan and Fatih Şen

Abstract Graphene is a two-dimensional allotrope of the carbon element, which is one of the most powerful materials of the 21st century. In order to facilitate the processing of the graphene, solvent-supported methods such as rotation coating, layer by layer assembly, and filtration are used. Single layer graphene prevents agglomeration of the material while reducing reactions occur. According to the studies in the literature, the chemical functionalization of graphene is performed by covalent and non-covalent modification techniques on substrate like copper. Besides, graphene can be used in many material production areas, such as polymer nanocomposites, drug delivery system, supercapacitor devices, solar cells, biosensors, and memory devices.

Keywords Graphene · Functionalization · Copper · Spectroscopy

1 Introduction

Graphene, known as the most studied material to date, is defined as two-dimensional sp^2-hybridized carbon [1–39]. The carbon atoms of this single atomic thickness, reminiscent of a honeycomb, have the characteristics of being the

M. Gülcan
Chemistry Department, Faculty of Science, Van Yüzüncü Yıl University, Zeve Campus, 65080 Van, Turkey
e-mail: mehmetgulcan65@gmail.com

A. Aygün · F. Almousa · H. Burhan · F. Şen (✉)
Sen Research Group, Department of Biochemistry, Dumlupinar University, 43100 Kütahya, Turkey
e-mail: fatihsen1980@gmail.com; fatih.sen@dpu.edu.tr

A. Khan
Chemistry Department, Faculty of Science, King Abdulaziz University, P.O. Box 80203, Jeddah 21589, Saudi Arabia

A. Khan
Center of Excellence for Advanced Materials Research, King Abdulaziz University, P.O. Box 80203, Jeddah 21589, Saudi Arabia

A. Khan et al. (eds.), *Graphene Functionalization Strategies*, Carbon Nanostructures, https://doi.org/10.1007/978-981-32-9057-0_13

thinnest, most powerful, and hardest material in the world which conducts heat with electricity perfectly. This two-dimensional material is much more promising in terms of application than other nanostructured and carbon-based materials [40]. After empirically demonstrating the electronic properties of graphene [41–84], scientists have focused on the development of effective synthesis pathways of graphene derivatives [85–148]. For instance, in the photocatalytic reduction of graphite [74], chemical vapor deposition [9, 58, 71], chemical [94], electrochemical [122], thermal [149] methods have been used for the preparation of graphene [86, 139, 146]. Single molecule detection and high carrier mobility are also very important for graphene and its application. [10, 66, 81, 85, 98, 126, 134]. Graphene and their applications in electronics, optical mechanics is also very important. Spesifically, the ambipolar field effect [91, 137] includes superior mechanical strength [21, 140], large surface area [79], high transparency [60, 136], and high thermal conductivity [91]. Graphene which has exceptional properties, is used in numerous areas, such as touch screens, batteries, sensors, capacitors, spintronic devices, transparent conductive films, fuel cells, high-frequency circuits, and the removal of toxic materials [1, 2, 3, 4, 7, 8, 11, 12, 15, 17, 18, 19, 20, 22, 23, 24, 25, 29, 30, 31, 32, 33, 34, 35, 36, 41, 42, 43, 44, 45, 46, 47, 48, 49, 56, 57, 59, 82, 87, 88, 90, 99, 100, 101, 102, 103, 104, 105, 106, 107, 108, 109, 110, 111, 112, 113, 114, 115, 116, 117, 118, 119, 120, 121, 132, 133, 141, 142, 143, 144, 145]. It has been observed that graphene-based nanostructures functionalized with biomolecules can create new research areas, especially in the field of biotechnology [62, 96, 97]. Due to its ability to resist graphene, organic dye and quantum dot [28], and rapid DNA sequencing [28, 73], it has a major role in the development of fluorescent resonance energy transfer (FRET) biosensors. The application potential has a wide graphene zero band gap and an inert chemical structure. The number of studies on the functionalization and modification of the surface of graphene and graphene derivatives with organic and inorganic reactions has increased day by day [64]. For functional nano-electronic devices, prolonging the graphene band space with doping, intercalation, and stripping are incredibly useful [55, 92]. The physical and chemical properties of graphene are described in Sect. 2. In Sect. 3, the basic approaches for the chemical functionalization of graphene are described in detail. Finally, graphene on the copper substrate and the spectroscopic methods used for this purpose are given in Sect. 4.

2 Physical and Chemical Properties of Graphene

Generally, graphene is a two-dimensional carbon allotrope, and each carbon atom is bonded to another carbon atom by sp^2 bonds. Monolayer graphene film thickness [84] is measured in the range of 1–1.1.6 and 0.33 nm [49]. Graphene is an incredibly strong material thanks to its 200 times more hardness than steel's. Graphene has a linear disintegration relationship at the Dirac point with zero-band spaced semiconductor whereby essentially zero-effect mass occur [28, 62].

Graphene has an electrical conductivity at room temperature of 7200 Sm^{-1} with ~200,000 mobility $cm^2\ Vs^{-1}$. Thermal conductivity values for single layer graphene at room temperature were determined as $(4.84 \pm 0.44) \times 10^3$ to $(5.30 \pm 0.48) \times 10^3$ W mK^{-1} [10]. Graphene with an aromatic structure with a high-density electron cloud is easy to interact with spherical p electrons of orbitals of organic molecules. Nucleophilic substitution is more difficult than [73] electrophilic substitution of graphene. Specific reaction classes in which graphene may be included are; cyclo-additions, carbene addition reactions and click reactions. Reactions on graphene surfaces prevent the planar structure of graphene. Disruption of the structure of sp^2 causes loss of electrical conductivity. The chemical activity of the geometrically stretched graphene lattice regions is explained by the easier displacement of the electron density, which is higher than the other regions, from the upper plane of the ring. Furthermore, the arm-chair edges of the graphene have lower chemical reactivity than the zig-zag edges.

3 Chemical Functionalization of Graphene

The carbon family was limited to diamond and graphite, and nowadays these limits have been developed by the discovery of materials such as fullerenes, 2D graphics, and CNTs [92]. Graphene, one of the carbon-based materials, attracts great interest from researchers due to its tremendous structural properties, morphological properties and its excellent performance in applications. Graphene surface modification is a popular research area among scientists. In graphene applications, the functionality and distribution of graphene layers are important. Solvent-assisted techniques, such as rotation coating, layer assembly, and filtration are generally used for the processing of functionalized graphene. To prevent agglomeration of monolayer graphite and to reduce solvent phase by chemical functionality of graphene, natural properties of graphene are preserved. Graphene oxide with the Hummer method is used as the starting material for graphene synthesis [55, 94]. The surfaces of the graphene oxide layers may alter the Van der Waals interactions depending on the functional groups, such as hydroxyl, epoxide, diol, ketone, carboxyl and the like, which provide solubility in water or other organic solvents [26, 27, 89, 94, 125]. The carboxyl and carbonyl groups are additionally present at the edges of the graphene layers (Fig. 1) and make the GO layers hydrophilic. This facilitates the spread of water [39, 69, 83, 128, 129]. Graphene is formed by thermal, chemical, and photochemical reduction of graphene oxide. The surface modification of the GO layers is performed covalently or non-covalently causing the process to collapse without the use of any stabilizers [37]. Reduction of the alkylamine modified graphene oxide in a characteristic organic solvent provides stable dispersions of the functionalized graphene layers. It is possible to obtain water-dispersible graphene layers by stimulating the sulfonate or carboxylic groups on the basal planes of the graphene [14, 63, 124]. Direct expression studies of graphene which can be dispersed from natural graphite [51, 72, 77, 148] were carried out. Electrochemically,

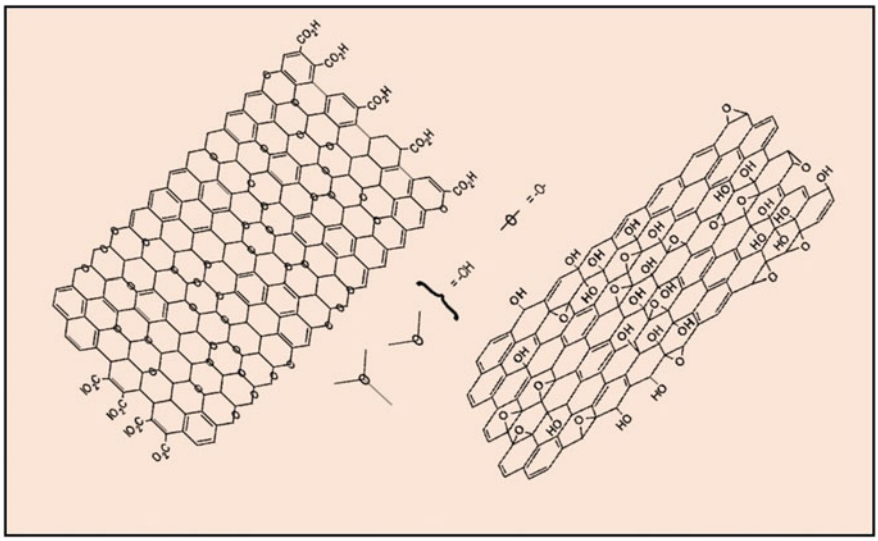

Fig. 1 Variations of the Lerf-Klinowski model, uncertainty about the presence or absence of carboxylic acids around the basal plane of graphene oxide platelets [27]

ionic fluid modified graphene is prepared using natural graffiti [74]. High-throughput synthesis methods for non-functional graphene are also reported in the literature [77].

3.1 Covalent Modification

In covalent functionalization, the structural change is performed at the end and/or surface of the graphene layers. The functionalization of the graphene surface is related to the loss of electronic conjugation and redistribution of the carbon atom in one or several sp^2 configurations to the sp^3 configuration [55]. Electrophilic addition, nucleophilic substitution, addition, and condensation are the four main methods used for covalent modification of graphene. By using different modifying agents, it is possible to vary the dispersibility and electrical conductivity of graphene in different solvents [92].

3.2 Non-covalent Functionalization

The non-covalent interactions of the physical adsorption of molecules suitable for the graphene surface require electrostatic forces and Van der Waals forces. Surface

modification of carbon-based nanomaterials is one of the known techniques for non-covalent functionalization and is common for the surface modification of sp^2 networks of carbon nanotubes [148]. According to the researches, the techniques applied to the graphene can also be applied using different organic modifiers [92].

3.3 Stabilization in an Ionic Medium

The functionalized graphene greatly reduces the electrical conductivity by the use of foreign stabilizer molecules. In order to prevent and maintain this reduction in electrical conductivity, it is necessary to reduce the graphene oxide in the ionic medium. In one study, the aqueous homogeneous suspension from chemically converted graphene (CCG) with electric conductivity was successfully prepared [93]. This method is based on dispersing the starting material of GO in water and then adding the potassium hydroxide solution to the medium. Groups in GO layers, such as reactive hydroxyl, carboxylic acid, and epoxy, can react with strong bases such as potassium hydroxide to form a large negative charge. Thus, negative charges and extensive coverage of the K^+ ions and the graphene surface are achieved. A homogeneous and long-term suspension is achieved by the addition of hydrazine monohydrate to the potassium hydroxide treated graphene oxide. In a recent study, stable aqueous colloids of graphene layers have been synthesized by a research group using electrostatic stabilization of graphene [70]. Hydrazine monohydrate is used to obtain an aqueous dispersion of graphene oxide. After the reduction process, 0.5% ammonia solution is used to remove excess hydrazine in the medium to produce the aqueous graphene dispersion. During this process, some of the stabilizers such as surfactant and polymeric materials are used.

3.4 Direct Synthesis from Graphite

The synthesis of graphene by chemical methods is more advantageous than highly oriented pyrolytic graphite (HOPG) and chemical vapor deposition (CVD) [58, 71]. A comparison of the CVD and HOPG processes with the chemical methods indicated a decrease in the surface area of the graphene. However, electronic application areas where a wide area of graphene is required should not be ignored. Therefore, such efforts have been made to synthesize graphene with large areas of direct graphite [52, 75, 148]. This method eliminates defects that may occur during oxidation.

4 Graphene Functionalizations on Copper

Graphene functionalizations on copper is an advantageous approach that can provide the covalent grafting technique, bandgap modulation, and simultaneous signaling with intermolecular interactions [65, 131, 135]. Chemical vapor deposition technique (CVD) is used for covalent grafting or functionalization. CVD is a method for the activation of gaseous reactants containing a chemical reaction and a stable solid on a substrate. Thermal, plasma-assisted or laser-assisted CVD sources, such as energy, heat, light, and electrical discharges are required for the chemical reaction. Precipitation may consist of two types of reactions; the first type of reaction is homogeneous gas phase reactions occurring in the gas phase, the second type of reaction is heterogeneous chemical reactions occurring on or near a heated surface that causes the formation of powders or films. Precipitation may consist of two types of reactions; the first is the homogeneous gas phase reaction and the second is the heterogeneous chemical reactions. Figure 2 schematically illustrates the working principle of CVD [80].

The Copper based CVD technique was used for high-quality graphene on a large surface area [6, 61]. Transfer of another substrate, such as Si/SiO_2 plates, with copper etching/polymer supported methods [50] is very improtant to perform its functionality and characterization. By this method, the procedure involves polymer, active, and reactant residues and contamination due to solvent additives [6, 76, 138]. Fouling inhibits slightly the homogeneous functionalization of the surface or the presence of high concentrations of contaminants, by preventing reaction on the graphene surface. It is essential to perform the functionalization reactions directly

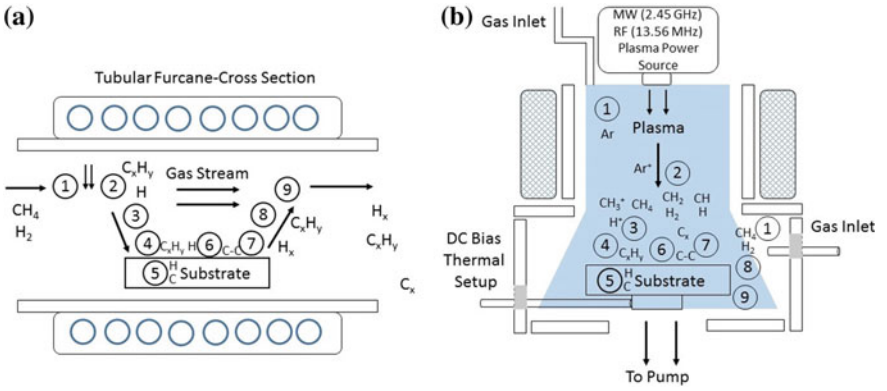

Fig. 2 Graphene shape of CH_4/H_2 mixtures. **a** Thermal CVD and **b** Plasma-supported diagrams of CVD. **1.** Transport of convection reactants **2.** Thermal **a** plasma **b** activation. **3.** Powder production in graphene synthesis, control of kinetic parameters (P, T, n). **4.** Adsorption of the reactants onto the substrate surface. **5.** Solubility and physical properties of a substrate by dissolution and bulk diffusion. **6.** The chemical catalytic reaction, surface activation, bonding, and heterogeneous surface reactions **7.** Superficial desorption from by-products. **8.** Diffusion transport from the boundary layer to the main gas flow from the by-products. **9.** Carrying by by-products [61]

on the copper, bypass the polymer-supported transfer, and achieve the synthesis and functionalization step in the gas phase. A wet process is avoided, and production is applied to a continuous line operation. Most of the graphene reactions placed on the metal with CVD are performed on Si/SiO_2 substrates which can be identified by optical imaging and/or spectroscopy. It has been shown that the substrates on the reactivity of graphene monolayer material have an essential role for covalent functionalization due to their effect. Good functionalization can be obtained for specific reaction conditions for a substrate [50].

4.1 Spectroscopic Techniques

Raman spectroscopy, surface-enhanced Raman spectroscopy (SERS), mass spectrometry (MS), X-ray diffraction (XRD), transmission electron microscopy (TEM), X-ray spectroscopy (EDX) with energy distributor, X-ray photoelectron methods, such as spectroscopy (XPS) and UV-visible spectroscopy are used to study the functionalization of copper-substrate graphene. Descriptive information on these methods is briefly described below.

4.1.1 Raman Spectroscopy

Raman spectroscopy analysis provides a structural and qualitative characterization of graphene quickly and easily. According to the results of Raman analysis, there are many defects in the graphene synthesized by the chemical oxidation-reduction method, while the graphite and micromechanical division of graphite prepared by CVD does not show any defects [92]. For Chemically reduced graphene, the double-degenerate zone shows an approximate peak of 1576 cm^{-1} (G band) corresponding to the E_{2g} mode. It relates to the vibration of sp^2-bound carbon atoms in a two-dimensional hexagonal cage. The 1326 cm^{-1} peak, known as the D band, is characterized by the deterioration and errors of chemically reduced graphene layers. However, the values of G-band 1580 cm^{-1} and 2D band 2700 cm^{-1} in the Raman spectrum vary due to the fact that graphite and graphene were prepared by different methods. In the Raman spectrometer of the graphene which has the disturbances, the second line region border phonon, i.e. 2D band, is not seen [5]. Such phonons cause a peak of about 1326 cm^{-1}. However, there is no such D-band in the center of the defect-free graphene. In Raman spectroscopy, the 2D band on the graphite is composed of two peaks while the monolayer graphite shows only one peak and the density of the monolayer graphene is lower than the graphene having more than one layer. A high number of layers of graphene affects the G band density. It is observed that the graphene with a high number of layers has a wider spaced and upwardly sloping 2D band than the graphene with a low number of layers. Ferrari et al. obtained Raman spectra to identify graphene up to five layers in the 514.5 and

633.0 nm range. It has been shown that Raman results can distinguish graphene from layers up to 5 layers of graphene [38, 138].

4.1.2 Surface Enhanced Raman Spectroscopy (SERS)

The introduction of Raman spectroscopy dates back 40 years. To date, many developments were achieved in Raman spectroscopy. Raman analysis is used in many fields such as electrochemistry, analytical chemistry, chemical physics, solid state physics, biophysics, and medicine [16]. The Raman analysis using SERS differs according to the other Raman spectroscopy results. The density of the bands seen in the Raman analysis decreases with increasing vibration frequency. The C-H extensions are relatively weak in SERS Raman analysis. Overtones and combination bands are not common. Selection rules are relaxed resulting in the appearance of normally forbidden Raman modes in the surface spectra [61]. The products of chemical derivatives of graphene are shown by SERS analysis. By this analysis method, chemical functional groups are determined by the fact that the vaccinated species show their specific bands. Thus, the composition of the monolayer molecules at only one molecule level can be determined exactly. With this situation, the critical problem of graphene functionalization analysis is solved [54, 61].

4.1.3 Mass Spectrometry (MS)

The mass spectrometry method is widely used to examine other materials including graphite and graphene. Thermally programmed desorption-electron ionization (TPD-EI) and superficial laser desorption ionization/flight time analyzer (SELDI) methods are used. In the study, graphene materials functionalized on copper and Si/SiO_2 substrates were investigated. As a result of the analysis with two different mass spectrometers, two different mass spectrometers are used to analyze the functional graphene structure. First, the detection of [M–H]—ions by using SELDI rather than TPD gives an idea about the non-covalent vaccination to result in non-covalent adsorption. Second, the overreaction of electron-rich reagents and diazonium vaccination can be accomplished by single-layer functionalization. Third, the mass spectra of thermal decomposition products at certain temperatures is the chemical transformation occurring on the graft surface. Finally, SELDI imaging is monitored on very large areas that cannot be observed by other methods, typically in the presence of species [50].

4.1.4 X-Ray Diffraction (XRD)

In the XRD analysis, which is one of the characterization methods used to define the graphene, graphite $2\theta = 26.6^{\circ}$ ($d_{spacing} = 0.335$ nm) shows a basal reflection (002) peak. ($d_{spacing} = 0.79$ nm) at a lower angle. Depending on functional oxygen

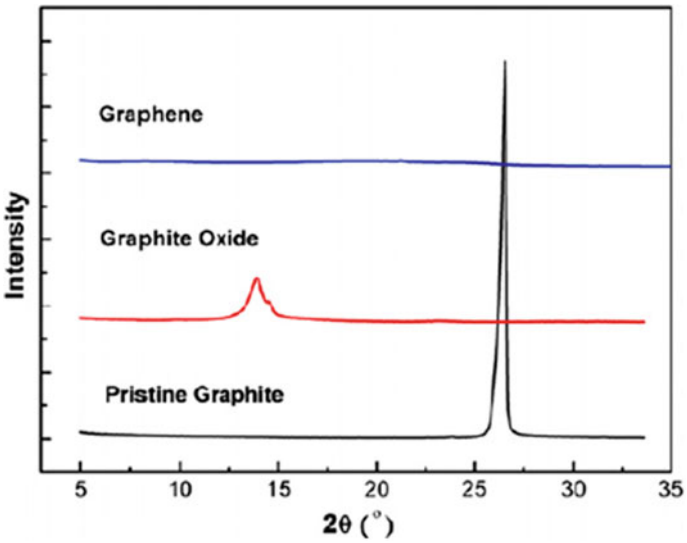

Fig. 3 X-ray diffraction patterns of pristine graphite, graphite oxide, and graphene [147]

formation in the interlayer layer of graphite and the intercalation of water molecules, an increase in D spacing is observed. If the graphite oxide is poured into a single graphene oxide layer, a straight line with no significant breaking peak is obtained in the XRD pattern (Fig. 3). The XRD image of a single layer of graphene oxide and monolayer graphene is the same suggesting that the periodic structure of graphite is removed and passes to completely separate layers [146].

XRD is one of the characterization methods used to describe the graphene. In XRD analysis, graphite $2\theta = 26.6°$ ($d_{spacing} = 0.335$ nm) shows a basal reflection (002) peak. The XRD result of the oxidized graphite changes to a lower angle at 002 reflectance peak $2\theta = 11.2°$ ($d_{spacing} = 0.79$ nm) according to the XRD result of intact graphite. An increase in $d_{spacing}$ was induced due to intercalation of oxygen and water molecules in the intermediate layer of graphite. At the XRD level, the formation of a refractive peak was obtained in order to pour the graphite oxide in a single GO layer (Fig. 3). The XRD image of the single layer graphene is the same as that of the single layer Graphene Oxide which suggests that the periodic structure of the graphite has disappeared and passes into completely separate layers [146].

4.1.5 Transmission Electron Microscopy

In order to obtain information about the magnitude of the graphene samples, the electron microscopy (TEM) was used. Hernandez et al. analyze the statistical data by analyzing the TEM image of a large number of samples and by making sure that the samples analyzed are similar. The presence of a single layer graphene structure

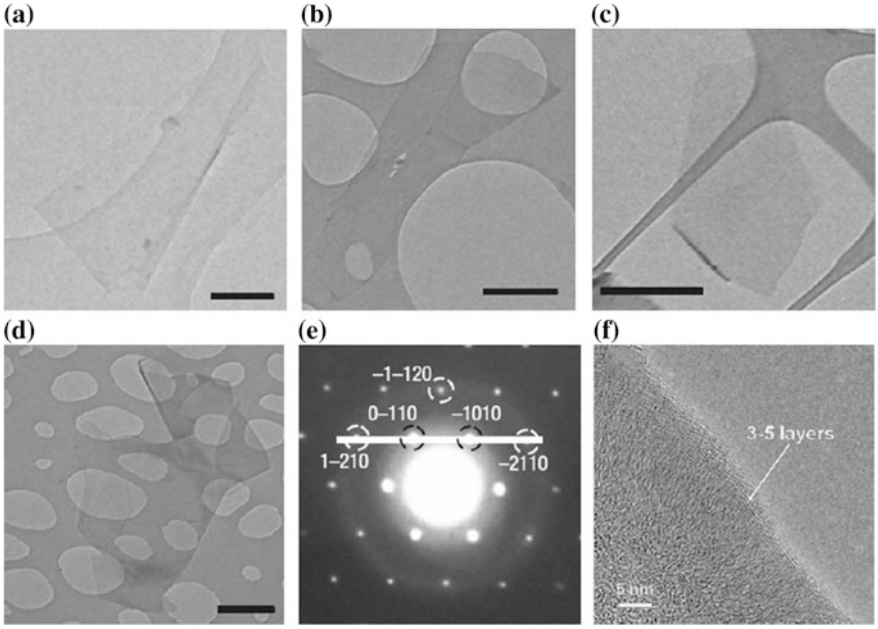

Fig. 4 **a–f** TEM and HR-TEM image of graphene [53]

was obtained by visualization of transparent and stable graphene layers provided by TEM analyzes. In order to obtain a cross-sectional view of the image on the received images, the edges of the suspended image should always be folded backward (Fig. 4a–f). Images of graphene layers of different sizes with high-resolution TEM are obtained accurately [53, 95]. A folded graphene sheet is locally parallel to the electron beam. For monolayer graphene, one layer is seen only as a dark line [78]. The number of layers in the graph is equal to the number of dark lines. A more precise definition of graphene can be made using the analysis of small-area electron diffraction (SAED) models. The SAED pattern of single-layer and two-layer graphene was successfully defined by Hernandez et al. [95]. TEM images and SAED models of the monolayer and two-layer graphene are shown in Fig. 4a–e. The SAED image of monolayer graphene (Fig. 4e) shows characteristic six-fold graphene symmetry.

4.1.6 X-Ray Photoelectron Spectroscopy (XPS)

Qualitative description of X-ray photoelectron spectroscopy, analytical methods for surface chemistry, and quantitative definition of the sample can also be made. Comparison reaction is made by inserting two heteroatoms into the graphene cage: XeF_2 during the nucleophilic exchange of thiophenol and fluorine in the activation of sulfur. In XPS analysis graphene clears the substrate atoms and spectra of carbon

well, and a more accurate quantitative measurement is made in the analysis of the complex C1 complex. Approximately 80% of the fluorine with XPS analysis remains with the used nucleophile. The nucleophile and substrate affect the reactivity. In the thiol series which exhibits a decrease in the thio acetic acid > thio phenol benzyl thiol sequence, the amount of fluorine is related to the acidity of the sulfur nucleophile used. Unlike the Si/SiO_2 substrate on the copper, the benzylthiol reacts and proceeds further. Thioacetate substitution on Si/SiO_2 causes copper foil fragmentation and wear of the graphene monolayer. The ability to control the substrate selection is considered to be an essential component in the adjustment of the chemical reaction kinetics. Similarly to fluorine or sulfur, nitrogen is visible in X-ray photoelectron spectroscopy. Diazonium double reactivity is a good example. Because of the distortion that the substrate can cause in the XPS analysis, a thin metallic film layer is used which prevents photoelectrons in the support substrate for the transfer process [50].

4.1.7 UV-Visible Spectroscopy

UV-visible spectroscopy was used as an analytical method to determine graphene formation and number of layers. Thanks to the UV-visible spectrum, the two-dimensional graphene oxide layer and the monolayer graphene oxide layer

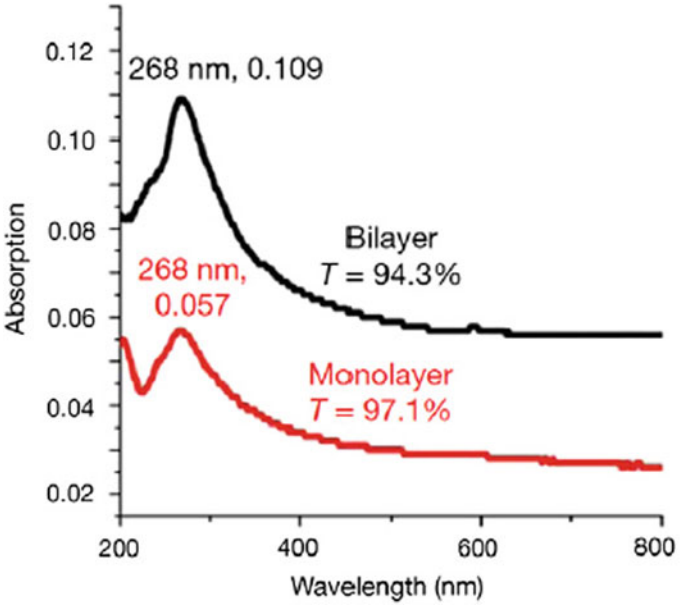

Fig. 5 UV permeability (T, %) UV visible absorption spectra of monolayer and bilayer graphene measured at 550 nm; The peaks are matched with the maximum absorption value and the maximum absorption wavelength [127]

gave wavelength UV peaks at 262 nm. The transmission of high carbon sp^2 carbons from the chemically reduced graphene results in a decrease in transmittance. In their study, Sun et al. determined that the monolayer graphene measured at the wavelength of 550 nm showed 97.1% of transmittance. Linear development in ultraviolet absorption, the permeability of bimodal graphite ($\lambda = 550$ nm) is 94.3%. (Figure 5). Graphene has six layer thicknesses showing a transmittance of 83% at the same wavelength [67, 68, 123, 127].

5 Conclusions

Generally, graphene and graphene based materials are the most powerful materials of the last century and they have been used in many material production areas, such as polymer nanocomposites, drug delivery system, supercapacitor devices, solar cells, catalytic applications, biosensors, and memory devices. To facilitate the processing of the graphene and graphene based materials, covalent and non-covalent modification techniques have been used and these modifications were analysed, identified by many spectroscopic techniques such as XRD, XPS, TEM, TEM-EDX, Raman etc. As a future mark, the importance of the identification and characterization of the graphene and graphene based materials after modifications will be increasing day by day due to increasing application areas of them.

References

1. Abrahamson, J.T., Sempere, B., Walsh, M.P., Forman, J.M., Şen, F., Şen, S., Mahajan, S.G., Paulus, G.L.C., Wang, Q.H., Choi, W., Strano, M.S.: Excess thermopower and the theory of thermopower waves. ACS Nano **7**, 6533–6544 (2013). https://doi.org/10.1021/nn402411k
2. Aday, B., Pamuk, H., Kaya, M., Sen, F.: Graphene Oxide as highly effective and readily recyclable catalyst using for the One-Pot synthesis of 1,8-Dioxoacridine derivatives. J. Nanosci. Nanotechnol. **16**, 6498–6504 (2016). https://doi.org/10.1166/jnn.2016.12432
3. Aday, B., Yıldız, Y., Ulus, R., Eris, S., Sen, F., Kaya, M.: One-Pot, efficient and green synthesis of Acridinedione derivatives using highly monodisperse platinum nanoparticles supported with reduced Graphene Oxide. New J. Chem. **40**, 748–754 (2016). https://doi.org/10.1039/C5NJ02098K
4. Akocak, S., Şen, B., Lolak, N., Şavk, A., Koca, M., Kuzu, S., Şen, F.: One-Pot three-component synthesis of 2-Amino-4H-Chromene derivatives by using monodisperse Pd nanomaterials anchored Graphene Oxide as highly efficient and recyclable catalyst. Nano-Struct. Nano-Objects **11**, 25–31 (2017). https://doi.org/10.1016/j.nanoso.2017.06.002
5. Al-Mashat, L., Shin, K., Kalantar-zadeh, K., Plessis, J.D., Han, S.H., Kojima, R.W., Kaner, R.B., Li, D., Gou, X., Ippolito, S.J., Wlodarski, W.: Graphene/Polyaniline nanocomposite for hydrogen sensing. J. Phys. Chem. C **114**, 16168–16173 (2010). https://doi.org/10.1021/jp103134u

6. Ambrosi, A., Pumera, M.: The CVD graphene transfer procedure introduces metallic impurities which alter the graphene electrochemical properties. Nanoscale **6**, 472–476 (2014). https://doi.org/10.1039/C3NR05230C
7. Ayranci, R., Baskaya, G., Guzel, M., Bozkurt, S., Ak, M., Savk, A., Sen, F.: Activated Carbon furnished monodisperse Pt nanocomposites as a superior adsorbent for methylene blue removal from aqueous solutions. Nano-Struct. Nano-Objects **11**, 13–19 (2017). https://doi.org/10.1016/j.nanoso.2017.05.008
8. Ayranci, R., Başkaya, G., Güzel, M., Bozkurt, S., Şen, F., Ak, M.: Carbon based nanomaterials for high performance optoelectrochemical systems. ChemistrySelect **2**, 1548–1555 (2017). https://doi.org/10.1002/slct.201601632
9. Bae, S., Kim, H., Lee, Y., Xu, X., Park, J.-S., Zheng, Y., Balakrishnan, J., Lei, T., Ri Kim, H., Song, YIl, Kim, Y.-J., Kim, K.S., Özyilmaz, B., Ahn, J.-H., Hong, B.H., Iijima, S.: Roll-to-roll production of 30-inch graphene films for transparent electrodes. Nat. Nanotechnol. **5**, 574–578 (2010). https://doi.org/10.1038/nnano.2010.132
10. Balandin, A.A., Ghosh, S., Bao, W., Calizo, I., Teweldebrhan, D., Miao, F., Lau, C.N.: Superior thermal conductivity of single-layer graphene. Nano Lett. **8**, 902–907 (2008). https://doi.org/10.1021/nl0731872
11. Baskaya, G., Esirden, İ., Erken, E., Sen, F., Kaya, M.: Synthesis of 5-Substituted-1H-Tetrazole derivatives using monodisperse carbon black decorated Pt nanoparticles as heterogeneous nanocatalysts. J. Nanosci. Nanotechnol. **17**, 1992–1999 (2017). https://doi.org/10.1166/jnn.2017.12867
12. Başkaya, G., Yıldız, Y., Savk, A., Okyay, T.O., Eriş, S., Sert, H., Şen, F.: Rapid, sensitive, and reusable detection of glucose by highly monodisperse nickel nanoparticles decorated functionalized multi-walled carbon nanotubes. Biosens. Bioelectron. **91**, 728–733 (2017). https://doi.org/10.1016/j.bios.2017.01.045
13. Berger, C., Song, Z., Li, X., Wu, X., Brown, N., Naud, C., Mayou, D., Li, T., Hass, J., Marchenkov, A.N., Conrad, E.H., First, P.N., de Heer, W.A.: Electronic confinement and coherence in patterned epitaxial graphene. *Science (80-) 312*, 1191–1196 (2006). https://doi.org/10.1126/science.1125925
14. Bourlinos, A.B., Gournis, D., Petridis, D., Szabó, T., Szeri, A., Dékány, I.: Graphite oxide: chemical reduction to graphite and surface modification with primary aliphatic amines and amino acids. Langmuir **19**, 6050–6055 (2003). https://doi.org/10.1021/la026525h
15. Bozkurt, S., Tosun, B., Sen, B., Akocak, S., Savk, A., Ebeoğlugil, M.F., Sen, F.: A hydrogen peroxide sensor based on TNM functionalized reduced graphene oxide grafted with highly monodisperse Pd nanoparticles. Anal. Chim. Acta **989**, 88–94 (2017). https://doi.org/10.1016/j.aca.2017.07.051
16. Campion, A., Kambhampati, P.: Surface-enhanced Raman scattering. Chem. Soc. Rev. **27**, 241–243 (1998). https://doi.org/10.1039/a827241z
17. Çelik, B., Başkaya, G., Sert, H., Karatepe, Ö., Erken, E., Şen, F.: Monodisperse Pt(0)/DPA@GO nanoparticles as highly active catalysts for alcohol oxidation and dehydrogenation of DMAB. Int. J. Hydrogen Energy **41**, 5661–5669 (2016). https://doi.org/10.1016/j.ijhydene.2016.02.061
18. Çelik, B., Erken, E., Eriş, S., Yıldız, Y., Şahin, B., Pamuk, H., Sen, F.: Highly monodisperse Pt(0)@AC NPs as highly efficient and reusable catalysts: the effect of the surfactant on their catalytic activities in room temperature dehydrocoupling of DMAB. Catal. Sci. Technol. **6**, 1685–1692 (2016). https://doi.org/10.1039/C5CY01371B
19. Çelik, B., Kuzu, S., Erken, E., Sert, H., Koşkun, Y., Şen, F.: Nearly monodisperse carbon nanotube furnished nanocatalysts as highly efficient and reusable catalyst for dehydrocoupling of DMAB and C1 to C3 Alcohol Oxidation. Int. J. Hydrogen Energy **41**, 3093–3101 (2016). https://doi.org/10.1016/j.ijhydene.2015.12.138
20. Çelik, B., Yildiz, Y., Sert, H., Erken, E., Koşkun, Y., Şen, F.: Monodispersed Palladium-Cobalt alloy nanoparticles assembled on Poly(N-vinyl-pyrrolidone) (PVP) as a highly effective catalyst for Dimethylamine Borane (DMAB). RSC Adv **6**, 24097–24102 (2016). https://doi.org/10.1039/c6ra00536e

21. Chen, D., Tang, L., Li, J.: Graphene-based materials in electrochemistry. Chem. Soc. Rev. **39**, 3157–3180 (2010). https://doi.org/10.1039/b923596e
22. Daşdelen, Z., Yıldız, Y., Eriş, S., Şen, F.: Enhanced electrocatalytic activity and durability of Pt nanoparticles decorated on GO-PVP Hybride material for methanol oxidation reaction. Appl. Catal. B Environ. **219**, 511–516 (2017). https://doi.org/10.1016/j.apcatb.2017.08.014
23. Demir, E., Savk, A., Sen, B., Sen, F.: A novel monodisperse metal nanoparticles anchored graphene oxide as counter electrode for dye-sensitized solar cells. Nano-Struct. Nano-Objects **12**, 41–45 (2017). https://doi.org/10.1016/j.nanoso.2017.08.018
24. Demir, E., Sen, B., Sen, F.: Highly efficient Pt nanoparticles and f-MWCNT nanocomposites based counter electrodes for dye-sensitized solar cells. Nano-Struct. Nano-Objects **11**, 39–45 (2017). https://doi.org/10.1016/j.nanoso.2017.06.003
25. Demirci, T., Çelik, B., Yildiz, Y., Eriş, S., Arslan, M., Sen, F., Kilbas, B.: One-pot synthesis of hantzsch dihydropyridines using a highly efficient and stable PdRuNi@GO catalyst. RSC Adv **6**, 76948–76956 (2016). https://doi.org/10.1039/c6ra13142e
26. Dikin, D.A., Stankovich, S., Zimney, E.J., Piner, R.D., Dommett, G.H.B., Evmenenko, G., Nguyen, S.T., Ruoff, R.S.: Preparation and characterization of graphene oxide paper. Nature **448**, 457–460 (2007). https://doi.org/10.1038/nature06016
27. Dreyer, D.R., Park, S., Bielawski, C.W., Ruoff, R.S.: The chemistry of graphene oxide. Chem. Soc. Rev. **39**, 228–240 (2010). https://doi.org/10.1039/b917103g
28. Eda, G., Chhowalla, M.: Graphene-based composite thin films for electronics. Nano Lett. **9**, 814–818 (2009). https://doi.org/10.1021/nl8035367
29. Eris, S., Daşdelen, Z., Sen, F.: Investigation of electrocatalytic activity and stability of Pt@F-VC catalyst prepared by in-situ synthesis for methanol electrooxidation. Int. J. Hydrogen Energy **43**, 385–390 (2018). https://doi.org/10.1016/j.ijhydene.2017.11.063
30. Eris, S., Daşdelen, Z., Sen, F.: Enhanced electrocatalytic activity and stability of monodisperse Pt nanocomposites for direct methanol fuel cells. J. Colloid Interface Sci. **513**, 767–773 (2018). https://doi.org/10.1016/j.jcis.2017.11.085
31. Eris, S., Daşdelen, Z., Yıldız, Y., Sen, F.: Nanostructured Polyaniline-rGO decorated platinum catalyst with enhanced activity and durability for methanol oxidation. Int. J. Hydrogen Energy **43**, 1337–1343 (2018). https://doi.org/10.1016/j.ijhydene.2017.11.051
32. Erken, E., Esirden, İ., Kaya, M., Sen, F.: A rapid and novel method for the synthesis of 5-Substituted 1H-Tetrazole catalyzed by exceptional reusable monodisperse Pt NPs@AC under the microwave irradiation. RSC Adv. **5**, 68558–68564 (2015). https://doi.org/10.1039/C5RA11426H
33. Erken, E., Pamuk, H., Karatepe, Ö., Başkaya, G., Sert, H., Kalfa, O.M., Şen, F.: New Pt(0) nanoparticles as highly active and reusable catalysts in the C1–C3 Alcohol Oxidation and the room temperature dehydrocoupling of Dimethylamine-Borane (DMAB). J. Clust. Sci. **27**, 9–23 (2016). https://doi.org/10.1007/s10876-015-0892-8
34. Erken, E., Yıldız, Y., Kilbaş, B., Şen, F.: Synthesis and characterization of nearly monodisperse Pt Nanoparticles for C 1 to C 3 Alcohol oxidation and dehydrogenation of Dimethylamine-borane (DMAB). J. Nanosci. Nanotechnol. **16**, 5944–5950 (2016). https://doi.org/10.1166/jnn.2016.11683
35. Ertan, S., Şen, F., Şen, S., Gökağaç, G.: Platinum nanocatalysts prepared with different surfactants for C1–C3 Alcohol oxidations and their surface morphologies by AFM. J. Nanoparticle Res. **14**, 922–934 (2012). https://doi.org/10.1007/s11051-012-0922-5
36. Esirden, İ., Erken, E., Kaya, M., Sen, F.: Monodisperse Pt NPs@rGO as highly efficient and reusable heterogeneous catalysts for the synthesis of 5-Substituted 1H-Tetrazole derivatives. Catal. Sci. Technol. **5**, 4452–4457 (2015). https://doi.org/10.1039/C5CY00864F
37. Fang, M., Wang, K., Lu, H., Yang, Y., Nutt, S.: Single-layer graphene nanosheets with controlled grafting of polymer chains. J. Mater. Chem. **20**, 1982–1992 (2010). https://doi.org/10.1039/b919078c

38. Ferrari, A.C., Meyer, J.C., Scardaci, V., Casiraghi, C., Lazzeri, M., Mauri, F., Piscanec, S., Jiang, D., Novoselov, K.S., Roth, S., Geim, A.K.: Raman spectrum of graphene and graphene layers. Phys. Rev. Lett. **97**, 187401–187404 (2006). https://doi.org/10.1103/PhysRevLett.97.187401
39. Gao, W., Alemany, L.B., Ci, L., Ajayan, P.M.: New Insights into the structure and reduction of graphite oxide. Nat. Chem. **1**, 403–408 (2009). https://doi.org/10.1038/nchem.281
40. Georgakilas, V., Otyepka, M., Bourlinos, A.B., Chandra, V., Kim, N., Kemp, K.C., Hobza, P., Zboril, R., Kim, K.S.: Functionalization of graphene: covalent and non-covalent approach. Chem. Rev. **112**, 6156–6214 (2012). https://doi.org/10.1021/cr3000412
41. Giraldo, J.P., Landry, M.P., Faltermeier, S.M., McNicholas, T.P., Iverson, N.M., Boghossian, A.A., Reuel, N.F., Hilmer, A.J., Sen, F., Brew, J.A., Strano, M.S.: Plant nanobionics approach to augment photosynthesis and biochemical sensing. Nat. Mater. **13**, 400–408 (2014). https://doi.org/10.1038/nmat3890
42. Göksu, H., Çelik, B., Yıldız, Y., Şen, F., Kılbaş, B.: Superior monodisperse CNT-Supported CoPd (CoPd@CNT) nanoparticles for selective reduction of nitro compounds to primary amines with NaBH4 in aqueous medium. ChemistrySelect **1**, 2366–2372 (2016). https://doi.org/10.1002/slct.201600509
43. Goksu, H., Sert, H., Kilbas, B., Sen, F.: Recent advances in the reduction of nitro compounds by heterogenous catalysts. Curr. Org. Chem. **21**, 794–820 (2017). https://doi.org/10.2174/1385272820666160525123907
44. Goksu, H., Yıldız, Y., Çelik, B., Yazici, M., Kilbas, B., Sen, F.: Eco-friendly hydrogenation of aromatic aldehyde compounds by tandem dehydrogenation of Dimethylamine-Borane in the presence of a reduced graphene oxide furnished Platinum nanocatalyst. Catal. Sci. Technol. **6**, 2318–2324 (2016). https://doi.org/10.1039/C5CY01462J
45. Göksu, H., Yıldız, Y., Çelik, B., Yazıcı, M., Kılbaş, B., Şen, F.: Highly efficient and monodisperse graphene oxide furnished Ru/Pd nanoparticles for the dehalogenation of Aryl Halides via Ammonia Borane. ChemistrySelect **1**, 953–958 (2016). https://doi.org/10.1002/slct.201600207
46. Goksu, H., Zengin, N., Karaosman, A., Sen, F.: Highly active and reusable Pd/AlO(OH) nanoparticles for the Suzuki Cross-coupling reaction. Curr. Organocatal. **5**, 34–41 (2018). https://doi.org/10.2174/2213337205666180614114550
47. Gulçin, İ., Taslimi, P., Aygün, A., Sadeghian, N., Bastem, E., Kufrevioglu, O.I., Turkan, F., Şen, F.: Antidiabetic and antiparasitic potentials: inhibition effects of some natural antioxidant Compounds on A-Glycosidase, A-Amylase and Human Glutathione S-Transferase enzymes. Int. J. Biol. Macromol. **119**, 741–746 (2018). https://doi.org/10.1016/j.ijbiomac.2018.08.001
48. Günbatar, S., Aygun, A., Karataş, Y., Gülcan, M., Şen, F.: Carbon-nanotube-based Rhodium nanoparticles as highly-active catalyst for hydrolytic dehydrogenation of Dimethylamineborane at room temperature. J. Colloid Interface Sci. **530**, 321–327 (2018). https://doi.org/10.1016/j.jcis.2018.06.100
49. Gupta, A., Chen, G., Joshi, P., Tadigadapa, S., Eklund, P.C.: Raman scattering from high-frequency phonons in supported N-Graphene layer films. Nano Lett. **6**, 2667–2673 (2006). https://doi.org/10.1021/nl061420a
50. Hallam, T., Berner, N.C., Yim, C., Duesberg, G.S.: Strain, bubbles, dirt, and folds: a study of graphene polymer-assisted transfer. Adv. Mater. Interfaces **1**, 1400115–1400122 (2014). https://doi.org/10.1002/admi.201400115
51. Hamilton, C.E., Lomeda, J.R., Sun, Z., Tour, J.M., Barron, A.R.: High-yield organic dispersions of unfunctionalized graphene. Nano Lett. **9**, 3460–3462 (2009). https://doi.org/10.1021/nl9016623
52. Hao, R., Qian, W., Zhang, L., Hou, Y.: Aqueous dispersions of TCNQ-Anion-stabilized graphene sheets. Chem. Commun. pp. 6576–6578 (2008). https://doi.org/10.1039/b816971c
53. Hernandez, Y., Nicolosi, V., Lotya, M., Blighe, F.M., Sun, Z., De, S., McGovern, I.T., Holland, B., Byrne, M., Gun'Ko, Y.K., Boland, J.J., Niraj, P., Duesberg, G., Krishnamurthy, S., Goodhue, R., Hutchison, J., Scardaci, V., Ferrari, A.C., Coleman, J.N.: High-yield

production of graphene by liquid-phase exfoliation of graphite. Nat. Nanotechnol **3**, 563–568 (2008). https://doi.org/10.1038/nnano.2008.215
54. Huang, S., Ling, X., Liang, L., Song, Y., Fang, W., Zhang, J., Kong, J., Meunier, V., Dresselhaus, M.S.: Molecular selectivity of graphene-enhanced raman scattering. Nano Lett. **15**, 2892–2901 (2015). https://doi.org/10.1021/nl5045988
55. Hummers, W.S., Offeman, R.E.: Preparation of graphitic oxide. J. Am. Chem. Soc. **80**, 1339 (1958). https://doi.org/10.1021/ja01539a017
56. Iverson, N.M., Barone, P.W., Shandell, M., Trudel, L.J., Sen, S., Sen, F., Ivanov, V., Atolia, E., Farias, E., McNicholas, T.P., Reuel, N., Parry, N.M.A., Wogan, G.N., Strano, M.S.: In vivo biosensing via tissue-localizable near-infrared-fluorescent single-walled carbon nanotubes. Nat. Nanotechnol. **8**, 873–880 (2013). https://doi.org/10.1038/nnano.2013.222
57. Karatepe, Ö., Yıldız, Y., Pamuk, H., Eris, S., Dasdelen, Z., Sen, F.: Enhanced electrocatalytic activity and durability of highly monodisperse Pt@PPy–PANI nanocomposites as a novel catalyst for the electro-oxidation of methanol. RSC Adv. **6**, 50851–50857 (2016). https://doi.org/10.1039/C6RA06210E
58. Kim, K.S., Zhao, Y., Jang, H., Lee, S.Y., Kim, J.M., Kim, K.S., Ahn, J.-H., Kim, P., Choi, J.-Y., Hong, B.H.: Large-scale pattern growth of graphene films for stretchable transparent electrodes. Nature **457**, 706–710 (2009). https://doi.org/10.1038/nature07719
59. Koskun, Y., Şavk, A., Şen, B., Şen, F.: Highly sensitive glucose sensor based on monodisperse palladium nickel/activated carbon nanocomposites. Anal. Chim. Acta. **1010**, 37–43 (2018). https://doi.org/10.1016/j.aca.2018.01.035
60. Kosynkin, D.V., Higginbotham, A.L., Sinitskii, A., Lomeda, J.R., Dimiev, A., Price, B.K., Tour, J.M.: Longitudinal unzipping of carbon nanotubes to form graphene nanoribbons. Nature **458**, 872–876 (2009). https://doi.org/10.1038/nature07872
61. Kovaříček, P., Bastl, Z., Valeš, V., Kalbac, M.: Covalent reactions on chemical vapor deposition grown graphene studied by surface-enhanced raman spectroscopy. Chem - A Eur J **22**, 5404–5408 (2016). https://doi.org/10.1002/chem.201504689
62. Kudin, K.N., Scuseria, G.E., Yakobson, B.I.: C2F, BN, and C nanoshell elasticity from AB initio computations. Phys. Rev. B **64**, 235406–235416 (2001). https://doi.org/10.1103/PhysRevB.64.235406
63. Kuila, T., Bose, S., Hong, C.E., Uddin, M.E., Khanra, P., Kim, N.H., Lee, J.H.: Preparation of functionalized graphene/linear low density polyethylene composites by a solution mixing method. Carbon N Y **49**, 1033–1037 (2011). https://doi.org/10.1016/j.carbon.2010.10.031
64. Kuila, T., Bose, S., Mishra, A.K., Khanra, P., Kim, N.H., Lee, J.H.: chemical functionalization of graphene and its applications. Prog. Mater Sci. **57**, 1061–1105 (2012). https://doi.org/10.1016/j.pmatsci.2012.03.002
65. Larisika, M., Kotlowski, C., Steininger, C., Mastrogiacomo, R., Pelosi, P., Schütz, S., Peteu, S.F., Kleber, C., Reiner-Rozman, C., Nowak, C., Knoll, W.: Electronic olfactory sensor based on *A. mellifera* odorant-binding protein 14 on a reduced graphene oxide field-effect transistor. Angew Chemie. Int. Ed. **54**, 13245–13248 (2015). https://doi.org/10.1002/anie.201505712
66. Lee, C., Wei, X., Kysar, J.W., Hone, J.: Measurement of the elastic properties and intrinsic strength of monolayer graphene. Science (80-) **321**, 385–388 (2008). https://doi.org/10.1126/science.1157996
67. Lee, D.Y., Khatun, Z., Lee, J.-H., Lee, Y., In, I.: Blood compatible graphene/heparin conjugate through noncovalent chemistry. Biomacromol **12**, 336–341 (2011). https://doi.org/10.1021/bm101031a
68. Lee, W.H., Park, J., Kim, Y., Kim, K.S., Hong, B.H., Cho, K.: Control of graphene field-effect transistors by interfacial hydrophobic self-assembled monolayers. Adv. Mater. **23**, 3460–3464 (2011). https://doi.org/10.1002/adma.201101340
69. Lee, W.H., Park, J., Kim, Y., Kim, K.S., Hong, B.H., Cho, K.: Control of graphene field-effect transistors by interfacial hydrophobic self-assembled monolayers. Adv. Mater. **23**, 3460–3464 (2011). https://doi.org/10.1002/adma.201101340

70. Li, D., Müller, M.B., Gilje, S., Kaner, R.B., Wallace, G.G.: Processable aqueous dispersions of graphene nanosheets. Nat. Nanotechnol. **3**, 101–105 (2008). https://doi.org/10.1038/nnano.2007.451
71. Li, X., Cai, W., An, J., Kim, S., Nah, J., Yang, D., Piner, R., Velamakanni, A., Jung, I., Tutuc, E., Banerjee, S.K., Colombo, L., Ruoff, R.S.: Large-area synthesis of high-quality and uniform graphene films on copper foils. Science (80-) **324**, 1312–1314 (2009). https://doi.org/10.1126/science.1171245
72. Liu, N., Luo, F., Wu, H., Liu, Y., Zhang, C., Chen, J.: One-step Ionic-liquid-assisted electrochemical synthesis of ionic-liquid-functionalized graphene sheets directly from graphite. Adv. Funct. Mater. **18**, 1518–1525 (2008). https://doi.org/10.1002/adfm.200700797
73. Loh, K.P., Bao, Q., Ang, P.K., Yang, J.: The chemistry of graphene. J. Mater. Chem. **20**, 2277–2289 (2010). https://doi.org/10.1039/b920539j
74. Lotya, M., Hernandez, Y., King, P.J., Smith, R.J., Nicolosi, V., Karlsson, L.S., Blighe, F.M., De, S., Zhiming, W., McGovern, I.T., Duesberg, G.S., Coleman, J.N.: Liquid phase production of graphene by exfoliation of graphite in surfactant/water solutions. J. Am. Chem. Soc. **131**, 3611–3620 (2009). https://doi.org/10.1021/ja807449u
75. Lotya, M., King, P.J., Khan, U., De, S., Coleman, J.N.: High-concentration, surfactant-stabilized graphene dispersions. ACS Nano **4**, 3155–3162 (2010). https://doi.org/10.1021/nn1005304
76. Lupina, G., Kitzmann, J., Costina, I., Lukosius, M., Wenger, C., Wolff, A., Vaziri, S., Östling, M., Pasternak, I., Krajewska, A., Strupinski, W., Kataria, S., Gahoi, A., Lemme, M. C., Ruhl, G., Zoth, G., Luxenhofer, O., Mehr, W.: Residual metallic contamination of transferred chemical vapor deposited graphene. ACS Nano **9**, 4776–4785 (2015). https://doi.org/10.1021/acsnano.5b01261
77. Matsuo, Y., Sakai, Y., Fukutsuka, T., Sugie, Y.: Preparation of pillared carbons by pyrolysis of silylated graphite oxide. Chem. Lett. **36**, 1050–1051 (2007). https://doi.org/10.1246/cl.2007.1050
78. Meyer, J.C., Geim, A.K., Katsnelson, M.I., Novoselov, K.S., Booth, T.J., Roth, S.: The structure of suspended graphene sheets. Nature **446**, 60–63 (2007). https://doi.org/10.1038/nature05545
79. Min, S.K., Kim, W.Y., Cho, Y., Kim, K.S.: Fast DNA sequencing with a graphene-based nanochannel device. Nat. Nanotechnol. **6**, 162–165 (2011). https://doi.org/10.1038/nnano.2010.283
80. Muñoz, R., Gómez-Aleixandre, C.: Review of CVD synthesis of graphene. Chem. Vap. Depos. **19**, 297–322 (2013). https://doi.org/10.1002/cvde.201300051
81. Nair, R.R., Blake, P., Grigorenko, A.N., Novoselov, K.S., Booth, T.J., Stauber, T., Peres, N. M.R., Geim, A.K.: Fine structure constant defines visual transparency of graphene. Science (80-) **320**, 1308–1308 (2008). https://doi.org/10.1126/science.1156965
82. Nemes-Incze, P., Osváth, Z., Kamarás, K., Biró, L.P.: Anomalies in thickness measurements of graphene and few layer graphite crystals by tapping mode atomic force microscop. Carbon N Y **46**, 1435–1442 (2008). https://doi.org/10.1016/j.carbon.2008.06.022
83. Nethravathi, C., Rajamathi, J.T., Ravishankar, N., Shivakumara, C., Rajamathi, M.: Graphite oxide-intercalated anionic clay and its decomposition to graphene-inorganic material nanocomposites. Langmuir **24**, 8240–8244 (2008). https://doi.org/10.1021/la8000027
84. Novoselov, K.S.: Electric field effect in atomically thin carbon films. Science (80-) **306**, 666–669 (2004). https://doi.org/10.1126/science.1102896
85. Novoselov, K.S., Geim, A.K., Morozov, S.V., Jiang, D., Katsnelson, M.I., Grigorieva, I.V., Dubonos, S.V., Firsov, A.A.: Two-dimensional gas of massless dirac fermions in graphene. Nature **438**, 197–200 (2005). https://doi.org/10.1038/nature04233
86. Novoselov, K.S., McCann, E., Morozov, S.V., Fal'ko, V.I., Katsnelson, M.I., Zeitler, U., Jiang, D., Schedin, F., Geim, A.K.: Unconventional quantum Hall effect and Berry's Phase of 2π in Bilayer Graphene. Nat. Phys. **2**, 177–180 (2006). https://doi.org/10.1038/nphys245

87. Ozturk, Z., Sen, F., Sen, S., Gokagac, G.: The preparation and characterization of nano-sized Pt-Pd/C catalysts and comparison of their superior catalytic activities for methanol and ethanol oxidation. J. Mater. Sci. **47**, 8134–8144 (2012). https://doi.org/10.1007/s10853-012-6709-3
88. Pamuk, H., Aday, B., Şen, F., Kaya, M.: Pt NPs@GO as a highly efficient and reusable catalyst for one-pot synthesis of acridinedione derivatives. RSC Adv. **5**, 49295–49300 (2015). https://doi.org/10.1039/C5RA06441D
89. Parades, J.I., Villar-Rodil, S., Martínez-Alonso, A., Tascón, J.M.D.: Graphene oxide dispersions in organic solvents. Langmuir **24**, 10560–10564 (2008). https://doi.org/10.1021/la801744a
90. Park, J., Jo, S.B., Yu, Y.-J., Kim, Y., Yang, J.W., Lee, W.H., Kim, H.H., Hong, B.H., Kim, P., Cho, K., Kim, K.S.: Single-gate bandgap opening of bilayer graphene by dual molecular doping. Adv. Mater. **24**, 407–411 (2012). https://doi.org/10.1002/adma.201103411
91. Park, J., Lee, W.H., Huh, S., Sim, S.H., Bin, Kim S., Cho, K., Hong, B.H., Kim, K.S.: Work-function engineering of graphene electrodes by self-assembled monolayers for high-performance organic field-effect transistors. J. Phys. Chem. Lett. **2**, 841–845 (2011). https://doi.org/10.1021/jz200265w
92. Park, M.J., Lee, J.K., Lee, B.S., Lee, Y.W., Choi, I.S., Lee, S.G.: Covalent modification of multiwalled carbon nanotubes with imidazolium-based ionic liquids: Effect of anions on solubility. Chem. Mater. **18**, 1546–1551 (2006). https://doi.org/10.1021/cm0511421
93. Park, S., An, J., Piner, R.D., Jung, I., Yang, D., Velamakanni, A., Nguyen, S.T., Ruoff, R.S.: Aqueous suspension and characterization of chemically modified graphene sheets. Chem. Mater. **20**, 6592–6594 (2008). https://doi.org/10.1021/cm801932u
94. Park, S., Ruoff, R.S.: Chemical methods for the production of graphenes. Nat. Nanotechnol. **4**, 217–224 (2009). https://doi.org/10.1038/nnano.2009.58
95. Reina, A., Jia, X., Ho, J., Nezich, D., Son, H., Bulovic, V., Dresselhaus, M.S., Jing, K.: Large area, few-layer graphene films on arbitrary substrates by chemical vapor deposition. Nano Lett. **9**, 30–35 (2009). https://doi.org/10.1021/nl801827v
96. Şahin, B., Aygün, A., Gündüz, H., Şahin, K., Demir, E., Akocak, S., Şen, F.: Cytotoxic effects of platinum nanoparticles obtained from pomegranate extract by the green synthesis method on the MCF-7 cell line. Colloids Surf. B Biointerfaces **163**, 119–124 (2018). https://doi.org/10.1016/j.colsurfb.2017.12.042
97. Şahin, B., Demir, E., Aygün, A., Gündüz, H., Şen, F.: Investigation of the effect of pomegranate extract and monodisperse silver nanoparticle combination on MCF-7 cell line. J. Biotechnol. **260**, 79–83 (2017). https://doi.org/10.1016/j.jbiotec.2017.09.012
98. Schedin, F., Geim, A.K., Morozov, S.V., Hill, E.W., Blake, P., Katsnelson, M.I., Novoselov, K.S.: Detection of individual gas molecules adsorbed on graphene. Nat. Mater. **6**, 652–655 (2007). https://doi.org/10.1038/nmat1967
99. Şen, B., Akdere, E.H., Şavk, A., Gültekin, E., Paralı, Ö., Göksu, H., Şen, F.: A novel thiocarbamide functionalized graphene oxide supported bimetallic monodisperse Rh-Pt nanoparticles (RhPt/TC@GO NPs) for Knoevenagel condensation of Aryl Aldehydes together with malononitrile. Appl. Catal. B Environ. **225**, 148–153 (2018). https://doi.org/10.1016/j.apcatb.2017.11.067
100. Şen, B., Aygün, A., Okyay, T.O., Şavk, A., Kartop, R., Şen, F.: Monodisperse palladium nanoparticles assembled on graphene oxide with the high catalytic activity and reusability in the dehydrogenation of Dimethylamine-borane. Int. J. Hydrogen Energy **43**, 20176–20182 (2018). https://doi.org/10.1016/j.ijhydene.2018.03.175
101. Şen, B., Demirkan, B., Levent, M., Şavk, A., Şen, F.: Silica-based monodisperse PdCo nanohybrids as highly efficient and stable nanocatalyst for hydrogen evolution reaction. Int. J. Hydrogen Energy **43**, 20234–20242 (2018). https://doi.org/10.1016/j.ijhydene.2018.07.080

102. Şen, B., Demirkan, B., Şavk, A., Karahan Gülbay, S., Şen, F.: Trimetallic PdRuNi nanocomposites decorated on graphene oxide: a superior catalyst for the hydrogen evolution reaction. Int. J. Hydrogen Energy **43**, 17984–17992 (2018). https://doi.org/10.1016/j.ijhydene.2018.07.122
103. Sen, B., Demirkan, B., Şimşek, B., Savk, A., Sen, F.: Monodisperse Palladium nanocatalysts for dehydrocoupling of Dimethylamineborane. Nano-Struct. Nano-Objects **16**, 209–214 (2018). https://doi.org/10.1016/j.nanoso.2018.07.008
104. Sen, B., Kuyuldar, E., Demirkan, B., Onal Okyay, T., Şavk, A., Sen, F.: Highly efficient polymer supported monodisperse ruthenium-nickel nanocomposites for dehydrocoupling of Dimethylamine Borane. J. Colloid Interf. Sci. **526**, 480–486 (2018). https://doi.org/10.1016/j.jcis.2018.05.021
105. Şen, B., Kuzu, S., Demir, E., Akocak, SüleymanŞSen F.: Highly monodisperse RuCo nanoparticles decorated on functionalized multiwalled carbon nanotube with the highest observed catalytic activity in the dehydrogenation of Dimethylamine–borane. Int. J. Hydrogen Energy **42**, 23292–23298 (2017). https://doi.org/10.1016/j.ijhydene.2017.06.032
106. Şen, B., Kuzu, S., Demir, E., Akocak, S., Şen, F.: Polymer-graphene hybride decorated Pt nanoparticles as highly efficient and reusable catalyst for the dehydrogenation of Dimethylamine–borane at room temperature. Int. J. Hydrogen Energy **42**, 23284–23291 (2017). https://doi.org/10.1016/j.ijhydene.2017.05.112
107. Sen, B., Kuzu, S., Demir, E., Onal Okyay, T., Sen, F.: Hydrogen liberation from the dehydrocoupling of dimethylamine–borane at room temperature by using novel and highly monodispersed RuPtNi nanocatalysts decorated with graphene oxide. Int. J. Hydrogen Energy **42**, 23299–23306 (2017). https://doi.org/10.1016/j.ijhydene.2017.04.213
108. Şen, B., Kuzu, S., Demir, E., Yıldırır, E., Şen, F.: Highly efficient catalytic dehydrogenation of dimethyl ammonia borane via monodisperse palladium-nickel alloy nanoparticles assembled on PEDOT. Int. J. Hydrogen Energy **42**, 23307–23314 (2017). https://doi.org/10.1016/j.ijhydene.2017.05.115
109. Şen, B., Lolak, N., Paralı, Ö., Koca, M., Şavk, A., Akocak, S., Şen, F.: Bimetallic PdRu/graphene oxide based catalysts for one-pot three-component synthesis of 2-amino-4H-chromene derivatives. Nano-Struct. Nano-Objects **12**, 33–40 (2017). https://doi.org/10.1016/j.nanoso.2017.08.013
110. Sen, B., Şavk, A., Kuyuldar, E., Karahan Gülbay, S., Sen, F.: Hydrogen liberation from the hydrolytic dehydrogenation of hydrazine borane in acidic media. Int. J. Hydrogen Energy **43**, 17978–17983 (2018). https://doi.org/10.1016/j.ijhydene.2018.03.225
111. Sen, B., Şavk, A., Sen, F.: Highly efficient monodisperse pt nanoparticles confined in the carbon black hybrid material for hydrogen liberation. J. Colloid Interf. Sci. **520**, 112–118 (2018). https://doi.org/10.1016/j.jcis.2018.03.004
112. Sen, F., Boghossian, A.A., Sen, S., Ulissi, Z.W., Zhang, J., Strano, M.S.: Observation of oscillatory surface reactions of Riboflavin, Trolox, and singlet oxygen using single carbon nanotube fluorescence spectroscopy. ACS Nano **6**, 10632–10645 (2012). https://doi.org/10.1021/nn303716n
113. Şen, F., Gökağaç, G.: Different sized platinum nanoparticles supported on carbon: An XPS study on these methanol oxidation catalysts. J. Phys. Chem. C **111**, 5715–5720 (2007). https://doi.org/10.1021/jp068381b
114. Şen, F., Gökağaç, G.: Improving catalytic efficiency in the methanol oxidation reaction by inserting Ru in face-centered cubic Pt nanoparticles prepared by a new surfactant, Tert-octanethiol. Energy Fuels **22**, 1858–1864 (2008). https://doi.org/10.1021/ef700575t
115. Şen, F., Gökağaç, G.: Pt nanoparticles synthesized with new surfactants: Improvement in C1-C3 alcohol oxidation catalytic activity. J. Appl. Electrochem. **44**, 199–207 (2014). https://doi.org/10.1007/s10800-013-0631-5
116. Şen, F., Gökağaç, G., Şen, S.: High performance Pt Nanoparticles prepared by new surfactants for C1 to C3 alcohol oxidation reactions. J Nanoparticle Res. **15**, 1979–1988 (2013). https://doi.org/10.1007/s11051-013-1979-5

117. Sen, F., Karatas, Y., Gulcan, M., Zahmakiran, M.: Amylamine stabilized Platinum(0) nanoparticles: Active and reusable nanocatalyst in the room temperature dehydrogenation of dimethylamine-borane. RSC Adv. **4**, 1526–1531 (2014). https://doi.org/10.1039/c3ra43701a
118. Şen, F., Şen, S., Gökağaç, G.: Efficiency enhancement of methanol/ethanol oxidation reactions on Pt Nanoparticles prepared using a new surfactant, 1,1-Dimethyl Heptanethiol. Phys. Chem. Chem. Phys. **13**, 1676–1684 (2011). https://doi.org/10.1039/c0cp01212b
119. Sen, S., Sen, F., Boghossian, A.A., Zhang, J., Strano, M.S.: Effect of reductive dithiothreitol and Trolox on nitric oxide quenching of single-walled carbon nanotubes. J. Phys. Chem. C **117**, 593–602 (2013). https://doi.org/10.1021/jp307175f
120. Sert, H., Yıldız, Y., Okyay, T.O., Gezer, B., Dasdelen, Z., Sen, B., Sen, F.: Monodisperse Mw-Pt NPs@VC as highly efficient and reusable adsorbents for methylene blue removal. J. Clust. Sci. **27**, 1953–1962 (2016). https://doi.org/10.1007/s10876-016-1054-3
121. Sert, H., Yıldız, Y., Onal Okyay, T., Sen, B., Gezer, B., Bozkurt, S., Ba, G., Sen, F.: Activated carbon furnished monodisperse Pt nanocomposites as a superior adsorbent for methylene blue removal from aqueous solutions. J. Nanosci. Nanotechnol. **17**, 1–6 (2017). https://doi.org/10.1166/jnn.2017.13776
122. Shao, Y., Wang, J., Engelhard, M., Wang, C., Lin, Y.: Facile and controllable electrochemical reduction of graphene oxide and its applications. J. Mater. Chem. **20**, 743–748 (2010). https://doi.org/10.1039/B917975E
123. Shukla, S., Saxena, S.: Spectroscopic investigation of confinement effects on optical properties of graphene oxide. Appl. Phys. Lett. **98**, 073104–073106 (2011). https://doi.org/10.1063/1.3555438
124. Si, Y., Samulski, E.T.: Synthesis of water soluble graphene. Nano Lett. **8**, 1679–1682 (2008). https://doi.org/10.1021/nl080604h
125. Stankovich, S., Dikin, D.A., Dommett, G.H.B., Kohlhaas, K.M., Zimney, E.J., Stach, E.A., Piner, R.D., Nguyen, S.B.T., Ruoff, R.S.: Graphene-based composite materials. Nature **442**, 282–286 (2006). https://doi.org/10.1038/nature04969
126. Stoller, M.D., Park, S., Yanwu, Z., An, J., Ruoff, R.S.: Graphene-based ultracapacitors. Nano Lett. **8**, 3498–3502 (2008). https://doi.org/10.1021/nl802558y
127. Sun, Z., Yan, Z., Yao, J., Beitler, E., Zhu, Y., Tour, J.M.: Growth of graphene from solid carbon sources. Nature **468**, 549–552 (2010). https://doi.org/10.1038/nature09579
128. Szabó, T., Berkesi, O., Forgó, P., Josepovits, K., Sanakis, Y., Petridis, D., Dékány, I.: Evolution of surface functional groups in a series of progressively oxidized graphite oxides. Chem. Mater. **18**, 2740–2749 (2006). https://doi.org/10.1021/cm060258+
129. Szabó, T., Szeri, A., Dékány, I.: Composite graphitic nanolayers prepared by self-assembly between finely dispersed graphite oxide and a cationic polymer. Carbon N Y **43**, 87–94 (2005). https://doi.org/10.1016/j.carbon.2004.08.025
130. Tasic, A., Sredovic-Ignjatovic, I., Ignjatovic, L., Andjelkovic, I., Antic, M., Rajakovic, L.: Investigation of different extraction procedures for the determination of major and trace elements in coal by ICP-AES and Ion chromatography. J. Serbian Chem. Soc. **81**, 403–417 (2016). https://doi.org/10.2298/JSC150429078T
131. Tehrani, Z., Burwell, G., Azmi, M.A.M., Castaing, A., Rickman, R., Almarashi, J., Dunstan, P., Beigi, A.M., Doak, S.H., Guy, O.J.: Generic epitaxial graphene biosensors for ultrasensitive detection of cancer risk biomarker. 2D Mater **1**, 025004–23 (2014). https://doi.org/10.1088/2053-1583/1/2/025004
132. Ulissi, Z.W., Sen, F., Gong, X., Sen, S., Iverson, N., Boghossian, A.A., Godoy, L.C., Wogan, G.N., Mukhopadhyay, D., Strano, M.S.: spatiotemporal intracellular nitric oxide signaling captured using internalized, near-infrared fluorescent carbon nanotube nanosensors. Nano Lett. **14**, 4887–4894 (2014). https://doi.org/10.1021/nl502338y
133. Ulus, R., Yıldız, Y., Eriş, S., Aday, B., Şen, F., Kaya, M.: Functionalized multi-walled carbon nanotubes (f-MWCNT) as highly efficient and reusable heterogeneous catalysts for the synthesis of acridinedione derivatives. ChemistrySelect **1**, 3861–3865 (2016). https://doi.org/10.1002/slct.201600719

134. Van Noorden, R.: Chemistry: The trials of new carbon. Nature **469**, 14–16 (2011). https://doi.org/10.1038/469014a
135. Varghese, S.S., Lonkar, S., Singh, K.K., Swaminathan, S., Abdala, A.: Recent advances in graphene based gas sensors. Sens. Actuators B Chem. **218**, 160–183 (2015). https://doi.org/10.1016/j.snb.2015.04.062
136. Wang, Q.H., Hersam, M.C.: Room-temperature molecular-resolution characterization of self-assembled organic monolayers on epitaxial graphene. Nat. Chem. **1**, 206–211 (2009). https://doi.org/10.1038/nchem.212
137. Wang, Y., Li, Z., Wang, J., Li, J., Lin, Y.: Graphene and graphene oxide: Biofunctionalization and applications in biotechnology. Trends Biotechnol. **29**, 205–212 (2011). https://doi.org/10.1016/j.tibtech.2011.01.008
138. Wang, Y., Ni, Z., Yu, T., Shen, Z.X., Wang, H., Wu, Y., Chen, W., Shen, W.A.T.: Raman studies of monolayer graphene: The substrate effect. J. Phys. Chem. C **112**, 10637–10640 (2008). https://doi.org/10.1021/jp8008404
139. Williams, G., Seger, B., Kamat, P.V.: TiO2-graphene nanocomposites. UV-assisted photocatalytic reduction of graphene oxide. ACS Nano **2**, 1487–1491 (2008). https://doi.org/10.1021/nn800251f
140. Yi, J.W., Park, J., Kim, K.S., Kim, B.H.: PH-responsive self-duplex of (Py)A-substituted oligodeoxyadenylate in graphene oxide solution as a molecular switch. Org. Biomol. Chem. **9**, 7434–7438 (2011). https://doi.org/10.1039/c1ob06037f
141. Yildiz, Y., Okyay, T.O., Sen, B., Gezer, B., Kuzu, S., Savk, A., Demir, E., Dasdelen, Z., Sert, H., Sen, F.: Highly monodisperse Pt/Rh nanoparticles confined in the graphene oxide for highly efficient and reusable sorbents for methylene blue removal from aqueous solutions. ChemistrySelect **2**, 697–701 (2017). https://doi.org/10.1002/slct.201601608
142. Yıldız, Y., Erken, E., Pamuk, H., Sert, H., Şen, F.: Monodisperse Pt nanoparticles assembled on reduced graphene oxide: highly efficient and reusable catalyst for methanol oxidation and dehydrocoupling of Dimethylamine-Borane (DMAB). J. Nanosci. Nanotechnol. **16**, 5951–5958 (2016). https://doi.org/10.1166/jnn.2016.11710
143. Yıldız, Y., Esirden, İ., Erken, E., Demir, E., Kaya, M., Şen, F.: Microwave (Mw)-assisted synthesis of 5-Substituted 1H-Tetrazoles via [3 + 2] cycloaddition catalyzed by Mw-Pd/Co nanoparticles decorated on multi-walled carbon nanotubes. ChemistrySelect **1**, 1695–1701 (2016). https://doi.org/10.1002/slct.201600265
144. Yıldız, Y., Kuzu, S., Sen, B., Savk, A., Akocak, S., Şen, F.: Different ligand based monodispersed Pt nanoparticles decorated with rGO as highly active and reusable catalysts for the methanol oxidation. Int. J. Hydrogen Energy **42**, 13061–13069 (2017). https://doi.org/10.1016/j.ijhydene.2017.03.230
145. Yıldız, Y., Pamuk, H., Karatepe, Ö., Dasdelen, Z., Sen, F.: Carbon black hybrid material furnished monodisperse platinum nanoparticles as highly efficient and reusable electrocatalysts for formic acid electro-oxidation. RSC Adv. **6**, 32858–32862 (2016). https://doi.org/10.1039/C6RA00232C
146. Zhang, H.B., Zheng, W.G., Yan, Q., Yang, Y., Wang, J.W., Lu, Z.H., Ji, G.Y., Yu, Z.Z.: electrically conductive polyethylene terephthalate/graphene nanocomposites prepared by melt compounding. Polymer (Guildf) **51**, 1191–1196 (2010). https://doi.org/10.1016/j.polymer.2010.01.027
147. Zhang, H., He, S., Chen, C., Zheng, W.Y.Q.: Electrical conductivity of melt compounded functionalized graphene sheets filled polyethyleneterephthalate composites. In: Physics and Applications of Graphene—Experiments. InTech. (2011)
148. Zhao, Y.-L., Stoddart, J.F.: Noncovalent functionalization of single-walled carbon nanotubes. Acc. Chem. Res. **42**, 1161–1171 (2009). https://doi.org/10.1021/ar900056z
149. Zhu, Y., Stoller, M.D., Cai, W., Velamakanni, A., Piner, R.D., Chen, D., Ruoff, R.S.: Exfoliation of graphite oxide in propylene carbonate and thermal reduction of the resulting graphene oxide platelets. ACS Nano **4**, 1227–1233 (2010). https://doi.org/10.1021/nn901689k

Chemically Functionalized Penta-Graphene for Electronic Device Applications: Journey from Theoretical Prediction to Practical Implementation

Kasturi Ghosh, Hafizur Rahaman and Partha Bhattacharyya

Abstract Penta-Graphene (PG), proposed in 2014 on the basis of theoretical simulations, is a two dimensional (2D) metastable carbon allotrope composed of carbon pentagons. PG is proposed to be synthesized by exfoliation from T12-carbon by hydrogen intercalation. Theoretical calculations confirm that PG is appreciably stable and can sustain the temperature as high as 1000 K. Unlike graphene which needs to be functionalized for opening a band gap, PG is itself a quasi-direct band gap semiconductor having a band gap of $\sim$3.25 eV. PG offers an unusual negative Poisson's ratio and very high mechanical strength exceeding than that of graphene. According to prediction, successful synthesis of penta-graphene may bring forth considerable makeover in future nano-electronics arena. However, synthesis of PG is still a challenge. It is not only difficult to isolate PG from the plethora of alternative isomers; it may rapidly restructure itself towards graphene in the presence of even a trace amount of specific catalytic impurities. Though unstable in its pure form, theoretical simulation shows suitable chemical functionalization stabilizes the penta-graphene structure by partially releasing the strain, which paves the path towards successful synthesis of penta-graphene considering its functionalized state as the precursor. In this book chapter, the strikingly interesting features/properties, procedure for predicting the characteristics through theoretical simulations, synthesis process, potential applications and critical bottlenecks of functionalized penta-graphene have been comprehensively discussed with special emphasis on its future prospects for next generation electronic device applications. Mainly three types of chemical functionalizations have been considered employing (i) hydrogen, (ii) fluorine and (iii) oxygen. Improvement of stability of functionalized PG, in terms of energy, lattice dynamics, mechanical and thermal in comparison to that of pristine PG have been discussed. Underlying mechanism

K. Ghosh · H. Rahaman
School of VLSI Technology, Indian Institute of Engineering Science and Technology (IIEST), Shibpur, India

P. Bhattacharyya (✉)
Department of Electronics and Telecommunication Engineering, Indian Institute of Engineering Science and Technology (IIEST), Shibpur, India
e-mail: pb_etc_besu@yahoo.com

A. Khan et al. (eds.), *Graphene Functionalization Strategies*, Carbon Nanostructures, https://doi.org/10.1007/978-981-32-9057-0_14

for the corresponding dramatic improvement in electronic, mechanical and thermal properties of PG for the above mentioned functionalization(s) have also been discussed. Hydrogenation and fluorination of PG changes the Poisson's ratio from negative to positive and turns the PG from a semiconductor to an insulator. Thermal conductivity of PG enhances dramatically on full hydrogenation. The three types of functionalizations mentioned above, improve mechanical strength of PG by enhancing the value of failure stress and failure strain. Chemical functionalizations widen the application potentiality of PG. Improvement in thermal conductivity of PG by partial functionalization facilitates its application in thermoelectric devices. Band gap tailoring by judicious chemical functionalization lays the foundation stone for future application of PG in the field of optoelectronic and photovoltaic devices. Hydrogen adsorption remarkably enhances the magnetic moment of PG which is useful for potential application in magnetic storage technology and next generation spintronic nano-devices. However, the practical implementation (synthesis and subsequent technology development to couple it successfully with device fabrication) is still in nascent stage and the future research endeavor of the researchers is inclined towards mitigating that bottleneck.

Keywords Penta-graphene · Chemical functionalization · Electronic property · Mechanical property · Magnetic property · Optical property · Thermal property

1 Introduction

Carbon, the most important and major constituent of the cycles on the Earth, is also an interesting and versatile element in the periodic table due to its enormous flexibility in bonding characteristics. The vast and ever expanding family of carbon allotropes, constructed with sp^3, sp^2 and sp hybridized orbitals, offer a wide range of hierarchical nano-structures ranging from three dimensional (3D) to zero dimensional (0D) variety (such as, diamond (3D), graphene (2D), nanotubes (1D) and bucky balls (0D)) [1]. Such carbon allotropes are also be characterized with diversified material properties (viz., the electronic property of Carbon allotropes can vary drastically over the range; from metal to insulator). Graphene, constructed with sp^2 hybridized carbon atoms arranged in a hexagonal honeycomb lattice (2D), has initiated a new era in nano-electronics due to its unprecedentedly advantageous electronic properties. The great success of graphene has triggered the interest of the researchers across the globe in exploring other 2D nanomaterials specially based on carbon [2]. Since then, a number of low-dimensional carbon allotropes have been proposed from theoretical consideration [3–5], among which Penta-Graphene (PG) is one of the most remarkable one. Zhang et al. first identified penta-graphene by simulation in 2014 [5]. It is a two dimensional metastable carbon allotrope and is constructed from a mixture of sp^2- and sp^3 hybridized carbon atoms arranged in pentagonal lattice which closely resembles to the well-known Cairo pentagonal tiling. The key difference between PG and graphene is that graphene is zero band

gap material whereas penta-graphene is a semiconductor with a finite band gap of ∼3.25 eV [5]. Although experimental synthesis of PG is still a crucial challenge, some of its unique electronic, thermal, mechanical, magnetic and optical features and their tunability through suitable functionalization (as predicted from theoretical studies) projected this material as a potential candidate for applications in nano-electronics and nano-mechanics for the coming era. Like graphene, PG can also form nanoribbon and nanotube structure which are beyond the scope of this chapter [6–9].

Prediction of either the existence of a material or the properties of a material (theoretically proposed or already existing) can be decided from "Density functional theory" (DFT) and "Molecular Dynamics" (MD) based calculations. DFT is the most successful ab initio/ first principle calculation which is based on the quantum mechanical description of the material and governed by the laws of condensed matter physics [10–12]. The underlying principle is that "the total energy of the system is a unique function of the electron density". DFT calculations are based on 'Kohn–Sham (KS)' method which is an independent particle method for many-body electron problem. The framework of DFT is based on computing the ground state energy and charge density of many body system of electron by solving a set of Schrödinger like equations representing a fictitious but simplified system of non-interacting electrons moving in an effective potential [11, 12]. "Effective potential consists of external potential, Coulomb potential and Exchange-correlation (XC) potential. The XC potential is a measure of the quantum mechanical exchange and correlation of the particles" [13]. XC potential plays critical role in DFT calculation. The ground state energy of the material is identified from DFT calculation. "Ab initio Molecular Dynamics" (AIMD) simulation calculate the dynamics for systems for which the interatomic forces are derived from DFT based calculations.

The possibility of existence of penta-graphene and its properties were first predicted by Zhang et al. with the help of DFT based AIMD simulations performed using Vienna Ab initio Simulation Package (VASP) [14]. Interactions between ion cores and valance electrons were treated with "Projector augmented wave" (PAW) basis set [15]. Proper choice of "exchange-correlation" (XC) potential function is important for predicting material properties using DFT based calculations. Zhang et al. [5] used "generalized gradient approximation" (GGA) with 'Perdew–Burke–Ernzerhof' XC potential for most of the calculations. Since, electronic band structure calculations demand high precision, Zhang et al. [5] used 'hybrid Heyd–Scuseria–Ernzerhof' (HSE06) XC potential [17] only for calculation of electronic band structure of penta-graphene. 'Phonopy package' was used to determine phonon properties of PG using finite displacement method.

It is well established that electronic, magnetic, optical and mechanical properties of graphene can be tuned effectively by chemical functionalization [18, 19]. This triggered the curiosity among the researchers to find a way of tuning of various properties of PG through chemical functionalization. Although, penta-graphene is proposed very recently and its research is in very nascent stage, it is found that chemical functionalization will significantly widen the application of PG in

electronic devices. Bonding characteristics (transformation from sp^2 to sp^3, change of bond length, angle etc.), electronic and phonon band structure of PG change upon chemical functionalization which is reflected in electronic, thermal, mechanical, optical and magnetic properties of the same. Thus, the properties of PG can be tuned for suitable electronic device application employing judicious chemical functionalizations. The property of PG can also be changed by doping which is out of scope of this book chapter [20–22].

2 Structure and Properties of PG

Penta-graphene was first theoretically proposed by Zhang et al. in 2014 by exfoliation of single layer from T12-carbon, whose existence is also recently predicted from DFT based calculations [5]. PG shows tetragonal lattice structure with six carbon atoms per unit cell having optimized lattice parameters; a = b = 3.64 Å. The carbon atoms in PG shows two types of hybridization viz. sp^3 and sp^2 which are customarily distinguished as C1 and C2, respectively [5].

Figure 1 shows the top and side view of the optimized structure of penta-graphene along with its the first Brillouin zone in reciprocal lattice space identifying the high symmetry path Γ–M–X–Γ where Γ = (0, 0, 0)2π/a, M = (1/2, 1/2, 0)2π/a and X = (0, 1/2, 0)2π/a. From the top view, PG looks like Cairo pentagonal tiling. Carbon-carbon bond lengths in PG are 1.55 Å (C1–C2) and 1.34 Å (C2–C2) which show pronounced character of single and double bonds, respectively. However, these bond lengths differ from the carbon-carbon bond length in diamond and graphite/graphene which are 1.54 and 1.42 Å, respectively. Thus, the bonding characteristics in

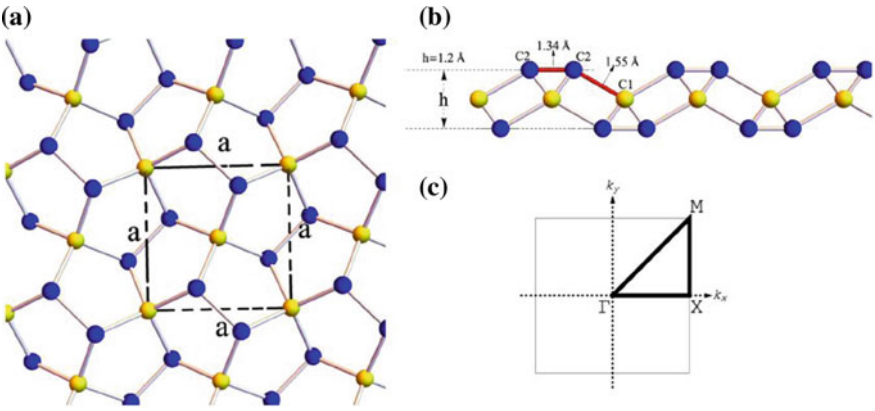

Fig. 1 **a** Top view, unit cell and **b** front view of the optimized structure of penta-graphene, Yellow, blue sphere represent C1 and C2 respectively, **c** first Brillouin zone and high symmetry points for 2-dimensional tetragonal lattice Γ = (0, 0, 0)2π/a, X = (0, 1/2, 0)2π/a and M = (1/2, 1/2, 0)2π/a All the figures are reprinted with permission from the Ref. [23]

PG are somewhat different than well-known diamond and graphite/graphene structure. The bond angle ($\theta_{C2–C1–C2}$) in PG is 134.2° which also indicate the distorted sp^3 character of C1 atoms. Since, sp^3 carbon bonds are tetrahedral in nature; penta-graphene is not truly a planner structure [23]. A buckling of 0.6 Å is observed from the side view of PG. Thus, PG is a two dimensional sheet having a thickness of 1.2 Å. The structure of PG can be viewed as a "multidecker sandwich", where the sp^3 hybridized C atoms (C1) are sandwiched between the sp^2 hybridized C atoms (C2). It is interesting to note that the structure of PG is similar to experimentally identified layered silver azide (AgN_3) [5].

2.1 Stability Issues

Whenever a material is proposed theoretically, the first question arise regarding the stability of the material which can also be viewed as the feasibility of practical existence/synthesis of the material. Study of stability includes identifying ground state energy from the calculation of total energy by DFT as well as the behavior of the system in other perturbation like thermal, mechanical etc. Ab initio MD simulation within the framework of DFT is essential in studying the behavior of the system in perturbation.

Energetic Stability Thermodynamic stability of penta-graphene has been examined by means of total energy calculation. PG is identified as metastable in comparison to graphene and other two dimensional carbon allotropes due to its violation of the IPR (isolated pentagon rule) [24]. However, it is more stable than some other nanostructures of carbon, like, 2D α-graphyne, 3D T-carbon and (3, 12)-carbon sheet [5].

Figure 2a shows the area dependence of total energy of penta-graphene along with graphene, graphyne, C_{20}, (3, 12)-carbon sheet, a-graphyne [5]. It can be envisaged that penta-graphene is energetically stable than some experimentally synthesized carbon nanostructures such as, the smallest carbon nanotube and C_{20} (smallest fullerene). This study, therefore, affirmatively, indicates towards possibility of synthesis of the 2D penta-graphene sheet. The structural unit of both of the carbon allotropes, C_{20} and penta-graphene is fused pentagons. Since C_{20} is a highly curved structure, all carbon atoms in it are in strained condition with distorted sp^2 hybridization. On the contrary, in penta-graphene, the curvature is reduced due to the presence of sp^3 hybridized carbon atoms along with sp^2 hybridized carbon atoms and thus the strain is released partially [5].

Dynamic Stability Calculation of lattice vibration gives the phonon dispersion curve which determines whether a crystalline structure is dynamically stable or not. For a dynamically stable crystal structure, there should not have any imaginary frequency in entire Brillouin zone [25]. Phonon band structure and phonon DOS of PG are shown in Fig. 2b. The dynamic stability of penta-graphene is confirmed

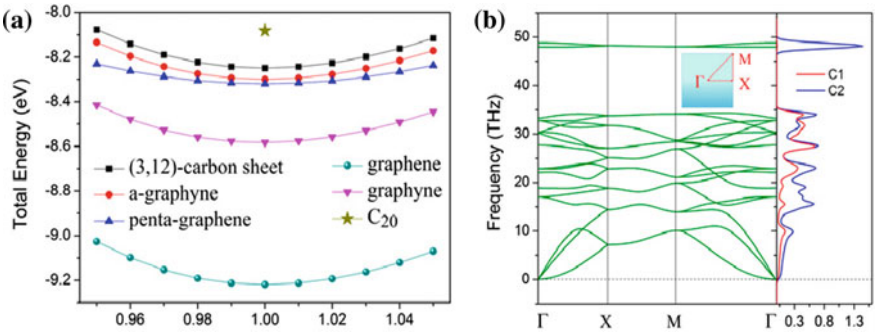

Fig. 2 **a** Area dependence of total energy per atom for some 2D carbon allotropes. The total energy of the experimentally identified dodecahedral C20 cage is also calculated and plotted here for comparison. **b** Phonon band structures and PhDOS of penta-graphene. (Inset) High-symmetric q-point paths: Γ (0, 0) → X (1/2, 0) → M (1/2, 1/2) → Γ (0, 0) All the figures are reprinted with permission from the Ref. [5]

from the absence of imaginary frequencies in entire Brillouin zone i.e. in all high symmetry directions. Like graphene, three distinct acoustic modes are observed in phonon band structure of PG [5].

Thermal Stability To ensure the thermal stability, Zhang et al. performed "Ab initio molecular dynamics" (AIMD) simulation (using canonical ensemble) of 2D supercell of penta-graphene [5]. No structural reconstruction is observed for 6 ps with a time step of 1 fs, at room temperature (300 K). It is revealed, penta-graphene can sustain temperatures as high as 1000 K. PG is found to be dynamically stable even in presence of different types of defects like Stone–Wales-like defect, mono and di-vacancies, edge atoms and adatoms [5].

Mechanical Stability To ensure the feasibility of practical existence of a theoretically proposed material, it is necessary to know the effect of lattice distortion on structural stability. The linear elastic constants of a mechanically stable crystal should follow the "Born–Huang criteria" to guarantee the positive-definiteness of strain energy caused by lattice distortion. Accordingly, the four nonzero 2D elastic constants viz., C_{11}, C_{22}, C_{12} and C_{66} should satisfy the criteria $C_{11}C_{22} - C_{12}^2$ and $C_{66} > 0$ in a mechanically stable 2D sheet [26]. From the calculation of the change of energy due to the in-plane strain (uniaxial and biaxial), PG was found to satisfy the above criteria [5].

2.2 *Properties of Pristine PG*

Confirmation of stability of the material invokes the curiosity regarding the properties of penta-graphene. Researches are in progress in investigating the electronic, thermal, mechanical, magnetic, optical properties of penta-graphene [5, 20, 23, 27–30].

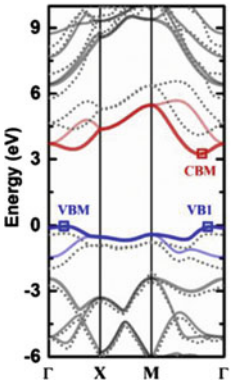

Fig. 3 Calculated HSE06 (solid lines) and GW_0 (dotted lines) band structures of monolayer PG. The figures are reprinted with permission from the Ref. [43]

Electronic Properties From the computation of band structure using—Scuseria–Ernzerhof (HSE06) potential functional, penta-graphene is found to be an indirect band-gap semiconductor with a band gap of ~3.25 eV (computed with HSE06 potential function) [5]. Figure 3 shows the electronic band structure of PG computed with hybrid HSE06 potential function (solid lines) and GW correction (dotted line). It is observed from the electronic band structure that the conduction band minimum lies on the M–Γ path whereas the valance band maximum (VBM) is located on the Γ–X path. However, there exists a sub-VBM on the M–Γ path whose energy value is very close to that of true VBM [5]. Thus, penta-graphene can also be considered as a "quasi-direct–band-gap" semiconductor. Analysis of partial DOS reveals that the major contribution of electronic states near the Fermi level is due to the sp^2 hybridized C2 atoms. In penta-graphene, the p_z orbitals of sp^2-hybridized C2 atoms are spatially separated by the sp^3-hybridized C1 atoms. Thus, full electron delocalization is hindered which gives rise to finite band gap. According to Zhang et al., there is possibility to achieve superconductivity in penta-graphene through hole doping since there are dispersion-less, partially degenerate valance bands which leads a high total DOS near the Fermi level [5, 31].

Mechanical Properties The elastic strain per unit area in a 2D material can be expressed as [5];

$$U = \frac{1}{2}C_{11}\varepsilon_{xx}^2 + \frac{1}{2}C_{22}\varepsilon_{yy}^2 + \frac{1}{2}C_{12}\varepsilon_{xx}^2\varepsilon_{yy}^2 + 2C_{66}\varepsilon_{xy}^2 \quad (1)$$

where the constants, C_{11}, C_{22}, C_{12} and C_{66} are the components of the elastic modulus tensor and can be obtained from second order partial derivative of strain energy as a function of strain. ε_{xx}, ε_{yy} and ε_{xy} are the components of strain tensor. C_{11}, C_{22}, C_{12} and C_{66} can be obtained by fitting the energy curves as a function of with uniaxial ($\varepsilon_{yy} = 0$) and equi-biaxial strains ($\varepsilon_{xx} = \varepsilon_{yy}$).

Young's modulus of a material is defined as $E = \left(C_{11}^2 - C_{12}^2\right)/C_{11}$ [5]. The value of Young modulus in penta-graphene is found to be 263.8 GPa nm whereas

the corresponding value is 345 GPa nm in case of graphene [32]. The value of Young modulus in penta-graphene is comparable to that of h-BN monolayer [33].

Another important parameter which articulates the mechanical property of a material is Poisson's ratio. It is defined as the negative ratio of the transverse strain to the corresponding axial strain. In case of most of the solids, this ratio is positive since under a uniaxial compression, solids expand in the transverse direction. Although the continuum mechanics theory does not discard the possibility of existence of negative Poisson's ratio (NPR) in a stable linear elastic material, it is rarely found in nature. Very few artificial materials are characterized with NPR. Materials with NPR, known as "auxetic materials", are of great scientific and technological interest [34, 35]. The major area of application of "auxetic materials" are in biomedical field as a material for structure/muscle/alignment anchors, surgical implant, prosthetic materials, dilator to open up blood vessels during heart surgery etc. Other application field of "auxetic materials" is piezoelectric sensors and actuators. Auxetic foams and fibers find application in filters and woven structures. Interestingly, penta-graphene exhibit negative Poisson's ratio viz., $\nu 12 = \nu 21 = C12/C11 = -0.068$ since C12 is negative for PG [5].

The NPR characteristics of PG has been testified comprehensively for both of the cases i.e. the lateral response in the x direction when the tensile strain is applied in the y direction and vice versa. Penta-graphene as a nano-auxetic material may have multiple applications in micro-mechanical and micro-electromechanical systems (MEMS).

In addition to in-plane stiffness, ideal strength (i.e. the maximum stress that a material can sustain) is also an important mechanical property of a nanomaterial. Figure 4a shows the stress–strain relationship of penta-graphene under equi-biaxial tensile strain [5]. It is observed from the curve that the strain at maximum stress is 21% (denoted by red arrow) beyond which the mechanical failure starts. However, the critical strain is less than 21% for penta-graphene since phonon instability i.e. phonon softening induced by Kohn anomaly occurs before the stress reaches its maximum [5, 36]. Figure 4b and c represent Phonon bands at the extreme of equi-biaxial strain of penta-graphene and graphene, respectively. It is found that in case of penta-graphene, phonon softening arise when the equi-biaxial strain reaches 17.2% whereas the corresponding value is 14.8% for graphene. Thus, the ideal strength of PG is higher than that of graphene. At the critical strained condition, the single bond lengths between C1 and C2 atoms are found to be ~ 1.77 Å, which is comparable with the experimentally and theoretically reported longest C–C bond length. Beyond critical strength, the structure fracture starts through breaking of the bonds between C1 and C2 atoms.

Thermal Property Thermal conductivity is an important physical parameter which asses heat dissipation ability of a material and high temperature application possibility. Joule heating is a major problem in electronic devices which affect performance, reliability and life time of the device. Moreover, lower heat capacity of nano-electronic devices is a critical issue. Hence, the device material should be thermally highly conductive so that the generated heat during device operation can

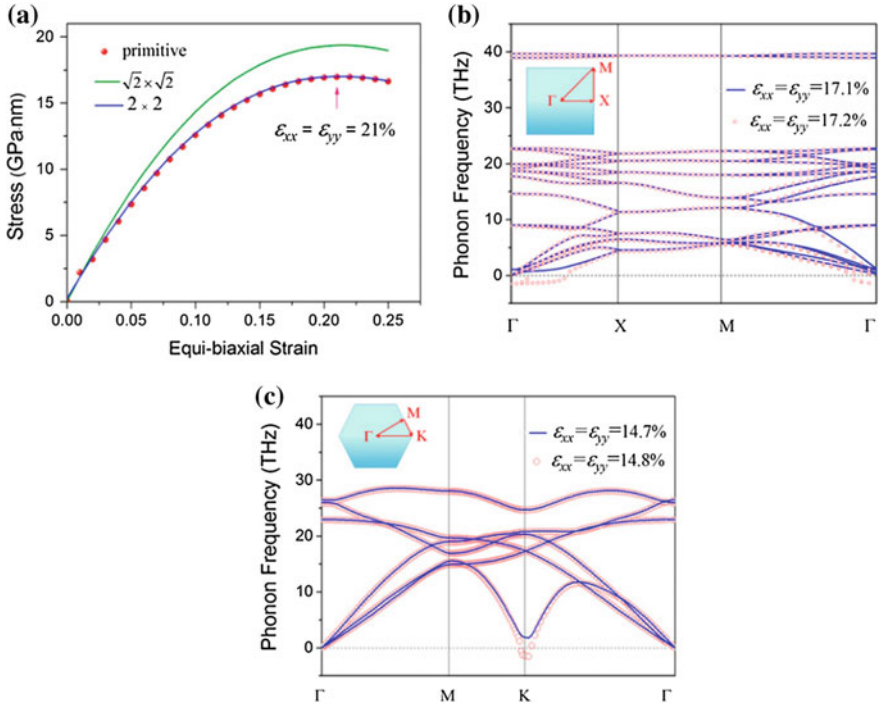

Fig. 4 **a** Stress–strain relationship under equi-biaxial tensile strain. The red arrow denotes the maximum strain. **b** Phonon bands of penta-graphene at the extreme of equi-biaxial strain. **c** Phonon bands of graphene at the extreme of equi-biaxial strain. Blue lines and red circles represent phonons before and after the failure, respectively. (Insets) The high-symmetry q-point paths in the reciprocal space All the figures are reprinted with permission from the Ref. [5]

dissipate fast. On the other hand, thermoelectric devices demands lower thermal conductivity. Although graphene is characterized with ultrahigh lattice thermal conductivity (3000–5800 W/mK), the absence of bandgap limits its application in most of the electronic devices including transistor. From the solution of linearized phonon "Boltzman transport equation" (BTE) with first principle calculation, lattice thermal conductivity of PG is found to be 645 W/mK at room temperature which is significantly lower in comparison to that of graphene. The presence of more scattering channels in buckled penta-graphene structure may be the possible reason behind significantly lower thermal conductivity of PG in comparison to that of graphene [27]. It is found that lattice thermal conductivity of stacked PG does not depend on the number of layers present. This characteristic of PG is also in sharp contrast to that of graphene. In metals, the thermal conductivity is mainly due to electrons while in semiconductors and insulators, phonons play a significant role in determining the resultant thermal conductivity.

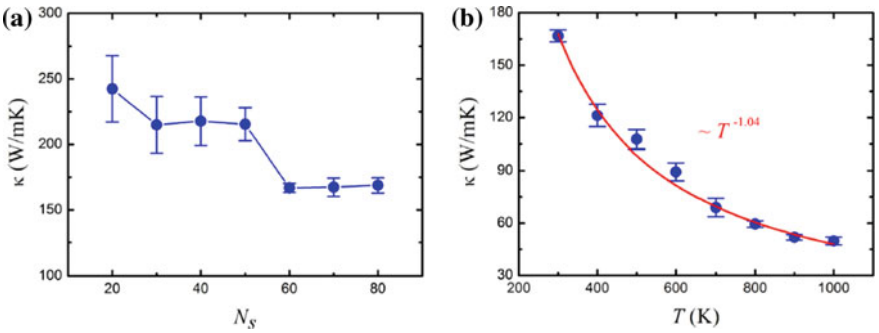

Fig. 5 **a** Thermal conductivity of penta-graphene at 300 K predicted by the Green-Kubo formula with respect to the size of simulating sample (Ns × Ns unit cells). **b** Thermal conductivity of penta-graphene as a function of temperature. The values are from simulations performed on the simulating sample of 60 × 60 unit cells. The red curve denotes the best-fitting All the figures are reprinted with permission from the Ref. [28]

From "classical equilibrium molecular dynamics simulations" using the original "Tersoff interatomic potential", the intrinsic thermal conductivity of PG is found to be 167 W/mK [28]. In PG, the acoustic phonon lifetimes are 20 ps and 1–10 ps for lower (1–5 THz) and higher (5–15 THz) frequency range, respectively which are comparable to that of the graphene. However, the remarkably lower thermal conductivity of PG, in comparison to graphene, arises from the lower phonon group velocities and fewer collective phonon excitations in PG.

In penta-graphene, the phonon scattering rate is proportional to temperature and consequently, the thermal conductivity is inversely proportional to the temperature [28]. The variation of thermal conductivity of PG as a function of size of the simulating sample for constant temperature (300 K) is shown in Fig. 5a. Figure 5b shows the variation of thermal conductivity of PG as a function of temperature for a fixed size of the simulating sample (60 × 60 unit cell). From non-equilibrium molecular dynamics (NEMD) simulations using ReaxFF force field, thermal conductivity of infinitely long penta-graphene is found to be 112.35 W/mK [37]. The cause behind the difference in results is due to the method of simulation and the type of interatomic force field employed. Researchers are still in search of appropriate potential for penta-graphene [3].

Optical Property Although Kohn-Sham DFT estimate ground state energy most successfully, it cannot assess optical absorption accurately since "Kohn-Sham DFT eigenvalues" do not consider the electron addition and removal energies. It is necessary to include the calculation of electron-hole interaction to get information regarding the optical spectra. GW (G_0W_0) approximation/correction is a "many-body perturbation theory" which can successfully predict the optical properties of the materials. In this method, ground state energy and electronic density are computed by DFT Kohn-Sham framework and then, G_0W_0 i.e. the green function G and dynamically screened interaction W is computed from the obtained Kohn-Sham

electronic structure. Applying G_0W_0 correction, the "quasi-direct band gap" of PG is found to lie in the range of 4.1–4.5 eV which corresponds to ultra-violet region (wavelength for optical absorption). Since visible light is not absorbed in PG, it is transparent in nature and photoelectron can't be produced easily in PG [23].

3 Hydrogen Functionalization of Penta-Graphene

Hydrogen functionalization is the most widely studied functionalization method for penta-graphene. It is found that hydrogen functionalization not only stabilize the structure of penta-graphene but also tune its property flexibly.

Among sp^3 (i.e. C1 atom) and sp^2 (i.e. C2 atom) hybridized carbon atoms in penta-graphene, only sp^2 hybridized carbon atoms are capable of adsorbing hydrogen. Figure 6 depicts the top and side views of the optimized structures of the fully hydrogenated penta-graphene. In fully hydrogenated penta-graphene, the ratio of C:H is 3:2, whereas this ratio is 1:1 in case of fully hydrogenated graphene. Li et al. [38] studied hydrogen functionalization of penta-graphene with the help of DFT based AIMD simulations using PAW method. Most of the calculations were performed using GGA-PBE exchange correlation (XC) potential functional whereas the hybrid HSE06 was considered for high precision electronic structure calculations. It is found that crystallographic symmetry of penta-graphene does not change even with full hydrogenation.

In fully hydrogenated PG, both of the bond lenghts (C1–C2 and C2–C2) are 1.55Å which resembles the single bond character. The bond angles $\theta_{C2-C1-C2}$ and $\theta_{C1-C2-C1}$ are 116.9° and 105.9°, respectively, indicating the distorted sp^3 hybridization of the carbon atoms [38]. Change of bond length of C2–C2 from 1.34 to 1.55 Å, indicates that the C2–C2 bond transforms from double bond to single

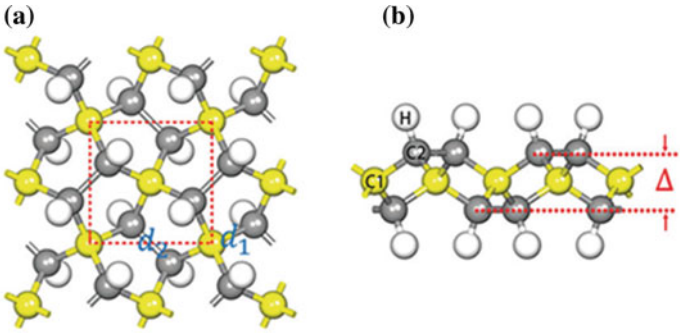

Fig. 6 **a** Top view of optimized fully hydrogenated penta-graphene. Unit cell is identified by square marked by red dashed lines and **b** side views of the optimized fully hydrogenated penta-graphene. Δ represent thickness of PG. Yellow, gray and white spheres represent C1, C2 and Hydrogen, atoms respectively All the figures are reprinted with permission from the Ref. [38]

bond due to hydrogenation. After hydrogenation of penta-graphene, the thickness buckling increases. Vertical distance between topmost and bottommost carbon atom in fully hydrogenated penta-graphene is 1.62 Å whereas the value is 1.20 Å for pristine penta-graphene.

3.1 Stability Issues

The binding energy of each hydrogen atom in penta-graphene is defined as [38];

$$E_b = -(E_{total} - E_{PG} - 4E_{adatom})/4 \tag{2}$$

where, E_{total}, E_{PG}, *and* E_{adatom} are total energy of the ground state configuration of the unit cell of fully hydrogenated penta-graphene, pristine penta-graphene, and isolated hydrogen atom, respectively. There are four adsorbed hydrogen atoms per unit cell. The calculated binding energy is 3.65 eV whereas the corresponding value is 2.47 eV for graphene. Thus, adsorption of hydrogen in penta-graphene is energetically favorable over that of graphene. In fully hydrogenated PG, all sp^2 hybridized carbon atoms are transformed into sp^3 hybridized atoms. C2–C2 bonds get elongated and bonding characteristic changes from double bond to single bond. The strain stored in pristine PG is released partially due to such hydrogenation leading towards more stability of functionalized PG than its pristine counterpart.

Figure 7 shows the variations of total potential energy of fully hydrogenated penta-graphene during the AIMD simulations for 300 K and 1000 K. It is found that the structures remain integrated and the average value of the total potential energies remains nearly constant throughout the simulation time for both the temperature 300 and 1000 K [38]. Thus, it can be inferred that hydrogenated PG sheets are not only thermally stable at room temperature, but it can also sustain at a temperatures as high as 1000 K.

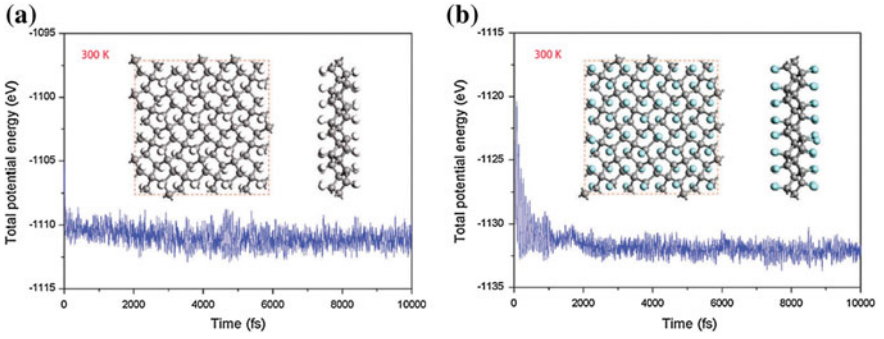

Fig. 7 The variations of total potential energy of full hydrogenated PG during the AIMD simulations at **a** 300 K and **b** 1000 K. The insets are snapshots of the top and side view of the structures at the end of simulations All the figures are reprinted with permission from the Ref. [38]

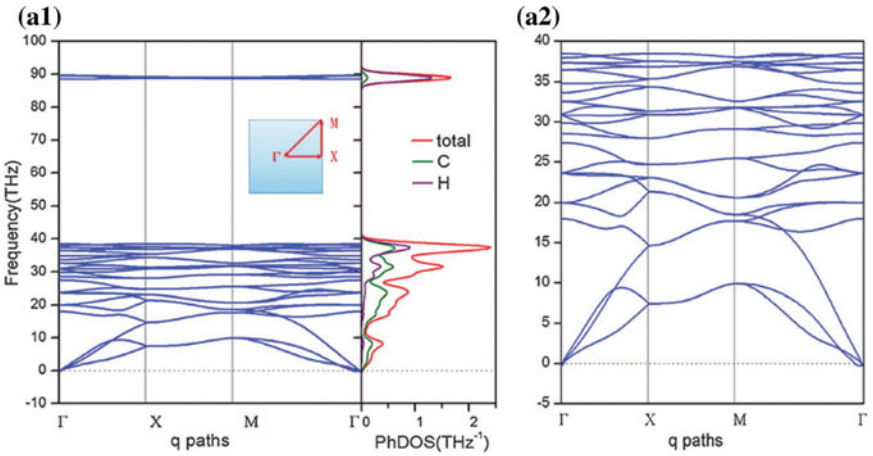

Fig. 8 **a1** Phonon band structures and corresponding atom-resolved PhDOS of fully hydrogenated PG. The inset represents the high-symmetric q-point paths: Γ (0, 0)–X (1/2, 0)–M (1/2, 1/2)–G (0, 0). **a2** Phonon band structures of fully hydrogenated PG in the low frequency region All the figures are reprinted with permission from the Ref. [38]

Figure 8 represents phonon band structure of fully hydrogenated PG along the high symmetric paths (Γ–X–M–Γ) in the first Brillouin zone. The dynamic stability of the hydrogenated penta-graphene is confirmed by the absence of imaginary frequencies in the entire Brillouin zone. Like penta- graphene, there exist three distinct acoustic modes and the two-fold degeneracy on the X–M path in hydrogenated penta-graphene also [38]. A large phonon gap is observed in phonon band structure of penta-graphene. From the vibrational activity at the Γ point in the Brillouin zone, Raman and Infrared (IR) spectra of hydrogenated penta-graphene can be studied. In hydrogenated penta-graphene, Raman-activity was found at 2945.89, 2911.14, 1267.57, 1179.84, 1115.23, 990.23 and 780.64 cm^{-1} and IR-activity was found at 2943.53 and 2911.14 cm^{-1}, respectively.

3.2 Properties of Hydrogenated Penta-Graphene

Electronic Property Like penta-graphene, fully hydrogenated PG is also characterized with indirect band gap since its conduction band minimum (CBM) and valence band maximum (VBM) are located at different k points in the momentum space. Figure 9a shows the electronic band structure and atom-decomposed partial DOS of fully hydrogenated penta-graphene computed with PBE and HSE06 functional. The computed band gap of fully hydrogenated penta-graphene with PBE and hybrid HSE06 functional are 4.29 and 5.35 eV, respectively. It is well known that calculation with PBE functional underestimate the bandgap of a material.

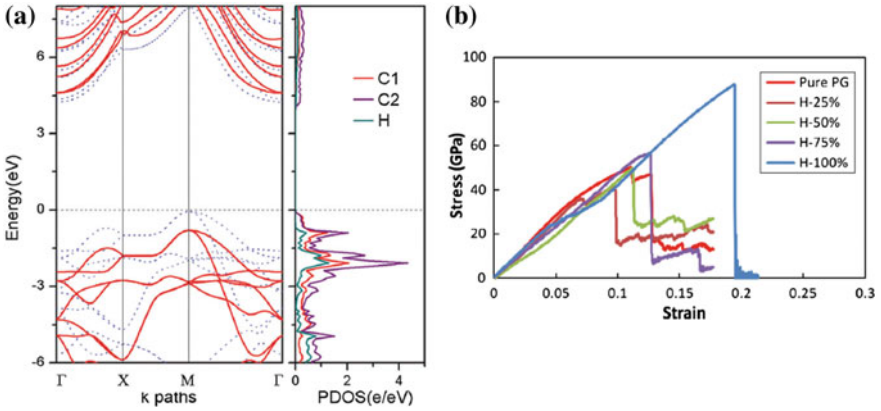

Fig. 9 **a** Electronic band structure and atom-decomposed partial DOS of fully hydrogenated PG. Blue dashed lines and red solid lines correspond to the PBE and HSE06 results, respectively. [38] **b** Stress–strain curves of pristine and hydrogenated PG at different hydrogen coverage [39] All the figures are reprinted with permission from the Ref. [38, 39]

Hydrogen functionalization changes penta-graphene from a semiconductor to an insulator [38]. Due to hydrogenation, the CBM/VBM of penta-graphene shifts from the M–Γ/Γ–X path to the M–Γ path. From the analysis of partial DOS of fully hydrogenated penta graphene, it is found that the electronic states near the Fermi level are mainly contributed from C1 and C2 atoms.

Mechanical Property Molecular Dynamics simulation confirms that hydrogenation significantly enhance the mechanical strength of penta-graphene [39]. Figure 9b shows stress–strain curves of pristine and hydrogenated PG with four different hydrogenation coverage of 25, 50, 75, and 100% at 300 K [39]. Stress increases linearly with the increase of tensile strain and attain a maximum after which stress drops sharply indicating a material degradation. The strain for which the stress is the maximum is identified as the failure strain and the corresponding strain is the failure stress. The simulated failure stress and failure strain value for pristine penta-graphene are 50.2 GPa and 0.127, respectively which are significantly lower than that of graphene (130 GPa and 0.25, found experimentally and 125.2 GPa and 0.191, found by MD simulations) [39]. It is revealed from Fig. 9 that fully hydrogenated PG is characterized with the highest value of failure stress and strain. This phenomenon is strikingly in contrast with graphene where hydrogenation (up to 30%) significantly reduces the value of failure stress and failure strain. For a hydrogenation range of 30–100%, mechanical properties of graphene are almost insensitive to functionalization [40].

The failure stress and failure strain of pristine and hydrogenated PGs are represented in the form of a bar diagram summarized in Fig. 10a and b, respectively. When PG is hydrogenated to 25%, the failure stress and failure strain decrease by 16.9 and 22.8%, respectively than that of pristine PG. With further increase of

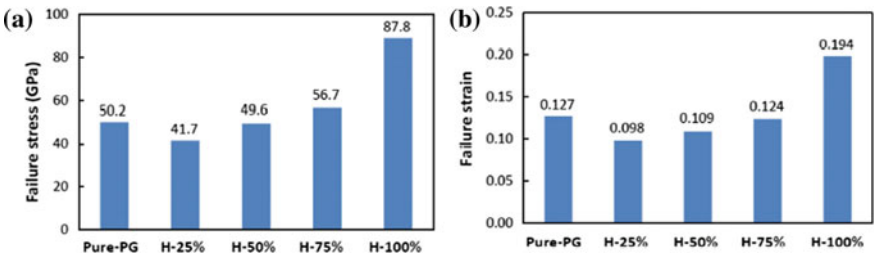

Fig. 10 **a** Failure stress and **b** failure strain of pristine and hydrogenated PGs with different hydrogenation functionalities All the figures are reprinted with permission from the Ref. [39]

hydrogenation, failure stress failure and strain increase monotonically. For 100% hydrogenated PG, failure stress and failure strain increase by 74.9 and 52.8% with respect to that of pristine PG.

Structural transformation from pentagon to polygon (6-, 7-, 8-, or more atom rings) is the cause behind the failure of pristine as well as partially hydrogenated PGs beyond failure strain [39]. For 100% hydrogenated PG, the failure mechanism is entirely different. Any structural transition induced failure is not observed in fully hydrogenated PG. In the 100% hydrogenated PG, all the sp^2-hybridized carbon atoms transforms to sp^3-hybridized. Thus, fully hydrogenated PG is more stable structure and is characterized with higher value of failure stress and failure strain (87.8 GPa and 0.194). In fully hydrogenated PG, the failure mechanism is initiated (for a strain 0.1944) with C–C bond breaking and a visible crack is formed in the structure [39]. With further increase of strain, the crack rapidly spreads in the direction perpendicular to the loading direction and causes fully hydrogenated PG to rupture finally [39].

These improvements in the mechanical properties of hydrogenated PG remain almost unaltered for the temperature range of 200–600 K. Figures 5a and b represent the failure stress and failure strain as a function of temperature for pristine and fully hydrogenated PG. It can be observed that with the increase in temperature from 200 to 600 K, the value of failure stress and failure strain decrease slightly for pristine as well as fully hydrogenated PGs (Fig. 11).

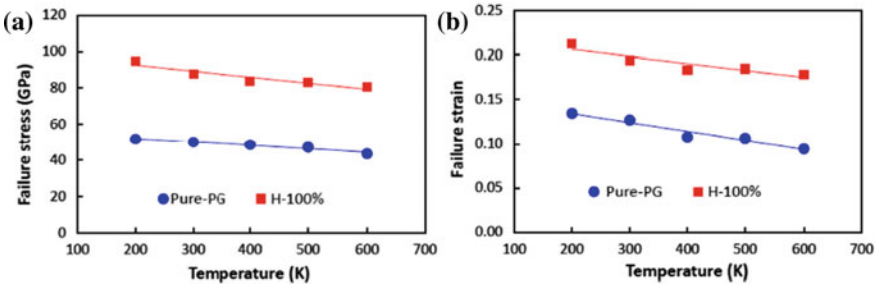

Fig. 11 Effect of temperature on **a** the failure stress and **b** the failure strain of pristine PG and fully hydrogenated PG All the figures are reprinted with permission from the Ref. [39]

Decrease of failure stress and failure strain with temperature can be caused by the stronger thermal vibration of atoms at higher temperature which renders the atomic bonds more likely to reach the critical bond length and subsequently to break. In spite of the degradation of the mechanical properties with increasing temperature, the failure stress and failure strain of fully hydrogenated PG are still much higher (about 71–88% higher) than that of pristine PG [39].

In Edge Hydroxyl, OP: The "in-plane Young's modulus" reduces to 205.50 GPa from 263.8 GPa upon full hydrogenation of PG [38]. In contrast to the pristine penta-graphene (−0.068), Poisson's ratio of fully hydrogenated PG is found to be positive (0.243) [38].

Thermal Property From first-principles lattice dynamics and iterative solution of the phonon "Boltzmann transport equation" (BTE), it is found that thermal conductivity of fully hydrogenated PG is increased by 76% compared to its pristine counterpart. This is in contrast to hydrogenated graphene which shows a dramatic decrease in thermal conductivity in comparison to pristine graphene. Figure 12a shows Variation of thermal conductivity as a function of sample length of penta-graphene and fully hydrogenated penta-graphene [41].

Another study based on non-equilibrium molecular dynamics simulations using 'ReaxFF force field' on hydrogenated penta-graphene at different levels of coverage shows that initially with increasing coverage (up to 25% hydrogen), thermal conductivity decreases (nearly 57%), but with further increase in the coverage, thermal conductivity increases [37]. Interestingly, the fully functionalized (100%) PG shows nearly the same thermal conductivity as that of the pristine one. The result is depicted in Fig. 20a. The difference in results may arise from the considered size of the sample for simulation since the results of MD simulations is sensitive to the model size due to the boundary scattering [42]. For reduced sample length, the associated phonon-boundary scattering is more which may reduce the simulated

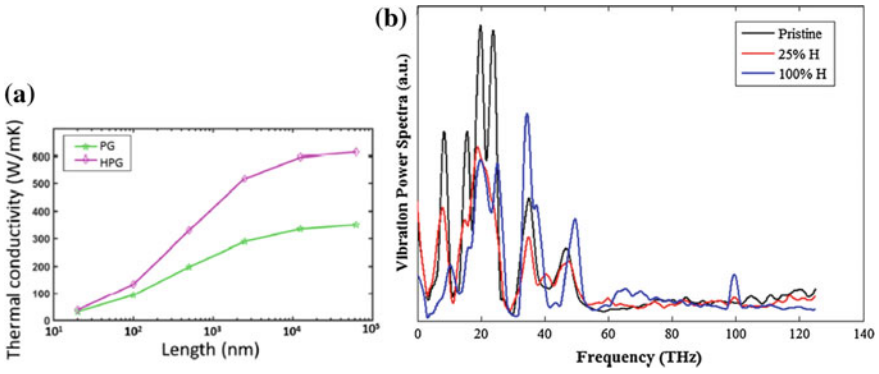

Fig. 12 **a** Variation of thermal conductivity as a function of length for penta-graphene and fully hydrogenated penta-graphene. **b** VPS of carbon atoms in pristine and hydrogenated PG All the figures are reprinted with permission from the Ref. [37, 41]

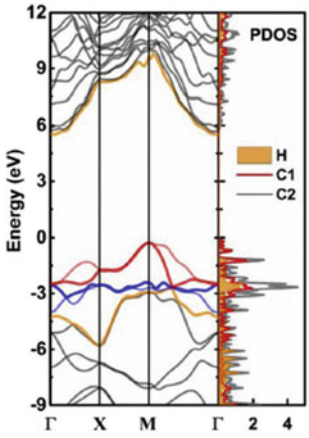

Fig. 13 Electronic band structure and partial densities of states of fully hydrogenated PG computed with GW approximation The figures are reprinted with permission from the Ref. [43]

value of thermal conductivity of hydrogenated PG. However, researches are in progress to optimize the simulation environment to obtain more realistic results.

Figure 12b shows the vibration power spectra (VPS) of carbon atoms in pristine and hydrogenated (25 and 100%) PG. In pristine graphene, peaks appear in VPS at low frequency domain. In case of 25% hydrogenated penta-graphene, peaks are significantly suppressed. Change in VPS leads to a local acoustic mismatch which leads to phonon scattering [37]. Consequently, thermal conductivity decreases. Although peaks are suppressed at low frequency in 100% hydrogenated graphene, there exist peaks at high frequencies (50 and 100 THz). Thus, higher thermal conductivity in 100% hydrogenated graphene is attributed to high frequency vibration [37].

Optical Property Like pristine PG, fully hydrogenated PG is also characterized by indirect band gap with CBM and VBM at M and Γ point respectively [43]. The computed band gap of with GW approximation is ∼5.78 eV. New bands are found at conduction band edge of fully hydrogenated PG which eventually leads to possible optical absorption (Fig. 13).

Magnetic Property From spin polarized DFT calculations, it is found that hydrogen adsorption induce magnetic moment in PG [44]. The magnetic moment of PG increases 137 times upon hydrogenation. This result indicates the potential application of PG in magnetic storage and next generation spintronic devices.

4 Fluorine Functionalization of Penta-Graphene

Like hydrogen functionalization, fluorine functionalization was also found to be very effective in tuning different physio-chemical and electronic properties of penta-graphene.

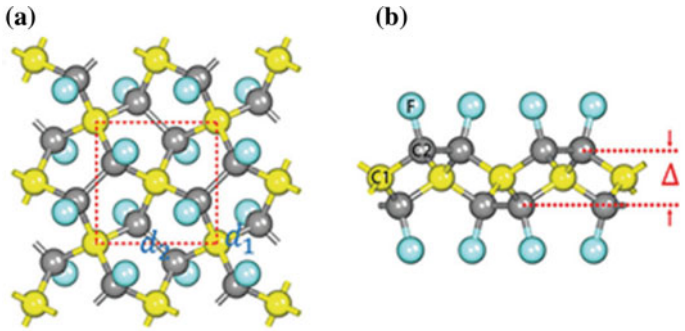

Fig. 14 **a** Top and **b** side views of the optimized structures of fluorinated penta-graphene. The square marked by red dashed lines denotes the unit cell. The yellow, gray and cyan spheres represent the C1, C2 and fluorine C atoms All the figures are reprinted with permission from the Ref. [38]

Figure 14 depicts the top and side views of the optimized structures of fluorinated penta-graphene. The structure of fluorinated penta-graphene is similar to that of hydrogenated PG, where C2-C2 bond changes from double bond to single bond and thus stabilizes the structure by releasing strain. In fluorinated penta-graphene, the bond lengths of C1–C2 and C2–C2 are 1.57Å and 1.58Å, respectively. Like hydrogen, fluorine also gets adsorb on sp^2 hybridized carbon atom. The bond angles $\theta_{C2-C1-C2}$ and $\theta_{C1-C2-C1}$ are 117.8° and 106.7°, respectively. The vertical distance between the topmost and the bottommost carbon atom in fully fluorinated PG is 1.6 Å [38].

4.1 Stability Issues

The binding energy of fluorine in fluorinated graphene is 4.22 eV which is higher than hydrogen functionalized PG [38].

Figure 15 shows the variations of total potential energy of 100% fluorinated penta-graphene during the AIMD simulations for 300 K and 1000 K, respectively. The insets are the top and the side view of the structure at the end of the simulation. The fully fluorinated PG sheet remains integrated and the average value of total potential energy remains almost constant during the MD simulations for both of the temperatures (300 and 1000 K). Thus, like 100% hydrogenated PG, fully fluorinated PG is also a stable structure and can withstand a temperature as high as 1000 K.

Figure 16a shows the phonon band structures and corresponding atom-resolved PhDOS of fully fluorinated penta-graphene [38]. Absence of imaginary frequency in the entire Brillouin zone confirms the dynamical stability of fluorinated penta-graphene. The phonon gap in fluorinated PG is less in magnitude than that of

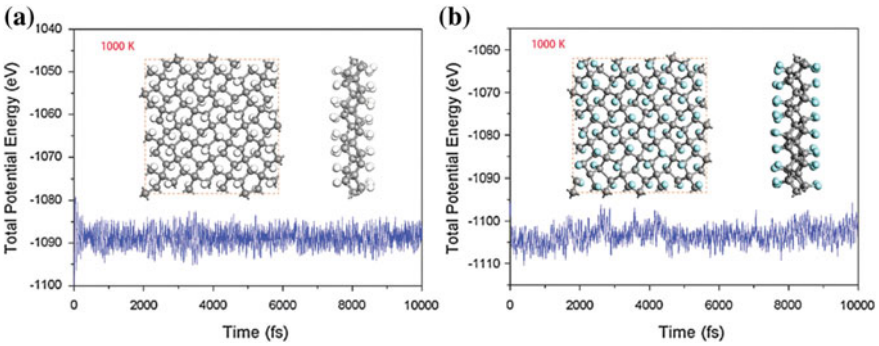

Fig. 15 The fluctuations of total potential energy of fully fluorinated penta-graphene during the AIMD simulations at **a** 300 K and **b** 1000 K. The insets are snapshots of the structures at the end of simulations All the figures are reprinted with permission from the Ref. [38]

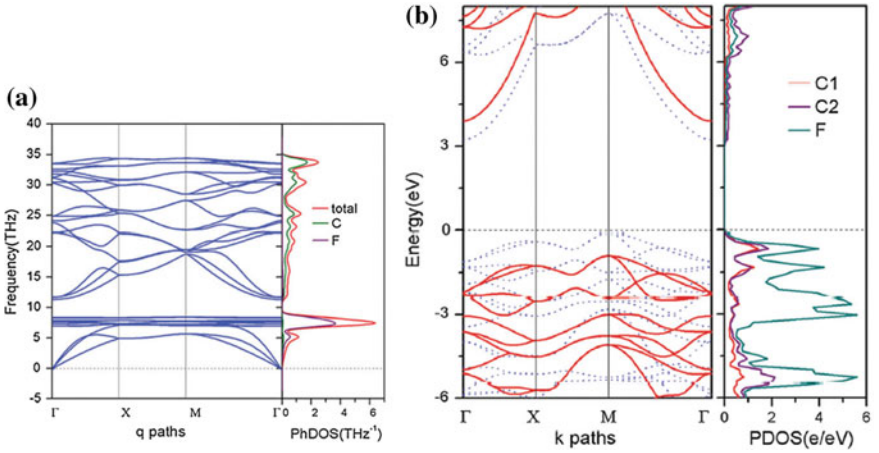

Fig. 16 **a** Phonon band structures and corresponding atom-resolved PhDOS of fully fluorinated penta-graphene. **b** Electronic band structure and atom-decomposed partial DOS of fluorinated penta-graphene. Blue dashed lines and red solid lines correspond to the PBE and HSE06 results, respectively All the figures are reprinted with permission from the Ref. [38]

hydrogenated PG. It is observed that high frequency (> 40THz) phonon modes are absent in fluorinated PG which is in contrast to the hydrogenated PG. The frequencies of pronounced Raman active modes of fluorinated PG are 1219.33, 1077.20, 1012.18 and 491.26 cm^{-1} while the IR-active modes are 1261.45, 1130.71 and 545.58 cm^{-1}.

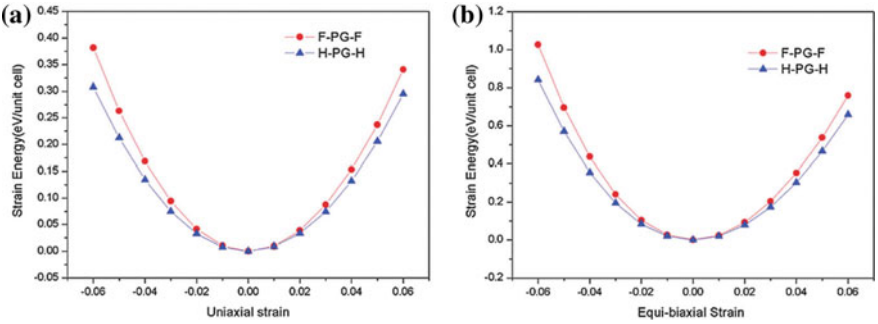

Fig. 17 Strain–energy relationship of the hydrogenated and fluorinated penta-graphene sheets under **a** uniaxial strain and **b** equi-biaxial strain All the figures are reprinted with permission from the Ref. [38]

4.2 Properties of Fluorinated Penta-Graphene

Electronic Property

Figure 16b represents the electronic band structure and atom-decomposed partial DOS of fluorinated penta-graphene [38]. Fluorinated PG is also characterized with indirect band gap. The computed band gap of fully fluorinated penta-graphene with PBE and hybrid HSE06 functional are 3.36 and 4.78 eV, respectively. From the analysis of partial DOS, it is found that, the states near Fermi level is more contributed by fluorine than C1 or C2.

Mechanical Property

Young's modulus of fluorinated PG is found to be 239.12 GPa which is lower than that of pristine PG but higher than that of hydrogenated PG. Poisson's ration of fluorinated PG is positive (0.236) [38]. Figure 17 represents strain–energy relationship of the fluorinated and hydrogenated penta-graphene sheets under uniaxial strain and equi-biaxial strain.

5 Oxygen Functionalization

Two type of oxygen functionalization is studied in penta-graphene viz. functionalization with epoxy group (–O–) and with hydroxyl group (–OH). Figure 18a and 18b represent top and side view of atomistic configurations of PG fully functionalized with epoxy (–O–) group and hydroxyl group (–OH), respectively. Hydroxyl group creates bond with single sp^2 hybridized C2 atom(s) whereas epoxy group creates bond with two C2 atom(s).

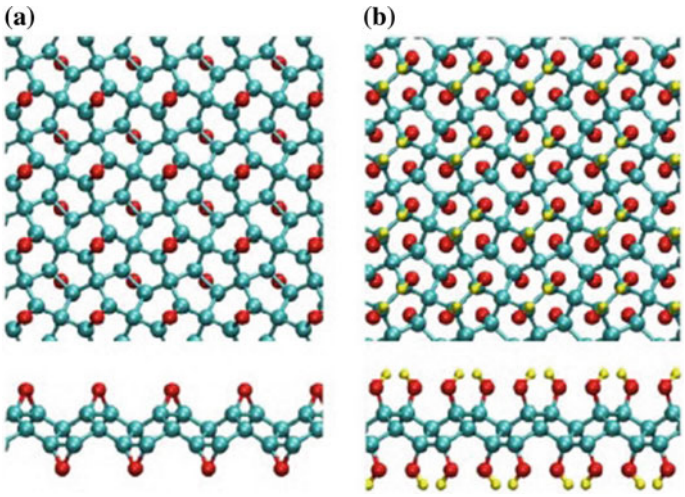

Fig. 18 Top and side view of atomistic configurations of PG fully functionalized with **a** epoxide group and **b** hydroxyl group. Cyan, red and yellow balls are carbon, oxygen and hydrogen atoms respectively All the figures are reprinted with permission from the Ref. [39]

5.1 Properties of Oxygenated Penta-Graphene

Mechanical property

Figure 19a depicts the stress-strain curves of fully functionalized PG with epoxy (–O–) and hydroxyl (–OH) groups along with that of pristine and fully hydrogenated PG for comparison. In terms of failure stress and failure strain, all functionalized PG structures outperform the pristine PG [39]. Among the three different functional groups, the fully functionalized PG with hydroxyl groups possesses the highest failure stress and failure strain (86.6 and 82.4%), followed by the PG having hydrogen (74.9 and 52.8%) and epoxy groups (49.3 and 45.2%) [39].

The lower failure stress and failure strain value of functionalized PG with epoxy group may be caused by the bonding characteristics of epoxy group with PG. Epoxy group is bonded with two carbon atoms in PG. As a result, the local sp^3 bonds of PG are distorted and stress is generated. It can be observed from Fig. 18a that there exists a non-zero initial stress in the stress-strain curve of epoxide-functionalized PG. It is also notable that beyond the failure stress, in epoxide-functionalized (100%) and hydroxyl-functionalized PG, the failure mechanism starts with bond breaking as in case of 100% hydrogenated PG.

Thermal property

Computation of thermal conductivity of oxygen functionalized PG for different percentage of coverage (of oxygen) in PG shows that, initially thermal conductivity decreases with increasing percentage of coverage (up to 25%). Beyond 25%, thermal conductivity increases with increasing percentage of coverage. Figure 20a

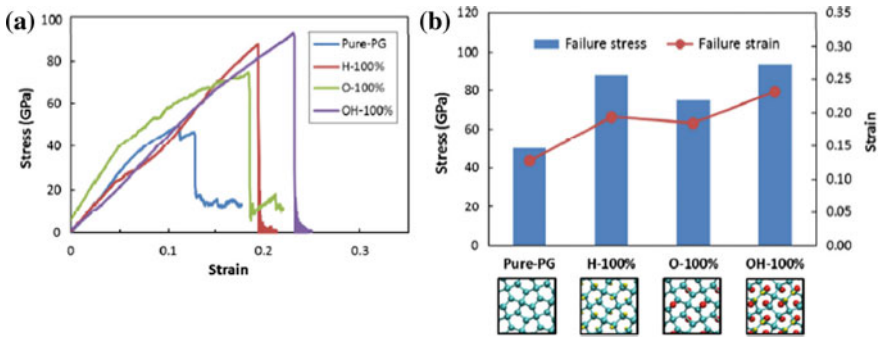

Fig. 19 **a** Stress-strain curves of pristine and fully functionalized PGs with different functional groups. **b** Failure stress and failure strain of pristine and fully functionalized PGs with different functional groups All the figures are reprinted with permission from the Ref. [39]

shows the normalized thermal conductivity of functionalized PG for different coverage of hydrogen and oxygen atoms [37]. It is observed that the trends of variation of thermal conductivity with percentage of coverage are similar for oxygen and hydrogen functionalization of PG. Thus, fully oxygenated PG is also characterized with nearly equal thermal conductivity of pristine PG [37].

Figure 20b shows the vibration power spectra (VPS) of carbon atoms in pristine and oxygenated (25 and 100%) PG. In 25% oxygenated PG, VPS peaks are also significantly suppressed as in case of hydrogenated PG. In case of 100% oxygenated PG, although peaks are suppressed in the lower frequencies (where pristine PG shows pronounced peaks), the same at higher frequencies is observed to be dominant [37].

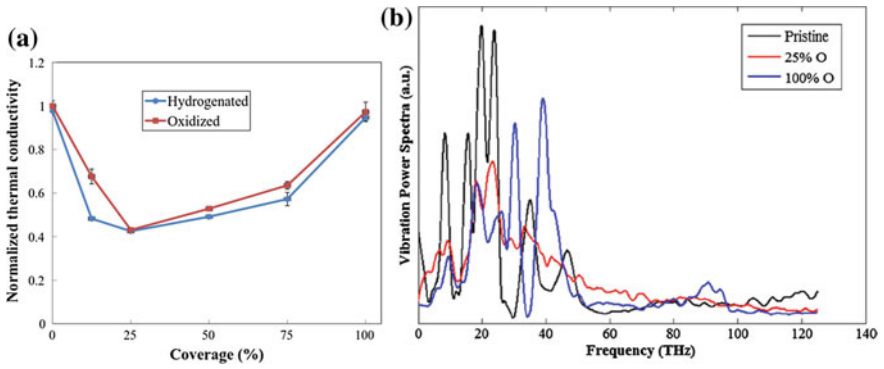

Fig. 20 **a** Normalized thermal conductivity of functionalized PG at different coverage of hydrogen and oxygen atoms. **b** VPS of carbon atoms in pristine and oxidized PG All the figures are reprinted with permission from the Ref. [37]

6 Challenges in Implementation and Future Direction of Research

A set of criteria has been put forward by Ewels et al. [45] whether or not the theoretically proposed penta-graphene can experimentally be synthesized. The experimental feasibility of synthesis of a theoretically proposed material not only demands that the energy of the structure should be at a minima on the local potential energy surface but also its energy should be isolated by high potential barrier from its related isomers [45]. Accordingly, after synthesis also, PG may rapidly restructure itself towards graphene in the presence of even a trace amount of specific catalytic impurities. Some of the researchers considered the growth of large-area aligned pentagonal graphene domains on Cu foils by chemical vapor deposition as the first step towards the experimental fabrication of PG [37, 46]. However, there exists lots of confusion/controversy regarding the effectiveness of this approach. However, theoretical simulation shows suitable chemical functionalization stabilizes penta-graphene. In most of the functionalizations i.e. hydrogen, fluorine and hydroxyl, sp^2 bonded carbon atoms of penta-graphene transforms to sp^3 bonded ones. Thus, these functionalizations stabilize the penta-graphene structure by partially releasing strain. The binding energy of hydrogen and fluorine in PG are also found to be higher than that of graphene. It suggests possible synthesis of penta-graphene considering its functionalized state as a precursor just like the case of experimentally synthesized dodecahedral C_{20} fullerene where hydrogenated or brominated C20 is considered as the precursor [38].

Guo et al. studied the characteristics of the vdW heterojunction composed of penta-graphene and graphene to explore the future device applications of PG [47]. For potential device application Hydrogen adsorption capability of PG steers the application of PG as a substrate for hydrogen spillover or hydrogen storage [48] where Pt_4, Pd_4 Ni_4, and Ti_4 can play the role of a catalyst. The oxygen adsorption capability of PG indicate the application of it as a potential, metal-free, and low-cost catalyst for low-temperature CO oxidation where CO transforms to CO_2 by the pre-adsorbed O_2 on the PG sheet [49]. This property can further be extended to gas sensor device development as the basic principle of operation is in line with the conventional chemi-resistive gas sensors [50–52]. Hydrogenation and fluorination transforms penta-graphene from semiconductor to insulator. High band gap of hydrogenated and fluorinated penta-graphene can find their possible application as dielectric layers in field effect transistors (FETs), relinquishing the requirement of conventional silicon oxides [38]. Hydrogen adsorbed magnetic penta-graphene (M–PG) and weakly magnetic penta-graphene (WM–PG) are predicted to be the most stable state among other hydrogen adsorbed PG. On hydrogen adsorption, the magnetic moment of the PG increases by 137 times which can be utilized in magnetic storage technology [44].

Band gap tailoring as well as appearance of new bands due to hydrogen passivation paves the path for future application of PG in the field of optoelectronic and photovoltaic devices also [43]. It is observed that CBM and VBM of PG shift along

momentum axis upon chemical functionalization. If indirect band gap PG can be transformed to direct band gap semiconductor by band tailoring through suitable chemical functionalization, then it would open new opportunities in the field of optoelectronic devices.

7 Conclusion

Penta-graphene is a two dimensional carbon allotrope which has been proposed theoretically very recently. Although, its practical synthesis/implementation is yet a crucial challenge, some of its unique electrical, thermal, mechanical, magnetic and optical properties highlighting promising application in nano-electronic devices have motivated researchers to study the material thoroughly. Zero bandgap characteristic of graphene limits its application in various cases whereas PG is a quasi-direct band gap semiconductor with a bandgap of $\sim$3.25 eV. It can withstand a temperature as high as 1000 K. Thermal conductivity of PG is significantly lower in comparison to graphene which enhances the possibility of using PG in thermoelectric devices. Mechanical strength of PG also outperforms graphene. There would have enormous application of PG in biomedical and sensor field as nano auxetic materials (having negative Poisson's ratio). However, in spite of such a wide spectra of interesting properties, practical realization of pristine PG is a crucial challenge. Judicious chemical functionalization could be possible solutions for achieving stable PG structure. Functionalized PG (hydrogenated and fluoridated) is shown to be (theoretically) more stable than its pristine counterpart suggesting the possibility of synthesis of PG functionalized state as a precursor. Interestingly, PG was proposed to be synthesized by hydrogen intercalation from T12-carbon in the pioneer work on PG. Moreover, electronic, mechanical, thermal, optical and magnetic property of PG can be significantly tailored by judicious chemical functionalization. Mechanical strength of PG was found to improve significantly upon chemical functionalization especially for hydrogen and hydroxyl groups. Thermal conductivity of PG dramatically increases upon hydrogenation which is in contrast to the graphene, where hydrogenation reduces thermal conductivity. Possibility of tuning thermal conductivity by varying the percentage of coverage of functional groups widens the application of PG in thermoelectric devices. Band gap tailoring of PG is also possible by suitable chemical functionalization which is of huge interest for nano-electronic devices. Magnetization can also be induced in PG by hydrogen functionalization which finds application in next generation spintronic devices. Mainly the effects of three types of functionalizations (hydrogen, fluorine and oxygen) of PG have been studied so far. There are many others in the queue (which are found to be effective in other 2D materials) to be studied. However, successful synthesis of PG, with desired stability and predicted properties, is still a crucial challenge.

References

1. Zhang, X., Wei, L., Tan, J., Zhao, M.: Prediction of an ultrasoft graphene allotrope with Dirac cones. Carbon **105**, 323–329 (2016). https://doi.org/10.1016/j.carbon.2016.04.058
2. Novoselov, K.S., Geim, A.K., Morozov, S.V., Jiang, D., Zhang, Y., Dubonos, S.V., Grigorieva, I.V., Firsov, A.A.: Electric field effect in atomically thin carbon films. Science **306**, 666–669 (2004). https://doi.org/10.1126/science.1102896
3. Winczewski, S., Shaheen, M.Y., Rybicki, J.: Interatomic potential suitable for the modeling of penta-graphene: molecular statics/molecular dynamics studies. Carbon **126**, 165–175 (2018). https://doi.org/10.1016/j.carbon.2017.10.002
4. Su, C., Jiang, H., Feng, J.: Two-dimensional carbon allotrope with strong electronic anisotropy. Phys. Rev. B **87**, 075453 (2013). https://doi.org/10.1103/PhysRevB.87.075453
5. Zhang, S., Zhou, J., Wanga, Q., Chend, X., Kawazoef, Y., Jenac, P.: Penta-graphene: a new carbon allotrope. PNAS **112**, 2372–2377 (2015). https://doi.org/10.1073/pnas.1416591112
6. He, C., Wanga, X.F., Zhang, W.X.: Coupling effects of the electric field and bending on the electronic and magnetic properties of penta-graphene nanoribbons. Phys. Chem. Chem. Phys. **19**, 18426–18433 (2017). https://doi.org/10.1039/c7cp03404k
7. Rajbanshi, B., Sarkar, S., Mandal, B., Sarkar, P.: Energetic and electronic structure of penta-graphene nanoribbons. Carbon **100**, 118–125 (2016). https://doi.org/10.1016/j.carbon.2016.01.014
8. Yuan, P.F., Zhang, Z.H., Fan, Z.Q., Qiu, M.: Electronic structure and magnetic properties of penta-graphene nanoribbons. Phys. Chem. Chem. Phys. **19**, 9528–9536 (2017). https://doi.org/10.1039/c7cp00029d
9. Quijano-Briones, J.J, Fernández-Escamilla, H.N, Tlahuice-Flores, A.: Chiral penta-graphene nanotubes: structure, bonding and electronic properties. Comput. Theor. Chem. **1108**, 70–75 (2017). http://dx.doi.org/10.1016/j.comptc.2017.03.019
10. Hasnip, P.J, Refson, K., Probert, M.I.J., Yates, J.R., Clark, S.J., Pickard, C.J.: Density functional theory in the solid state. Philos. Trans. Royal Soc. Math. Phys. Eng. Sci. vol. **372** (2014). https://doi.org/10.1098/rsta.2013.0270
11. Hohenberg, P., Kohn, W.: Inhomogeneous electron gas. Phys. Rev. **136**, B864–B87 (1964). https://doi.org/10.1103/Phys-Rev.136.B864
12. Kohn, W., Sham, L.J.: Self-consistent equations including exchange and correlation effects. Phys. Rev. **140**, A1133–A1138 (1965). https://doi.org/10.1103/PhysRev.140.A1133
13. Ghosh, K., Rahaman, H., Bhattacharyya, P.: Potentiality of density-functional theory in analyzing the devices containing graphene-crystalline solid interfaces: a review. IEEE Trans. Electron Dev **64**, 4738–4745 (2017). https://doi.org/10.1109/TED.2017.2755688
14. Kresse, G., Furthmüller, J.: Efficient iterative schemes for abinitio total-energy calculations using a plane-wave basis set. Phys. Rev. B, Condens. Matt. **54**, 11169–11186 (1996). https://doi.org/10.1103/Phys.RevB.54.11169
15. Blöchl, P.E.: Projector augmented-wave method. Phys. Rev. B: Condens. Matter **50**, 17953–17979 (1994). https://doi.org/10.1103/PhysRevB.50.17953
16. Perdew, J.P, Burke, K., Ernzerhof, M.: Generalized gradient approximation made simple. Phys. Rev. Lett. **77**, 3866–3868 (1996). https://doi.org/10.1103/physrevlett.77.3865
17. Heyd, J., Scuseria, G.E., Ernzerhof, M.: Erratum: hybrid functionals based on a screened Coulomb potential. J. Chem. Phys. **124**, 219906 (2006). https://doi.org/10.1063/1.1564060
18. Kuila, T., Bose, S., Mishra, A.K., Khanra, P., Kim, N.H., HeeLe, J.: Chemical functionalization of graphene and its application. Prog. Mater Sci. **57**, 1061–1105 (2012). https://doi.org/10.1016/j.pmatsci.2012.03.002
19. Maity, I., Ghosh, K., Rahaman, H., Bhattacharyya, P.: Selectivity tuning of graphene oxide based reliable gas sensor devices by tailoring the oxygen functional groups: a DFT study based approach. IEEE Trans. Dev. Mater. Reliab. **17**, 738–745 (2017). https://doi.org/10.1109/TDMR.2017.2766291

20. Berdiyorov, G.R., Dixit, G., Madjet, M.E.: Band gap engineering in penta-graphene by substitutional doping: first-principles Calculations. J. Phys.: Condens. Matter **28**, 475001 (2016)
21. Enriquez, J.I.G., Villagracia, A.R.C.: Hydrogen adsorption on pristine, defected, and 3d-block transition metal-doped penta-graphene. Int. J. Hydrogen Energy **41**, 12157–12166 (2016). https://doi.org/10.1016/j.ijhydene.2016.06.035
22. Quijano-Briones, J.J., Ferna´ndez-Escamilla, H.N., Tlahuice-Flores, A.: Doped penta-graphene and hydrogenation of its related structures: a structural and electronic DFT-D study. Phys. Chem. Chem. Phys. **18**, 15505—15509 (2016). https://doi.org/10.1039/c6cp02781d
23. Einollahzadeh, H., Dariani, R.S., Fazeli, S.M.: Computing the band structure and energy gap of penta-graphene by using DFT and G_0W_0 approximations. Solid State Commun. **229**, 1–4 (2016). https://doi.org/10.1016/j.ssc.2015.12.012
24. Tan, Y.Z., Xie, S.Y., Huang, R.B., Zheng, L.S.: The stabilization of fused-pentagon fullerene molecules. Nat. Chem. **1**, 450–460 (2009). https://doi.org/10.1038/nchem.329
25. Togo, A., Tanaka, I.: First principles phonon calculations in materials science. Scripta Mater. **108**, 1–5 (2015). https://doi.org/10.1016/j.scriptamat.2015.07.021
26. Ding, Y., Wang, Y.: Density functional theory study of the silicene-like SiX and XSi3 (X = B, C, N, Al, P) honeycomb lattices: The various buckled structures and versatile electronic properties. J. Phys. Chem. C **117**, 18266–18278 (2013). https://doi.org/10.1021/jp407666m
27. Wang, F.Q., Yu, J., Wang, Q., Kawazoe, Y., Jena, P.: Lattice thermal conductivity of penta-graphene. Carbon **105**, 424–429 (2016). https://doi.org/10.1016/j.carbon.2016.04.054
28. Xu, W., Zhang, G., Li, B.: Thermal conductivity of penta-graphene from molecular dynamics study. J. Chem. Phys. **143**, 154703 (2015). https://doi.org/10.1063/1.4933311
29. Le, M.Q.: Mechanical properties of penta-graphene, hydrogenated penta-graphene, and penta-CN2 sheets. Comput. Mater. Sci. **136**, 181–190 (2017). https://doi.org/10.1016/j.commatsci.2017.05.004
30. Sun, H., Mukherjee, S., Singh, C.V.: Mechanical properties of monolayer penta-graphene and phagraphene: a first-principles study. Phys. Chem. Chem. Phys. **18**, 26736–26742 (2016). https://doi.org/10.1039/c6cp04595b
31. Savini, G., Ferrari, A.C., Giustino, F.: First-principles prediction of doped graphane as a high-temperature electron-phonon superconductor. Phys. Rev. Lett. **105**, 037002 (2010). https://doi.org/10.1103/physrevlett.105.037002
32. Lee, C., Wei, X., Kysar, J.W., Hone, J.: Measurement of the elastic properties and intrinsic strength of monolayer graphene. Science **321**(5887), 385–388 (2008). https://doi.org/10.1126/science.1157996
33. Andrew, R.C., Mapasha, R.E., Ukpong, A.M., Chetty, N.: Mechanical properties of graphene and boronitrene. Phys. Rev. B **85**, 125428 (2012). https://doi.org/10.1103/PhysRevB.85.125428
34. Jiang, J.W, Park, H.S.: Negative Poisson's ratio in single-layer black phosphorus. Nat. Commun. **5**, 4727 (2014). doi.org/10.1038/ncomms5727
35. Greaves, G.N., Greer, A.L., Lakes, R.S., Rouxel, T.: Poisson's ratio and modern materials. Nat. Mater. **10**, 823–837 (2011). https://doi.org/10.1038/nmat3134
36. Marianetti, C.A., Yevick, H.G.: Failure mechanisms of graphene under tension. Phys. Rev. Lett. **105**, 245502 (2010). https://doi.org/10.1103/PhysRevLett.105.245502
37. Zhang, Y.Y., Pei, Q.X., Cheng, Y., Zhang, Y.W., Zhang, X.: Thermal conductivity of penta-graphene: the role of chemical functionalization. Comput. Mater. Sci. **137**, 195–200 (2017). https://doi.org/10.1016/j.commatsci.2017.05.042
38. Li, X., Zhang, S., Wang, F.Q., Guo, Y., Liu, J., Wang, Q.: Tuning the electronic and mechanical properties of penta-graphene via hydrogenation and fluorination. Phys. Chem. Chem. Phys. **18**, 14191 (2016). https://doi.org/10.1039/c6cp01092j

39. Zhang, Y., Pei, Q., Sha, Z., Zhang, Y., Gao, H.: Remarkable enhancement in failure stress and strain of penta-graphene via chemical functionalization. Nano Res. **10**, 3865–3874 (2017). https://doi.org/10.1007/s12274-017-1600-9
40. Pei, Q.X., Zhang, Y.W., Shenoy, V.B.: A molecular dynamics study of the mechanical properties of hydrogen functionalized graphene. Carbon **48**, 898–904 (2010). https://doi.org/10.1016/j.carbon.2009.11.014
41. Wu, X., Varshney, V., Lee, J., Zhang, T., Wohlwend, J.L., Roy, A.K., Luo, T.: Hydrogenation of penta-graphene leads to unexpected large improvement in thermal conductivity. Nano Lett. **16**, 3925–3935 (2016). https://doi.org/10.1021/acs.nanolett.6b01536
42. Schelling, P.K., Phillpot, S.R., Keblinski, P.: Comparison of atomic-level simulation methods for computing thermal conductivity. Phys. Rev. B **65**, 144306 (2002). https://doi.org/10.1103/PhysRevB.65.144306
43. Wang, Z., Dong, F., Shen, B., Zhang, R.J., Zheng, Y.X., Chen, L.Y., Wang, S.Y., Wang, C. Z., Ho, K.M., Fan, Y.J., Jin, B.Y., Su, W.S.: Electronic and optical properties of novel carbon allotropes. Carbon **101**, 77–85 (2016b). https://doi.org/10.1016/j.carbon.2016.01.078
44. Liu, L.L., Wang, Y., Chen, C.P., Yu, H.X., Zhao, L.S., Wang, X.C.: Tuning the electronic and magnetic properties of penta-graphene using a hydrogen atom: a theoretical study. RSC Adv. **7**, 40200 (2017). https://doi.org/10.1039/c7ra06956a
45. Ewels, C.P., Rocquefelte, X., Kroto, H.W., Rayson, M.J., Briddon, P.R., Heggie, M.I.: Predicting experimentally stable allotropes: Instability of penta-graphene. PNAS **112**, 15609–15612 (2015). https://doi.org/10.1073/pnas.1520402112
46. Xia, K., Artyukhov, V.I., Sun, L., Zheng, J., Jiao, L., Yakobson, B.I., Zhang, Y.: Growth of large-area aligned pentagonal graphene domains on high-index copper surfaces. Nano Res. **9**, 2182–2189 (2016). https://doi.org/10.1007/s12274-016-1107-9
47. Guo, Y., Wang, F.Q., Wang, Q.: An all-carbon vdW heterojunction composed of penta-graphene and graphene: tuning the Schottky barrier by electrostatic gating or nitrogen doping. Appl. Phys. Lett. **111**, 073503 (2017). https://doi.org/10.1063/1.4986604
48. Guo, J.H., Liu, D.D., Li, X.D., Liu, H.Y., Chen, G.: Pt4, Pd4, Ni4, and Ti4 catalyzed hydrogen spillover on penta-graphene for hydrogen storage: the first-principles and kinetic Monte Carlo study. Int. J. Hydrogen Energy **43**, 2247–2255 (2018). https://doi.org/10.1016/j.ijhydene.2017.11.169
49. Krishnan, R., Su, W.S., Chen, H.T.: A new carbon allotrope: penta-graphene as a metal-free catalyst for CO oxidation. Carbon **114**, 465–472 (2017). https://doi.org/10.1016/j.carbon.2016.12.054
50. Bhowmik, B., Manjuladevi, V., Gupta, R.K., Bhattacharyya, P.: Highly selective low-temperature acetone sensor based on hierarchical 3-D TiO_2 nanoflowers. IEEE Sensors J. **16**, 3488–3495 (2018). https://doi.org/10.1109/JSEN.2016.2530827
51. Bhattacharyya, P., Basu, P.K., Mukherjee, N., Mondal, A., Saha, H., Basu, S.: Deposition of nanocrystalline ZnO thin films on p-Si by novel galvanic method and application of the heterojunction as methane sensor. J. Mater. Sci. Mater. Electr. **18**, 823–829 (2007). https://doi.org/10.1007/s10854-006-9105-4
52. Ghosh, K., Hahapatra, N.S., Rahaman H., Bhattacharyya, P.: Prediction of adsorption probability of oxidizing and reducing species on 2-D hybrid junction of rGO-ZnO from first principle analysis. IEEE Trans. Nanotechnol. **18**, 119–125 (2019). https://doi.org/10.1109/TNANO.2018.2884171

3D Graphene and Its Nanocomposites: From Synthesis to Multifunctional Applications

Xin Tong, G. Zhang, Jai Prakash and Shuhui Sun

Abstract 3D graphene based nanomaterials have been extensively used in various fields due to their excellent and tunable physio-chemical properties such as electrical conductivity, higher surface area, strength etc. Extensive research has been achieved for the built of 3 Dimensional graphene and its nanocomposites with excellent properties for multidisciplinary applications. The applications of these nanomaterials have been increased dramatically in the energy field for the recent years and it has become a rapidly developing area. This chapter focuses on the latest developments of these novel 3D graphene-based nanomaterial and their multifunctional applications in field of energy i.e. fuel cells and lithium-ion batteries.

1 Introduction

Nowadays 2 Dimensional graphene materials and their composites have been broadly used in energy field because of tunable and excellent physical, chemical and surface properties such as higher electrical conductivity, strength, specific surface area (SSA) and surface chemistry, which have been reviewed previously [1–4]. Such properties are very important in electrocatalysis processes. In spite of all these excellent properties of 2D graphene based nanomaterials, aggregation and restacking of pristine graphene layers diminish their properties affecting the proper utilization. In addition, pristine graphene has lack of functional edges and is

X. Tong · G. Zhang · J. Prakash (✉) · S. Sun (✉)
Department of Energy, Materials and Telecommunications, Institut National de La Recherche Scientifique (INRS), Montreal J3X 1S2, Canada
e-mail: jaip@nith.ac.in

S. Sun
e-mail: shuhui@emt.inrs.ca

J. Prakash
Department of Chemistry, National Institute of Technology Hamirpur, Hamirpur 17005, India

A. Khan et al. (eds.), *Graphene Functionalization Strategies*,
Carbon Nanostructures, https://doi.org/10.1007/978-981-32-9057-0_15

unacceptable to deploy them in practical. Therefore, the center and forefront in this research area have moved into the research of heteroatoms doped or functionalized graphene materials, dimension-controlled graphene derivatives and the nano-sized materials supported on graphene composites [4–8].

Graphene is the basic material for building any other graphitic materials such as graphite, carbon nanotubes (CNTs) and fullerene [9] that results in several difference in the properties of these materials. Along with this, 2D graphene has also been shown to form various other nanostructures [10] using several physical and chemical routes. For example, graphene has been modifying in different structures and is being used as graphene quantum dots (GQDs), graphene nanoribbons (GNR) and scaffold into 3D graphene networks (3D-GNs). In these materials with new structures the intrinsic properties of graphene are maintained. Furthermore, they show outstanding electrochemical performance to overcome the shortage of the pristine graphene.

3D-GNs are such 3D structures with interconnected networks constructed by individual graphene sheets [5, 11–15]. The graphene sheets could be bonded together to assembly into macroscopic 3D materials. The name such as porous graphene [16], graphene aerogels [17], graphene sponges [18], graphene hydrogels [19], and graphene foams [20] are used in previous literatures when refer to these 3D-GNs materials. Although these materials have some slight differences in their microscopic morphology and performance, they all present similar properties such as huge SSA, excellent electrical conductivity, high mechanical strengths, rapid electron and transport kinetics.

The researches about construction of these 3D graphene structures and application in energy field has increased dramatically in the past few years and become a rapidly developing area. The summary on this topic is essential and beneficial to create significant breakthrough in the future. Although, there are already some excellent review articles on the syntheses and applications such as energy field, environmental-related area and biological applications of these new materials [5, 11–15, 21–27]. In this review, the current research in this rapidly developed filed are updated and the application of these novel 3 dimensional graphene-based material in fuel cell and lithium-ion battery are spotlighted.

2 The Fabrication Strategy of 3D Graphene

The fabrication of 3D graphene is carried out mainly by chemical self-assembly, template assisted chemical and Chemical Vapor Deposition (CVD) methods (Fig. 1) [12, 14, 15, 22, 24].

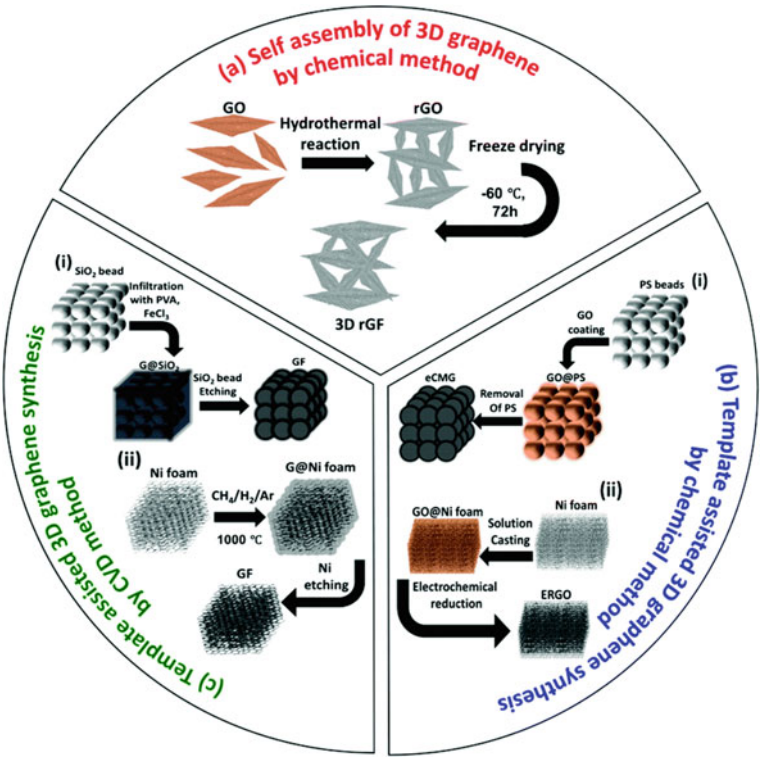

Fig. 1 Fabrication methods for 3D graphene. Reproduced with permission [28]. Copyright © 2015, Royal Society of Chemistry

2.1 Chemical Self-assembly Method

The typical process of assembly of graphene oxide (GO) method is as follow. Firstly, the GO are dispersed in a solution where existing a hydrophilic–hydrophobic balance between the electrostatic repulsive force from functional groups such as hydroxyl, epoxy and carboxyl groups on GO and the attractive van der Waals force between graphene layers. There are delicate hydrophilic–hydrophobic balance between graphene sheets. Then a series of procedures (i.e. ultrasonic treatment, changing the PH or adding surfactant) are held to break down this balance and then gelation process subsequently occurs. After reduction process, these routes share a special drying process, to get the macroscopic 3D structure.

The construction of GO or graphene hydrogel is the starting material for generation 3D-GNs. There are ample techniques such as hydrothermal processes [19], sol-gel method [17], speed vacuum centrifugation [29], ferrous ion induced self-assembly method [30], dip coating method [18], chemical reduction [31] and electrochemical reduction [32] for the treatment of GO dispersion. As shown in Fig. 2, the graphene hydrogel, which containing 97.4 wt% water (just 2.6 wt%

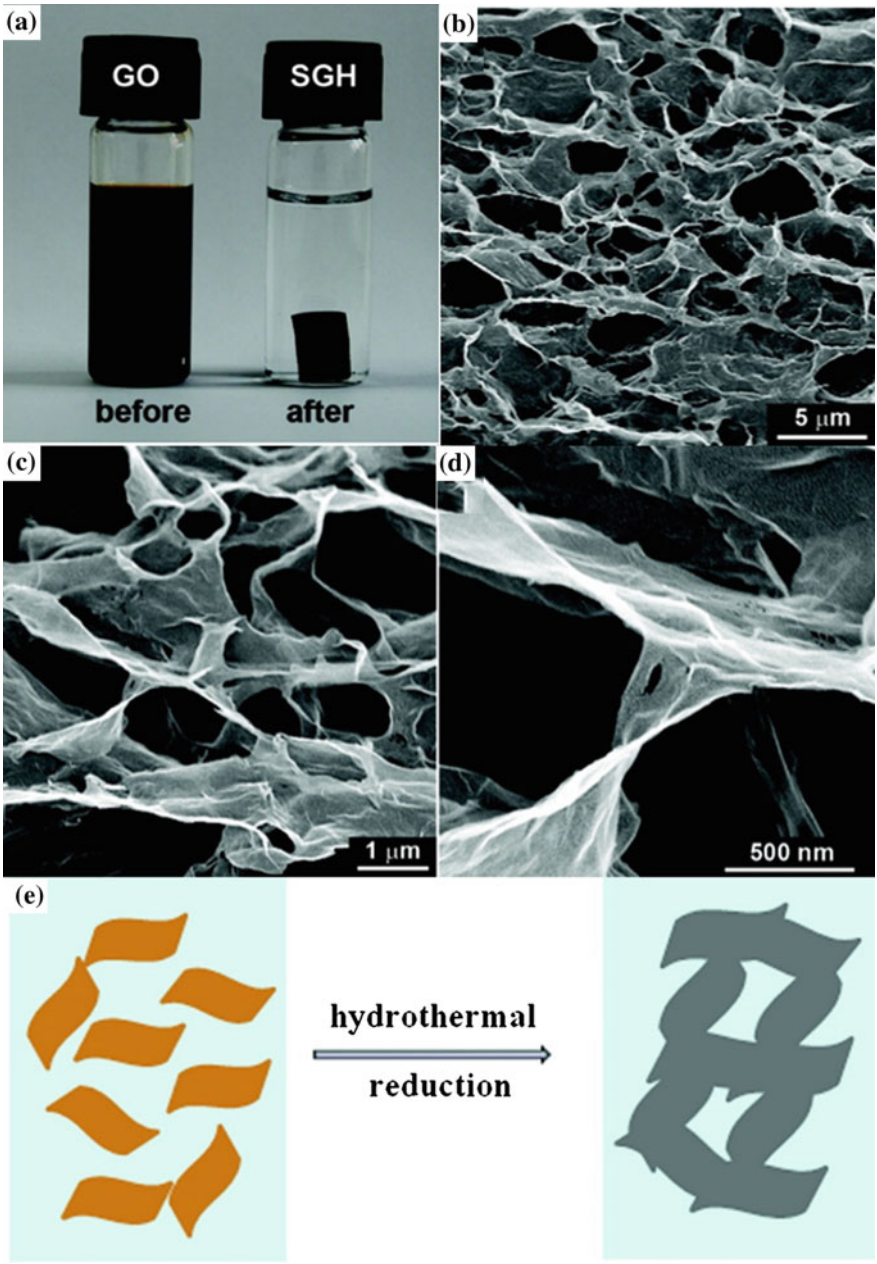

Fig. 2 **a** The photos of GO aqueous dispersion before and after hydrothermal process. **b–d** SEM images of the 3D graphene structure in different magnifications. **e** The schematic diagram for the formation mechanism of graphene hydrogel [19]. Copyright © 2010, American Chemical Society

graphene), was got by hydrothermal process. In SEM images, the pore sizes of 3D porous structure range from sub-micrometer to several micrometers. Partially coalescing or overlapping of the graphene layers may be the main reasons for the formation of 3D framework. Unlike the randomly dispersion in water of GO, the combined effects of electrostatic repulsion and van der Waals force caused a 3D random stacking during the hydrothermal processes.

2.2 Template Assisted Chemical Method

For controlling pore sizes in these materials, the PS beads and Ni foam is generally used to be as the template to get a controlled porous structure [33, 34]. In the research of Zhang et al. Ni foam were used as the template to prepare 3D graphene by a simple solution casting method as shown in Fig. 3. After electrochemical reduction, the GO can be reduced into 3D graphene structure, and the brown-colored GO foam turned into black. Moreover, the MnO_2 NPs can be electrochemical reduced and electrodeposited simultaneously on the 3D graphene to get MnO_2/3D graphene composite. This method offers several advantages in term of easy to scale up, simply, low-cost and efficient and the thinness and dimension of the graphene can be controlled freely to adjust different seized template or different volume of GO dispersion.

2.3 Chemical Vapor Deposition Method

The direct growth on catalyst supports route could provide a fundamentally different bottom-up method for the fabrication of 3D-GNs. The basic idea of this methodology is to firstly produce the layer of graphene on catalyst's surface under the effect of high temperature and then the catalyst support is removed finally.

The 3D metal catalyst are used as the catalyst and substrate for the assembly of 3D-GNs, while the flat metal substrates are used in conventional CVD method for graphene growth. In general, Ni has been used for this purpose in several reports [35–39]. Also, the ZnO [40] pyrolyzed photoresist films [41], anodic aluminum oxide [42] could also be taken as the scaffold in building the 3D nanostructure. As shown in Fig. 4 [35], the catalyst was a porous nickel foam and the carbon source were methane. After the methyl methacrylate (PMMA) coating, Ni etching, PMMA dissolving and infiltration process, a monolith of graphene 3D network was obtained. Choosing different Ni foams would be better to control the structure of 3D-GNs. In addition, the Cu catalyst can be used to produce the 3D-GNs with monolayer graphene. This template-directed CVD technique could be a promising method for the fabrication of 3D-GNs with excellent properties.

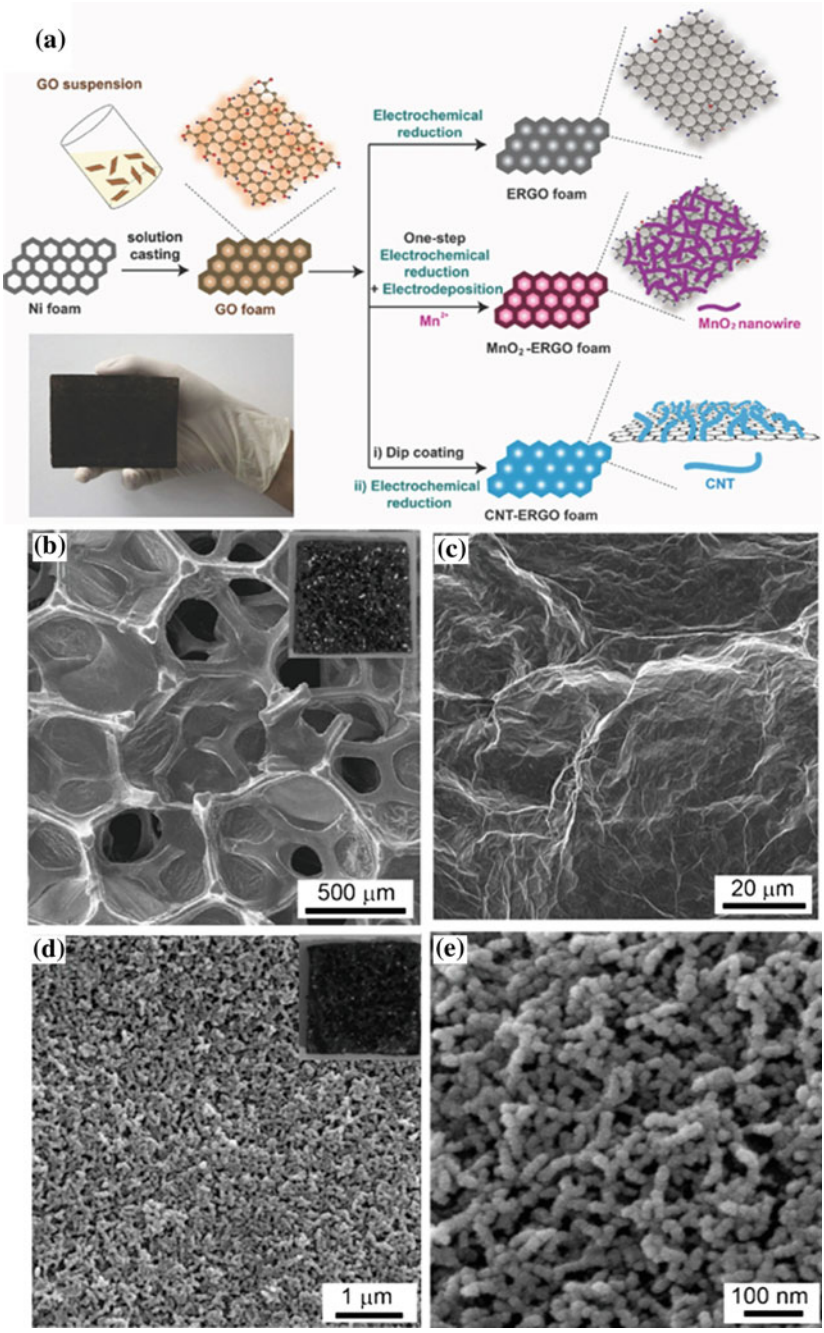

Fig. 3 **a** Illustration of the preparation of different foams. SEM images of **b**, **c** 3D graphene foam and **d**, **e** MnO_2–3D graphene foam composite with different magnification [34]. Copyright © 2014, John Wiley and Sons

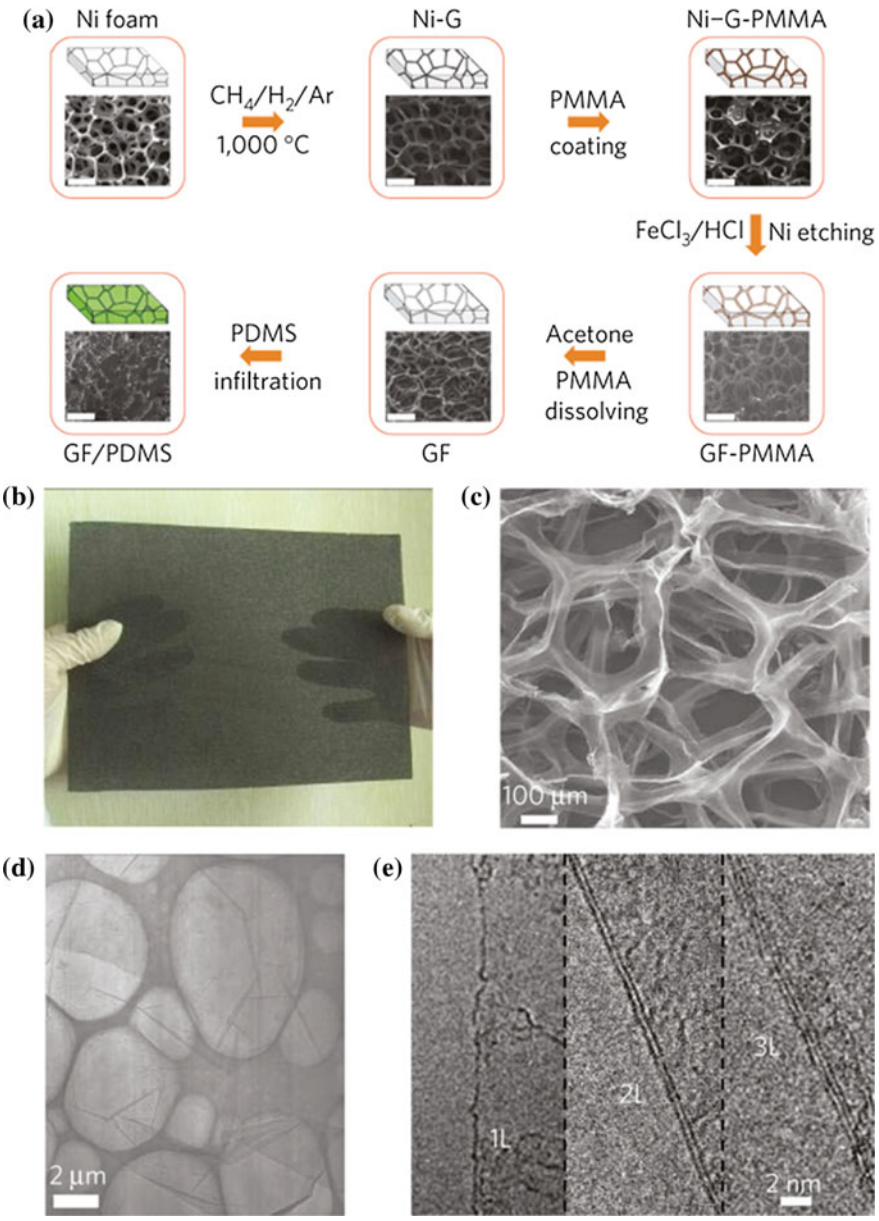

Fig. 4 **a** Schematic representation for the produce procedure of GF. **b** The photos, **c** SEM image and **d**, **e** TEM images of graphene Foams [35]. Copyright © 2011, Rights Managed by Nature Publishing Group

3 3D Graphene for Fuel Cells

Currently, the use of fuel cells is regarded as one of the most promising solutions for various environmental issues because these are environmentally friendly and highly efficient [4, 7, 44–46]. A powerful catalyst for facilitating the kinetically sluggish oxygen reduction reaction (ORR), is crucial to convert chemical energy directly into electricity in fuel cells. The ORR usually occurs by two distinct pathways in acid electrolytes: the 2-electron ($2e^-$) step by step reduction of O_2 with H_2O_2 as an intermediate product and the 4-electron ($4e^-$) directly reduction of O_2 to H_2O [47, 48], as shown in Fig. 5. The catalysts based on Pt metal are one of the promising catalysts which are being used in the industries. It conducts through $4e^-$ pathway with higher onset potential as well as large current density. The practical application is still not so viable in the industry because of the higher cost of Pt. Along with this, there are other issues such as stability. Consequently, finding another way for commercializing Pt/C catalyst, which is qualified to efficiently accelerating the ORR, with high stabilities, at low cost, has become into the central stage of this research topic [3, 49, 50]. In this regard, 3D graphene materials are the excellent candidate for ORR owing to their supreme properties including excellent electronic conductivity, huge SSA, as well as supreme thermal, optical and mechanical strength [51].

With rich interconnected macroporous framework and facilitated ion diffusion in multidimensional graphene structure are extremely required for facilitating involvement of catalysts and providing ample active sites for the reaction to processed [7, 14, 15, 23, 28, 49, 53, 54]. Moreover, these 3D materials could also be

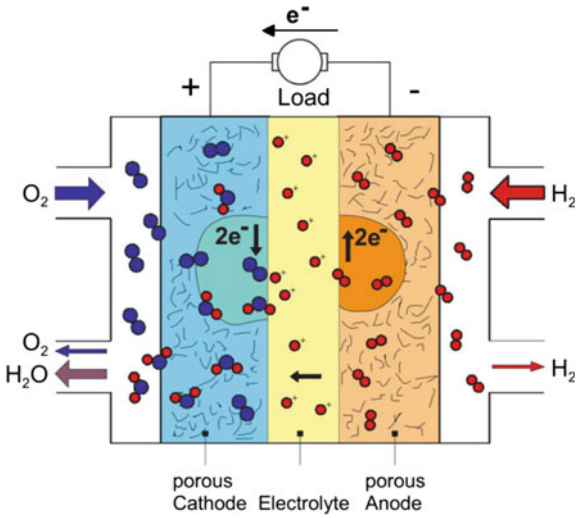

Fig. 5 The construction and reaction of PEMFC [43]. Copyright © 2018 MDPI

doped with other atoms (e.g. N, S, P) that enhance its catalytic efficiency. Qiao et al. fabricated such a doped 3D graphene i.e. N and S dual-doped mesoporous graphene (3D-N,S-G) [55]. It exhibited higher activity and number of active sites attributed to higher ORR catalytic activity and higher reaction current along with more positive onset potential. Figure 6 shows 3D graphene/pyrrole (Py) nanocomposite. A 3D graphene framework with high nanohole density and uniform pore size can be observed in electron microscopy micrographs. It was observed that the reduction peak of the nanocomposite was at −0.1 V (vs. Ag/AgCl) when reaction was taken place in the O_2-saturated potassium hydroxide solution. The nanocomposite also showed a high onset potential of about 0.04 V, which was found to be equivalent to as reported in case of Pt/C (20%) catalysts. The n value was found to be approximately 3.6 which exhibited a dominant $4e^-$ oxygen reduction process. The peroxide yield on the doped 3D graphene nanomaterial was found to be less than 15%. These results were attributed to the unique structure, functional active sites and multidimensional electron transport path as a result of doping. There are a number of reports available in the literature based on doped 3D graphene as metal-free catalysts for ORR.

As discussed above, with the porous structure and non-agglomerated morphology, the 3D graphene is an excellent support material to allow the utilization of the unique features. A great deal of carbon materials and metals or metal oxide nanoparticles are used to build graphene based 3D structure. For instance, Feng et al. fabricated a 3D N-doped graphene aerogel supported Fe_3O_4 nanoparticles (3D Fe_3O_4/N-GAs) by a one-pot hydrothermal method for the first time. The Fe_3O_4 nanoparticles were uniformly deposited on the interconnected macroporous graphene structure enhancing the interface contact and suppressing the agglomeration along with the dissolution of nanoparticles. The 3D-Fe_3O_4/N-G exhibited a remarkable ORR activity associated with a more positive onset potential (−0.19 V vs. Ag/AgCl), higher electron transfer number, and lower H_2O_2 yield in alkaline media. Besides, 3D graphene prepared by CVD are used as supporting material for the mesoporous $NiCo_2O_4$ nanoplate on ORR. The 3D graphene foam was immersed in the precursor solution and then maintained at 160 °C for 3 h. As show in Fig. 7, the as-formed $NiCo_2O_4$ nanoparticles grown vertically and uniformly covered on the graphene surface to create a loose porous structure. An obvious reduction peak at 0.75 V (vs. RHE) occured in the O_2-saturated 0.1 M KOH solution. The 3D-$NiCo_2O_4$/G material outperformed the commercial Pt/C (20%) in terms of half-wave potential and limiting current. The n value for GQDs/GNR was found to be 4.0, exhibiting a dominant $4e^-$ oxygen reduction process. Due to the morphology and structure stability, the 3D-$NiCo_2O_4$/G showed better stability than commercial Pt/C.

In summary, with large porous channel size, huge surface area and high electrical conductivity, the role of the 3D graphene inspires more exciting developments [12, 52, 56–87].

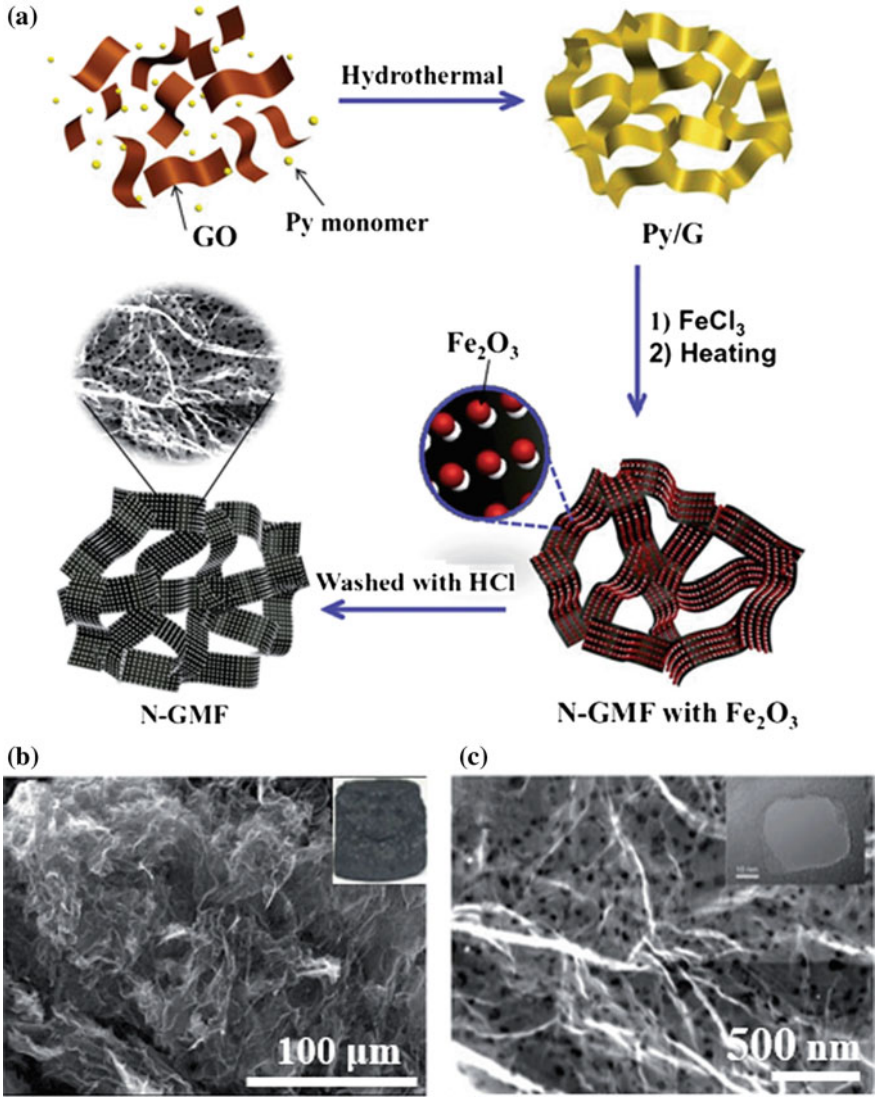

Fig. 6 **a** Steps for the synthesis, **b** SEM micrograph of N-GMF (nitrogen-doped graphene nanomeshes foam). **c** Scanning transmission electron microscopy image of N-GMF. **d** CV curves of N-S-GMF (N and S codoped graphene nanomesh foam) and N-S-GF (N and S codoped graphene foam) in O_2-saturated 0.1 M KOH solution. **e** LSV curves of different electrocatalysts (1600 rpm). **f** RDE measurement of N-S-GMF in oxygen saturated 0.1 M KOH with different rotating speed. The inset shows the K-L plots from LSVs. **g** The n and HO_2^- production of the N–S-GMF. Reproduced with permission [52]. Copyright © 2014, Royal Society of Chemistry

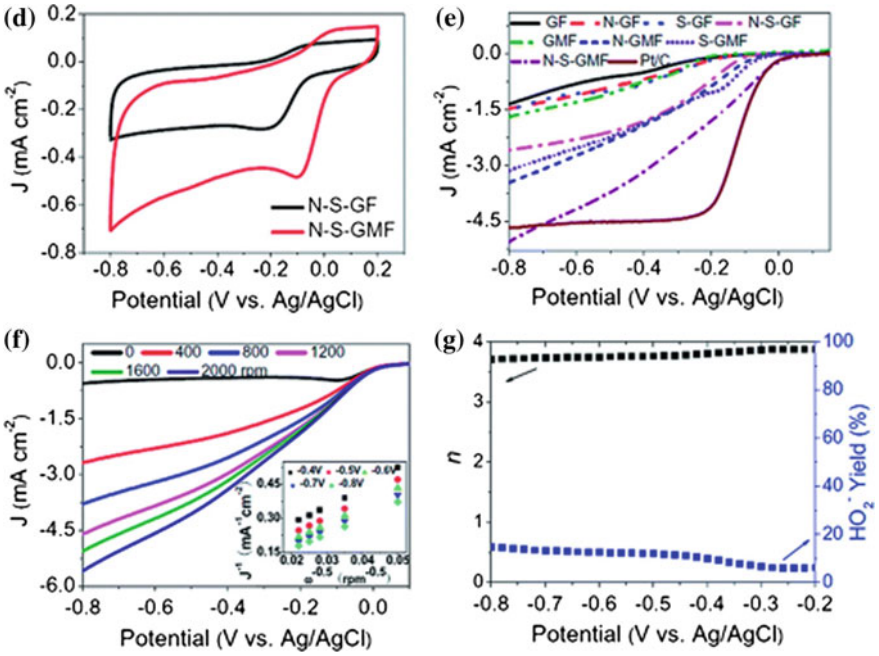

Fig. 6 (continued)

4 3D Graphene for Lithium-Ion Battery

Once the lithium-ion battery (LIB) adopted commercially in 1990s [88], it play a dominant role in portable electronic devices and is considered as one of the effective power sources. The LIB presents superior performance including high power and energy density (the weight and volumetric density can reach 130 Wh/kg and 370 Wh/cm^3), excellent charge retention capacity (self-discharge <10%/month), high output voltage, long cycling life and low maintenance [89–95]. As shown in Fig. 8, during charge and discharge process the lithium-ion can reversibly shuttle between the anode and the cathode of LIB.

When charging, the Li-ions move form cathode to anode, transforming electricity energy into chemical energy. While discharge process, supplying power to external electronic device, the direction of the Li-ions are from anode to cathode. The chemical energy are thus transformed into electricity energy. Therefore, the active electrode materials on each sides can mainly affect the performances of LIBs [96–100]. With the rapid development of portable electric device and commercial realization of electric vehicles, it puts forward higher requirements on the battery technology on high energy density, excellent cycling performance, and fast charging-discharging capacity [99, 101–105]. As a result, research on finding new

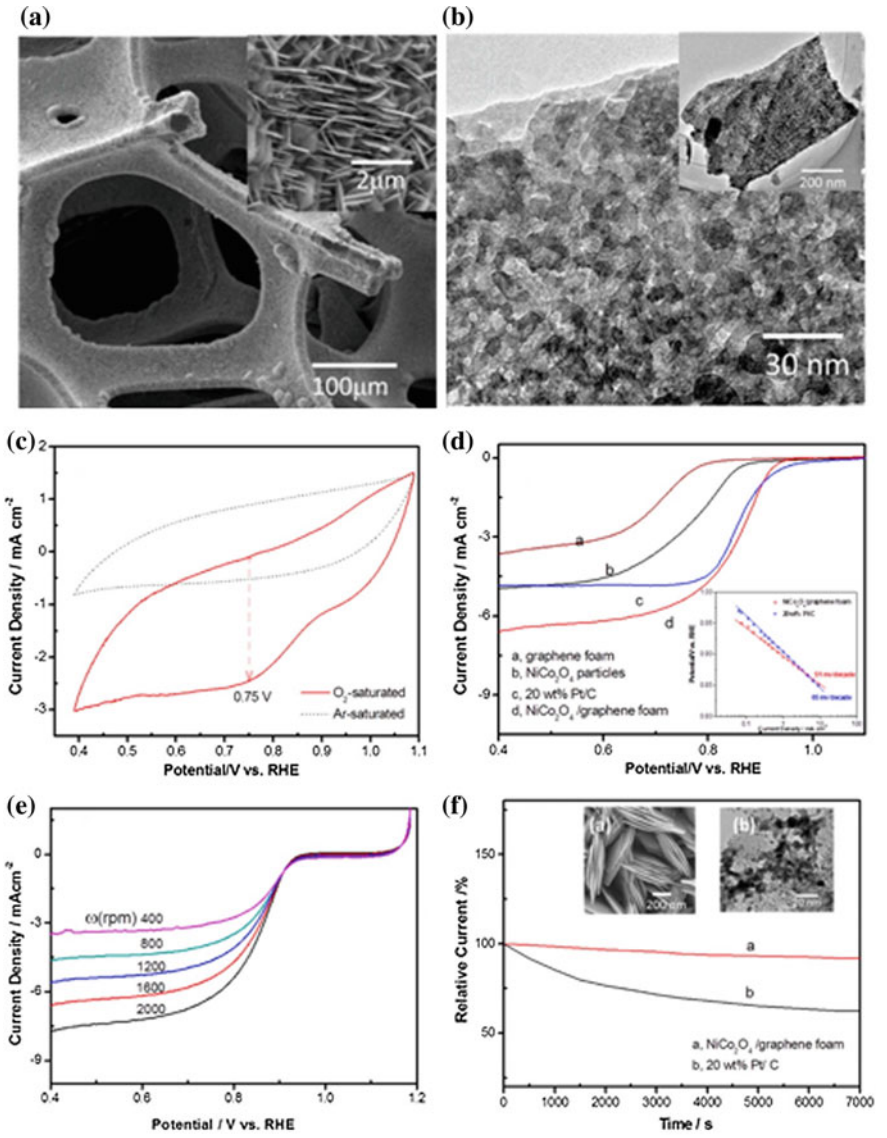

Fig. 7 **a** SEM images of $NiCo_2O_4$/3D-graphene. The inset shows that the as-prepared NPs grow vertically on the surface of 3D-G. **b** TEM image of $NiCo_2O_4$/3D-G. The inset is the TEM image with low magnification. **c** CV curves of $NiCo_2O_4$/3D-G in O_2- and Ar-saturated 0.1 M KOH solution. **d** LSV curves of different electrocatalysts (1600 rpm). **f** The stability test for $NiCo_2O_4$/3D-G and Pt/C (20%), measured by the current at 0.75 V. The insets are the SEM image of the **a** $NiCo_2O_4$/3D-G and **b** Pt/C after the test. Reproduced with permission [56]. Copyright © 2016, American Chemical Society

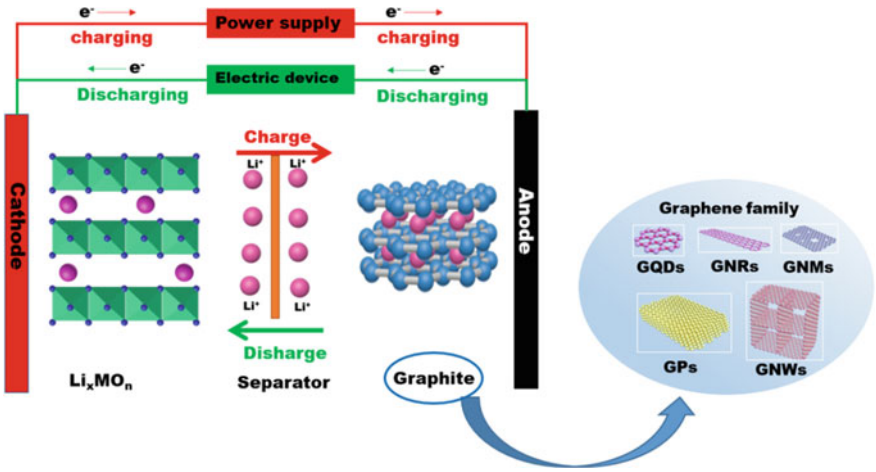

Fig. 8 The Schematic representation of Lithium-ion battery

electrode materials and improving the existing materials to provide better electrochemical performance while lower cost has always been a hotspot.

Graphite, which possessing laminate structure and could allow the lithium-ion intercalate and deintercalate reversibly, is definitely the commercialized anode. However, the theoretical lithium-ion storage of graphite is only 372 mAh/g (calculated as LiC_6) and shows low Li-ion transport rate between graphite layers (10^{-12}–10^{-14} cm^2/s). Hence, there are great needs to exploring alternative anode materials with higher reversible capacity, energy and power density. Compared with graphite, graphene shows a series extraordinary performance such as large specific area, superior electron conductivity, excellent mechanical flexibility and high lithium-ion storage capacity [106, 107]. Therefore, tremendous efforts applied the graphene based hybrid materials in lithium-ion battery, not only using in anode but also as an additive in cathode [93, 94, 108–117]. However, because of strong Van Der Waals forces between graphene layers, the 2D graphene could easily restack and aggregate, which significantly diminish the surface area and hinder the rapid electron transport and ion diffusion. Furthermore, pristine graphene usually shows limited cross-plane diffusion of ion and electron, which result in fast capacity fade under high charge/discharge current density. In addition, a limited number of reactive sites can be found in pristine graphene, which affect the lithium storage capacity and high-rate discharge performance. The optimal candidate for LIB materials should have high lithium storage capability and robust structural stability for charge/discharge cycles. The 3D graphene materials can be used in LIBs due to their excellent conductivity, high elasticity, mechanical and electrochemical stability. 3D-GNs can highly improve the electrochemical performance of electrode in LIBs [12, 14, 15, 22–24, 118, 119].

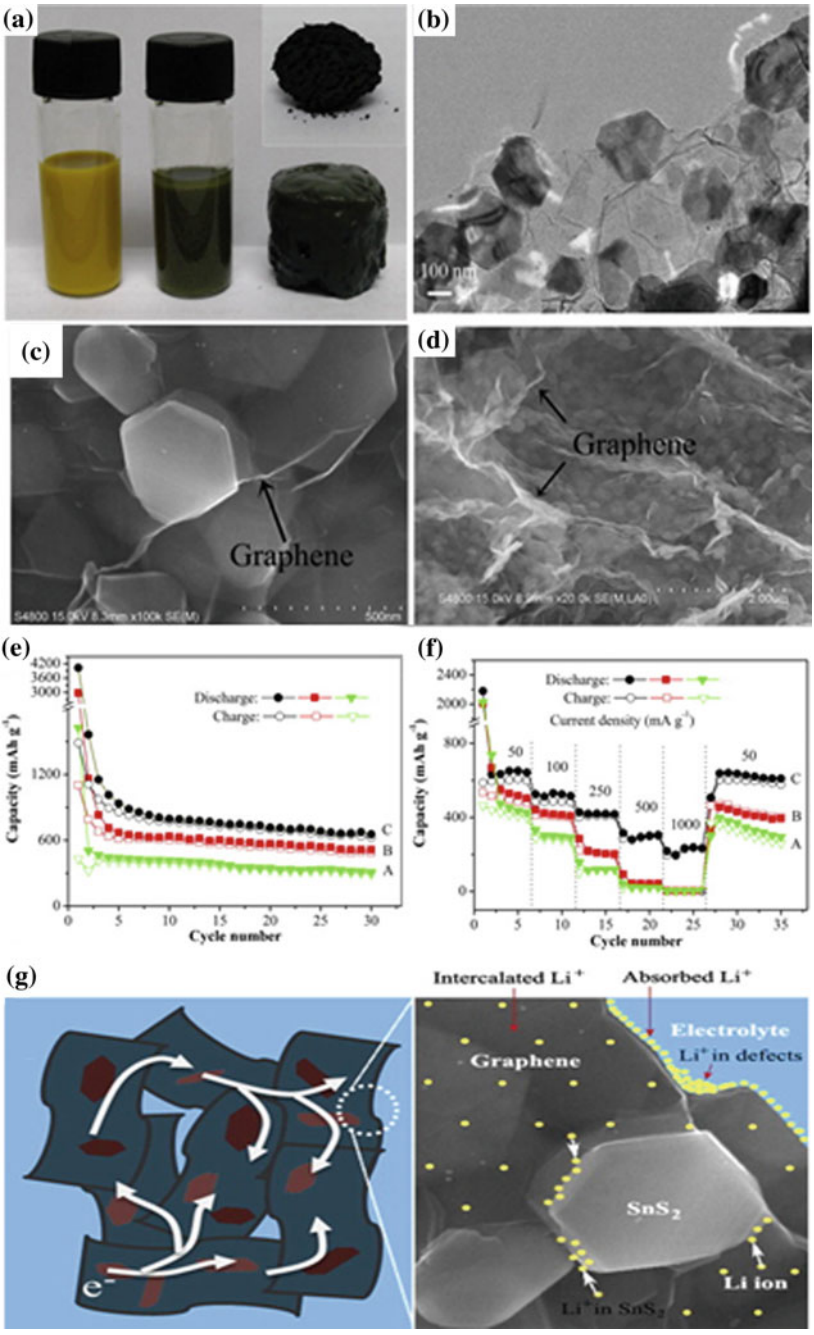
(a)
(b)
100 nm
(c)
Graphene
(d)
Graphene
(e)
Discharge:
Charge:
Capacity (mAh g-1)
Cycle number
C
B
A
(f)
Discharge:
Charge:
Current density (mA g-1)
50
100
250
500
1000
50
Capacity (mAh g-1)
Cycle number
(g)
Intercalated Li+
Absorbed Li+
Electrolyte
Li+ in defects
Graphene
SnS2
Li ion
Li+ in SnS2
e-

◂**Fig. 9** **a** The photo of SnS_2, SnS_2/G-Hs, the SnS_2/G-As samples before lyophilization. The inset is the SnS_2/G-As after lyophilization. **b** TEM image, SEM images on **c** up-side and **d** cross section direction of SnS_2/G-As. **e** Charge–discharge curves and **f** Cycle and rate performance of SnS_2 NPs (A), SnS_2/G-Hs (B) and SnS_2/G-As (C). **g** Schematic diagram of lithium ions storage and electron transmission in composites [122].

3D GNs-based porous composite have been demonstrated as attractive materials for high-performance LIBs, both in anode [16, 20, 120–151] and cathode materials [152]. Firstly, the 3D-GNs show high SSA and supply more lithium-ion store space, leading to a higher energy density. Besides, the opening porous structures in 3D-GNs could shorten the diffusion distance of Li^+ ions and facilitate electron transportation, thus enhance the fast charging/discharging capacity. Furthermore, the 3D-GNs could avoid the aggregation and restrain the crumbling and cracking of active material, which accounts for the long cycling life.

As seen from Fig. 9, SnO_2/3D-GNs were fabricated by self-assembly of graphene and SnS_2 in a hydrothermal and lyophilization process. During the hydrothermal process, the built of 3D network architectures and the synthesis of SnS_2 are achieved at the same time. The resultant SnS_2/3D-GNs were about 20 mm in height and 15 mm in diameter (the water content is around 94.3 wt%). The 3D structure was maintained almost the same with the undried one after lyophilization. As seen from the SEM, the graphene sheets were partial overlapping or coalescing and thus form the 3D network with homogeneously dispersing the SnS_2 nanoparticles. The reversible capacity of the composites is 656 mAh/g at a current density of 50 mA/g. Even the current density is 1000 mA/g it shows excellent rate capability (240 mAh/g). It is explained as follows. (i) The 3D-GNs can supply rich active sites for absorbing Li^+ ions. (ii) The pores of the 3D-GNs can allow effective ion migration to enhance ionic diffusion. (iii) The 3D-GNs can also serve as buffers for suppress the volume change of SnS_2 during Li^+ insertion/extraction process.

In Fig. 10, 3D-G network was synthesized by 3D porous Ni templated CVD method. The 3D-G materials display high conductivity of ~ 600 S cm^{-1} and low square resistance of 1.6 Ω sq^{-1}. The 3D graphene network can served as excellent conducting substrate for electrode materials because of its few defects and grain boundaries. The SEM showed that the $LiFePO_4$ particles was coated on both out and inside surface of the 3D graphene interconnected network was generally maintained during synthesis process. Because 3D graphene network could supply the tunnel for the electrons cathode to fast transport, the $LiFePO_4$/3D-G shows high rate charge–discharge capacity, suggesting potential application in high charge–discharge rate LIBs.

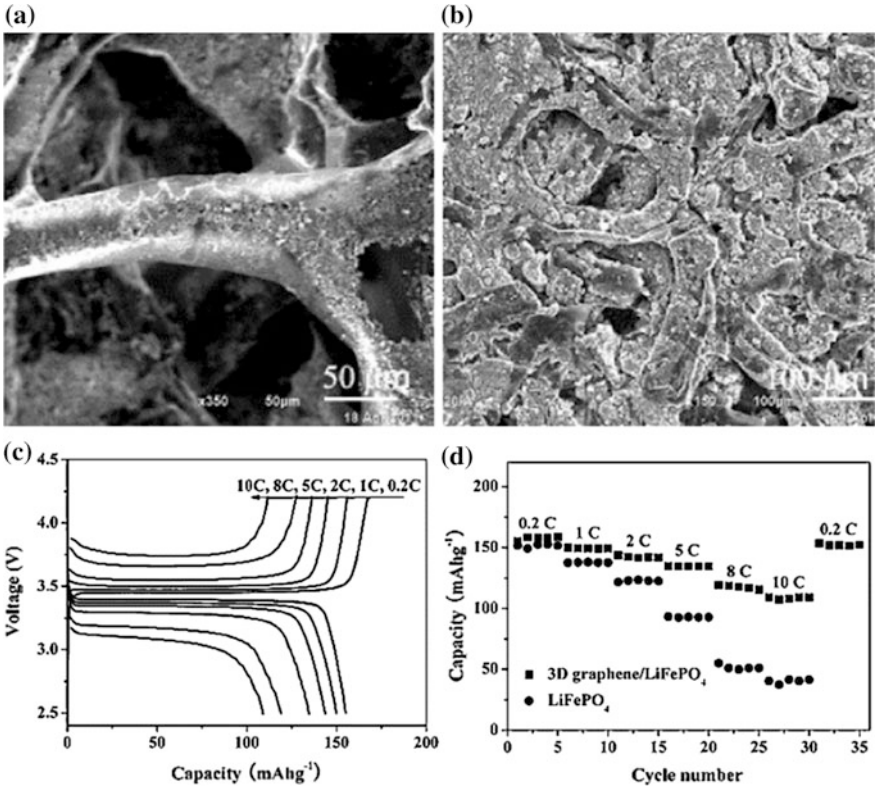

Fig. 10 **a** SEM images of (**a**) as prepared $LiFePO_4$/3D graphene composite. **b** SEM images of the surface of $LiFePO_4$/3D graphene electrode. **c** The charge–discharge curves for $LiFePO_4$/3D graphene composite at different current densities. **d** Rate performance of $LiFePO_4$ with and without 3D graphene.

5 Conclusions and Future Outlook

Because of the flexible structure and tunable functionalities, graphene can be considered as a versatile building block to the other dimension materials. The graphene family materials show some excellent properties, which are assisted of the excellent intrinsic properties of pristine graphene such as a high surface area and mechanical strengths. Although, there are various forms in graphene derivatives, they share something in common. The large specific area, superior electron conductivity and excellent mechanical flexibility of these material are beneficial for the application in energy filed. The finding of these new structures of graphene can expand the boundary of graphene material and made the investigation of the application of these material. Predictably the different structure of these materials will allow them suitable for various situations.

Although numerous efforts have been devoted, research about 3D materials fabrication and their applications in energy field are still in its infancy. The following challenges still remain and need to resolve in the future. Firstly, the electrical conductivity is a key factor applying in the energy filed. The synthesis route from GO is a simply and widely used to fabricate the 3D graphene material. There is still no very effective way to deoxidize graphene without breaking the pristine structure. Furthermore, the structure of graphene derivative material predetermines its properties. It is urgently need to improve the production route to make more precise control. For instance, we need to find a proper method to synthesize the 3D-GNs with controlled pore size distribution. Last but not the least, the applications of these materials can be used in other fields such as environment or biology area.

Acknowledgements The authors (JP, SS) acknowledge the financial supports from the Natural Sciences and Engineering Research Council of Canada (NSERC), Fonds de Recherche du Québec-Nature et Technologies (FRQNT). JP would like to acknowledge FRQNT for Merit Scholarship (Ranked#1, 2017–2018), department of science and technology (DST), India for the prestigious award of INSPIRE faculty (IFA/2015/MS-57), and Shastri Indo-Canadian Institute for SSTSG (2017–18) award.

References

1. Choi, H.J., Jung, S.M., Seo, J.M., Chang, D.W., Dai, L.M., Baek, J.B.: Graphene for energy conversion and storage in fuel cells and supercapacitors. Nano Energy **1**(4), 534–551 (2012). https://doi.org/10.1016/j.nanoen.2012.05.001
2. Zhang, J., Zhao, F., Zhang, Z., Chen, N., Qu, L.: Dimension-tailored functional graphene structures for energy conversion and storage. Nanoscale **5**(8), 3112–3126 (2013). https://doi.org/10.1039/c3nr00011g
3. Wang, D.W., Su, D.S.: Heterogeneous nanocarbon materials for oxygen reduction reaction. Energy Environ. Sci. **7**(2), 576–591 (2014). https://doi.org/10.1039/c3ee43463j
4. Geng, D.S., Ding, N., Hor, T.S.A., Liu, Z.L., Sun, X.L., Zong, Y.: Potential of metal-free "graphene alloy" as electrocatalysts for oxygen reduction reaction. J. Mater. Chem. A **3**(5), 1795–1810 (2015). https://doi.org/10.1039/c4ta06008c
5. Chabot, V., Higgins, D., Yu, A.P., Xiao, X.C., Chen, Z.W., Zhang, J.J.: A review of graphene and graphene oxide sponge: material synthesis and applications to energy and the environment. Energy Environ. Sci. **7**(5), 1564–1596 (2014). https://doi.org/10.1039/c3ee43385d
6. Holade, Y., Sahin, N.E., Servat, K., Napporn, T.W., Kokoh, K.B.: Recent advances in carbon supported metal nanoparticles preparation for oxygen reduction reaction in low temperature fuel cells. Catalysts **5**(1), 310–348 (2015). https://doi.org/10.3390/catal5010310
7. Wei, Q.L., Tong, X., Zhang, G.X., Qiao, J.L., Gong, Q.J., Sun, S.H.: Nitrogen-doped carbon nanotube and graphene materials for oxygen reduction reactions. Catalysts **5**(3), 1574–1602 (2015). https://doi.org/10.3390/catal5031574
8. Ni, J.F., Li, Y.: Carbon nanomaterials in different dimensions for electrochemical energy storage. Adv. Energy Mater. **6**(17), 1600278-n/a. UNSP 1600278 (2016). https://doi.org/10.1002/aenm.201600278
9. Geim, A.K., Novoselov, K.S.: The rise of graphene. Nat. Mater. **6**(3), 183–191 (2007). https://doi.org/10.1038/nmat1849

10. Cong, H.P., Chen, J.F., Yu, S.H.: Graphene-based macroscopic assemblies and architectures: an emerging material system. Chem. Soc. Rev. **43**(21), 7295–7325 (2014). https://doi.org/10.1039/c4cs00181h
11. Li, C., Shi, G.: Three-dimensional graphene architectures. Nanoscale **4**(18), 5549–5563 (2012). https://doi.org/10.1039/c2nr31467c
12. Fang, Q.L., Shen, Y., Chen, B.L.: Synthesis, decoration and properties of three-dimensional graphene-based macrostructures: a review. Chem. Eng. J. **264**, 753–771 (2015). https://doi.org/10.1016/j.cej.2014.12.001
13. Gao, H., Duan, H.: 2D and 3D graphene materials: preparation and bioelectrochemical applications. Biosens. Bioelectron. **65**, 404–419 (2015). https://doi.org/10.1016/j.bios.2014.10.067
14. Ma, Y.F., Chen, Y.S.: Three-dimensional graphene networks: synthesis, properties and applications. Natl. Sci. Rev. **2**(1), 40–53 (2015). https://doi.org/10.1093/nsr/nwu072
15. Mao, S., Lu, G., Chen, J.: Three-dimensional graphene-based composites for energy applications. Nanoscale **7**(16), 6924–6943 (2015). https://doi.org/10.1039/c4nr06609j
16. Wang, Z.L., Xu, D., Wang, H.G., Wu, Z., Zhang, X.B.: In situ fabrication of porous graphene electrodes for high-performance energy storage. ACS Nano **7**(3), 2422–2430 (2013). https://doi.org/10.1021/nn3057388
17. Worsley, M.A., Pauzauskie, P.J., Olson, T.Y., Biener, J., Satcher Jr., J.H., Baumann, T.F.: Synthesis of graphene aerogel with high electrical conductivity. J. Am. Chem. Soc. **132**(40), 14067–14069 (2010). https://doi.org/10.1021/ja1072299
18. Nguyen, D.D., Tai, N.H., Lee, S.B., Kuo, W.S.: Superhydrophobic and superoleophilic properties of graphene-based sponges fabricated using a facile dip coating method. Energy Environ. Sci. **5**(7), 7908–7912 (2012). https://doi.org/10.1039/c2ee21848h
19. Xu, Y., Sheng, K., Li, C., Shi, G.: Self-assembled graphene hydrogel via a one-step hydrothermal process. ACS Nano **4**(7), 4324–4330 (2010). https://doi.org/10.1021/nn101187z
20. Wei, W., Yang, S., Zhou, H., Lieberwirth, I., Feng, X., Mullen, K.: 3D graphene foams cross-linked with pre-encapsulated Fe3O4 nanospheres for enhanced lithium storage. Adv. Mater. **25**(21), 2909–2914 (2013). https://doi.org/10.1002/adma.201300445
21. Shen, J., Zhu, Y., Yang, X., Li, C.: Graphene quantum dots: emergent nanolights for bioimaging, sensors, catalysis and photovoltaic devices. Chem. Commun. (Camb.) **48**(31), 3686–3699 (2012). https://doi.org/10.1039/c2cc00110a
22. Xu, Y., Shi, G., Duan, X.: Self-assembled three-dimensional graphene macrostructures: synthesis and applications in supercapacitors. Acc. Chem. Res. **48**(6), 1666–1675 (2015). https://doi.org/10.1021/acs.accounts.5b00117
23. Wang, H., Yuan, X., Zeng, G., Wu, Y., Liu, Y., Jiang, Q., Gu, S.: Three dimensional graphene based materials: synthesis and applications from energy storage and conversion to electrochemical sensor and environmental remediation. Adv. Colloid Interface Sci. **221**, 41–59 (2015). https://doi.org/10.1016/j.cis.2015.04.005
24. Yan, Z., Yao, W., Hu, L., Liu, D., Wang, C., Lee, C.S.: Progress in the preparation and application of three-dimensional graphene-based porous nanocomposites. Nanoscale **7**(13), 5563–5577 (2015). https://doi.org/10.1039/c5nr00030k
25. Mao, M., Hu, J.Y., Liu, H.T.: Graphene-based materials for flexible electrochemical energy storage. Int. J. Energy Res. **39**(6), 727–740 (2015). https://doi.org/10.1002/er.3256
26. Zhang, Y.Z., Wang, Y., Cheng, T., Lai, W.Y., Pang, H., Huang, W.: Flexible supercapacitors based on paper substrates: a new paradigm for low-cost energy storage. Chem. Soc. Rev. **44**(15), 5181–5199 (2015). https://doi.org/10.1039/c5cs00174a
27. Zheng, X.T., Ananthanarayanan, A., Luo, K.Q., Chen, P.: Glowing graphene quantum dots and carbon dots: properties, syntheses, and biological applications. Small **11**(14), 1620–1636 (2015). https://doi.org/10.1002/smll.201402648
28. Patil, U., Lee, S.C., Kulkarni, S., Sohn, J.S., Nam, M.S., Han, S., Jun, S.C.: Nanostructured pseudocapacitive materials decorated 3D graphene foam electrodes for next generation supercapacitors. Nanoscale **7**(16), 6999–7021 (2015). https://doi.org/10.1039/c5nr01135c

29. Liu, F., Seo, T.S.: A controllable self-assembly method for large-scale synthesis of graphene sponges and free-standing graphene films. Adv. Funct. Mater. **20**(12), 1930–1936 (2010). https://doi.org/10.1002/adfm.201000287
30. Cong, H.-P., Ren, X.-C., Wang, P., Yu, S.-H.: Macroscopic multifunctional graphene-based hydrogels and aerogels by a metal ion induced self-assembly process. ACS Nano **6**(3), 2693–2703 (2012). https://doi.org/10.1021/nn300082k
31. Chen, W., Li, S., Chen, C., Yan, L.: Self-assembly and embedding of nanoparticles by in situ reduced graphene for preparation of a 3D graphene/nanoparticle aerogel. Adv. Mater. **23** (47), 5679–5683 (2011)
32. Sheng, K., Sun, Y., Li, C., Yuan, W., Shi, G.: Ultrahigh-rate supercapacitors based on eletrochemically reduced graphene oxide for ac line-filtering. Sci. Rep. **2**, 247 (2012). https://doi.org/10.1038/srep00247
33. Choi, B.G., Yang, M., Hong, W.H., Choi, J.W., Huh, Y.S.: 3D macroporous graphene frameworks for supercapacitors with high energy and power densities. ACS Nano **6**(5), 4020–4028 (2012)
34. Zhang, Z., Xiao, F., Qian, L., Xiao, J., Wang, S., Liu, Y.: Facile synthesis of 3D MnO2–graphene and carbon nanotube-graphene composite networks for high-performance, flexible, all-solid-state asymmetric supercapacitors. Adv. Energy Mater. **4**(10), 1400064 (2014)
35. Chen, Z., Ren, W., Gao, L., Liu, B., Pei, S., Cheng, H.M.: Three-dimensional flexible and conductive interconnected graphene networks grown by chemical vapour deposition. Nat. Mater. **10**(6), 424–428 (2011). https://doi.org/10.1038/nmat3001
36. Cao, X., Shi, Y., Shi, W., Lu, G., Huang, X., Yan, Q., Zhang, Q., Zhang, H.: Preparation of novel 3D graphene networks for supercapacitor applications. Small **7**(22), 3163–3168 (2011). https://doi.org/10.1002/smll.201100990
37. Dong, X., Wang, X., Wang, J., Song, H., Li, X., Wang, L., Chan-Park, M.B., Li, C.M., Chen, P.: Synthesis of a MnO2–graphene foam hybrid with controlled MnO2 particle shape and its use as a supercapacitor electrode. Carbon **50**(13), 4865–4870 (2012). https://doi.org/10.1016/j.carbon.2012.06.014
38. Ito, Y., Tanabe, Y., Qiu, H.J., Sugawara, K., Heguri, S., Tu, N.H., Huynh, K.K., Fujita, T., Takahashi, T., Tanigaki, K.: High-quality three-dimensional nanoporous graphene. Angew. Chem. Int. Ed. **53**(19), 4822–4826 (2014)
39. Li, W., Gao, S., Wu, L., Qiu, S., Guo, Y., Geng, X., Chen, M., Liao, S., Zhu, C., Gong, Y., Long, M., Xu, J., Wei, X., Sun, M., Liu, L.: High-density three-dimension graphene macroscopic objects for high-capacity removal of heavy metal ions. Sci. Rep. **3**, 2125 (2013). https://doi.org/10.1038/srep02125
40. Mecklenburg, M., Schuchardt, A., Mishra, Y.K., Kaps, S., Adelung, R., Lotnyk, A., Kienle, L., Schulte, K.: Aerographite: ultra lightweight, flexible nanowall, carbon microtube material with outstanding mechanical performance. Adv. Mater. **24**(26), 3486–3490 (2012). https://doi.org/10.1002/adma.201200491
41. Xiao, X., Beechem, T.E., Brumbach, M.T., Lambert, T.N., Davis, D.J., Michael, J.R., Washburn, C.M., Wang, J., Brozik, S.M., Wheeler, D.R., Burckel, D.B., Polsky, R.: Lithographically defined three-dimensional graphene structures. ACS Nano **6**(4), 3573–3579 (2012). https://doi.org/10.1021/nn300655c
42. Zhou, M., Lin, T., Huang, F., Zhong, Y., Wang, Z., Tang, Y., Bi, H., Wan, D., Lin, J.: Highly conductive porous graphene/ceramic composites for heat transfer and thermal energy storage. Adv. Func. Mater. **23**(18), 2263–2269 (2013)
43. Lv, Y., Wang, X., Mei, T., Li, J., Wang, J.: Single-step hydrothermal synthesis of N, S-dual-doped graphene networks as metal-free efficient electrocatalysts for oxygen reduction reaction. ChemistrySelect **3**(11), 3241–3250 (2018). https://doi.org/10.1002/slct.201800098
44. Yang, Z., Nie, H., Xa, Chen, Chen, X., Huang, S.: Recent progress in doped carbon nanomaterials as effective cathode catalysts for fuel cell oxygen reduction reaction. J. Power Sources **236**, 238–249 (2013). https://doi.org/10.1016/j.jpowsour.2013.02.057
45. Wu, G., Zelenay, P.: Nanostructured nonprecious metal catalysts for oxygen reduction reaction. Acc. Chem. Res. **46**(8), 1878–1889 (2013). https://doi.org/10.1021/ar400011z

46. Yang, Z., Ren, J., Zhang, Z., Chen, X., Guan, G., Qiu, L., Zhang, Y., Peng, H.: Recent advancement of nanostructured carbon for energy applications. Chem. Rev. **115**(11), 5159–5223 (2015). https://doi.org/10.1021/cr5006217
47. Guo, S., Zhang, S., Sun, S.: Tuning nanoparticle catalysis for the oxygen reduction reaction. Angew. Chem. Int. Ed. Engl. **52**(33), 8526–8544 (2013). https://doi.org/10.1002/anie.201207186
48. Nie, Y., Li, L., Wei, Z.: Recent advancements in Pt and Pt-free catalysts for oxygen reduction reaction. Chem. Soc. Rev. **44**(8), 2168–2201 (2015). https://doi.org/10.1039/c4cs00484a
49. Dai, L., Xue, Y., Qu, L., Choi, H.J., Baek, J.B.: Metal-free catalysts for oxygen reduction reaction. Chem. Rev. **115**(11), 4823–4892 (2015). https://doi.org/10.1021/cr5003563
50. Song, Z.X., Cheng, N.C., Lushington, A., Sun, X.L.: Recent progress on MOF-derived nanomaterials as advanced electrocatalysts in fuel cells. Catalysts **6**(8), 116 (2016). https://doi.org/10.3390/catal6080116
51. Sun, D.M., Liu, C., Ren, W.C., Cheng, H.M.: A review of carbon nanotube-and graphene-based flexible thin-film transistors. Small **9**(8), 1188–1205 (2013)
52. Zhao, Y., Hu, C.G., Song, L., Wang, L.X., Shi, G.Q., Dai, L.M., Qu, L.T.: Functional graphene nanomesh foam. Energy Environ. Sci. **7**(6), 1913–1918 (2014). https://doi.org/10.1039/c4ee00106k
53. Wang, X., Sun, G., Chen, P.: Three-dimensional porous architectures of carbon nanotubes and graphene sheets for energy applications. Front. Energy Res. **2**(33) (2014). https://doi.org/10.3389/fenrg.2014.00033
54. Qiu, H.J., Liu, L., Wang, Y.: Template-directed fabrication of 3D graphene-based composite and their electrochemical energy-related applications. Sci. Bull. **61**(6), 443–450 (2016). https://doi.org/10.1007/s11434-016-1024-z
55. Liang, J., Jiao, Y., Jaroniec, M., Qiao, S.Z.: Sulfur and nitrogen dual-doped mesoporous graphene electrocatalyst for oxygen reduction with synergistically enhanced performance. Angew. Chem. Int. Ed. Engl. **51**(46), 11496–11500 (2012). https://doi.org/10.1002/anie.201206720
56. Tong, X., Chen, S., Guo, C., Xia, X., Guo, X.Y.: Mesoporous $NiCo_2O_4$ nanoplates on three-dimensional graphene foam as an efficient electrocatalyst for the oxygen reduction reaction. ACS Appl. Mater. Interfaces **8**(42), 28274–28282 (2016). https://doi.org/10.1021/acsami.5b10044
57. Jin, Z., Nie, H., Yang, Z., Zhang, J., Liu, Z., Xu, X., Huang, S.: Metal-free selenium doped carbon nanotube/graphene networks as a synergistically improved cathode catalyst for oxygen reduction reaction. Nanoscale **4**(20), 6455–6460 (2012). https://doi.org/10.1039/c2nr31858j
58. Liu, J., Daio, T., Sasaki, K., Lyth, S.M.: Defective nitrogen-doped graphene foam: clarifying the role of nitrogen in non-precious ORR catalysts. Polym. Electrolyte Fuel Cells 14 **64**(3), 271–280 (2014). https://doi.org/10.1149/06403.0271ecst
59. Liu, J., Sasaki, K., Lyth, S.M.: Defective nitrogen-doped graphene foam: a non-precious electrocatalyst for the oxygen reduction reaction in alkaline medium. Polym. Electrolyte Fuel Cells 14 **64**(3), 1161–1172 (2014). https://doi.org/10.1149/06403.1161ecst
60. Liu, J.F., Takeshi, D., Orejon, D., Sasaki, K., Lyth, S.M.: Defective nitrogen-doped graphene foam: a metal-free, non-precious electrocatalyst for the oxygen reduction reaction in acid. J. Electrochem. Soc. **161**(4), F544–F550 (2014). https://doi.org/10.1149/2.095404jes
61. Liu, J., Takeshi, D., Sasaki, K., Lyth, S.M.: Platinum-decorated nitrogen-doped graphene foam electrocatalysts. Fuel Cells **14**(5), 728–734 (2014). https://doi.org/10.1002/fuce.201300258
62. Qin, Y., Li, J., Yuan, J., Kong, Y., Tao, Y.X., Lin, F.R., Li, S.: Hollow mesoporous carbon nitride nanosphere/three-dimensional graphene composite as high efficient electrocatalyst for oxygen reduction reaction. J. Power Sources **272**, 696–702 (2014). https://doi.org/10.1016/j.jpowsour.2014.09.017

63. Wang, L., Sofer, Z., Ambrosi, A., Simek, P., Pumera, M.: 3D-graphene for electrocatalysis of oxygen reduction reaction: Increasing number of layers increases the catalytic effect. Electrochem. Commun. **46**, 148–151 (2014). https://doi.org/10.1016/j.elecom.2014.07.002
64. Yuan, W., Li, J., Wang, L., Chen, P., Xie, A., Shen, Y.: Nanocomposite of N-doped TiO_2 nanorods and graphene as an effective electrocatalyst for the oxygen reduction reaction. ACS Appl. Mater. Interfaces **6**(24), 21978–21985 (2014). https://doi.org/10.1021/am507890h
65. Chen, R.W., Yan, J., Liu, Y., Li, J.H.: Three-dimensional nitrogen-doped graphene/MnO nanoparticle hybrids as a high-performance catalyst for oxygen reduction reaction. J. Phys. Chem. C **119**(15), 8032–8037 (2015). https://doi.org/10.1021/acs.jpcc.5b00306
66. Chen, S., Duan, J.J., Tang, Y.H., Jin, B., Qiao, S.Z.: Molybdenum sulfide clusters-nitrogen-doped graphene hybrid hydrogel film as an efficient three-dimensional hydrogen evolution electrocatalyst. Nano Energy **11**, 11–18 (2015). https://doi.org/10.1016/j.nanoen.2014.09.022
67. Cheng, J.H., Li, Y.Y., Huang, X.D., Wang, Q.Q., Mei, A., Shen, P.K.: Highly stable electrocatalysts supported on nitrogen-self-doped three-dimensional graphene-like networks with hierarchical porous structures. J. Mater. Chem. A **3**(4), 1492–1497 (2015). https://doi.org/10.1039/c4ta05552g
68. Lee, K.J., Sa, Y.J., Jeong, H.Y., Bielawski, C.W., Joo, S.H., Moon, H.R.: Simple coordination complex-derived three-dimensional mesoporous graphene as an efficient bifunctional oxygen electrocatalyst. Chem. Commun. (Camb.) **51**(31), 6773–6776 (2015). https://doi.org/10.1039/c5cc01123j
69. Liu, Y., Li, J., Li, W.Z., Li, Y.M., Chen, Q.Y., Zhan, F.Q.: Nitrogen-doped graphene aerogel-supported spinel $CoMn_2O_4$ nanoparticles as an efficient catalyst for oxygen reduction reaction. J. Power Sources **299**, 492–500 (2015). https://doi.org/10.1016/j.jpowsour.2015.09.042
70. Wang, M., Wang, J., Hou, Y., Shi, D., Wexler, D., Poynton, S.D., Slade, R.C., Zhang, W., Liu, H., Chen, J.: N-doped crumpled graphene derived from vapor phase deposition of PPy on graphene aerogel as an efficient oxygen reduction reaction electrocatalyst. ACS Appl. Mater. Interfaces **7**(13), 7066–7072 (2015). https://doi.org/10.1021/acsami.5b01025
71. Wang, Z., Cao, X., Ping, J., Wang, Y., Lin, T., Huang, X., Ma, Q., Wang, F., He, C., Zhang, H.: Electrochemical doping of three-dimensional graphene networks used as efficient electrocatalysts for oxygen reduction reaction. Nanoscale **7**(21), 9394–9398 (2015). https://doi.org/10.1039/c4nr06631f
72. Ye, D.X., Wang, L., Zhang, R., Liu, B.H., Wang, Y., Kong, J.L.: Facile preparation of N-doped mesocellular graphene foam from sludge flocs for highly efficient oxygen reduction reaction. J. Mater. Chem. A **3**(29), 15171–15176 (2015). https://doi.org/10.1039/c5ta03060a
73. Yun, S., Lee, S., Shin, C., Park, S., Kwon, S.J., Park, H.S.: One-pot self-assembled, reduced graphene oxide/palladium nanoparticle hybrid aerogels for electrocatalytic applications. Electrochim. Acta **180**, 902–908 (2015). https://doi.org/10.1016/j.electacta.2015.08.157
74. Zhou, X.J., Bai, Z.Y., Wu, M.J., Qiao, J.L., Chen, Z.W.: 3-dimensional porous N-doped graphene foam as a non-precious catalyst for the oxygen reduction reaction. J. Mater. Chem. A **3**(7), 3343–3350 (2015). https://doi.org/10.1039/c4ta06538g
75. Fu, X., Choi, J.Y., Zamani, P., Jiang, G., Hoque, M.A., Hassan, F.M., Chen, Z.: Co-N decorated hierarchically porous graphene aerogel for efficient oxygen reduction reaction in acid. ACS Appl. Mater. Interfaces **8**(10), 6488–6495 (2016). https://doi.org/10.1021/acsami.5b12746
76. Guo, W.H., Ma, X.X., Zhang, X.L., Zhang, Y.Q., Yu, D.L., He, X.Q.: Spinel $CoMn_2O_4$ nanoparticles supported on a nitrogen and phosphorus dual doped graphene aerogel as efficient electrocatalysts for the oxygen reduction reaction. RSC Adv. **6**(99), 96436–96444 (2016). https://doi.org/10.1039/c6ra16337h
77. Ma, X.X., He, X.Q.: Cobalt oxide anchored on nitrogen and sulfur dual-doped graphene foam as an effective oxygen electrode catalyst in alkaline media. Appl. Mater. Today **4**, 1–8 (2016). https://doi.org/10.1016/j.apmt.2016.04.002

78. Tang, S., Zhou, X.J., Xu, N.N., Bai, Z.Y., Qiao, J.L., Zhang, J.J.: Template-free synthesis of three-dimensional nanoporous N-doped graphene for high performance fuel cell oxygen reduction reaction in alkaline media. Appl. Energy **175**, 405–413 (2016). https://doi.org/10.1016/j.apenergy.2016.04.074
79. Wang, M., Fang, Z., Zhang, K., Fang, J., Qin, F., Zhang, Z., Li, J., Liu, Y., Lai, Y.: Synergistically enhanced activity of graphene quantum dots/graphene hydrogel composites: a novel all-carbon hybrid electrocatalyst for metal/air batteries. Nanoscale **8**(22), 11398–11402 (2016). https://doi.org/10.1039/c6nr02622b
80. Wang, M., Hou, Y., Slade, R.C., Wang, J., Shi, D., Wexler, D., Liu, H., Chen, J.: Core-shell Co/CoO integrated on 3D nitrogen doped reduced graphene oxide aerogel as an enhanced electrocatalyst for the oxygen reduction reaction. Front. Chem. **4**, 36 (2016). https://doi.org/10.3389/fchem.2016.00036
81. Wu, M., Dou, Z.Y., Chang, J.J., Cui, L.L.: Nitrogen and sulfur co-doped graphene aerogels as an efficient metal-free catalyst for oxygen reduction reaction in an alkaline solution. RSC Adv. **6**(27), 22781–22790 (2016). https://doi.org/10.1039/c5ra22136f
82. Yan, W.N., Cao, X.C., Tian, J.H., Jin, C., Ke, K., Yang, R.Z.: Nitrogen/sulfur dual-doped 3D reduced graphene oxide networks-supported $CoFe_2O_4$ with enhanced electrocatalytic activities for oxygen reduction and evolution reactions. Carbon **99**, 195–202 (2016). https://doi.org/10.1016/j.carbon.2015.12.011
83. Zhu, Z., Yang, Y., Guan, Y., Xue, J.H., Cui, L.L.: Construction of a cobalt-embedded nitrogen-doped carbon material with the desired porosity derived from the confined growth of MOFs within graphene aerogels as a superior catalyst towards HER and ORR. J. Mater. Chem. A **4**(40), 15536–15545 (2016). https://doi.org/10.1039/c6ta05196k
84. Yu, D.L., He, X.Q.: 3D cobalt-embedded nitrogen-doped graphene xerogel as an efficient electrocatalyst for oxygen reduction reaction in an alkaline medium. J. Appl. Electrochem. **47**(1), 13–23 (2017). https://doi.org/10.1007/s10800-016-1008-3
85. Han, J., Huang, G., Wang, Z., Lu, Z., Du, J., Kashani, H., Chen, M.: Low-temperature carbide-mediated growth of bicontinuous nitrogen-doped mesoporous graphene as an efficient oxygen reduction electrocatalyst. Adv. Mater. **30**(38), e1803588 (2018). https://doi.org/10.1002/adma.201803588
86. Xue, Q., Ding, Y., Xue, Y.Y., Li, F., Chen, P., Chen, Y.: 3D nitrogen-doped graphene aerogels as efficient electrocatalyst for the oxygen reduction reaction. Carbon **139**, 137–144 (2018). https://doi.org/10.1016/j.carbon.2018.06.052
87. Zhang, T., Li, Z., Wang, L., Sun, P., Zhang, Z., Wang, S.: Spinel $MnCo_2O_4$ nanoparticles supported on three-dimensional graphene with enhanced mass transfer as an efficient electrocatalyst for the oxygen reduction reaction. Chemsuschem **11**(16), 2730–2736 (2018). https://doi.org/10.1002/cssc.201801070
88. Nishi, Y.: The development of lithium ion secondary batteries. Chem. Rec. **1**(5), 406–413 (2001). https://doi.org/10.1016/S0378-7753(01)00887-4
89. Tarascon, J.M., Armand, M.: Issues and challenges facing rechargeable lithium batteries. Nature **414**(6861), 359–367 (2001). https://doi.org/10.1038/35104644
90. Scrosati, B., Garche, J.: Lithium batteries: status, prospects and future. J. Power Sources **195**(9), 2419–2430 (2010). https://doi.org/10.1016/j.jpowsour.2009.11.048
91. Chen, J.S., Lou, X.W.: SnO_2-based nanomaterials: synthesis and application in lithium-ion batteries. Small **9**(11), 1877–1893 (2013). https://doi.org/10.1002/smll.201202601
92. Goodenough, J.B., Park, K.S.: The Li-ion rechargeable battery: a perspective. J. Am. Chem. Soc. **135**(4), 1167–1176 (2013). https://doi.org/10.1021/ja3091438
93. Srivastava, M., Singh, J., Kuila, T., Layek, R.K., Kim, N.H., Lee, J.H.: Recent advances in graphene and its metal-oxide hybrid nanostructures for lithium-ion batteries. Nanoscale **7**(11), 4820–4868 (2015). https://doi.org/10.1039/c4nr07068b
94. Zhao, Y., Li, X.F., Yan, B., Li, D.J., Lawes, S., Sun, X.L.: Significant impact of 2D graphene nanosheets on large volume change tin-based anodes in lithium-ion batteries: a review. J. Power Sources **274**, 869–884 (2015). https://doi.org/10.1016/j.jpowsour.2014.10.008

95. Etacheri, V., Marom, R., Elazari, R., Salitra, G., Aurbach, D.: Challenges in the development of advanced Li-ion batteries: a review. Energy Environ. Sci. **4**(9), 3243–3262 (2011). https://doi.org/10.1039/c1ee01598b
96. Ji, L.W., Lin, Z., Alcoutlabi, M., Zhang, X.W.: Recent developments in nanostructured anode materials for rechargeable lithium-ion batteries. Energy Environ. Sci. **4**(8), 2682–2699 (2011). https://doi.org/10.1039/c0ee00699h
97. Zhang, W.J.: A review of the electrochemical performance of alloy anodes for lithium-ion batteries. J. Power Sources **196**(1), 13–24 (2011). https://doi.org/10.1016/j.jpowsour.2010.07.020
98. Hu, M., Pang, X.L., Zhou, Z.: Recent progress in high-voltage lithium ion batteries. J. Power Sources **237**, 229–242 (2013). https://doi.org/10.1016/j.jpowsour.2013.03.024
99. Reddy, M.V., Subba Rao, G.V., Chowdari, B.V.: Metal oxides and oxysalts as anode materials for Li ion batteries. Chem. Rev. **113**(7), 5364–5457 (2013). https://doi.org/10.1021/cr3001884
100. Goriparti, S., Miele, E., De Angelis, F., Di Fabrizio, E., Zaccaria, R.P., Capiglia, C.: Review on recent progress of nanostructured anode materials for Li-ion batteries. J. Power Sources **257**, 421–443 (2014). https://doi.org/10.1016/j.jpowsour.2013.11.103
101. Zhou, X., Wan, L.J., Guo, Y.G.: Binding SnO_2 nanocrystals in nitrogen-doped graphene sheets as anode materials for lithium-ion batteries. Adv. Mater. **25**(15), 2152–2157 (2013). https://doi.org/10.1002/adma.201300071
102. Kucinskis, G., Bajars, G., Kleperis, J.: Graphene in lithium ion battery cathode materials: a review. J. Power Sources **240**, 66–79 (2013). https://doi.org/10.1016/j.jpowsour.2013.03.160
103. Ma, D., Cao, Z., Hu, A.: Si-based anode materials for Li-ion batteries: a mini review. Nanomicro Lett. **6**(4), 347–358 (2014). https://doi.org/10.1007/s40820-014-0008-2
104. Tucek, J., Kemp, K.C., Kim, K.S., Zboril, R.: Iron-oxide-supported nanocarbon in lithium-ion batteries, medical, catalytic, and environmental applications. ACS Nano **8**(8), 7571–7612 (2014). https://doi.org/10.1021/nn501836x
105. Choi, N.S., Chen, Z., Freunberger, S.A., Ji, X., Sun, Y.K., Amine, K., Yushin, G., Nazar, L.F., Cho, J., Bruce, P.G.: Challenges facing lithium batteries and electrical double-layer capacitors. Angew. Chem. Int. Ed. Engl. **51**(40), 9994–10024 (2012). https://doi.org/10.1002/anie.201201429
106. Xin, S., Guo, Y.G., Wan, L.J.: Nanocarbon networks for advanced rechargeable lithium batteries. Acc. Chem. Res. **45**(10), 1759–1769 (2012). https://doi.org/10.1021/ar300094m
107. Han, S., Wu, D., Li, S., Zhang, F., Feng, X.: Graphene: a two-dimensional platform for lithium storage. Small **9**(8), 1173–1187 (2013). https://doi.org/10.1002/smll.201203155
108. Pumera, M.: Graphene-based nanomaterials for energy storage. Energy Environ. Sci. **4**(3), 668–674 (2011). https://doi.org/10.1039/c0ee00295j
109. Sun, Y.Q., Wu, Q.O., Shi, G.Q.: Graphene based new energy materials. Energy Environ. Sci. **4**(4), 1113–1132 (2011). https://doi.org/10.1039/c0ee00683a
110. Brownson, D.A.C., Kampouris, D.K., Banks, C.E.: An overview of graphene in energy production and storage applications. J. Power Sources **196**(11), 4873–4885 (2011). https://doi.org/10.1016/j.jpowsour.2011.02.022
111. Guo, S., Dong, S.: Graphene nanosheet: synthesis, molecular engineering, thin film, hybrids, and energy and analytical applications. Chem. Soc. Rev. **40**(5), 2644–2672 (2011). https://doi.org/10.1039/c0cs00079e
112. Xu, C.H., Xu, B.H., Gu, Y., Xiong, Z.G., Sun, J., Zhao, X.S.: Graphene-based electrodes for electrochemical energy storage. Energy Environ. Sci. **6**(5), 1388–1414 (2013). https://doi.org/10.1039/c3ee23870a
113. Bonaccorso, F., Colombo, L., Yu, G., Stoller, M., Tozzini, V., Ferrari, A.C., Ruoff, R.S., Pellegrini, V.: 2D materials. Graphene, related two-dimensional crystals, and hybrid systems for energy conversion and storage. Science **347**(6217), 1246501 (2015). https://doi.org/10.1126/science.1246501

114. Raccichini, R., Varzi, A., Passerini, S., Scrosati, B.: The role of graphene for electrochemical energy storage. Nat. Mater. **14**(3), 271–279 (2015). https://doi.org/10.1038/nmat4170
115. Wang, X.L., Shi, G.Q.: Flexible graphene devices related to energy conversion and storage. Energy Environ. Sci. **8**(3), 790–823 (2015). https://doi.org/10.1039/c4ee03685a
116. Raccichini, R., Varzi, A., Wei, D., Passerini, S.: Critical insight into the relentless progression toward graphene and graphene-containing materials for lithium-ion battery anodes. Adv. Mater. **29**(11), 1603421-n/a (2017). https://doi.org/10.1002/adma.201603421
117. Sun, Y., Tang, J., Zhang, K., Yuan, J., Li, J., Zhu, D.M., Ozawa, K., Qin, L.C.: Comparison of reduction products from graphite oxide and graphene oxide for anode applications in lithium-ion batteries and sodium-ion batteries. Nanoscale **9**(7), 2585–2595 (2017). https://doi.org/10.1039/c6nr07650e
118. Xia, X.H., Chao, D.L., Zhang, Y.Q., Shen, Z.X., Fan, H.J.: Three-dimensional graphene and their integrated electrodes. Nano Today **9**(6), 785–807 (2014). https://doi.org/10.1016/j.nantod.2014.12.001
119. Zai, J.T., Qian, X.F.: Three dimensional metal oxides-graphene composites and their applications in lithium ion batteries. RSC Adv. **5**(12), 8814–8834 (2015). https://doi.org/10.1039/c4ra11903g
120. Cao, X., Shi, Y., Shi, W., Rui, X., Yan, Q., Kong, J., Zhang, H.: Preparation of MoS_2-coated three-dimensional graphene networks for high-performance anode material in lithium-ion batteries. Small **9**(20), 3433–3438 (2013). https://doi.org/10.1002/smll.201202697
121. Gong, Y., Yang, S., Liu, Z., Ma, L., Vajtai, R., Ajayan, P.M.: Graphene-network-backboned architectures for high-performance lithium storage. Adv. Mater. **25**(29), 3979–3984 (2013). https://doi.org/10.1002/adma.201301051
122. Jiang, X., Yang, X.L., Zhu, Y.H., Shen, J.H., Fan, K.C., Li, C.Z.: In situ assembly of graphene sheets-supported SnS_2 nanoplates into 3D macroporous aerogels for high-performance lithium ion batteries. J. Power Sources **237**, 178–186 (2013). https://doi.org/10.1016/j.jpowsour.2013.03.048
123. Luo, J., Liu, J., Zeng, Z., Ng, C.F., Ma, L., Zhang, H., Lin, J., Shen, Z., Fan, H.J.: Three-dimensional graphene foam supported Fe_3O_4 lithium battery anodes with long cycle life and high rate capability. Nano Lett. **13**(12), 6136–6143 (2013). https://doi.org/10.1021/nl403461n
124. Xiao, L., Wu, D., Han, S., Huang, Y., Li, S., He, M., Zhang, F., Feng, X.: Self-assembled Fe_2O_3/graphene aerogel with high lithium storage performance. ACS Appl. Mater. Interfaces **5**(9), 3764–3769 (2013). https://doi.org/10.1021/am400387t
125. Choi, S.H., Kang, Y.C.: Fe_3O_4-decorated hollow graphene balls prepared by spray pyrolysis process for ultrafast and long cycle-life lithium ion batteries. Carbon **79**, 58–66 (2014). https://doi.org/10.1016/j.carbon.2014.07.042
126. Jiang, Y., Jiang, Z.J., Cheng, S., Liu, M.L.: Fabrication of 3-dimensional porous graphene materials for lithium ion batteries. Electrochim. Acta **146**, 437–446 (2014). https://doi.org/10.1016/j.electacta.2014.09.059
127. Qin, J., He, C., Zhao, N., Wang, Z., Shi, C., Liu, E.Z., Li, J.: Graphene networks anchored with sn@graphene as lithium ion battery anode. ACS Nano **8**(2), 1728–1738 (2014). https://doi.org/10.1021/nn406105n
128. Qiu, B., Xing, M., Zhang, J.: Mesoporous TiO_2 nanocrystals grown in situ on graphene aerogels for high photocatalysis and lithium-ion batteries. J. Am. Chem. Soc. **136**(16), 5852–5855 (2014). https://doi.org/10.1021/ja500873u
129. Wang, R., Xu, C., Sun, J., Gao, L.: Three-dimensional Fe_2O_3 nanocubes/nitrogen-doped graphene aerogels: nucleation mechanism and lithium storage properties. Sci. Rep. **4**, 7171 (2014). https://doi.org/10.1038/srep07171
130. Wang, R., Xu, C., Sun, J., Gao, L., Yao, H.: Solvothermal-induced 3D macroscopic SnO_2/nitrogen-doped graphene aerogels for high capacity and long-life lithium storage. ACS Appl. Mater. Interfaces **6**(5), 3427–3436 (2014). https://doi.org/10.1021/am405557c

131. Deng, J.W., Chen, L.F., Sun, Y.Y., Ma, M.H., Fu, L.: Interconnected MnO_2 nanoflakes assembled on graphene foam as a binder-free and long-cycle life lithium battery anode. Carbon **92**, 177–184 (2015). https://doi.org/10.1016/j.carbon.2015.04.021
132. Ren, Z.M., Yu, S.Q., Fu, X.X., Shi, L., Sun, C.X., Fan, C.Y., Liu, Q., Qian, G.D., Wang, Z. Y.: Coordination-driven self-assembly: construction of a Fe_3O_4-graphene hybrid 3D framework and its long cycle lifetime for lithium-ion batteries. RSC Adv. **5**(50), 40249–40257 (2015). https://doi.org/10.1039/c5ra04837k
133. Sui, Z.-Y., Wang, C., Shu, K., Yang, Q.-S., Ge, Y., Wallace, G.G., Han, B.-H.: Manganese dioxide-anchored three-dimensional nitrogen-doped graphene hybrid aerogels as excellent anode materials for lithium ion batteries. J. Mater. Chem. A **3**(19), 10403–10412 (2015). https://doi.org/10.1039/C5TA01508A
134. Tang, H., Sui, Y., Zhu, X., Bao, Z.: Synthesis of Mn_3O_4-based aerogels and their lithium-storage abilities. Nanoscale Res. Lett. **10**(1), 960 (2015). https://doi.org/10.1186/s11671-015-0960-x
135. Ye, J.C., Charnvanichborikarn, S., Worsley, M.A., Kucheyev, S.O., Wood, B.C., Wang, Y. M.: Enhanced electrochemical performance of ion-beam-treated 3D graphene aerogels for lithium ion batteries. Carbon **85**, 269–278 (2015). https://doi.org/10.1016/j.carbon.2014.12.097
136. Wang, Y., Jin, Y., Zhao, C., Pan, E., Jia, M.: 1D ultrafine SnO_2 nanorods anchored on 3D graphene aerogels with hierarchical porous structures for high-performance lithium/sodium storage. J. Colloid Interface Sci. **532**, 352–362 (2018). https://doi.org/10.1016/j.jcis.2018.08.011
137. Zhao, B., Wang, Z., Chen, F., Yang, Y., Gao, Y., Chen, L., Jiao, Z., Cheng, L., Jiang, Y.: Three-dimensional interconnected spherical graphene framework/SnS nanocomposite for anode material with superior lithium storage performance: complete reversibility of Li_2S. ACS Appl. Mater. Interfaces **9**(2), 1407–1415 (2017). https://doi.org/10.1021/acsami.6b10708
138. Zhang, Y., Chen, P., Gao, X., Wang, B., Liu, H., Wu, H., Liu, H., Dou, S.: Nitrogen-doped graphene ribbon assembled core-sheath MnO@Graphene scrolls as hierarchically ordered 3D porous electrodes for fast and durable lithium storage. Adv. Funct. Mater. **26**(43), 7754–7765 (2016). https://doi.org/10.1002/adfm.201603716
139. Zhang, X., Zhang, Q.W., Sun, Y.F., Zhang, P.Y., Gao, X., Zhang, W., Guo, J.X.: MoS_2-graphene hybrid nanosheets constructed 3D architectures with improved electrochemical performance for lithium-ion batteries and hydrogen evolution. Electrochim. Acta **189**, 224–230 (2016). https://doi.org/10.1016/j.electacta.2015.12.082
140. Zhang, C., Yu, J.S.: Morphology-tuned synthesis of $NiCo_2O_4$-coated 3D graphene architectures used as binder-free electrodes for lithium-ion batteries. Chemistry **22**(13), 4422–4430 (2016). https://doi.org/10.1002/chem.201504386
141. Yu, H., Ye, D., Butburee, T., Wang, L., Dargusch, M.: Green synthesis of porous three-dimensional nitrogen-doped graphene foam for electrochemical applications. ACS Appl. Mater. Interfaces **8**(4), 2505–2510 (2016). https://doi.org/10.1021/acsami.5b09030
142. Luo, B., Qiu, T.F., Hao, L., Wang, B., Jin, M.H., Li, X.L., Zhi, L.J.: Graphene-templated formation of 3D tin-based foams for lithium ion storage applications with a long lifespan. J. Mater. Chem. A **4**(2), 362–367 (2016). https://doi.org/10.1039/c5ta08508j
143. Liu, Y., Wang, X., Wan, W., Li, L., Dong, Y., Zhao, Z., Qiu, J.: Multifunctional nitrogen-doped graphene nanoribbon aerogels for superior lithium storage and cell culture. Nanoscale **8**(4), 2159–2167 (2016). https://doi.org/10.1039/c5nr05909g
144. Liu, L., Yang, X., Lv, C., Zhu, A., Zhu, X., Guo, S., Chen, C., Yang, D.: Seaweed-derived route to Fe_2O_3 hollow nanoparticles/N-doped graphene aerogels with high lithium ion storage performance. ACS Appl. Mater. Interfaces **8**(11), 7047–7053 (2016). https://doi.org/10.1021/acsami.5b12427

145. Jiang, L., Lin, B., Li, X., Song, X., Xia, H., Li, L., Zeng, H.: Monolayer MoS_2-graphene hybrid aerogels with controllable porosity for lithium-ion batteries with high reversible capacity. ACS Appl. Mater. Interfaces **8**(4), 2680–2687 (2016). https://doi.org/10.1021/acsami.5b10692
146. He, J.R., Li, P.J., Lv, W.Q., Wen, K.C., Chen, Y.F., Zhang, W.L., Li, Y.R., Qin, W., He, W. D.: Three-dimensional hierarchically structured aerogels constructed with layered MoS_2/graphene nanosheets as free-standing anodes for high-performance lithium ion batteries. Electrochim. Acta **215**, 12–18 (2016). https://doi.org/10.1016/j.electacta.2016.08.068
147. He, D., Li, L., Bai, F., Zha, C., Shen, L., Kung, H.H., Bao, N.: One-pot synthesis of pomegranate-structured Fe_3O_4/carbon nanospheres-doped graphene aerogel for high-rate lithium ion batteries. Chemistry **22**(13), 4454–4459 (2016). https://doi.org/10.1002/chem.201504429
148. Gu, X.Y., Wu, F.L., Lei, B.B., Wang, J., Chen, Z.L., Xie, K., Song, Y., Sun, D.L., Sun, L. X., Zhou, H.Y., Fang, F.: Three-dimensional nitrogen-doped graphene frameworks anchored with bamboo-like tungsten oxide nanorods as high performance anode materials for lithium ion batteries. J. Power Sources **320**, 231–238 (2016). https://doi.org/10.1016/j.jpowsour.2016.04.103
149. Bai, D., Wang, F., Lv, J., Zhang, F., Xu, S.: Triple-confined well-dispersed biactive $NiCo_2S_4$/$Ni_{0.96}S$ on graphene aerogel for high-efficiency lithium storage. ACS Appl. Mater. Interfaces **8**(48), 32853–32861 (2016). https://doi.org/10.1021/acsami.6b11389
150. Zhang, W., Zhu, J., Ang, H., Zeng, Y., Xiao, N., Gao, Y., Liu, W., Hng, H.H., Yan, Q.: Binder-free graphene foams for O_2 electrodes of Li-O_2 batteries. Nanoscale **5**(20), 9651–9658 (2013). https://doi.org/10.1039/c3nr03321j
151. Ye, S., Feng, J., Wu, P.: Deposition of three-dimensional graphene aerogel on nickel foam as a binder-free supercapacitor electrode. ACS Appl. Mater. Interfaces **5**(15), 7122–7129 (2013). https://doi.org/10.1021/am401458x
152. Tang, Y.F., Huang, F.Q., Bi, H., Liu, Z.Q., Wan, D.Y.: Highly conductive three-dimensional graphene for enhancing the rate performance of $LiFePO_4$ cathode. J. Power Sources **203**, 130–134 (2012). https://doi.org/10.1016/j.jpowsour.2011.12.011

Enhanced Electrocatalytic Activity and Durability of PtRu Nanoparticles Decorated on rGO Material for Ethanol Oxidation Reaction

Esra Kuyuldar, Hakan Burhan, Aysun Şavk, Buse Güven, Ceren Özdemir, Sultan Şahin, Anish Khan and Fatih Şen

Abstract Direct ethanol fuel cells (DEFCs) use ethanol as a fuel to obtain energy in a low temperature. This makes them one of the most important among fuel cells. However, in order to increase the efficiency of these fuel cells, highly effective catalysts should be developed. These catalysts may be of a wide variety of nanoparticles like platinum-based nanoparticles as a most efficient fuel cell catalyst. Generally, the nanoparticles related to the catalyst are obtained using functionalized carbon derivatives. The catalyst obtained in this study shows a higher electrocatalyst activity than the Pt and demonstrates excellent electrocatalytic performance for ethanol oxidation reaction. In this chapter, the reduced graphene oxide was used as a support and a composite material was obtained by synthesizing platinum–ruthenium nanoparticles (PtRu@rGO) with the help of chemical reduction method. The resultant PtRu@rGO nanoparticles were characterized by X-ray diffraction (XRD), transmission electron microscopy (TEM), X-ray photoelectron spectroscopy (XPS), and Raman spectroscopy. The electrochemical activity of the catalyst was determined using chronoamperometry (CA) and cyclic voltammetry (CV) techniques for ethanol oxidation reaction. The results showed that the prepared nanocomposite has a high catalytic activity for alcohol oxidation reaction.

Keywords Direct ethanol fuel cells · PtRu@rGO · Nanocatalyst · Ethanol oxidation

E. Kuyuldar · H. Burhan · A. Şavk · B. Güven · C. Özdemir · S. Şahin · F. Şen (✉)
Biochemistry Department, Sen Research Group, Dumlupinar University,
43100 Kütahya, Turkey
e-mail: fatihsen1980@gmail.com

A. Khan
Chemistry Department, Faculty of Science, King Abdulaziz University,
P.O. Box 80203, Jeddah 21589, Saudi Arabia

A. Khan
Center of Excellence for Advanced Materials Research,
King Abdulaziz University, P.O. Box 80203, Jeddah 21589, Saudi Arabia

A. Khan et al. (eds.), *Graphene Functionalization Strategies*,
Carbon Nanostructures, https://doi.org/10.1007/978-981-32-9057-0_16

1 Introduction

In order to solve the problems related to the global warming and environmental pollution, scientists are now focusing on the development of renewable energy resources that can be an alternative to fossil fuels. With the increase in environmental problems, it has become imperative to develop renewable, clean, and environmentally friendly energy resources with low carbon dioxide emissions [1–47]. Energy production from natural resources in the 21st century is an important problem [12]. Hydrogen gas is known as an environmentally friendly, toxic substance-free gas that can carry plenty of energy. However, it is still difficult to store this gas safely and efficiently [12]. The main reason for this is the long-term economic disadvantages of hydrogen storage [32]. The interest in this energy has become a serious necessity by experiencing climatic changes. For this reason, some of the alternative energy sources have been searching to be able to get a clean energy. Fuel cells are one of the most important energy sources for these types of applications. Among the types of fuel cells, direct Alcohol fuel cells are one of the most important ones. For instance, alcohol can be considered as a convenient liquids fuel in terms of easy transportability and volumetric density [27]. The aim of direct alcohol fuel cells that can be defined as electrochemical devices is to convert the chemical energy stored in liquid alcohol into electrical energy [46]. This energy transformation is also a potential solution to current problems [27]. Methanol (MeOH), ethanol (EtOH), ethylene glycol (EgOH), glycerol (GlOH), 1-propanol, 2-propanol, and butanol are also liquid alcohols that are conceivable for alcohol fuel cells [25, 46]. Direct alcohol fuel cells can be used in mobile sensors, laptops, and other electronic devices in addition to being used as alcohol sensors [19, 46]. Additionally, if we examine the structure of the alcohol fuel cells, we usually see the anode, cathode, and ion exchange membrane [41]. Generally, ethanol with high energy density has become one of the most important renewable energy sources with its easy transportation and reliability [3]. At the same time, low cost, easy handling and low toxicity have made ethanol the most attractive alternative to electrochemical batteries and fossil fuel based engines [22, 38]. However, in order to increase the efficiency of these fuel cells, highly effective catalysts should be developed. These catalysts may be of a wide variety of nanoparticles like platinum-based nanoparticles as a most efficient fuel cell catalyst. The reason why Platin is a promising catalyst is its positive catalytic properties and high electrochemical stability. The formation of platinum-based alloys has become a very important factor to increase these properties and to change the electronic structure of the platinum. The reports have proved the positive effects of platinum on some other metals (Co, Ni, Cu, Fe etc.). However, even small amounts of positive catalytic effects caused by platinum increase orientation [5, 39]. This orientation results from the use of homogeneously dispersed platinum-containing nanoparticles [1, 4, 6, 8, 9, 15, 17, 30, 43, 47] directly in alcohol fuel cells because it has a large specific surface area and a more active center [16]. A strong effort has been made to strengthen the catalytic performance of platinum-based nanocatalysts. The metal or

metal oxide-containing design of these platinum nanocatalysts is thought to be a means for influencing the catalytic performance of the anode catalysts. Platinum nanocatalyst has been developed with effectively improved catalytic performance of platinum nanocatalysts with alkali metals, such as Mo, Ir, Ag, Mn, V, Rh, and Pb [21]. For this aim, in this study, we have prepared reduced graphene oxide supported Pt–Ru nanoparticles (PtRu@rGO) in a simple way and characterized by several techniques such as XRD, XPS, TEM, Raman etc. The characterized nanoparticles have been performed for ethanol oxidation reaction with the help of electrochemical techniques such as CV (cyclic voltammetry) and CA (chronoamperometry).

2 Materials and Methods

2.1 The Synthesis of Pt@rGO and PtRu@rGO NPs

For the synthesis of the novel PtRu@rGO nanocatalyst; 30 mg of reduced graphene oxide (rGO) was added to 30 mL of distilled water and stirred for 1 h. After mixing of them, 2 mL (0.01 M) of $PtCl_4$ and $RuCl_3$ salts were added to the mixture and the resulting mixture was allowed to stir for another 30 min. DMAB (148 mg) was then added to reduce and then allowed to mix in an ultrasonic bath. After that, reflux was carried out at 90 °C for 12 h to obtain PtRu@rGO nanocatalyst. This nanocatalyst was washed with a pure water-ethanol mixture and allowed to dry under vacuum. Pt@rGO catalyst were also prepared by the same way for the comparison of the catalysts.

3 Results and Discussion

Pt@rGO and PtRu@rGO nanoparticles were prepared by the chemical reduction method as shown in materials and method section. The characterization of the prepared new nanocatalyst was carried out using spectroscopic techniques, such as Transmission Electron Microscope (TEM), X-ray Diffraction (XRD), Raman Spectroscopy, and X-ray Photoelectron Spectroscopy (XPS). The surface morphologies and structures of Pt@rGO and PtRu@rGO nanocomposites were characterized using TEM and High-Resolution TEM (HRTEM). Pt and PtRu nanoparticles were homogenously distributed over the rGO support material. In the HRTEM analysis, the mean size of PtRu@rGO nanoparticles was found to be 3.98 nm.

The crystal structure of the prepared catalysts was also analyzed by using XRD, and typical peaks are shown in Fig. 1a. The XRD peaks at about 2Θ = 39.930, 46.800, 67.920, 81.400, and 86.250 that are related to the PtRu (111), (200), (220), (311), and (222) planes. There is a small shift to higher 2 theta values compared to the

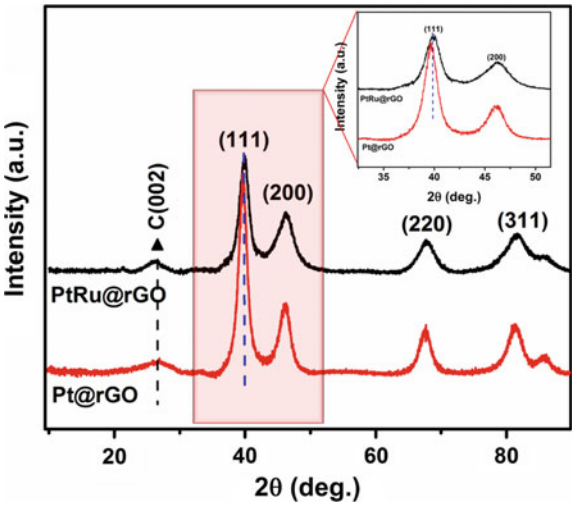

Fig. 1 XRD pattern of as-prepared Pt@rGO and PtRu@rGO catalyst

monometallic Pt nanoparticles which confirm the alloy formation in PtRu nanoparticles. These characteristic diffraction peaks show that PtRu nanoparticles have a face-centered cubic structure. Furthermore, the Scherrer Formula was used to calculate the PtRu particle size [20, 44, 45]. The average particle size for PtRu@rGO was found to be 3.87 nm, which is in good agreement with TEM results.

Raman spectroscopy is also a powerful and effective technique to understand the structural properties, composition, sequential, and irregular carbon structure of carbonaceous materials [2, 11, 24, 26]. Raman spectroscopic analysis for rGO and PtRu@rGO was performed as shown in Fig. 2. According to the obtained Raman spectrum, rGO and PtRu@rGO exhibit two distinct scattering peaks at 1350 and

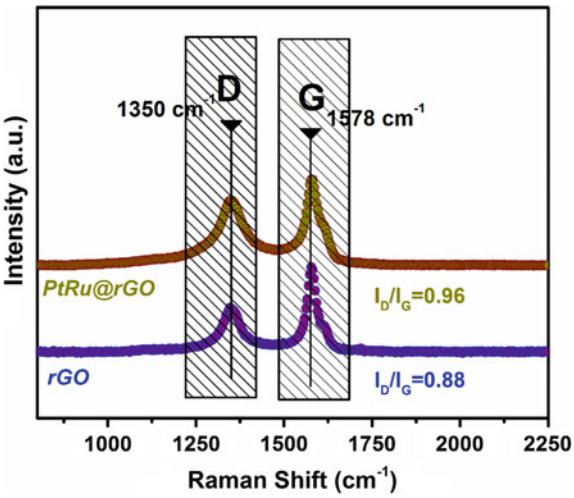

Fig. 2 Raman analysis of prepared materials

1578 cm^{-1}, corresponding to the D band and G band. The ratio of the group D and the G band for rGO and PtRu@rGO were found to be 0.88 and 0.96, respectively. The increasing D/G band ratio shows the functionalization of rGO with prepared nanomaterials [18, 31].

X-ray photoelectron spectroscopy (XPS) was also used to investigate the oxidation state of metals in prepared catalyst. For this aim, the Pt 4*f* region of the prepared catalysts were examined in detail [23, 40]. In these measurements, the Shirley shaped background analysis and the Gaussian-Lorentzian method were used in order to analyze the spectrum. In these spectrum, Pt 4*f* and Ru 3*p* regions were examined in detail and it was seen that Platinum and Ruthenium are mostly in zero oxidation state in prepared nanomaterials as shown in our previous publications [13, 14, 28, 34, 36]. However, there are also some unreduced and/or oxidized species such as Pt (II), Pt (IV), Ru (IV) etc. in prepared materials as shown in Fig. 3 [7, 29, 33, 35].

After fully characterization of prepared nanomaterials, the electrocatalytic activity of the prepared catalysts showing ethanol oxidation is indicated in Fig. 4 (in 0.5 M sulfuric acid solution saturated with nitrogen gas containing 0.5 M ethanol). Two different oxidation peaks were observed in two-way potential scans, both forward and reverse. The main oxidation peak of ethanol in PtRu@rGO is about −0.30 V in forward scanning and, the peak current density in the same potential is 20 mA. The oxidation current on PtRu@ rGO decreased significantly at about −0.20 V due to the formation of Pt oxides. Because of the removal of oxidized carbonaceous species formed during further screening electro-oxidation; the main oxidation peak in reverse scans is about -0.50 V. When the electrocatalytic performances of the prepared catalysts were compared, it was observed that PtRu@rGO was approximately 1.53 times more active than Pt@rGO. As a result of this observation; with the presence of more active sites with second metal and rGO

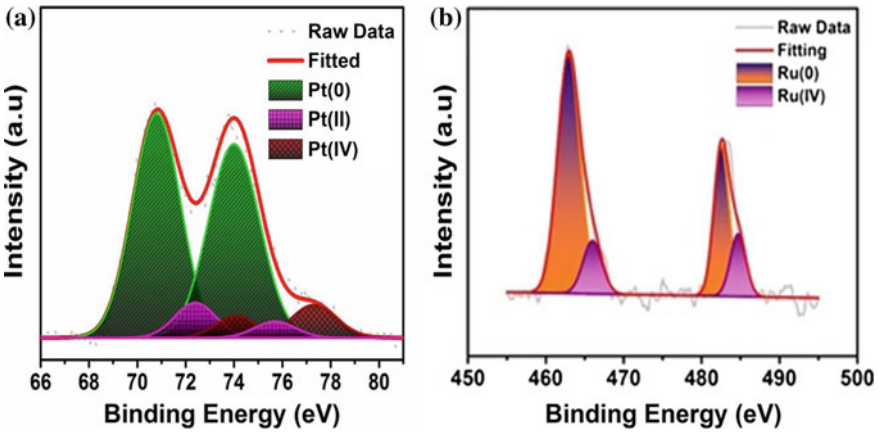

Fig. 3 **a** X-ray photoelectron spectra of Pt 4*f*; **b** Ru 3*p* spectrum in prepared nanomaterials

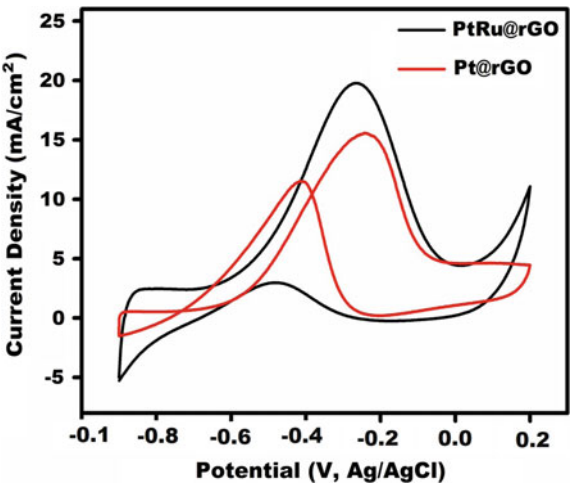

Fig. 4 Cyclic voltammograms of PtRu@rGO and Pt@rGO in nitrogen saturated solution of 0.5 M KOH containing 0.5 M C_2H_5OH (Scan rate = 50 mV s^{-1})

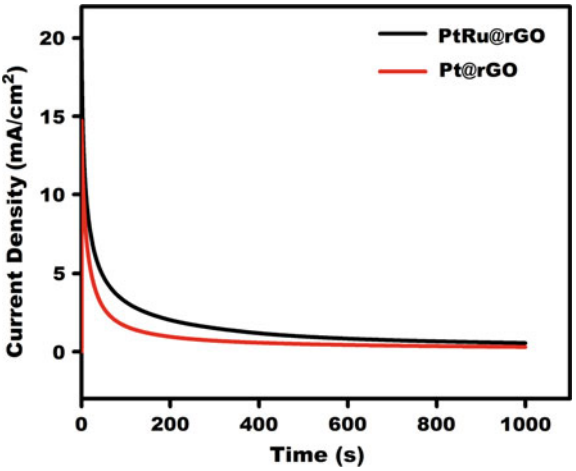

Fig. 5 Chronoamperometric curves of PtRu@rGO and Pt@rGO, in nitrogen saturated solution of 0.5 M KOH containing 0.5 M C_2H_5OH at −0.30 V

composites and with the help of these active sites, more alcohol adsorbability on the surface of PtRu@rGO catalyst is observed for ethanol oxidation.

According to the results, it was determined that PtRu@rGO showed high efficiency in alcohol oxidation reaction. We have also checked the stability of the prepared materials with the help of chronoamperometry techniques. For this reason, After obtaining the highest anodic peak potential, chronoamperometry (CA) was used for the stability tests of prepared catalysts, and the currents between the 1st and 1000th cycles were compared for the long-term stability test by cyclic voltammetry (Fig. 5). It was investigated that there was sudden drop in the activity and stability of the prepared structures due to the accumulation of the carbonaceous structures on the surface of the electrode. However, the use of the second metal prevented the

poisoning on the surface of the metal in the ethanol oxidation reaction, and the resulting catalytic activity of bimetallic nanomaterial was higher than the individual metal-carbon catalysts.

4 Conclusions

In summary, Pt and PtRu based catalysts were synthesized by a facile and efficient method in the presence of GO. A combination of sonochemical and chemical reduction methods were used during synthesis as an environmentally friendly methodology. PtRu@GO exhibits outstanding performance as catalysts for the electrooxidation of ethanol as compared to Pt@GO. The reason for this is the high active surface areas, because it contains high amount of Pt (0) compared to the other one. In addition to providing a large surface area, the synergistic effect of second metal has significantly increased the catalytic activity. Since the method is easy and controllable, it can be seen as a highly efficient way to prepare new nanocatalysts with high catalytic activity, and various applications can be performed directly using these types of catalysts synthesized by this method.

References

1. Aday, B., Pamuk, H., Kaya, M., Sen, F.: Graphene oxide as highly effective and readily recyclable catalyst using for the one-pot synthesis of 1,8-dioxoacridine derivatives. J. Nanosci. Nanotechnol. **16**, 6498–6504 (2016). https://doi.org/10.1166/jnn.2016.12432
2. Akhairi, M.A.F., Kamarudin, S.K.: Catalysts in direct ethanol fuel cell (DEFC): an overview. Int. J. Hydrogen Energy **41**, 4214–4228 (2016)
3. Altarawneh, R.M., Brueckner, T.M., Chen, B., Pickup, P.G.: Product distributions and efficiencies for ethanol oxidation at PtNi octahedra. J. Power Sources **400**, 369–376 (2018). https://doi.org/10.1016/j.jpowsour.2018.08.052
4. Ayranci, R., Başkaya, G., Güzel, M., Bozkurt, S., Şen, F., Ak, M.: Carbon based nanomaterials for high performance optoelectrochemical systems. ChemistrySelect **2**, 1548–1555 (2017). https://doi.org/10.1002/slct.201601632
5. Bo, Z., Hu, D., Kong, J., Yan, J., Cen, K.: Performance of vertically oriented graphene supported platinum-ruthenium bimetallic catalyst for methanol oxidation. J. Power Sources **273**, 530–537 (2015). https://doi.org/10.1016/j.jpowsour.2014.09.125
6. Çelik, B., Kuzu, S., Erken, E., Sert, H., Koşkun, Y., Şen, F.: Nearly monodisperse carbon nanotube furnished nanocatalysts as highly efficient and reusable catalyst for dehydrocoupling of DMAB and C_1 to C_3 alcohol oxidation. Int. J. Hydrogen Energy **41**, 3093–3101 (2016). https://doi.org/10.1016/j.ijhydene.2015.12.138
7. Daşdelen, Z., Yıldız, Y., Eriş, S., Şen, F.: Enhanced electrocatalytic activity and durability of Pt nanoparticles decorated on GO-PVP hybride material for methanol oxidation reaction. Appl. Catal. B Environ. **219**, 511–516 (2017). https://doi.org/10.1016/j.apcatb.2017.08.014
8. Demir, E., Savk, A., Sen, B., Sen, F.: A novel monodisperse metal nanoparticles anchored graphene oxide as counter electrode for dye-sensitized solar cells. Nano-Struct. Nano-Objects **12**, 41–45 (2017). https://doi.org/10.1016/j.nanoso.2017.08.018

9. Demirci, T., Çelik, B., Yildiz, Y., Eriş, S., Arslan, M., Sen, F., Kilbas, B.: One-pot synthesis of Hantzsch dihydropyridines using a highly efficient and stable PdRuNi@GO catalyst. RSC Adv. (2016). https://doi.org/10.1039/c6ra13142e
10. Dong, L., Gari, R.R.S., Li, Z., Craig, M.M., Hou, S.: Graphene-supported platinum and platinum-ruthenium nanoparticles with high electrocatalytic activity for methanol and ethanol oxidation. Carbon **48**, 781–787 (2010). https://doi.org/10.1016/j.carbon.2009.10.027
11. Dresselhaus, M.S., Jorio, A., Saito, R.: Characterizing graphene, graphite, and carbon nanotubes by Raman spectroscopy. Annu. Rev. Condens. Matter Phys. **1**, 89–108 (2010). https://doi.org/10.1146/annurev-conmatphys-070909-103919
12. Eris, S., Daşdelen, Z., Sen, F.: Enhanced electrocatalytic activity and stability of monodisperse Pt nanocomposites for direct methanol fuel cells. J. Colloid Interface Sci. **513**, 767–773 (2018). https://doi.org/10.1016/j.jcis.2017.11.085
13. Eris, S., Daşdelen, Z., Yıldız, Y., Sen, F.: Nanostructured polyaniline-rGO decorated platinum catalyst with enhanced activity and durability for methanol oxidation. Int. J. Hydrogen Energy **43**, 1337–1343 (2018). https://doi.org/10.1016/j.ijhydene.2017.11.051
14. Ertan, S., Şen, F., Şen, S., Gökağaç, G.: Platinum nanocatalysts prepared with different surfactants for C_1–C_3 alcohol oxidations and their surface morphologies by AFM. J Nanopart. Res. (2012). https://doi.org/10.1007/s11051-012-0922-5
15. Esirden, I., Erken, E., Kaya, M., Sen, F.: Monodisperse Pt NPs@rGO as highly efficient and reusable heterogeneous catalysts for the synthesis of 5-substituted 1H-tetrazole derivatives. Catal. Sci. Technol. (2015). https://doi.org/10.1039/c5cy00864f
16. Galal, A., Atta, N.F., Hassan, H.K.: Graphene supported-Pt-M (M=Ru or Pd) for electrocatalytic methanol oxidation. Int. J. Electrochem. Sci. **7**, 768–784 (2012)
17. Gökağaç, G., Yildirim, L.T., Sonsuz, M., Şen, F.: Spectroscopic, magnetic and crystal structure analysis of diammine-bis(2,6-dibromo-4-chlorophenolato-O)copper(II). *Zeitschrift für Naturforschung B*, J Chem Sci **60**(5), 543–547 (2005)
18. Goksu, H., Yildiz, Y., Çelik, B., Yazici, M., Kilbas, B., Sen, F.: Eco-friendly hydrogenation of aromatic aldehyde compounds by tandem dehydrogenation of dimethylamine-borane in the presence of a reduced graphene oxide furnished platinum nanocatalyst. Catal. Sci. Technol. (2016). https://doi.org/10.1039/c5cy01462j
19. Jurzinsky, T., Cremers, C., Jung, F., Pinkwart, K., Tübke, J.: Development of materials for anion-exchange membrane direct alcohol fuel cells. Int. J. Hydrogen Energy **40**, 11569–11576 (2015)
20. Karatepe, Ö., Yıldız, Y., Pamuk, H., Eris, S., Dasdelen, Z., Sen, F.: Enhanced electrocatalytic activity and durability of highly monodisperse Pt@PPy–PANI nanocomposites as a novel catalyst for the electro-oxidation of methanol. RSC Adv. **6**, 50851–50857 (2016). https://doi.org/10.1039/C6RA06210E
21. Lee, S.H., Kakati, N., Jee, S.H., Maiti, J., Yoon, Y.S.: Hydrothermal synthesis of PtRu nanoparticles supported on graphene sheets for methanol oxidation in direct methanol fuel cell. Mater. Lett. **65**, 3281–3284 (2011). https://doi.org/10.1016/j.matlet.2011.07.025
22. Liu, J., Luo, Z., Li, J., Yu, X., Llorca, J., Nasiou, D., Arbiol, J., Meyns, M., Cabot, A.: Graphene-supported palladium phosphide PdP_2 nanocrystals for ethanol electrooxidation. Appl. Catal. B Environ. **242**, 258–266 (2019). https://doi.org/10.1016/j.apcatb.2018.09.105
23. Liu, M., Zhang, R., Chen, W.: Graphene-supported nanoelectrocatalysts for fuel cells: synthesis, properties, and applications. Chem. Rev. **114**, 5117–5160 (2014)
24. Malard, L.M., Pimenta, M.A., Dresselhaus, G., Dresselhaus, M.S.: Raman spectroscopy in graphene. Phys. Rep. **473**, 51–87 (2009)
25. Martins, C.A., Ibrahim, O.A., Pei, P., Kjeang, E.: Towards a fuel-flexible direct alcohol microfluidic fuel cell with flow-through porous electrodes: assessment of methanol, ethylene glycol and glycerol fuels. Electrochim. Acta **271**, 537–543 (2018). https://doi.org/10.1016/j.electacta.2018.03.197

26. Ozturk, Z., Sen, F., Sen, S., Gokagac, G.: The preparation and characterization of nano-sized Pt-Pd/C catalysts and comparison of their superior catalytic activities for methanol and ethanol oxidation. J. Mater. Sci. **47**, 8134–8144 (2012). https://doi.org/10.1007/s10853-012-6709-3
27. Qi, J., Benipal, N., Liang, C., Li, W.: PdAg/CNT catalyzed alcohol oxidation reaction for high-performance anion exchange membrane direct alcohol fuel cell (alcohol = methanol, ethanol, ethylene glycol and glycerol). Appl. Catal. B Environ. **199**, 494–503 (2016). https://doi.org/10.1016/j.apcatb.2016.06.055
28. Şahin, B., Aygün, A., Gündüz, H., Şahin, K., Demir, E., Akocak, S., Şen, F.: Cytotoxic effects of platinum nanoparticles obtained from pomegranate extract by the green synthesis method on the MCF-7 cell line. Colloids Surf. B Biointerfaces (2018). https://doi.org/10.1016/j.colsurfb.2017.12.042
29. Şen, B., Akdere, E.H., Şavk, A., Gültekin, E., Paralı, Ö., Göksu, H., Şen, F.: A novel thiocarbamide functionalized graphene oxide supported bimetallic monodisperse Rh-Pt nanoparticles (RhPt/TC@GO NPs) for Knoevenagel condensation of aryl aldehydes together with malononitrile. Appl. Catal. B Environ. **225**, 148–153 (2018). https://doi.org/10.1016/j.apcatb.2017.11.067
30. Sen, B., Kuzu, S., Demir, E., Akocak, S., Sen, F.: Polymer-graphene hybride decorated Pt nanoparticles as highly efficient and reusable catalyst for the dehydrogenation of dimethylamine–borane at room temperature. Int. J. Hydrogen Energy **42**, 23284–23291 (2017). https://doi.org/10.1016/j.ijhydene.2017.05.112
31. Sen, B., Kuzu, S., Demir, E., Onal Okyay, T., Sen, F.: Hydrogen liberation from the dehydrocoupling of dimethylamine–borane at room temperature by using novel and highly monodispersed RuPtNi nanocatalysts decorated with graphene oxide. Int. J. Hydrogen Energy **42**, 23299–23306 (2017). https://doi.org/10.1016/j.ijhydene.2017.04.213
32. Sen, B., Kuzu, S., Demir, E., Yıldırır, E., Sen, F.: Highly efficient catalytic dehydrogenation of dimethyl ammonia borane via monodisperse palladium–nickel alloy nanoparticles assembled on PEDOT. Int. J. Hydrogen Energy (2017). https://doi.org/10.1016/j.ijhydene.2017.05.115
33. Sen, B., Şavk, A., Sen, F.: Highly efficient monodisperse Pt nanoparticles confined in the carbon black hybrid material for hydrogen liberation. J. Colloid Interface Sci. **520**, 112–118 (2018). https://doi.org/10.1016/j.jcis.2018.03.004
34. Şen, F., Gökağaç, G.: Different sized platinum nanoparticles supported on carbon: an XPS study on these methanol oxidation catalysts. J. Phys. Chem. C **111**, 5715–5720 (2007). https://doi.org/10.1021/jp068381b
35. Şen, F., Gökağaç, G.: Improving catalytic efficiency in the methanol oxidation reaction by inserting Ru in face-centered cubic Pt nanoparticles prepared by a new surfactant, tert-octanethiol. Energy Fuels **22**, 1858–1864 (2008). https://doi.org/10.1021/ef700575t
36. Sen, F., Karatas, Y., Gulcan, M., Zahmakiran, M.: Amylamine stabilized platinum(0) nanoparticles: active and reusable nanocatalyst in the room temperature dehydrogenation of dimethylamine-borane. RSC Adv. **4**, 1526–1531 (2014). https://doi.org/10.1039/C3RA43701A
37. Sharma, S., Ganguly, A., Papakonstantinou, P., Miao, X., Li, M., Hutchison, J.L., Delichatsios, M., Ukleja, S.: Rapid microwave synthesis of CO tolerant reduced graphene oxide-supported platinum electrocatalysts for oxidation of methanol. J. Phys. Chem. C **114**, 19459–19466 (2010). https://doi.org/10.1021/jp107872z
38. Tan, J.L., De Jesus, A.M., Chua, S.L., Sanetuntikul, J., Shanmugam, S., Tongol, B.J.V., Kim, H.: Preparation and characterization of palladium-nickel on graphene oxide support as anode catalyst for alkaline direct ethanol fuel cell. Appl. Catal. A Gen. **531**, 29–35 (2017). https://doi.org/10.1016/j.apcata.2016.11.034
39. Wang, H., Du, J., Yao, Z., Yue, R., Zhai, C., Jiang, F., Du, Y., Wang, C., Yang, P.: Facile fabrication, characterization of Pt-Ru nanoparticles modified reduced graphene oxide and its high electrocatalytic activity for methanol electro-oxidation. Colloids Surf. A Physicochem. Eng. Aspects **436**, 57–61 (2013). https://doi.org/10.1016/j.colsurfa.2013.06.020

40. Xu, X., Zhou, Y., Lu, J., Tian, X., Zhu, H., Liu, J.: Single-step synthesis of PtRu/N-doped graphene for methanol electrocatalytic oxidation. Electrochim. Acta **120**, 439–451 (2014). https://doi.org/10.1016/j.electacta.2013.12.062
41. Yi, Q., Chen, Q., Yang, Z.: A novel membrane-less direct alcohol fuel cell. J. Power Sources **298**, 171–176 (2015). https://doi.org/10.1016/j.jpowsour.2015.08.050
42. Yi, Q., Zou, T., Zhang, Y., Liu, X., Xu, G., Nie, H., Zhou, X.: A novel alcohol/iron (III) fuel cell. J. Power Sources **321**, 219–225 (2016). https://doi.org/10.1016/j.jpowsour.2016.04.134
43. Yıldız, Y., Erken, E., Pamuk, H., Sert, H., Şen, F. Monodisperse Pt nanoparticles assembled on reduced graphene oxide: highly efficient and reusable catalyst for methanol oxidation and dehydrocoupling of dimethylamine-borane (DMAB). J. Nanosci. Nanotechnol. (2016). https://doi.org/10.1166/jnn.2016.11710
44. Yıldız, Y., Esirden, İ., Erken, E., Demir, E., Kaya, M., Şen, F.: Microwave (Mw)-assisted synthesis of 5-substituted 1H-tetrazoles via [3 + 2] cycloaddition catalyzed by Mw-Pd/Co nanoparticles decorated on multi-walled carbon nanotubes. ChemistrySelect **1**, 1695–1701 (2016). https://doi.org/10.1002/slct.201600265
45. Yıldız, Y., Kuzu, S., Sen, B., Savk, A., Akocak, S., Şen, F.: Different ligand based monodispersed Pt nanoparticles decorated with rGO as highly active and reusable catalysts for the methanol oxidation. Int. J. Hydrogen Energy **42**, 13061–13069 (2017). https://doi.org/10.1016/j.ijhydene.2017.03.230
46. Zakil, F.A., Kamarudin, S.K., Basri, S.: Modified Nafion membranes for direct alcohol fuel cells: an overview. Renew. Sustain. Energy Rev. **65**, 841–852 (2016). https://doi.org/10.1016/j.rser.2016.07.040
47. Zhang, J., Landry, M.P., Barone, P.W., Kim, J.H., Lin, S., Ulissi, Z.W., Lin, D., Mu. B., Boghossian, A.A., Hilmer, A.J., Rwei, A., Hinckley, A.C., Kruss, S., Shandell, M.A., Nair, N., Blake, S., Şen, F., Şen, S., Croy, R.G., Li, D., Yum, K., Ahn, J.H., Jin, H., Heller, D.A., Essigmann, J.M., Blankschtein, D., Strano, M.S.: Molecular recognition using corona phase complexes made of synthetic polymers adsorbed on carbon nanotubes. Nat. Nanotechnol. (2013). https://doi.org/10.1038/nnano.2013.236